Dyadic and Triadic Porphyrin Monomers for Electropolymerization and Pyrazine-Containing Architectures for Solar Energy Harvesting and Mediating Photoinduced Electron Transfer

by

Brian Lyndon Watson

A Dissertation Presented in Partial Fulfillment
of the Requirements for the Degree
Doctor in Philosophy

Approved November 2013 by the
Graduate Supervisory Committee:

John Devens Gust, Chair
Ana L. Moore
Ian Gould

ARIZONA STATE UNIVERSITY

December 2013

ABSTRACT

Natural photosynthesis dedicates specific proteins to achieve the modular division of the essential roles of solar energy harvesting, charge separation and carrier transport within natural photosynthesis. The modern understanding of the fundamental photochemistry by which natural photosynthesis operates is well advanced and solution state mimics of the key photochemical processes have been reported previously. All of the early events in natural photosynthesis responsible for the conversion of solar energy to electric potential energy occur within proteins and phospholipid membranes that act as scaffolds for arranging the active chromophores. Accordingly, for creating artificial photovoltaic (PV) systems, scaffolds are required to imbue structure to the systems.

An approach to incorporating modular design into solid-state organic mimics of the natural system is presented together with how conductive scaffolds can be utilized in organic PV systems. To support the chromophore arrays present within this design and to extract separated charges from within the structure, linear pyrazine-containing molecular ribbons were chosen as candidates for forming conductive linear scaffolds that could be functionalized orthogonally to the linear axis. A series of donor-wire-acceptor (D-W-A) compounds employing porphyrins as the donors and a C_{60} fullerene adduct as the acceptors have been synthesized for studying the ability of the pyrazine-containing hetero-aromatic wires to mediate photoinduced electron transfer between the porphyrin donor and fullerene acceptor. Appropriate substitutions were made and the necessary model compounds useful for dissecting the complex photochemistry that the series is expected to display were also synthesized.

A dye was synthesized using a pyrazine-containing heteroaromatic spacer that features two porphyrin chromophores. The dye dramatically outperforms the control dye featuring the same porphyrin and a simple benzoic acid linker. A novel, highly soluble 6+kDa extended phthalocyanine was also synthesized and exhibits absorption out to 900nm. The extensive functionalization of the extended phthalocyanine core with dodecyl groups enabled purification and characterization of an otherwise insoluble entity.

Finally, in the interest of incorporating modular design into plastic solar cells, a series of porphyrin-containing monomers have been synthesized that are intended to form dyadic and triadic molecular-heterojunction polymers with dedicated hole and electron transport pathways during electrochemical polymerization.

This dissertation is dedicated to my mother, Lesley, for her endless love, support and sacrifice shown in raising me.

Thank you.

ACKNOWLEDGEMENTS

Professor Devens Gust for supervision and guidance in conducting this work and for giving me the freedom to play with new ideas. Dr Paul Liddell and Dr Yuichi Terazono for hours of conversations in troubleshooting problems encountered in synthesis. Dr Christopher Madden, Dr Maxime Fournier and Dr Benjamin Sherman for conducting electrochemical experiments, solar cell manufacture and testing.

This research was supported through the Center for Bio-Inspired Solar Fuel Production, an Energy Frontier Research Center funded by the U.S. Department of Energy, Office of Science, Office of Basic Energy Sciences under Award Number DE-SC0001016.

LIST OF TABLES

Table Page

LIST OF FIGURES

Figure Page

Figure Page

Figure Page

Figure Page

Figure Page

Figure Page

Figure Page

Figure Page

Figure Page

LIST OF SCHEMES

Scheme Page

Scheme Page

Scheme Page

TABLE OF CONTENTS

Page

Page

Page

Page

Page

Chapter 1: Introduction

1.1 Energy, Fossil Fuels and the Environment

During a period of global atmospheric cooling, Wally Broecker published his seminal 1975 *Science* paper[1], "*Climatic Change: Are we on the brink of a pronounced global warming?*" in which the term "global warming" was used for the first time. At the time, high concentrations of particulate matter in the atmosphere resulting from increased anthropogenic activity were reflecting insolation away from the earth resulting in a decline of the mean global temperature. Broecker predicted that, as a result of increasing levels of carbon dioxide in the atmosphere originating from the combustion of fossil fuels to power man's activity, this period of cooling would succumb to "a pronounced period of atmospheric warming."[1]

Though political debate continues today[2], the strong correlation between increased atmospheric CO_2 concentrations and increased mean annual temperature is widely accepted within the international scientific community[3-11]. The long-term effects of climate change are difficult to predict and require complex models. Nevertheless the observed effects of the increasing levels of CO_2 appear to be worse than the initial predictions[5]. The long-term effects of climate change resulting from CO_2 emissions will be, largely, irreversible for 1000 years[6].

The CO_2 emissions in the atmosphere to date have been generated by a small fraction of the world's population[12,13]. The majority of the global population does not enjoy the standard of living afforded by the high level of energy consumption present in

western societies. It is of utmost importance that technology is invented that will enable the third world to develop in a manner that does not contribute further to the levels of CO_2 in the atmosphere and oceans[14].

In Lewis and Nocera's paper[15], *Powering the Planet: Chemical challenges in solar energy utilization*, they give insight to the scenarios developed by the Intergovernmental Panel on Climate Change that project the future global energy consumption. In 2001, the worldwide primary energy consumption was 425 x 10^{18} J which corresponds to a rate of energy consumption of 13.5TW[15]. Alarmingly, 86% of this energy was derived from fossil fuels[15]. Using the formula:

$$E = N.(GDP/N) \, . \, (E/GDP) \qquad (1.1)$$

in which E is the rate of energy consumption, N is the global population, and GDP is the gross domestic product, they outlined how projections for future energy consumption could be calculated using annual rates of increase in N and GDP from known values in 2001. The global population in 2001 was 6.1 billion and the global per capita GDP average was $7500. The projected annual rate of increase for the per capita GDP was expected to be 0.9% while the projected annual rate of population growth was 0.9%, giving a 2.3% yr^{-1} increase in energy consumed. Their calculation included an attenuation of this increase to account for technological advancements that improve the efficiency with which energy is utilized. This reduced the rate of increase to 1.5%. Based on 2001 values, they projected a 27TW consumption rate by 2050 and a 43TW consumption rate by 2010TW[15]. For comparison, there are proven fossil fuel reserves available to provide a

global energy consumption rate of 25-30TW[15] for several centuries implying that a carbon intensive future is possible if man chooses so, but likely, with disastrous consequences to the planet[5,10,11]. Factoring in the transition to combustion of fossil fuels with higher hydrogen to carbon ratios, such as natural gas and oil, Lewis and Nocera reported that a business as usual scenario would likely cause the annual emissions of CO_2 to increase from 6.6 $(GtC)yr^{-1}$ to 13.5$(GtC)yr^{-1}$ in 2050[15].

In 1h, 4.3 $x10^{20}$ J of solar energy strikes the earth's surface. The 2001 rate of energy usage was 13.5 TW which integrated over a year gives an annual consumption $4.1x10^{20}$ J. The implication is that more solar energy strikes the surface of the earth in an hour than was consumed in an entire year[15]. Solar energy however is diffuse and fluctuates daily and seasonally. Consequently for effective utilization of solar energy, the technology utilized must exhibit a high efficiency/surface area for conversion, and a high storage capacity while still being cheap.

Fossil fuels are an incredibly energy dense fuel and can be obtained with current technology at remarkably low price points. In 2006, the cost of electricity was approximately \$0.02-0.05 $[kW.hr^{-1}]$ while the cost for electricity derived from silicon solar cells cost \$0.35$[kW.hr^{-1}]$, considering the cost of the panels against the projected lifetime of operation[15]. These price comparisons do not take into account the required cost of an energy storage system to buffer against the diurnal and seasonal fluctuations in solar energy. Consequently, considerable progress is required to increase the efficiency of conventional solar panels employing low cost materials and similarly develop a cheap means for storing this energy.

1.2 Thermodynamics of Solar Energy Conversion

Absorption of light by the active material in photovoltaic (PV) devices occurs via interactions of photons of electromagnetic radiation, of which the light is comprised, with materials within the device. In a molecule, absorption of a photon typically results in a transition of an electron from a ground state orbital to an excited state. In line with the conservation of energy, the energy gained by the electron on absorption of the photon by the molecule or material is equal to the energy of the photon. Transitions can only occur between quantum states of the molecule or the material. Thus, only photons with energies that mach the energy gaps between the ground state and higher energy states are absorbed. Consequently, photons with energy less than the HOMO-LUMO energy gap of a molecule or the band gap of a semiconductor will pass through the molecule or material unabsorbed. In line with Kasha's Rule[16], which states that "Polyatomic molecular entities luminesce with appreciable yield only from the lowest excited state of a given multiplicity"[17], molecules excited to states of energy greater than the lowest excited state will relax thermally to the lowest excited state very quickly. The implication of this, in the context of photovoltaics, is that the maximum electronic potential energy that can be produced from a PV device will correspond to the energy of the lowest excited state of the active material. Consequently in converting solar energy to electrical potential energy, the magnitude the lowest energy transition of the active material must be carefully considered.

Solar radiation is a spectrum of light of different wavelengths, the intensities of which vary across the spectrum. For optimal conversion of the photonic energy of this

spectrum to electrical potential energy by a single or multiple band gap device, the energy gap(s) of the devise must be considered against this spectrum. If the lowest energy absorption is too large, all light in the spectrum with insufficient energy to promote the transition will pass through the active layers unabsorbed. If the energy gap is too small, photons with energy greater than that of the lowest energy excited state that are absorbed by transitions to higher energy states will relax thermally to the lowest energy excited state, giving off the excess energy as heat. Consequently, there is an optimal energy in which the trade-off between low energy photons being transmitted is weighed against the losses of higher energy photons relaxing thermally to the edge of the lowest energy excited state[18].

The American Society for Testing and Materials together with US government laboratories have developed two solar spectra used in testing photovoltaic devices[19]. Apart from obvious variances resulting from the time of day and weather conditions, insolation at the earths surface exhibits variance resulting from the thickness of the atmosphere through which the insolation passes prior to impinging on the earth's surface. The AM1.5 spectrum shown in red in figure 1.1 was developed as a standard spectrum for testing solar cells devices for the United States[19]. It represents an annual average spectral irradiance on the surface of the earth at a solar zenith angle of 48.19^{o} for a surface tilted at 37^{o} towards the equator. The spectrum is named the AM1.5 spectrum since the light effectively passes through an air mass the thickness of 1.5 atmospheres to strike the latitude 41.81^{o} for which the spectrum is calculated. The deviations present between the AM1.5 spectrum and the extraterrestrial spectrum or AM0 spectrum shown in black in firgure 1.1 result from absorptions by molecular oxygen, water and carbon

dioxide present in the atmosphere[20]. The AM0 spectrum roughly follows the spectrum of a black body radiator at 5777K, the temperature of the sun.

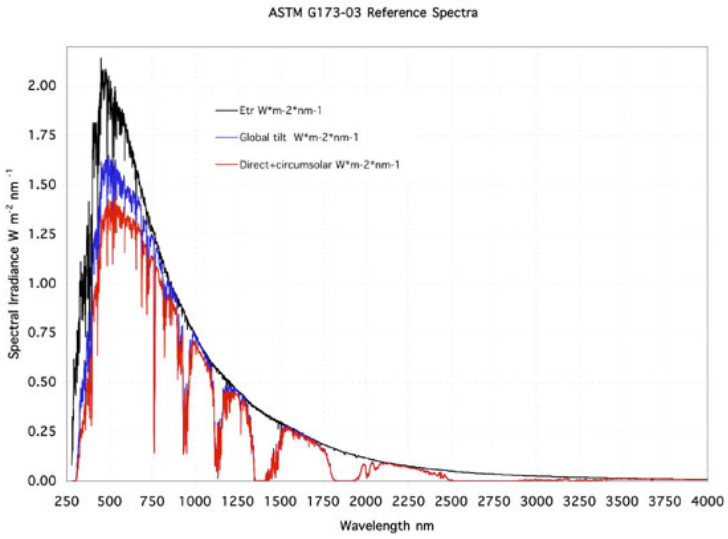

Figure 1.1 The solar spectrum in $W.m^2.nm^{-1}$ at the edge of the atmosphere the AM0 or extraterrestrial spectrum (black), at the equator, the AM1 spectrum (blue) and at latitude 41.81^o AM1.5 (red). Figure obtained from http://rredc.nrel.gov/solar/spectra/am1.5/

In 1960 Shockley and Queisser[18] published their detailed balance approach to determining the optimal energy gap for a solar cell operating at 300K irradiated by the spectrum from a black body radiator at 6000K, approximating the sun. From their calculations they concluded that the upper-limit conversion efficiency possible for a single band gap solar cell was 30%, which would be achieved by a band gap of 1.1eV. This energy corresponds to a photon with a 887nm wavelength. In 1996, Martí and Auaújo[21] refined this calculation to be based on the AM1.5 spectrum. For single band gap cells operating without concentration or reflectance, the optimal band gap was concluded to be 1.3eV. This corresponds to an upper limit conversion efficiency of 32.5%[21]. This limit is commonly referred to as the Shockley-Queisser limit. Higher conversion

efficiencies can be achieved if devices employ multiple band gaps or molecules with various HOMO-LUMO gaps arranged in series. The calculated upper limit efficiencies and corresponding energy gaps are 44.3% for two gaps positioned at 0.94 and 1.64eV, 49.7% for three gaps, each at 0.71, 1.16 and 1.83 eV and finally a 53% for four gaps, each at 0.71, 1.13, 1.55 and 2.13 eV[21].

1.3 Design Strategies for Forming Integrated Artificial Photosynthetic PV Systems

Natural photosynthesis is a wonderful example how various molecules, together with supporting structures can be used to convert solar energy, to electrochemical potential energy, electrochemical gradients and finally chemical energy in the form of bonds. The natural systems feature beautiful, highly ordered arrays of accessory pigments housed within proteins that capture various portions of the solar spectrum, transferring the resulting excitation energy efficiently to reaction centers with near unity quantum yields under low light conditions. Excitation of the P_{680} reaction center of PSII produces a P_{680}^{*} excited state that decays with a 3ps lifetime by donating an electron to a primary electron acceptor, pheophytin[22,23]. A nearby immobile quinone, Q_A, subsequently accepts (250-300ps) this electron from the pheophytin, extending the distance over which the charge is separated[22,23]. A tyrosine residue adjacent to the P_{680} reaction center acts as a secondary electron donor, donating an electron to satisfy the hole residing on P_{680}^{+} with a 20ns-35μs lifetime[22,23]. The hole of the tyrosine residue is ultimately filled by electrons from the nearby manganese water oxidation complex on a 50μs-1.3ms timescale[22,23]. With the charges well separated, the electron residing on Q_A can be donated to a second

quinone, Q_B, which occurs on a much slower 100-200μs timescale[22,23]. After two cycles of this process, Q_B, having been reduced twice and having accepted two protons from the lumen of the thylakoid space, can exit and become part of the plastoquinone/hydroquinone pool within the thylakoid[22,23].

This process clearly exhibits how a cascade of acceptors and donors positioned on either side of a reaction center can act to increase the distance over which charges are separated following the primary charge transfer event. With each successive transfer, the Coulombic force of attraction that promotes charge recombination is diminished, and so increases the overall yield of charge separation. Each successive charge transfer requires a small thermodynamic driving force in order to occur quickly, and so, a small energy penalty is paid to achieve the long-lived charge separated state. In each successive electron transfer along the acceptor cascade, the high-energy electron produced on absorption of a photon moves to a LUMO with lower and lower energy, diminishing the resulting reduction potential of the electron. Similarly, each successive donation of ground state electrons from $HOMO_{donor}$ to $HOMO_{acceptor}$ causing the hole to move away from the reaction center diminishes the oxidation potential of the resulting hole.

Silicon solar cells are to date, the cheapest and most widely employed photovoltaic technology. The contrast between the simplicity of these cells with regard to composition, form and function in comparison to the natural photosynthetic machinery responsible for the related roles of light absorption and charge separation is quite astonishing. In neglecting a considerable portion of the photosynthetic machinery responsible for the conversion of absorbed photon energy into chemical potential energy as chemical bonds, and simply focusing on the elements responsible for the early events

in photosynthesis, specifically, absorption of photons and conversion of photons to electric potential energy, it is clear how incredibly complex and diverse the composition, form and function of the natural systems are.

The antenna systems employ a variety of complex pigments arranged in very specific orientations within protein scaffolds. The proteins themselves are arranged within phospholipid membranes that perform a structural role to house the proteins and compartmentalize the chloroplast matrix into the stroma and lumen between which electrochemical gradients can be generated. As already described, the function of the reaction employs a variety of pigments and a cascade of acceptors and donors to facilitate charge separation. All of these are contained and ordered very specifically within highly tuned proteins.

The essential point is that in trying to mimic the complex functioning of the natural photosynthetic machinery responsible for solar energy harvesting and conversion to electric potential energy with molecular constructs, one quickly moves away from the simple bulk material sandwich of the pn-junction silicon solar cell. Creating molecular systems designed to mimic and exploit the fundamental photophysics and electronics of the natural photosynthetic systems will likely, even in the simplest form, feature many different components and materials, each of which needs to be assembled into a complex and fully functional system.

To reduce the complexity of artificial systems and the number of components employed, the components of the system can be designed to perform more than one role. Coupling an elementary functional role such as light absorption or mediating charge transfer with a structural role is one such example and provides a way to negate the need

for the complex protein scaffolds present in the natural systems. Designing integrated organic systems in which the organic molecules employed are required to perform both the necessary photophysical or electronic roles and act as a structural entity imposes an additional selection criterion on the chromophores, donors, acceptors and semiconductors to be used in the systems. If the structural properties of the organic components required for carrying out the requisite light harvesting, charge separation and carrier transporting functions are not exploited, then additional molecules or materials are required to structure the system, adding to the number of elements required for building it.

An example in which a structural and a functional role are coupled in present artificial technologies is the use of mesoporous TiO_2 in dye-sensitized solar cells[24]. The mesoporous TiO_2 acts as a high-surface area structural support to which dyes are attached and as a semiconductor, accepting high-energy electrons from excited dyes and transporting them to the electrodes for collection[25]. The structural role of the mesoporous TiO_2 must not be underestimated. It enables the chemist to create a device in which millions of dye molecules can be positioned densely within a minimal volume to achieve the necessary cross-sectional absorbance but are still spatially separated from one another to enable the solution state electrolyte to access and interact with the dye molecules directly. Mesoporous TiO_2 however, is an inorganic material and not an organic molecule or polymer. It is still a very disordered material and so, is difficult to interface with solid state, hole-conducting materials. Cell works best with liquids that can access the porous structure to perform the necessary electrochemistry[26].

Very crudely, the essential functions required for conversion of solar energy to electric potential energy are: absorption of photons from sunlight to produce an excited

state of a molecular entity or of a bulk material; movement of this excitation energy to a reaction center or donor-acceptor interface, at which point electron transfer can occur; separation of the electron-hole pair resulting from the primary electron transfer event, and finally; collection of the respective electrons and holes by a conductor[27].

Form an engineering standpoint, designing systems in a modular fashion allows for each component to be optimized separately in accordance with a dedicated role assigned to the component. There is a tradeoff between designing systems in a modular fashion in which each component performs a single, specific role and can be optimized independently of the other components, and simple systems that feature only a few components, each of which is responsible for a multitude of roles to achieve the overall function of solar energy conversion. These latter systems are harder to optimize. Modifying a given component to optimize one function without impacting the functionality relating to other roles performed by the same component is difficult.

Modern organic chemistry has developed to a level of sophistication that allows the synthetic chemist to synthesize incredibly complex molecules from a wide library of commercially available starting materials. The atoms commonly present in organic molecules are earth abundant and relatively cheap. Consequently, a molecular approach to designing complex systems out of organic molecules could be a very promising route to producing cheap, scalable, photovoltaic technologies. The architectures designed could be continuously optimized through incremental changes or completely overhauled and redesigned along completely different design strategies that couple different functional requirements into separate components.

Considerable work has been conducted by members of the groups led by Gust, Moore and Moore[28-40], Lindsey[41-48], in mimicking various elements of the complex photophysics present in the early events in natural photosynthesis. These include the synthesis of molecular assemblies that exhibit energy transfer between the constituent chromophores, (dyads, triads and pentads) that both mimic antenna functionality and exhibit sequential electron transfer events characteristic of donor and acceptor cascades. The potential applications of the photophysical knowledge uncovered over the years through these studies are broad. In the context of photovolatics, they can be of particular importance for engineering the next generation of solar cells to exhibit high spectral responses by using antenna arrays and high internal quantum yields of energy conversion by using donor and acceptor cascades to facilitate separation of electron hole pairs following the initial electron transfer event.

There are two advantages to using antennas in systems. The first is that many chromophores can act to absorb solar radiation, while only a small number of the chromophores present in the system perform the dedicated role of charge separation in reaction centers. This separates the function of harvesting light from the role of creating the charge-separated state. Secondly antennas enable more of the solar spectrum to be captured and utilized. A central assumption of calculations by which the Shockley-Quessier limit is derived is that all photons with energy greater than that of the band gap are absorbed, and all equally so. This assumes that there is a continuity of states above the LUMO orbital. This is often not the case for molecules, the absorptions of which show considerable variance across the spectrum. For absorption to occur there must be a transition from the ground state to a higher energy state that matches the energy of the

photon. Consequently for molecular systems designed for solar conversion, accessory antenna systems will be necessary to complement the spectrum of the pigment that acts as the reaction center and exhibits the lowest energy 1st excited state.

Secondly, antennas can be used to reduce the quantity of material required to mediate carrier transport. Excitation energy generated within an antenna array can be transferred by coherently or by successive energy transfer events to a reaction center. If an alternative system is considered in which each chromophore acts as a reaction center, transferring an excited electron to an electron or n-type semiconductor, then a considerable quantity of the n-type semiconductor will need to be present in order to extract the excited electrons from the system. An efficient antenna system that "funnels" the excitation energy to dedicated reaction center chromophores thus minimizes the quantity of charge transporting material required in the system.

Very complex systems can be envisaged in which chromophores would be arranged in ordered and specific geometries to act as antennas, funneling excitation energy to a reaction center, at which point charge separation would occur. Secondary and higher order donors could be present in a donor cascade to quickly remove the positive charge away from the primary donor chromophores in the reaction center and similarly, secondary and tertiary acceptors that could shuttle the accepted negative charge away from the positively charged hole. Finally, n-type or electron conducting and p-type or hole conducting organic or organometallic wires arranged in an ordered fashion could facilitate the transport of the separated charges at the end of the donor or acceptor cascades to the terminal electrodes. Creating a regularly ordered system that maintains long-range order over the necessary distance to effectively absorb the solar radiation is a

very challenging task. Despite the incredible progress that has been made in mimicking various aspects of the natural photosynthetic system, integrating the mimics into a functional and highly ordered systems has not been attempted and would be difficult without having the correct structural support that maintains the arrangement of each functional component relative to the next.

Two broad challenges stand in the way of creating artificial photosynthetic mimics of natural systems that couple the fundamental functional roles required for solar energy conversion with the constraint that the elements that perform these functions must also perform the structural role. Broadly these challenges are designing and synthesizing the structures and finding a way to assemble them. The following section briefly reviews a few of the areas in which organic chemistry has been employed in PV technologies.

1.4 Prominent Organic PV Technologies

Organic chemistry has been widely employed in the development of future photovoltaic technologies. Organic materials are relatively cheap and feature earth abundant atoms. The three major types of solar cells in which organic materials feature prominently are organic (or plastic) solar cells[49], hybrid solar cells[50-52] and dye sensitized solar cells[25] (DSSCs). Each of these types of cells have areas in which bio-inspired mimics of the natural photosynthetic process can be incorporated into the designs to improve their efficiencies.

The bulk heterojunction solar cell is a good starting point for understanding the essential features of organic solar cells. Two bulk-phases exist, sandwiched between two

conductive contacts. Typically one phase acts as the donor phase and is usually responsible the majority of the spectral response of the cell. The donor phase is comprised of an organic molecule, oligomer or polymer such as a derivative of polythiophene. Under irradiation, electrons within the donor-phase are excited to form an excited state or Frënkel exciton. The exciton will then migrate through the donor-phase until it reaches the donor-acceptor interface, at which point, electron transfer from the donor-phase into the acceptor phase can occur. The negatively charged electron in the acceptor-phase, commonly PCBM, a C_{60} derivative, must then diffuse through the bulk acceptor phase to the anode. Similarly, the hole residing in the donor phase must diffuse though the bulk-donor phase to the cathode.

Immediately following the electron transfer event at the junction, the hole and electron residing in the donor and acceptor phases respectively will still experience an electrostatic attraction to one another that is attenuated by the dielectric constant of the organic material between the two charges. As organic materials often do not exhibit very large dielectric constants, these charges will still experience significant attraction to one another[27]. This can act to cause the two carriers to recombine, releasing heat in the process.

Excitation can also occur within the acceptor phase. In this scenario, for a photovoltaic response to be derived from this excitation, the exciton would need to migrate to the phase junction and then oxidize the donor phase. This establishes the same situation as that which followed electron transfer resulting from donor-phase excitation.

Hybrid solar cells utilize a high-surface area semiconducting metal oxide such as mesopourous TiO_2 or ZnO nanorods[52] as the electron acceptor and an organic material as

the donor phase. Ideally, the organic material would make good contact with the surface area of the metal oxide, filling the pores and crevices of the structure[53]. In practice this is quite difficult to achieve. The predefined, continuous and rigid structure of the metal oxide semiconductor does however offer the advantage over fully organic bulk heterojunction solar cells in that in assembly, a bi-continuous phase already exist and the problem of creating phase islands is negated. In hybrid cells, the organic material acts as both the donor phase and hole conducting material, sensitizing the semiconducting metal oxide. During cell function, the organic donor phase absorbs light to form an exciton which, as in the bulk heterojucntion cell, diffuses to the donor-acceptor interface, at which point, electron transfer from the organic donor phase into the metal-oxide can occur. Provided recombination does not occur, the residual hole in the organic phase must diffuse back through the organic donor phase towards the cathode for collection. The electron injected into the conduction band of the metal oxide must diffuse to the anode for collection.

Dye sensitized solar cells[24,25,54] feature organic-dye molecules adhered to a high surface area semiconducting oxide surface. The high surface area of the semiconducting oxide allows for many dye molecules to be present in a given volume of the semiconductor material[24]. The additive effect of all of the extinction co-efficients of the adsorbed dyes produces a material that absorbs a considerable fraction of the solar spectrum. Under normal cell function, a photon will be absorbed by a given dye molecule causing a transition of a ground state electron from the HOMO to the LUMO of dye. The LUMO is designed to be more energetic than the conduction band edge of the semiconducting metal oxide and so can inject the excited electron into the conduction

band of the semiconducting oxide. This electron will then travel through the metal oxide until it reaches the metal anode for collection. Turning attention back to the dye molecule, the hole residing in the HOMO of the oxidized dye must be reduced by a solution state electrolyte, returning the dye to its neutral ground state ready for subsequent excitations. The oxidized form of the electrolyte or Red-Ox mediator will then diffuse through the solution to the cathode, typically a platinum metal surface, where it will be reduced. The difference in energy between the conduction band of the semiconducting oxide in the photoanode and the oxidation potential of the oxidized Red-Ox mediator will determine V_{OC} produced by the cell.

1.5 Scaffolds that Mediate Carrier Transport

The efficiencies of plastic organic solar cells have not yet been able to match the efficiencies obtained by dye-sensitized solar cells[26]. The latter technology is arguably more complex and utilizes a modular design together with coupling of structural and functional elements. It is not coincidental that the more complex system exhibits higher conversion efficiencies; researchers have been able to systematically optimize each component of the modular DSSC over the last two decades with great success. As mentioned earlier, DSSCs feature a structural component that also performs a vital functional requisite for solar energy conversion that of carrier transport. The high surface area of mesoporous TiO_2, once functionalized with organic dyes, produces a hybrid material with an incredibly high cross-sectional absorption, exhibits a high reaction center density and is capable of electron transport over considerable distances[24,25,54]. A

drawback of mesoporous TiO_2 in with the view of forming a system as shown in figure 1.2 is the disordered and unpredictable structure of the material.

The intrinsic disorder means that holes present on dye molecules following injection must be transported by a solution state Red-Ox mediator or a solid state hole-conducting material that can be deposited in the liquid sate, and so interface well with the highly porous material. The high surface area, ease of functionalization, well positioned band edges and good carrier mobilities of TiO_2, the backbone of DSSCs technology has resulted in DSSCS showing a dominant presence in the literature for the past two decades. Room still exists for designing new dyes for use in DSSC to feature secondary and tertiary donors generating functional triads and tetrads if the TiO_2 is views as the primary acceptor. Large antenna arrays could be synthesized and covalently bound to a primary reaction center chromophore, but due to the variance in pore size of the mesoporous surface, the possibility exists that smaller pores will not be able to accommodate the larger antenna arrays. The variance in the surface structure of mesoporous metal oxides also prohibits systems in which the long-range order of the scaffold (in this case TiO_2) can be utilized as a scaffold from which ordered arrangements of antennas can be synthesized.

The pioneering work by Omar Yaghi and Michael O'Keeffe in developing reticular chemistry for the synthesis covalent organic frameworks and metal-organic frameworks (MOFs) in the last two decades has demonstrated how materials with considerable long range order can created by using organic building blocks tailored with the specificity afforded by the organic chemists remarkable toolbox[55-64]. The stepwise synthesis of MOFs has also been achieved[65-68], allowing for MOFs to be grown from

surfaces using sequential dipping. It is foreseeable that the MOF structures could be engineered to be conductive, forming a porous material with long-range order and with very specific pore sizes. These structures could then be utilized to perform a role analogous to TiO_2 in DSSCs but would offer the advantage of exhibiting a higher degree of order. Functionalizing the organic building blocks with chromophores to fill these pores with pigments would produce 3-D materials with very strong light absorbing properties.

MOF's have already been synthesized to feature porphyrin chromophores that exhibit efficient energy transfer from porphyrins through the MOF as a result of the high degree of order that they exhibit, transferring excitation to a terminal energy acceptor[69]. It is conceivable that a conductive MOF or COF backbone could be synthesized that acts as an electron acceptor and semiconductor to transport excited electrons from pendant chromophores to a metallic contact. The oxidized chromophores could be reduced by a Red-Ox mediator in solution or by a secondary donor connected to an intercalating p-type semiconducting MOF. Central to this objective is the presence of an n-type semiconducting organic backbone that can be incorporated into a MOF and can be easily functionalized to subtend organic chromophores.

1.6 Polymeric, Triadic Molecular Heterojunctions

The production of bulk heterojuntion solar cells is a challenging task. To increase the surface area at which charge separation can occur, and so, reduce the distance over which excitons need to migrate before charge separation can occur, intimate mixing of

the bulk phases is required. Achieving a high degree of interpenetration in a manner in which phase islands are not produced limits the degree to which this interpenetration can be achieved. Following charge separation at a phase interface, the respective carriers must travel through the respective phases to the appropriate electrodes. If phase islands are produced in the manufacture of the cells, carriers formed at the edge of these islands will have no means by which to travel to the appropriate electrode resulting ultimately in recombination and losses in efficiency.

Chapter 2 presents a more detailed analysis of the functioning of molecular heterojunction solar cells and some of the problems that are inherent in the lack of complexity inherent in their design. The design of a system that seeks to overcome some of these problems is presented. In line with some of the design principles of the molecular approach to artificial photosynthesis discussed already, the system proposed, the requisite monomers for which have been synthesized, is designed to exhibit triadic functionality and forms a polymer with dedicated hole and electron conduction pathways, negating the need for mixing of two phases. This design increases the complexity of the plastic cell in comparison to the bulk heterojunction by engineering components responsible for dedicated roles into the system, separating the functions of absorption and conduction and altogether mitigating the need for exciton diffusion by drastically increasing the reaction center density within the material.

1.7 Designs for Organic Artificial PV Systems Incorporating Mimics of Natural Systems

Porphyrin chromophores have featured prominently in the model compounds produced to mimic the photophysics of natural photosynthesis. They exhibit strong cross-sectional absorbencies and their spectra can be modified by varying the functionality present at the *beta* and *meso* positions, or through metallation of the core with different atoms. In line with the need for components for use in artificial systems that exhibit good structural properties, the geometry of porphyrins is particularly convenient. The *meso* positions can be easily and diversely functionalized to subtend four axes that meet at the center of the porphyrin, forming the centre of a square planar geometry. Very few organic molecules exhibit this property. Consequently, when viewed as a structural building block, the porphyrin macrocycle could serve as a convenient unit for constructing arrays that exhibit long-range order.

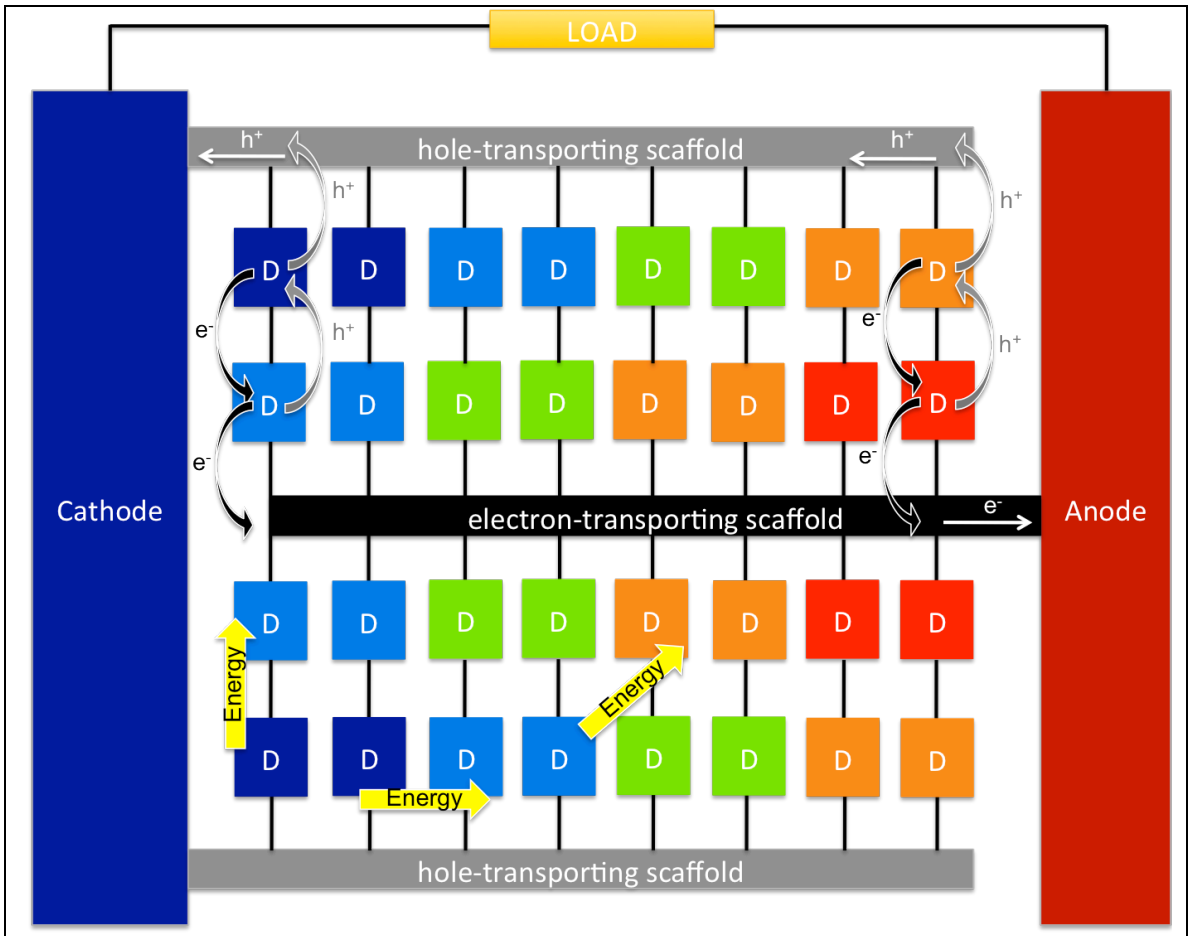

Figure 1.2 Design of an idealized organic photovoltaic device featuring chromophores that act as donor and acceptor cascades and as an antenna array. Hole and electron transporting scaffolds support the array and mediate carrier transport.

Figure 1.2 shows an idealized depiction of a design for an organic photovoltaic device that employs a variety of chromophores (possibly porphyrins) that complement one another spectrally and are arranged in an array that would funnel excitation energy from the more blue absorbing chromophores to the more red absorbing chromophores. The electron transporter shown in black is intended to act as the primary electron acceptor for all of the choromphores bound directly to it and as secondary or final electron acceptor for chromophores acting as secondary donors to the primary donors. This transporter or

semiconductor is intended to exhibit both a structural role and to mediate the transport of carriers. The function of the electron transporter shown in black can be relaxed to perform simply a structural role without requiring it to act as a charge carrier if the transfer of energy through the antenna array created is efficient at directing excitation to the red-most absorbing dye closest to the photoanode. The structure shown in black is thus a scaffold first, and a carrier transporter second.

When the scaffold shown in black acts as an electron transporter, the array of chromophores acts as a two dimensional donor and acceptor cascade as well as an antenna array. Holes generated following electron transfer into the scaffold can be replenished by subsequent electron transfers from the HOMO orbitals of adjacent chromophores and finally from the valence band of the hole transporting scaffold. The linear and parallel arrangement of the electron and hole transporters further structures the material produced, fixing the array in place. This is indeed a very strict design prerequisite if the transporters are polymeric entities comprised of regular repeat units. It requires that the dimensions of the repeat units of the corresponding transporters match exactly. This design constraint can be relaxed if the charge transport function of each transporter is replaced by adjacent iso-energetic acceptors or donors between which charges can move by incoherent charge-hopping.

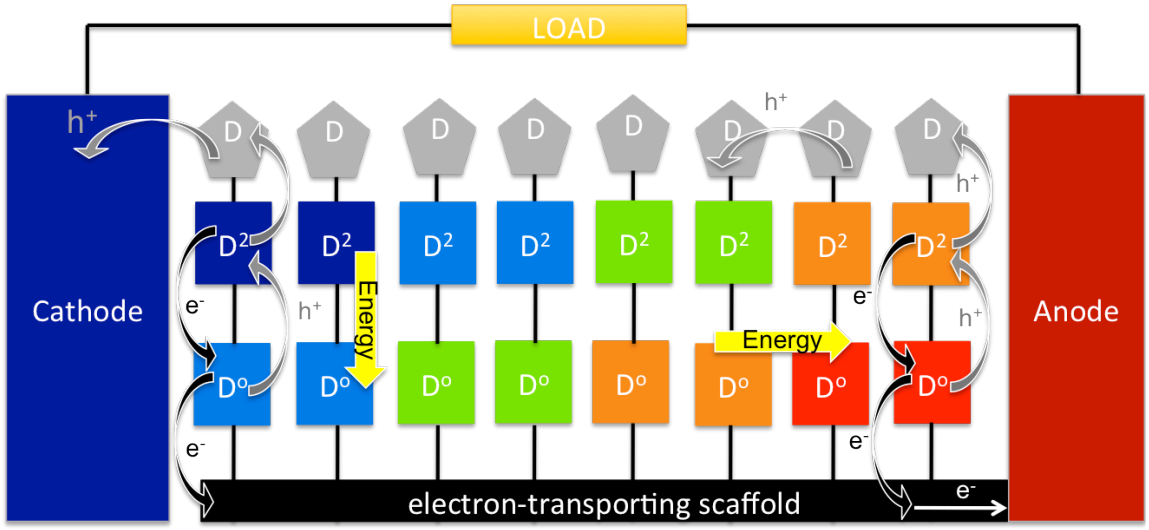

a

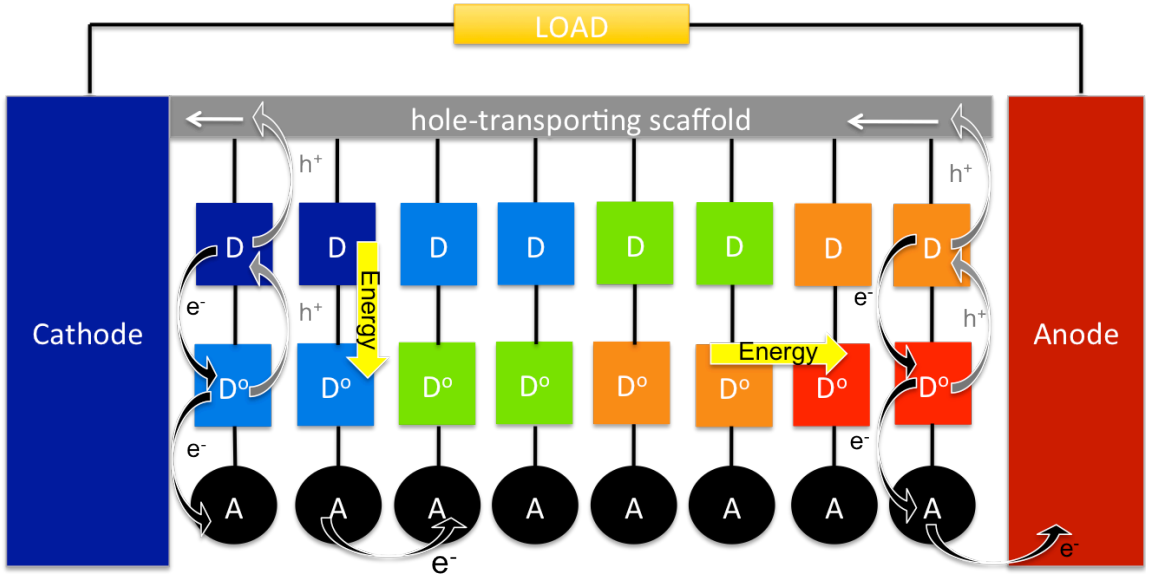

b

Figure 1.3 a.) Design of an idealized organic photovoltaic device featuring chromophores that act as donor and acceptor cascades and as an antenna array. An electron-transporting scaffold supports the array and mediates electron transport. Hole transport is mediated by hopping along the terminal isoenergetic donors of the array. b.) Similarly, a hole-transporting scaffold supports the array and mediates hole transport. Electron transport is mediated by hopping along the terminal isoenergetic acceptors of the array.

If this substitution is made, as shown in figure 1.3.a and b, the demands on the remaining carrier transporting scaffold to act as a structural support and to confer order to the system are increased. A rigid entity exhibiting minimal rotation between any subunits would be required.

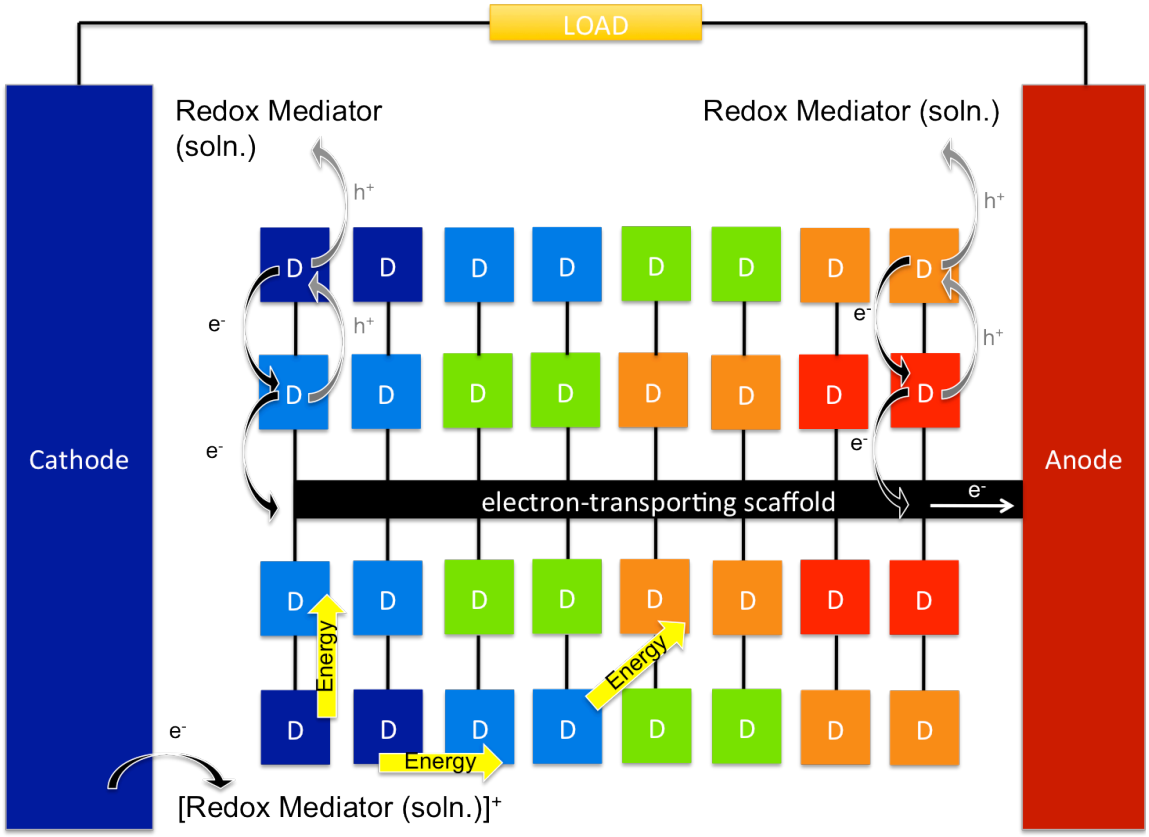

Figure 1.4 Design of an idealized organic photovoltaic device featuring chromophores that act as donor and acceptor cascades and as an antenna array. An electron-transporting scaffold supports the array and mediates electron transport. Hole-transport is mediated by a solution state Red-Ox mediator.

Figure 1.4 shows the system simplified even further. The hole-transporting scaffold of figure 1.2 and the terminal donor along which holes hop in figure 1.3 have been removed and the cell now features a solution state Red-Ox mediator responsible for reducing the terminal donors of the cascade and transporting holes to the cathode by

diffusion. Common to all three systems in figure 1.2, 1.3a and 1.4 is the electron-conducting scaffold shown in black.

The necessary attributes of the conducting scaffold shown in black are that it is rigid, can be functionalized orthogonally to the longitudinal axis, features a conduction band or LUMO orbital that is sufficiently stabilized to accept electrons from excited state chromophores such as porphyrins, a band gap that is larger than that of the choromophores employed in the array to prevent fluorescence quenching of the donor chromophores and finally, exhibits good electron mobilities for conduction of the accepted charges to the anode.

1.8 Charge Transfer Across Organic Bridges and Wires

Organic molecules are able to mediate the transfer of charges across space. There is some variance in the terminology used with regard to the molecular entity by which charge transfer is mediated with the terms, bridge and wire featuring prominently. Weiss *et al.* point out[70] the liberty with which the term molecular wire has been used in the literature, ranging from a broad definition; "a molecule connected between two reservoirs of electrons"[71]; more specifically as "a molecule that conduct(s) electrical current between two electrodes"[72], and finally according to the characteristics of the wire as a species that conducts in a regime "wherein the distance dependence [of electron transfer] may be very weak"[73].

Three basic approaches exist for studying organic structures for their ability to mediate the transfer of charge between two points. The first approach uses molecules

functionalized with sulfur atoms on two opposite termini. Sulfur exhibits a strong binding affinity for gold and so provides a means to covalently bind a molecule between two gold electrodes, forming a junction. The conductances of the molecules can thus be tested by varying the Fermi-levels of the two respective gold contacts that they span and measuring the resulting current.[71,72,74-79]. The second approach still employs a gold electrode to which one side of the molecule is bound by a gold atom while the opposite terminus is functionalized with an electroactive compound such as ferrocene. The charge transport across the "wires" can then be studied by AC voltammetry[80]. The third broad approach involves the synthesis of soluble covalent donor-wire-acceptor (D-W-A) compounds in which the donors are chromophores that are known to exhibit good photoinduced electron transfer characteristics and the acceptors are molecules capable of accepting an electron from the donors, exhibiting good spectroscopic signatures in the reduced state[73,81-88]. In this latter strategy, the study is performed in the solution state and inferences about the wire or bridge are made from the electron transfer rates and dark charge recombination rates exhibited by the compound. Extensive theory has been developed to understand the transport of charge across the junctions and enables researchers to make comparisons between the conductances obtained through the electrode based experiments and electron transfer rates obtained from the D-W-A compounds [89].

Electron transfer through shorter molecular bridges typically occurs via tunneling processes. In the superexchange mechanism[90,91], electron transfer occurs via a tunneling process between donor and acceptor moieties, between which the orbital overlap without the bridge present is largely negligible. In this type of transfer process, the presence of the bridge contributes high lying virtual orbitals that serve to mix with the donor and

acceptor orbitals between which the transfer occurs. The role of the bridge, the orbtials of which are energetically inaccessible by the fermion being transferred, is largely to enhance the coupling of donor and acceptor orbitals[70,92]. No nuclear motion occurs in the bridge during the charge transfer process[70].

Electron transfer over long distances is an inherently nonadiabatic process, the rate of which is determined by a combination of tunneling, which exhibits a strong distance dependence and inchoherent processes, which exhibit markedly weaker distance dependences[70]. In the superexchange mechanism[91,93] of charge transfer across bridges, the electron tunnels from the donor to the acceptor. The rates of electron transfer from donors to acceptors across bridges via the superexchange mechanism exhibit three broad trends[78,79]. The rate of charge transfer decreases with increasing length of the bridge. There is a strong correlation between the degree of conjugation of the bridge and the rate of charge transfer. Finally, the smaller the energy gap between bridge virtual states and donor and acceptor orbitals between which the charge transfer occurs, the higher the charge transfer rate. Consequently, shorter, highly conjugated bridges with LUMO energies more closely matching those of the donor and acceptor will exhibit higher electron transfer rates[78,79].

The electron transfer rate across bridges and wires is often modeled using the exponential function:

$$k = k_0 \, e^{-\beta(r-R)} \tag{4.1}$$

in which (r-R) is the separation of the donor and acceptor (the length of the bridge less the van der Waals contact distance). The pre-exponetial factor k_o is the rate for electron

transfer at the van der Waals contact distance, ~3.5Å and β is the attenuation factor. The electron transfer is consequently an exponentially decaying function dampened by the attenuation factor β[78,79,94].

In this type of transfer the coupling between the donor and the acceptor, V_{DA}, by the bridge can be described by

$$V_{DA} = (V_{DB}V_{BA}/\Delta E_{DB}) (V_{BB}/\Delta E_{DB})^{N-1} \quad (4.2)$$

in which V_{DB} is the matrix element for the coupling between the donor and bridge, V_{BB} for that between the N equivalent subunits of the bridge and V_{BA}, for that between the bridge and acceptor. The energy gap between the donor and bridge states is ΔE_{DB}.[78,79,94] Accordingly, for superexchange, β is described as a function of this energy gap, the coupling between the donor and the first bridge subunit, the bridge-bridge subunit coupling, and the length of the bridge subunit R_B [70,91,94]

$$\beta = (2/R_B) \ln(\Delta E_{DB}/V_{BB}). \quad (4.3)$$

In incoherent charge transfer, the electronic states of the wire are accessible by the electron being transferred. The transfer process involves the wire actually accepting the electron and real intermediate states are involved in the transfer process. These are coupled to the nuclear motion of wire[70]. The mechanism of incoherent charge transfer is thermally activated hopping in which the electron hops sequentially, incoherently from intermediate state to state. Each short transfer is in itself a tunneling event. Incoherent

charge hopping exhibits much weaker distance dependence than charge transfer that occurs via superexchange. While values for the attenuation factor β should be used in the description of exponentially decaying process, the use of eq. 4.1 as a benchmark for characterizing the behavior of molecules in mediating charge transfer has become common practice. β values are frequently used as a measure to give insight to if they mediate charge transfer by super-exchange, intermediately via incoherent charge transfer or coherently, as true wires, exhibiting coherent wire-like charge transfer[70].

Inspection of eq. 4.3 reveals the importance of the electronic coupling between subunits of a wire or bridge. If the subunits are able to rotate relative to one another, the Pi-systems will be able to decouple, increasing the value of β. For this reason it is important that in the design of molecular wires, the structures are engineered to either prevent rotation or be free from significant decoupling during normal molecular motion, such as when benzene rings are used in conjunction with alkynes. Similarly, the alignment of the donor and wire orbital energies is a central factor, implying that systems D-W-A systems designed for solution state analysis of a given type of wire must be engineered precisely to match the orbital energies of the donor and wire.

1.9 Pyrazine-Containing Structures as Candidates for Electron-Transporting Scaffolds

As discussed, organic structures featuring extended conjugation can facilitate charge transfer over very long distances via incoherent charge hopping processes. P-type organic semiconducting materials feature prominently in the literature, but there are considerably fewer examples of n-type organic semiconducting materials[95]. A basic rule

of thumb for carrier transport by organic materials is that holes travel through HOMO orbitals and electrons travel through LUMO orbitals. The energetic positions of these HOMOs or LUMOs relative to those of other electron donors and acceptors or Fermi-levels of metallic conductors present in the cell architecture will play a role in determining if they acts as hole transporters or electron transporters. Essentially, an organic material being described as being hole-conducting or electron conducting can be a relative description. The unbalanced presence of hole conducting materials in the literature over electron conducting materials is likely due to the difference in how the HOMOs and LUMOs are destabilized and stabilized respectively with increasing conjugation as monomeric units are added to form longer and longer oligomers. The HOMO-LUMO gaps of extended aromatics and polyenes steadily decrease with increasing conjugation. The HOMO orbitals are destabilized as conjugation is increased resulting in HOMO orbitals that are suited to act as electron donors, or as p-type semiconductors. Similarly LUMO orbitals are increasingly stabilized, yet, as a broad generalisation not as quickly as the HOMO orbitals are destabilized. For an extended aromatic or polyene to act as an n-type conductor it must act as an electron acceptor presenting states with intermediate energy between the two reservoirs of charges between which it is mediating electron transfer. To achieve this, the LUMO orbital must be stabilized to bring it into an energy region where it is appropriately poised to accept electron density from donor chormophores. This can be achieved by extending the degree of aromaticity or length of the polyene. As a prerequisite for acting as an electron acceptor and a conductor, the scaffold shown in black in the PV designs of figures 1.2, 1.3 and 1.4 must present a LUMO with an appropriately poised energy to be able to

accept electrons from the excited chromophores. It must also exhibit a HOMO-LUMO energy gap of energy greater than those of the donor chromophores. This is to prevent the wire from quenching the excitation energy by acting as a fluorescence energy acceptor.

Stabilization of the LUMO orbitals of conjugated molecules can be achieved by using electronegative atoms. There are only three second row atoms that are more electronegative than carbon. They are oxygen, nitrogen and fluorine. Of these, nitrogen, the atom with the highest valency is the only one that can be incorporated into an extended conjugated motif of alternating single and double bonds, the minimum valency for which, is conveniently three. Nitrogen present in the form of amines undergoes reversible reactions with carbonyl compounds to form Schiff-bases. Condensing an aromatic *o*-diamine with an *o*-diketone produces a heteroaromatic pyrazine.

GAO-6

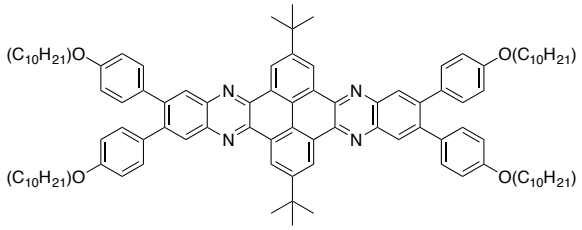

GAO-8

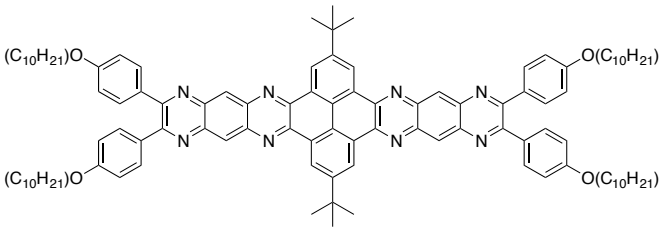

GAO-11

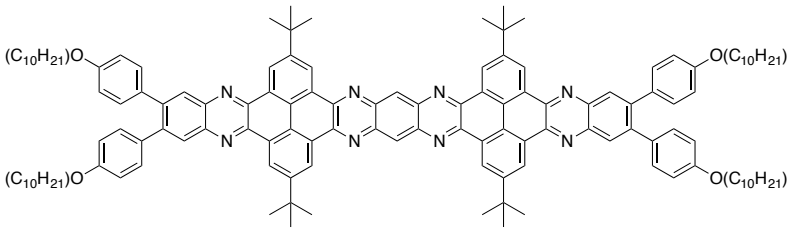

GAO-13

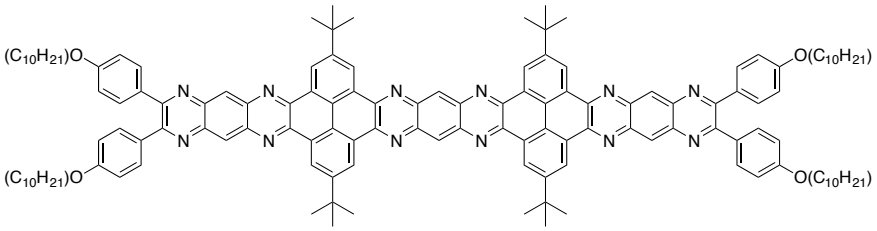

GAO-16

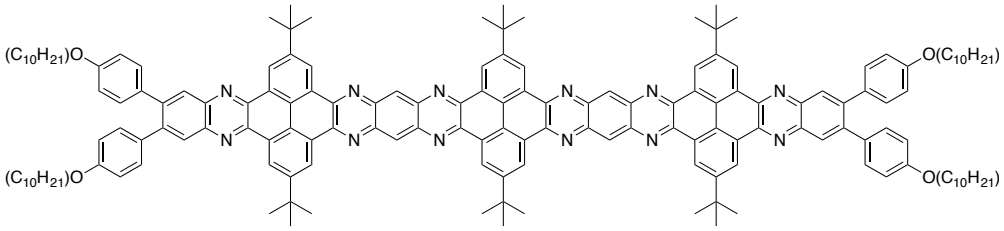

Figure 1.5 Pyrazine-containing rectilinearly fused molecular ribbons published by Gao *et al*.[95]

Gao *et al*. published[95] a series of rectilinearly-fused heteroaromatic ribbons shown in figure 1.5 that were synthesized by condensing various *o*-diketones with aromatic *o*-amines. The longest of the reported ribbons contained 16-rectilinearly fused aromatic rings shown in figure 1.5 as **GAO-16**. The molecules in the series all feature electron deficient pyrazine rings and pyrene cores. Table 1.1, reproduced from the report by Gao *et al*. shows data for the UV-Vis absorptions, fluorescence, and electrochemistry of the ribbons.

An attractive property of the ribbons is the pyrazine core, which can be functionalized to subtend various functionalities orthogonal to the axis of the ribbon, as is required for the electron-conducting scaffold shown in figures 1.2, 1.3, and 1.4. The nitrogen atoms present in the ribbons serve to stabilize LUMO orbitals as can be seen from the reduction potentials in ($E^{red}_{1/2}$) Table1.1. Analysis of the first reduction potentials together with the onset reduction potentials and the HOMO-LUMO gap, one notices that as the length of the ribbons increases, the HOMO-LUMO energy gaps begin to level off. The energy gaps to not diminish as quickly with increasing length for the longer ribbons. **GAO-16** exhibits E_{gap} = 2.18 eV and the first reduction potential ($E_{1/2}{}^{1}$) of the series stabilizes towards a value near -0.71 V (vs Ag/AgCl). This data indicated that these types of molecular ribbons may be suitable for use with appropriately tuned porphyrin chromophores for use as the required electron conducting scaffold. **GAO-16** is still remarkably short compared to the length that would be required to achieve a reasonable absorption cross section when functionalized with chromophores. The E_{gap}, at 2.18eV was considerably larger than the Shockly-Queisser limit of 1.3eV, indicating sufficient room for play if E_{gap} did diminish further as the ribbons' lengths were increased

to appreciable lengths and still not quench the excitation of a chromophore with a HOMO-LUMO gap close to 1.3eV.

Table 1.1

UV-Vis absorption Maxima (λ_{abs}), Photoluminescence Maxima (λ_{em}), Photoluminesence Quantum Yields (Φ), Energy Gaps (E_{gap}), Reduction Potentials ($E^{red}_{1/2}$) and Onsets (E^{red}_{onset}), and LUMO Energy Levels of compounds in the GAO series.

compd	λ_{abs} ($\varepsilon/10^{-5}$[mol/L.cm])[a]		λ_{em} (nm)	Φ[b](%)	E_{gap}[c] (eV)	$E^{red}_{1/2}$[d]			E^{red}_{onset}[e] (V)	LUMO[f] (eV)
	$\lambda_{abs}^{(0-1)}$	$\lambda_{abs}^{(0-0)}$				$E_{1/2}^{1}$(V)	$E_{1/2}^{2}$(V)	$E_{1/2}^{3}$(V)		
GAO-6	418(0.59)	443(0.88)	480	91	2.65	-1.22	-1.40		-1.16	-3.24
GAO-8	471(1.04)	500(1.64)	533	82	2.35	-0.78	-1.37		-0.69	-3.70
GAO-11	494(0.50)	525(0.59)	652	4	2.25	-0.78	-1.38		-0.67	-3.73
GAO-13	500(1.36)	529(0.83)			2.22	-0.73	-1.23	-1.47	-0.64	-3.76
GAO-13	508(0.47)	538(0.34)			2.18	-0.71	-1.22	-1.42	-0.62	-3.78

[a]Measured in chloroform with a concentration of 2.0 x 10^{-6}mol/L. [b]Measured in chloroform with Nile red in 1,4-dioxane (Φ = 68%) as a reference. [c]Estimated from absorption onset. [d]Obtained from differential pulse voltammetry experiments. [e]Calculated from cyclic voltammograms. [f]Estimated from E^{red}_{onset}.

Pyrene is believed to act, to a degree, as a cross-conjugating center[79,95]. If A is conjugated with B and B conjugated with C, but C is not conjugated with A through B, then A is cross-conjugated with C through B, a cross-conjugating center[79]. Figure 1.6 shows an example of this cross-conjugation. It was proposed by Gao *et al*. that the cross-conjugating pyrene centers present in the molecules of figure 1.5 are involved in the observed leveling-off of the energy gap with increasing length. In 2010 Ricks and co-workers published[79] an interesting investigation into the effect of cross-conjugation on the transmission and photoinduced electron transfer rates through simple molecular bridges comprising conjugated, non-conjugated, σ-bonded and cross-conjugated centers

that spanned two benzene rings. While the results did require some discussion, the cross-conjugated bridges appeared to exhibit considerably diminished transmission and rates for both photoinduced charge-separation and dark charge-recombination processes in comparison to the fully conjugated bridges. Nevertheless the cross-conjugated bridges still performed better than the unconjugated σ-bonded bridges studied. It is worth noting that this study investigated the effect of cross-conjugation on charge transport across bridges by the superexchange mechanism and not across longer molecular wires that would occur by inchoherent charge hopping. In the charge hopping mechanism, the electron hops from site to site along the wire[70]. The cross conjugation present in the ribbons in figure 1.5 may serve to break up the ribbons into subunits between which the electrons can hop incoherently. The study by Ricks *et al*. also concluded that that rigidity of the bridges has significant implications in mediating charge transfer by superexchange[79] with more rigid structures exhibiting better conductances due to minimized torsional decoupling. Many molecular wires studied[73,81-88] exhibit rotational motion between the various subunits present, effectively decoupling the subunits from one another to various degrees. The rigidity of fully aromatic ribbons is thus a favorable feature as they are free from this electronic decoupling.

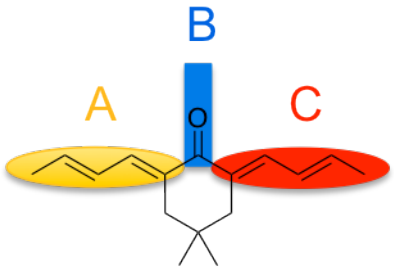

Figure 1.6. An example of cross-conjugation.

In light of the favorable electronic and optical properties of the molecules presented by Gao *et al.*, together with the convenience of orthogonal functionalization of the pyrene core, a study to synthesize a series of D-W-A compounds was proposed to investigate the rates of photoinduced electron transfer and recombination across the various wires. The constructs would employ porphyrins as the donors and a new C_{60} fullerene as the acceptor. If it was found that the wires produced did not exhibit good conductances, the synthetic methodology developed would not be useless and the structures could still be utilized as scaffold for constructing antenna arrays.

If the initial project proved to be successful, further synthetic attempts could be made to extend the synthetic methodology developed to synthesizing more complex donor-wire-acceptor architectures such as those shown in figure 1.7, which feature lateral functionalization of the molecular wires.

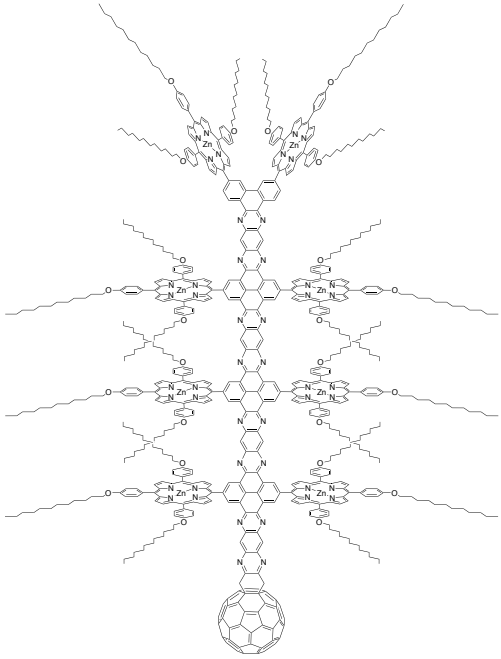

Figure 1.7 A structure of laterally functionalized molecular ribbon to act as a D-W(D_n)-A system. Success in the preliminary studies of this work would enable compounds of this type to be studied, a step towards the more complex architectures like that shown in figure 1.2.

1.10 Efforts Towards the Synthesis of Pyrazine-Containing Structures

Chapter 3 of this work presents the synthetic attempts at testing the feasibility of producing a D-W-A construct to test the waters regarding the synthetic protocols utilized and properties of the final compound. Chapter 4 presents the synthesis of three porphyrin-wire-fullerene constructs together with the necessary model compounds for studying their photophysics. The lessons learned in the synthesis of the target molecule of chapter 3 are incorporated into the design of the twelve target molecules of this chapter.

In the interest of putting the molecular ribbons to work in a functional device, the fullerene acceptor terminus of the donor-wire-acceptor compounds of figure 1.8 can be substituted with an appropriate anchoring group to produce a dye for use in dye-

sensitized solar cells. Chapter 5 investigates the use of a very short pyrazine-containing heteroaromatic spacer as a first attempt at building dyes that feature many chromophoric units, further increasing the effective loading of chromophores on the TiO_2 surface, enabling co-sensitization and antenna functionality, and preventing recombination at this interface. This effort is a step towards complex systems like those shown in figure 1.4.

In the course of synthesizing the many compounds required for the target molecules of chapters 4 and 5, an observation was made that some of the intermediates could be used to produce an extended phthalocyanine. Many chromophores used in artificial photosynthesis exhibit a lowest energy transition at a far higher energy than the optimum Shockley-Queisser energy gap of 1.3eV. Motivation existed to attempt the synthesis of the highly conjugated extended phthalocyanine to investigate how extension of the aromatic phthalocyanine core would affect the absorption properties. The materials proposed to be used in the synthesis also featured extensive functionalization with solubilizing groups which would facilitate the purification and characterization of the phthalocyanine produced. As is presented in chapter 6, the structure obtained features 24 dodecyloxy groups around the periphery of the pthalocyanine that makes it a potential candidate for forming discotics. The core structure is also a suitable scaffold for use in forming antenna arrays and higher order structures.

Chapter 2: Synthesis of Porphyrin Monomers for Electrochemical Polymerization to Form Dyadic and Triadic Polymers

2.1 Bulk Heterojunction Solar Cells

Organic solar cells offer several advantages over their silicon counterparts, specifically, cost, flexibility, processability and the use of earth abundant materials. The cost involved in obtaining the degree of purity required for manufacturing and obtaining the high efficiency of silicon solar cells has been a prohibitive factor in the economic viability of silicon technologies to date. Nevertheless, silicon based solar cells still dominate the solar photovoltaic market as the efficiencies of organic solar cells are still low.

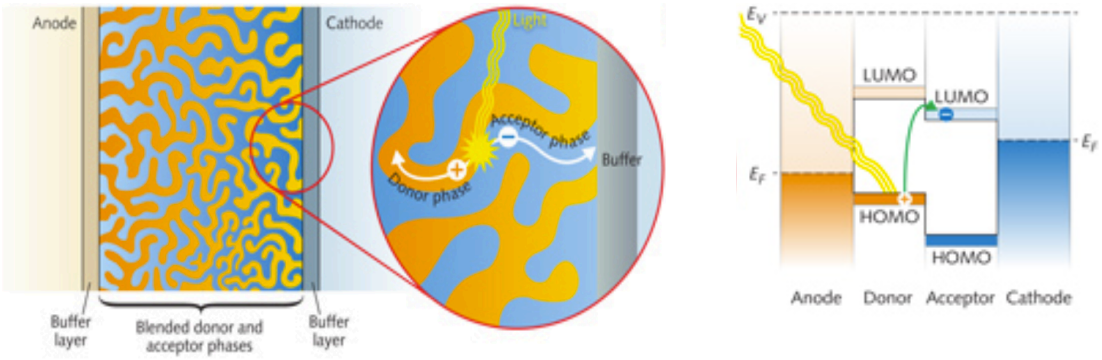

a.) b.)

Figure 2.1.a.) A simplified representation of a bulk-heterojunction solar cell. b.) Orbital energy diagram of the constituent phases of a bulk-heterojnuction solar cell and electrodes. Image reproduced from laserfocusworld.com[96].

Bulk heterojunction (figure 2.1.a) solar cells typically feature two layers of bulk organic materials along with several smaller layers of organic or inorganic materials that

act as electron or hole blocking layers, improving carrier collection characteristics at the electrodes. Typically, a donor phase is responsible for absorbing solar energy and ultimately injecting a hot electron into the acceptor phase. Consideration must be given to tuning the relevant electronics of the cell's constituent phases to ensure efficient functioning[97]. A cell employing a donor phase that features a lowest energy absorption beyond the red or even infa-red end of the solar spectrum will absorb a considerable portion of the solar spectrum but will not effectively utilize the absorbed photonic energy[98].

Electrons excited by photons will relax thermally to the conduction band edge, giving off the excess energy as heat[97]. Consideration must also be given to the relative positions of the LUMO orbitals or conduction band edges of the donor and acceptor phases. Broadly speaking, the conduction band edge should be positioned to be slightly more energetic than the acceptor phase so that there is some thermodynamic driving force for the charge transfer from donor to acceptor phases. It is important, though, that the donor and acceptor phases are not chosen such that there is too much driving force[99]. Firstly, the difference in energy between electrons collected at the anode and holes collected at the cathode will determine the maximum voltage that can be generated by the cell[97]. The energy of the LUMO orbitals of the donor phase sets the upper limit for the electron energy that can be collected at the anode[97] and any losses of electronic potential energy that are incurred in the excited electrons journey from its point of generation in the donor phase to collection at the anode will diminish the overall voltage that can be generated by the cell. It is not desirable to unnecessarily discard electrical potential energy beyond what is required to achieve efficient electron transfer. In addition, Marcus

theory[99] predicts that as the thermodynamic driving force for electron transfer increases beyond a certain point, the rate of electron transfer will be inhibited. This is the characteristic behavior of the Marcus-inverted[100] region for intramolecular electron transfer[49,97,99,101-107]. These two factors alone warrant careful consideration of the relative energies of the donor and acceptor phase conduction band edges.

For quantum conversion in bulk-heterojunction solar cells four core processes[27,97] need occur. Absorption of a photon by the donor or acceptor material results in the formation of a localized excited state or Frenkel exciton. This excitation energy must diffuse through the bulk material until a donor-acceptor interface is encountered, at which point charge transfer can occur. If the excitation is generated in the donor-phase, electron transfer to the acceptor phase results, while if the excitation is generated in the acceptor phase, hole transfer to the donor phase can occur. Following charge separation at the phase boundary, each of the carriers must migrate through the respective phases until they reach a conductive electrode, at which point the carriers can be collected[27,98].

The spectral response and absorption coefficient of the active materials play a role in determining the overall power efficiency of the cell. Inefficiencies associated with each of the steps outlined above result in losses of internal quantum efficiencies of the cell affecting the J_{SC} of the cell. Each phase will exhibit a characteristic excitation lifetime. If the migrating exciton fails to encounter a phase boundary during this lifetime, the excitation energy will be lost as thermal energy. Minimizing the thickness of the phases utilized is important for obtaining high yields of charge separation and carrier collection. When the materials exhibit poor absorbencies, considerable material is required to absorb a reasonable fraction of the insolation. Consequently, excitons

generated far from the phase boundary would then have to diffuse a considerable distance before charge transfer could occur. The product of the exciton lifetime and diffusion speed must exceed the thickness of the phase for charge transfer to be possible. Immediately following charge transfer, the electron-hole pair resides at the phase boundary and the respective carriers experience a strong coulombic attraction that can lead to recombination.

The low dielectric-constant of organic materials does not screen the carriers in adjacent donor and acceptor phases well that would otherwise serve to promote carrier separation[27,97]. Carrier collection relies on the assumption that separated electron-hole pairs can move freely to the electrode along a thermodynamically favorable gradient. Underpinning this is the basic assumption that the electron or hole conducting medium exists uninterrupted between the phase interface and electrode.

The J_{SC} of the cell is linked to the internal quantum efficiency of a solar cell. As stated, the operation of bulk-heterojunction solar cells is complex[27,99]. With this complexity arises opportunity for losses that impair the internal quantum efficiency of the cells. In summary, not considering many finer details, effective conversion of absorbed photons necessitates that: the excitation generated on absorption must diffuse to a phase boundary within the lifetime of the Frënkel-exciton generated; electron transfer from the exciton in the donor phase to the acceptor phase or hole transfer from the exciton in the acceptor phase must proceed to generate an electron hole pair at the phase boundary; the respective carriers of the electron hole pair at the phase boundary must escape the Coulombic attraction for one another and migrate though the respective phases for collection at the appropriate electrodes.[27,97]

2.2 Molecular Heterojunctions

Obtaining long-lived charge-separated states in solution state model compounds has been achieved in high efficiency by using donor and acceptor cascades[36]. Triads, tetrads, pentads which feature a thermodynamic gradient for achieving long lived charge separated states in high yield pay a small energy penalty to separate the high energy electron formed on absorption and the resulting hole. Separating the two charges diminishes the columbic force that acts to cause them to recombine and so increases the lifetime of the state. The donor and acceptor cascades present within these models, if incorporated into materials for organic solar cells could provide a means for weakening the electrostatic attraction between the electron and hole of the polaron formed following the primary charge transfer event by providing a thermodynamic gradient to further separate the charges prior to relying on diffusion for further carrier separation.

As outlined above, in a simple bulk heterojunction solar cell, each phase is responsible for a variety of functionalities. It is possible to envisage new, complex polymers or phases that feature added components, each of which is designated to fulfill a specific functionality. Modularly diversifying the composition of the materials to specify functionality would enable one to optimize the components responsible for specific functionalities independently within the complex multi-component polymer. For example, complex polymers could be designed that feature components, each responsible for a unique function such as light absorption, charge separation, charge screening, hole conduction and electron conduction. Donor and acceptor cascades could be engineered into the materials to achieve high-yielding charge separation. The components of the

polymer can also work in unison to achieve, not only carrier separation and transport, but energy harvesting, acting as arrays, shuttling excitation energy to reaction centers present in the material. Modular design in this fashion reduces the requisite function performed by each component as more components are added.

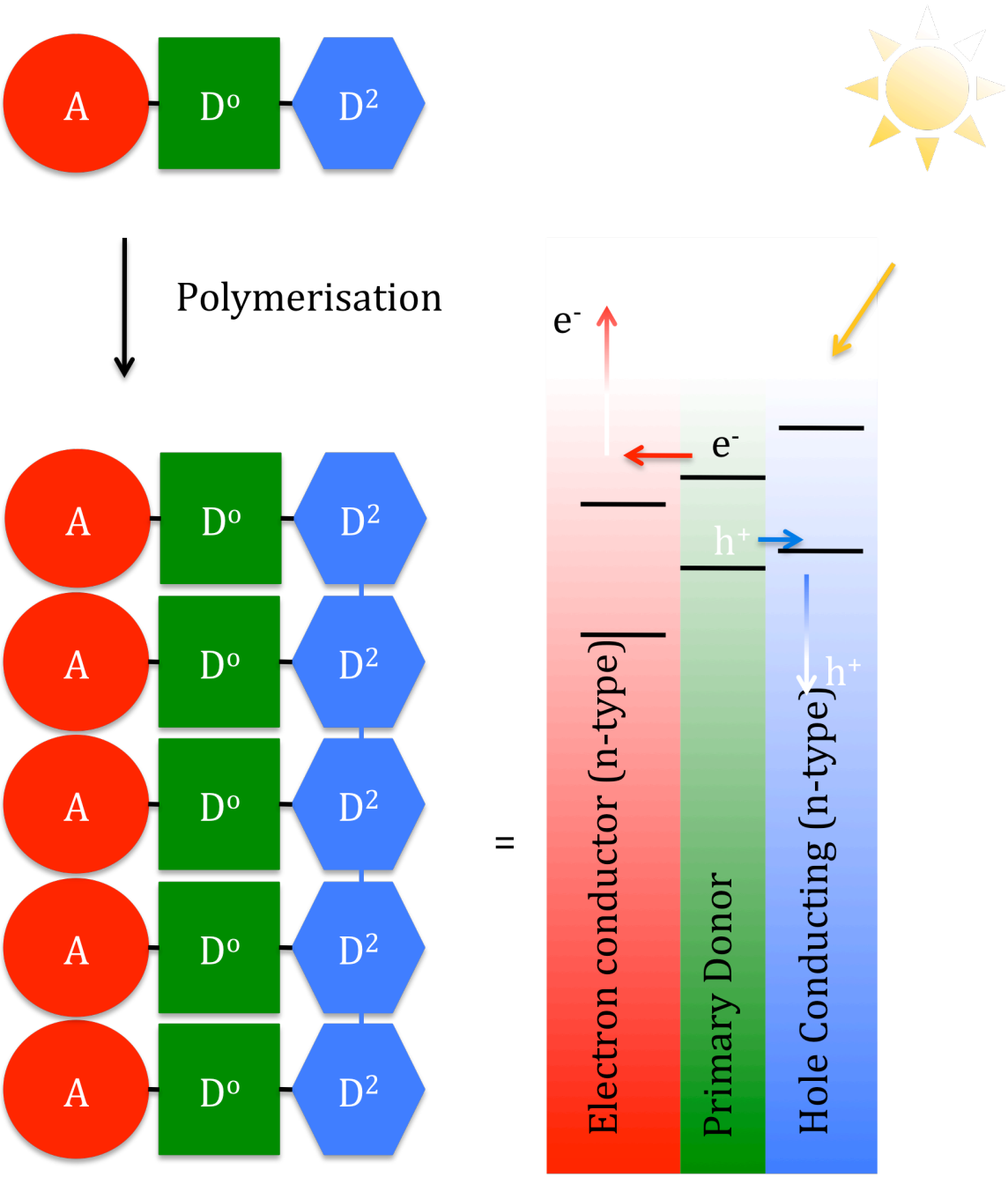

Figure 2.2. A multicomponent tryadic polymer featuring a designated light-absorbing and primary donor component (green) an electron accepting/conducting component (red) and a secondary donor/hole conducting component (blue).

Figure 2.2 shows a design strategy in which a triadic-molecular heterojunction polymer has been formed through polymerization of an appropriately designed monomer. In a molecular heterojunction, charge separation occurs between donor and acceptor molecules covalently bound to one another and present throughout the material. The donor-acceptor pair act as a reaction center, a point for charge separation. This is the continuous interface between red and greed layers in figure 2.2. Employing a molecular heterojunction in the design of organic solar cells drastically increases the reaction center density within the material formed in comparison to bulk heterojunction cell designs since charge separation occurs at the interface between the two bulk materials, the surface area of which is reduced in comparison. A central advantage of this strategy is that following absorption of light by the primary donor chromophore, electron transfer to the acceptor covalently bound to it can occur immediately without any requirement for exciton diffusion. Consequently a loss mechanism that impairs cell efficiency is completely eliminated. Molecular heterojunctions can be engineered to feature donor and acceptor cascades like the mimics of artificial reaction centers[36], employing secondary donor and acceptor cascades to further separate charge. The idealized molecular heterojunction shown in figure 2.2 is designed to function as a triad, with two sequential electron transfer events separating the two charges. If the primary acceptor shown in red is in close proximity to adjacent acceptors, the electron can diffuse away by hopping successively to adjacent acceptor molecules. Polymerization of the monomeric tryad is

thus intended to form a pathway for electrons to diffuse away from the site of light absorption and charge separation. Similarly, through polymerization of the monomeric triad, the covalently linked secondary donors, shown in blue, form a hole-conducting medium for transporting positive charges away from the sight of light absorption and carrier generation. The layer shown in green is expected to be responsible for the majority of the spectral response of the material and to act as the primary donor chromophore. The polymerization of the molecular triads shown in figure 2.2 occurs by connecting the secondary donors shown in blue, implying that the resulting electron transport pathway must occur via hopping of electrons between adjacent acceptor molecules that are not connected by covalent bonds. The system could be altered so that the polymers were formed by linking of the acceptors shown in red, in which case, hole conduction would be forced to occur by hopping of holes between adjacent units.

The orbital energies of monomers are frequently very different from those of the polymer formed. Consequently, the system must be tuned so that the appropriate electronics required to achieve the necessary photophysics are present in the material formed, and not within monomer.

2.3 Porphyrin Monomers for the Formation of Dyadic and Triadic Electropolymers

Figure 2.3 shows four monomers that have been designed to form molecular heterojunction polymers through electrochemical polymerization. Monomer **2.1** features a porphyrin that is designed to act as the primary donor chromophore and primary light absorber. The aniline moiety attached to the *meso* position of the porphyrin *ortho* to the

aniline amine is designed to form polyaniline via oxidative electrochemical polymerization. The polymerization would produce an aniline backbone that is intended to act as the secondary electron donor and hole-conductor. Finally, the C_{60} fullerenes present are designed to act as the primary electron acceptors within the system. While the C_{60} fullerenes present do not form a polymer during oxidation, it is expected that the high density of fullerenes in close proximity to each other would likely enable electron transport away from the site of charge separation by hopping to adjacent fullerenes, as in the PCBM phase of a bulk heterojunction solar cell[101].

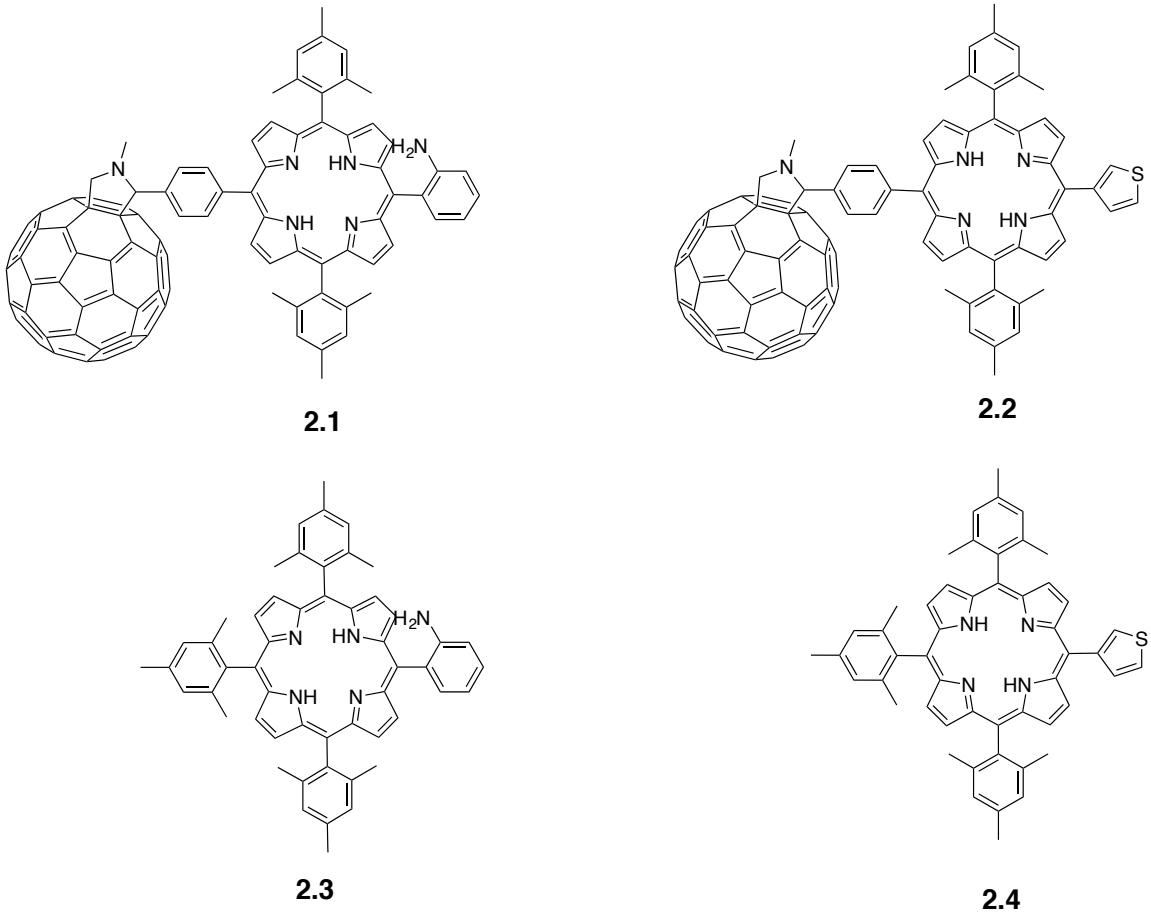

Figure 2.3. Aniline (**2.1** and **2.3**) and thiophene (**2.2** and **2.4**) functionalized porphyrin monomers synthesized for use in forming electropolymers.

Figure 2.4. shows a drastically idealized drawing of the proposed polymer formed by electroploymerization of **2.1**. Figure 2.4.b also shows an idealized depiction of a polymer formed by the oxidative polymerization of monomer **2.2**. Much like aniline, thiophene can be polymerized oxidatively to form polythiophene. Polythiophenes feature prominently in the literature of bulkheterojunction solar cells and act as the donor layers and hole-conducting materials[101,103,108]. Similar to the polymer proposed to be formed in the polymerization of **2.1** the polymer proposed to be formed through the polymerization of **2.2** would operate as a tryadic molecular heterojunction with the polythiophene formed acting as the secondary donor and hole-conductor. In both polymers there is a degree of gambling as to what the final electrochemical characteristics of the polyaniline and polythiophene formed will be. With increasing conjugation, the HOMO and LUMO energies of the resulting polymer are expected to shift. The resulting HOMO energy is important as it is from this orbital that an electron must be donated to an oxidized porphyrin in order for the molecular heterojunctions to exhibit tryadic behavior. In addition, if the HOMO-LUMO gap of the polyaniline and polythiophene formed was smaller than that of the HOMO-LUMO gap of the porhyrin molecules, they could act as energy acceptors, quenching the excitation of excited porphyrins.

a b

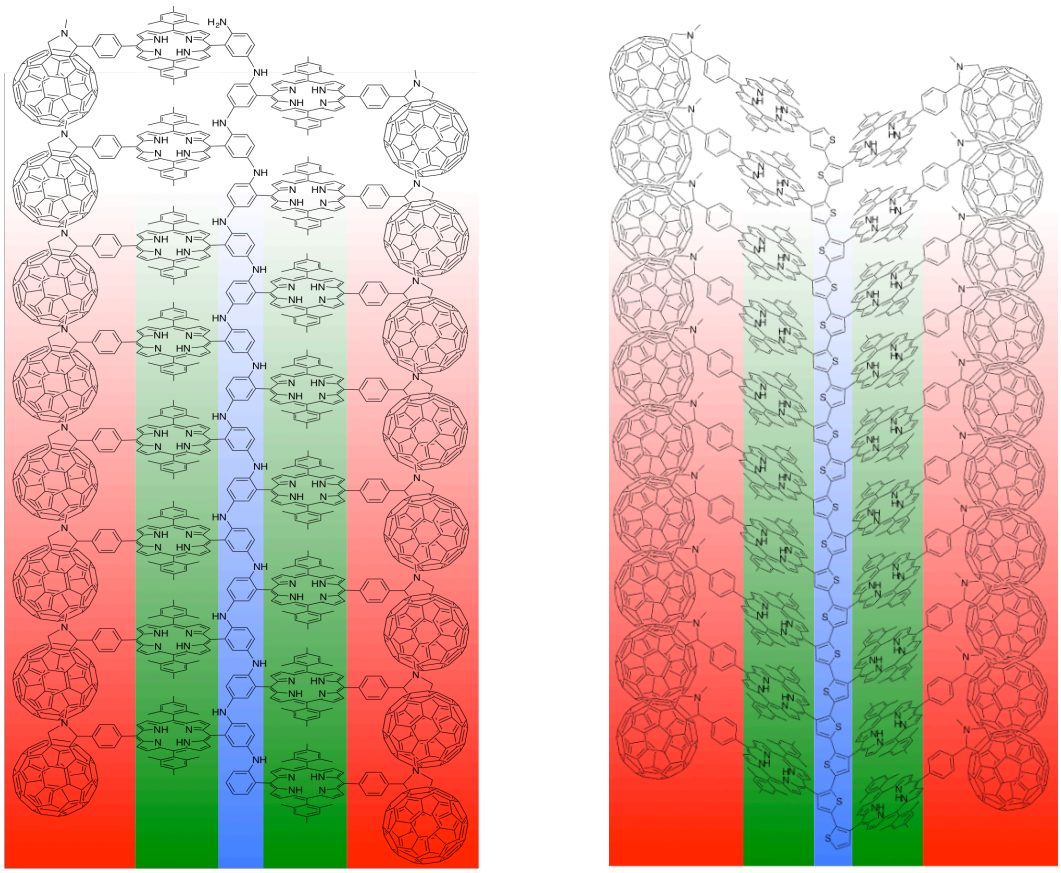

Figure 2.4. Idealised structures of triadic polymers designed to form during oxidative electrochemical polymerization of **2.1** (a) and **2.2** (b). Polyaniline and polythiophene sub-polymers (blue) formed are intended to act as secondary donors and hole conductors, porphyrin pigments (green) are intended to act as the primary light absorbers and donors and fullernes (red) are intended to act as the electron acceptors and electron conductors.

Monomers **2.3** and **2.4** shown in figure 2.3 were designed to act as controls for comparison to the polymers formed through polymerization of **2.1** and **2.2**. The polymers that would be formed by polymerization of **2.3** and **2.4** could still exhibit dyadic properties, with oxidation of the polyaniline or polythiophene strands occurring following excitation of the porphyrin molecules. This may still provide a means for creating a charge separated state, but it is expected that the material formed would exhibit poor

electron mobilities due to the lack of defined electron conducting pathway. These control monomers thus serve to investigate the carrier transport properties of fullerenes present in the polymers formed from **2.1** and **2.2**.

2.4 Synthesis of Triadic Monomers

The synthesis of the core porphyrin macrocycles for all compounds was achieved via $BF_3.OEt_2$ catalyzed 2+2 condensations of the appropriate dipyrromethanes and aryl aldehydes in chloroform containing 0.75% EtOH. The intermediate condensation products were oxidized by 2,3-dichloro-4,5-dicyanobenzoquinone (DDQ) to produce the red porphyrin products. In condensations of two equivalents of a given dipyrromethane or given aldehyde with two different aldehydes or dipyrromethanes respectively, to form the desired A_2BC porphyrins three porphyrin products are expected with a 1:2:1 relative product distribution-assuming that both of the aldehydes or dipyrromethanes exhibit similar reactivity.

Scheme 2.1

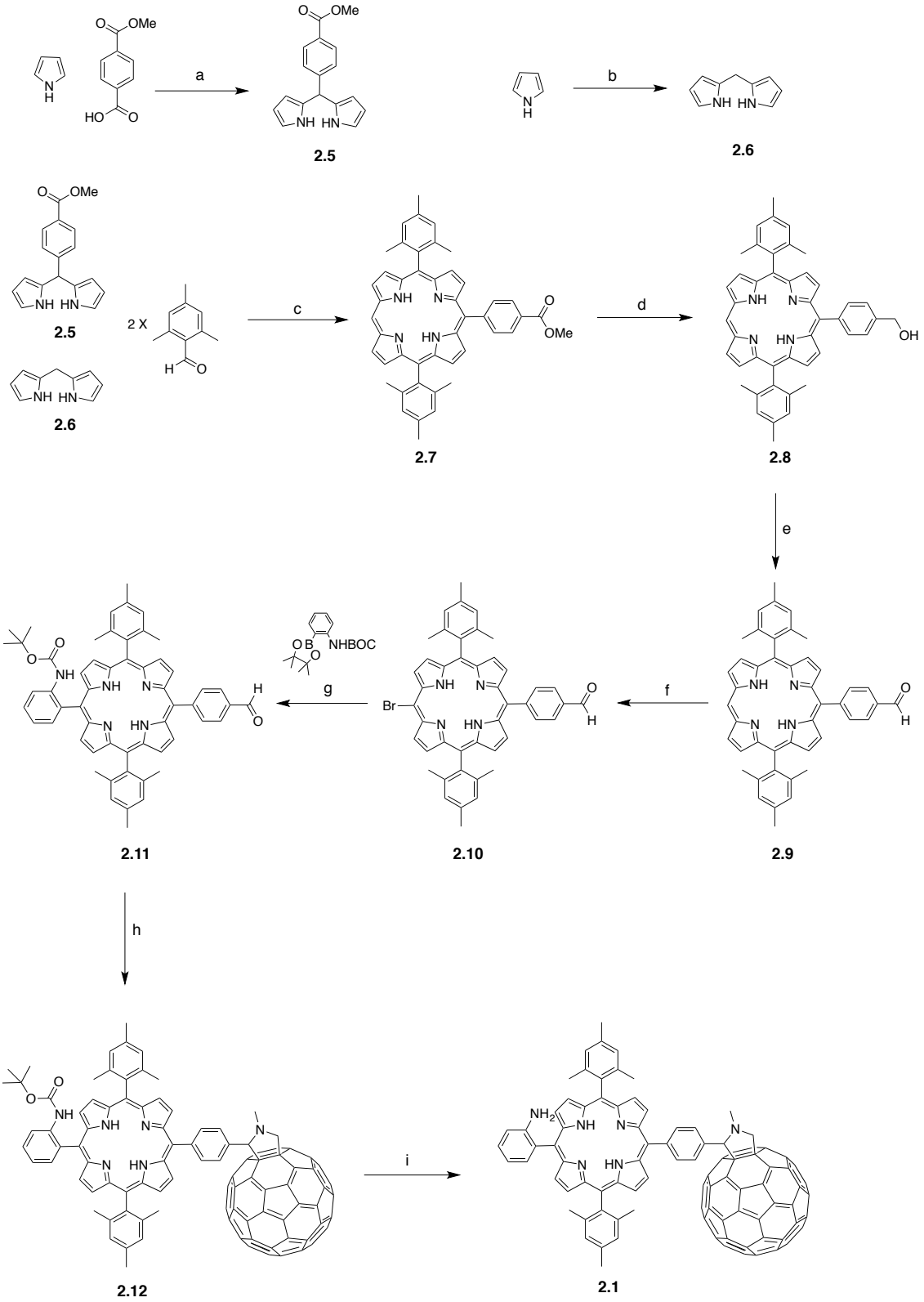

a.) i 0.18M HCl, RT, 4h **ii** NaOH, 28% yield **b.) i** $InCl_3$, 40°C, 3h **ii** NaOH, RT, 1h **c.) i** $BF_3.OEt_2$, $CHCl_3$/ 0.75% EtOH, RT 1.5h; **ii** DDQ, RT, 30min, 12% yield; **d.)** $LiAlH_4$, THF, 0°C → RT, 1h, 92% yield; **e.)** MnO_2, dichloromethane, RT, 1.5h, 80% yield; **f.)** NBS, $CHCl_3$, RT; 98% yield **g.)** $Pd(PPh_3)_4$, K_3PO_4, THF, 75°C, Ar, 84h, RT, 54% yield; **h.)** Toluene, reflux, 16h, 57% yield; **i.)** TFA:dichloromethane (1:1), RT, 30min., 97% yield.

The synthetic protocol required to make the monomer **2.1** is shown in scheme 2.1. *Meso*-(4-methylbenzoate)dipyrromethane (**2.5**) and dipyrromethane (**2.6**) were required for the synthesis of the porphyrin core. The synthesis of **2.5** utilized the reported literature procedure[97,109], an aqueous, hydrochloric acid-catalyzed condensation of 4-formyl-methylbenzoate with pyrrole on water. The reaction produced the necessary dipyrromethane with a low yield of 28%. Other higher yielding reports[99,110] of the synthesis of **2.5** exist but employ pyrrole as the solvent, and as such, use considerably higher quantities of an expensive reagent. Despite this attractive feature of the protocol, the literature yield[100,109] (89%) reported for this aqueous method to produce **2.5** could not be replicated on further attempts. The synthesis of dipyrromethane followed the method reported[111] by Lindsey et al. employing pyrrole as the solvent and $InCl_3$ as the Lewis-acid catalyst. This dipyrromethane is light sensitive and care must be taken to remove any residual pyrrole from the crude product residue prior to chromatographic purification.

Condensation of dipyrromethanes **2.5** and **2.6** with mesitaldehyde and subsequent oxidation produced the three expected porphyrins from which **2.7** was isolated by silica gel chromatography with a 12% yield. The methylester functionality present on **2.7** was reduced by $LiAlH_4$ to produce the alcohol **2.8** (92% yield) and subsequently oxidized to form the aldehyde **2.9** (71%) yield. The free *meso* position present on **2.9** was brominated using *N*-bromosuccinimide in chloroform to obtain the bromo-poprhyrin **2.10** (98%

yield) required for the subsequent Suzuki coupling. Commercially available *tert*-butyl-*N*-[2-(4,4,5,5-tetramethyl-1,3,2-dioxaborolan-2-yl)phenyl]-carbamate was coupled with **2.10**, employing $Pd(PPh_3)_4$ as the catalyst and tribasic-potassium phosphate as the base to obtain **2.11** in 54% yield.

With the amine functionality present in protected form, the aldehyde of **2.11** was used in a Prato reaction[112], a 1,3-dipolar cycloaddition reaction with sarcosine and ten equivalents of C_{60} fullerene to give **2.12** in 57% yield. Finally, acidic deprotection of the *tert*-butyl carbamate afforded the triadic monomer **2.1** in 97% yield. The overall synthesis is clean, with all products lending themselves to efficient purification by silica gel chromatography.

The overall synthesis of the thiophene-functionalized triadic monomer **2.2** shown in scheme 2 is considerably shorter and simpler than the synthesis of **2.1**. The central difference is that while the synthesis of **2.1** required introduction of the aniline functionality via a Suzuki-cross coupling reaction in the protected form of the amine and deprotection of the reactive amine following the Prato reaction, the thiophene functionality can be introduced during formation of the porphyrin macrocycle and is sufficiently robust that the synthesis of **2.2** requires no consideration for degradation or reactivity in either the synthesis of the porphyrin core or addition to C_{60}. *Meso*-(mesityl)dipyrromethane (**2.13**) was synthesized in a solvent free condensation of mesitaldehyde with pyrrole catalyzed by trifluoracetic acid. Two equivalents of **2.13** were condensed with thiophene-3-carboxaldehyde and formyl-4-methylbenzoate and oxidized to give a mixture of porphyrin products. The resulting porphyrin products were separated by column chromatography giving **2.14** in 8.5% yield. The methyl ester functionality was

reduced to the alcohol by $LiAlH_4$ and after a short work-up, oxidized to the corresponding aldehyde, **2.15**, by MnO_2 in an overall yield of 80% for the two steps. The final product, **2.2** was obtained via a Prato reaction involving reflux of **2.15** with C_{60} and sarcosine in Toluene. Distinct from the similar Prato reaction for the synthesis of **2.12**, more Prato side products were evident in the TLC and MALDI-TOF mass spectral analysis of the crude reaction mixture. The presence of adducts in which two or more cycloadditions of **2.15** to a single C_{60} fullerene had occurred were evident. The generation of these byproducts explains the low yield of 19% for **2.2** in comparison to the appreciably more satisfactory yield of 57% for **2.12**.

Scheme 2.2

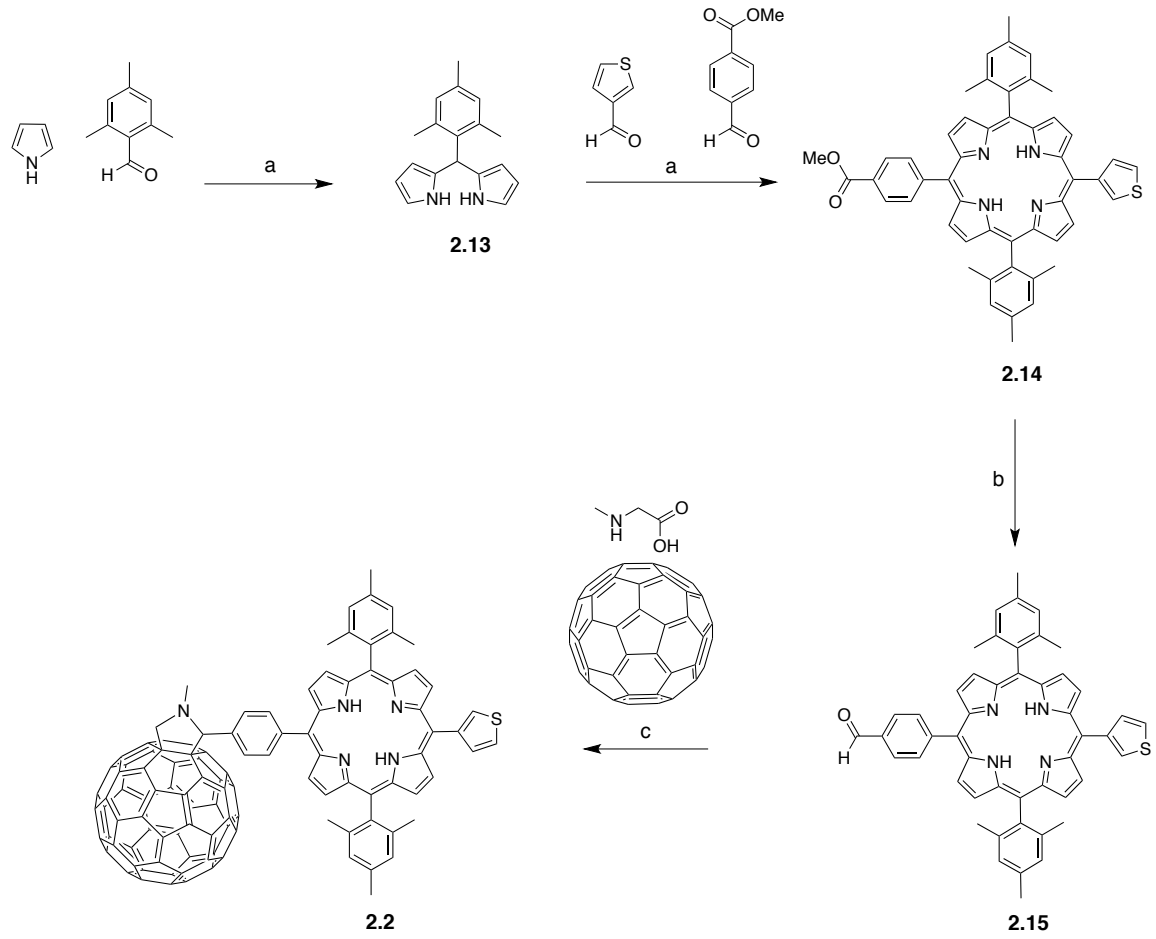

a.) TFA, NaOH, RT, 2h, 38% yield **b.)** $BF_3.OEt_2$, $CHCl_3$-0.75%EtOH, RT, 5h; **ii**. DDQ, RT, 45min, 8.5% yield **b.) i.** $LiAlH_4$, THF, $0^oC \rightarrow$ RT, 1h **ii**. Dichloromethane, MnO_2, 80% yield **c.)** Toluene, reflux, 16h, 19% yield.

2.5 Synthesis of Dyadic Monomers

The synthesis of the of **2.3** shown in scheme 2.3 required condensation of two equivalents of *meso*-(mesityl)dipyrromethane (**2.13**) with one equivalent of mesitaldehyde and 2-nitrobenzaldehyde. To generate the amino functionality, the nitro group present on **2.16** was reduced using zinc dust in the presence of acetic acid. The Zn

dust oxidized to Zn(II) in this reaction is readily coordinated by the porphyrin macrocycle. Subsequent demetallation of the crude product from this reaction using trifluoracetic acid and subsequent chromatographic purification yielded the final free-base amino porphyrin with an 85% yield.

Scheme 2.3

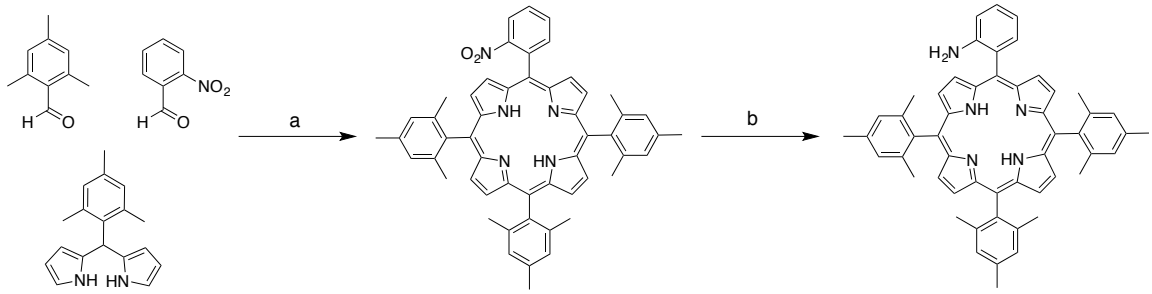

2.13 **2.16** **2.3**

a) i. $BF_3.OEt_2$, $CHCl_3$-0.75%EtOH, RT, 3h; **ii**. DDQ, RT, 1h; **b) i**. CH_3COOH, Zn (dust), 60^oC, 1h; **ii**. Dichloromethane:TFA (1:1), RT, 10min., 85% yield.

The synthesis of **2.4** shown in scheme 2.4 required metallation of the mixture of porphyrin products obtained from the condensation and subsequent oxidation of **2.13** with thiophene-3-carboxaldehyde and mesitaldehyde. The bright pink mixture of zincatoporphyrins produced was very sensitive to solvent polarity and showed an even higher propensity to crystallize in the presence of hexanes than the mixture obtained in the synthesis of **2.16**. Three passes of the mixture though a silica gel column were required to obtain **2.17** in pure form with an 11% yield. Treatment of **2.17** with a 1:1 mixture of TFA and dichloromethane afforded the free base product **2.4**.

Scheme 2.4

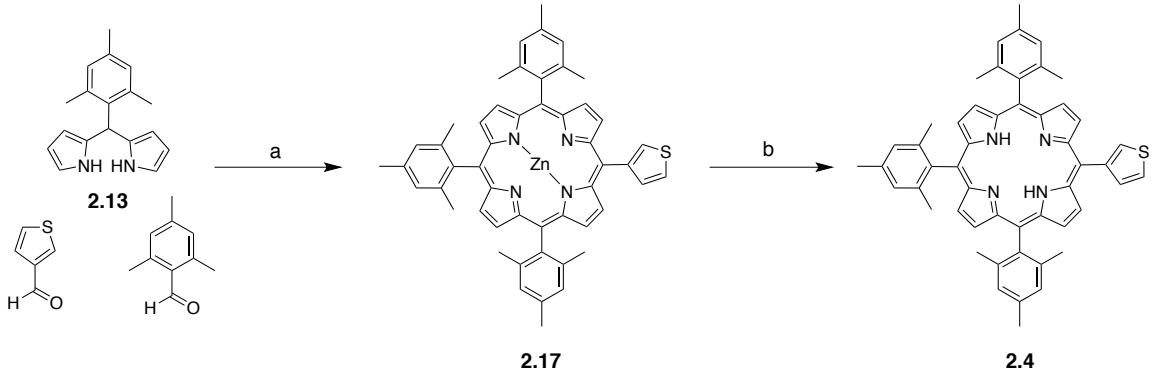

a.) i. $BF_3.OEt_2$, $CHCl_3$-0.75%EtOH, RT, 3h, **ii**. DDQ, RT, 1h, **iii**. $Zn(OAc)_2.2H_2O$, dichloromethane/MeOH, reflux, 16h,11.2% yield; **b.)** TFA:dichloromethane (1:1), RT, 1h.

2.6 Electrochemical Polymerization of Monomers

Having successfully synthesized and characterized the necessary monomers, the polymerization of the aniline substituted monomers was investigated via cyclic voltammetry. Many attempts at polymerization failed completely. Success was achieved when careful attention was paid to solvent preparation, revealing that distillation of the dichloromethane solvent over CaH was an essential prerequisite to achieving film growth. Figure 2.3 shows the cyclic voltammegram for the oxidative polymerization of **2.3** in dichloromethane. The results are not very encouraging. While the anodic peak around 1V vs Ag/AgCl does grow on successive scans, indicative on film growth, the spacing between successive scans is not linear with the increase in anodic current decreasing with scan number. This indicates a degree of passivation of the electrode.

With subsequent scans the peak of the anodic peak shifts to less positive potentials. This is in line with how the HOMO energies of conjugated polymers shift to

more negative potentials with increasing length. The anodic scan, by which polymerization of the aniline substituent is proposed to occur is largely irreversible. This is an encouraging result as the product formed during the normal radical mechanism of oxidative polymerization is neutral and so does not require subsequent reduction[113]. In comparison the electrochemical polymerization of **2.1** shown in figure 2.6, the film produced in the polymerization of **2.3** (shown in figure 2.5) did not adhere to the electrode well and either dissolved or flaked off the electrode readily. Further work is required to optimize the conditions for the polymerization of **2.3** to enable further study.

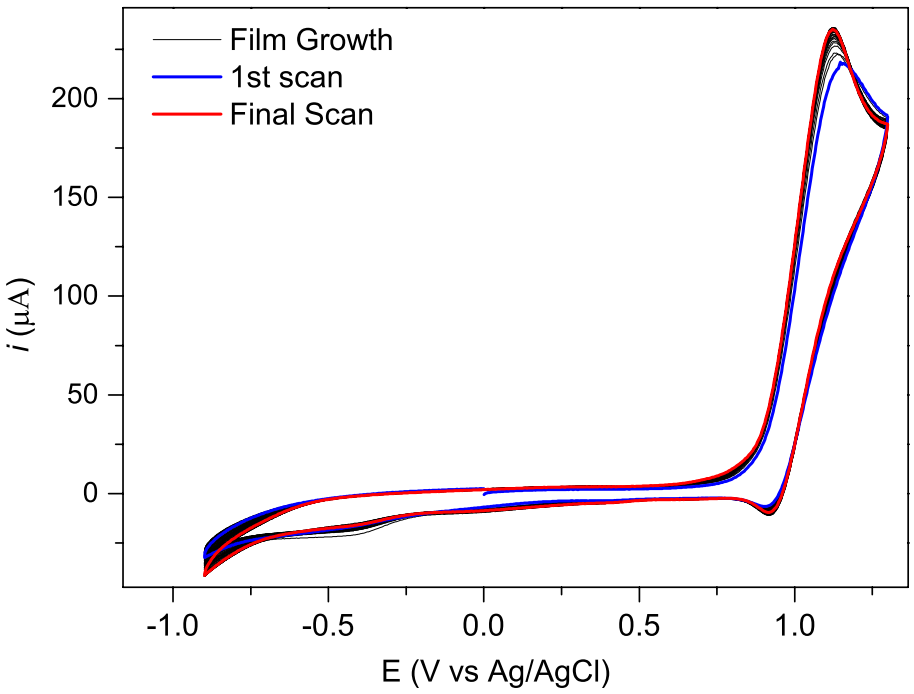

Figure 2.5 Cyclic-voltammegram for film growth of aniline monomer **2.3**. on a FTO slide in freshly distilled DCM using 100mM $TBAPF_6$ supporting electrolyte with a Ag/AgCl reference electrode and platinum gauze auxiliary electrode.

Comparably, the polymerization of **2.1** proceeded far more simply. It is likely that the insolubility imparted to the film through the presence of the fullerene of **2.1** inhibits the film formed from dissolving off the electrode. The anodic peak of polymerization is also irreversible characteristic of the polymerization chemistry. The increase in anodic current with subsequent scans is more pronounced for **2.1** than for **2.3** indicating that the film, for some unknown reason, is more conductive and does not passivate the electrode as quickly. Again the anodic peak shows a shift to more negative potentials with subsequent scans indicating formation of longer and longer chains of the aniline polymeric backbone. The cyclic voltammogram for the polymerization of **2.1** also reveals a largely reversible cathodic peak centered at 0.62V vs Ag/AgCl, indicative of the 1st reduction of the C_{60} Fullerene.

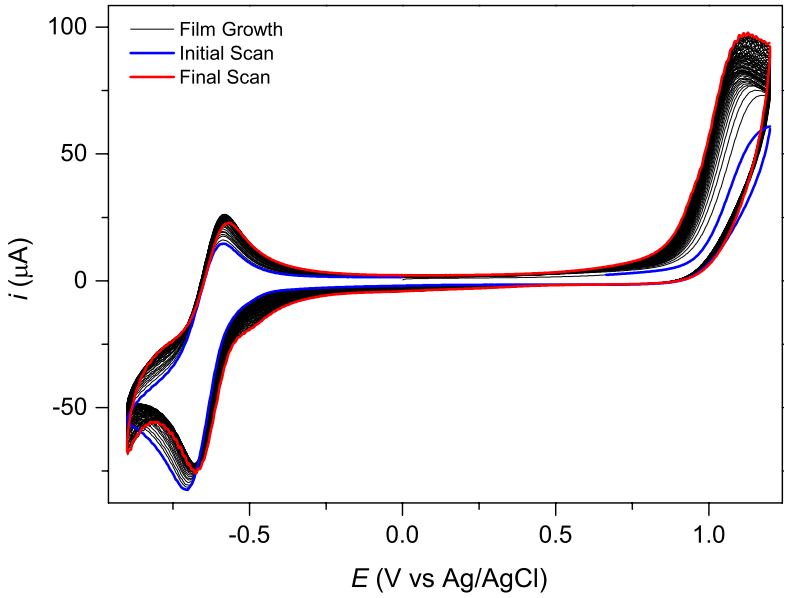

Figure 2.6 Cyclic-voltammegram for film growth of aniline monomer **2.1**. on an FTO slide in freshly distilled DCM, using 100mM $TBAPF_6$ supporting electrolyte with a Ag/AgCl reference electrode and platinum gauze auxiliary electrode.

Figure 2.7 shows the UV-Vis spectrum of an FTO slide on which polymeric **2.1** deposited with increasing scan number. The inset shows how the intensity of the absorption of the Soret absorption within the films formed scales with increasing scan number. One can observe that film growth is not linear with increasing number. The quick rate of film growth succumbs to a lower rate after the data point acquired at 20 scans. Intermediate scans were not acquired and a film was allowed to grow over 500 scans. The intensity of the absorption at 430nm of this film indicated that film growth between 20 and 500 scans was not linear either, however, the electrode was not completely passivated showing that the film formed is still conductive.

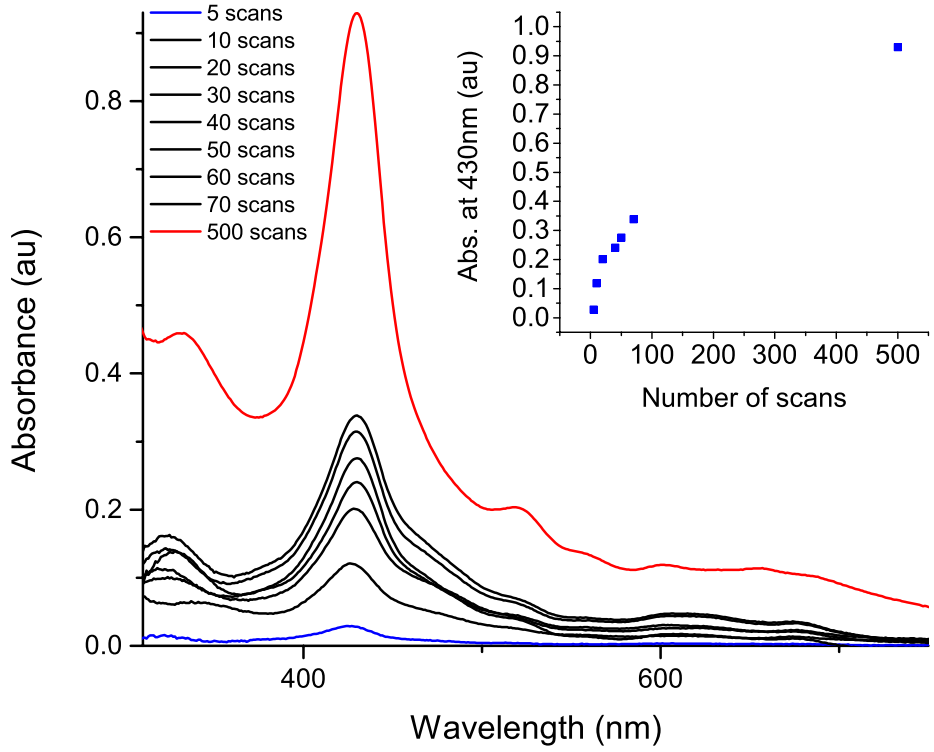

Figure 2.7 UV-Vis spectrum of poly-**2.1** on FTO for various scan numbers. Inset shows the absorbance at 430nm vs number of scans for the same polymerization.

Attempts were made to polymerize the thiophene-functionalized monomers **2.2** and **2.4** on FTO electrodes. Similar to the aniline analogue of **2.4**, **2.3**, **2.4** did not exhibit good film formation. More work must be conducted to optimize the solvent conditions to promote film formation for this monomer. **2.2** Did exhibit film growth during electrochemical polymerization. The film formed, however, appeared to passivate the electrode more quickly than the aniline analogue, **2.1**. More work is required to optimize the conditions for polymerization of **2.2**. Figure 2.8 shows oxidative and reductive scans of the monomer **2.2** together with a reductive scan of a film formed revealing the characteristic C_{60} peaks of **2.2** present within the film.

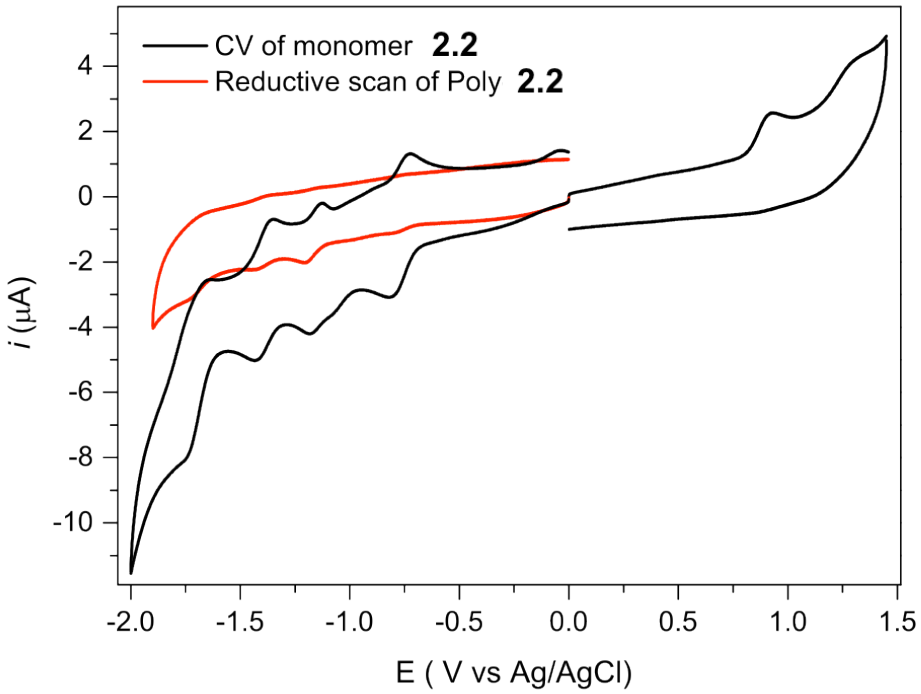

Figure 2.8 Oxidative and reductive scans of monomer **2.2** (black) on a platinum disc electrode and a reductive scan of a film formed from polymerization of **2.2** formed on an FTO slide. Electrochemistry conducted in freshly distilled DCM using 100mM $TBAPF_6$ supporting electrolyte with a Ag/AgCl reference electrode and platinum gauze auxiliary electrode.

2.7 Materials and Methods

2.7.1 General

Dichloromethane, chloroform, hexanes, ethylacetate, tetrahydrofuran and toluene were purchased from BDH and 200 PROOF ethanol and methanol from KOPTEC. Solvents were used without purification unless stated otherwise. Tetrahydrofuran was

distilled over CaH under argon. Pyrrole, formyl-4-methylbenzoate, sarcosine, mesitaldehyde and 2-nitrobenzaldehyde starting materials were acquired from Sigma-Aldrich. Thiophene-3-carboxaldehyde and *tert*-butyl-*N*-[2-(4,4,5,5-tetramethyl-1,3,2-dioxaborolan-2-yl)phenyl]-carbamate were acquired from Oakwood Products Inc. C_{60} fullerene was acquired from M.E.R corporation. Manganese dioxide was acquired from Fluka and $LiAlH_4$, *N*-bromosuccinimide, 1,2-dicholoro-4,5-benzoquinone, $BF_3.OEt_2$, $Pd(PPh_3)_4$ and K_3PO_4 reagents were purchased from Sigma Aldrich. Silica for silica gel chromatography was purchased from Silicycle.

Matrix assisted laser desorption/ionization time of flight (MALDI-TOF) mass spectra were acquired using an Applied Biosystems Voyager-DE STR workstation and acquired in reflector mode using terthiophene, diphenylbutadiene or dithranol as the matrix. NMR spectroscopy was conducted using a Varian (Agilent) MR 400 MHz NMR spectrometer operating at a 1H Lamor frequncy of 399.87 MHz, equipped with a 5 mm Broadband Observe Z-gradient probe. UV-Vis spectra were acquired using a Shimadzu UV-2550 UV-Visible spectrophotometer.

2.7.2 Synthesis of Monomers

Monomer 2.1. 0.127g (0.08mmol) of **2.12** was dissolved in 100ml dichloromethane. With stirring, 80ml of TFA was added and the solution was left to stir for 1h. The solution was diluted with 100ml dichloromethane and then transferred to a separating funnel and washed with water, saturated $NaHCO_3$ and brine. The organic layer was collected and concentrated and the residue purified by column chromatography using

neat dichloromethane as the eluting solvent yielding 0.115g (0.772mmol, 97%) of **2.1**. ^{1}H NMR (400 MHz, $CDCl_3$): δ 8.83 (d, J = 4.8 Hz, 4H), 8.67 (d, J = 4.8 Hz, 4H), 8.25 (m, 4 H), 7.86 (d, J = 7.5 Hz, 1 H), 7.57 (t, J = 9.0, 1 H), 7.25 (s, 4H), 7.16 (t, J = 7.7 Hz, 1 H), 7.09 (d, J = 8.1, 1 H), 5.23 (s, 1H), 5.05 (d, J = 9.1 Hz, 1 H), 3.57 (s, 2 H), 3.07 (s, 3 H), 2.59, (s, 6 H), 1.81 (m, 12 H), -2.62 (s, 2 H). MS (MALDI-TOF): m/z obsd 1488.5058 $[M]^+$, calcd 1488.3935.

Monomer 2.2. 0.261g (0.356 mmol) **2.15** was dissolved in 50ml of toluene along with 0.513g (0.712 mmol) of C_{60} and 0.317g (3.56 mmol) of sarcosine. The solution was heated to reflux overnight after which it was cooled at filtered through a pad of celite. The celite was washed with toluene and the filtrates concentrated. The brown residue obtained was taken up in CS_2 and loaded onto a silica gel column and chromatographed with DCM:CS_2 (1:4) yielding 0.102g (0.069 mmol, 19% yield). ^{1}H NMR (400 MHz, $CDCl_3$): δ 8.87 (d, J = 4.4 Hz, 2H), 8.61 (d, J = 4.4 Hz, 2 H), 8.56 (bs, 2 H), 8.22 (m, 4H), 7.94 (bs, 2 H), 7.67 (t, J = 3.6 Hz, 1 H), 7.21 (s, 4 H), 5.28 (s, 1 H), 5.10 (d, J = 9.0 Hz, 1 H), 4.44 (d, J = 9.0 Hz, 1 H), 3.12 (s, 3 H), 2.59 (s, 6 H), 1.80 (s, 6 H), 1.78 (s, 6 H), -2.69 (s, 2 H). MS (MALDI-TOF): m/z obsd 1479.0915 $[M]^+$, calcd 1479.3390

Monomer 2.3. 66mg (0.084 mmol), of **2.16** was dissolved in 50ml of acetic acid. 0.3g of Zn dust was added and the solution was heated to 60^{o}C and allowed to stir for 1h. On cooling to RT, the solution was filtered through a pad of celite, the celite washed with DCM and the combined filtrates transferred into a separating funnel to be washed with H_2O and extracted with DCM. The organic layer was concentrated and then dissolved in 100ml DCM. 100ml TFA was added and allowed to stir for 10 minutes. The solution was transferred to a separating funnel, diluted with 100ml DCM and washed with water,

saturated $NaHCO_3$ and finally brine. The organic layer was concentrated, taken up in DCM:Hexane (1:1), loaded onto a silica gel column and eluted with DCM:Hexanes (1:1to 9:1) yielding 55mg (0.0715 mmol, 85%) **2.3**. ^{1}H NMR (400 MHz, $CDCl_3$): δ 8.82 (d, J = 4.7 Hz, 2 H), 8.68 (d, J = 4.7 Hz, 2 H), 8.63 (s, 4 H), 7.86 (d, J = 6.8 Hz, 1 H), 7.57 (t, J = 7.7 Hz, 1 H), 7.27 (s, 6 H), 7.14 (t, J = 7.4 Hz), (s, 9 H), 1.86 (s, 9 H), 1.84 (s, 9 H), -2.53 (s, 2 H). ^{13}C NMR (100 MHz, CDCl3): δ 147.01, 139.65, 139.58, 139.53, 138.35, 138.34, 137.88, 134.96, 130.65 (broad), 129.69, 127.94, 127.92, 127.35, 118.31, 118.08, 117.63, 115.35, 114.77, 21.90, 21.88, 21.63. MS (MALDI-TOF): m/z obsd 755.3880 $[M]^+$, calcd 755.3982.

Monomer 2.4. **2.17** (208mg, 0.258mmol) was dissolved in 20ml of dichloromethane. To this, 20ml of TFA was added causing the pink solution to turn green. The reaction was stirred for 1 hour at RT and then transferred to a separating funnel, diluted with 100ml DCM and washed with water, then saturated $NaHCO_3$ and finally brine. The organic layer was concentrated, taken up in dichloromethane and passed through short silica gel column, being eluted with DCM. One concentration, 183mg (0.245mmol, 95% yield) of a purple solid was obtained. ^{1}H NMR (400 MHz, $CDCl_3$): δ 8.89 (d, J = 4.7 Hz, 2 H), 8.68 (d, J = 4.7 Hz, 2 H), 8.62 (bs, 4 H), 7.98 (m, 1 H), 7.95 (d, J = 4.8 Hz, 1 H), 7.63 (dd, J = 4.73, 3.0 Hz, 1 H), 7.26 (s, 4 H), 7.24 (s, 2 H), 2.59 (s, 6 H), 2.58 (s, 3 H), 1.86 (s, 18 H), -2.43 (s, 2 H). ^{13}C NMR (100 MHz, CDCl3): δ 142.61, 139.70, 139.69, 138.68, 138.48, 137.93, 134.68, 131.22 (broad), 130.53 (broad), 130.19 (broad), 128.24, 128.00, 123.49, 118.27, 118.17, 113.82, 21.84, 21.80, 21.59. MS (MALDI-TOF): m/z obsd 746.3398 $[M]^+$, calcd 746.3438.

***Meso*-(p-methylbenzoate)dipyrromethane (2.5)** The synthesis of **2.5** was based on the literature[109] procedure reported by Rohand and co-workers. Freshly distilled pyrrole (3.122ml, 45mmol) and 2.46g (15mmol) of methyl-4-formylbenzoate were added to 100ml of vigorously stirred 0.18M HCl. The reaction solution was stirred in the dark for 4h following which point the solution was filtered to isolate the off-white crystals that had formed. A dark rubber solid had coated the stirrer bar and portions of the reaction vessel. This rubber product was dissolved in dichloromethane and transferred to a separating funnel. Containing the filtrate that had been neutralized with NaOH. More dichloromethane was added and the organic layer was isolated and concentrated. The residue was purified by silica gel chromatography employing Hex:DCM:EtOAc (7:2:1) as the eluting solvent. The product obtained was combined with the crystals obtained on filtration and recrystallized from DCM/hexanes yielding 11.91g (4.25mmol, 28% yield) of **5**. ^{1}H NMR (400 MHz, $CDCl_3$): δ 7.97 (bs, 4H), 6.71 (bs, 2H), 6.16 (bs, 2H), 65.88 (bs, 2H), 5.51 (bs, 1H), 3.90 (s, 3H). MS (MALDI-TOF): m/z obsd 280.1039 $[M]^+$, calcd 280.1206.

Dipyrromethane (2.6) A large-scale synthesis of **2.6** was conducted in which the same reaction was repeated three times. The same pyrrole was used as the solvent and reactant in each reaction and recovered and reused subsequent iterations of the same procedure. While the volume of pyrrole decreased slightly on each recovery, the quantities of paraformaldehye and $InCl_3$ catalyst were not altered. The procedure followed for each reaction is as follows. Freshly distilled pyrrole (500ml, 7.21mol) was deoxygenated in the dark by bubbling argon through it for 20 minutes. Paraformaldehyde (2.164g, 72.1mmol) was added and the solution heated to aid dissolution of the white

powder. Once dissolved, the reaction was cooled to 45^{o}C and 1.6g (7.21mmol) of anhydrous $InCl_3$ was added and allowed to stir at 45^{o}C in the dark for 1.5h under argon. Following this, the solution was allowed to cool to RT and 8.65g (0.2162mmol) of finely powdered NaOH was added and allowed to stir for 45minutes. The solution was filtered through a pad of celite. The celite was washed with dichloromethane to recover any residual pyrrole and product and the filtrates were combined and concentrated, first removing the dichloromethane which was discarded and then collecting the evaporated pyrrole for use in the next iteration of the reaction. The residue obtained from three iterations of this procedure was dried on hi-vac overnight to remove any residual pyrrole and then purified using silica gel chromatography employing hexane:DCM:EtOAc (7:2:1) as the eluting solvent. The appropriate fractions were concentrated and the product recrystallized from DCM/Hexanes to obtain 17.13g (54%) of fluffy white crystals. ^{1}H NMR (400 MHz, $CDCl_3$): δ 7.66 (bs, 2H), 6.58 (q, J = 2.56 Hz, 2 H), 6.13 (d, J = 2.92 Hz, 2 H), 6.02, (d, J = 0.56 Hz, 2 H), 3.91 (s, 3 H). ^{13}C NMR (100 MHz, $CDCl_3$): δ 129.22, 117.48, 108.40, 106.58, 26.43. MS (MALDI-TOF): m/z obsd 146.04 $[M]^{+}$, calcd 146.08.

Porphyrin 2.7. A mixture 2l of $CHCl_3$ and 15ml of EtOH in a 3l RBF was deoxygenated by bubbling argon for 15minutes. Mesitaldehyde (2.17ml, 14.7mmol), **2.5** (2.06g, 7.35 mmol) and **2.6** (1.075g, 7.35 mmol) were added followed by dropwise addition of $BF_3.OEt_2$ (0.39ml, 3.1 mmol) which caused the solution to turn red. The solution was allowed to stir for 1.5 h at RT in the dark following which DDQ (5.01g, 22.06 mmol) was added and the solution allowed to stir for a further 45 minutes. The solution was filtered through a pad of celite and concentrated. The residue was passed

through a pad of silica with dichloromethane as the eluting solvent, concentrated and purified by silica gel chromatography, again using dichloromethane as the eluting solvent affording 0.58g (0.85 mmol, 12% yield). ^{1}H NMR (400 MHz, $CDCl_3$): δ 10.14 (s, 1H), 9.28 (d, J = 4.6 Hz, 2 H), 8.83 (d, J = 4.6 Hz, 2H), 8.75 (m, 4H), 8.41 (d, J = 8.1 Hz, 4 H), 8.3 (d, J = 8.24 Hz, 2 H), 7.30 (s, 4 H), 4.10 (s, 3 H), 2.64 (s, 6 H), 1.84 (s, 12 H), -2.91 (s, 2 H). MS (MALDI-TOF): m/z obsd 680.3844 $[M]^+$, calcd 680.3146.

Porphyrin 2.8. 0.5795g (0.851 mmol) Of **2.7** was dissolved in 100ml of freshly distilled THF. Small spatula-tipfuls of $LiAlH_4$ were added stepwise at RT and the reaction monitored by TLC (dichloromethane). When no more of **2.7** was present by TLC, the reaction was quenched by the addition of small quantities of crushed ice until no further evolution of hydrogen was evident. The reaction solution was filtered through a pad of celite and concentrated. The residue was pushed through a short pad of silica using dichloromethane as the eluting solvent. The fractions containing porphyrin were concentrated yielding 0.511g (0.782 mmol, 92% yield) of crude product. The product was not characterized further and was subsequently oxidized in the next step. MS (MALDI-TOF): m/z obsd 652.3719 $[M]^+$, calcd 652.3197.

Porphyrin 2.9. 478 mg (0.733 mmol) Of **2.8** were dissolved in 50ml of dichloromethane. Small spatula-tipfuls of MnO_2 were added over a period of 1h. The reaction was monitored by TLC (dichloromethane). When all of the alcohol had been consumed to form the corresponding alcohol, the reaction solution was filtered through celite, the celite washed with dichloromethane and concentrated. The purple residue was purified by silica gel chromatography employing DCM:Hexanes (4:1) as the eluting solvent yielding 0.339g (0.5219 mmol, 71%) of **2.9**. ^{1}H NMR (400 MHz, $CDCl_3$): δ

10.36 (s, 1 H), 10.14 (s, 1 H), 9.26 (d, J = 4.6 Hz, 2 H), 8.83 (d, J = 4.5 Hz, 2 H), 8.76 (m, 4 H), 8.39 (d, J = 7.7 Hz, 2 H), 8.24 (d, J = 7.9, 2 H), 2.63 (s, 6 H), 1.84 (s, 4 H), -2.89 (s, 2 H). MS (MALDI-TOF): m/z obsd 650.2657 $[M]^+$, calcd 650.3040.

Porphyrin 2.10. 0.307g (0.472 mmol) Of **2.9** was dissolved in 250ml of chloroform and 0.084g (0.472mmol) of NBS were added and allowed to stir at RT for 1h in the dark. The reaction solution was concentrated, the residue taken up in dichloromethane and loaded onto a silica gel column and chromatographed using dichloromethane as the solvent yielding 0.299g (0.409mmol, 98%) of a purple residue that was used in the subsequent step without further characterization. MS (MALDI-TOF): m/z obsd 728.1946 $[M]^+$, calcd. 728.2145

Porphyrin 2.11. 0.2985g (0.409 mmol) Of the purple residue, **2.10**, was dissolved in 50ml of freshly distilled THF, 1.737g (8.181 mmol) of K_3PO_4 was added and the system deoxygenated with bubbling argon for 20 minutes. 1.044g (3.27 mmol) of *tert*-butyl-*N*-[2-(4,4,5,5-tetramethyl-1,3,2-dioxaborolan-2-yl)phenyl]-carbamate was added followed by 4.7mg (0.0409 mmol) of $Pd(PPh_3)_4$. The vessel was fitted with a reflux condenser and allowed to reflux under an argon atmosphere for 84h. Upon cooling, the solution was filtered through a pad of celite. The celite was washed with DCM and the filtrates concentrated. The residue was purified using silica gel chromatography using neat dichloromethane as the solvent system giving 0.1847g (0.219 mmol, 53% yield) of **2.11**. ^{1}H NMR (400 MHz, $CDCl_3$): δ 10.38 (s, 1 H), 8.33 (m, 8 H), 8.46 (m, 2 H), 8.35 (d, J = 7.8 Hz , 1 H), 8.27 (m, 2 H), 8.01 (d, J = 7.5 Hz, 1 H), 7.79 (t, J = 7.9 Hz, 1 H), 7.43 (t, J = 7.4 Hz, 1 H), 7.29 (s, 2 H), 7. 28 (s, 2 H), 6.07 (s, 1 H), 2.53 (s, 6 H), 1.87 (s,

6 H), 1.82 (s, 6 H), 1.03, (s, 9 H), -2.61 (s, 2 H). MS (MALDI-TOF): m/z obsd 841.173 $[M]^+$, calcd 841.3986.

Porphyrin 2.12. 0.119g (0.141 mmol) Of **2.11** was dissolved in toluene along with 203mg (0.282 mmol) of C_{60} and 0.126g (1.41 mmol) of sarcosine. The reaction was heated to reflux and left to stir overnight. The vessel was removed from heat and allowed to cool to room temperature. The solution was filtered through celite, which was subsequently washed with toluene. The filtrates were combined and concentrated. The residue was purified by silica gel chromatography using neat dichloromethane as the solvent. The appropriate fractions were concentrated yielding 0.127g (0.080 mmol, 57% yield) of **2.12**. ^{1}H NMR (400 MHz, $CDCl_3$): δ 8.71 (m, 8 H), 8.46, (d, J = 8.3 Hz, 1 H), 8.29 (d, J = 6.3 Hz, 1 H), 8.23 (d, J = 6.7 Hz, 1 H), 7.98 (d, J = 7.6 Hz, 2 H), 7.77 (t, J = 8 Hz, 1 H), 7.41 (t, J = 7.1 Hz, 1 H), 7.25 (bs, 4 H), 6.11 (s, 1H), 5.19 (s, 1 H), 5.00 (d, J = 9.0, 1 H), 4.30 (d, J = 9.1 Hz, 1 H), 3.04 (s, 3H), 2.58 (s, 6H), 1.83 (m, 12 H), 1.01 (s, 9 H), -2.61 (s, 2 H).

***Meso*-(mesityl)dipyrromethane (2.13)**. 22.222g (149.95 mmol) of mesitaldehyde was added to 500ml (7.707mol) of pyrrole followed by 1.15ml (15mmol) of TFA and stirred at RT for 2h in the dark. 17.99g (449.84 mmol) of finely crushed NaOH was added to the solution and allowed to stir for 1h further. The solution was then filtered through celite and the celite washed with dichloromethane. The filtrates were combined, concentrated *en vacuo* and dried overnight on hi-vac. The sticky dark residue was taken up in dichloromethane passed through two short pads of silica. The eluents were concentrated to a volume of 200ml and 600ml of hexanes were added. The dichloromethane was slowly removed on the rotary evaporator causing further

precipitation of crystals from the dark green solution. The yellow crystals were isolated by filtration, washed with hexanes and dried on hi-vac overnight yielding 14.98g (56.66 mmol, 38%) of product. ^{1}H NMR (400 MHz, $CDCl_3$): δ 7.93 (bs, 2H), 6.86 (s, 2H), 6.66 (d, J = 1.36 Hz, 2H), 6.17 (d, J = 2.96, 2H), 6.00 (s, 2H), 5.92 (s, 2H), 2.28(s, 3H), 2.06 (s, 6H). ^{13}C NMR (100 MHz, CDCl3): δ 137.73, 136.71, 131.37, 131.37, 130.47, 116.26, 108.26, 108.79, 106.63, 38.45, 20.67. MS (MALDI-TOF): m/z obsd 264.2307 $[M]^+$, calcd 264.1621.

Porphyrin 2.14. *Meso*-(mesityl)dipyrromethane (**2.13**) (1.8g, 6.808mmol, 2 equiv.), 3-thiophene carboxaldehye (0.404g, 2.723mmol, 0.8 equiv.) and methyl-4-formylbenzoate (0.671g, 4.085mmol, 1.2 equiv.) were added to 3l of chloroform containing 22.5ml EtOH. In the dark, $BF_3.OEt_2$ (0.18 ml, 1.43mmol) was added slowly and left to stir for 5 h. DDQ (2.32g, 10.212mmol) was then added, allowed to stir for 45 minutes further, after which the dark, 3l solution was passed through a pad of silica and concentrated. The residue was taken up in DCM:hexanes (4:1) and chromatographed on a silica gel column using the same solvent system as the eluent. 0.3413g (0.231 mmol, 8.5% yield) of **2.14** was obtained on concentration of the relevant fractions. ^{1}H NMR (400 MHz, $CDCl_3$): δ 8.95 (t, J = 2.3 Hz, 2 H), 8.74 (m, 6 H), 8.44 (d, J = 8 Hz, 2 H), 8.34 (d, J = 8 Hz, 2 H), 7.98 (bs, 1 H), 7.95 (d, J = 4.8 Hz, 1 H), 7.58 (t, J = 3.4 Hz, 1 H), 7.23 (s, 4H), 4.04 (s, 3 H), 2.56 (s, 6 H), 1.84 (s, 12 H), -2.52 (s, 2 H). ^{13}C NMR (100 MHz, CDCl3): δ 167.49, 147.11, 142.16, 139.52, 138.52, 137.98, 134.74, 134.60, 131.36 (broad), 130.60 (broad), 129.72, 128.46, 128.14, 127.99, 123.69, 118.83, 118.16, 114.41, 52.54, 21.83, 21.63. MS (MALDI-TOF): m/z obsd 762.5173 $[M]^+$, calcd 762.3023.

Porphyrin 2.15. **2.14** (340mg, 446 mmol) Was dissolved in 25ml of freshly distilled THF and the solution cooled to 0^{o}C. 4.2mg (0.111 mmol) of $LiAlH_4$ was added under an argon blanket and allowed to warm to RT over the course of 1h at which point the reaction was quenched with a small quantity of crushed ice and filtered through a pad of celite that was washed with dichloromethane to recover all of the product. The filtrates were combined, concentrated and the alcohol product isolated by silica gel chromatography employing DCM/1% MeOH as the eluting solvent. The residue obtained on concentration of the relevant fractions from the column was dissolved in 150ml of DCM and small spatula-tipfulls of MnO_2 were added as required and the oxidation to the aldehyde (**2.15**) was monitored by TLC (DCM). Once all starting material had been consumed, the solution was filtered through a pad of celite that was subsequently washed with dichloromethane. The filtrates were concentrated and the product isolated by silica gel chromatography using neat DCM as the solvent. 0.263g (0.358g mmol, 80% yield) of **2.15** was obtained as a purple residue. ^{1}H NMR (400 MHz, $CDCl_3$): δ 8.94 (d, J = 4.1 Hz, 2 H), 8.72 (bs, 6 H), 8.38 (d, J = 7.5 Hz, 2 H), 8.23 (d, J = 7.6 Hz, 2 H), 8.01 (bs, 1 H), 8.22 (d, J = 4.4 Hz, 1 H), 7.27 (s, 4 H), 2.61 (s, 6 H), 1.84 (s, 12 H), -2.58 (2 H, s). ^{13}C NMR (100 MHz, CDCl3): δ 192.54, 148.70, 142.10, 139.55, 139.50, 138.42, 138.01, 135.72, 135.29, 134.61, 130.47 (broad), 128.49, 128.17, 127.97, 123.70, 118.88, 117.59, 114.54, 21.79, 21.63. MS (MALDI-TOF): m/z obsd 732.2951 $[M]^{+}$, calcd 732.2917

Porphyrin 2.16. *Meso*-(mesityl)dipyrromethane (**2.13**) (0.917, 3.67 mmol), mesitaldehyde (2.57g, 1.733 mmol) and 2-nitrobenzaldehyde (0.262g, 1.733 mmol) were added to 3l of deoxygenated chloroform containing 22.5ml of EtOH. With stirring, 0.091ml (0.728 mmol) of $BF_3.OEt_2$ were added and left to stir in the dark for 3h before

1.18g (5.2 mmol) of DDQ were added and allowed to stir for a further hour. The solution was passed through a pad of silica and concentrated. The components of the dark purple residue were separated via silica gel chromatography employing DCM:hexanes (2:3→ 1:1) as the eluting solvent. Concentration of the appropriate fractions yielded 66.6mg (0.0847 mmol, 4.9% yield) of **2.16**. ^{1}H NMR (400 MHz, $CDCl_3$): δ 8.66 (d, J = 4.7 Hz, 2 H), 8.62 (s, 4 H), 8.56 (d, J = 4.7 Hz, 2 H), 8.44 (dd, J = 8.1, 1.5 Hz, 2 H), 8.17 (dd, J = 7.0, 1.6 Hz, 2H), 7.90 (m, 2 H), 7.27 (s, 3 H), 7.26 (s, 3 H), 2.61 (s, 9 H), 1.89 (s, 3 H), 1.86 (s, 6 H), 1.84 (s, 6 H), 1.82 (s, 3 H), -2.50 (s, 2H).

Porphyrin 2.17. **2.13** (0.68g, 2.572 mmol), mesitaldehyde (0.191g, 1.29 mmol) and thiophen-3-carboxyaldehye (0.144g, 1.29 mmol) were added to 3l of deoxygenated chloroform containing 22.5ml EtOH followed by $BF_3.OEt_2$ (0.077g, 0.54 mmol) and allowed to stir in the dark for 3h. After this period, DDQ (0.867g, 3.86 mmol) was added and left to stir for an additional minutes before being passed through pad of silica and concentrated to yield a dark purple residue. The residue was dissolved in 500ml DCM and 1.13g of $Zn(OAc)_2.2H_2O$ dissolved in 50ml of MeOH was added, heated to reflux and left to react for 16 hours. The solution was transferred to a separating funnel and washed with water. The organic layer was collected and concentrated. Silica gel chromatography employing Hexanes:DCM (7:3) was used to isolate **2.17** (0.117g, 0.144mmol, 11%) as a bright pink solid once concentrated. ^{1}H NMR (400 MHz, $CDCl_3$): δ 9.00 (d, J = 2.2 Hz, 2 H), 8.78 (d, J = 4.5 Hz, 2 H), 8.72 (s, 4 H), 7.98 (m, 2 H), 7.64 (m, 2H), 7.27 (s, 4 H), 7.26 (s, 2 H), 2.61 (s, 6 H), 2.60 (s, 3 H), 1.86 (s, 6 H), 1.85 (s, 12). ^{13}C NMR (100 MHz, CDCl3): δ 150.33, 150.07, 150.05, 149.96, 143.17, 139.46, 139.24, 139.14, 134.69, 132.07, 131.34, 131.27, 130.87, 127.83, 123.20, 119.07, 118.91,

114.65, 21.95, 21.86, 21.65. MS (MALDI-TOF): m/z obsd 808.2364 $[M]^+$, calcd 808.2573.

2.7.3 Electrochemistry

Polymerization of monomers was conducted using a CH Instruments Electrochemical Workstation. Dichloromethane solvent was distilled before use over CaH and stored under argon. FTO glass slides were cleaned by sequential sonication in water, ethanol and dichloromethane and dried in an oven at 180^{o}C prior to use. Polymerization was achieved using a standard 3-electrode cell using an FTO slide as the working electrode, a Ag/AgCl reference electrode and a platinum gauze auxiliary electrode.

Chapter 3: Optimizing the Solvent System for the Synthesis of a Porphyrin-Wire-C_{60} Construct Using a Tetraaminodiquinoxalpyrene Building Block

3.1 Design of a Trial Porphyrin-Wire-C_{60} system

The pyrazine-containing heteroaromatic ribbons shown figure 1.5, as reported by Gao *et al*.[95] show promise as candidates for use as conductive scaffolds. It was envisaged that pyrene moieties present within these ribbons could be functionalized to subtend chromophores orthogonal to the primary axis of the ribbons, thus providing a starting point for the synthesis of higher order arrays for use in photovoltaic technologies using square intersections of the various components.

The molecules reported by Gao *et al*. are not simple repeats of a common unit and feature variance in the number of pyrazine rings present between the pyrene centers and termini. The core repeat unit of interest is that shown in figure 3.1, which presents a possible strategy for the synthesis of a polymer of this repeat unit by condenstion of a simple monomeric unit.

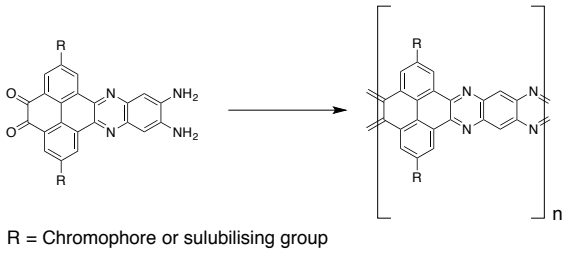

Figure 3.1 The core repeat unit of interest for the synthesis of an orthogonally functionalized linear conductive scaffold.

In the interest of systematically studying the ability of such structures to mediate long distance photoinduced electron transfer, an appropriate donor-acceptor system needed to be developed between which heteroaromatic wire units of varying length could be positioned and the electron transfer rates determined for determination of the characteristic attenuation factor, β for electron transfer across the wires.

There is a good precedent in the literature for the use of porphyrins as donors and substituted fullerenes as the acceptors in such studies[81,85-88,114-116]. The pyrazine-containing heteroaromatic wires of interest feature a high degree of symmetry and were also reported to exhibit incredibly high association constants[95]. The fortunate symmetry provided an opportunity to navigate an anticipated solubility problem for conducting solution state studies. A suitable end-cap that allowed for the terminal substitution of the wires with two porphyrin moieties was sought. It was thought that designing the system to feature porphyrin moieties that would rotate relative to the plane of the wire, would inhibit the aggregation of the wires. An *o*-diketone aromatic terminus was designed that would append two porphyrins directly onto the wires without the presence of any intermediate benzene rings that could otherwise rotate and decouple the porphyrins from the wire.

While extensive synthetic methodology exists for producing aryl substituted porphyrins, which can subsequently be incorporated into systems using palladium coupling methodologies, since the attenuation factors of the wires were sought, the design required that the porphyrin donors must be attached directly to the fused aromatic wires without any moieties such as benzene rings present between the donor and wires.

Equally, an appropriate acceptor terminus was required that would not feature significant separation between a fullerene acceptor and the end of the wire but would still provide sufficient electronic decoupling so as to retain the separate identities of the wire and acceptor entities. With the symmetry present in the wires and the decision to use two porphyrins on the donor terminus, a fullerene building block was required that also preserved the symmetry of the system, and so, ensured that the two porphyrin donors would remain identical.

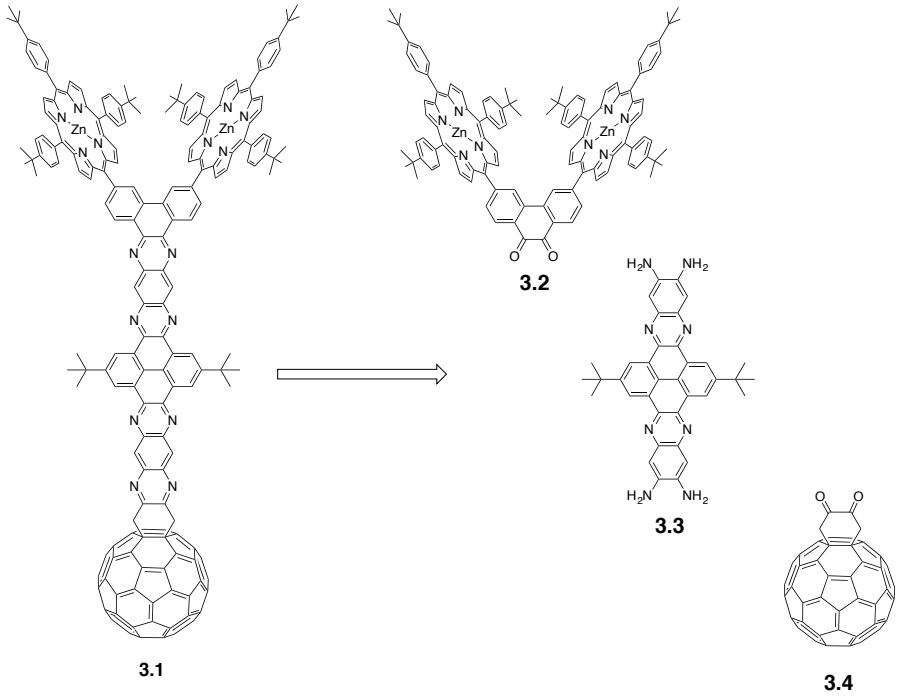

Figure 3.2 A retrosynthetic scheme of the first D-W-A construct **(3.1)** designed as a step towards determining the attenuation factor of the fused heteroaromatic wires.

Figure 3.2 shows the first D-W-A system designed (**3.1**) to satisfy these constraints. The requisite porphyrin-substituted phenanthrenedione donor terminus building block **3.2** is shown together with the tetraaminodiquinoxalpyrene building block (**3.3**) that chosen as the shortest unit of interest for use in constructing the first D-W-A

system for this investigation. The diketone fullerene adduct, **3.4**, was selected for use as the acceptor terminus.

The donor terminus building block (**3.2**) was synthetically feasible and provided a simple means for appending the porphyrin donors to *o*-diamino aromatic building blocks of the wire, continuing the characteristic fused aromatic nature of the wire. The 3,6 substitution of phenanthrenedione with porphyrins shown was chosen so to best preserve the linearity of the system and to force steric interactions between the two porphyrins. This was incorporated into the design to prevent the porphyrins from flattening into the plane of the wire formed and so inhibit aggregation. The porphyrins chosen for use in **3.2** feature *para*-(*t*-butyl)benzene rings. The bulky *t*-butyl groups were selected to increase the steric interactions between adjacent porphyrins on **3.2** and to enhance the solubility of the resulting construct.

The *o*-diketone fullerene adduct, **3.4**, satisfied the requirements for a building block to append the wires as the acceptor terminus of the structures. The *o*-diketone could be condensed with aromatic-*o*-diamines to form the final pyrazine moiety of the fused wire in **3.1**.

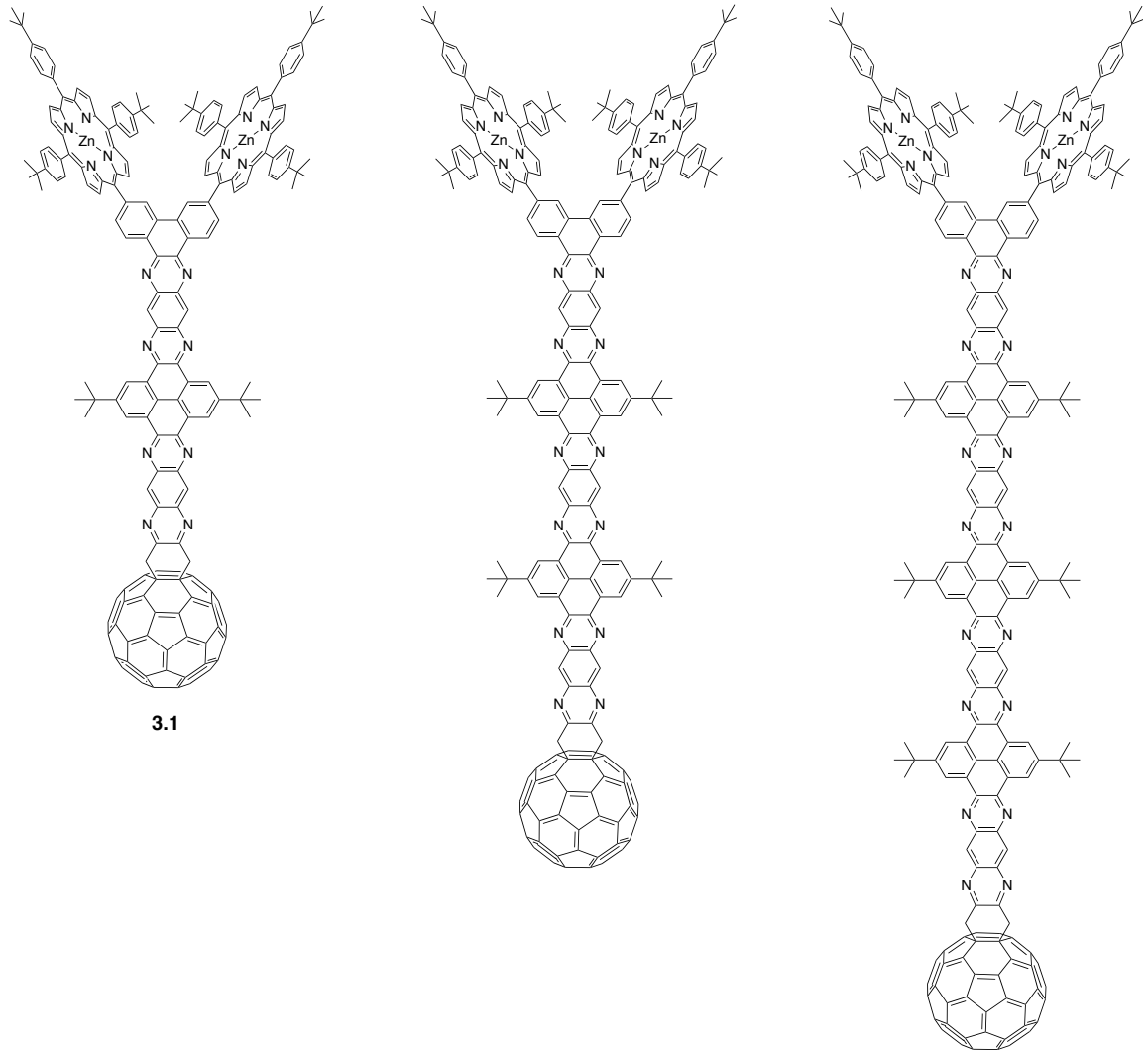

Figure 3.3 A series of D-W-A complexes proposed for determining the attenuation factor *β* of the wires shown utilizing the porphyrin donor terminus **3.2** and acceptor terminus **3.3**.

Figure 3.3 shows a series of donor wire acceptor compounds that could be synthesized by using the donor and acceptor termini **3.2** and **3.4,** respectively, for determining the attenuation factors of wires of the type shown in figure 3.1. With the system designed, a synthetic protocol for the synthesis of **3.2** was created. **3.3**[117] and **3.4**[118] are known literature compounds along with building blocks required for their synthesis.

3.2 Synthesis of the Porphyrin-Substituted-Phenerenedione Donor Terminus

For the synthesis of **3.2** the porphryin, **3.6** shown in scheme 3.1 is required for Suzuki-coupling with 3,6-dibromophenanthrene-9,10-dione. The synthesis of the core porphyrin macrocycle was achieved by condensing *meso*-(*p*-*tert*-butylphenyl)dipyrromethane (**3.5**) with dipyrromethane (**2.6**) and *p*-(*t*-butyl)benzaldehyde using BF_3OEt_2 as the Lewis acid catalyst. It was found that the mixture of porphyrin products could not be separated efficiently by silica gel chromatography. The three products did not exhibit significant differences in mobility when a dichloromethane/hexanes solvent system was used to elute the products. Increasing the percentage of hexanes within the system to slow down the mobility under chromatographic purification promoted crystallization of the porphyrin products, negating the effectiveness of the strategy to increase the R_f differences of the products. Inserting zinc into the porphyrin product mixture did not result in the mixture exhibiting significant differences in R_f. The product mixture resulting from bromination of the free meso positions present on molecules in the mixture also failed to produce a separable mixture. Consequently, the synthesis of **3.6** was achieved in four successive steps before the products present in the mixture could be separated by column chromatography. Following metallation with zinc and bromination using NBS, a palladium catalyzed coupling of pinacolborane to the brominated *meso* positions of the porphyrins afforded a mixture that was separable. The resulting mono- and di-boronic ester products exhibited lower mobilities during silica gel chromatography, which enabled separation.

Scheme 3.1

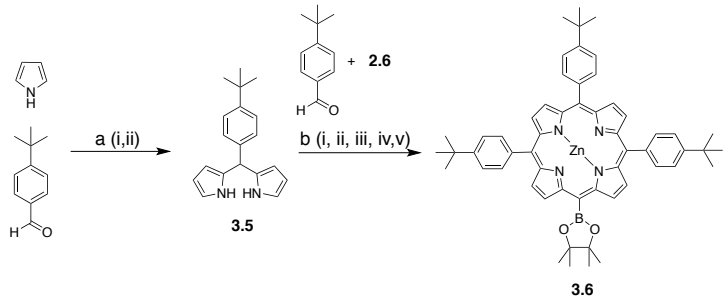

a) i $InCl_3$, RT, 3h. **ii** NaOH, RT, 1h. **b) i** $BF_3.OEt_2$, $CHCl_3$/0.75% EtOH, RT, 3h **ii** DDQ, RT, 1h. **iii** $Zn(OAc)_2.2H_2O$, DCM/60% MeOH, reflux, overnight. **iv** NBS, $CHCl_3$/0.1% Pyridine, RT, 1h. **v** Pinacolborane, $Pd(PPh_3)_2Cl_2$, Et_3N, 1,2-dichloroethane, Ar., reflux, overnight. Overall yield: 8%

Scheme 3.2 shows how the product mixture following the initial condensation is transformed in the successive steps in the synthesis of **3.6**.

Scheme 3.2

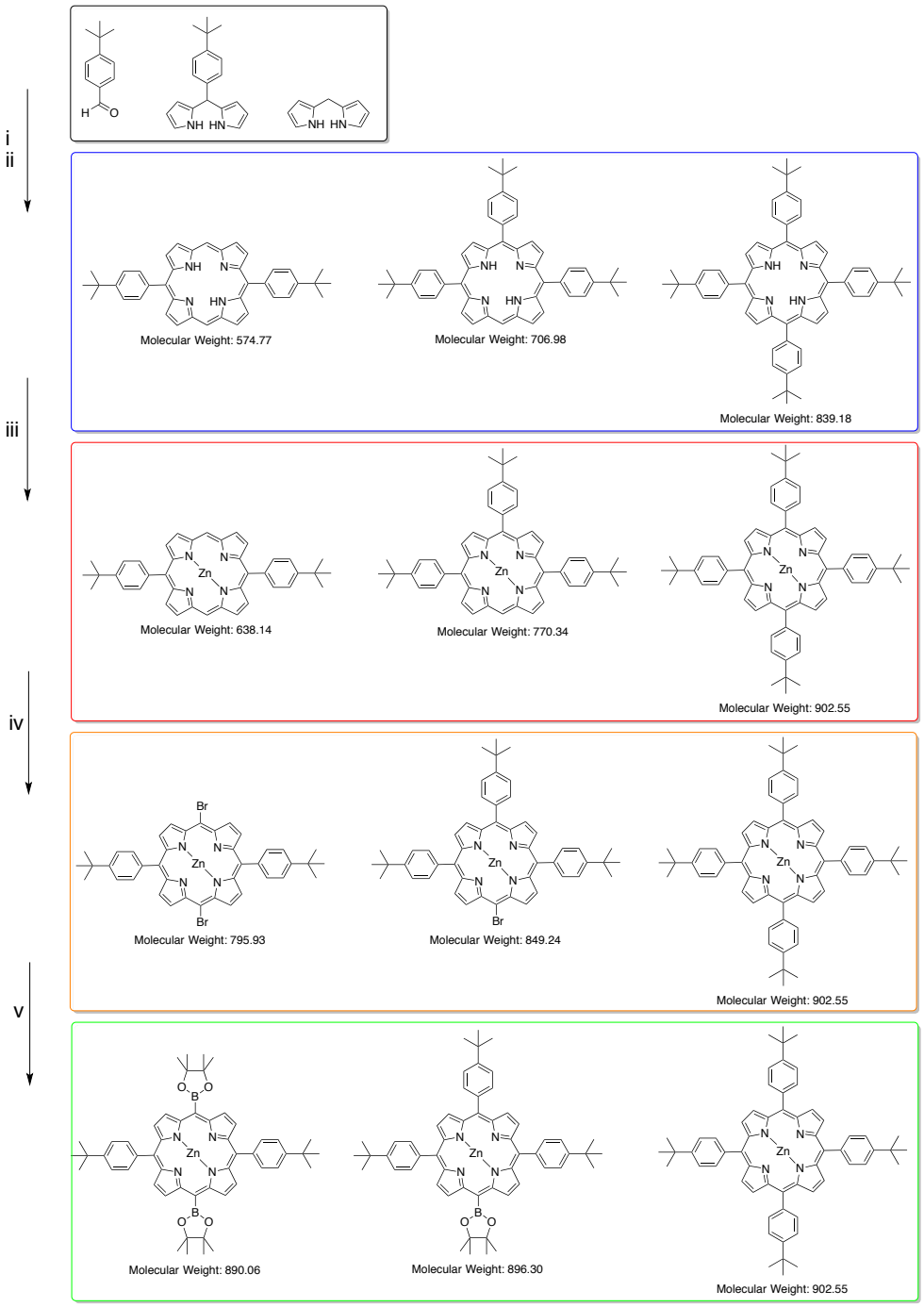

Products produced in the synthesis of **3.2** showing how each byproduct is converted in each step until the product mixture is separable (green rectangle). **i** $BF_3.OEt_2$, $CHCl_3$/0.75% EtOH, RT, 3h **ii** DDQ, RT, 1h. **iii** $Zn(OAc)_2.2H_2O$, DCM/60% MeOH, reflux, overnight. **iv** NBS, $CHCl_3$/0.1% Pyridine, RT, 1h. **v** Pinacolborane, $Pd(PPh_3)_2Cl_2$, Et_3N, 1,2-dichloroethane, Ar., reflux, overnight.

The necessary aryl bromide for Suzuki-coupling with **3.6** is 3,6-dibromo-9,10-phenanthrenedione, **3.7**. The synthesis of **3.7** shown in scheme 3.3 is achieved by a light activated radical bromination of 9,10-phenanthrenedione with bromine in nitrobenzene[119].

Scheme 3.3

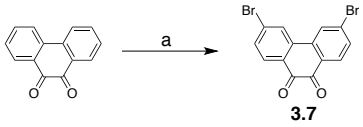

3.7

a) Br_2, Nitrobenzene, hυ (60 W-tungsten lamp), 60→150°C, 3h, 72 % yield

The synthesis of **3.7** proceeded simply by coupling **3.6** with **3.7** using $Pd(PPh_3)_4$ as the catalyst. The reaction was conducted using THF as the solvent and in a pressure tube at 120°C as shown in scheme 3.4.

Scheme 3.4

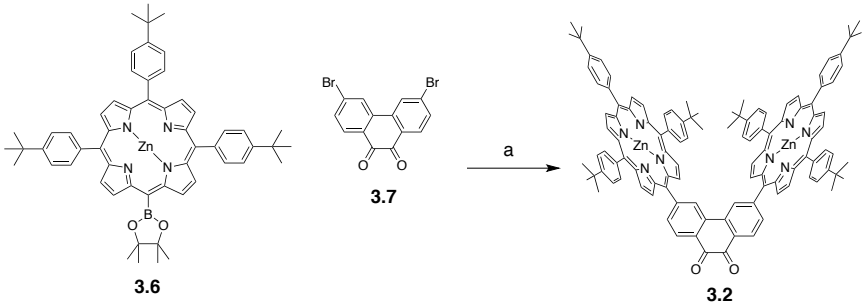

3.6 **3.7** **3.2**

a) $Pd(PPh_3)_4$, Cs_2CO_3, THF, 120°C, 20h

3.3 Temperature Dependent NMR Investigation of the Porphyrin-Substituted Phenanthrenedione Donor Terminus

The room temperature ^{1}H NMR spectrum of **3.2** in $CDCl_3$ displayed interesting signals for the protons of the phenyl rings attached to the two porphyrins. While a C_2 symmetry axis is present in the molecule, the protons on the phenyl rings present at the 10 and 20 positions (equatorial phenyl rings colored red and blue in fig.3.6.a) did not exhibit the expected set of two doublets. Rather, four doublets were observed revealing that at room temperature the phenyl rings experienced two distinct environments.

Consequently a sample of **3.2** in DMSO-*d*6, a high boiling-point solvent was created. Figure 3.4 shows the aromatic portion of the spectra acquired as the temperature was increased stepwise from 25^{o}C to 120^{o}C. The signals for the phenyl rings are present between 8.2 and 7.5 ppm. At room temperature two larger doublets are present around 8 and 7.74 ppm. These are the signals of the phenyl rings drawn in green in figure 3.6. The chemical shifts and relative intensities of these two doublets do not show any significant changes as the temperature is raised from 25^{o}C to 120^{o}C, yet they are obscured by the coalescence of the signals of the equatorial phenyl rings at intermediate temperatures.

The doublets assigned to the equatorial phenyl rings shown in red and blue in figure 3.6 coalesce as the temperature is raised, finally producing a pair of doublets around 7.92 and 7.65ppm.

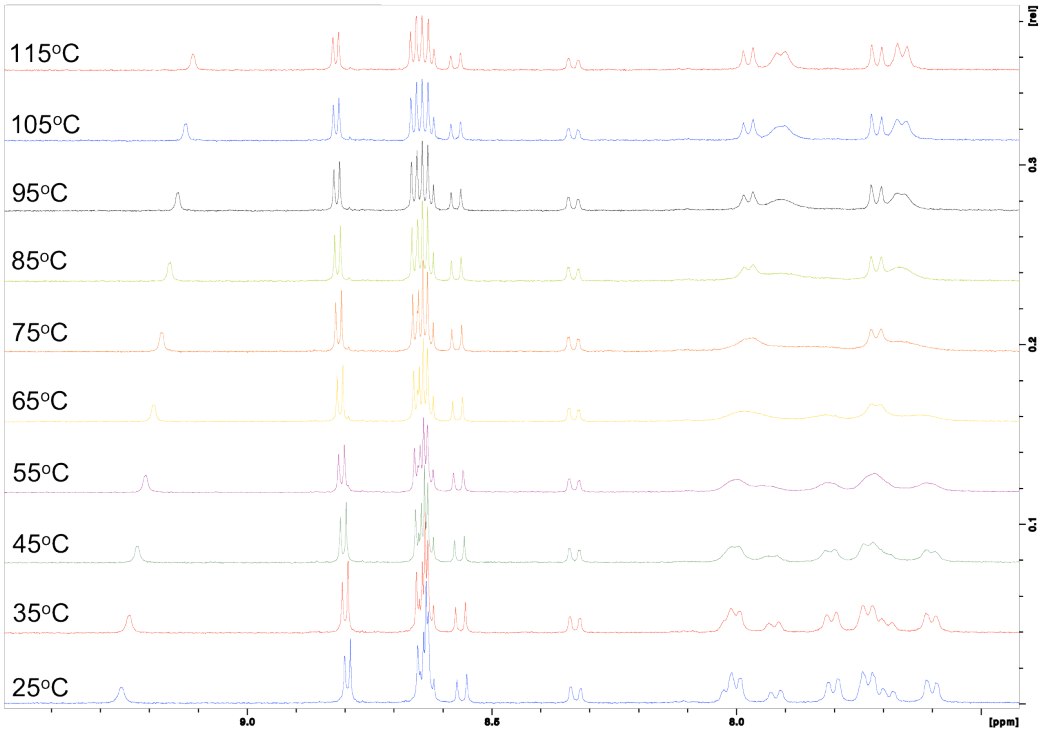

Figure 3.4 The behavior of the aromatic region of the ^{1}H NMR spectrum of **3.2** in DMSO is shown as the temperature is increased incrementally from room temperature to 115°C.

As stated previously, apart from the obvious donor role of the porphyrins in the D-W-A construct of **3.1**, the presence of the porphyrin substituents in **3.2** was intended to imbue solubility to the compounds formed. The proximity of the porphyrins to each other was intended to force steric interactions that would poise the porphyrins in a configuration similar to that shown in figure 3.5.a. In this configuration, stacking of the D-W and D-W-A constructs through wire-wire interactions would be somewhat inhibited as shown by the drawing in figure 3.5.b. Analysis of the NMR spectra shown in figure 3.4 shows that the opposite may well be true. Instead of the porphyrins exhibiting a RT configuration like that in figure 3.5a, which would cause the protons on the benzene rings

in the 5 and 20 positions of the porphyrins to exhibit like chemical shifts, it appears that **3.2** exhibits a room temperature configuration something like that shown in figure 3.5.c in which there is an attractive π-π interaction between the phenyl rings on adjacent porphyrins. This is problematic as it implies that aggregation of the wire portions of the D-W-A constructs would be markedly less obstructed when the porphyrins rested in this configuration, as shown by the drawing in figure 3.5.d.

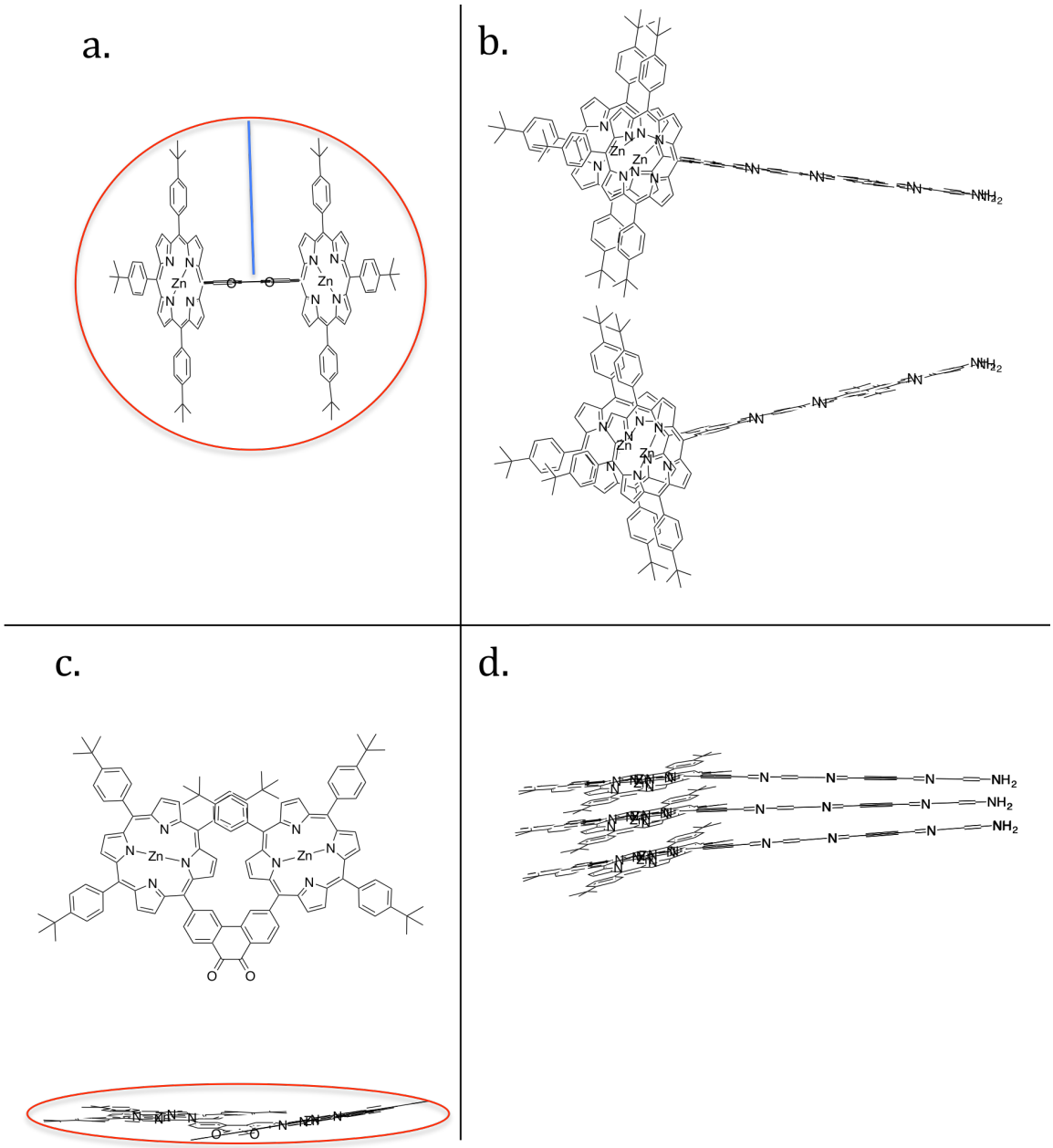

Figure 3.5 a.) Shows **3.2** drawn in a conformation in which the space between the porphyrins is maximized so as to minimize the steric interactions between them, effectively increasing the space occupied orthogonal (blue line) to the plane of phenanthrenedione. b.) Shows **3.2** in the same conformation connected to a long fused heteroaromatic wire. When arranged side by side the spacing between the wires is evident. c.) The porphyrins on **3.2** are drawn so as so to flatten into the plane created by phenanthrenedione in **3.2**. d.) Shows how a wire construct featuring this flattened conformation enables the long heteroaromatic wires to come closer together to stack.

Figure 3.6 shows how the thermal energy available with increasing temperature increases the conformational variability exhibited within the NMR timescale of **3.6** to produce the observed NMR spectra shown in figure 3.4. While the positioning of the porphyrins in close proximity to one another on phenanthrenedione does inhibit their rotation, the RT conformation is most likely that shown in figure 3.5.c and not 3.5.a. This conclusion was only reached later in the study after further synthesis had been conducted.

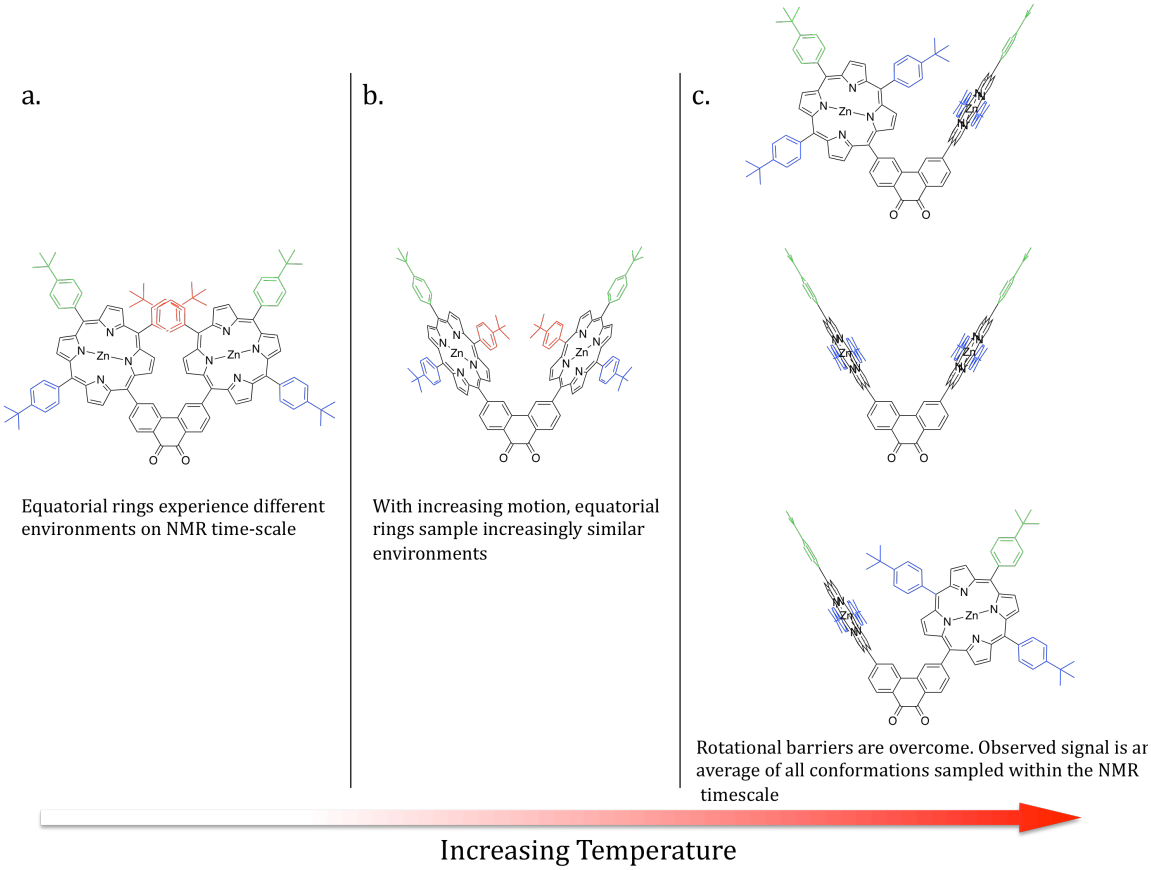

Figure 3.6 a.) Shows the proposed RT conformation of **3.2**. Phenyl rings in red rest in a different magnetic environment to those of shown in blue producing differnent signals for the corresponding protons b.) Shows a conformation in which the rotation about the phenanthrene-porphyrin bond is restricted. Both of the blue and red environments can be sampled on the NMR time-scale causing coalescence of the representative peaks. c.) At higher-temperatures the rotational barrier is overcome and phenyl rings rotate to sample all of the possible conformers. The resulting spectrum is shows signals from both rings representing an average of the magnetic environment of all conformers.

3.4. Synthesis of the Tetraaminodiquinoxalpyrene Wire Building Block and the Requisite Precursors

Scheme 3.5 shows the stepwise synthesis of **3.9**, a known literature[120] compound. Friedel-Crafts alkylation of pyrene using *t*-butylchloride and $AlCl_3$ afforded 2,7-*t*-butylpyrene (**3.8**) in 64% yield[121]. Oxidation of **3.8** to produce 2,7-*t*-butyl-4,5,9,10-tetraketopyrene (**3.9**) was achieved using $RuCl_3.xH_2O$ as the catalyst and $NaIO_4$ to provide the oxidation potential. The reaction employed a solvent system of dichloromethane to dissolve the pyrene, water to dissolve the $RuCl_3.xH_2O$ catalyst and $NaIO_4$ and CH_3CN in which both of these solvents are miscible. Over the course of this work, this literature procedure was carried out numerous times. The reported literature yields for **3.9** were never achieved. On each occasion, a significant amounts of partially oxidized **3.8** determined to be 2,7-*t*-butyl-4,5-diketopyrene was obtained in significant quantities. 2,7-*t*-butyl-4,5-diketopyrene can be readily oxidized to form the tetraketone as would be required in the direct oxidation of **3.8** to form **3.9**. In the report by Hu *et al.*, two variables in the reaction are controlled to determine if the diketone or tetraketone is produced, specifically the equivalents of the oxidant, $NaIO_4$, that are added and the temperature. To produce the diketone, four equivalents of $NaIO_4$ are used and the reaction conducted is at RT. Synthesis of the tetraketone employs eight equivalents of $NaIO_4$ and is conducted at 30-40^oC[120]. Consequently, in practice, if high yields of **3.9** were required, a two-step procedure was employed. First 2,7-*t*-butyl-4,5-diketopyrene was first synthesized using the reported literature procedure for the synthesis of the diketone[120]. The crude product from this reaction was then further oxidized to the

tetraketone, again using four equivalents of $NaIO_4$ but at an elevated temperature of 40°C. A literature report[122] for a higher-yielding procedure affording the tetraktopyrenes exists but requires sonication and heating. Considering the number of times that the tetraketopyrenes were synthesized in this work, acquiring the necessary equipment to be able to use this procedure would be a worthwhile investment.

Scheme 3.5

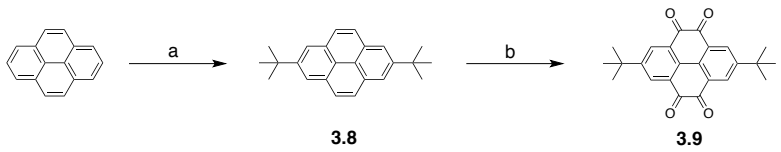

a) $AlCl_3$, *t*-BuCl, dichloromethane, RT, 4h, 64% yield. **b)** $RuCl_3.xH_2O$, $NaIO_4$, CH_3CN, dichloromethane, H_2O, 50°C, 47% yield.

The overall synthesis of 2,3,11,12,-tetraminodiquinoxal[2, 3-e, 2', 3'-1]pyrene (**3.3**) developed by Arnold[117] as shown in scheme 3.7. 1,2-Diamino-4,5-(*p*-toluenesulfamido)benzene (**3.9)** is an important compound which enables a high-yielding two-step synthesis of **3.3** from **3.9** and **3.6**. In concept, **3.3** could be produced from reaction of **3.9** with 1,2,4,5-tetraaminobenzene tetrahydrochloride. This however would require a high excess of 1,2,4,5-tetraaminobenzene tetrahydrochloride to prevent polymerization from occurring and the products and remaining starting materials would be difficult, if not impossible to separate and purify. The tosyl protecting groups of **3.9** enable the synthesis of **3.3** without requiring an excess of the *o*-diamine employed, and so, negate the need for a difficult separation of largely insoluble aromatic compounds from one another following the reaction.

Scheme 3.6

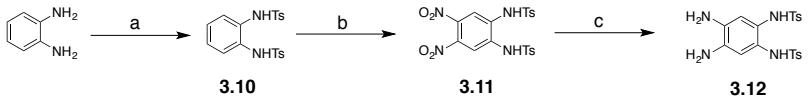

a) TosCl, dichloromethane, pyridine, 0°C→RT, 5h, 88% yield. **b)** HNO_3, AcOH, 70°C, 2h, 66% yield **c)** H_2 (60 psi), 10% Pd/C, EtOH, 78% yield.

1,2-(*p*-Toluenesulfamido)benzene (**3.10**) was produced by a low temperature protection of *o*-phenylenediamine with toluenesulfonylchloride in ice cold DCM using pyridine to mop up the acid produced over the course of the reaction. This was in accordance with the report[123] by Proust and Paquette. With the robust tosyl protecting groups present, synthesis of 1,2-dinitro-4,5-(*p*-toluenesulfamido)benzene (**3.11)** was achieved by treating **3.10** with nitric acid in acetic acid at 70°C as reported by Cheesman[124]. The nitro groups of **3.10** were subsequently reduced in a Pd/C catalyzed hydrogenation using a Parr apparatus at 60psi loosely following the report[125] by Shirai and co-workers. Isolation of **3.12** from the Pd/C catalyst according to the reported protocol did not proceed as cleanly as was described. The purification protocol was improved on by dissolving the product present in the cake obtained on filtration of the crude reaction solution with DMSO with subsequent recovery of the product by precipitation from this solvent using water.

Scheme 3.7

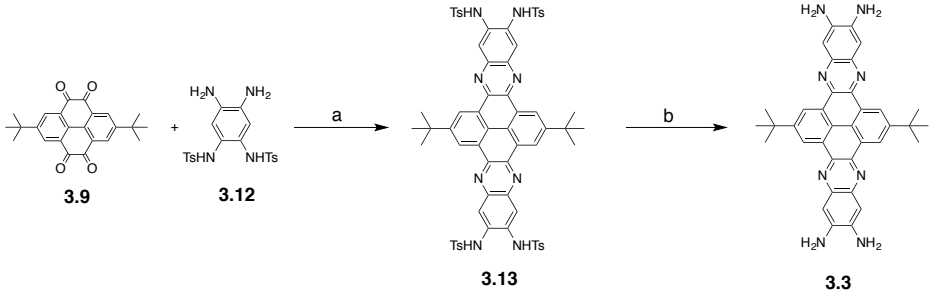

a) AcOH, 60°C, Ar., 8h, 73% yield. **b)** H_2SO_4, RT, 6h.

Synthesis of **3.13** was readily achieved by condensing **3.9** with **3.12** in glacial acetic acid at 60°C as described by Arnold[117]. The amines of **3.13** were deprotected to form **3.3** by treatment with deoxygenated H_2SO_4. The reported[117] work-up was followed closely and every effort was made to dry the final compound. Nonetheless, over 100% yield was achieved indicating that the product had trapped solvent within the solid product formed or that the deprotection reaction had not occurred to completion. Nevertheless, either option would not have serious consequence on subsequent reactions and the product was used without further purification.

3.5 Synthesis of the Diketone Fullerene Acceptor Terminus

In 1997 Torres-Garcia and co-workers published a report on a "*Versatile Route to Subsituted 1,4-Diazine-Fused [60]Fullerenes*"[118]. This report detailed the synthesis of a convenient alternative to the common Bingel and Prato[112] attachments for incorporating C_{60} fullerenes onto simple diamines and aromatic *o*-amines.

The diketone **3.4** (shown in figure 3.4) was the perfect candidate for the project at hand as it negated the need for the synthesis of an aromatic *o*-diketone functionalized with a fullerene through by a Bingel or Prato[112] attachment that would break the C_2 symmetry of the overall D-W-A formed using attachments. While a tandem Bingel addition could produce such a compound[126], the use of **3.4** was far simpler. Furthermore, the methane groups of the diketone, **3.13**, when condensed onto the end of an *o*-diamine-terminated aromatic wire would decouple the orbitals of the wire from the fullerene to preserve the electronic identity of the two species. Of the known methodologies for incorporating C_{60} fullerenes into organic molecules, the use of **3.4** would position the fullerene closest to the terminus of wire, thus the rate constants derived for electron transfer from donor to acceptor would more closely represent electron transfer across the wire and not through the additional intermediary space that the other attachments to C_{60} feature.

The general literature procedure[118] used for the syntheses of some simple 1,4-diazine-fused [60] fullerenes do not isolate the diketone **3.4** prior to condensation with the respective *o*-diamines. The established protocol simply uses crude mixtures obtained after following a one pot, three-step procedure for the synthesis of **3.4**. For the purposes of this work, attempts were made to isolate **3.4** in pure form. Following the synthesis in accordance with the literature procedure shown in scheme 3.8, purification attempts were made that were largely successful at removing C_{60} from the product mixture giving a crude product enriched in **3.4**. MALDI-TOF mass spectral analysis confirmed the presence of **3.4** in a brown fraction obtained by column chromatography. Given the precedent in the literature in using **3.4** as a crude isolate, further attempts at

characterizing **3.4** were abandoned when the first ^{1}H NMR spectrum acquired revealed the presence of several impurities. The most complex 1,4-diazine-fused [60] fullerene synthesized in the report[118] followed was [5,6]fullereno-C_{60}-Ih-[1,9-*b*]-10′,11′,12′,13′-tetrahydro-dibenzo[*a*,*c*]phenazine which was achieved with a poor 6% yield based on fullerene used. It was thus concluded that for the synthesis of considerably more complex compounds using **3.4**, the modified protocol would be used, even though a completely pure sample was not obtained.

Scheme 3.8

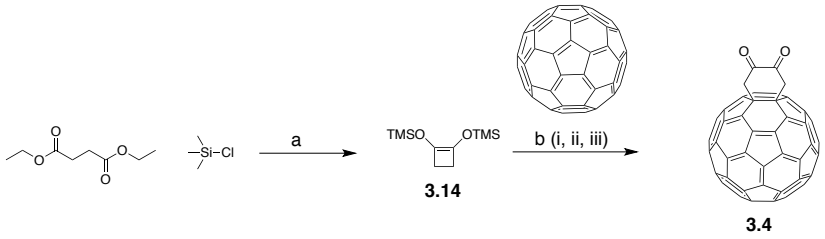

a) Na (metal), Toluene, reflux, overnight. 54% yield. **b) i** 1,2-Dichlorobenzene, reflux, 1h. **ii** Br_2, CS_2, -78^{o}C, 1.5h. **iii** $Et_3N.HF$, 1,2-dichlorobenze, RT, 1h. 23%

Synthesis of **3.4** requires the synthesis of 1,2-bis(trimethylsiloxy)cyclobutene (**3.14**) from diethylsuccinate. This was achieved by following the established method published by Hazen[127]. The reduction employed exposing diethylsuccinate to molten sodium metal in refluxing toluene together with trimethylsilylchloride (TMSCl). The three-step, one-pot synthesis of **3.4** involves heating **3.14** in 1,2-dichlorobenzene to 180^{o}C which causes ring opening to form the corresponding butadiene, which then undergoes a [4+2] Diels-Alder cycloaddition with C_{60} present in solution[118]. A subsequent low temperature bromination of the resulting cyclohexene double bond created in the cycloaddition primes the protected alcohols with α-bromo leaving groups

that can eliminate from ketones on deprotection. As such, treatment of the TMS-protected alcohols present on the brominated intermediate with $Et_3N.HF$ resulted in the formation of **3.4**.

3.6 Optimization of Solvent for the Synthesis of the Porphyrin-Wire-C_{60} Construct

With the necessary building blocks in hand, the first attempts at the synthesis of **3.1** were conducted. There is a considerable precedent in the literature for condensing *o*-diketones with aromatic *o*-diamines to form the corresponding pyrazine moiety[95,128-138]. Amongst the methods present many of them are achieved by reflux of the *o*-diketone and *o*-diamine together in EtOH, AcOH or *m*-cresol[95]. Ethanol is not a good solvent for larger aromatic molecules as their poor solubility inhibits them from partaking in the reaction. Acetic acid is consequently a better solvent for conducting condensations of larger aromatic diketones and diamines, which exhibit better solubility within it. In addition, the acidity of AcOH acts to activate the ketones, priming them for nucleophillic attack by the amines. For this reason the first attempt made to condense **3.2** with **3.3** followed by subsequent condensation with **3.4** employed acetic acid as the solvent.

Scheme 3.9

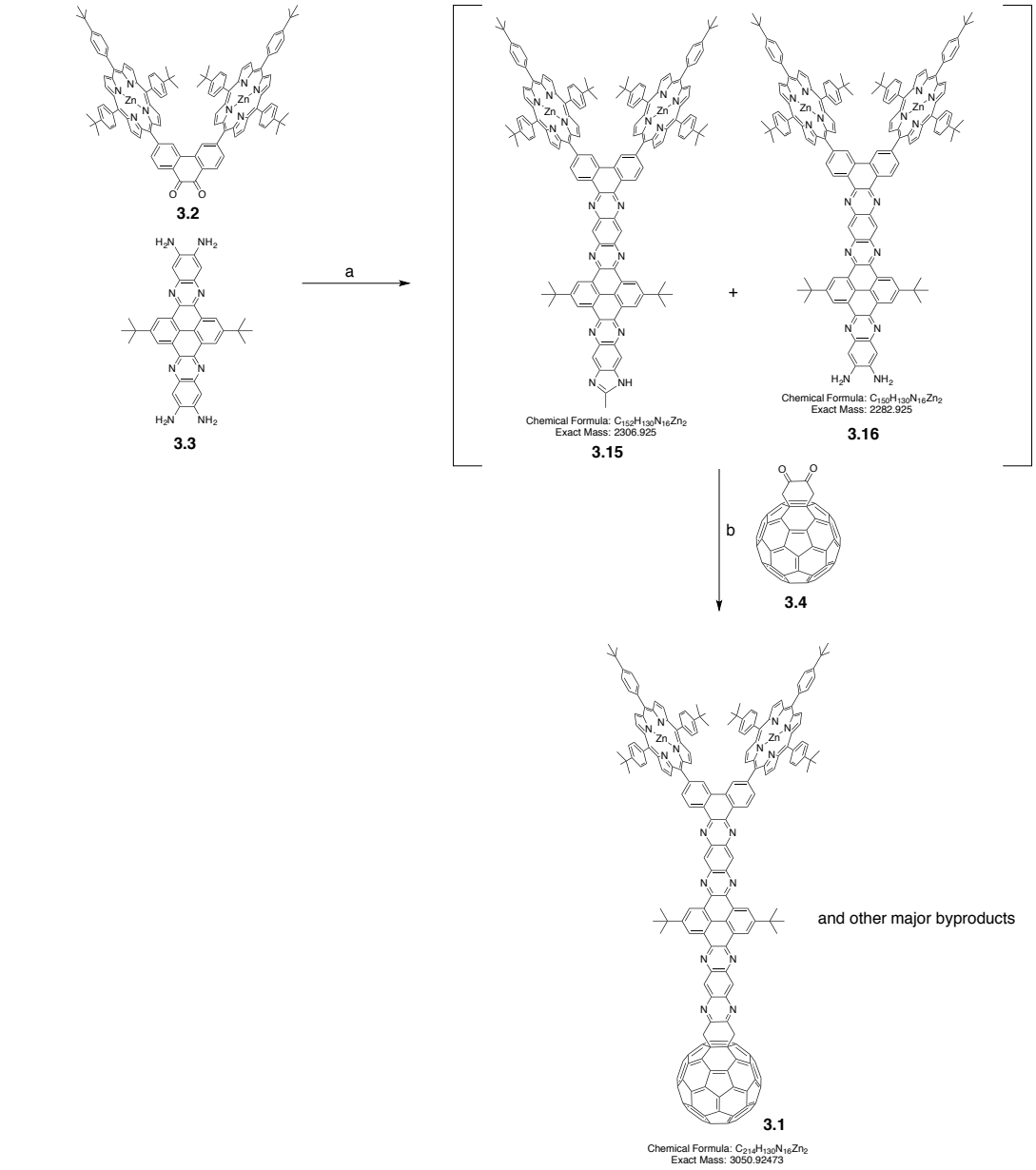

a) AcOH, reflux, overnight **b)** AcOH, 1,2-dichlorobenzene, reflux, overnight.

The AcOH used was thoroughly deoxygenated by freeze-pump-thaw cycles with argon owing to concern regarding the oxygen sensitivity of **3.3**. MALDI-TOF mass-spectral analysis of the crude reaction mixture following overnight reflux of **3.2** with **3.3**

(figure 3.7.a) revealed incomplete consumption **3.2** (peak at 1744 Da). Also evident was that considerable single and double demetallation of **3.2** had occurred and that little to none of the desired intermediate product, **3.16** (peak around 2282 Da), was present.

An unexpected byproduct peak around 2310 Da appeared to be the only real product that had formed at this stage. Figure 3.7.b shows a comparison of the observed spectrum obtained from the crude solution at this point with the theoretical peak for the byproduct **3.15**. It is thought that AcOH reacts with the intermediate product, **3.16**, to produce **3.15** by eliminating water twice. While little to no **3.16** was present at this stage, **3.4** dissolved in 1,2-dichlorobenzene was added. It was thought that the formation of the byproduct **3.15** may be reversible and that hydrolysis of **3.15** would liberate **3.16** into solution to react with the **3.4**, producing **3.1**.

a.)

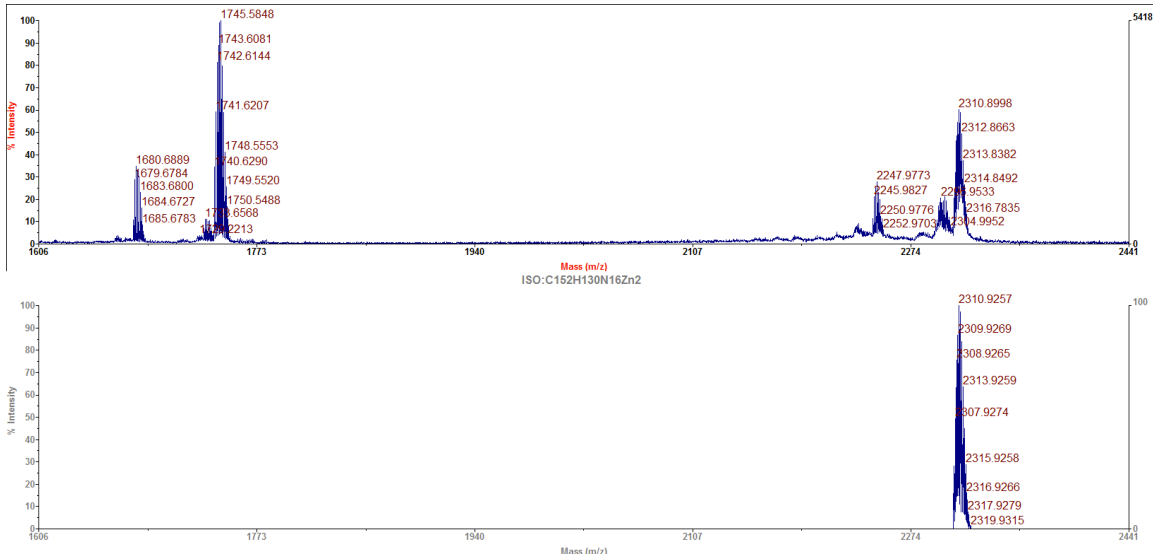

b.)

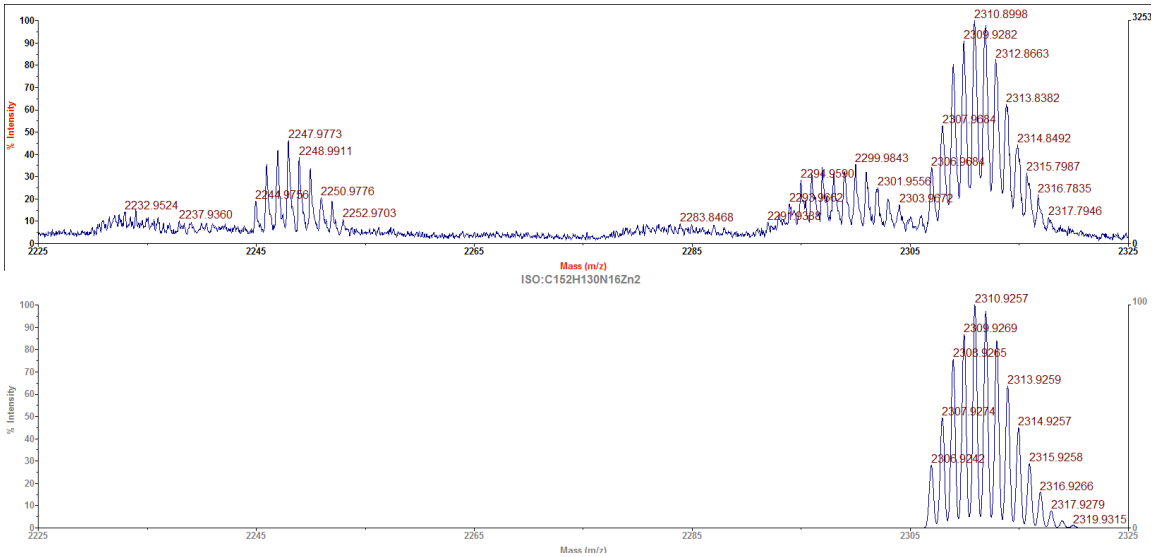

Figure 3.7. a.) Top trace: MALDI-TOF mass spectrum of the reaction of scheme 3.9 theoretical spectra of the reaction of scheme 3.9 prior to addition of **3.13**. Bottom trace: Theoretical spectrum for **3.15**. b.) Same as for (a) but zoomed in to reveal the resolution of isotope splitting. Top trace is the observed spectrum of the crude reaction mixture and the bottom trace the theoretical spectrum for **3.15.**

In addition, as so much starting material appeared to still be present (peak at 1745 Da in figure 3.7.a), there was a chance that if unreacted **3.2** reacted with **3.3** to form **3.16**, that with **3.4** present, the kinetics of the reaction of **3.16** with **3.4** to form **3.1** may be better than the competing reaction with acetic acid to form **3.15**. Following the addition of **3.13** and overnight reaction at reflux, MALDI-TOF analysis of the crude reaction mixture revealed that a dominant peak at ca. 2310 Da persisted. There was question as to if **3.3** had even been sufficiently dissolved to be present in solution and so able to react with **3.15** to form **3.1.** No traces of the product **3.16** were present in the crude reaction solution at the end of the reaction period. Nonetheless, analysis of some fractions of a column conducted following a short work up revealed the presence of a small amount of

3.1 (figure 3.8, top trace). This encouraging result confirmed that **3.1** could be synthesized, but that the reaction conditions needed to be drastically optimized.

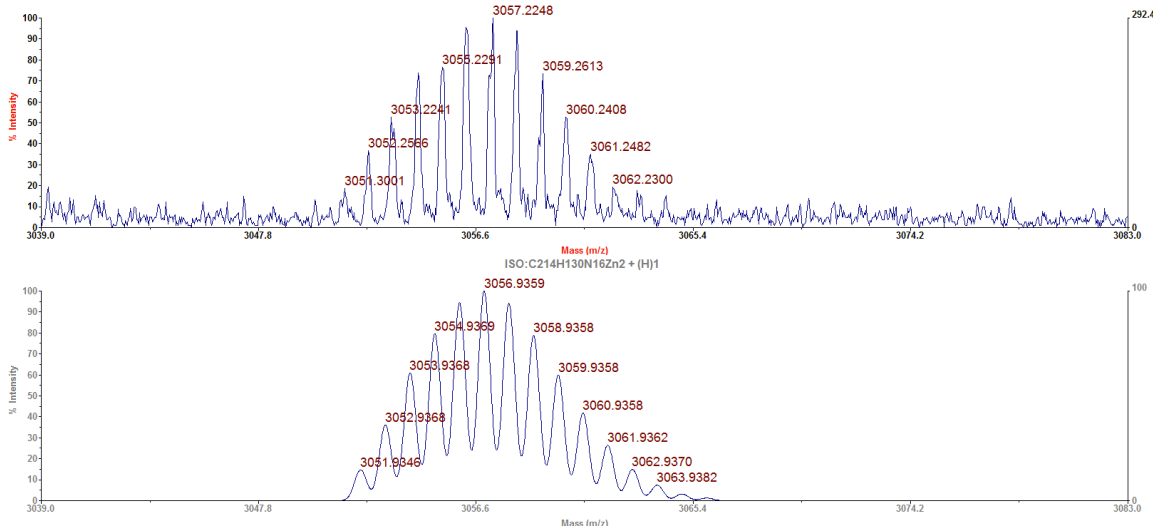

Figure 3.8. Top trace: the observed MALDI-TOF mass spectrum of **3.1**. Bottom trace: the theoretical spectrum shown for comparison $[M+H]^+$ of **3.1**.

Not only had acetic acid failed as a solvent to mediate the condensation of **3.2** with **3.3** to form the intermediate **3.15**, reaction of acetic acid with **3.16** or possibly free **3.3** that would subsequently react with **3.2** to form **3.15** resulted in the unwanted and irreversible formation of **3.15**. Reports in the literature[95] of using *m*-cresol as a catalytic solvent for these types of condensations existed. The stepwise synthetic protocol was repeated substituting AcOH with *m*-cresol.

Mass spectral analysis of the crude reaction mixture after 14h and again at 36h prior to the addition of **3.13** revealed the presence of two unwanted byproducts, a dominant peak around 2495 Da and a smaller peak around 1836 Da. Distinct from the acetic acid reaction, the use of *m*-cresol did allow for the complete consumption of starting material **3.2** after 36h of reaction. It is worth noting that this reaction was

conducted at a considerably higher temperature, specifically, 180°C as was the reported temperature for a similar reaction when this solvent was used[95].

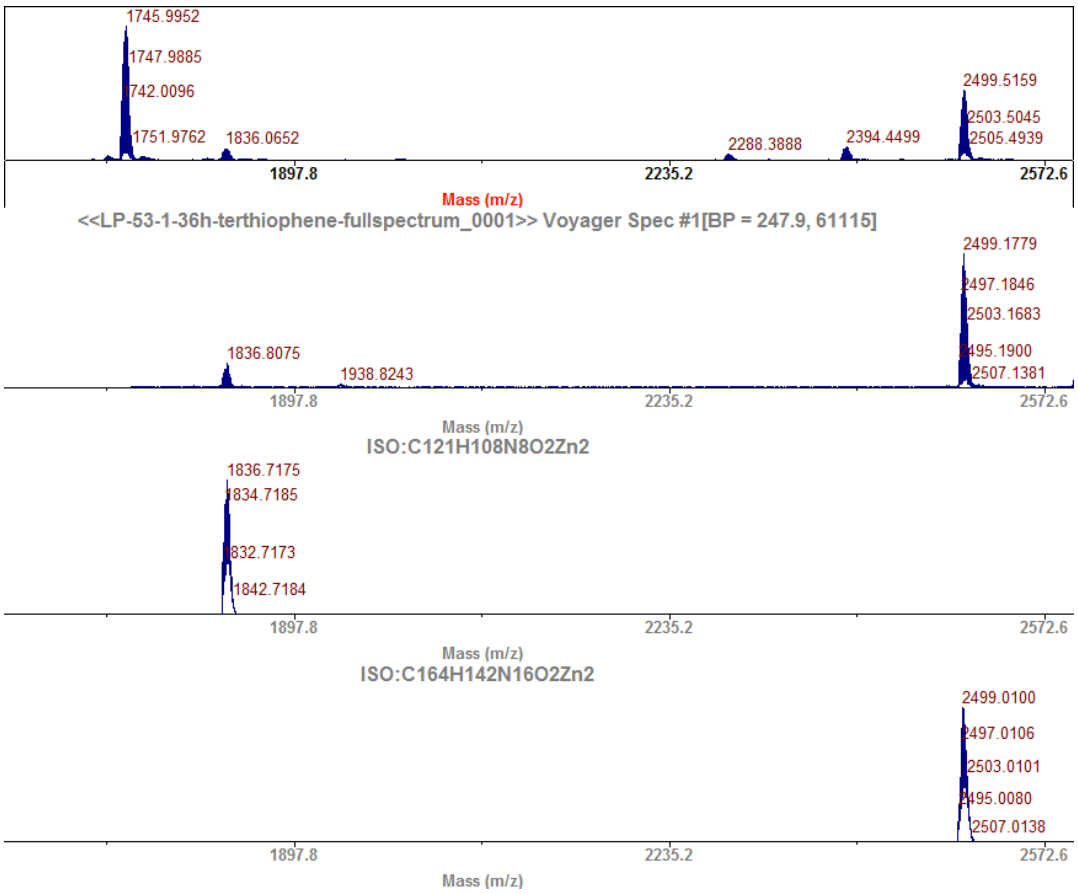

Figure 3.9 From top to bottom: MALDI-TOF mass spectrum of the crude reaction mixture after 14h. Second trace: crude solution after 36h of reaction. Third trace: the theoretical peak for **3.17** (scheme 3.10). Bottom trace: theoretical peak for **3.18** (scheme 3.10).

Close analysis of the peak distribution of two byproduct peaks indicated that *m*-cresol had interacted with the starting materials to form the observed byproducts, though matching the isotopic peak distribution observed in the MALDI-TOF spectra was not a simple task. The only plausible structures that could be created, given the peak patterns observed, are shown as structures **3.17** and **3.18** (scheme 3.10). At the time of conducting

the reaction, it was not possible to determine if the byproduct peaks present were simply co-ordination products of the *m*-cresol with zinc in the porphyrins or byproducts and if their formation was reversible or not. Consequently, **3.4** was added and allowed to react.

Scheme 3.10

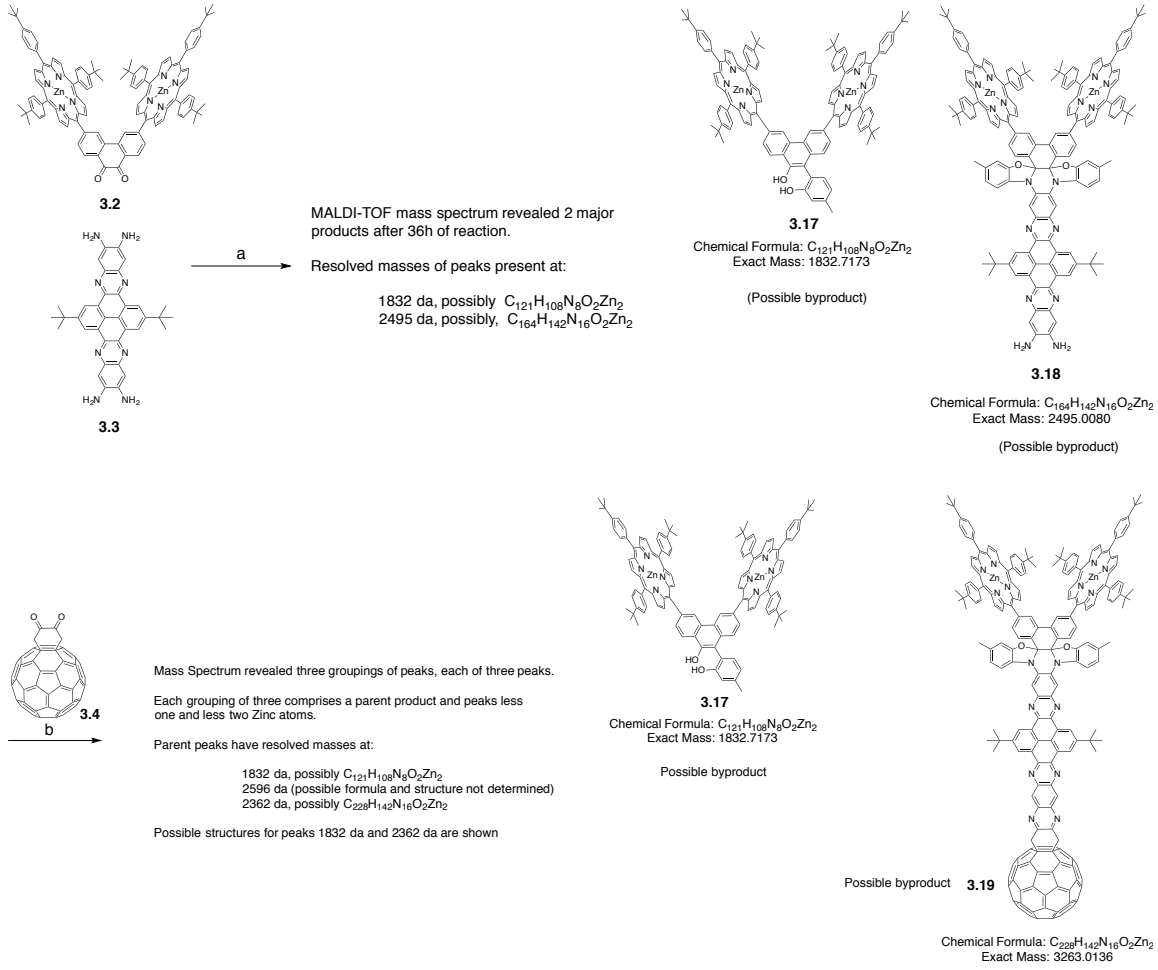

a) *m*-Cresol, 180°C, 36h. **b)** *m*-cresol, 1,2-dichlorobenzene, 180°C, 28h.

Analysis of the MALDI-TOF spectrum of the crude reaction mixture after termination revealed an interesting result. Three groupings of peaks were present. Each grouping itself was comprised of three sets of peaks, corresponding to a parent product

peak and then two trailing peaks corresponding to singular and double losses of zinc (figure 3.10, top trace). The parent peaks were present at 1832Da, the same molecular species proposed to be **3.17**, at 2596Da. and 3266Da. The two latter peaks were analyzed and determined to correspond to molecular formulae $C_{164}H_{142}N_{16}O_2Zn_2$ and $C_{228}H_{142}N_{16}O_2Zn_2$ respectively. The absence of the byproduct **3.18** in the solution following addition of **3.4** and the new peak at 3266da suggested that the presence of the terminal *o*-diamino functionality of **3.18** was correct and that **3.18** had reacted with **3.4** to form **3.19**.

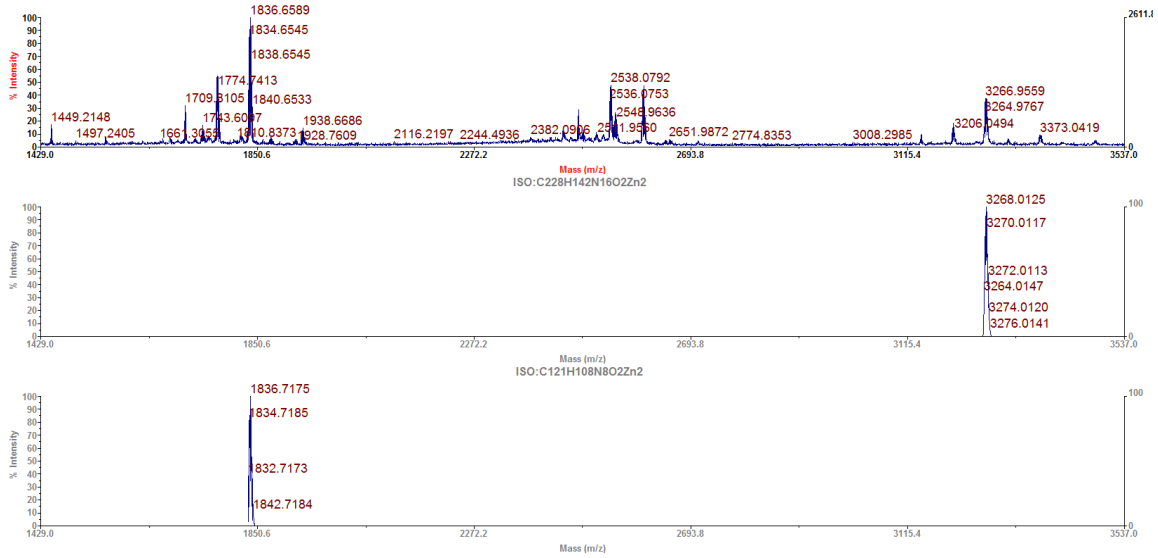

Figure 3.10. Top trace shows the MALDI-TOF mass spectrum of the crude reaction mixture obtained at the end of the reaction shown in scheme 3.10. For comparison middle trace shows the theoretical peak for **3.19**. Bottom trace shows the theoretical peak for **3.17**.

The mass of the parent peak present at 2596Da (figure 3.10) suggested that an additional *m*-cresol molecule had reacted with **3.18**. Alignment of the chemical formula of any reasonable structure conjured up with the isotope pattern of the observed mass spectrum could not be achieved. Following a short work up, the product mixture was

treated with TFA to rule out the existence of the peak at 3263da existing as a complex of *m*-cresol with zinc within the porphyrin macrocycles or as hydrolysable entity. The peak corresponding to the structure of **3.19**, less two zinc atoms was obtained, indicating the strong covalent nature with which two cresols had reacted to form the product with mass at ~3263 da, possibly structure **3.19**.

a b

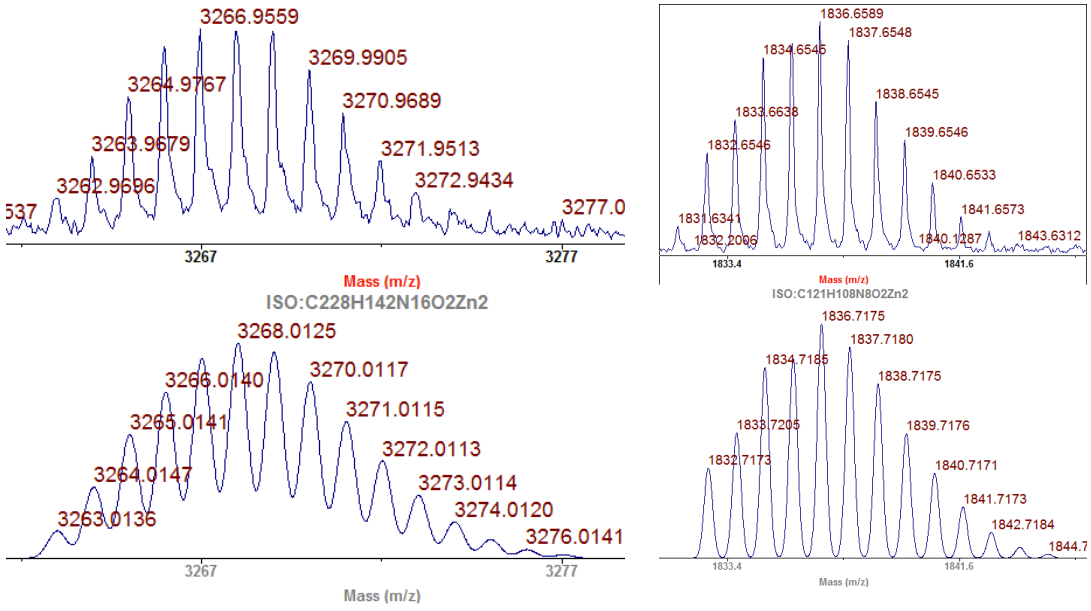

Figure 3.11. a.) MALDI-TOF spectrum of the byproduct peak assigned as structure **3.19** (top trace) and theoretical spectrum (bottom trace) for $C_{164}H_{144}N_{16}O_2Zn_2$ (**3.19**). b.) Observed (top trace) and theoretical spectrum (bottom trace) assigned as structure **3.17**.

Having achieved complete consumption of the starting material **3.4** in the use of *m*-cresol at 180°C, it was thought that the aromatic nature of the solvent, along with the high temperature may have facilitated the observed reactivity. Consequently, a reaction employing a 1:1 mixture of 1,2-dichlorobenzene as a high boiling aromatic solvent and acetic acid for acid-catalysis was conducted. It is questionable if the internal temperature

of the reaction solution reached a temperature much higher than the 111^{o}C boiling point of acetic acid.

Scheme 3.11

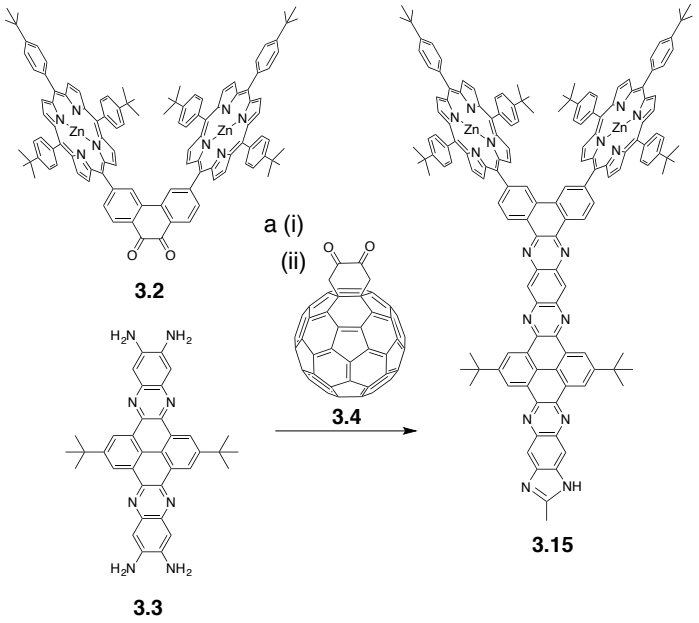

a) i AcOH:1,2-Dichlorobenzene (1:1), 180^{o}C. **ii** AcOH:1,2-dichlorobenzene.

Good results were achieved indicating complete consumption of the starting material **3.2**. Figure 3.6 shows the MALDI-TOF spectrum of the crude solution following 14h of reaction. It is evident that while no **3.2** is present, the desired product peak is absent and a dominant peak with mass ~2311 Da is present. The product, **3.16**, appears to have has been converted to the unfortunate acetic acid adduct **3.15** along with some demetallation thereof (figure 3.12). This is a similar observation for the previous 1,2-dichlorobenzene-free reaction. Again **3.4** was added and the solution allowed to react further in the event that the required **3.15** peak was present but possibly was not observed because it did not fly well in the mass spectrometer. Analysis of the final reaction

solution and products obtained following work-up and chromatography revealed that no **3.1** was present.

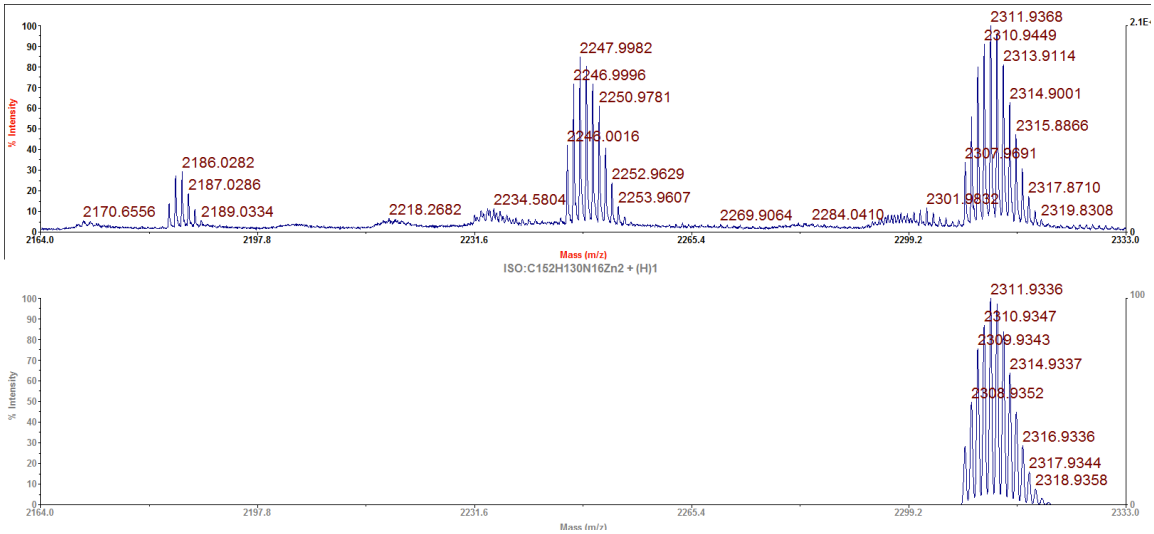

Figure 3.12. Top trace shows the MALDI-TOF mass spectrum of the crude reaction solution of scheme 3.11. The three peaks correspond to the structure

Finally, to test if the excessive temperature may be providing the thermal energy for the unwanted acetic acid adduct, **3.15**, to form, a lower temperature reaction was conducted though still using a 1:1 mixture of 1,2-dichlorobenzene with acetic acid. The possibility existed that it was the presence of 1,2-dichlorobenene and not the higher temperature that had enabled the complete consumption of the starting material **3.2**. Consequently, lowering the temperature could allow for complete consumption of **3.2** to form **3.16**, but would not provide sufficient energy for the production of **3.15**. Sadly, very similar results were obtained for a reaction conducted at 90^{o}C (figure 3.13), as for that conducted at 180^{o}C, and while the product mixture obtained did show that all the starting material, **3.2**, had been consumed, the acetic acid adduct was essentially the only product

formed. Interestingly, little to no demetallation of the poprhyrins was evident, as could be expected from the lower temperature at which the reaction was conducted.

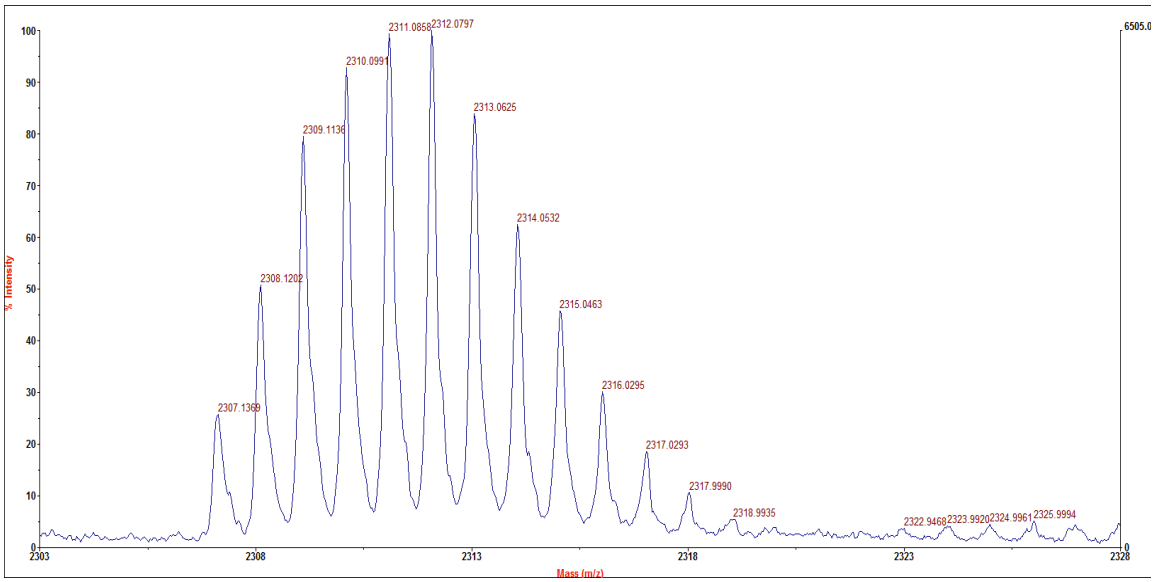

Figure 3.13. MALDI-TOF mass spectrum of **3.15** obtained through the lower temperature reaction in 1,2-dichlorobenzene and AcOH at 90°C.

After briefly investigating the effects of using TsOH as an acid catalyst, with less than desirable results having been obtained, attention was turned back to acetic acid as the proton source to catalyze the reaction and an investigation into if adding ethanol to the solvent system may help was conducted.

Scheme 3.12

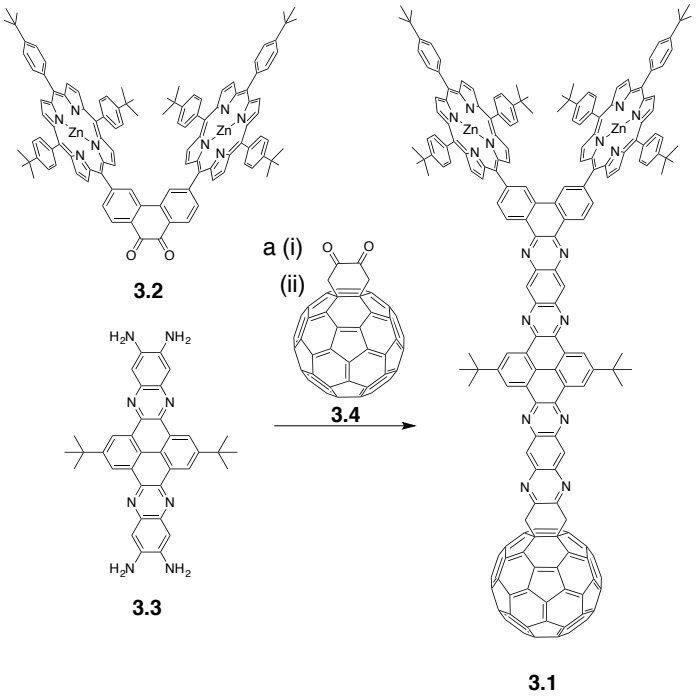

a) **i** AcOH:1,2-Dichlorobenzene:EtOH (1:1:1), reflux, 2.5 h **ii** AcOH:1,2-Dichlorobenzene:EtOH (1:1:1), reflux overnight.

An equal quantity of ethanol was added to the solvent system of 1,2-dichlorobenzene and AcOH that had proven effective to promote the condensation of **3.2** with **3.3** and the same reaction was attempted, reacting **3.2** with **3.3** followed by addition of **3.4** (scheme 3.12). It was found that the presence of ethanol significantly inhibited the unwanted formation of the acetic acid adduct **3.15**. MALDI-TOF mass spectral analysis of the crude reaction solution acquired after just 2.5h of reflux (figure 3.13) revealed that all of the starting material **3.2** had been consumed to produce the intermediate, **3.16**. Isolation of the intermediate product formed at this point was not attempted.

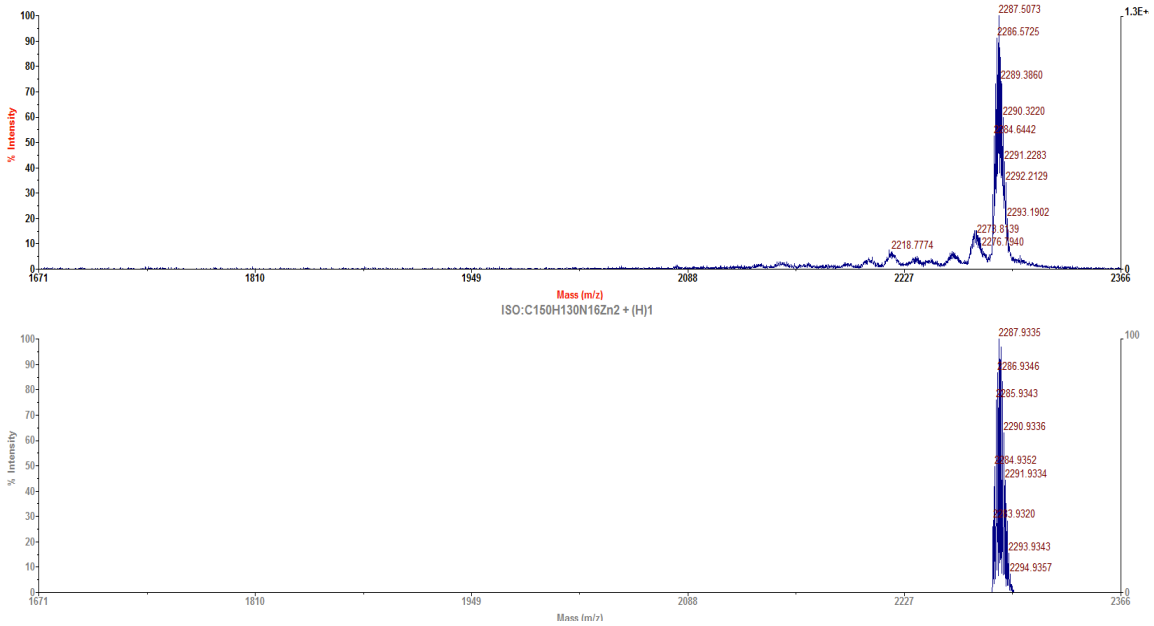

Figure 3.14. Top trace: MALDI-TOF mass spectrum of the crude reaction solution of the reaction from scheme 3.12 showing complete consumption of starting material. Bottom trace: theoretical mass spectrum of **3.16** for comparison.

To determine if the solvent system was also effective for formation of **3.1**, **3.4** was added and the reaction was left to reflux overnight. The addition of alcohols like methanol and ethanol generally alter the polarity of a given solution sufficiently to cause fullerene adducts to precipitate out of solution. Consequently, there was some concern as to if the presence of ethanol in solution would cause **3.4** to precipitate out of solution rendering it unable to react. Analysis of the crude mixture after overnight reflux indicated significant formation of the desired product **3.1**. The temperature and presence of acetic acid and 1,2-dichlorobenzene appeared to have allowed for sufficient dissolution of **3.4** despite the ethanol present so that it could react to form **3.1**. It was evident, however, that a fraction of the product mixture had been demetallated in the course of the reaction. Consequently, following a short work up, the crude isolate was treated with $Zn(AcO)_2$ to remetallate the products.

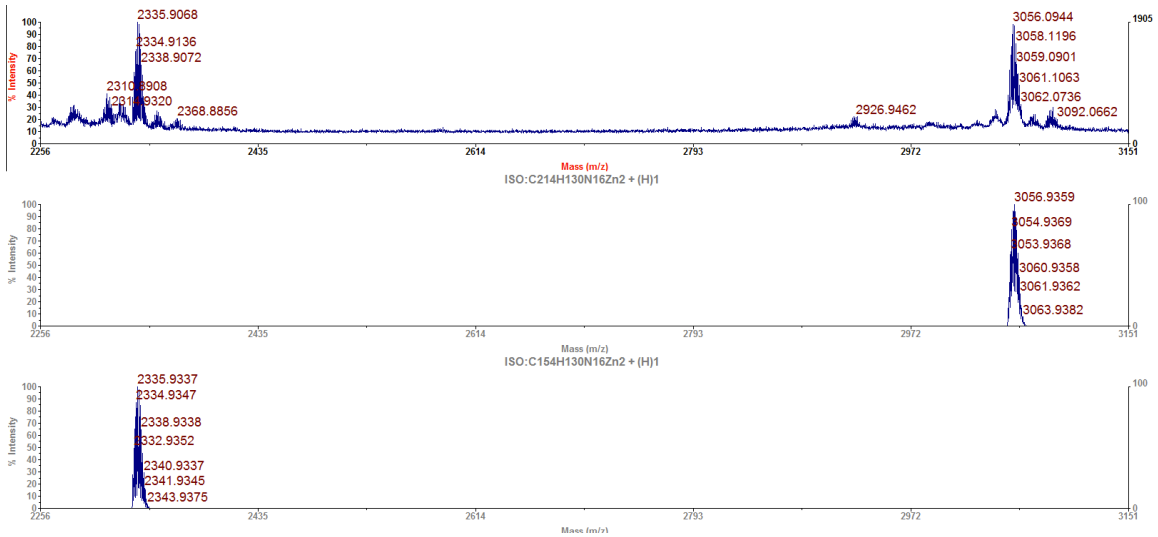

Figure 3.15. Top trace shows the MALDI-TOF mass spectrum of the product obtained from reaction shown in scheme 3.12. Middle trace: Theoretical peak for **3.1** $[M+H]^+$. Bottom trace shows the theoretical peak for the fragment formed in the mass-spectrometer in which C_{60} is blown off of **3.1**.

Despite best efforts, the poor solubility and propensity for **3.1** to precipitate on contact with silica gel or preparative TLC plates rendered the complete purification of **3.1** impossible. Nonetheless, when loaded onto a preparative TLC plate, and developed for hours, the immobile baseline did show improved purity by mass-spectral analysis as the more mobile impurities moved up the plate with the mobile phase. Isolation of this brown band revealed the best purity of **3.1** achieved in this work. The ^{1}H NMR spectrum of this product was acquired, and while characteristic peaks of porphyrins and some additional aromatic peaks are present, the poor solubility of the product in solution meant that impurities dominated the spectrum and that any peaks arising from **3.1** present in solution were broad. It is worth pointing out at this stage that the mass spectra of products formed by reaction of an *o*-diamine with **3.4** will typically yield three indicative peaks in a MALDI-TOF mass spectrum, specifically, the parent peak and then two fragment peaks,

that for C_{60} at 720Da. and the mass of the parent peak less 720Da. This can be seen clearly in figure 3.15 which shows the mass spectrum of **3.1** obtained from the baseline of the prep-TLC. The product peak around 3056Da and fragment peak at approximately 2335Da are clearly visibly.

Having shown that the addition of ethanol to the reaction solution was effective for forming **3.16** and **3.1**, an attempt was made to synthesize, isolate and characterize **3.16**. Care was taken to eliminate oxygen from the system and the reaction was allowed to proceed in AcOH:EtOH (3:5) without the presence of 1,2-dichlorobenze. Following work up and isolation, a relatively pure isolate of **3.16** was obtained in 73% yield. Nevertheless, the purest form of **3.16** isolated failed to yield an NMR spectrum of acceptable quality. It was determined that poor solubility was impairing characterization even of **3.16** that does not even feature a fullerene moiety. This corresponds to the likely stacking shown by the drawing in figure 3.5.d. It is likely that the considerable presence of aromatic moieties present in the structure of **3.16** by which it could align and π-stack is not effectively overcome by interactions with solvent. While no scattering of laser light was evident from the solution used for NMR analysis, which would indicate the presence of small particulates, one cannot rule out small-scale stacking sufficient to hinder effective NMR characterization.

After finding a solvent system that facilitated the formation of both **3.16** and **3.1**, attention was turned to modifying the design of the porphyrins employed in **3.2** to confer a higher degree of solubility to the system. Considering the length of the wire used in **3.1**, efforts were made to make smaller donor-wire-acceptor systems that employed shorter pyrazine-containing wires to test if a good NMR spectrum of a porphyrin-wire construct

could be obtained prior to condensation with the C_{60} adduct **3.4**. This work is presented in chapter 4.

3.7 Materials and Methods

3.7.1 General

Dichloromethane, chloroform, acetonitrile, hexanes, ethylacetate, tetrahydrofuran and toluene were purchased from BDH and 200 PROOF ethanol from KOPTEC. 1,2-dichloroethane was acquired from Avantor; DMF, DMSO and DMA solvents from Alfa Aesar and were all stored over molecular sieves. Nitrobenzene was purchased from Alfa-Aesar. Carbon disulfide and 1,2-dichlorobenzene were purchased from Sigma-Aldrich. Solvents were used without purification unless stated otherwise. Tetrahydrofuran was distilled over CaH under argon. Pyrrole, trimethylsilylchloride and 4,4,5,5-tetramethyl-1,3,2-dioxaboralane starting materials were purchased from Sigma-Aldrich. Pyrene, *tert*-butylchoride, *o*-phenylenediamine, toluenesulfonylchloride, diethylsuccinate and 9,10-phenanthrenedione starting materials were purchased from Alfa Aesar. C_{60} fullerene was purchased from M.E.R Corporation. 4-*tert*-butylbenzaldehyde was obtained from Combi-Blocks. *N*-bromosuccinimide, $CsCO_3$, $BF_3.OEt_2$, $Pd(PPh_3)_2Cl_2$ and $Pd(PPh_3)_4$ reagents were purchased from Sigma-Aldrich. $Et_3N.HF$ reagent was obtained from Alfa Aesar.

Matrix assisted laser desorption/ionization time of flight (MALDI-TOF) mass spectra were acquired using an Applied Biosystems Voyager-DE STR workstation and acquired in reflector mode using terthiophene, diphenylbutadiene or dithranol as the

matrix. High resolution mass spectra were acquired using a Thermo LTQ-FT Ultra spectrometer. NMR spectroscopy was conducted using a Varian (Agilent) MR 400 MHz NMR spectrometer operating at a 1H Lamor frequncy of 399.87 MHz, equipped with a 5 mm Broadband Observe Z-gradient probe.

3.7.2 Synthetic Protocols.

3.1 By reaction of scheme 3.12 16mg (9,16μmol) Of **3.2** was dissolved in 1ml of 1,2-dichlorobenzene. 10.6mg (18.32μmol) Of **3.3** was added along with 1ml of EtOH and 1ml of AcOH. The solution was set to reflux for 2.5h at which point 22.1mg (27.5μmol) of **3.4** was added. The solution was left to stir at reflux overnight after which it was cooled and concentrated *in vacuo*. The residue was taken up in 1,2-dichlorobenzene and a spatula tipful of $Zn(AcO)_2.2H_2O$ along with a few drops of methanol. The solution was heated to 60^oC and left to stir for 5 hours following which it was cooled, washed with 50ml H_2O, extracted with dichloromethane and concentrated. Efforts were made to isolate the product by silica gel chromatography and preprative TCL using toluene:CS_2 (1:1) as the solvent system. The most pure form of **3.1** was achieved by recovering an immobile band on the baseline of the prep. TLC. Mass spectral analysis after 2.5h, major product: MS (MALDI-TOF): m/z obsd 2283.6681 $[M+H]^+$, calcd 2283.9320. Mass spectral analysis of baseline prep. TLC: MS (MALDI-TOF): m/z obsd 3051.1272 $[M+H]^+$, calcd 3051.9346. (**3.1**) and obsd 2331.9083 $[M+H]^+$, calcd 2331.9320. [M of **3.1 lessC_{60}**]+.

3.2. **3.6** (0.517g, 0.577mmol) And **3.7** (70.4mg, 0.192mmol) were added to a reaction tube in 80ml THF along with Cs_2CO_3 (0.188g, 0.577mmol). The solution was thoroughly deoxygenated by bubbling with argon for 20min. Under a stream of argon $Pd(PPh_3)_4$ was added and the tube sealed with a Teflon screw cap. The tube was heated to 120^oC and left to stir at that temperature for 20h. On cooling the solution was concentrated and the residue purified by silica get chromatography employing DCM to DCM/1%MeOH as the solvent system. Relevant fractions were concentrated giving 0.213g (0.122mmol, 63% yield) of **3.2**. ^1H NMR (400 MHz, DMSO, 120^oC): δ 9.11 (s, 2H), 8.82 (d, J = 4.6Hz, 4H), 8.64 (m, 12H), 8.57 (d, J = 7.9Hz, 2H), 8.33 (d, J = 7.5Hz, 2H), 7.98 (d, J = 8Hz, 4H), 7.91 (d, J = 6.8Hz, 8H), 7.71 (d, J = 8.2Hz, 4H), 7.66 (d, J = 8Hz, 8H), 1.54 (s, 18H,) 1.53 (s, 36H). MS (MALDI-TOF): m/z obsd 1740.991 $[M]^+$, calcd 1740.655.

3.3 In line with the literature procedure[117] 5.97g (4.994mmol) of **3.13** was placed in a RBF. 80ml H_2SO_4 was deoxygenated with bubbling argon and then added to the flask containing **3.13**. The viscous purple solution was left to stir at RT for 6h, following which, it was poured over 500g of crushed ice. A red ppt. formed and was isolated by filtration. The tacky red filtrand was transferred to a 1.5l solution of 20% $(NH_4)_2CO_3$ and stirred for 30 minutes. The solid was again isolated by filtration and recrystallized from deoxygenated DMA, isolated by filtration, washed with EtOH and dried on hi-vac giving reddish brown solid in quantitative yield. HRMS: m/z obsd 579.298 $[M+H]^+$, calcd 579.298.

3.4 The literature[118] procedure for the synthesis of **3.4** produces it as an intermediate and does not make attempts to isolate or characterize this intermediate. The

literature procedure was followed with deviation towards the end to attempt to isolate and purify the product. 3.8g (5.28mmol) of C_{60} fullerene was dissolved in 500ml 1,2-dichlorobenzene and deoxygenated with bubbling argon for 30minutes. 2.433g (10.555mmol) of **3.14** was added and argon bubbled through the solution for 10 minutes further. The solution was heated to 180^{o}C and stirred at that temperature under argon for 1h. The solution was concentrated and in vacuo and dried on hi-vac briefly. A portion of carbondisulphide was cooled to -78^{o}C and deoxygenated with bubbling argon for 20minutes. 300ml of this cooled deoxygenated CS_2 was added to the residue, and Br_2 (0.272ml, 5.28mmol) added at -78^{o}C and stirred at that temperature for 1h under argon. The reaction solution was concentrated *in vacuo* and then redissolved in 200ml of 1,2-dichlorobenzene to which (1.29ml, 7.92mmol) of $Et_3N.HF$ was added at RT and allowed to stir for 1h under argon before a volume equivalent of methanol was added. The precipitate formed was isolated by filtration over a pad of cilite and was washed with 200ml of methanol. The brown solid was redissolved in a minimum amount of CS_2 and loaded onto a silica gel column and eluted with CS_2:Toluene (2:3) and concentrated yielding 1.650g (2.051mmol, 39% yield) of a brown solid. This residue was chromatographed a second time, with some solid precipitating out on contact with silica. Concentration of relevant fractions produced 0.981g (1.219mmol, 23% yield). MS (MALDI-TOF): m/z obsd 803.9971 $[M]^+$, calcd 804.0206.

***Meso*-(*p-tert*-butylphenyl)dipyrromethane (3.5)** They synthesis of **3.5** is reported in the literature[139]. Accordingly, 250ml (3.6mol) of freshly distilled pyrrole was deoxygenated with bubbling argon for 20minutes before 6.03ml (36.03mmol) of *p-t*-butylbenzaldehyde and 0.8g (3.603mmol) was added and allowed to stir in the dark under

an argon atmosphere for 2 h. 4.234g (108.1mmol) of finely crushed NaOH was added and allowed to stir for 1h more. The solution was filtered through a pad of celite that was washed with dichloromethane. The filtrates were pooled and concentrated and dried on hi-vac. overnight. The solid residue obtained was dissolved in a minimal amount of hot ethanol, water added until precipitation was visible and then cooled and stored at 4^{o}C overnight. The considerable mass of white crystals formed was isolated by filtration and dried on hi-vac. yielding 9.162g (32.91mmol) 91% yield. ^{1}H NMR (400 MHz, $CDCl_3$): δ 7.89 (bs, 2H), 7.32 (d, J = 8.3Hz, 2H), 7.14 (d, J = 8.1Hz, 2H), 6.68 (s, 2H), 6.15 (d, J = 2.7Hz, 2H), 5.93 (s, 2H), 5.44 (s, 1H), 1.30 (s, 9H). MS (MALDI-TOF): m/z obsd 278.2427 $[M]^{+}$, calcd 278.1778.

3.6 The multi-step procedure for the synthesis of **3.6** began with addition of **2.6** (3g, 20.52mmol) of **3.5** (5.71g, 20.52mmol) and *t*-butylbenzaldehyde (6.66g, 1.04mmol) to a solution 3.12L of $CHCl_3$ containing 24ml of EtOH. To this stirred solution $BF_3.OEt_2$ (1.22g, 8.62mmol) was added dropwise and the solution allowed to stir for 2 hours at RT. At this point, DDQ (13.974g, 61.56mmol) was added and the reaction left to stir for 1 hour further. The crude solution was filter through 10cm x 16cm pad of silica topped with a 5cm thick pad of celite. The eluent was concentrated and subsequently taken up in 500ml of DCM to which 300ml of methanol was added followed by $Zn(AcO)_2.H_2O$ (18.02g, 82.08mmol). The solution was left to reflux overnight after which it was cooled and transferred to a separation funnel, washed with water and the organic layer collected and concentrated. The residue was dissolved in dichloromethane and passed through a pad of silica and further eluted with dichloromethane. The eluent was concentrated and dissolved in 500 ml dichloromethane and 0.5ml of pyridine followed by NBS (1g,

5.619mmol) were added. The solution was allowed to stir for 1 hour at RT in the dark before being concentrated and the residue passed through a pad of silica, eluted with dichloromethane. The eluent was concentrated and dried on hi-vac. The residue was then taken up in 400ml of 1,2-dichloroethane to which Et_3N (10.96ml, 78mmol) was added and the solution deoxygenated with bubbling argon for 20minutes. $Pd(PPh_3)Cl_2$ (0.211g, 0.3mmol) was added followed by pinacolborane (8.71ml, 60mmol) and the solution warmed to reflux for 20h under an argon atmosphere. The reaction solution was subsequently concentrated and dried on hi-vac prior to purification by silica gel chromatography employing DCM:Hexanes (1:1) as the eluting solvent. Concentration of the appropriate fractions afforded 1.455g (1.623mmol, 8% yield) of **3.6** was obtained as a purple residue. ^{1}H NMR (400 MHz, $CDCl_3$): δ 9.90 (d, J = 4.68Hz, 2H), 9.12 (d, J = 2.5Hz, 2H), 8.98 (m, 4H), 8.14 (d, J = 8.1Hz, 4H), 8.14 (d, J = 8.2Hz, 2H), 7.75 (d, J = 8.2Hz, 2H), 7.75 (d, J = 8.1Hz, 4H), 7.74 (d, J = 8.1Hz), 1.84 (s, 12H), 1.61 (s, 18H), 1.60 (s, 9H). MS (MALDI-TOF): m/z obsd 893.447 $[M]^+$, calcd 893.405.

3,6-dibromophenanthrene-9,10-quinone (3.7) The synthesis of **3.7** was conducted according to a reported literature[119] procedure with a few deviations. As such, phenanthrenedione (20g, 96.05mmol) was added to a 2-neck round bottom flask along with 120ml nitrobenzene and heated to 130^{o}C to increase the dissolution of phenanthrenequinone. The solution was cooled to 60^{o}C and bromine (10.4ml, 201.92mmol) was added and irradiated with a 60W tungsten light for 15minutes causing the solution to bubble vigorously, liberating HBr gas. The solution was left to stir at 150^{o}C for 3h with stirring and then cooled and stored at 4^{o}C overnight. The crystals formed were isolated by filtration and washed with 2x200ml 5% $Na_2S_2O_3$, ethanol,

toluene, acetic acid then finally recrsytallized from acetic acid. The crystals isolated were washed with water, ethanol and dried on hi-vac. yielding 25.43g (69.48mmol, 72% yield) of **3.3** as small yellow crystals. ^{1}H NMR (400 MHz, $CDCl_3$): δ 8.12 (d, J = 1.7Hz, 1H), 8.08 (d, J = 8.32 Hz, 1H), 7.67 (dd, J = 8.3, 1.8Hz, 1 H). MS (MALDI-TOF): m/z obsd 364.880$[M]^+$, calcd 364.910. HRMS: m/z obsd 364.881 $[M+H]^+$, calcd 364.881.

2,7-di-*tert*-butylpyrene (3.8). A procedure reported in a patent[121] was followed with some deviations. A comparable yield was not obtained, possibly due to the scale on which the reaction was conducted. 400ml of dichloromethane was cooled to 0^{o}C and deoxygenated with argon for by bubbling. 40g (0.198mmol) of pyrene and 2.645(0.0198mmol) $AlCl_3$ were added. 47.96ml (0.435mmol) of *t*-BuCl in 60ml of dichloromethane was added to the solution at 0^{o}C with stirring under argon and allowed to warm to RT and stir for 4h. The solution was washed with water and extracted with dichloromethane. Purification of the residue by silica gel chromatography using hexane as the eluting solvent was unsuccessful. The residue form chromatography was boiled in 500ml of EtOH for an hour and then cooled to 4^{o}C and filtered yielding 39.5g (0.126mmol, 64% yield) of a white crystal. ^{1}H NMR (400 MHz, $CDCl_3$): δ 8.18 (s, 4H), 8.02 (s,4H), 1.58 (s,18H). ^{13}C NMR (100 MHz, $CDCl_3$): δ 148.71, 130.92, 127.56, 123.00, 122.14, 35.36, 32.12. MS (MALDI-TOF): m/z obsd 314.278 $[M]^+$, calcd 314.203.

2,7-di-*tert*-butyl-4,4,9,10-tetraketopyrene (3.9) The literature procedure[120] for the oxidation of **3.8** was followed with slight deviation in the work up. As such, 20g (63.6mmol) of **3.8** was dissolved in 250ml of dichloromethane and 250ml of acetonitrile was added. $RuCl_3.xH_2O$ (0.717g, 3.18mmol) dissolved in 320ml of deionized water was

added followed by 108.828g (508.8mmol) of $NaIO_4$. The reaction vessel was fitted with a condenser and the solution left to stir at 50°C overnight. The solution was filtered and the filter paper washed with dichloromethane. The filtrates were transferred to a separating funnel and washed with water and then concentrated. The residue was purified by silica gel chromatography employing DCM→ DCM 1%MeOH. Concentration of the relevant fractions yielded 11.207g (29.93mmol, 47%) of the orange product. ^{1}H NMR (400 MHz, $CDCl_3$): δ 8.45 (s, 4H), 1.43 (s, 18H). MS (MALDI-TOF): m/z obsd 375.1876 $[M+H]^+$, calcd 375.1591. HRMS: m/z obsd 375.1591 $[M+H]^+$, calcd 375.1591.

3.10 The synthesis of **3.10** followed a procedure described in the literature[123]. 5.79g (53.4mmol) of *o*-phenylenediamine was added to a round bottom flask containing 150ml pyridine and 8.63ml (107.8mmol) pyridine and cooled to 0°C. 20.417g (107.8mmol) of *p*-toluenesulfonylchloride was added over 5min. causing the solution to turn an orange-red color. The solution was allowed to warm to RT with stirring and stirred at RT for 5h. The reaction solution was transferred to a separating funnel and washed with 120ml 2M HCl twice, brine twice and sat. $NaHCO_3$ twice. The solid was isolated by filtration and recrystallized twice from ethanol. 19.57g (46.99mmol, 88% yield) of pale pink crystals were obtained. ^{1}H NMR (400 MHz, DMSO): δ 8.41 (s, 2H), 6.73 (d, J = 8.3Hz, 4H), 6.48 (d, J = 8.04Hz, 4H), 6.12 (s, 4H), 1.49 (s, 6H). HRMS: m/z obsd 833.180 $[2M+H]^+$, calcd 833.180.

3.11 The literature procedure[124] for the synthesis of **3.11** from **3.10** was followed. 15g (36.013mmol) of **3.10** was added to a RBF along with 110ml of glacial acetic acid and warmed to 60°C. A mixture of HNO_3 (3.025ml, 72.026mmol) and 3.61ml acetic acid was created and added to the reaction over the course of 15 minutes. 50ml more acetic

acid was added to aid stirring of the thick solution and the solution left to stir at 70°C for 2h following which the reaction was cooled to 0°C, the crystal solid isolated by filtration and washed with water. The product was recrystallized from glacial acetic acid and again from EtOH affording 11.98g (23.65mmol, 66%) of pale yellow crystals. ^{1}H NMR (400 MHz, DMSO): δ 7.69 (s, 2H), 7.65 (d, J = 8.28, H4), 7.33 (d, J = 8.04, H4), 2.35 (s, 6H). HRMS: m/z obsd 1013.119 $[2M+H]^+$, calcd 1013.120.

3.12. Reduction of **3.11** to form **3.12** was conducted in a Parr apparatus at 60 psi H_2. A suspension of 20g (39.49mmol) of **3.11** was added to the vessel containing 300ml EtOH along with 2g of 10 w% Pd/C. The vessel was purged with H_2 five times before being left to react under 60Psi H_2 at RT for 24hours. The solution was filtered and the cake obtained was washed with DMSO (800ml) to recover the product. An equivalent volume of H_2O was added to the DMSO filtrate causing a precipitant to form that was isolated by filtration. The ethanol filtrate was concentrated and the residue pooled with the precipitant from the DMSO solution. The combined solids were recrystallized twice from MeOH yielding 13.68g (30.665mmol, 78%yield) of **3.12** as an off-white solid. ^{1}H NMR (400 MHz, DMSO): δ 8.51 (s, 2H), 7.50 (d, J = 8.2Hz, 4H), 7.30 (d, J = 8.2Hz, 4H), 5 (s, 4H), 2.34 (s, 6H). ^{13}C NMR (100 MHz, DMSO): δ 143.04, 136.29, 133.64, 129.46, 126.95, 120.06, 110.85, 21.06. HRMS: m/z obsd 469.098 $[M+Na]^+$, calcd 469.097.

3.13 The literature[117] procedure for the synthesis of **3.13** was followed closely. Accordingly, 250ml of acetic acid was deoxygenated by bubbling with argon, 3.357g (8.966) of **3.9** and 8g (17.933mmol) of **3.12** were added. The mixture was heated to 60°C and left to stir at that temperature overnight under argon. The solution was then cooled,

filtered and the solid obtained washed with water, ethanol and diethyl ether. The solid was dried overnight on hi-vac. yielding 7.79g (6.52mmol, 73%) of the yellow solid. ^{1}H NMR in tetrachloroethane confirmed the identity of the product while some small impurities were present at δ 2.99, 2.91 and 2.06. ^{1}H NMR (400 MHz, 1,1,2,2-tetrachloroethane-*d*2): δ 9.42 (s, 4H), 8.01 (s, 4H), 7.72(d, J = 8.3Hz, 8H), 7.44 (s, 4H), 7.29 (d, J = 8.3Hz, 8H), 2.39 (s, 12H), 1.66 (s, 18H). HRMS: m/z obsd 1195.336 $[M+H]^{+}$, calcd 1195.835 and obsd 1206.827 $[M+Na]^{+}$, calcd 1206.826.

1,2-Bistrimethoxysiloxy-1-cyclobutane (3.14) The literature[127] procedure for the synthesis of **3.14** was followed closely. A stirrer bar was placed in a 3-neck RBF fitted with an addition funnel, a condenser topped with an argon line and was charged with 180ml of dry toluene. 14g Of sodium in cubed form was added and the vessel heated to reflux with vigorous stirring, causing the sodium to melt. Diethylsuccinate (24.96ml, 0.15mol) and TMS-Cl (85.67ml, 0.675mol) in 25ml of dry toluene were added slowly over 15 min via the dropping funnel so as to maintain reflux at all times. The solution was left to stir at reflux overnight. In the morning the solution was cooled to RT, filtered and the filter paper washed with ether. The filtrates were concentrated in vacuo and the residue distilled yielding 18.52g (80.37mmol, 54% yield) of a clear oil, bp. 98-103^{o}C. NMR (400 MHz, $CDCl_3$): δ 2.10 (s,4H), 0.16 (2,18H). ^{13}C NMR (100 MHz, $CDCl_3$): δ 120.22, 26.16, 0.438.

Procedure of scheme 3.9 30ml of deoxygenated glacial acetic acid was added to a 100ml round bottom flask along with 12.4mg(0.0071mmol) of **3.2** and 6.13mg(0.0106mmol) of **3.3**. The flask was fitted with a reflux condenser and left to reflux under argon overnight. Concurrently a side reaction for the synthesis of crude **3.4**

was carried out. As such, 0.1635g(0.7098mmol) of **3.14** along with 0.256g (0.346mmol) C_{60} was carried through the synthetic protocol for the synthesis of **3.4** as described above. However, methanol was not added at the final step to precipitate the product. Rather, the crude reaction solution was simply added to the reaction involving **3.2** and **3.3** and allowed to stir at 120^{o}C overnight under argon. 100ml of MeOH was added to the resulting solution and the precipitant formed was isolated by filtration through pad of celite. The residue was taken up in carbon disulfide, loaded onto a silica gel column and eluted with Toluene:CS_2:EtOAc (50:49:1). MALDI-TOF analysis of some fractions revealed the presence of **3.1** MS (MALDI-TOF): m/z obsd 3051.3001 $[M+H]^+$, calcd 3051.9346, while starting material and **3.15** MS (MALDI-TOF): m/z obsd 2306.9684 $[M]^+$, calcd 2306.9684, were present in significantly larger quantities.

Reaction of Scheme 3.10 A 100ml RBF was charged with 50ml *m*-cresol and purged of oxygen by three freeze-pump-thaw cycles using argon. 0.077g (0.0442mmol) **3.2** And 0.077g (0.1325mmol) of **3.3** were added, a condenser was fitted and the solution was heated to 180^{o}C and allowed to stir for 32h under argon. The solution was cooled to RT and 0.356g (0.442mmol) of **3.4** dissolved in 30ml of oxygen-free 1,2-dichlorobenzene was added. The solution was put through three freeze-pump-thaw cycles using argon and subsequently heated to 180^{o}C for 28h. On cooling, 1.5 volume equivalents of methanol were added and the precipitate was isolated by filtration through a pad of celite. The solid isolated was loaded onto a silica gel column and chromatographed using toluene:CS_2 (3:2). Analysis of the crude solution along with fractions obtained through silica gel chromatography revealed the presence of the intermediates and products reported.

3.15 by scheme 3.11 1,2-dichlorobenzene:AcOH (1:1) was deoxygenated by three freeze-pump-thaw cycles using argon. 30ml of the deoxygenated solvent system was transferred to a pressure tube containing 73.5mg (0.0421mmol) of **3.2** and 73mg (0.126mmol) of **3.3**. Argon was bubbled through the solution for 5 minutes before being sealed with a Teflon screw cap. The vessel was heated to 180^{o}C and stirred at that temperature for 14h. The vessel was cooled and 0.339g (0421mmol) dissolved in 20ml of deoxygenated 1,2-dichlorobenzene was added, the vessel was purged with argon, sealed and warmed to stir at 180^{o}C overnight. The solution was then cooled and 200ml of methanol was added causing precipitation of the product that was isolated by filtration through a pad of celite. The residue was taken up in CS_2, loaded onto a silica gel column and eluted with Toluene:CS_2:EtOAc (50:49:1). **3.15** was present as the major product of the purification. MS (MALDI-TOF): m/z obsd 2307.9691 $[M+H]^+$, calcd 2307.9320.

Chapter 4. Synthesis of a Series of Porphyrin-Wire-C_{60} Constructs Using Pyrazine-Containing Wires and Their Model Compounds For Photophysical Analysis.

4.1 Design of Porphyrin-Wire-C_{60} Compounds and the Respective Model Compounds in Series A, B, C

Having determined that the t-butyl groups present on the porphrin groups of **3.1** were not sufficient to overcome the aggregative behavior of **3.1** and enable facile solution-state purification and characterization, the porphyrin moieties were redesigned to feature dodecyloxy groups in place of the *tert*-butyl groups. In addition, shorter bis-*o*-diamino aromatic building blocks were sought to at least allow for proof that the core project design that centered around condensing a porphyrin-functionalised aromatic diketone with a fullerene diketone around a bis(*o*-diamino) aromatic wire was feasible for producing a characterizable entity.

This objective is slightly removed from the initial objective of studying long pyrene-containing heteroaromatic wires presented in *chapter 1* as molecular wires for mediating photoinduced electron transfer. It is expected that the LUMOs of the shorter heteroaromatics included in the study would not be suitably poised to accept an electron from the porphyrin donor. In this case, the shorter wires would be expected to mediate electron transfer by the superexchange mechanism with the aromatic bridges serving only to mix the roughly exponentially decaying molecular orbitals of the donor with the acceptor[70,92]. It was expected that later in the study, if the longer pyrene-containing heteroaromatic D-W-A structures could be synthesized, a change in the distance dependence for the photoinduced electron transfer rates across the bridges would change

as the LUMO energies of the wires dropped to an energy suitable for accepting an excited electron from the porphyrin and so, being able to mediate the electron transfer via the hopping-mechanism. Incoherent charge hopping typically exhibits a weaker distance dependence for which wire-like behavior can be ascribed. Consequently, it was expected that the synthesis of the shorter wire constructs would be useful for compiling a complete data set in which the transition from electron transfer via superexchange to incoherent hopping may be observed.

The photophysics of pyrazine-containing fused aromatic structures that feature as the wire moieties in this work have as yet not been determined. Furthermore, the photophysics between the individual wire structures and porphyrins or fullerenes have also not been determined. Consequently, the initial challenge to simply construct a series of porphyrin-wire-acceptor compounds featuring wires of different lengths was increased to include the necessary model compounds that would enable the investigator to dissect the complex photophysics expected to be present in such multi-component systems

Based on the electrochemical data in the literature[95] of rectilinearly fused pyrazine-containing heteroaromatic polyacenes, it was roughly expected that only much longer aromatic wires of this type of fused aromatic could accept an electron from the of S_1 excited state of a zincated porphyrin. It was therefore initially of interest to construct donor-wire-acceptor compounds with very long aromatic wires, featuring 9 to 18 rectilinearly fused aromatic rings in the series and then to obtain the attenuation factor for electron transfer from the two porphyrins to the fullerene acceptor across such wires. The hope was that if the attenuation factor was weak and that the HOMO-LUMO gap of longer and longer wires beyond 18-fused aromatic units in length did not collapse, that

the wires may serve as candidates for building larger D-W(D_n)-A structures comprised of long wires with the edges functionalized with porphyrin or other appropriate chromophores as shown in figure 1.7.

The three series of molecules are shown in figures 4.1, 4.2 and 4.3 were proposed to be synthesized; they are series A, B and C respectively. Compound **4.4** of series A, **4.8** of series B and **4.12** of series C are the complete donor-wire-acceptor molecules of each series. The remaining molecules of each series are designed to act as model compounds to isolate the properties the interactions between the wires, porphyrins and C_{60}.

Series A

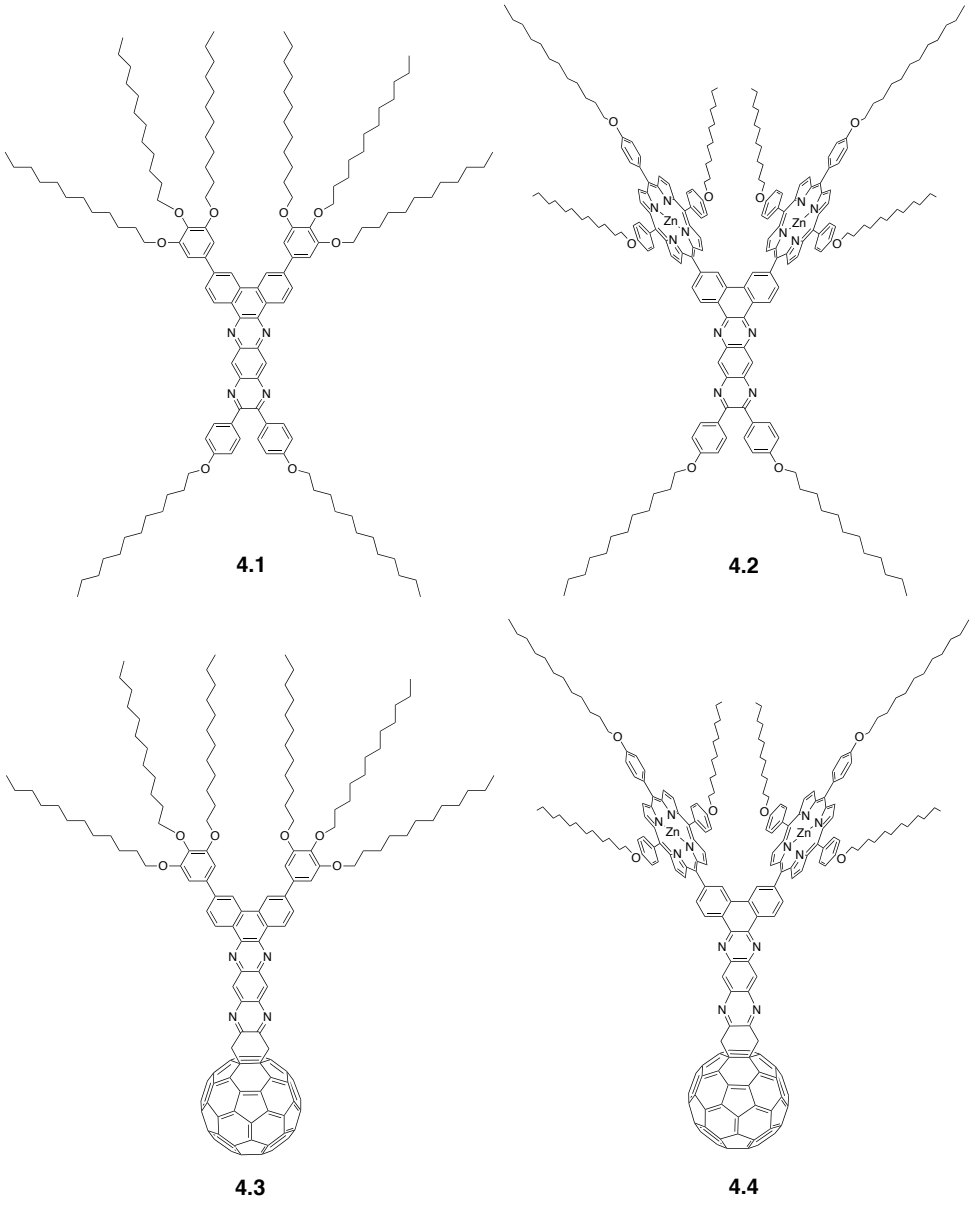

Figure 4.1 Series A compounds all employing 1,2,4,5-tetraaminobenzene as the wire building block to create a heteroarmoatic wire containing four rectilinearly fused aromatic units.

Series A features the shortest wire or bridge comprised of four rectilinearly fused aromatic rings which can be formed through condensation of 1,2,4,5-tetraaminobenzene

with the appropriate *o*-diketones. Tetraaminobenzene is commercially available as the tetrahydrochloride salt, and is relatively cheap.

Series B

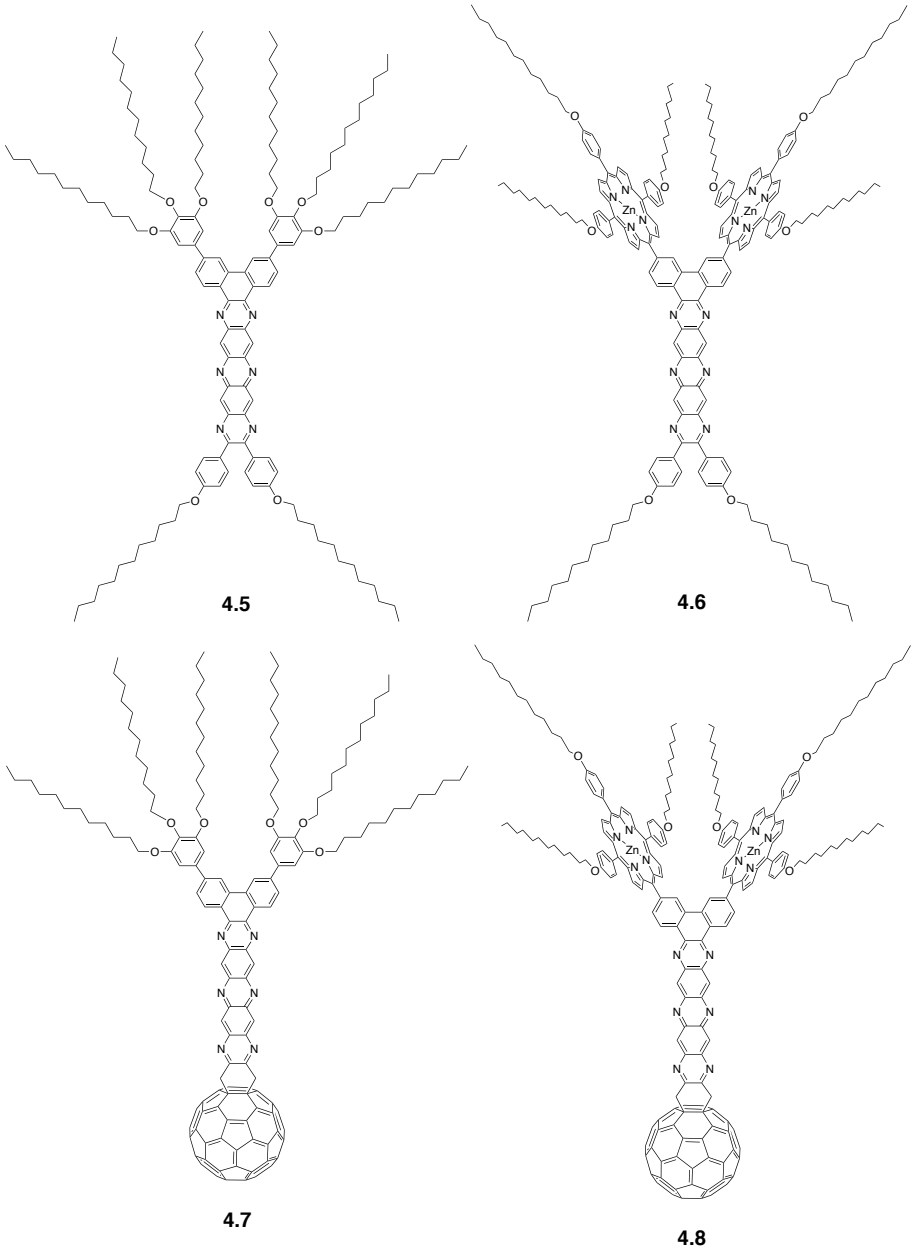

Figure 4.2 Series B compounds featuring a heteroaromatic wire containing six rectilinearly fused aromatic rings and notably, three pyrazine units.

Series B shown in figure 4.2 employs a fused heteroaromatic wire or bridge that features six rectilinearly fused aromatic rings. The synthesis of this structure can be achieved through condensation of tetraaminophenazine with the appropriate *o*-diketones. Tetraaminophenazine can be synthesized in one step from tetraaminobenzene. Consequently, employing the same *o*-diketones required for the synthesis of the molecules of series C (figure 4.3), the molecules of series A and B could be achieved only requiring the synthesis of one additional building block, specifically, tetraaminophenazine.

Series C

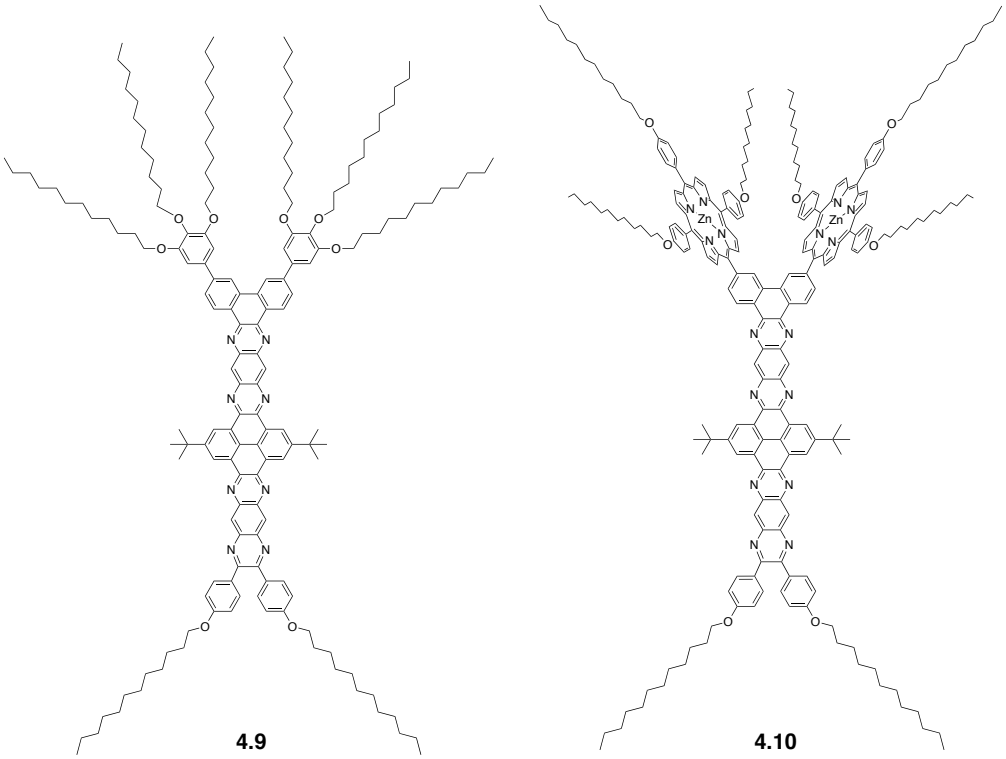

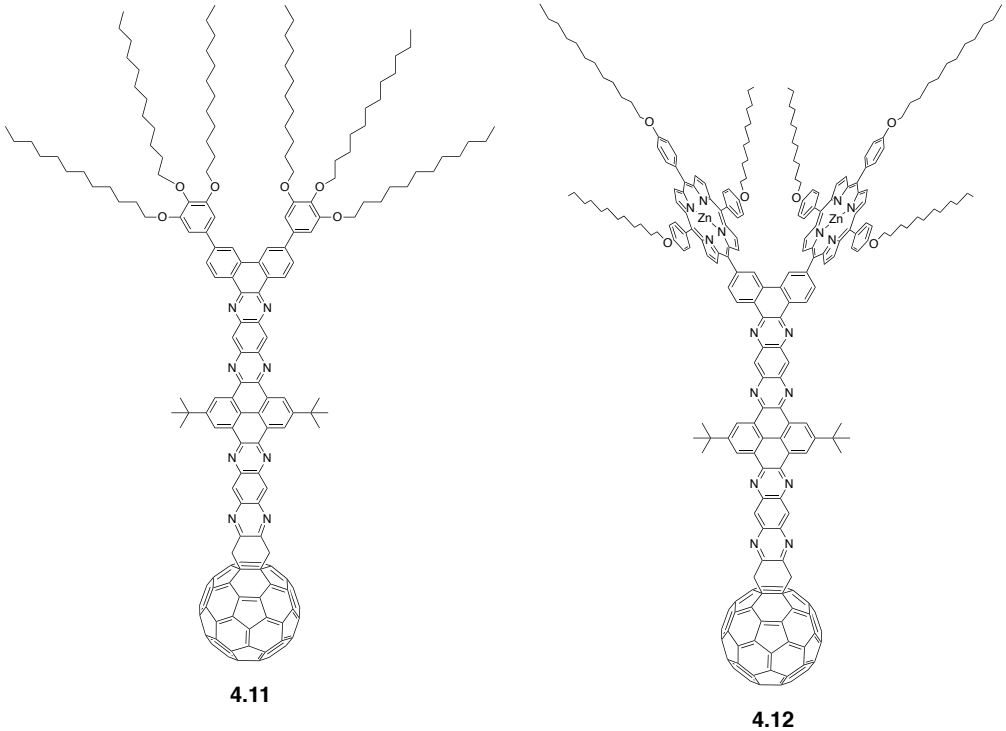

Figure 4.3. Series C compounds all employing a heteroaromatic wire that is nine rectilinearly fused aromatic units long and contains a pyrene cross-conjugated center.

Molecules **4.1**, **4.5** are **4.9** are designed to model properties of the wires present in the respective D-W-A compounds. The 3,4,5-tris(dodecyloxy)benzene rings positioned in place of porphyrins at the donor termini and *p*-dodecyloxybenzene groups substituted at the acceptor termini are intended to imbue solubility to the planar wire molecules without changing the structure of the core wire molecule enabling solution state studies.

Molecules **4.2**, **4.6** and **4.10** are designed to isolate the photophysical interactions between the porphyrin donors and respective wires. Again *p*-dodecyloxybenzene groups are employed to imbue the acceptor terminus with solubility without significantly altering the wire cores. Finally, molecules **4.3**, **4.7** and **4.11** are designed to isolate the photophysical interactions between the respective wires and fullerene acceptors present.

4.2 Synthesis of Building-Blocks for the Synthesis of the Molecules of Series A, B and C

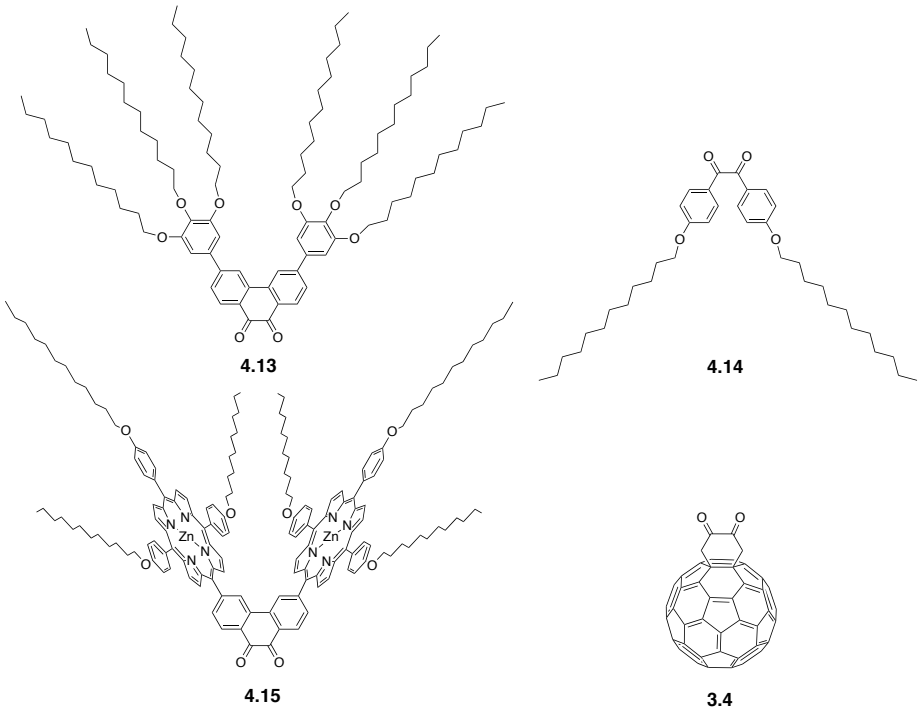

Figure 4.4 Essential building blocks for the synthesis of the molecules of series A, B and C.

The synthesis of series A, B and C all require the four *o*-diketones shown in figure 4.4. The initial plan for the synthesis of the compounds of series A, B and C was to simply condense these four *o*-diketones with the corresponding tetraamino heteroaromatic wire building blocks appropriate for the synthesis of each specific compound. 1,2,4,5-tetraminobenze, as stated earlier, is commercially available while the synthesis of the necessary tetraamino wire core **3.3** was shown in chapter 3. Consequently the synthesis of 2,3,6,7-tetraaminophenazine was the only other building block required before initial attempts at the assembly of the compounds by the appropriate condensations could be achieved.

Scheme 4.1

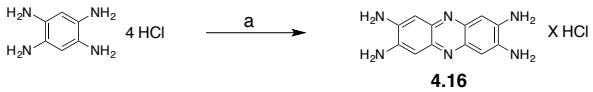

4.16

a) Na(AcO), H_2O, O_2, 100°C, 5h, 96% yield (x = 0) or 78% (x= 1.5) [140]

The synthesis of 2,3,6,7-tetraaminophenazine (**4.16)** shown in scheme 4.1 was achieved in accordance with a known literature procedure[140]. The reaction involves an aqueous reflux of the tetrahydrochloride salt of 1,2,4,5-tetraaminobenzine with fourteen equivalents of sodium acetate. The reaction is conducted with constant bubbling of air through the solution. The oxygen in the air serves to oxidize the intermediate dihydrophenzine to form the aromatic phenazine core. The literature procedure reports a quantitative yield but not the mass of product obtained. The product in the reported procedure is claimed, based on elemental analysis, to be the 1.5HCl salt. It is, however, unlikely that a quantitative yield can be obtained in this procedure as the tetraaminobenzene starting material is incredibly soluble and the filtrate from which the product is isolated remains bright red after filtration. The correlation of calculated and experimentally determined elemental composition is not very close, and as such, throws some doubt into what the protonation state of the actual product is. An unlikely quantitative yield is an indication that the product is certainly not the free tetraminophenazine but rather the 1.5HCl salt or a salt with a higher HCl composition than what was reported in the literature.

The protonation state of the tetraamino aromatics is important for the work at hand as the reaction conditions employed to condense an aromatic *o*-diamine with an *o*-

diketone varies depending on if a bare *o*-amine is used, in which the reaction is carried out in mildly acidic conditions, or if a hydrochloride salt of the *o*-amine is employed, in which case basic conditions are used. When a tetrahydrochloride salt is employed, the amine exists in the protonated form, preventing the nitrogen lone pair of electrons from participating in a nucleophillic attack of the carbonyl carbons of the *o*-diketone to form the corresponding pyrazine moiety. The amines are thus considered to be deactivated when employed as a hydrochloride salt. Consequently, basic conditions are employed to deprotonate the amines, enabling them to act as the necessary nucleophiles. This is exemplified in the reaction of scheme 4.1, which uses a large excess of sodium acetate as the base to shift the equilibrium to favor the presence of the free amines originally present as hydrochloride salts, and to deprotonate the reaction intermediates.

The yield for the reaction shown in scheme 4.1 was 96% if the product is the free tetraaminophenazine or 78% if it is the 1.5HCl salt. Effort was not taken to determine the exact elemental composition as a ratio of 1.5HCl to one tetraminophenazine implies that two amines are still free to react. As no protocol in this work requires all four amines to react in a given reaction, and that reaction of all four amines would be an undesirable reaction given the synthetic objectives at hand, the uncertainty as to the nature of the product was not deemed a concern. For the purposes of establishing the correct reaction conditions for condensations with this product, it was assumed to be that of the reported literature product, the 1.5 HCl salt.

Scheme 4.2

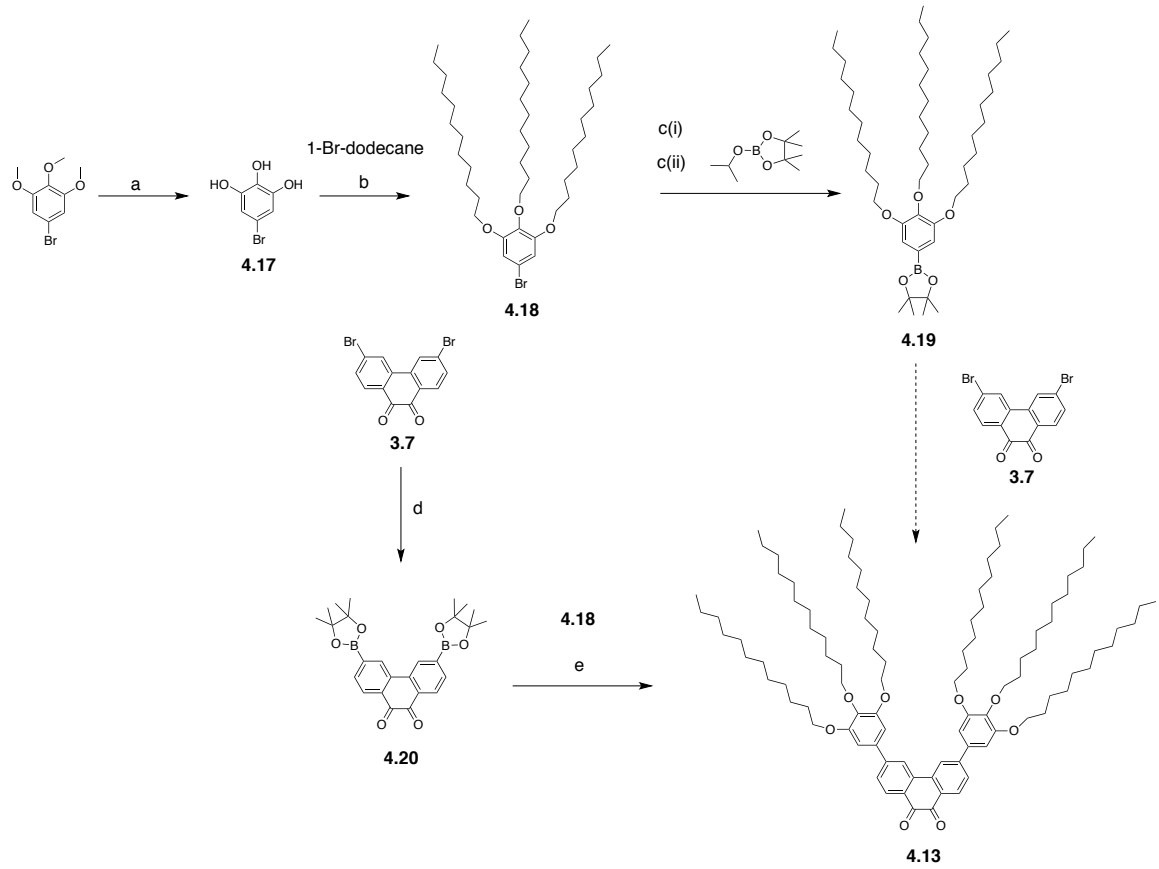

a) BBr_3, DCM, -78°C → 96% **b)** K_2CO_3, DMF, 70°C, overnight, 61% yield **c) i** 1.6M *n*-BuLi, THF -78°C, 1h **ii** -78°C → RT 20 h, 56% yield **d)** $Pd(PPh_3)_4$, Et_3N, 1,2-dichloroethane, 90°C, overnight, 28% yield **e)** $Pd(PPh_3)_4$, Cs_2CO_3, THF, 90°C (pressure tube), overnight, 32% yield

Several different routes for the synthesis of the solubilizing phenanthrenedione based end-cap **4.13** were investigated, not by choice, but due to difficulty in executing literature reports for the synthesis of a key synthetic step[141]. Considering that the building block **4.13** is required for the synthesis of eight of the twelve target molecules of series A, B and C, obtaining **4.13** in high yield and in gram quantities was a necessary goal for achieving the overall aims of the project, allowing for the necessary test reactions for the assembly of the final compounds to be performed without having to continuously repeat

the synthesis of **4.13**. On this basis, molecules upstream of **4.13**, would be required in even greater quantities. **4.13** was initially proposed to be synthesized in an analogous fashion to the synthesis of **3.4**. Consequently, a high yielding route to the boronic acid or boronic ester, **4.19**, was necessary. A literature[141] procedure for the synthesis of **4.19** from the arylbromide, **4.18**, involving a lithium-halogen exchange and subsequent reaction with 2-isopropoxy-4,4,5,5-tetramethyl-1,3,2-dioxaborolane was reported to proceed with a 46% yield. While this low yield was not ideal, it appeared to be the best way forward. The report also detailed high yielding reactions for the synthesis of the requisite precursors, specifically **4.17** which was produced in 96% yield by a BBr_3 cleavage of 1-bromo-3,4,5-trimethoxybenene and the subsequent Williamson-ether synthesis of the 1-bromo-3,4,5-(trisdodecyloxy)benzene (**4.18**) obtained in 61% yield.

With gram quantities of **4.18** on hand, the synthesis of **4.19** was attempted. A significant problem was encountered in that on cooling a THF solution of the heavily alkylated aryl bromide, **4.18**, down to -78^{o}C, the solution turns to a thick slurry, and if vigorous stirring is not maintained, turns into a solid waxy lump. As the protocol requires addition of the *n*-butyllithium reagent and subsequent reaction at -78^{o}C for an hour, the added *n*-butyllithium will not react with the frozen solid until the temperature is raised, at which point the ideal conditions for reaction are broken. A satisfactory yield was obtained on one occasion giving a yield of 41%. This was on the second attempt but further attempts to reproduce the results failed, with the starting material being recovered. Attempts were made to allow the reaction to warm with quick addition of *n*-butyllithium and subsequent cooling, but these attempts were unsuccessful at producing the product in good yield.

Consequently, attempts were made to invert the presence of the boronic ester and bromide group on the two aryl groups that required coupling to form **4.13** (scheme 4.2). 3,6-dibromophenanthrene-9,10-dione (**3.7**) was successfully transformed to the corresponding diboronic ester, **4.20**, using pinacolborane via a palladium mediated coupling in the same way that the boronic ester was introduced to the porphyrin **3.6**. This reaction produced **4.20** in a 28% yield following purification by silica gel chromatography. **4.20** was successfully coupled with **4.18** to produce **4.13** in 32% yield, a still unsatisfactory yield for obtaining **4.13** in appreciable quantities.

Scheme 4.3

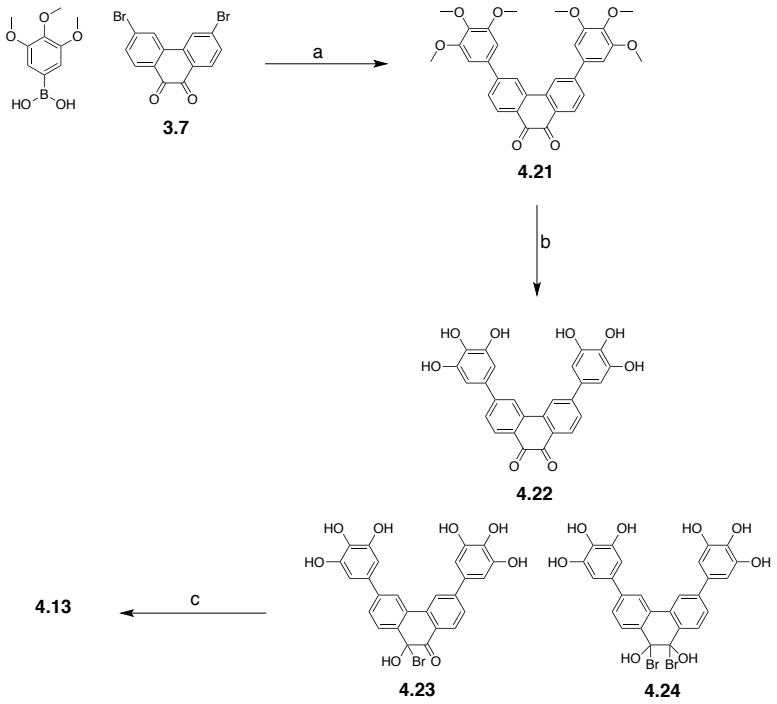

a) $Pd(PPh_3)_4$, Cs_2CO_3, THF, 67°C, overnight, >66% yield. **b)** BBr_3, DCM, -78°C→ RT, yield 101%.**c)** 1-bromododecane, K_2CO_3, DMF, 70°C, overnight, 4% yield.

Efforts were turned to couple the aryl constituents of **4.13** prior to generation of the dodecyloxy functionalities. 3,4,5-trimethoxyphenylboronic acid is available commercially and was successfully coupled to **3.7** (scheme 4.3) to give **4.22** in 66% yield. Unfortunately, attempts to cleave the methoxy groups utilizing similar methodology employed in the synthesis of **4.17** was not straightforward. The yield of the reaction was 101% and the MALDI-TOF mass spectrum indicated that the product mixture featured the desired product along with byproducts exhibiting masses indicative of the addition of one and two bromine atoms. The identity of the byproducts was not determined conclusively but it is suspected that they are the byproducts **4.23** and **4.24** shown in scheme 4.3 produced by a nucleophillic attack of bromide to the ketone moiety.

This is feasible as the boron atom of BBr_3 could coordinate to the oxygen atom of the ketone, activating the carbonyl carbon for such an attack.

The two byproducts present could not be separated from **4.22**. In hopes that the byproducts were unstable and could decompose to produce the diketone functionality, a reaction was attempted utilizing a portion of the product mixture to alkylate the hydroxyl functional groups present to generate **4.13**. **4.13** was successfully obtained, however, the bromo adducts remained present in product mixture, though now alkylated. The desired product mixture was separable and **4.13** was isolated apart from the two byproducts with a terrible yield of 4%. It was concluded that the excessive side reaction of BBr_3 with the diketone present on **4.21** deemed this route to **4.13** unsuitable. Other attempts at generating **4.22** from **4.21** involving heating of **4.21** in pyridine hydrochloride or in acetic acid with HBr proved unsuccessful.

Scheme 4.4

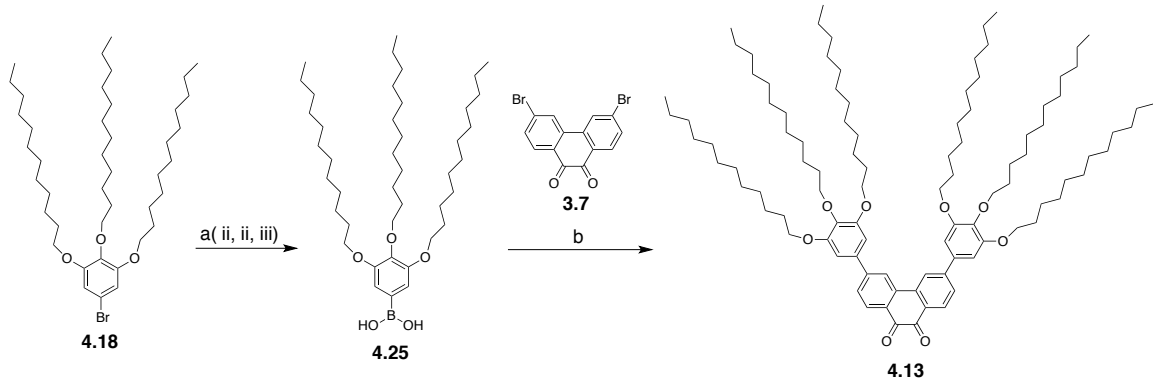

a) i 1.6M *n*-BuLi, THF -78°C, 5h, → 0°C, 5min **ii** $B(OMe)_3$, -78°C → RT 24 h **iii** 1M HCl. 51% yield **b)** $Pd(PPh_3)_4$, Cs_2CO_3, THF, 80°C, overnight, 67% yield.

Given the initial, yet unreproducable success of synthesizing the boronic ester **4.19** utilizing *n*-butyllithium, efforts were made to revisit the protocol, but with some

changes. Trimethylborate was used as the boron source and the final product was to be isolated as the boronic acid as opposed to a boronic ester. The reaction still required cooling to -78°C. Extra care was made to avoid the thick slurry produced at this temperature from turning solid. A typical three step procedure was carried out for this type of reaction, specifically a lithium-halogen exchange employing *n*-butyllithium, treatment of the lithiated intermediate with $B(OMe)_3$ and finally hydrolysis of the boronic ester produced to yield the boronic acid product **4.25** which was acquired in 51% yield. The boronic acid was easily coupled to **3.7** utilizing $Pd(PPh_3)_4$ as the catalyst and Cs_2CO_3 as the base to afford the desired **4.13** in 67% yield, as shown in scheme 4.3.

Scheme 4.5

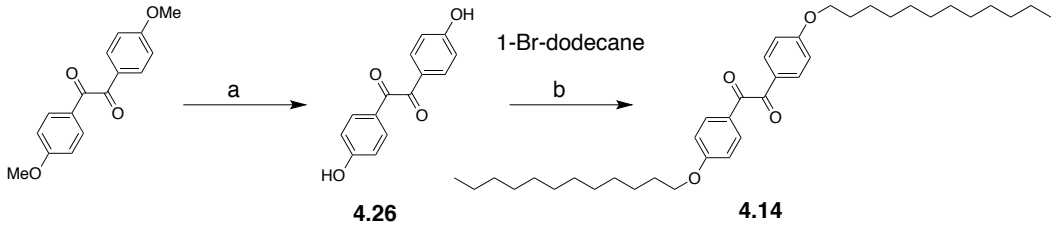

a) Pyridine.HCl, 220°C, 3h, 94% yield[142]. **b)** K_2CO_3, DMF, 70°C, overnight, >100% yield

With the requisite phenanthrenedione end-cap in hand, a series of quick literature procedures were followed to produce **4.14** in very high yield. The literature procedure[142] to cleave the methoxy groups generating **4.27** involved heating 4,4'-dimethoxybenzil in Pyr.HCl at 220°C for 3 hours. **4.14** was readily produced from **4.27** and 1-bromododecane by a Williamson-ether synthesis in DMF using K_2CO_3 as the base. The white waxy solid was obtained in over 100% yield that may have been due to the presence of residual bromododecane or byproducts thereof that co-eluted with the

product during chromatographic purification. This impurity was not expected to pose any problems in subsequent steps and no further effort was made to purify the compound further.

Scheme 4.6

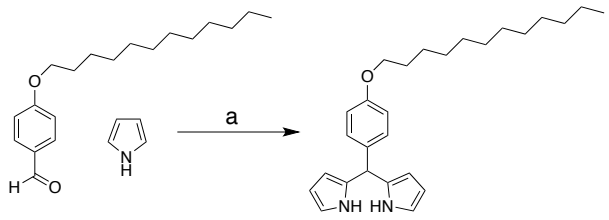

4.27

a) TFA, RT, 1h 45min, NaOH, 30min 79%[143]

The porphyrin moieties present on **4.15** required *meso*-(*p*-dodecyloxyphenyl)dipyrromethane, **4.27**, for their synthesis. A literature[143] procedure existed for this compound but reported that it could not be isolated in pure form owing to co-elution of the tripyrromethane byproduct. Following the literature procedure, the purification protocol was modified slightly to enable isolation of pure **4.27** in 79% yield. The tripyrromethane byproduct was expected to be less stable than the dipyrromethane product and consequently could be degraded in solution by exposure to light while air was bubbled through the solution. The degraded tripyrromethane is green and is less mobile during silica gel chromatography when employing chloroform as the mobile phase, the same solvent used in the literature protocol.

Scheme 4.7

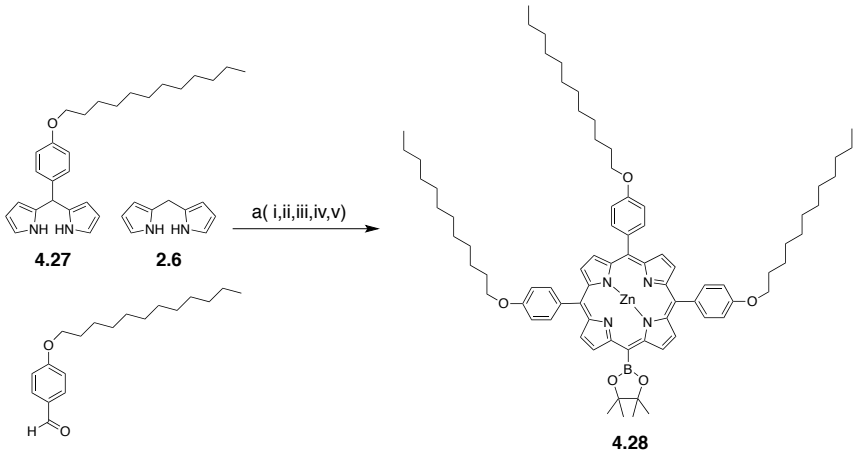

a) i $BF_3.OEt_2$, $CHCl_3$, RT, 3h. **ii** DDQ, RT, 1h. **iii** $Zn(OAc)_2.2H_2O$, DCM:MeOH (2:5), reflux, overnight. **iv** NBS, $CHCl_3$, RT, 2h. **v** 4,4,5,5-Tetramethyl-1,3,2-dioxaborolane, $Pd(PPh_3)_2Cl_2$, Et_3N, 1,2-dichloroethane, Ar., reflux, overnight.

The synthesis of the requisite boronic ester porphyrin **4.28** required for the Suzuki cross-coupling to produce **4.15** was anything but elegant and just like the synthesis of **3.6** required several transformations before the products from the initial condensation in which the macrocyle was formed were separable by column chromatography. In an analogous manner, dipyrromethane, **2.6**, was condensed with **4.27** and 4-dodecyloxybenzaldehyde in chloroform using $BF_3.OEt_2$ as the Lewis acid catalyst. The macrocylic intermediates formed were oxidized by DDQ and the porphyrin product mixture isolated, metallated with zinc and brominated using NBS. The electron rich porphyrin mixture is susceptible to over-bromination, even at low temperatures, and coupling products are present in the mass spectrum even at this stage of the synthesis representing dimers of the various porphyrins present. Care was thus taken to conduct the bromination step with a minimal amount of NBS and was monitored carefully by TLC

and MALDI-TOF mass spectral analysis. Finally, palladium mediated coupling of pinacolborane to the brominated product mixture produced a mixture of porphyrin boronic esters from which the desired product, **4.28**, could be isolated by silica gel chromatography in 9.75% yield for all of the steps combined. It is worth noting that while this protocol was repeated on many occasions, the best yield was obtained when unequal molar equivalents of the two dipyrromethanes required were employed. 2.4 Molar equivalents of **2.6** to **4.27** were used in the reaction that typically gives the product in 6-7% yield when an equimolar ratio of the two dipyrromethanes is used.

Scheme 4.8

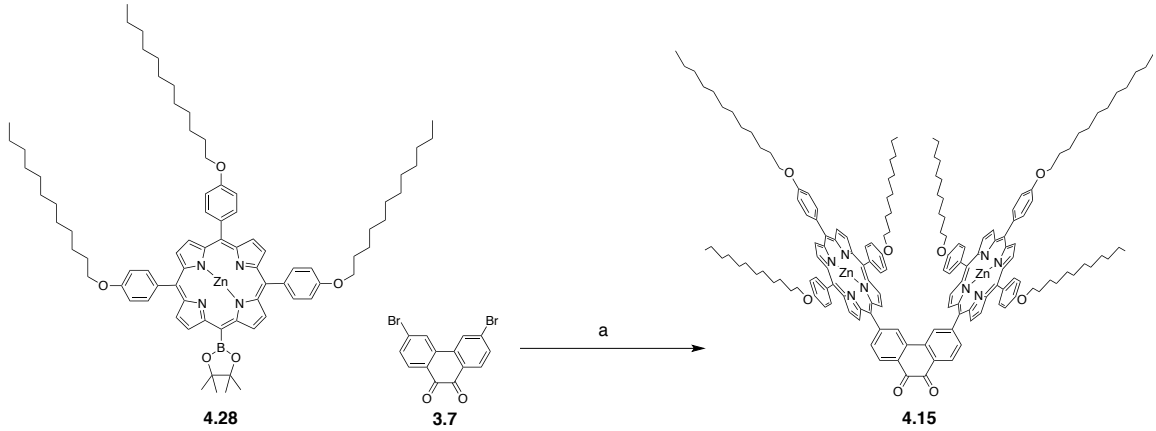

a) $Pd(PPh_3)_4$, Cs_2CO_3, THF, 90°C, overnight, 68%.

The synthesis of the final building block for the assembly of the molecules of series A, B and C was achieved by coupling **4.28** to **3.7** employing $Pd(PPh_3)_4$ as the catalyst. **4.15** Was obtained in 68% yield and was easily isolated by silica gel chromatography. ^{1}H NMR spectra of **4.15** at various temperatures also revealed that rotation of the porphyrin moieties of **4.15** is inhibited and that at room temperature the inherent symmetry of the molecule is not reflected in the NMR spectrum.

4.3 Synthesis of Series A

Scheme 4.9

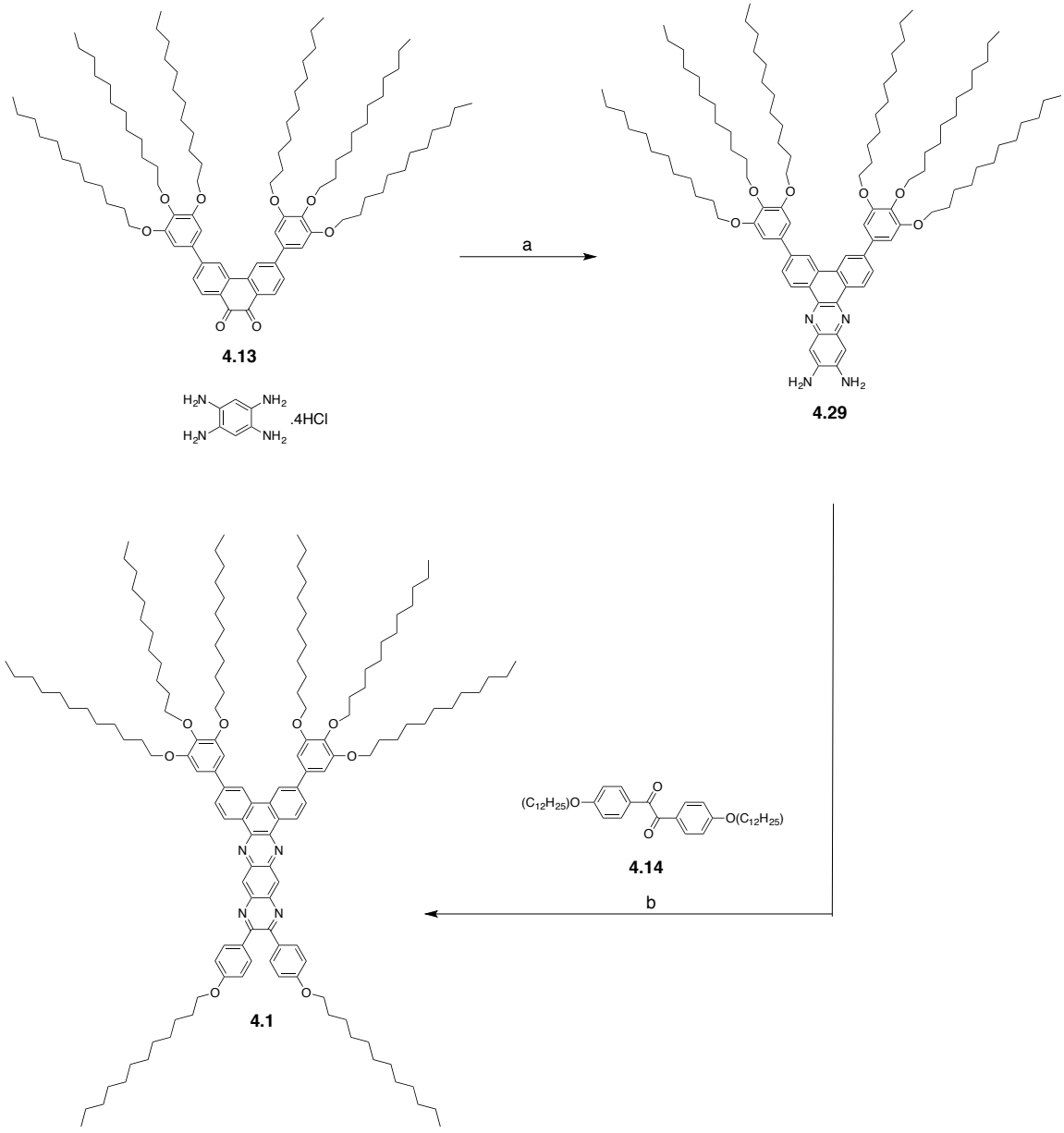

a) NaOAc, 1,4-dioxane, reflux, 20h, 92% yield. **b)** 1,4-Dioxane, AcOH, DCM, reflux, 20h, 51% yield.

The synthesis of 4.1 shown in scheme 4.9 from the building blocks on hand proceeded quite simply. A ten-fold excess of tetraaminobenzene tetrahydrochloride was condensed with **4.13** to produce **4.29**. The excess was used to prevent the double condensation product from forming. Since tetraaminobenzene has essentially two sites that can condense with free **4.13** in solution, it is important that an excess of the tetraamine is used to prevent two molecules of **4.13** from reacting with a single molecule of tetraaminobenzene to form the double condensation product.

Importantly, this reaction does not employ any acid in solution to activate the ketones present. Rather, for every HCl molecule present on the tetrahydrochloride salt, an equivalent of NaOAc was added. Reaction of the acid and base produces sodium chloride and AcOH in solution. Trial reactions in which the tetrahydrochloride salt of the tetraamine was added without any base present did not proceed to produce the desired product. The amine functionality, as stated earlier, is deactivated when protonated and base must be added to liberate the free aromatic amine to partake in nucleophillic attack of ketones present in solution. Product **4.29** was isolated in a very a good 92% yield and subsequently condensed with *p,p'*-didocecyloxybenzil (**4.14**), this time, in an acetic acid catalyzed reaction employing 1,4-dioxane as the solvent. A small amount of dichloromethane was added to facilitate dissolution of **4.14** and also to prevent the solution from getting too hot during reflux. Ethanol was not used in this reaction to prevent the formation of the unwanted acetic acid adduct as had been observed in the synthesis of **3.16**. There was concern that ethanol would hinder the dissolution of **4.14** which has a tendency to float as small waxy lumps in the reaction solution. Fortunately, the byproduct was not detected despite the lack of ethanol and the product was obtained

in 51% yield. The reaction to form **4.1** was also achieved using thiamine hydrochloride as the catalyst[144]. The desired product was detected by MALDI-TOF mass spectral analysis of the crude reaction solution but was not worked-up or purified as sufficient quantities had been obtained in the previous reaction.

Scheme 4.10

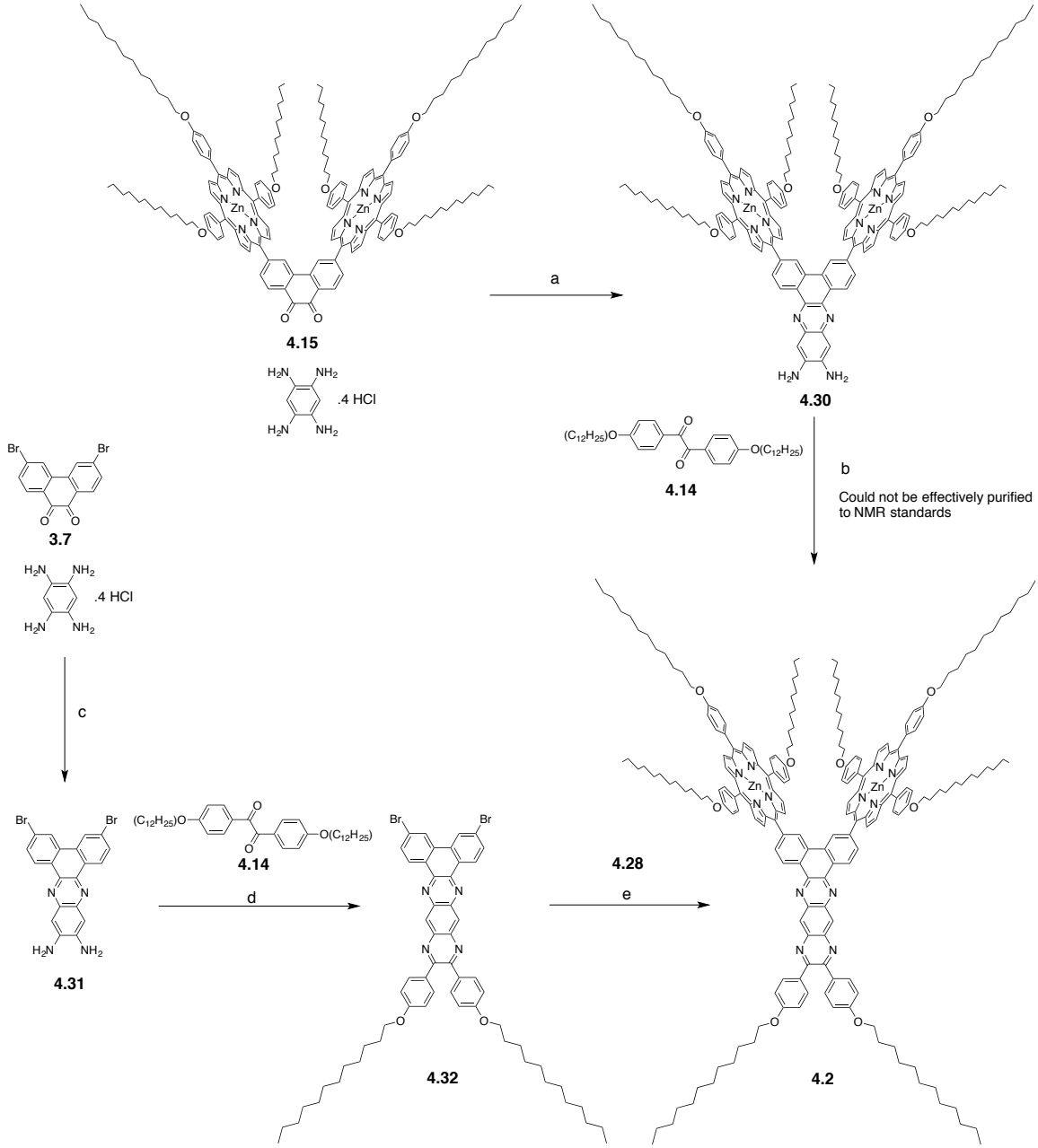

a) NaOAc, 1,4-dioxane, EtOH, reflux, overnight, 69% yield. **b)** $TsOH.H_2O$, toluene, reflux, overnight, yield not determined. **c)** NaOAc, 1,4-dioxane, reflux, overnight, 95% yield. **d)** $TsOH.H_2O$, 1,2-dichlorobenzene, reflux, overnight, 41% yield. **e)** $Pd(PPh_3)_4$, Cs_2CO_3, THF, 80°C, 20% yield.

The synthesis of **4.2** was in no way a simple task. A strategy similar to that for the synthesis of **4.1** was attempted, but failed to produce **4.2** satisfactorily. The first

condensation proceeded smoothly, again employing a ten-fold excess of tetraaminobenzene relative to the diketone, **4.15**, and a corresponding equivalent of NaOAc for every protonated amine introduced to the reaction. This strategy afforded **4.30** in 70% yield. The next step, distinct from the condensation to form **4.1**, employed toluenesulfonic acid as the proton source for catalysis. The reaction yielded enough of the product that an apparently pure fraction of **4.2** was obtained after considerable effort via chromatography. The identity of the compound present in the fraction obtained was confirmed by MALDI-TOF mass spectral analysis to be **4.2**. However, NMR analysis of the sample obtained was unsatisfactory and an alternative strategy was employed to obtain **4.2**. The problem with this reaction is that the product co-elutes with **4.14** that was added in a ten-fold excess to promote reactivity. In general, during the course of this work it was observed that **4.14** exhibits less reactivity than the diketones **3.13**, **4.13** and **4.15**. Many of the products formed by reactions in which **4.14** was used eluted with similar R_f values to **4.14**, which also exhibits a propensity to streak slightly. As a result, obtaining pure samples of products free from unreacted **4.14** was a time consuming task.

An alternative strategy was employed to achieve the two condensation reactions in which the complete wire core of **4.2** is formed on a larger scale. Compound **4.15** is a precious starting material and performing test reactions with it is difficult as the quantities available for testing were so small that the corresponding catalytic quantities of acid or Lewis acid catalysts that needed to be added are very difficult to weigh out. **4.14** and **3.7** had both been obtained in significant quantities. Attempting to obtain high quantities of the wire core from these starting materials to which the precious porphyrin, **4.28**, could be coupled later seemed like a better strategy.

3.7 and tetraaminobenzene tetrahydrochloride were condensed to from **4.31** in 95% yield, again using 1,4-dioxane as the solvent and sodium acetate as the base. The product was isolated as a brown solid, which was soluble in DMSO, but very little else. The next step employed a five-fold excess of **4.14** and was carried out in 1,2-dichlorobenzene, a high boiling solvent with aromatic properties appropriate for aiding the dissolution of solid **4.31**. TsOH was employed as the acid catalyst and the product was obtained in 42% yield. While the yield was not ideal, 139 mg of **4.32** was obtained. This is an appreciable quantity in comparison to the quantities of **4.15** that were available to start the synthesis of **4.2** by the previously described synthetic pathway.

Despite the dibromo functionality and the extent of the fused aromaticity present in **4.32**, the two dodecyloxy chains imbue sufficient solubility to the molecule to render it soluble in toluene and enable the necessary purification by chromatography.

With the synthesis of the core wire structure complete, **4.28** was coupled to **4.32** employing $Pd(PPh_3)_4$ as the catalyst. The yield achieved following purification was not as high as expected based on the analogous coupling of **4.38** to **3.7** to form **4.15**. The exact yield of the reaction was not determined, yet the quantity of **4.2** that could be obtained in pure form represented a 20% yield. The product exhibited good solubility in chlorinated solvents and a satisfactory ^1H NMR spectrum was obtained.

Scheme 4.11

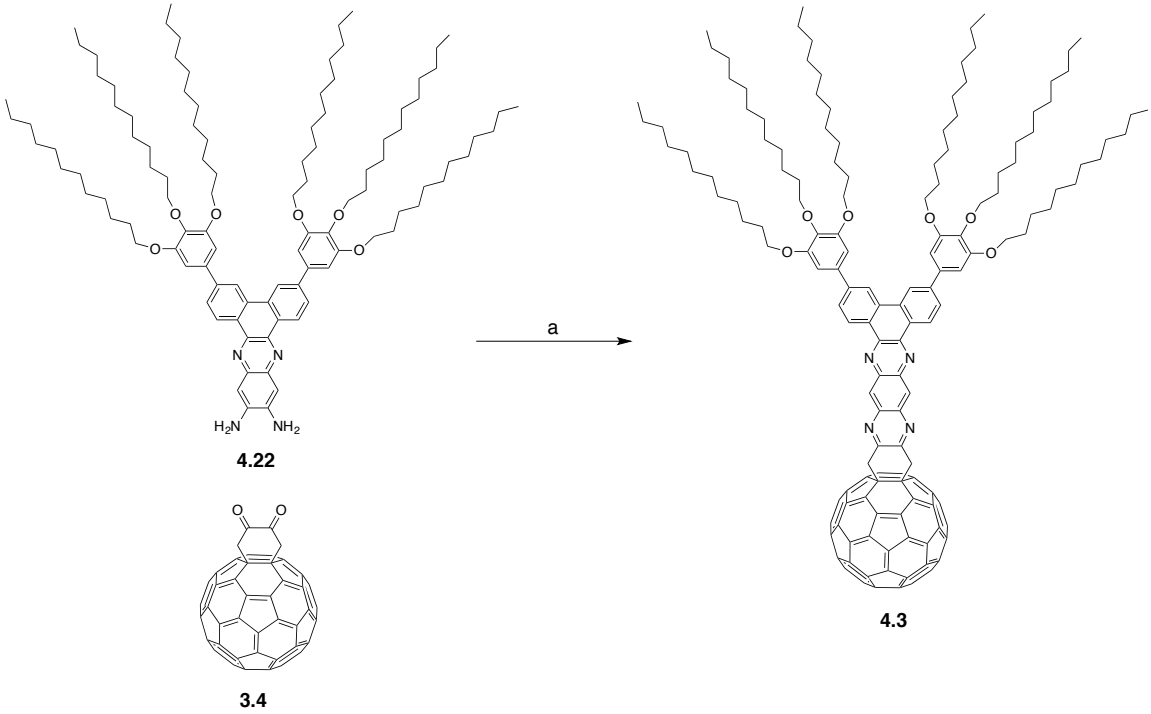

a) AcOH, 1,2-dichlorobenzene, EtOH, reflux, overnight, yield not determined due to extensive processing.

The synthesis of **4.3** (scheme 4.10) was achieved simply. **4.22** was refluxed with an excess of **3.13** using the solvent system developed in chapter 3 comprised of acetic acid, ethanol and 1,2-dichlorobenzene. The product was obtained in good yield with mass spectral analysis conducted as the reaction proceeded, which indicated appreciable consumption of the starting material, **4.22**. The product was processed extensively until pure and less pure samples had been pooled. Subsequently, the actual yield of the reaction was not determined, but satisfactory quantities of the required product could be obtained by this method. The procedure can be repeated in future work to determine the actual yield for the reaction.

Scheme 4.12

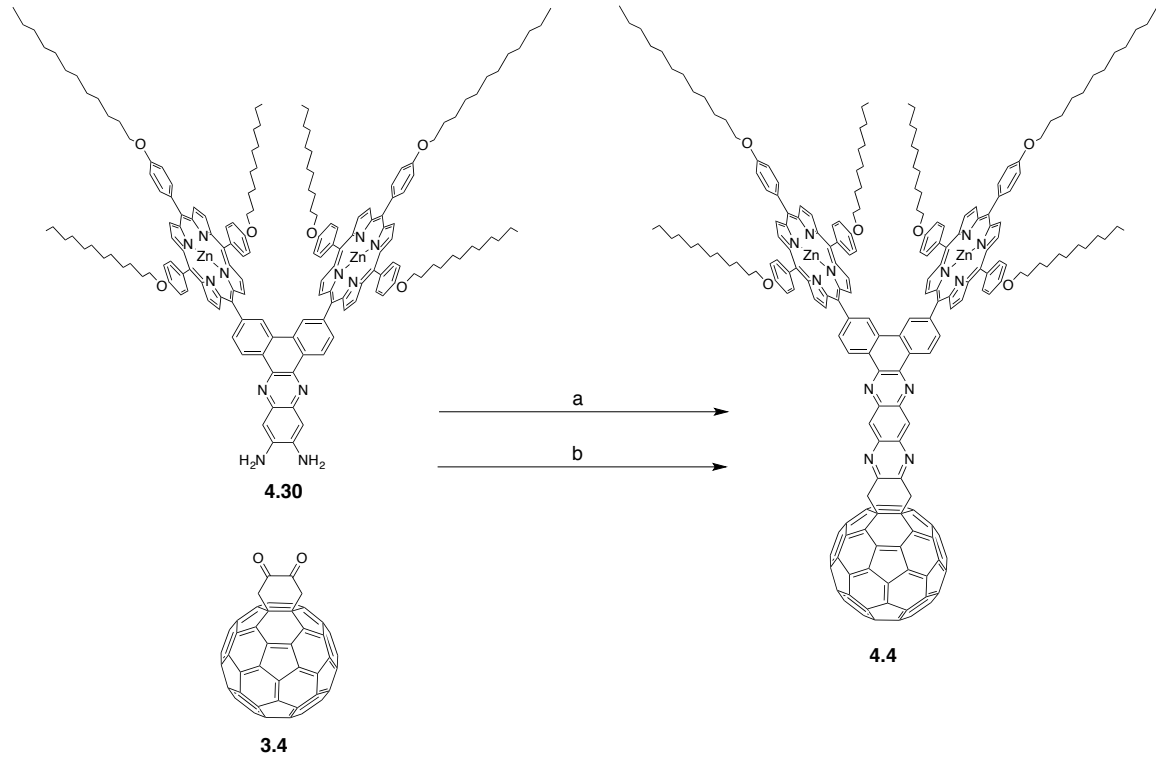

a) AcOH:1,2-Diclorobenzene:EtOH (1:2:1), reflux under argon, 36h, 73% yield. **b)** 1,2-dichlorobenzene:EtOH (5:1), TsOH.H_2O, reflux under argon, 18 h, 85% yield.

Two methods (scheme 4.12) were investigated for the synthesis of **4.4**, the most important molecule of series A. These involved condensing **4.30** with **3.4**. In the first reaction, acetic acid was used as the acid catalyst together with ethanol to prevent the formation of the acetic acid adduct. In the second reaction, TsOH was employed as the acid catalyst. Both reactions produced the desired product in good yield though ^{1}H NMR characterization of products from both reactions proved difficult. A higher scale reaction was performed for the TsOH catalyzed reaction and a high temperature ^{1}H NMR spectrum could be acquired with the additional material produced in this procedure. Even at 110^{o}C, peaks are broad indicating aggregation of the compound in solution.

A common problem experienced in this work is that poor solubility of the compounds synthesized relative to the miscibility or solubility of trace impurities results in a misrepresentative signal ratio in the NMR spectrum between product and impurities. Despite considerable effort being given to purifying compounds, the NMR spectra of the larger target molecules, especially those featuring fullerenes appear to contain significant quantities of impurities while it is likely that it is just the relative differences in solubility that causes this observation. It is useful to compare the intensity of the TMS signal, present in 0.03% v/v to the intensity of the product and impurity signals to gauge, proportionately how much of the added material is NMR active.

It is also worth paying attention to the difference in the integration between the signals of the aromatic protons and dodecyloxy groups present in the molecules of this work. Frequently, the integration does not match perfectly, while mass spectral characterization affirms the identity and purity of the compound, and while the chemical shift of peaks in the NMR spectra, and splitting patterns also confirm the identity, the freely moving alkyl groups tend to integrate for more than they should when compared to the integrations of the aromatic signals.

4.4 Synthesis of Series B

Scheme 4.13

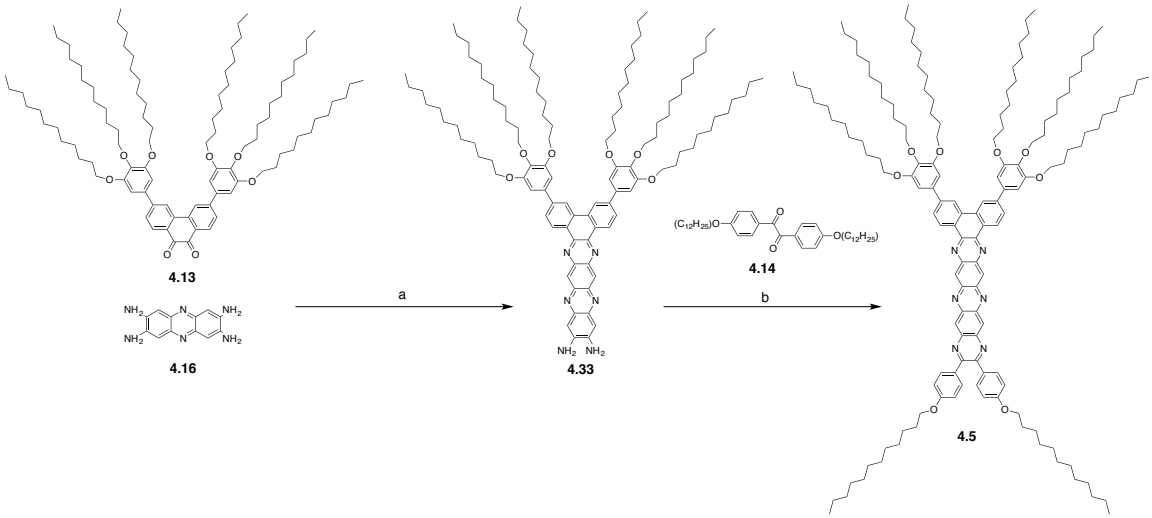

a) NaOAc, 1,4-Dioxane, EtOH, reflux, overnight, 94% yield. **b)** $TsOH.H_2O$, Toluene, reflux, 4 days, 49% yield.

Scheme 4.12 shows the synthesis of **4.5** the series B analogue to **4.1** of series A. Molecules of series B employ the tetraaminophenazine wire core, the synthesis of which was shown in scheme 1. The reaction for the synthesis of **4.33** from **4.13** and **4.16** did not employ the same calculated methodology employed in the synthesis of **4.29**. Considering that the identity of **4.16** was most likely similar to that reported in the literature, and so the 1.5 HCl salt, the use of three equivalents of NaOAc per equivalent of tetraaminophenazine introduced was essentially twice as much NaOAc than was required. Fortunately, the reaction still proceeded to produce product, **4.33**, in 94% yield, a 2% better yield than that for **4.29**. Ethanol was added to the solvent system in this reaction, which was another distinction from the reaction for the synthesis of **4.1**.

The subsequent step was slightly more tricky and required four days of reflux of the reactants, **4.16** and **4.33** in toluene using TsOH as the acid catalyst, producing the product in 49% yield. The longer reaction time required was the first indication that the single condensation products of tetraaminophenazine showed less reactivity than their tetraaminobenzene counterparts of series A. The reduced reactivity may come from how the phenazine core features two electronegative nitrogen atoms, and so withdraws electron density from the terminal amines, rendering them less nucleophillic than the tetraaminobenzene analogues.

An observation about the high yield in scheme 4.1 for the synthesis of **4.16** confirms this suspicion. The synthesis of **4.16** involves the attack of the amino carbons of tetraaminobenzene by two amines of another tetraamino molecule. The reaction does not continue to form larger heteroacenes that would be produced by attack of the nitrogen atoms of tetraaminophenazine on tetraaminobenzene free in solution. This is possibly because the nucleophilicity of the tetraaminophenazine nitrogen atoms is diminished inhibiting such a reaction.

Scheme 4.14

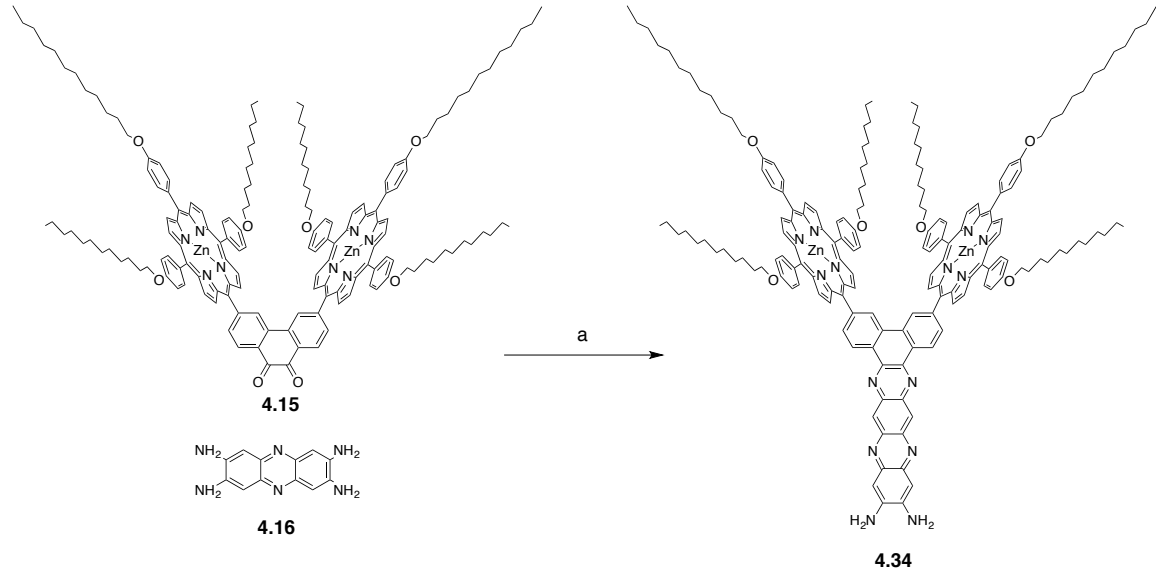

a) NaOAc, 1,4-Dioxane, EtOH, 1,2-dichloroenzene (3:2:3), reflux, 18h, 67% yield.

4.34 could be produced simply in a similar fashion to the reaction for the synthesis of **4.33** as shown in scheme 4.14. This time, the amount of NaOAc used was reduced to just two equivalents per tetraaminophenazine used in the reaction. As with the synthesis of **4.33**, ten equivalents of the tetraamine was used to minimize formation of the double condensation product. The yield of the reaction was 67%, not as high as that for **4.33**, and interestingly, very similar to that for the analogous tetraaminobenzene reaction (69%) indicating a similar difference in yield between condensations of **4.13** (92% and 94%) and **4.15** (69% and 67%) with a given aryl-*ortho*-amine. This was not an expected result.

Scheme 4.15

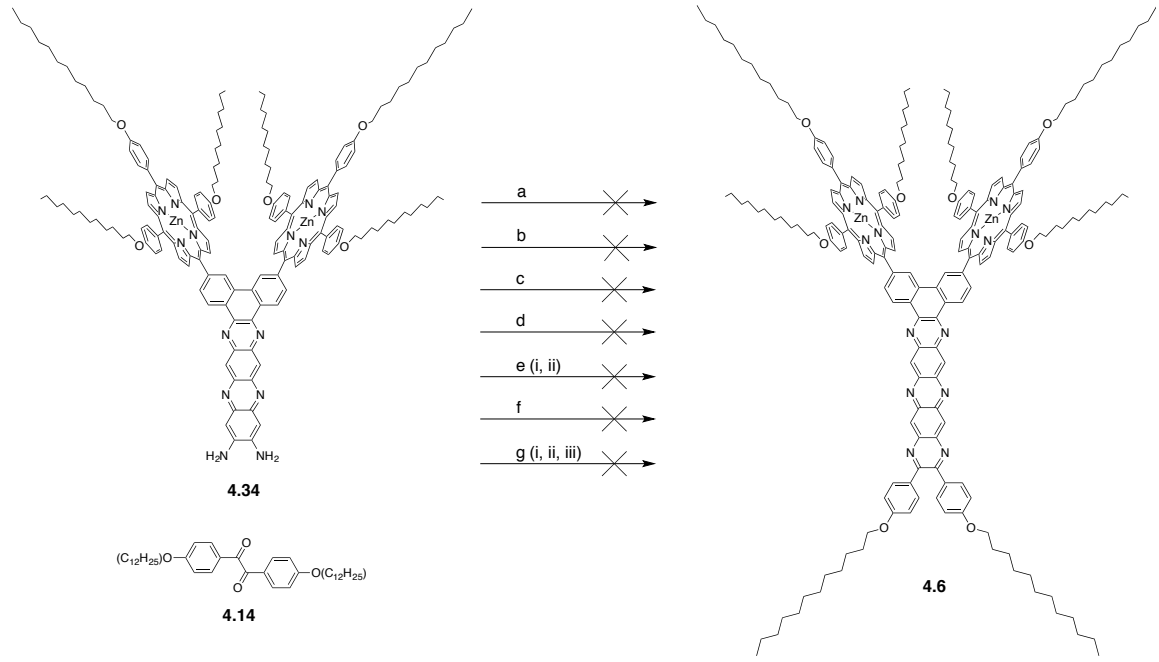

a) 1,2-Dichlorobenzene:EtOH:AcOH (2:2:1), reflux, overnight. **b)** $TsOH.H_2O$, toluene, reflux, overnight. **c)** I_2, DMSO:1,2-dichloroethane (5:3), RT (1day) $\rightarrow 100^oC$ (1 day). **d)** IBX, AcOH:1,1,2,2-tetrachloroehane (2:1), reflux overnight. **e) i** 1M HCl, **ii** NaOAc, 1,4-dioaxane, reflux, overnight. **f)** Pyridine, reflux, overnight. **g) i** DCM:TFA (1:1), 15min, RT. **ii** Toluene, 4N HCl, 1,4-dioxane, reflux, overnight **iii** pyridine, reflux, overnight.

The synthesis of **4.6** was not achieved. Numerous efforts to react **4.34** as shown in scheme 4.15 were attempted. None produced the desired compound in appreciable yield, if any traces were even detected. The literature was searched extensively for reactions in which quinoxaline functionality was produced from an aromatic *o*-diamine and an *o*-diketone. Every attempt made failed, which included acid catalyzed reactions employing AcOH, TsOH, IBX in AcOH and HCl (with zinc removed in a previous step) and base catalyzed reactions employing NaOAc or pyridine as the base. Efforts were even made to create the hydrochloride salt of **4.34** and subsequently conduct the reaction under basic conditions as for the synthesis of **4.3**.

With no success on this path, a similar strategy to that by which **4.2** was synthesized was attempted. This required synthesis of the dibromo wire core, **4.36**, as shown in scheme 4.16, prior to attachment of the porphyrins by Suzuki cross-coupling methodology.

Scheme 4.16

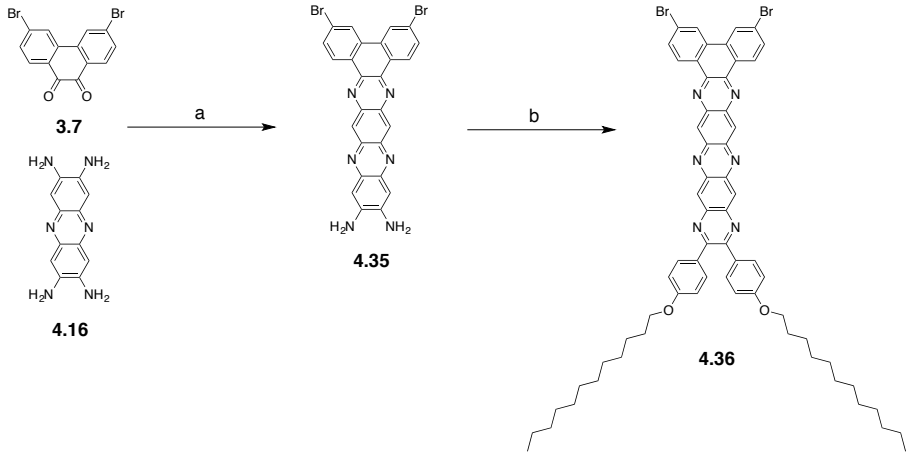

a) NaOAc, 1,4-dioxane, reflux, overnight, 97% yield. **b)** 4N HCl:THF:DMSO (2:7:20), reflux 48h.

While the synthesis of **4.35** proceeded simply, similarly to, and in an analogously high yield to the synthesis of **4.33**, the subsequent step to produce **4.36** was almost as tricky as that for the synthesis of **4.6** from **4.34**. A central problem was that **4.35** is largely insoluble in most common organic solvents. After numerous test reactions, a reaction employing a solvent system of THF and DMSO, to which 4N HCl was added and allowed to reflux for 2 days, produced the desired product, as was evidenced by MALDI-TOF mass spectrometry. From previous attempts at isolating **4.36** from test reactions, it was known to exhibit poor solubility in chlorinated solvents, but to be soluble in DMF. DMF is a difficult solvent to recover such products from, and while they

can be precipitated by addition of water or sometimes alcohols, filtration of DMF-H_2O mixtures can be very messy and time consuming. Consequently, attempt was not made to isolate and purify the product. The crude product obtained following isolation of a precipitated product by filtration and subsequent washing and drying showed a good presence of the product as determined by MALDI-TOF analysis. A Suzuki-coupling reaction was attempted in DMF but no traces of **4.6** could be detected. No further attempts were made to synthesize **4.6**.

Scheme 4.17

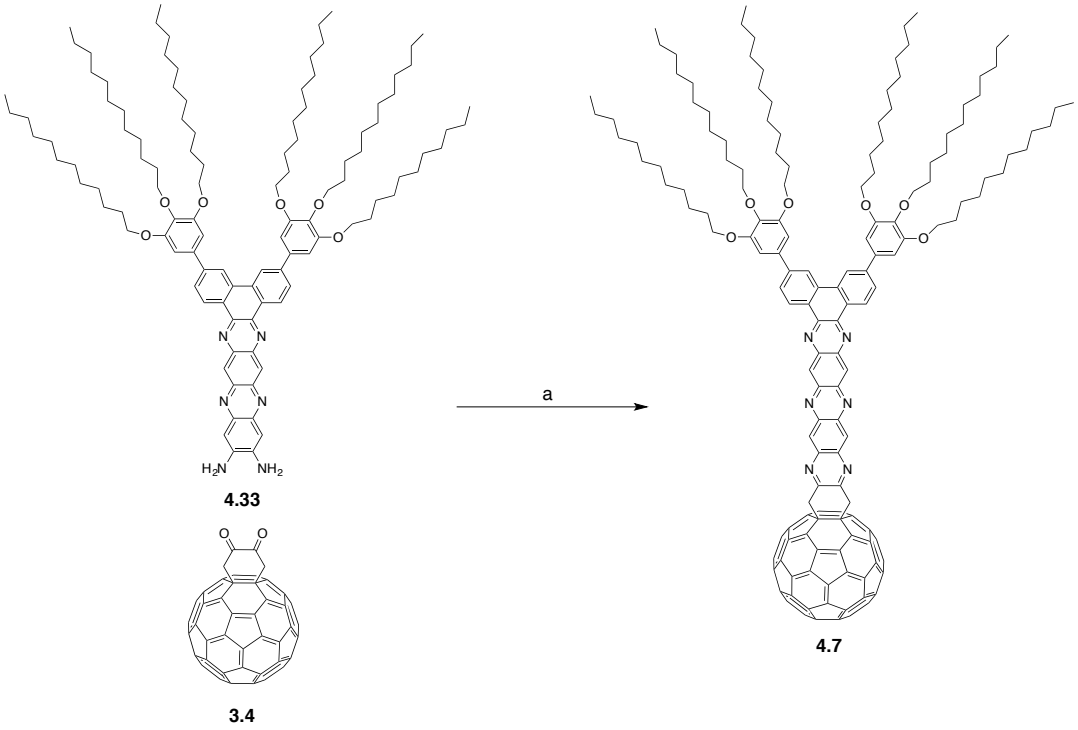

a) TsOH.H_2O, Toluene, reflux, overnight.

Scheme 4.17 shows the synthesis of **4.7**, which proceeds by simply condensing **4.33** with **3.4** in a TsOH catalyzed reaction in toluene. The product is soluble in dichloromethane and can be purified by silica gel chromatography with this solvent.

Scheme 4.18

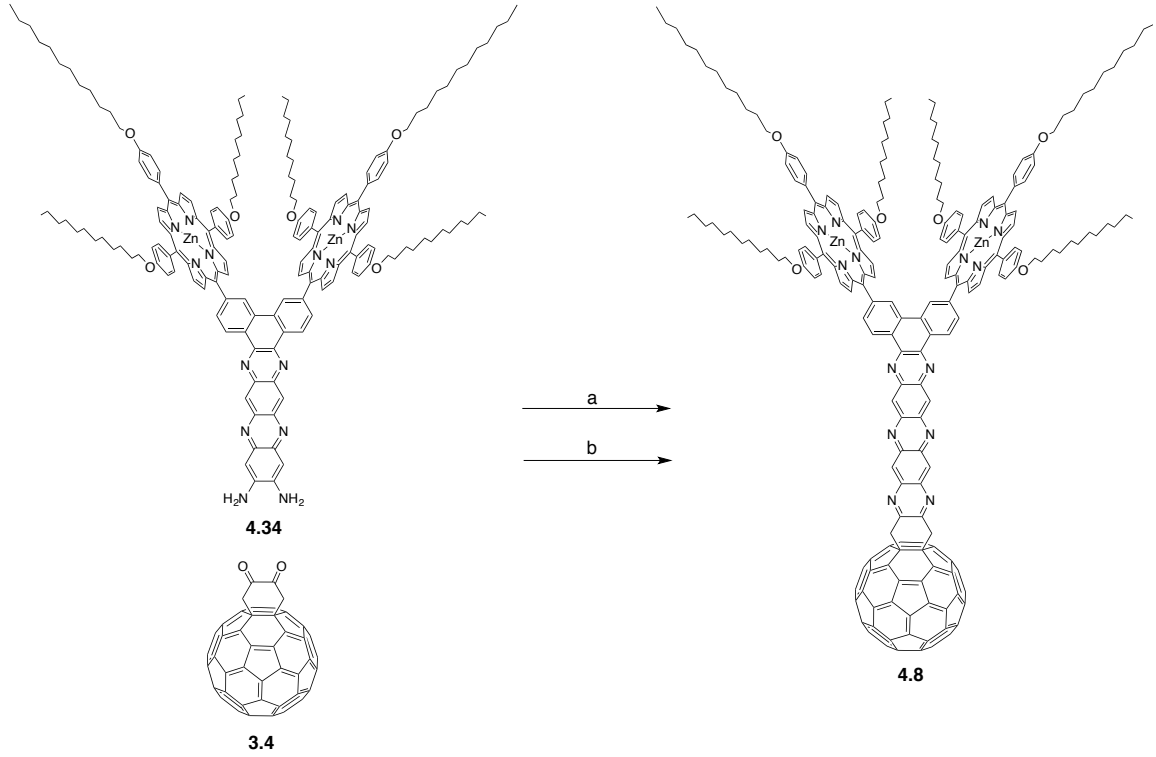

a) TsOH.H_2O, 1,2-dichlorobenzene:Toluene (2:1), reflux, overnight, 15% yield **b)** AcOH:1,2-dichlorobenzene:EtOH (1:2:1), reflux, 16 h, no yield determined.

Two methods for the synthesis of **4.8** were conducted as shown in scheme 4.18. These were a TsOH catalyzed reaction conducted in 1,2-dichlorobenzene and an acetic acid catalyzed reaction in 1,2-dichlorobenze and ethanol, again used to inhibit formation of the problematic acetic acid adduct. Both reactions produced the product in poor yield, and as a result of the small scale on which the second reaction (scheme 4.18.b) was conducted, a yield of the pure isolate obtained after extensive processing was in no way a representation of the yield of the reaction. NMR characterization of the product was not possible as a result of what appears to be extensive aggregation. Further work must be conducted to obtain higher quantities of **4.8** for attempts at making single crystals for

conclusive characterization. At this stage, MALDI-TOF mass spectral data and the acquired UV-Vis. spectra serve as the only evidence for the synthesis of **4.8**.

It is thought that the electron withdrawing nature of the phenazine core employed in the molecules of series B reduce the nucleophillicity of the terminal amines which results in diminished reactivity with *o*-diketones and consequently, the lower yields observed.

4.5 Synthesis of Series C

Unlike the synthesis of the molecules of series B, those of series C were synthesized simply and obtained in good yield. It is thought that the cross-conjugated pyrene center in **3.3** breaks up the conjugation, and so, despite the presence of two pyrazine rings in **3.3** and three pyrazine rings in the single condensation products of **3.3** with *o*-diketones, the pyrene center acts to isolate the electron withdrawing effect of the pyrazine structures on either side of it, minimizing the cumulative electron withdrawing effect that would otherwise result. Consequently, the nucleophillicity of structures synthesized from **3.3** does not appear to be as diminished as for those synthesized from **4.16**. Essentially, the terminal amines if **3.3** behave more like those of **4.29** and less like those of **4.33**. This is encouraging since the goal of this work is to make steps towards synthesizing considerably large architechtures of long heteroaromatic wires functionalized with many chromophores, the excited electrons of which could be collected by these wires and transmitted to an electrode. If the cumulative electron-withdrawing effect of the pyrazine rings present within longer and longer ribbons

increasingly diminished the nucleophilicity of the terminal amines, then the synthesis of such structures would not be possible.

Scheme 4.19

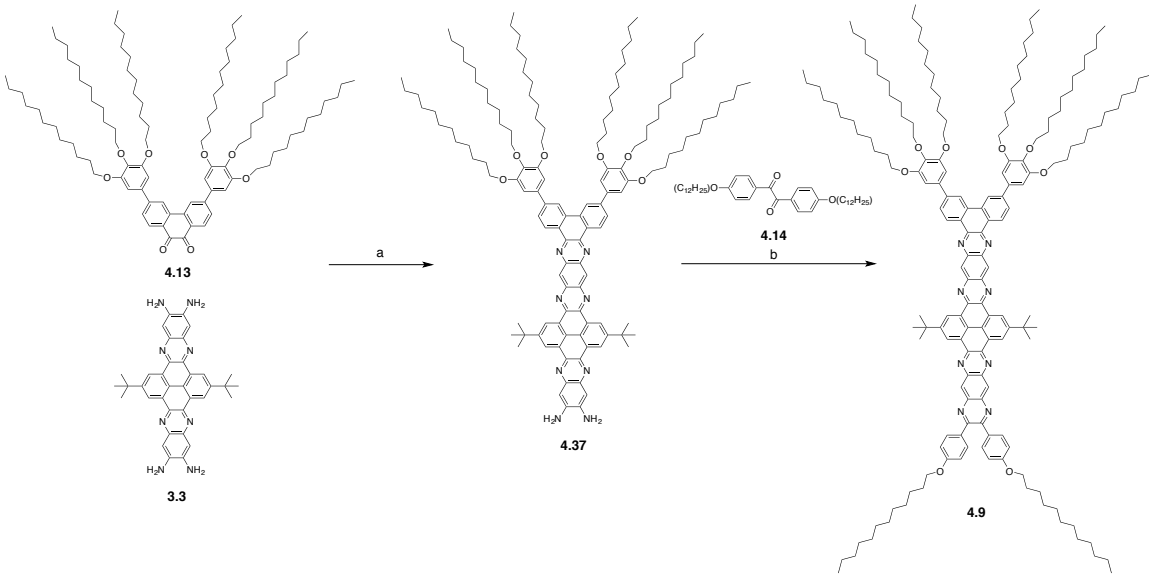

a) AcOH:EtOH:1,2-dichlorobenzene (1:2:2), reflux, 3.5 h, 56% yield. **b)** $TsOH.H_2O$, 1,2-dichlorobenzene, reflux, overnight, 75% yield.

The favorable reactivity of **3.3** is exemplified by the synthesis of **4.9**, as shown in scheme 4.19. **4.37** Was produced by an acetic acid catalyzed reaction of **4.13** with **3.3** in 56% yield. **4.37** Was then reacted with **4.14** in 1,2-dichlorobenzene using TsOH as the acid catalyst. A good yield of 75% was achieved, which is notably better than that for the first step to produce **4.37**, which employed the solvent system developed in chapter 3 of this work.

Scheme 4.20

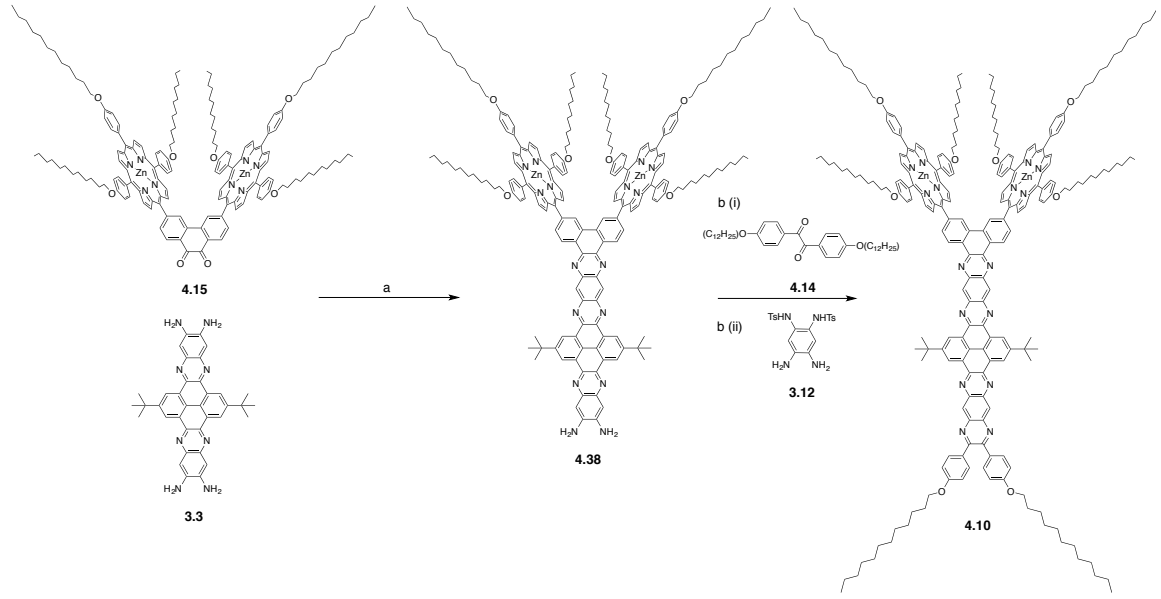

a) AcOH:EtOH:1,2-dichlorobenzene (1:2:2), 100^{o}C (pressure tube), overnight, 70% yield. **b) ii** AcOH:1,2-dichlorobenzene (3:4), 80^{o}C, overnight. **ii** AcOH:1,2-dichlorobenzene (3:4), 80^{o}C, overnight, yield not determined.

The synthesis of **4.10** proceeded simply too, distinct from the remarkable difficulty experienced in synthesizing the analogous compounds of series A and B. First, **4.15** was condensed with **3.3** in an acetic acid catalyzed reaction. The reaction was carried out in a pressure tube sealed with a Teflon screw cap at 100^{o}C. The higher internal temperature achieved in this manner was a concern as extra energy would be available for the acetic acid adduct to form. This was not the case and implies that the presence of ethanol in solution does not inhibit the undesirable acetic acid adduct from forming simply by virtue of its lower boiling point. It must have something to do with ethanol being a polar, protic solvent. The second condensation, that of **4.38** with an excess of **4.14** to produce **4.10**, required an additional step to facilitate effective

purification. The product, **4.10** coeluted with the remaining **4.14**. Consequently an excess of **3.12** was added to condense with the unreacted **4.14** present in solution. The tosyl groups present on **3.12** exhibit a strong affinity for silica gel, and consequently, retard the motion of the product obtained from reaction of **3.12** with **4.14**. Performing this second reaction enabled isolation of **4.10** free of **4.14**. Despite this additional reaction, the synthesis of **4.10** was markedly simpler than the attempts at producing the series B analog **4.6**.

Scheme 4.21

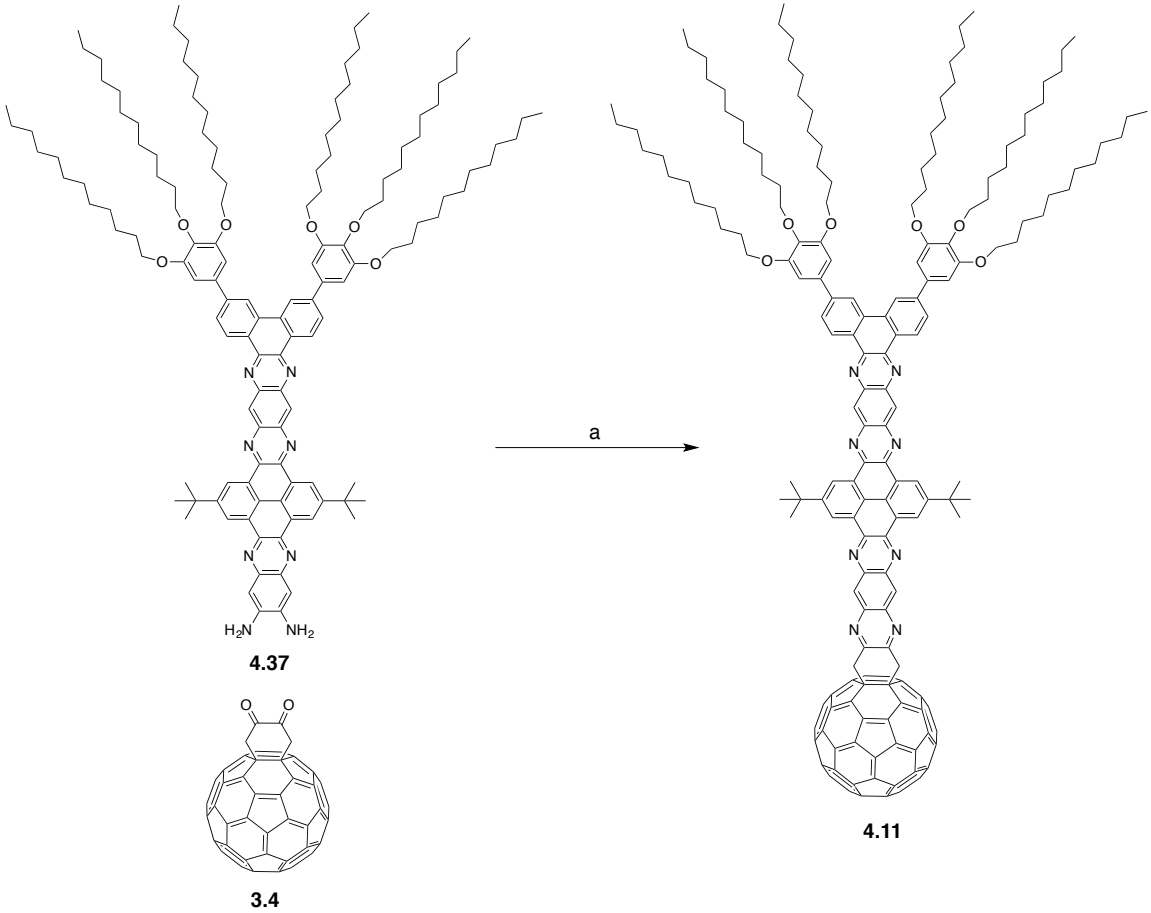

a) $TsOH.H_2O$, 1,2-dichlorobenzene, 100°C, 42% yield.

Having already synthesized **4.37**, **4.11** was obtained by adding an excess of **3.4** to a solution of 1,2-dichlorobenzene containing **4.37**. The reaction was catalyzed by TsOH. The yield obtained was low, 42%, which may be as a result of the comparably lower temperature at which the reaction was conducted, 100^{o}C, as opposed to that used for the synthesis of **4.10** (reflux, 181^{o}C).

Scheme 4.22

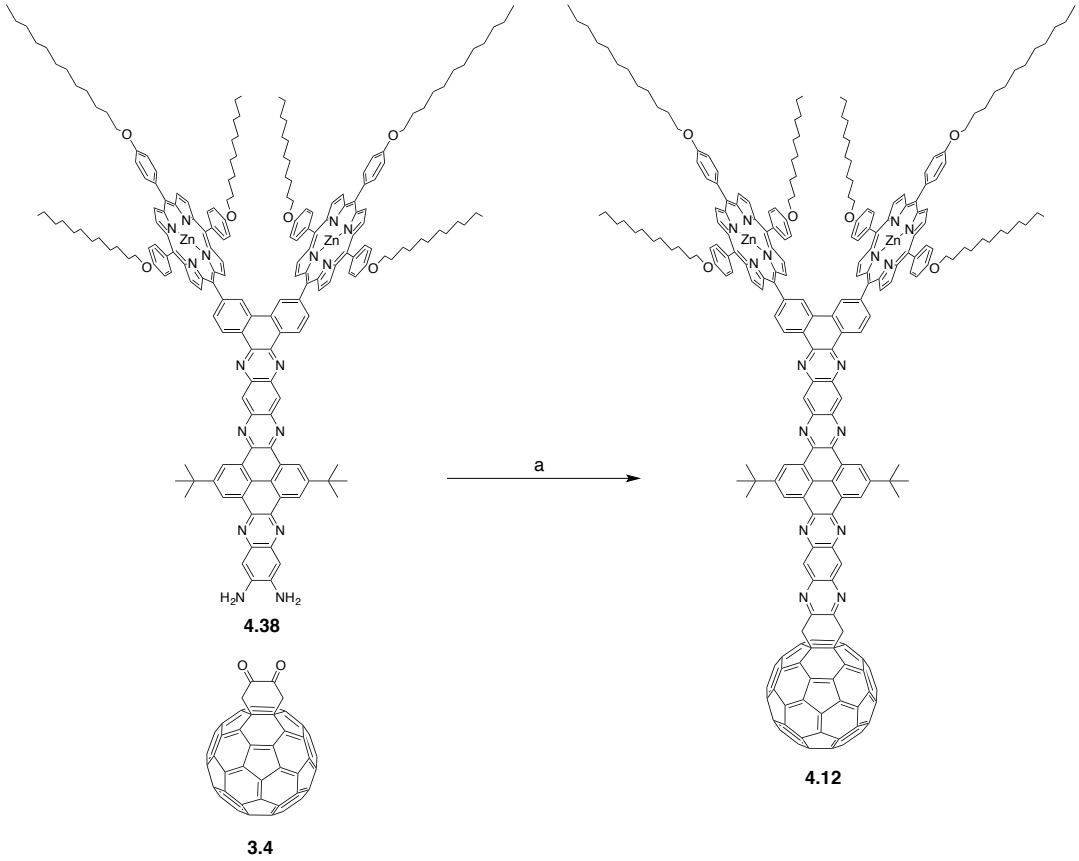

a) 1,2-dichlorobenzene:AcOH: EtOH (2:1:1), reflux, 18h.

Finally, the key compound of series C was synthesized by condensing **4.38** with **3.4** in an acetic acid catalyzed reaction. The product was difficult to purify and the compound obtained in pure form was not in any way an actual representation of the true

reaction yield. NMR characterization of **4.12** proved very difficult and despite efforts to characterize **4.12** in CS_2 spiked with 1,1,2,2-tetrachloroethane-D2, employing a 850MHz NMR spectrometer, considerable peak broadening, most likely due to aggregation, prevented characterization by this method. Many efforts were made to grow single crystals of **4.12**. While some success in growing small single crystals from dichloromethane was achieved, the crystals were too small or too delicate to mount effectively. The synthesis of **4.12** needs to be repeated to obtain higher yields for growing larger crystals or the design modified to substitute the *t*-butyl groups present on the pyrene core with bis(*ortho*-dodecyloxy)benzene groups that could potentially inhibit aggregation by wrapping the aromatic wire core with a small "grease" layer.

4.6 UV-Vis spectra of Compounds of Series A, B and C

Figure 4.5 shows the normalized UV-Vis absorption spectra of the wire model compounds of series A, B and C, **4.1**, **4.5** and **4.9** together with the emission spectra adjusted to the value of the lowest energy absorption. It was expected that with increasing length of the "wire" molecules, the lowest energy transitions would occur at longer and longer wavelengths. This is not observed with **4.5**, which is of intermediate length, but exhibits the lowest energy transition. This is a very encouraging result and may be explained by the presence of the pyrene cross-conjugating center present in **4.9**, which breaks up the full conjugation of the fused heteroaromatic core, causing it to exhibit a lowest energy transition that is at shorter wavelengths than expected.

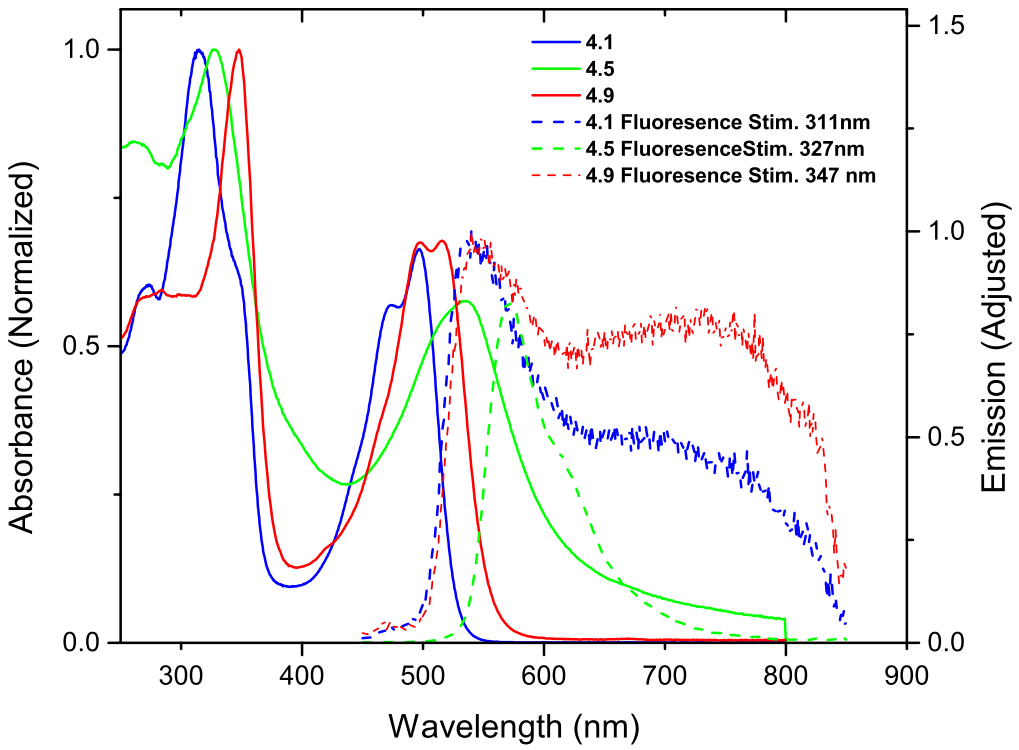

Figure 4.5. Normalized UV-Vis and fluorescence spectra of model compounds **4.1**, **4.5** and **4.9** in dichloromethane.

The values for the HOMO-LUMO gaps determined from the intersection of the absorption and emission spectra are shown in table 4.1. The difference in E_{gap} between **4.1** and **4.5** is 0.11eV in which **4.5** is two fused aromatic units longer than **4.1** while that between **4.1** and **4.9** is only 0.06eV despite **4.9** being five fused aromatic units longer.

Table 4.1
Lowest energy absorption values of wire model compounds **4.1**, **4.5** and **4.11** in dichloromethane

Compound	λ_{abs} [a] (nm)	E_{gap} [b] (nm)	E_{gap} [b] (eV)
4.1	496.7	514.8	2.41
4.5	533.9	558.9	2.30
4.11	516.6	527.7	2.35

a. Lowest energy absorption maximum *b*. Calculated from intersection of Absorption and emission spectra

The model compound **4.6** could not be synthesized. Nonetheless the UV-Vis absorption spectra of other two porphyrin-wire model compounds, **4.2** and **4.10** in dichloromethane are shown in figure 4.6 below. The absorption spectra have been normalized to the prominent Soret transition of the porphyrins. The characteristic wire absorptions shown in figure 4.5 are considerably broadened, though still present.

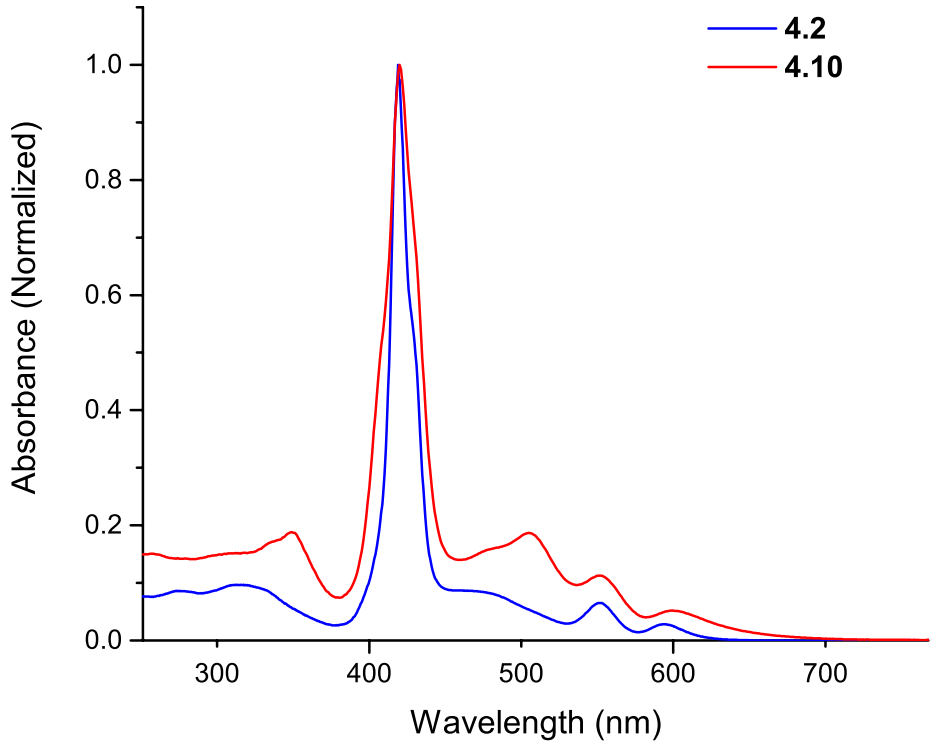

Figure 4.6. UV-Vis spectrum of **4.2** and **4.10** in dichloromethane normalized at the Soret band of the porphyrins.

Figure 4.6 shows the UV-Vis absorption spectra for the Wire-C_{60} model compounds **4.3**, **4.7** and **4.11** in dichloromethane. The spectra have been normalized at the highest energy transition characteristic of fullerene absorption. Again the lower energy transitions characteristic of the fused heteroaromatics are markedly broadened in comparison to those obtained for the compounds free of C_{60} shown in figure 4.4.

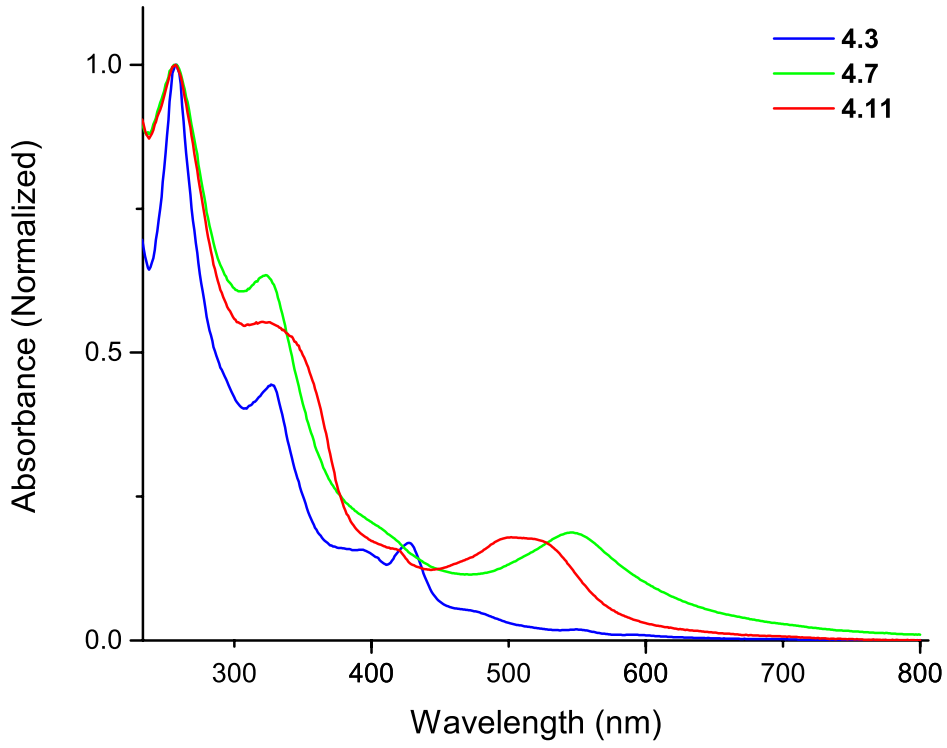

Figure 4.7 UV-Vis absorption spectra of **4.3**, **4.7** and **4.11** normalized to the highest energy transition of C_{60} present.

Finally, figure 4.7 shows the UV-Vis absorption spectra of the complete P-Wire-C_{60} compounds **4.4**, **4.8** and **4.12** shown in dichloromethane. The spectra are normalized at the Soret transition of the porphyrins on the respective D-W-A compounds. The absorption spectra are dominated by the characteristic transitions of the porphyrins and C_{60} moieties present for compounds **4.4** and **4.12**. The spectrum obtained for **4.8** is strange with a dominant absorption at 316nm, which is blue shifted 7nm relative to the same absorption of the free wire **4.5** at 323nm. The corresponding transitions in **4.4** and **4.12** are less intense than those of the respective Soret bands of each molecule.

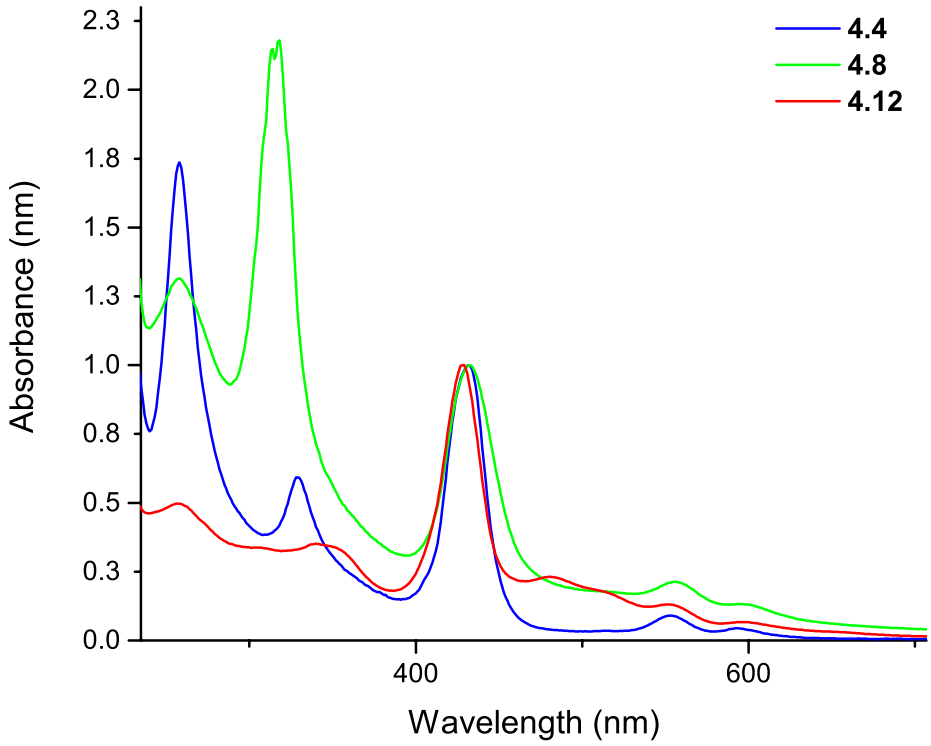

Figure 4.8 UV-Vis absorption spectra of the three P-Wire-C_{60} compounds **4.4**, **4.8** and **4.12**.

4.7 Materials and Methods

4.7.1 General

Dichloromethane, chloroform, hexanes, ethyl acetate, tetrahydrofuran, methanol and toluene were purchased from BDH. 200 PROOF ethanol was purchased from KOPTEC. DMF was purchased from Alfa Aesar and stored over sieves prior to use. 1,2-dichlorethane was purchased from Macron and stored over sieves. Carbon disulfide, 1,2-dichlorobenzene and 1,4-dioxane were purchased from Sigma-Aldrich. Solvents were

used without purification unless stated otherwise. Tetrahydrofuran was distilled over CaH under argon. Pyrrole, 4,4,5,5-trimethyl-1,3,2-dioxaborolane and 1,2,4,5-tetraaminobenzene tetrahydrochloride starting materials were purchased from Sigma-Aldrich. 1-bromo-3,4,5-trimethoxybenzene, 1-bromododecane, trimethylborate and *p*-dodecyloxybenzaldehyde were obtained for Alfa Aesar. 4,4'-dimethoxybenzil, 2-isopropoxy-4,4,5,5-tetramethyl-1,3,2-dioxaborolane and 3,4,5-trimethoxyphenylboronic acid were procured from Combi-Blocks. Et_3N and 1.6M *n*-butyllithium reagents were obtained from Alfa Aesar. $TsOH.H_2O$, *N*-bromosuccinimide, 2,3-dicholoro-5,6-benzoquinone, $BF_3.OEt_2$, $Pd(PPh_3)_4$, $Pd_2(PPh_3)_2Cl_2$, Cs_2CO_3, BBr_3 and Pyr.HCl reagents were purchased from Sigma Aldrich. Silica for silica gel chromatography was purchased from Silicycle.

Matrix assisted laser desorption/ionization time of flight (MALDI-TOF) mass spectra were acquired using an Applied Biosystems Voyager-DE STR workstation and acquired in reflector mode using terthiophene, diphenylbutadiene or dithranol as the matrix. NMR spectroscopy was conducted using a Varian (Agilent) MR 400 MHz NMR spectrometer operating at a 1H Lamor frequncy of 399.87 MHz, equipped with a 5 mm Broadband Observe Z-gradient probe. UV-Vis spectra were acquired using a Shimadzu UV-2550 UV-Visible spectrophotometer.

4.7.2 Synthesis of Compounds

4.1. A 100ml RBF containing a magnetic stirrer bar was charged with **4.29** (53mg, 0.0338mmol), **4.14** (58.7mg, 0.1014mmol), 1,4-dioxane (18ml), AcOH (0.4ml)

and DCM (4ml). The solution was heated to reflux for 20h. On cooling, the solution was concentrated *in vacuo* and the residue purified by silica gel chromatography using DCM:Hex (7:3) as the eluent. Several columns are necessary to effectively separate unreacted **4.14** from the product. 36.5mg (0.0173mmol, 51%) of **4.29** was obtained as a waxy orange residue. ^{1}H NMR (400 MHz, 1,1,2,2-tetrachloroethane-*d*2): δ 9.53 (d, J = 8.32, 2H), 9.23 (s, 2H), 8.73 (s, 2H), 8.00 (d, J = 8.6 Hz, 2H), 7.64 (d, J =8.6Hz, 4H), 6.98 (s, 4H), 6.96 (d, J = 8.8Hz, 4H), 4.12 (t, J = 6.2 Hz, 8H), 4.5 (m, 8H), 1.84 (m, 16H), 1.53 (m, 16H), 1.42-1.20 (m,128H), 0.89 (m, 24H). ^{1}H NMR (100 MHz, $CDCl_3$): δ 161.34, 160.50, 154.97, 153.81, 144.52, 144.32, 141.63, 140.32, 138.88, 136.41, 132.89, 132.50, 131.67, 131.45, 129.43, 128.24, 127.72, 114.85, 114.50, 106.62, 73.84, 69.62, 68.31, 64.28, 34.19, 33.00, 32.11, 32.09, 32.07, 30.61, 29.96, 29.95, 29.94, 29.89, 29.88, 29.85, 29.84, 29.81, 29.78, 29.77, 29.72, 29.70, 29.67, 29.64, 29.60, 29.57, 29.54, 29.52, 29.49, 29.40, 29.34, 28.93, 26.38, 26.22, 25.97, 22.87, 22.85, 22.84. MS (MALDI-TOF): m/z obsd 2110.9957 $[M+H]^+$, calcd 2110.7004.

4.2 An oven dried pressure tube containing a magnetic stirrer bar was charged with **4.28** (200mg, 0.156mmol) dissolved in 80ml of freshly distilled THF, **4.32** (63mg, 0.0624mmol), Cs_2CO_3 (61mg, 0.1872mmol) and deoxygenated with bubbling argon for 20min. $Pd(PPh_3)_4$ (14.4mg, 0.0125mmol) was added, the tube filled with argon, sealed and heated to internal reflux to stir overnight. On cooling, the solution was concentrated and the residue purified by silica gel chromatography first using DCM:Hex. (2:1) for the first column and then DCM:Hex. (6:4→7:3→9:1→ 1:0) as the eluent for the second column. Fractions containing pure **4.2** were pooled yielding 37.5mg (0.0119mmol, 20%) of a purple residue. ^{1}H NMR (400 MHz, 1,1,2,2-tetrachloroethane-*d2*): δ 9.98 (s,2H),

9.48 (s,2H), 9.06 (s, 4H), 8.91 (m, 12H), 8.74 (s, 2H), 8.06 (m, 8H), 7.87 (s, 4H), 7.70 (d, *J* = 8.3Hz, 4H), 7.22 (s, 8H), 7.10 (s, 4H), 6.99 (d, *J* = 8.6Hz, 4H), 4.18 (m, 12H), 4.06 (t, *J* = 6.2Hz, 4H), 1.94 (m, 12H), 1.86 (m, 12H), 1.65 (m, 4H), 1.59 (m, 12H), 1.31 (m, 128H), 0.91 (m, 24H). MS (MALDI-TOF): m/z obsd 3153.8053 $[M]^+$, calcd 3153.8609.

4.3 To a 100ml RBF containing 1,2-dichlorobenzene (15ml), EtOH (4ml), and AcOH (1ml), **4.22** (59.7mg, 0.0381mmol) and **3.13** (61.2mg, 0.0761mmol) were added and the flask fitted with a reflux condenser. The solution was heated to reflux and left to stir at that temperature overnight. On cooling, 80ml MeOH was added to the solution, causing precipitation, and the precipitant isolated by filtration through a pad of celite. The isolated precipitant was redissolved using dichloromethane and concentrated. The residue was taken up in toluene, loaded onto the top of a silica gel column and eluted with toluene. MS (MALDI-TOF): m/z obsd 2335.1412 $[M]^+$, calcd 2335.2802.

4.4 as per scheme 4.12.a 1,2-dichlorobenzene (5ml), EtOH (2.5ml) and AcOH (2.5ml) were added to a 100ml RBF containing a residue of **4.30** (10mg, 3.82μmol). **3.4** (15mg, 19.11μmol) was added and the solution heated to reflux overnight. On cooling, 90ml of MeOH was added causing precipitation of the product. The precipitant was isolated by filtration through a pad of celite and redissolved in a 1:1 solution of DCM and CS_2, and concentrated. Analysis of the crude product my MALDI-TOF MS revealed that some of the desired product was present without Zn in a porphyrin macrocycle. Consequently, the residue was taken up in 50ml DCM and $Zn(AcO)_2.2H_2O$ (84mg, 0.038mmol) in 1ml was added and the solution heated to reflux overnight. The soltion was then concentrated to 50% volume and 75ml MeOH added. The precipitant formed was isolated by filtration though a pad of celite and recovered using DCM. The DCM

filtrate was concentrated, taken up in DCM:CS_2:Hex. (2:2:1) and purified by silica gel chromatography using DCM:CS_2:Hex. (2:2:1→ 1:0:0) as the eluting solvent. Concentration of relevant fraction afforded (9.4mg, 2.78μmol,73%). MS (MALDI-TOF): m/z obsd 3379.3710 $[M]^+$, calcd 3379.4529.

4.4 as per scheme 4.12.b 1,2-Dichlrobenzene (20ml) and EtOH) 5ml was added to a 100ml RBF containing a residue of **4.30** (43mg, 0.0164mmol). TsOH.H_2O (1.5mg, 0.00822mmol) and **3.4** (0.0661g, 0.0822mmol) were added and the solution heated to reflux under argon for 18h. Following reaction, the solution was concentrated and taken up in neat DCM and purified by silica gel chromatography. Concentration of relevant fraction afforded 47.5mg (0.014mmol, 85%) of **4.4** as a purple residue. ^{1}H NMR (400 MHz, 1,1,2,2-tetrachloroethane-*d2*, 110^{o}C): δ 10.23 (m, 2H), 9.44 (s, 2H), 9.14 (bs, 4H), 9.05 (d, J = 6.5Hz, 2H), 8.80 (m, 12H), 8.44 (s, 2H), 8.45 (s, 2H), 8.33-7.54 (m, 12H), 7.54-7.09 (m, 12H), 4.32 (m, 12H), 2.06 (m, 12H), 1.88-1.11 (m, 96H), 0.96 (m,18H). MS (MALDI-TOF): m/z obsd 3379.2382 $[M]^+$, calcd 3379.4529.

4.5 A magnetic stirrer bar was added to a RBF containing a residue of **4.33** (0.109g, 65,3 μmol) along with **4.14** (0.0756g, 0.131mmol), TsOH.H_2O (1mg, 5.27μmol) and Toluene (20ml). The flask was fitted with a reflux condenser and the solution heated to reflux for 4 days. On cooling, 50ml toluene was added and the solution washed with sat. $NaHCO_3$ solution and the organic layer concentrated and dried on hi-vac. The purple residue was taken up in DCM and purified by silica gel chromatography using DCM/1% MeOH as the eluting solvent. Concentration of relevant fractions afforded 70.7mg (31.9μmol, 49%) of a waxy purple residue. MS (MALDI-TOF): m/z obsd 2211.7482 $[M]^+$, calcd 211.7144.

Trial syntheses of 4.6:

4.6 as per Scheme 4.14(a) To a 100ml RBF containing a magnetic stirrer bar, **4.34** (34.7mg, 12.8μmol), **4.14** (36.95mg, 63.8μmol), 1,2-dichlorobenzene (10ml), AcOH (5ml) and EtOH (10ml) were added, the flask fitted with a reflux condensor and heated to reflux overnight. MALDI-TOF MS analysis revealed that no product had been formed.

4.6 as per Scheme 4.14(b) To a 100ml RBF containing a magnetic stirrer bar, **4.34** (315mg, 5.52μmol), **4.14** (6.4mg, 1.1μmol), $TsOH.H_2O$ (0.2mg, 1.1μmol) and toluene (10ml) were added, the flask fitted with a reflux condensor and heated to reflux overnight. MALDI-TOF MS analysis of the crude reaction solution revealed that no product had been formed.

4.6 as per scheme 4.14(c) To a 100ml RBF containing a magnetic stirrer bar, **4.34** (15.3mg, 5.63μmol), **4.14** (19.5mg, 33.77μmol), 1,2-dichloroethane (3ml) and DMSO (5ml) were added and the solution sonicated to ensure dissolution of reactants. I_2 (18mg) was added and the solution allowed to stir at RT for 1 day. MALDI-TOF MS analysis of the crude reaction solution revealed that no product had been formed. Subsequently, the temperature was raised to 100^oC and allowed to stir for 1 day at that temperature. Analysis of the crude solution again revealed no product formation.

4.6 as per scheme 4.14(d) To a 100ml RBF containing a magnetic stirrer bar, **4.34** (34.4mg, 12.7μmol), **4.14** (7.3mg, 12.7μmol), 1,1,2,2-tetrachloroethane (2.5ml) and AcOH (5ml) were added successively and the solution sonicated to ensure dissolution of reactants. 40% w/w IBX (0.2mg, 0.8μmol) was added and the solution heated to reflux and left to stir overnight. MALDI-TOF MS analysis of the crude reaction solution following this period revealed that no product had been formed.

4.6 as per scheme 4.14(e) **4.34** (19.4mg, 7.14μmol) present as a residue within a 100ml RBF was taken up in THF 5ml. 1M HCl (2ml) was added and the mixture allowed to stir for 30minutes. The solution was concentrated *in vacuo* and dried on hi-vac. overnight. NaOAc (1.2mg, 14.3μmol) and 1,4-dioxane (5ml) was added and the solution heated to reflux overnight. MS (MALDI-TOF) analysis of the crude reaction mixture revealed no product had been formed.

4.6 as per scheme 4.14(f) To a 100ml RBF containing a magnetic stirrer bar, **4.34** (14mg, 5.15μmol), **4.14** (30mg, 51,5μmol) and pyridine (10ml) were added, the flask fitted with a reflux condensor and the solution heated to reflux and left to react overnight. MS (MALDI-TOF) analysis of the crude reaction mixture revealed no product had been formed.

4.6 as per scheme 4.14(g) To a 100ml RBF containing **4.34** (97.4mg, 35.83μmol) as a residue, DCM (20ml) and TFA (20ml) were added successively and left to stir at RT for 15min. The dark green solution was transferred to a separating funnel, diluted with DCM (50ml) and washed with water (200ml). The organic layer was collected and transferred to a RBF and 12M HCl (1ml) was added and concentrated *in vacuo* and dried on hi-vac overnight. **4.14** (30mg, 51.8μmol) and toluene (30ml) were added, the flask fitted with a reflux condenser and heated to reflux overnight. MS (MALDI-TOF) analysis of the crude reaction mixture revealed no product had been formed at this point. A solution of 1:1 4N HCl (1ml) was added allowed to reflux overnight. Again, MS (MALDI-TOF) analysis of the crude reaction mixture revealed no product had been formed. Consequently, 4ml pyridine was added and again left to reflux overnight.

4.7 To 100ml RBF containing **4.33** (58mg, 34.7μmol) as a residue, toluene (10ml), **3.13** (55.8mg, 69.4μmol) and finally $TsOH.H_2O$ (0.7mg, 3.5μmol) were added. The flask was fitted with a reflux condenser and heated to reflux with stirring overnight. On cooling, the solution was diluted with 80ml toluene, washed with sat. $NaHCO_3$ (aq.) and the organic layer collected and concentrated *in vacuo*. The residue was taken up in DCM and purified by silica gel chromatography. MS (MALDI-TOF): m/z obsd 2437.8988 $[M]^+$, calcd 2437.3021.

4.8. 40mg (14.7μmol) Of **4.34**, 42mg (52.2μmol) of **3.4**, 1,2-dichlorobenzene (5ml), toluene (10ml) were added to a RBF containing a magnetic stirrer bar. 10mg (52.57μmol) $TsOH.H_2O$ was added and the solution heated to reflux overnight. On cooling, the solution was diluted with 60ml toluene and washed with sat. $NaHCO_3$ (aq.) and concentrated. MALDI-TOF MS analysis revealed that demetallation of some of the product had occurred. The residue was thus taken up in 20ml DCM and a small spatula-tip of $Zn(AcO)_2.2H_2O$ was added in 2ml of MeOH. The solution was heated to reflux for 5h, cooled, washed with water and concentrated. The residue was purified by silica gel chromatography using DCM→ DCM/1%MeOH as the eluting solvent yielding 7.7mg (2.21μmol, 15% yield). MS (MALDI-TOF): m/z obsd 3482.3919 $[M+H]^+$, calcd 3482.4853.

4.9. 18mg (9.1μmol) of **4.37** and 26.37mg (45.5μmol) of **4.14** was added to a RBF containing 5ml toluene. 2mg (10.5μmol) was added and heated to reflux overnight. On cooling, the solution was concentrated *in vacuo* and the product purified by silica gel chromatography using DCM/1→3% MeOH as the eluting solvent. Yield: 17.5mg (6.86μmol, 75%). MS (MALDI-TOF): m/z obsd 2551.0734 $[M+H]^+$, calcd 2550.9007.

4.10 A 100ml RBF containing 33mg(10.8μmol) of **4.38** was charged with 4ml of 1,2-dichlorobenzene, 3ml AcOH and 64.2mg (110.91μmol) of **4.14**. The flask was heated to 80^{o}C and left to stir overnight at that temperature. In the morning the solution was concentrated *in vacuo* and dried on hi-vac.. A first attempt was made to isolate the product by silica gel chromatography but attempts were futile due to co-elution of unreacted **4.14** with the product. Fractions containing the desired product were concentrated down and isolated as a residue in a 100ml RBF. 44.7mg of **3.9** was added followed by the 20ml of 1,2-dichlorobenzen:AcOH:EtOH (2:1:1) . The solution was heated to 100^{o}C and left to stir overnight. Concentration *in vacuo* and purification by silica gel chromatography employing DCM:Hexanes (3:2→9:1) afforded a purple residue. MS (MALDI-TOF): m/z obsd 3595.3022 $[M+H]^+$, calcd 3595.079.

4.11 To a 100ml RBF containing 22mg (11μmol) **4.37**, 5ml of 1,2-dichlorobenzene, 44.3mg (55μmol) of **3.4** and 5mg (26.29μmol) TsOH.H_2O were added. The solution was heated to 100^{o}C and left to stir overnight. On cooling, 20mg (0.244mmol) NaOAc was added and the reaction was left to stir for 2 hours, subsequently concentrated *in vacuo* and dried on hi-vac. overnight. The residue was then taken up in CS_2 and purified by silica gel chromatography employing CS_2/10% EtOAc as the eluting solvent, yielding 12.9mg (4.64mmol, 42%) of an orange/brown residue. MS (MALDI-TOF): m/z obsd 2775.4612 $[M]^+$, calcd 2775.4810. (overlap of $[M]^+$ and $[M+H]^+$ observed).

4.12 **4.38** (0.201g, 33.6μmol), **3.4** (0.135g, 0.168mmol) were added to a 100ml RBF containing a magnetic stirrer bar followed by 1,2-dichlorobenzene (20ml), EtOH (10ml) and AcOH (10ml). The flask was fitted with a reflux condenser and heated to

reflux overnight (18h) with stirring. On cooling, 50ml MeOH was added, promoting precipitation. The precipitant was isolated by filtration through a celite pad. The precipitant was recovered using CS_2 and the filtrate concentrated. The residue was taken up in DCM and purified by silica gel chromatography once using DCM as the eluting solvent and a second time using toluene:CS_2:Hexanes (6:1:3). Concentration of relevant fractions afforded a purple/brown residue.

4.13 as per **scheme 4.2**. An oven dried pressure tube was charged with **4.18** (3.63g, 4.738mmol), **4.20** (0.545g, 1.184mmol), Cs_2CO_3 (1.157g, 3.552mmol) and 90ml dry THF. Argon was bubbled through the solution for 20min prior to addition of $Pd(PPh_3)_4$ (0.342g, 0.296mmol). The tube was sealed with a Teflon screw cap, heated to 90^oC and left to stir at that temperature overnight. On cooling the reaction solution was concentrated *in vacuo* and the product isolated in pure form by silica gel chromatography (eluent:DCM:Hexanes = 7:3) yielding 0.561g, 0.3826mmol, 32%). ^1H NMR (400 MHz, $CDCl_3$): δ 8.22 (d, J = 8.1Hz, 2H), 8.15 (s, 2H), 7.60 (d, J = 8.7Hz, 2H), 6.83 (s, 4H), 4.06 (m, 12H), 1.84 (m, 12H), 1.51 (m, 12H), 1.42-1.97 (m, 96H), 0.88 (m, 18H). ^{13}C NMR (100 MHz, $CDCl_3$): δ 180.17, 153.86, 149.39, 139.62, 136.18, 135.06, 131.21, 129.87, 128.56, 122.68, 106.40, 73.83, 69.65, 32.09, 32.07, 30.55, 29.91, 29.90, 29.96, 29.81, 29.78, 29.64, 29.62, 29.54, 29.51, 26.31, 26.31, 22.84, 22.83, 14.24. MS (MALDI-TOF): m/z obsd 1466.2366 $[M+H]^+$, calcd 1466.2186.

4.13 as per **scheme 4.2** 0.414g of the mixture from demethylation of **4.21** was placed in an oven-dried RBF containing a magnetic stirrer bar along with K_2CO_3 (1.504g, 10. 885mmol), DMF (100ml) and 1-Br-dodecane (1.742ml, 7.257mmol) and heated to 70^oC to be stirred at that temperature overnight. Following the reaction period, the

solution was added to a separating funnel along with 500ml H_2O, extracted with EtOAc, dried over anhydrous Na_2SO_4, filtered, concentrated and purified by silica gel chromatography (eluent: DCM:Hexanes = 7:3). 55.7mg (0.038mmol, 4%) of the product was obtained as a deep orange residue. %). ^{1}H NMR (400 MHz, $CDCl_3$): δ 8.26 (d, J = 8.1Hz, 2H), 8.16 (s, 2H), 7.62 (d, J = 8.2Hz, 2H), 6.83 (s, 4H), 4.05 (m, 12H), 1.83 (m, 12H), 1.5 (m, 12H), 1.42-1.20 (m, 96H), 0.87 (m, 18H). ^{13}C NMR (100 MHz, $CDCl_3$): δ 180.22, 153.88, 149.43, 139.64, 135.08, 131.27, 129.90, 128.61, 122.70, 106.43, 73.85, 69.67, 32.10, 32.07, 30.55, 29.92, 29.91, 29.86, 29.82, 29.79, 29.64, 29.62, 29.55, 29.52, 26.32, 26.31, 22.85, 22.83, 14.26. MS (MALDI-TOF): m/z obsd 1466.5031 $[M+H]^+$, calcd 1466.2186.

4.13 as per **scheme 4.4. 33** (0.465g, 1.27mmol) and **4.25** (3g, 4.445mmol) and Cs_2CO_3 was added to oven dried pressure tube along with 80ml of dry THF. Argon was bubbled through the solution for 20minutes after which $Pd(PPh_3)_4$ (0.27g, 0.234mmol) was added, the tube sealed with a Teflon screw-cap under argon, heated to 90^{o}C and left to stir overnight. On cooling, the solution was concentrated in vacuo and the residue purified by silica gel chromatography (eluent: DCM:Hexanes = 7:3) yielding 1.26g (0.86mmol, 68%) of a orange-red waxy solid. ^{1}H NMR (400 MHz, $CDCl_3$): δ 8.17 (d, J = 8.12, 2H), 8.13 (s, 2H), 7.57 (d, J = 8.16, 2H), 6.84 (s, 4H), 4.08 (m, 12H), 1.85 (m, 12H), 1.51 (m, 12H), 1.26 (m, 96 H), 0.88 (m, 18H). ^{13}C NMR (100 MHz, $CDCl_3$): δ 180.09, 153.83, 149.31, 139.57, 136.09, 135.10, 129.81, 128.47, 122.65, 106.35, 73.79, 69.60, 32.07, 32.05, 30.54, 29.90, 29.89, 29.85, 29.80, 29.77, 29.64, 29.61, 29.53, 29.50, 26.32, 26.29, 22.82, 22.81. MS (MALDI-TOF): m/z obsd 1466.5012 $[M+H]^+$, calcd 1466.2186.

***p,p'*-didodecyloxybenzil 4.14. 4.26** (9g, 138.205mmol), K_2CO_3 (20.54g, 148.62mmol) and dry DMF (350ml) were added to an oven dried RBF containing a magnetic stirrer bar under argon. 1-Br-dodecane (24.09ml, 100.32mmol) was added and the vessel heated to react overnight at 70°C under argon. The solution was cooled to RT, DCM (350ml) was added and washed with water (2 x 300ml). The organic layer was concentrated and the product purified by silica gel chromatography (1:1 = DCM:hexanes) yielding 21.199g (36.62mmol, 99%) of **4.14**. ^{1}H NMR (400 MHz, $CDCl_3$): δ 7.92 (d, J = 8.7 Hz, 4H), 6.94 (d, J = 8.7Hz, 4H), 4.02 (t, J = 6.56Hz, 4H), 1.80 (m, 4H), 1.44 (m, 4H), 1.38-1.21 (m, 32H), 0.88 (t, J = 7.04, 6H).). MS (MALDI-TOF): m/z obsd 578.3548 $[M]^+$, calcd 578.4330.

4.15. An oven dried pressure tube containing a magnetic stirrer bar was charged with Cs_2CO_3 (0.1924g, 0.5904mmol), **3.7** (7.2mg, 0.197mmol), **4.28** (0.630g, 0.492mmol) and freshly distilled THF (80ml). Argon was bubbled through the solution for 20min following which $Pd(PPh_3)_4$ (45.5mg, 0.039mmol) was added, the reaction sealed with a Teflon screw cap and heated to 90°C to stir overnight. On cooling, the solution was concentrated and the residue purified by silica gel chromatography (DCM: Hex. 4:1→ 9:1) and concentrated yielding 0.338g (0.134mmol, 68%) of a shiny purple residue. ^{1}H NMR (400 MHz, $CDCl_3$ 55°C): δ 8.84 (d, J = 8.8Hz, 18H), 8.65 (d, J = 7.9Hz, 2H), 8.34 (d, J = 8.0Hz, 2H), 7.94 (m, 8H), 7.73 (d, J = 7.9Hz, 4H), 7.14 (m, 8H), 6.97 (d, J =7.6Hz, 4H), 4.15 (t, J = 6.4Hz, 4H), 4.10 (t, J = 6.5Hz, 8H), 1.89 (m, 12H), 1.55 (m, 12H), 1.50-1.22 (m, 96H), 0.89 (m, 18H). MS (MALDI-TOF): m/z obsd 2509.5530 $[M]^+$, calcd 2509.3755.

2,3,6,7-Tetraaminophenazine (4.16). The synthesis of 2,3,6,7-tetraaminophenazine was carried out according to the reported literature procedure[140]. 0.5g (1.761mmol) Of 1,2,4,5-tetraaminobenzene tetrahydrochloride was added to a 2-necked RBF containing 2.022g (24.65mmol) NaOAc. The flask was fitted with a reflux condenser and left to reflux with a constant stream of air bubbled through the solution while stirred. After 5 hours, the solution was cooled to 0^{o}C and filtered. The black crystal product obtained was washed with 30ml cold water. The product was dried on hi-vac. overnight yielding 0.203g (0.688mmol, 78%) of **4.16**. ^{1}H NMR (400 MHz, DMSO): δ 6.84 (s, 4H), 6.05 (bs, 8H). MS (MALDI-TOF): m/z obsd 240.1657 $[M]^{+}$, calcd 240.1118.

1-bromo-2,4,5-trihydroxybenzene (4.17). The reported literature[141] procedure for the synthesis of **4.17** was followed closely. 1-Bromo-2,4,5-trimethoxybenzene (20g, 80.942mmol) was added to RBF containing 125ml of dried dichloromethane and cooled to -78^{o}C. BBr_3 (23.02ml, 242.83mmol) was added dropwise under a steady stream of argon. The vessel was allowed to warm to RT slowly and left to stir overnight. The solution was poured into 300ml of crushed ice, 300ml of EtOAc was added and separated. The organic layer was dried over anhydrous Na_2SO_4, filtered and concentrated. The solid residue was recrystallized from EtOAc/Hexanes affording 15.9g (77.56mmol, 96% yield) of **4.17**. ^{1}H NMR (400 MHz, DMSO-*d6*): δ 9.24 (bs, 2H), 8.29 (bs, 1H), 6.39 (s, 2H). ^{13}C NMR (100 MHz, DMSO-*d6*): δ 147.31, 132.71, 109.83, 109.08.

1-Bromo-2,4,5-tridodecyloxybenzene (4.18). A reported literature[141] procedure for the synthesis of **4.18** was followed closely. Accordingly, a 1l RBF was charged with **4.17** (14.5g, 70.729mmol), K_2CO_3 (58.65g, 424.37mmol), dry DMF (400ml) and finally

1-Br-dodecane(67.93ml, 282.92mmol). The solution was heated to 70^{o}C and left to stir at that temperature under argon for 24h. The solution was cooled, poured into water and extracted with hexanes. The organic layer was dried over anhydrous Na_2SO_4, filtered and concentrated and dried on hi-vac. overnight. The residue obtained was purified by silica gel chromatography employing hexane:EtOAc (10:1) as the eluent. Concentration of relevant fractions afforded 50.13g (70.608mmol, 99.8% yield) of **4.18** as a white waxy solid. ^{1}H NMR (400 MHz, $CDCl_3$): δ 6.67 (s, 2H), 3.92 (m, 6H), 1.76 (m, 6H), 1.45 (m, 6H), 1.26 (m, 48H), 0.88 (t, J = 7.0Hz, 9H). ^{13}C NMR (100 MHz, $CDCl_3$): δ 153.96, 137.57, 115.69, 110.26, 73.58, 69.42, 32.10, 32.08, 30.42, 29.91, 29.89, 29.88, 29.85, 29.81, 29.78, 29.74, 29.55, 29.52, 29.42, 26.25, 26.19, 22.85. MS (MALDI-TOF): m/z obsd 708.7223 $[M]^+$, calcd 708.5051.

4.19. The synthesis of **4.19** was reported in the literature[141]. As stated earlier, the literature yields were not reproducible and significant problems were encountered with this synthesis. In line with the report[141] by Yasuda co-workers, an oven dried 3-neck RBF containing a magnetic stirrer bar was charged with **4.18** (2.35g, 3.31mmol) and 125ml dry THF. The solution was cooled to -78^{o}C under argon with vigorous stirring to prevent formation of a solid. 1.6M (in Hexanes) *n*-butyllithium was added dropwise via a syringe under a constant stream of argon. Stirring was continues at -78^{o}C for 2h before 2-isopropoxy-4,4,5,5-tetramethyl-1,3,2-dioxaborolane (1.69ml, 8.75mmol) was added and the reaction allowed to warm slowly to RT and stir at that temperature for 22h. The solution was then transferred to a separating funnel containing 500ml water and extracted with EtOAc (3 x 200ml). The extract was dried over anhydrous Na_2SO_4, filtered, concentrated and purified by silica gel chromatography using Hexanes/1.5% EtOAc as

the eluent. **4.19** (1.141g, 1.507mmol, 56% yield) was obtained as a white waxy solid. ^{1}H NMR (400 MHz, $CDCl_3$): δ 6.99 (s, 2H), 4 (m, 4H), 3.87 (m, 2H), 1.76 (m, 6H), 1.46 (m, 6H), 1.33 (s, 12H), 1.26 (s, 48H), 0.88 (t, J = 7.04Hz, 9 H). HRMS: m/z obsd 756.692 $[M+H]^+$, calcd 756.691.

4.20. A 1l RBF flask containing a magnetic stirrer bar was charged with 400ml of dry 1,2-dichloroethane, 17.75ml (112.95mmol) of Et_3N, and 1.59g (4.34mmol) of **3.7**. Argon was bubbled through the solution for 20minutes prior to the addition of 0.3049g (0.434mmol) $Pd(PPh_3)_2Cl_2$ and 12.606ml (86.88mmol) of 4,4,5,5-tetramethyl-1,3,2-dioxaborolane. The flask was fitted with a condenser and left to reflux overnight under argon. The reaction solution was concentrated *in vacuo* and the product isolated by silica gel chromatography (eluent = DCM/ 1% MeOH) yielding 0.557g (1.21mmol, 28%) of an orange solid. ^{1}H NMR (400 MHz, $CDCl_3$): δ 8.51 (s, 2H), 8.1 (d, J = 7.68 Hz, 2H), 7.89 (d, J = 7.68Hz, 2H), 1.42 (s, 24H). ^{13}C NMR (100 MHz, $CDCl_3$): δ 180.87, 135.63, 134.99, 132.55, 130.34, 129.27, 84.65, 24.88. MS (MALDI-TOF): m/z obsd 459.257 $[M+H]^+$, calcd 459.237.

4.21 An oven-dried pressure tube containing a magnetic stirrer bar was charged with **3.7** (3g, 8.197mmol), 3,4,5-trimethoxyphenylboronic acid (5.213g, 24.59mmol), Cs_2CO_3 (8.012g, 24.59mmol) and 90ml dry THF. Argon was bubbled through the solution for 20min. followed by addition of $Pd(PPh_3)_4$. The tube was sealed with a Teflon screw-cap under argon, heated to 100^{o}C and left to stir for 24h. The reaction was cooled and diluted with 100ml DCM, washed with water (2x1L) and concentrated. The residue was taken up in 400ml DCM, sonicated and filtered. The orange solid obtained was put aside while the filtrate was concentrated and purified by silica gel chromatography

(eluent = DCM/ 5% MeOH). The product obtained from chromatography was combined with the product obtained on filtration and recrystallized from DCM/Hexanes and filtered yielding 3.389g (6.269mmol, 76%) of a bright orange solid **4.21**. ^{1}H NMR (400 MHz, 1,1,2,2-tetrachloroethane-*d2*): δ 8.27 (d, J = 8.1Hz, 2H), 8.21 (s, 2H), 7.68 (d, J = 8.2Hz, 2H), 6.85 (s, 4H), 3.95 (s, 12H), 3.90 (s, 6H). ^{1}H NMR (100 MHz, $CDCl_3$): δ 180.14, 154.00, 149.23, 136.20, 135.63, 131.39, 130.09, 128.67, 122.76, 105.00, 61.22, 56.58. MS (MALDI-TOF): m/z obsd 541.330 $[M+H]^+$, calcd 541.186.

4.22 (1.939g, 3.59mmol) was added to flask containing 15ml dry DCM. The flask was cooled to -78^{o}C under argon and BBr_3 (2.04ml, 21.523mmol) was added. The reaction was allowed to warm to RT and stirred overnight under an argon atmosphere. The solution was poured into 200ml crushed ice, the precipitant was isolated by filtration and washed with water. The purple-brown solid was recrystallized from DMSO/H_2O and 1,4-dioxane/hexanes yielding 1.655g (3.626, 101%) of the product mixture.

4.25 To and oven-dried flask containing a magnetic stirrer bar, 9.08g (12.816mmol) of **4.18** was added along with 120ml dry THF. The vessel was purged of oxygen via a needle inserted through the rubber septum with which the flask was sealed and argon bubbled through the solution. The solution was cooled to -78^{o}C carefully under argon with vigorous stirring maintained at all times to prevent formation of an immobile solid. 14.4ml of 1.6M *n*-butyllithium in hexanes was added drop-wise via syringe and the solution stirred for 3h at that temperature. The vessel was then removed from the cold bath, allowed to warm slowly to 0^{o}C and allowed to stir for 5min before being cooled back to -78^{o}C. Trimethylborate (7ml) was added via syringe and allowed to warm to RT under argon and left stir at that temperature for 24h. 80ml of 1M HCL was added and

stirred for 10min. The product was extracted with petroleum ether and dried over Na_2SO_4, filtered and concentrated *in vacuo* to yield 4.4194g (6.55mmol, 51%) of a white waxy solid that was used without further purification. ^{1}H NMR (400 MHz, $CDCl_3$): δ 7.39 (s, 2H), 4.08 (m, 6H), 1.85 (m, 6H), 1.51 (m, 6H), 1.42-1.20 (m, 48H), 0.88 (t, J = 5.48Hz, 9H). ^{1}H NMR (100 MHz,$CDCl_3$): δ 153.08, 142.84, 114.84, 114.06, 107.10, 73.66, 69.36, 32.09, 30.52, 29.91, 29.86, 29.68, 29.55, 26.28, 22.85, 14.25.

4,4'-dihydroxybenzil (4.26). 4.26 Was synthesized according to the procedure reported in the literature[142]. Accordingly, 15g (55.5mmol) *p*-anisil was added to a RBF along with 6 equivalents of pyridinium hydrochloride (38.48g, 332.99mmol), heated to 220^{o}C and stirred at that temperature for 3h. The solution was cooled to 80^{o}C and 100ml H_2O was added dropwise. The solution was filtered while hot to isolate the white crystal product in suspension that was then dissolved in EtOAc and purified by silica gel chromatography using EtOAc:petroleum ether (6:4). Concentration of relevant fractions yielded a pale yellow solid that was taken up in EtOAc, precipitated with hexanes, isolated by filtration and dried on hi-vac. yielding 12.68g (52.38mmol, 94%) of **4.26**. ^{1}H NMR (400 MHz, MeOD): δ 7.79 (d, J = 8.64, 4H), 6.89 (d, J = 6.89, 4H), 4.88 (s, 2H). ^{1}H NMR (100 MHz, MeOD): δ 195.66, 165.52, 133.58, 126.28, 116.91.

***Meso*-(*p*-dodecyloxybenzene)dipyrromethane (4.27).** The literature procedure[143] for the synthesis of **4.27** was used with some modifications. Accordingly, argon was bubbled through 400ml of freshly distilled pyrrole for 20minutes. 5g (17.215mmol) of 4-dodecyloxybenzaldehyde was added followed by 0.132ml (1.7215mmol) of TFA and left to stir in the dark under argon at RT for 1h45min. 5g of finely crushed NaOH was added and left to stir for 30min prior to filtration through a pad

of celite. The celite pad was washed with DCM and the filtrates pooled and concentrated. The residue was dried on hi-vac overnight to remove residual pyrrole. The residue was purified by silica gel chromatography using chloroform. The fractions containing the product and tripyrromethane byproduct were concentrated, taken up in 500ml dichloromethane and aerated under laboratory lighting for 1h. The solution was concentrated, purified by silica gel chromatography, again using chloroform, and the eluent concentrated yielding 5.505g (13.54mmol, 79%) of pure **4.27**. ^{1}H NMR (400 MHz, $CDCl_3$): δ 7.73 (s, 2H), 7.04 (d, J = 8.7Hz, 2H), 6.79 (d, J = 8.7Hz, 2H), 6.57 (q, J = 2.6Hz, 2H), 6.11 (q, J = 3Hz, 2H), 5.85 (s, 2H), 3.89 (t, J = 6.6Hz, 2H), 1.74 (quin, J = 7.9Hz, 2H), 1.42 (m, 2H), 1.37-1.21 (m, 16H), 0.88 (t, J = 7.0Hz, 3H). ^{13}C NMR (100 MHz, $CDCl_3$): δ 158.13, 134.07, 133.04, 129.40, 117.19, 114.59, 108.37, 107.15, 68.12, 43.14, 32.01, 29.76, 29.73, 29.70, 29.68, 29.50, 29.44, 29.38, 26.15, 22.78, 14.72. HRMS: m/z obsd 407.306 $[M+H]^+$, calcd 407.306.

4.28 The synthesis of **4.28** was achieved over several steps, the products of which were not separated or characterized until reasonable differences in mobility on silica gel chromatography were observed. *p*-Dodecyloxybenzaldehyde (5g, 17.215mmol), **4.27** (2.05g, 5.047mmol) and **3.5** (1.779g, 12.168mmol) were added to a 3l RBF containing deoxygenated $CHCl_3$(2l) and EtOH (15ml). $BF_3.OEt_2$ (0.454ml, 3.615mmol) was added and the reaction was left to stir in the dark for 3h prior to addition of DDQ (5.86g, 25.823mmol) after which, stirring continued for 1h more. The solution was then passed through a thick pad of silica gel, concentrated and the porphyrin product mixture purified by silica gel chromatography (neat hexanes→ hexanes:DCM = 1:1). The eluent was concentrated and then taken up in 500ml of DCM to which $Zn(AcO)_2.2H_2O$ (9.447g,

43.04mmol) in MeOH (200ml) was added. The solution was warmed to reflux overnight, cooled, washed with water, the organics concentrated and passed through a large pad of silica using DCM:Hex. (1:1) as the eluting solvent. Concentration of porphyrin-containing fractions produced a purple residue that was dissolved in $CHCl_3$ (0.5l), NBS (0.613g, 3.44mmol) added and left to stir at RT in the dark for 2h. The solution was concentrated, taken up in a minimal amount of DCM and passed through a large silica gel pad being eluted with DCM. The brominated porphyrin mixture obtained was concentrated and dried on hi-vac. in a 1l RBF. 1,2-dichloroethane (450ml) and Et_3N (7.26ml, 52mmol) was added and argon bubbled through the solution for 20min after which, $Pd(PPh_3)_2Cl_2$ (0.14g, 0.2mmol) and 4,4,5,5-tetramethyl-1,3,2-dioxaborolane (5.80ml, 40mmol) were added, the solution warmed to reflux and left to stir overnight under argon. The solution was then cooled, concentrated and the residue purified by silica gel chromatography using a gradient solvent system DCM:Hex (3:7→8:2) allowing separation of the various products and isolation of 0.630g (0.492mol, 9.7%) of **4.28** as a pure product. ^{1}H NMR (400 MHz, $CDCl_3$): δ 9.90 (d, J = 4.68Hz, 2H), 9.10 (d, J = 4.68Hz, 2H), 8.97 (m, 4H), 8.08 (m, 6H), 7.20 (m, 6H), 4.15 (m, 6H), 1.92 (m, 6H), 1.84 (s, 12H), 1.58 (m, 6H), 1.50-1.21 (m, 48 H), 0.89 (m, 9H). ^{13}C NMR (100 MHz, $CDCl_3$): δ 158.93, 158.89, 154.51, 150.92, 150.42, 149.78, 135.61, 135.49, 135.28, 135.17, 133.11, 132.78, 132.24, 131.59, 112.73, 112.70, 85.31, 68.47, 32.12, 29.89, 29.86, 29.85, 29.70, 29.56, 26.39, 25.50, 22.89, 14.31. MS (MALDI-TOF): m/z obsd 1277.6402 $[M]^+$, calcd 1277.7655.

4.29. 4.13 (0.11g, 0.0761mmol) Was added to a100ml RBF along with 30ml 1,4-dioxane, 1,2,4,5-tetraaminobenzene tetrahydrochloride (108mg, 0.3802mmol) and

NaOAc (125mg, 1.521mmol). The flask was fitted with a condenser connected to an argon line and refluxed for 20h. The reaction solution was concentrated, taken up in dichloromethane, sonicated, loaded onto a silica gel column and eluted with DCM. Concentration of relevant fractions yielded 110mg (0.07mmol, 92%) of **4.19**. ^{1}H NMR (400 MHz, $CDCl_3$): δ 9.34 (d, J = 8.4Hz, 2H), 8.71 (s, 2H), 7.87 (d, J = 7.8Hz, 2H), 7.40 (s, 2H), 6.96 (s, 4H), 4.11 (t, J = 6.4Hz, 8H), 4.06 (t, J = 6.6Hz, 4H), 1.85 (m, 12H), 1.52 (m, 12H), 1.42-1.64 (m, 96H), 0.87 (m, 12H). ^{1}H NMR (400 MHz, $CDCl_3$): δ 153.71, 142.25, 141.00, 140.31, 139.46, 138.45, 136.97, 131.44, 130.14, 127.07, 126.08, 121.31, 109.87, 106.58, 73.82, 69.56, 32.10, 32.07, 29.94, 29.93, 29.92, 29.87, 29.86, 29.83, 29.81, 29.71, 29.66, 29.55, 29.52, 26.37, 22.85, 22.83, 14.25, 14.24. MS (MALDI-TOF): m/z obsd 1567.1017 $[M]^+$, calcd 1567.2802.

4.30 1,2,4,5-tetraaminobenzene tetrahyrdochloride (0.117g, 0.412mmol), **4.15** (0.1036g, 0.041mmol), NaOAc (0.135g, 1.65mmol), 1,4-dioxane (15ml) and EtOH (5ml) were added to a RBF that was subsequently fitted with a condenser and heated to reflux with stirring under argon overnight. Following reflux, the solution was concentrated *in vacuo* and purified by silica gel chromatography using DCM:Hexanes (7:3) as the eluting solvent. Concentration of appropriate fractions yielded 74.7mg (0.029mmol, 69%) of a purple residue. ^{1}H NMR (400 MHz, $CDCl_3$): δ 10.19 (s, 2H), 9.53 (s, 2H), 9.32 (s, 2H), 8.91 (bs, 4H), 8.80 (s, 4H), 8.62 (bs, 4H), 7.92 (s, 8H), 7.29 (d, J = 8.8Hz, 2H), 7.20 (m, 8H), 7.00 (m, 4H), 5.14 (bs, 4H), 4.24 (t, J = 6.3Hz, 4H), 4.13 (m, 8H), 1.98 (m, 4H), 1.89 (m, 8H), 1.61 (m, 4H), 1.54 (m, 8H), 1.45-1.12 (m, 96H), 0.86 (m, 18H). ^{1}H NMR (100 MHz, $CDCl_3$): δ 158.88, 158.73, 150.29, 150.20, 149.65, 144.84, 140.82, 135.58, 135.37, 135.05, 134.94, 132.23, 131.94, 131.64, 131.07, 130.88, 130.22, 128.73, 128.55,

124.23, 120.70, 120.45, 112.68, 112.53, 112.37, 68.48, 68.33, 32.10, 32.05, 29.89, 29.86, 29.81, 29.78, 29.75, 29.66, 29.55, 29.48, 26.44, 26.34, 22.86, 22.82. MS (MALDI-TOF): m/z obsd 2611.9980 $[M]^+$, calcd 2611.4450.

4.31. 3.7 (0.515g, 1.408mmol), 1,2,4,5-tetraaminobenzene tetrahydrochloride (1g, 3.521), NaOAc (1.155g, 14.08mmol) and 1,4-dioxane (20ml) were placed in a 100ml RBF containing a magnetic stirrer bar, a condenser was fitted and the solution heated to reflux overnight. On cooling, 200ml H_2O was added to the solution, the precipitate isolated by filtration and washed with water and ethanol. The brown solid was then sonicated in ethanol, isolated by filtration and dried on hi-vac. overnight yielding 0.669g (1.337mmol, 95%) of a brown solid that was soluble in DMSO. ^{1}H NMR (400 MHz, DMSO-*d*6): δ 9.05 (d, J = 8.7Hz, 2H), 8.99 (d, J = 1.0Hz, 2H), 7.88 (dd, J = 8.7, 1.0Hz, 2H), 7.09 (s, 2H). ^{13}C NMR (100 MHz, DMSO-*d*6): δ 143,54, 140.10, 135.60, 130.98, 130.45, 129.91, 126.41, 122.41, 103.70, 66.34. MS (MALDI-TOF): m/z obsd 465.8642 $[M]^+$, calcd 465.9423.

4.32. **4.31** (183mg, 0.327mmol), **4.14** (946mg, 1.634mmol), 1,2-dichlorobenzene (50ml) and $TsOH.H_2O$ (24.2mg, 0.127mmol) were added to a 100ml RBF containing a magnetic stirrer bar. The flask was fitted with a reflux condenser and heated to reflux under argon overnight. In the morning, the solution was cooled, concentrated and the product isolated by silica gel chromatography (eluent = toluene → toluene/2% EOAc) yielding 0.1395g (0.134mmol, 41%). ^{1}H NMR (400 MHz, $CDCl_3$, 45^{o}C): δ 9.22 (d, J = 8.6Hz, 2H), 9.01 (s, 2H), 8.49 (s, 2H), 7.85 (d, J = 8.6Hz, 2H), 7.61 (d, J = 8.24Hz, 4H), 6.91 (d, J = 8.4Hz, 2H), 4.02 (t, J = 6.48Hz, 4H), 1.82 (quin, J = 7.36Hz, 4H), 1.28 (s, 32H), 0.89 (t, J = 6.8Hz, 6H). ^{13}C NMR (100 MHz, $CDCl_3$) 160.61, 155.24, 143.17,

141.09, 140.45, 132.77, 132.03, 131.70, 131.28, 129.44, 128.76, 128.34, 126.22, 114.53, 68.34, 32.09, 29.84, 29.81, 29.78, 29.76, 29.60, 29.52, 29.40, 26.22, 22.85, 14.28.

4.33. A 100ml RBF containing a magnetic stirrer bar was charged with **4.13** (0.175g, 0.121mmol), **4.16** (0.2907g, 0.988mmol), NaOAc (0.2978g, 3.63mmol) and a 50ml of a 1:1 mixture of EtOH and 1,4-dioxane. The flask was fitted with a reflux condenser, the solution heated to maintain a steady reflux and left to stir overnight. In the morning, the solution was concentrated *in vacuo* and the residue dried on hi-vac. The purple residue was then taken up in a minimal amount of DCM and purified by silica gel chromatography using DCM/2→4% MeOH as the eluting solvent yielding 0.1902g (0.1139mmol, 94%) of **4.33**, a waxy purple residue. ^{1}H NMR (400 MHz, $CDCl_3$, 58^{o}C): δ 9.48 (d, J = 8.0Hz, 2H), 9.16 (s, 2H), 8.64 (s, 2H), 7.90 (d, J = 8.5Hz, 2H), 7.28 (s, 2H), 6.97 (s, 4H), 4.31 (s, 4H), 4.12 (t, J = 6.2 Hz, 8H), 4.64 (t, J = 6.6Hz, 4H), 1.85 (m, 12H), 1.60-1.06 (m, 108H), 0.87 (m, 18H). MS (MALDI-TOF): m/z obsd 1669.4372 $[M]^+$, calcd 1669.3020.

4.34. A 100ml RBF containing a magnetic stirrer bar was charged with **4.15** (0.1135g, 0.0451mmol), **4.16** (0.228g, 0.773), NaOAc (0.2978g, 3.63mmol) and a 50ml of a 1:1 mixture of EtOH and 1,4-dioxane. The flask was fitted with a condenser and heated to reflux with stirring for 18h. Following reaction, the solution was concentrated *in vacuo* and dried on hi-vac prior to purification by silica gel chromatography using DCM/1→4% MeOH as the eluting solvent. Concentration of relevant fractions afforded 0.0819g (0.03012mmol, 67%) of a dark purple residue. ^{1}H NMR (400 MHz, $CDCl_3$, 45^{o}C): δ 10.08 (d, J = 8.1Hz, 2H), 9.48 (s, 2H), 9.44 (s, 2H), 9.05 (m, 4H), 8.91 (m, 14H), 8.01 (m, 12H), 7.22 (m, 12H), 6.47 (s, 2H), 4.25 (m, 12H), 2.00 (m, 12H), 1.65 (m,

12H), 1.58-1.17 (m, 96H), 0.95 (m, 18H). MS (MALDI-TOF): m/z obsd 2713.9702 $[M]^+$, calcd 2713.4671.

4.35. **3.7** (51.2mg, 0.14mmol) and **4.16** (84mg, 0.285mmol) were added to a RBF containing a magnetic stirrer bar along followed by 1,4-dioxane (18ml) and NaOAc (57mg, 0.7mmol). The solution was stirred and heated to reflux overnight. On cooling to RT, 80ml H_2O was added and precipitant formed isolated by filtration and washed with water, MeOH, EtOH and finally DCM. The dark brown/black solid isolated was dried on hi-vac. overnight yielding 78mg (0.137mmol, 97% yield). Traces of unreacted **3.7** were present in the NMR spectrum. High temperature NMR in DMSO was required to obtain the proton spectrum. The ^{13}C NMR spectrum was not acquired for **4.35**. ^1H NMR (400 MHz, DMSO-*d*6, 120^{o}C): δ 9.24 (d, J = 8.6Hz, 2H), 8.94 (d, J = 1.3Hz, 2H), 8.84 (s, 2H), 7.99 (dd, J = 8.6, 1.3Hz, 2H), 6.95 (s, 2H), 6.51 (s, 4H). MS (MALDI-TOF): m/z obsd 567.8672 $[M]^+$, calcd 567.9641.

4.36. To a 100ml containing **4.35** (40mg, 70.1μmol) as a residue, **4.14** (100mg, 0.173mmol), THF (7ml) and DMSO (20ml) were added. The solution was sonicated and while stirred, 4N HCl (2ml) was added. The RBF fitted with a reflux condenser. The solution was heated to reflux and left to stir for 2days. On cooling, 100ml H_2O was added and the precipitant isolated by filtration. MS (MALDI-TOF) of the crude reaction mixture revealed that a mixture of products and unreacted starting materials were present at that point. The filtrand was washed with 100ml H_2O, methanol and finally DCM. The crude product obtained was soluble in DMF and DMSO. No attempt was made to purify it further. MS (MALDI-TOF): m/z obsd 1110.5808 $[M+H]^+$, calcd 1111.3843.

4.37. To a RBF flask containing 90ml of a 2:5:2 mixture of 1,2-dichlorobenzene:AcOH:EtOH, 0.152g (0.1037mmol) of **4.13** and 0.6g (1.037mmol) of **3.3** were added, the flask fitted with a condenser and the solution heated to 90^{o}C and left to stir for 3.5h. The solution was concentrated and the product purified by silica gel chromatography using DCM/0→2%MeOH as the mobile phase. Yield: 0.116g (0.0577mmol, 56%). ^{1}H NMR (400 MHz, $CDCl_3$): δ 9.55 (s, 2H), 9.34 (s, 2H), 9.06 (d, *J* = 2H), 8.61 (s, 2H), 8.15 (s, 2H), 7.85 (d, *J* = 7.92, 2H), 7.08 (s, 4H), 6.90 (s, 2H), 4.23 (t, *J* = 5.8Hz, 8H), 4.12 (t, *J* = 6.1Hz, 4H), 3.76 (s, 4H), 1.92 (m, 24H), 1.57 (m, 30H), 1.47-1.21 (m, 84H), 0.89 (m, 18H). MS (MALDI-TOF): m/z obsd 2008.2212 $[M+H]^{+}$, calcd 2008.4881.

4.38. To a pressure tube containing a magnetic stirrer bar, 0.2036g (81μmol) of **4.15**, 0.1172g (0.2025mmol) of **3.3** along with a 50ml of a 2:1:2 mixture of 1,2-dichlorobenzene:AcOH:EtOH. Argon was bubbled through the solution for 20minutes and the tube sealed with a Teflon screw cap and heated to 100^{o}C and allowed to stir overnight. The solution was transferred to a RBF using DCM, concentrated *in vacuo* and dried on the hi-vac overnight. The residue was purified by silica gel chromatography using DCM:Hexanes (3:2→9:1) as the solvent system. 173.3mg (56.7μmol, 70%) of **4.38** was obtained as a purple residue. ^{1}H NMR (400 MHz, 1,1,2,2-tetrachloroethane-*d*6): δ 10.47-9.29 (8H), 9.29-8.38 (18H), 8.38-7.51 (14H), 7.51-6.51(14H), 4.25 (12H), 3.02-1.84 (24H), 1.34-0.65(18H). MS (MALDI-TOF): m/z obsd 3052.2573 $[M+H]^{+}$, calcd 3052.6552.

Chapter 5: Synthesis of Pyrazine-Containing Fused Aromatic Cores as Spacers in Dyes for Dye Sensitized Solar Cells.

5.1 Design of a Dicarboxylic Heteroaromatic Spacer for Use in Dye-Sensitized Solar Cells

Since O'Regan and Grätzel's seminal paper[24] the efficiencies of dye-sensitized solar cells (DSSCs) have steadily improved as researchers etched away at the variety of challenges inherent in the complex functioning of the cells.[24,25,145-147] Particular focus has been paid to the design and optimization of the dyes employed to sensitize the TiO_2 semiconductor, with numerous dyes having been tested, leading to steady improvements in cell efficiencies[148-162]. DSSCs are a good example of how progressive increases in solar energy conversion efficiencies have been achieved through stepwise optimization of the various components within the cell design. Even within dyes, modular design as allowed for anchors, chromophores and secondary donors to be optimized. An example of a common design motif present within dyes employed in DSSC is the Donor-π-Acceptor (D-π-A) design[148,151,154,157-159,163]. When a core aromatic chromophore, such as a porphyrin, is sandwiched as the **π** functionality between an electron rich donor and an electron deficient anchoring moiety, push-pull functionality is inferred to the chromophore.[164-166]

The push functionality is commonly provided by a form of tertiaryamine that acts as a secondary donor, satisfying the hole generated on excitation of, or charge transfer from, the π-chromophore. An electron deficient anchoring group, commonly cyanoacetic acid, serves as the electron-deficient pull-anchor. In these systems, the HOMO of the dye

produced lies towards the secondary-donor end of the molecule while the LUMO resides towards the accepting terminus of the dye.[159,166,167] This distribution of the HOMO and LUMO orbitals away from the center of the π-chromophore has two effects: it facilitates injection, since the excited electron occupies an orbital closer to the TiO_2 surface, and inhibits recombination by poising the hole generated further away from the conduction band electrons.[159]

Co-adsorbing spectrally complementary dyes is an effective strategy for extending the spectral response of a DSSC.[168-172] Effective co-sensitization increases the photocurrent of the cell and the overall power conversion efficiency.[170] Ensuring an even distribution or a desired ratio of co-adsorbed dyes is, however, a challenging task, especially when the dyes exhibit physical differences, such as size or binding affinity, or exhibit differences in the propensity to interact with like dyes, resulting in aggregative accumulation of one dye in a local environment. If one dye is intended to serve as an energy donor for a second dye, the requirement for an even distribution of the two chromophores on the TiO_2 surface within close proximity to one another and possibly, even to be positioned so as to optimize the alignment of the respective transition dipole moments is a stringent objective for the adsorption process. This specificity cannot be achieved for all dyes without covalent linking of the two dyes to arrange them in a preordered fashion.

In the interest of increasing the modularity with which dyes for DSSCs can be designed and synthesized, we sought to design a rigid rectifying spacer that would improve the characteristics of the dye-TiO_2 interface, inhibit aggregation of dyes, increase the number of active chromophores bound to a given binding site on TiO_2 and

would enable even and defined co-adsorption of different chromophores onto the TiO_2 surface. This goal was a first-step towards the synthesis of larger architectures like those presented in figure 1.4 in which an array is arranged around a conductive scaffold through which electrons can travel to reach the anode, in the case of DSSC, the TiO_2 electrode. Figure 5.1 shows an image of a dicarboxylic heteraromatic spacer (**A(COOH)$_2$**) functionalized with two planar and spectrally complementary chromophores.

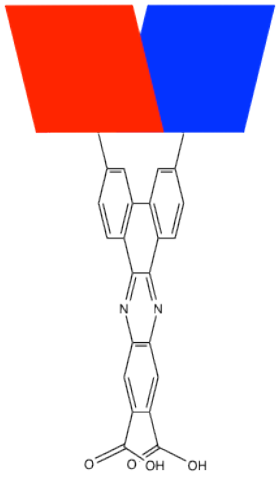

Spacer A(COOH)$_2$

Figure 5.1. Spacer **A(COOH)$_2$** functionalized with two planar chromophores.

Structurally spacer **A(COOH)$_2$** (fig. 5.1) is designed to bring a degree of order to the TiO_2-dye interface, inhibit aggregation of dyes and increase the regularity and strength with which dyes adsorb to the TiO_2 surface. The spacer is planar and very rigid in comparison to other alkane, alkene, alkyne and benzene based spacers that exhibit rotational freedom between the components of the spacers. In the event that a dye employing spacer **A(COOH)$_2$** is adsorbed by both carboxylic acid anchoring groups, the

bending modes of the dye relative to the TiO_2 surface will be restricted. In addition, cooperative binding of each carboxylic acid will increase the strength by which each chromophore on the dye is bound to the TiO_2 surface in comparison to a single chromophore anchored by a single benzoic acid anchor.

The efficiency of solar cells employing large planar dyes are often impaired by aggregation of the dyes at the metal oxide surface[25,173,174]. Employing co-adsorbants[162,175-177] or re-engineering the dyes' structure to inhibit aggregation[178,179] is often required to overcome this problem. It is expected that the variance with which a dye employing spacer **A(COOH)$_2$** could orient relative to the TiO_2 surface would be somewhat restricted, and so prevent bending movements that would enable alignment for aggregation. The inherent regularity with which **A(COOH)$_2$** subtends the chromophores bound to it ensures that the planar surfaces of the two chromophores can not align to stack with chromophores on adjacent dyes. Dyes that feature an umbrella-shaped structure, as would be produced by coupling chromophores to spacer **A(COOH)$_2$**, have been thought to screen the TiO_2 surface from the oxidized electrolyte present in solution, preventing recombination.[180]

Spacer **A(COOH)$_2$** provides a defined spacing and dictates the relative orientation between the transition dipole moments of the chromophores bound to it. This favorable, fixed alignment of transition dipole moments of distinct chromophores within the same dye could satisfy the requirements for efficient Förster resonance energy transfer[181,182] allowing one chromophore to act as an antenna for the next, moving beyond the limitations inherent in co-sensitization through co-adsorption of complementary dyes.[181]

Dyes constructed with large chromophores on the spacer cannot rotate to flatten completely into a conformation that would be more favorable for stacking.

5.2 Theoretical Considerations of Spacer Orbital Energies in the Operations of Dyes in a DSSC.

A key process in the operation of DSSCs is injection of an electron from an excited dye into the conduction band of TiO_2. Recombination at the TiO_2-dye interface is a source of efficiency loss. Electrons injected into the conduction band can recombine with the positively charged hole in the HOMO of the dye. Several considerations to the electronic properties of a spacer designed for use in dye-sensitized solar cells must made. Placing a spacer between a chromophore and TiO_2 increases the distance through which an electron must travel from a dye to TiO_2 during injection. As this is such a key event, diminishing the yield of this process in any way is undesirable. There is concern that while positioning a spacer between the chromophore and TiO_2 may favorably inhibit recombination of TiO_2 conduction band electrons with holes residing on the oxidized chromophore, it would unfavorably inhibit injection too. It is thus important to engineer a spacer to exhibit molecular orbitals that facilitate injection and inhibit charge recombination. In this way, the spacer could act as a rectifier. A second important consideration regarding the energy levels of a spacer designed for use in dyes of DSSCs is the HOMO-LUMO gap, or energy of the lowest energy transition of the spacer. A spacer must not quench the excitation energy of the chromophores bound to it and it would be preferable if the spacer acted as an energy donor for the chromophores.

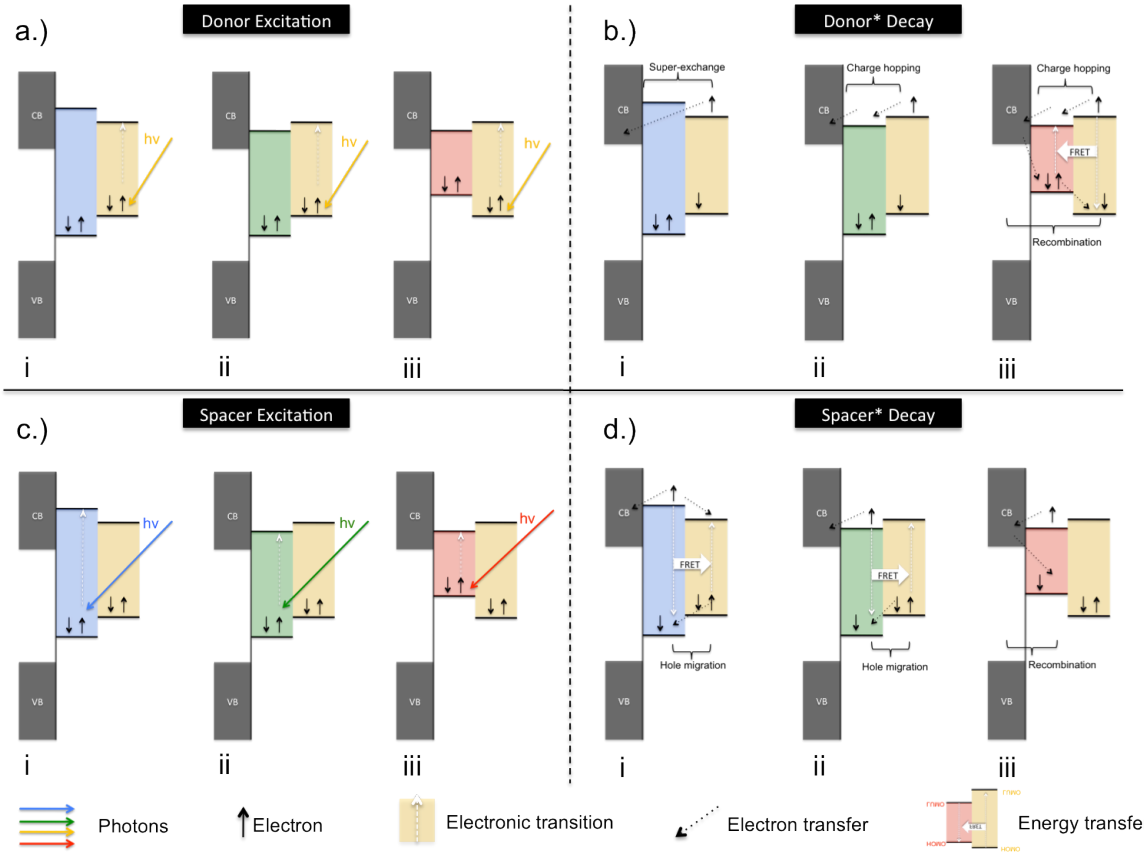

Figure 5.2. Energy level diagram showing the (a) excitation and (b) decay of dyes bound to TiO_2 by three hypothetical spacers that differ in HOMO-LUMO gaps and positions (**i**, **ii**, **iii**) along with the (c) excitation of the spacers and (d) resulting decay pathways. Scenarios **i** and **ii** do not allow for oxidation of the spacer by the dye, ensuring that the spacer serves its purpose in separating the hole from conduction band electrons in the TiO_2.

Figure 5.2 shows three hypothetical scenarios **i**, **ii** and **iii** in which three distinct dyes are constructed by positioning three different spacers with varying HOMO-LUMO potentials and consequently, differing HOMO-LUMO gaps (red, blue and green) between a common donor chromophore (yellow) and TiO_2 (charcoal). The positions of the HOM and LUM orbitals of the spacers present in the three dyes, **i**, **ii**, and **iii** along with the resulting HOMO-LUMO gaps of the spacer are important for the dynamics of the dyes in

solar cell function: their ability to absorb light, accept or donate excitation energy and accept or donate electrons or holes in the ground or excited state must be considered. Figure 5.2 also summarizes some of the photophysical processes that can occur (fig.5.2.b and d) following excitation of the chromophores (fig.5.2.a) or the spacer moieties (fig.5.2.c).

As stated earlier it is thought that if the increased distance between the chromophore and TiO_2 afforded by a spacer does not significantly inhibit injection, possibly by exhibiting bridge-like properties, mediating electron transfer over the increased distance via superexchange, it could reduce recombination of TiO_2 conduction band electrons with holes residing in the HOMOs of photooxidized dyes. In the hypothetical dye, **i**, the $LUMO_{spacer} > (LUMO_{chromophore} + k_BT)$ and so injection from the excited chromophore must proceed via tunneling across the space occupied by the spacer (figure 5.2.b, **i**). When $LUMO_{spacer} < LUMO_{chromophore}$ (**ii** and **iii**), the excited electron can be accepted by the spacer prior to injection. While this may better facilitate injection by diminishing the distance through which the electron must tunnel, it will likely also reduce the V_{OC} of the cell by approximately $(LUMO_{chromophore}-LUMO_{spacer})V$.

In **i** and **ii** the HOMO-LUMO energy gap of the spacer is greater than that of the chromophore and so prevents quenching of an excited chromophore via energy transfer to the spacer as is possible in **iii**.

The hypothetical dyes **i** and **ii** are constructed such that $HOMO_{spacer} < HOMO_{chromophore}$, preventing oxidation of the spacer by the excited dye, as is possible for dye **iii** (figure 5.2.b, **iii**). This ensures that holes generated by injection from an excited

spacer move thermodynamically downhill, to reside on the chromophore, away from the TiO_2 surface (Figure 5.21, **i** and **ii**).

In summary the position of the spacer LUMO relative to the chromophore is important for efficient injection. The position of the spacer HOMO is important for preventing recombination and keeping holes generated away from the TiO_2 surface. Finally the HOMO-LUMO gap of the spacer should always be more blue absorbing than the chromophore present in the dye to prevent energy transfer from the chromophore to the spacer.

5.3 Electrochemically Reduced Nitro Groups for Use as Anchoring Groups in DSSC.

Recently, Cong *et al.* proposed[183] that nitro groups, when reduced electrochemically, may serve as good anchoring groups for use in DSSC. Theoretically, the neutral nitro group is one of the worst anchoring groups, exhibiting a comparatively low affinity for the TiO_2 employed in DSSC[184]. In the Cong paper, an observation was reported of how a DSSC changed color during cell testing. The dye employed in the cell was anchored to TiO_2 by a carboxylic acid group, but the dye featured a terminally positioned nitro group. It was proposed that the color change observed during cell testing was as a result of the nitro group being reduced by electron density present within the TiO_2 conduction band and concomitant binding of this reduced nitro species to TiO_2. Interestingly, they also observed an increase in cell performance following the color change. No further work was reported in which a dye was specifically synthesized with

just a nitro group as the designated anchoring group to further probe the viability using electrochemically reduced nitro groups as anchoring groups.

The ability to generate an anchoring group from an otherwise low affinity group electrochemically would allow for an orthogonal step-wise assembly of electrochemical cells in which a dye-catalyst complex could be synthesized using interactions between catalytically active metal oxides and high affinity anchoring groups like carboxylic acids, and then subsequent attachment of these complexes to TiO_2 via reduction of the nitro groups. To investigate the use of spacers in dyes for DSSC applications and to investigate the viability of attaching a dye to TiO_2 electrochemically a series of four dyes was designed that utilize materials from previous chapters.

5.4 Design of a Series of Dyes Allowing for the Dual Investigation of Spacer **A** and the Electrochemical Attachment of Nitro Anchoring Groups.

To investigate both the idea of using the heteroaromatic spacer **A** in dye sensitized solar cells and to investigate the viability of using nitro groups as anchoring groups in DSSC through electrochemical reduction, a set of four dyes were designed that would allow for four comparisons to be made between the dyes. Figure 5.3 shows the dyes designed. All dyes employ the same triaryl zinc porphyrins to so that the weight of the comparisons made between the dyes can be attributed solely to the differences between the dyes. Dye **5.1** serves as the primary control dye. It features the common triaryl porphyrin chromophore and a benzoic acid moiety. Dye **5.2** features two of the triaryl porphyrin chromophores which are bound to spacer **A(COOH)$_2$**. Comparisons

made between **5.1** and **5.2** (red arrow) allow for investigating the effect of spacer **A(COOH)$_2$**. Dye **5.3** features the common chromophore bound to *p*-nitrobenzene. This serves as the control dye for investigating the effects of spacer **A(NO$_2$)$_2$** which is present in dye **5.4** (yellow arrow).

Comparisons between **5.1** and **5.3** (green arrow) allow for the differences between single nitro and carboxylic acid anchoring groups to be extracted whilst comparisons made between dyes **5.2** and **5.4** (blue arrow) would allow for comparisons to be made between *o*-dicarboxylic acid and or *o*-dinitro anchoring groups to me made.

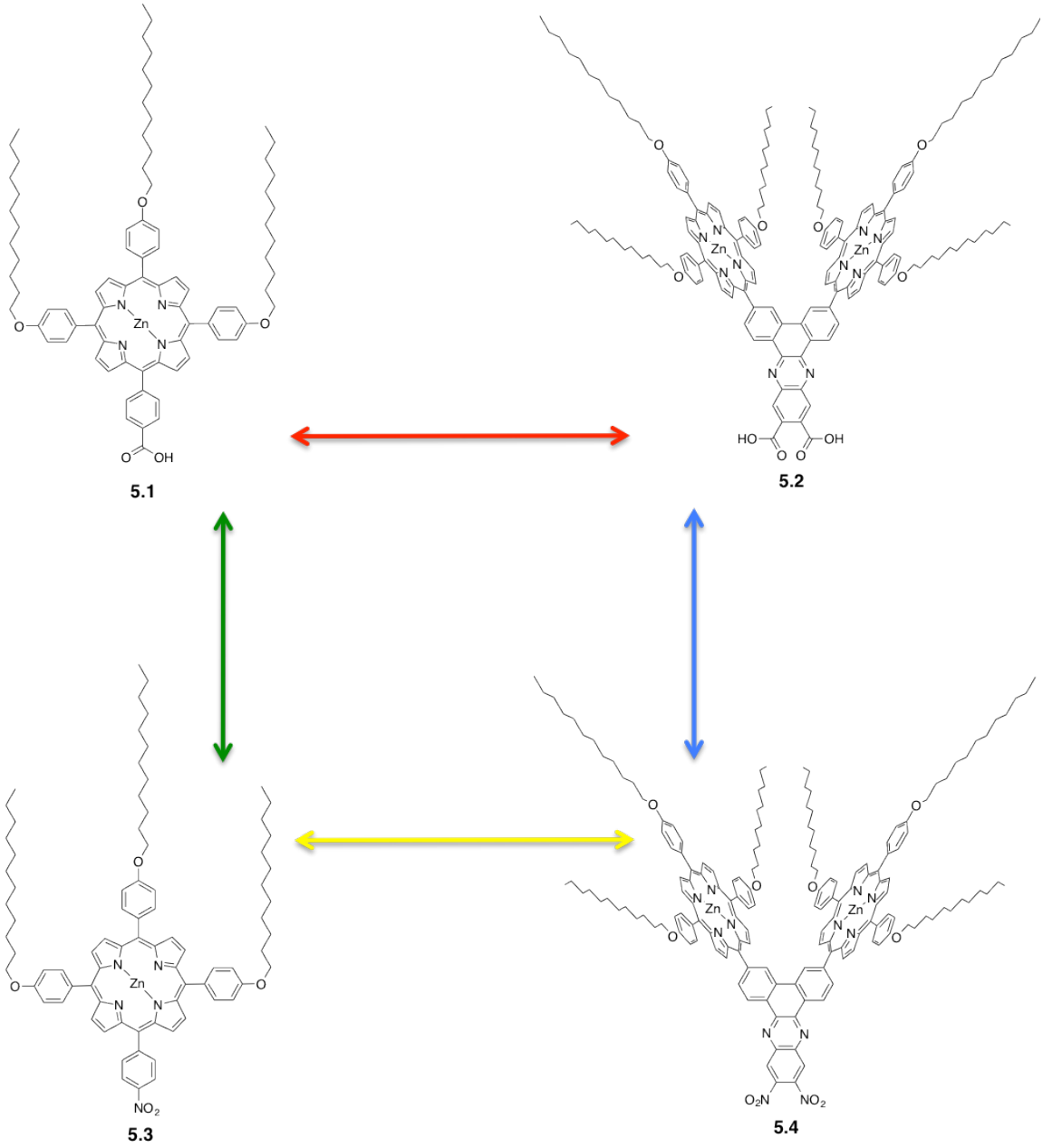

Figure 5.3 Dyes synthesized for comparison with one another to investigate the utility of spacers **A(COOH)$_2$** and **A(NO$_2$)$_2$** (red and yellow arrows) and the viability of electrochemically reduced nitro groups (green and blue arrows) as anchoring groups for use in DSSCs.

5.5 Synthesis of Dyes

The simple 3-step synthesis of **5.1** is shown in scheme 5.1 below. The porphyrin macrocycle was achieved by condensing equivalents of *p*-dodecyloxybenzaldehyde and formyl-4-methylbenzoate with two equivalents of *meso*-(*p*-dodecyloxybenzene)dipyrromethane (**4.27**) in a $BF_3.OEt_2$ catalyzed reaction to produce **5.5**. The methyl ester of **5.5** was hydrolyzed by reflux in an *iso*-propanol solution to which KOH was added to produce the carboxylic acid functionality of **5.6**. Finally, metallation of **5.6** using $Zn(AcO)_2.2H_2O$ in an overnight reflux in dichloromethane produced **5.1** in 94% yield.

Scheme 5.1

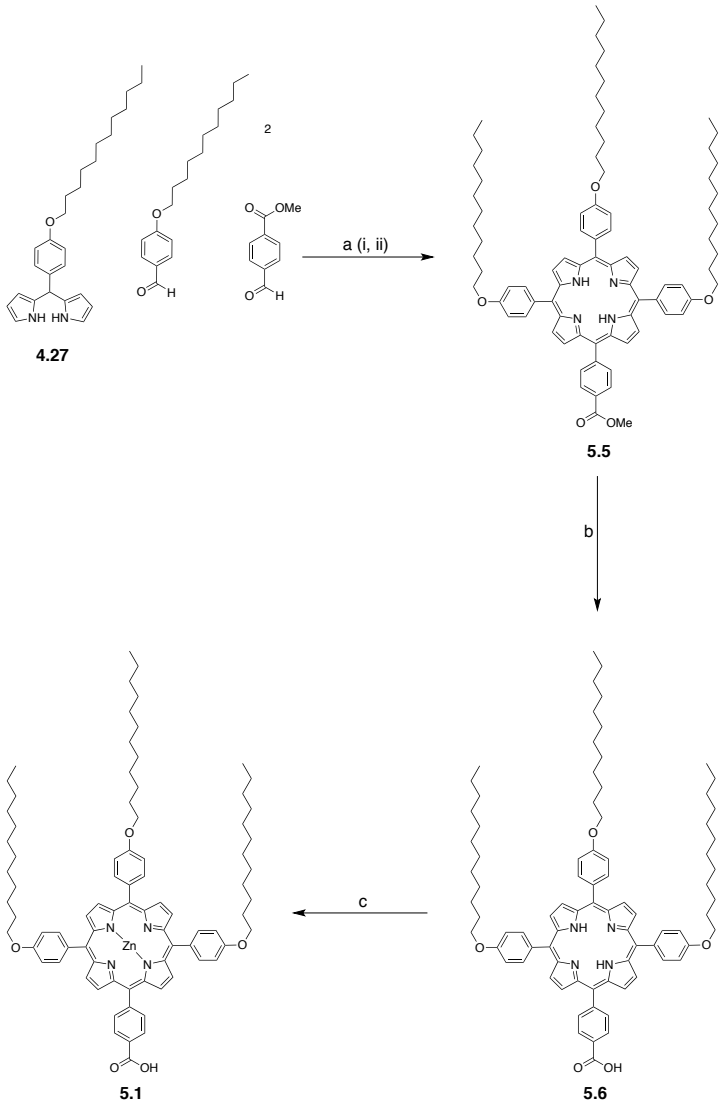

a) i $CHCl_3$/0.75%, EtOH, $BF_3.OEt_2$, 3h, RT. **ii** DDQ, RT, 1h, 11%. **b)** KOH, *iso*-propanol, H_2O, reflux, 5h, 88%. **c)** $Zn(AcO)_2.2H_2O$, DCM/MeOH, reflux, 16h, 94%.

The synthesis of **5.2** was anything but elegant. Condensation of 4,5-diaminophthaleonitrile with the porphyrin-functionalized phenanthrene-9,10-dione, **4.15**, synthesized in chapter 4 afforded **5.7** in high yield. Hydrolysis of the dinitrile functionality of **5.7** employed very harsh conditions in which a sealed pressure tube containing **5.7** and a 1:1 mixture of 12 N HCl and TFA was heated to internal reflux for 6

days. While the nitrile groups were successfully hydrolyzed to produce the desired *o*-dicarboxylic acid functionality, the harsh acidic conditions resulted in cleavage of some of the dodecyloxy functionalities present on the porphyrin macrocycles, together with removal of the chelated zinc metal atoms as evidenced by MALDI-TOF mass spectrometry. The product and byproducts were not isolated from each other at this stage. A Williamson-ether reaction of the product mixture with 1-bromododecane was employed to regenerate the dodecyloxy groups hydrolysed in the previous step, and subsequent basic reflux in THF was employed to hydrolyze any dianhydride that had formed, ensuring the presence of the dicarboxylic acid functionality. Finally, reflux of the residue in dichloromethane with a methanolic solution of zinc acetate and subsequent work-up and chromatographic purification produced **5.2**. This synthesis was in no way elegant, but was sufficient to produce the necessary dye for the study at hand.

Scheme 5.2

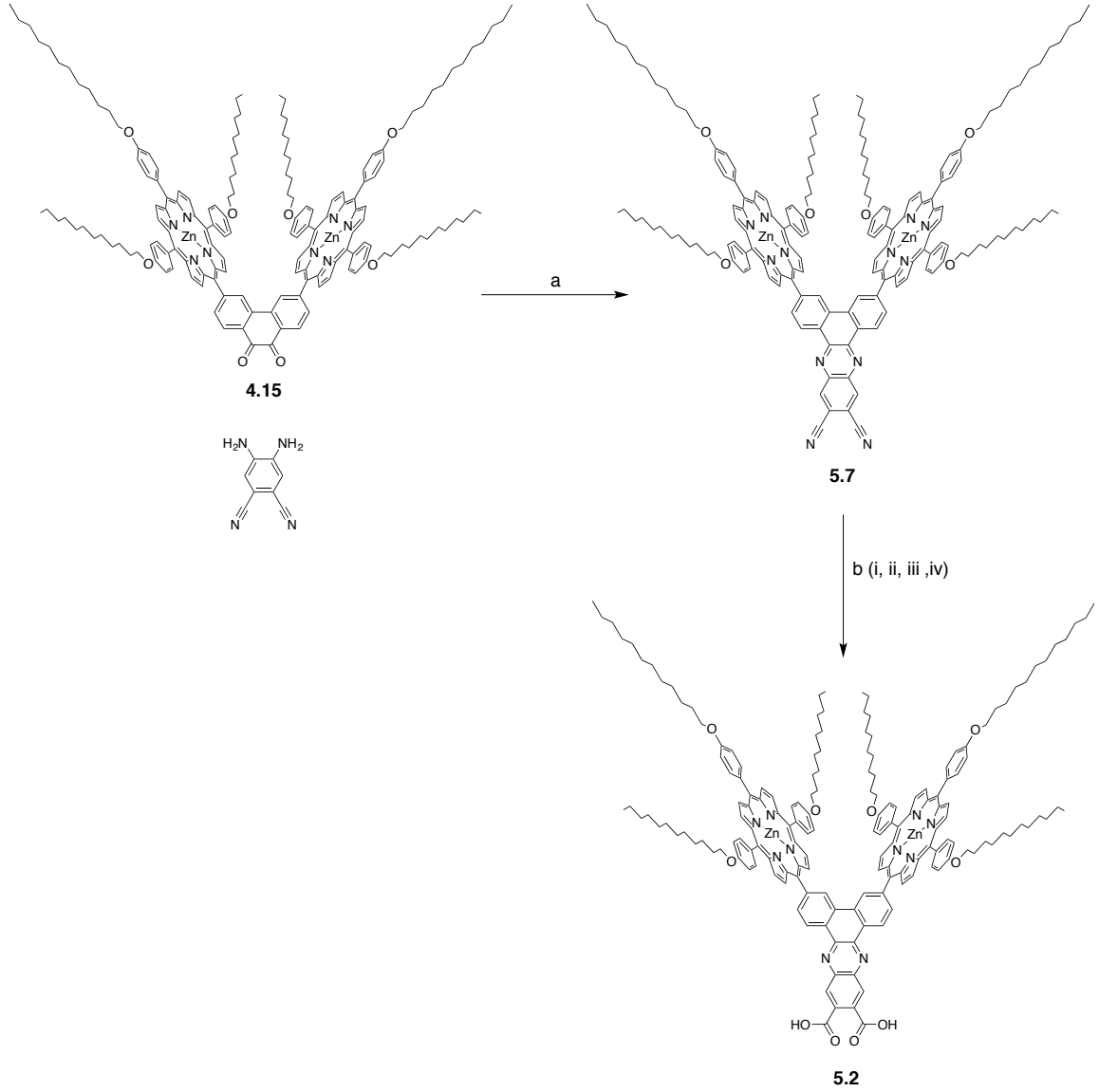

a) AcOH:EtOH:Toluene (1:1:2), 100°C, 20h, 93%. **b) i** TFA:12N HCl (1:1), pressure tube, reflux, 6 days. **ii** 1-bromododecane, DMF, K_2CO_3, 70°C, overnight. **iii** $Zn(OAc)_2$, MeOH, DCM, reflux, overnight. **iv** THF, KOH, H_2O, reflux, overnight.

The synthesis of **5.3** is shown in scheme 5.3. The porphyrin macrocycle is produced by condensing two equivalents of **4.27** with equivalents of *p*-dodecyloxybenzaldehye with 4-nitrobenzaldehye using $BF_3.OEt_2$ as the Lewis-acid catalyst. The free-base porphyrin was converted to the zinc porphyrin by refluxing a

solution of dichloromethane to which a methanolic solution of $Zn(AcO)_2$ was added yielding the product in 91%.

Scheme 5.3

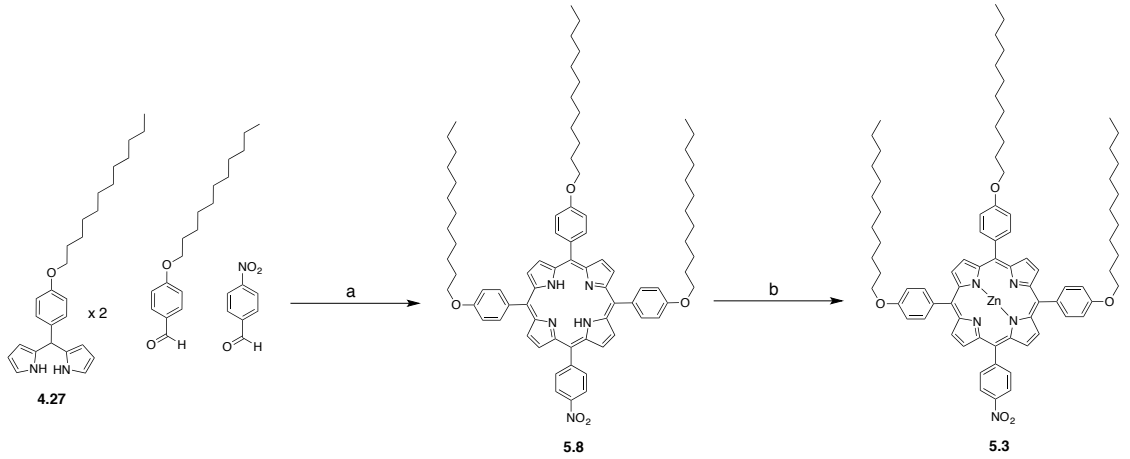

a) i BF_3OEt_2, $CHCl_3$/0.75% EtOH, RT, 3h. **ii** DDQ, RT, 1h, 14% **b)** DCM/MeOH, $Zn(AcO)_2$, 91%.

The synthesis of **5.4** (shown in scheme 5.4) is achieved in 96% yield simply by condensing the *o*-diamine, **5.9**, with **4.15** in toluene:EtOH:AcOH solvent at reflux. The requisite *o*-diamine is obtained by removal of the tosyl protecting groups of **3.11**, the synthesis for which was described in chapter 3. This was achieved in 50% yield by heating **3.11** in aqueous sulfuric acid in accordance with a reported literature procedure[185].

Scheme 5.4

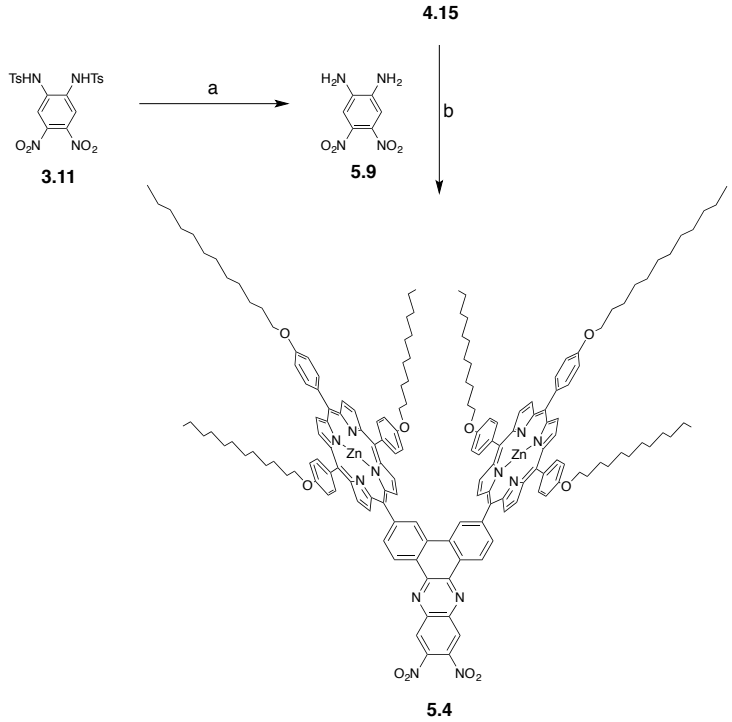

a) H_2SO_4/H_2O, 100°C, 3.5h, 50%. **b)** Toluene:AcOH:EtOH (2:1:1), reflux, overnight, 96%.

5.6 Performance of Carboxylic Acid Dyes **5.1** and **5.2** in Dye-Sensitized Solar Cells

The work presented in section 5.3 was conducted by Dr Benjamin J. Sherman. The UV absorbance spectra of the TiO_2 electrodes modified with dyes **5.1** and **5.2** (figure 5.4) show relatively similar dye loadings, with slightly higher absorption observed for **5.2**. It should be noted that effort was not taken to normalize for scattering effects of the TiO_2 films, and the increased absorption of the electrode with **5.2** may in part be due to this. Despite relatively comparable loadings, the DSSC with **5.2** exhibited improved performance as compared to **5.1**. The photocell with **5.2** showed steady photocurrent of 6.42 mA cm^{-2} and achieved an open circuit voltage (V_{oc}) of 0.53 V with a fill factor (FF)

of 0.60. In comparison, the cell with **5.1** produced a steady photocurrent of 2.28 mA.cm^{-2}, V_{oc} of 0.41 V, and FF 0.62. In addition, IPCE measurements clearly show greater performance of **5.2** over **5.1** throughout the entire spectral range of the porphryin absorption spectrum. This improved IPCE cannot simply be attributed to a higher surface coverage of dye given the comparable loading observed in the UV-Vis spectra.

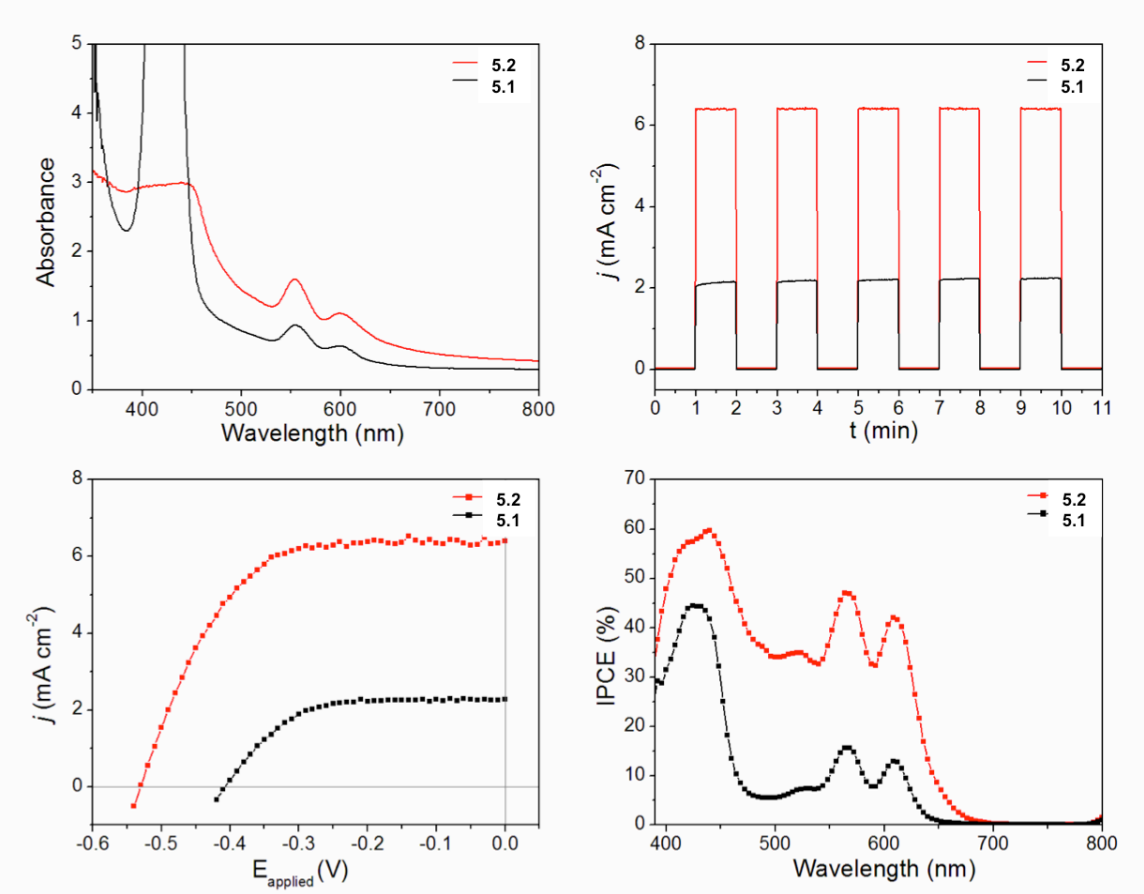

Figure 5.4. Absorption spectra (upper left), photocurrent (upper right), photocurrent-photovoltage (*jV*) (bottom left), and IPCE measurements (bottom right) for DSSCs using dyes **5.1** (black traces) and **5.2** (red traces).

Electrochemical analysis of **5.1** and **5.2** by cyclic voltammetry shown in figure 5.5 and listed in table 5.1 revealed that the potentials of the porphyrin moieties are largely

unaltered in the two dyes. The first oxidation and reduction potentials of **5.2** are characteristic of the porphyrins present.

Table 5.1

Oxidation and reduction potentials of dyes **5.1** and **5.2** (V vs SCE).

Dye	$E_{1/2}^{1ox}$ (ΔEp)	$E_{1/2}^{2ox}$ (ΔEp)	$E_{1/2}^{red}$ (ΔEp)
5.1	0.74 V (75 mV)	1.07 (70 mV)	-1.40 (75 mV)
5.2	0.76 V (55 mV)	1.05 V (55 mV)	-1.41 (53 mV)

Cyclic voltammetry was conducted in dichloromethane using 100mM $TBAPF_6$ supporting electrolyte. A three-electrode cell using a platinum disc electrode, platinum gauze reference electrode and Ag/AgCl pseudo reference electrode was used.

This implies that the oxidation and reduction potentials of the HOMO-LUMO gap of the spacer is greater than that of the porphyrins attached to it. Consequently, spacer **A(COOH)$_2$** is unlikely to quench the photo-excited porphyrin, be reduced by the porphyrin excited state or reduce the photo-oxidized porphyrin following photoinduced electron transfer into TiO_2, making it an ideal spacer as far as the orbital energy considerations are concerned.

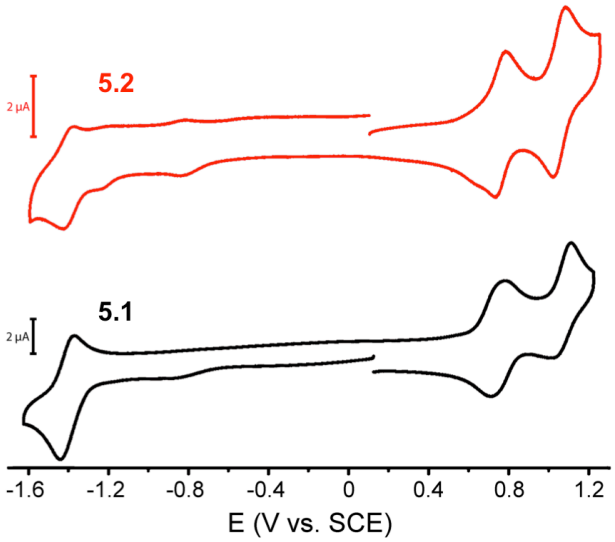

Figure 5.5 Cyclic voltammograms of **5.1** (black) and **5.2** (red).

Comparison of the *JV* curves obtained from cells using **5.1** and **5.2** (Fig. 5.4, bottom left) show that, despite injection originating form similarly energetic excited state porphyrins (as revealed from the reduction potentials, oxidation potentials and similar absorbance characteristics of **5.1** and **5.2**), the V_{OC} of **5.2** (0.53 V) is greater than that of **5.1** (0.41 V), showing a 29% improvement. The improved V_{OC} could indicate the rectifying behavior of spacer in **5.2**, enabling the Fermi-level of the TiO_2 to be raised without recombination occurring, or may simply be as a result of a higher loading of porphyrin chromophores in the cell using **5.2**. The steady state photocurrent (*j*) of **5.2** (6.41 mA cm^{-2}) is substantially higher than that of cell of **5.1** (j = 2.28 mA cm^{-2}), exhibiting a 181% improvement for the cell employing spacer **A(COOH)$_2$**. The fill-factors of the two cells are very similar. The control cell of **5.1** exhibits a FF = 0.62 just outperforming that of **5.2** with FF = 0.60. The dramatic difference in $j_{\text{steady state}}$ and V_{OC} along with similar fill-factors results in an improved overall efficiency for the cells with

5.2 over that with **5.1**. Using the spacer boosts the efficiency (η) of the porphyrin-based DSSC, η = 0.57% for **5.1** to η = 2.04% for **5.2**, a 258% increase.

Analysis of the IPCE spectra obtained from cells **5.1** and **5.2** (fig. 5.4, bottom right) reveals that the increased efficiency is largely derived from the spectral response of the porphyrin chromophore and not from the spacer. The IPCE values of the Q-band peaks in the region 550-650 nm are significantly greater for **5.2** (~50%) as compared to **5.1** (~17%). While the absorbance spectrum of the TiO_2 electrode of **5.1** does imply ~25% more porphyrin present in the cell with **5.2** than with **5.1**, this higher loading cannot account for the ~233% increase in Q-band IPCE near 555 nm in comparison of the two dyes.

As stated earlier, the cyclic voltammogram of **5.2**, (figure 5.5) implies that dye **5.2** satisfies the conditions of the hypothetical dye construct **i** shown in figure 5.2. While the improvement in cell performance has, as yet, not been attributed to any one factor, it is likely that it is derived from a combination of several factors, such as inhibited aggregation of the dye at the TiO_2 surface, increased dye loading, rectification of the dye-TiO_2 interface and improved shielding of the TiO_2 surface from the oxidized mediator by the umbrella-shaped dye.

The increased V_{OC} reveals that the Fermi-level within the TiO_2 can be raised to a higher energy without recombination occurring to both the hole on the porphyrin or the oxidized redox mediator present in solution. Similarly the increased photocurrent exhibited by **5.2** and IPCE values corroborate that recombination may be inhibited. It is also expected that the bulky shape of dye **5.2** could screen the TiO_2 surface from oxidized redox mediator.

The electrostatic potential of the spacer may also play a role in producing the desired rectifying behavior. The spacer presented in this work features two carboxylic anchoring groups along with an electronegative pyrazine moiety which may produce an gradient along the axis of the spacer that facilitates injection and inhibits recombination.

5.7 Design and Synthesis of a Dye for High Performance DSSC

Having shown that using the spacer **A(COOH)$_2$** can improve the efficiency of a solar cell for a simple porphyrin chromophore, an attempt was made to see if the efficiency of the record setting YD2-*o*-C8[26] dye shown could be improved by substituting the benzoic acid spacer with **A(COOH)$_2$** to produce the dye, **5.10**, as shown in figure 5.6, analogous to the substitution in dye **5.1** to form **5.2**. The HOMO-LUMO gap of **5.1** (and **5.2**) is very far from the optimal thermodynamic energy gap for a single band gap PV cell[18]. The presence of the triple bond in YD2-*o*-C8 shifts the red-most absorption into the red, and consequently, shifts the HOMO-LUMO gap energy closer to the optimal value of 887nm. In addition, YD2-*o*-C8 features an alkyl-substituted diphenylamine group at the far terminus of the dye, acting as an electron donor, imparting "push" functionality to the porphyrin dye. Finally, the phenyl rings at the 5 and 20 *meso* positions of the porphyrin macrocycle in YD2-*o*-C8 are bis-*ortho* substituted with octalkoxy groups. With these phenyl rings rotated relative to the plane of the porphyrin macrocycle, the alkoxy groups are able to wrap around the porphyrin, occupying space around the macrocycle. It is thought that this layer of "grease" inhibits the redox mediator from making contact with the TiO_2 electrode, preventing unwanted recombination.

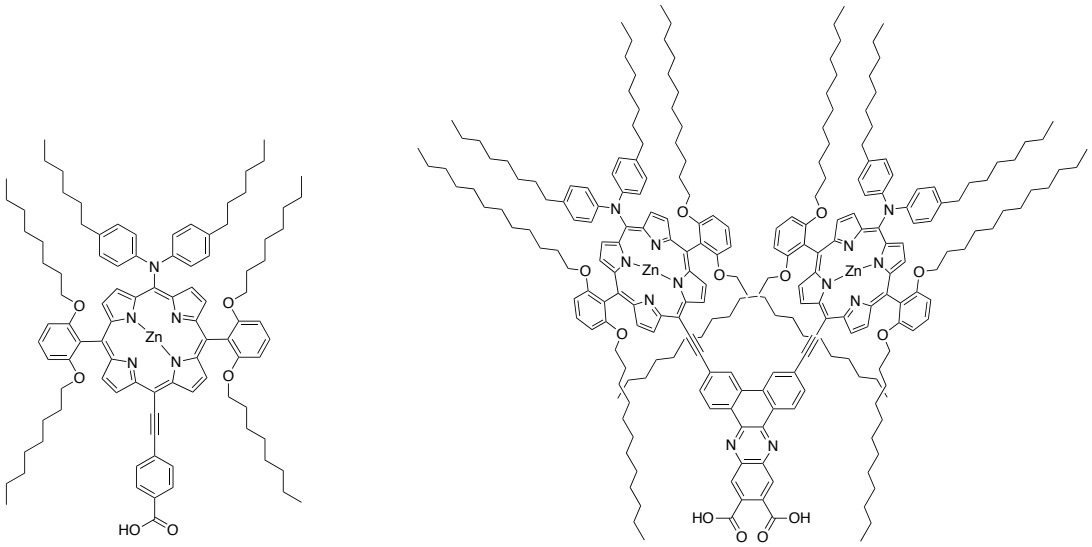

Figure 5.6 The structures of **YD2-*o*-C8** and **5.10**

The dye, **5.10**, does not employ the exact same porphyrin as is used in YD2-*o*-C8. The octyloxy groups were lengthened to be dodecyloxy groups, which could increase the insulating presence of the 8 alkoxy groups that would be present on the dye **5.10**. In a similar manner, the alkyl groups present on the diphenylamine group were extended from the hexyl groups used in **YD2-*o*-C8** to be octyl groups in **5.10**. This substitution was made because of the commercial availability of the p,p'-dioctyldiphenylamine unlike that for p,p'-dihexyldiphenylamine which requires several synthetic steps to obtain. The synthesis of the requisite tri-*iso*-propylsilyl protected alkynyl porphyrin, **5.18** (scheme 5.5) was synthesized using a similar synthetic strategy used to synthesize **YD2-*o*-C8** as outlined in the Science paper[26] by Yella *et al*.

Scheme 5.5

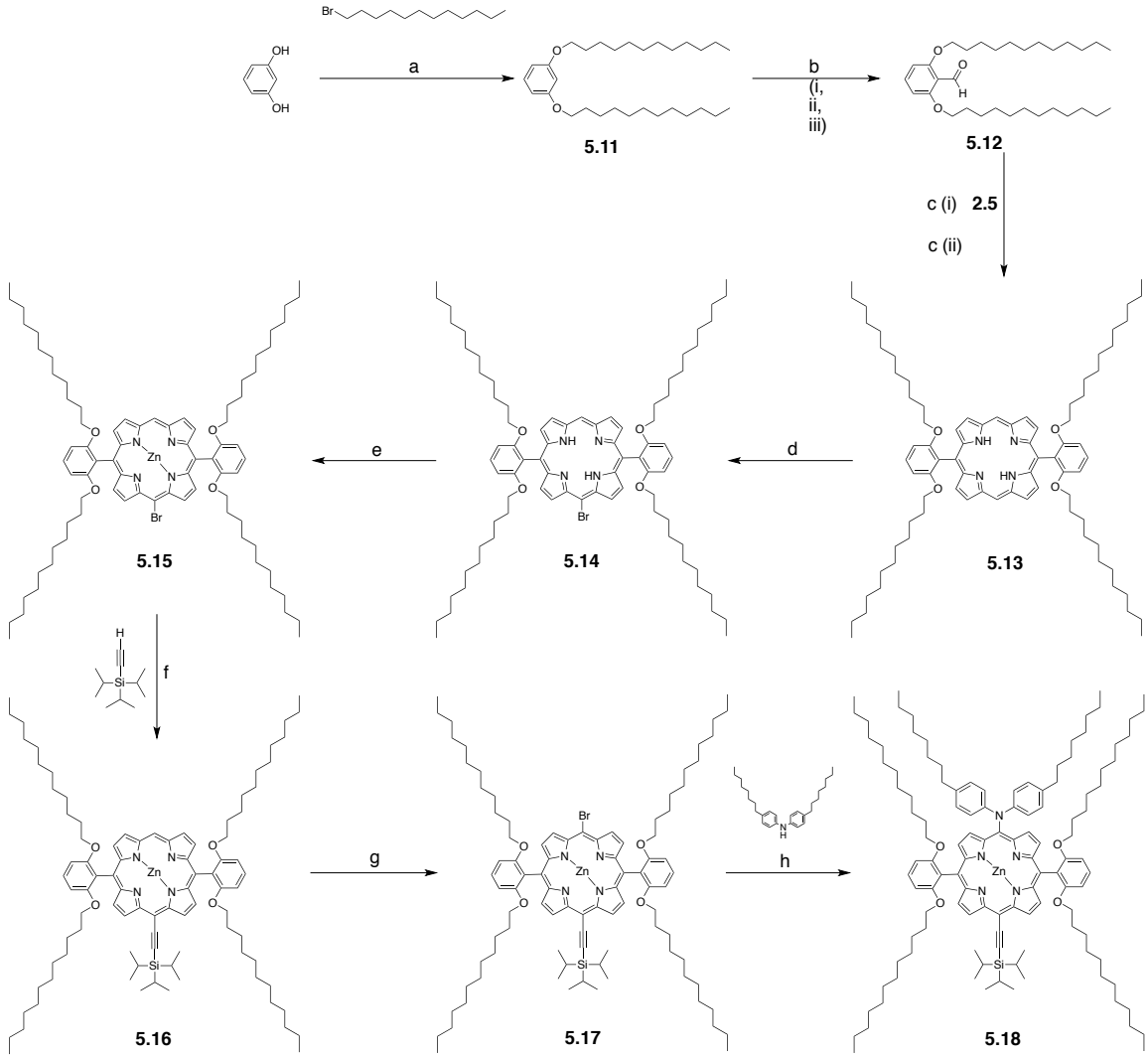

a) DMF, K_2CO_3, 80°C, overnight, Ar., 57%. **b) i** THF, TMEDA, 0°C, *n*-BuLi (1.6M), 1h, 0°C→ RT, 3h. **ii** DMF, 0°C→ RT, 16h, >100%. **c) i** $CHCl_3$/0.75% EtOH, $BF_3.OEt_2$, RT, 3h, dark. **ii** DDQ, RT, 1h, 54%. **d)** $CHCl_3$, NBS, 1h, RT, 59 %. **e)** DCM/MeOH, $Zn(AcOH).2H_2O$, reflux, overnight, 100%. **f)** THF (dry), Et_3N, CuI, $Pd(PPh_3)_2Cl_2$, Ar., reflux, 14h, 85%. **g)** $CHCl_3$/pyridine, NBS, 30min, RT, 87%. **h)** THF (dry), $Pd(OAc)_2$, DPEphos, Cs_2CO_3, Ar., 80°C, overnight. 13%.

A literature method for the synthesis of **5.11** exists in which DMSO is used as the solvent, and not DMF, as was used in this case. The synthesis of **5.11** was performed in an analogous fashion to many of the similar Williamson-Ether syntheses in this work and

like that for the analogous 1,3-bisoctyloxybenzene used in the synthesis of **YD2-*o*-C8** in the work by Yella *et al*[26]. The yield of this reaction was poor and purification was made difficult by the scale on which the reaction was conducted and the incredible chromatographic mobility of the compound, even when neat hexanes is used as the eluting solvent.

The aldehyde group present on **5.12** was introduced by generation of an aryl carbanion using *n*-BuLi at 0^{o}C and subsequent treatment with DMF. With the necessary bisdodecyloxy-substituted aryl aldeyhyde in hand, the core porphyrin macrocyle was synthesized using $BF_3.OEt_2$ as the Lewis-acid catalyst. The single porphyrin product **5.13** produced by condensing *meso*-(free)-dipyrromethane with the aldehyde **5.12** was easily purified. The four dodecyloxy groups present on the porphyrin confer significant mobility and solubility to it, even to the extent that it is soluble in neat hexanes and requires only 10% dichloromethane in hexanes to achieve mobility on silica gel. This is a stark contrast to mesityl and tolyl-substituted porphyrins that crystallize readily out of dichloromethane solutions as increasing amounts of hexanes are added.

In the synthesis of **5.18**, the alkyne groups and the diphenylamino group are both introduced by palladium-catalysed cross-couplings with the appropriate *meso*-brominated porphyrin. Care must be taken in the first bromination of **5.13** to **5.14**. Since two free *meso* positions are present, addition of excess *N*-bromosuccinimide will result in both free positions being brominated, along with the *beta* positions of the porphryin. The reaction must be carefully monitored by TLC to ensure that the stepwise addition of NBS is stopped once equal quantities of the di-*meso*-free porphyrin and the di-*meso*-brominated porphyrins are obtained, thus producing the optimal yield of the mono-*meso*-

brominated porphyrin **5.14**. The two brominatin products and residual starting material can be separated by silica gel chromatography with careful control of the solvent system using a very a-polar mixture of hexanes with 10% dichloromethane.

Prior to the copper(I) catalyzed reaction in the next step, zinc was introduced to the porphyrin macrocycle of **5.14** by addition of a methanolic solution of $Zn(AcO)_2.2H_2O$ to a solution of **5.14** in dichloromethane, and subsequent overnight reflux to produce **5.15**.

The TIPS-alkynyl group was introduced by a CuI, $Pd(PPh_3)_2Cl_2$ Sonogashira cross coupling reaction of TIPS-acetylene with **5.15**. It is important that the Zn atom was introduced in the previous step to prevent any Cu(II) generated during the reaction from being chelated by the porphyrin. Cu is difficult to remove from porphyrin macrocycles and requires harsh acidic conditions. The Sonogashira reaction proceeded in good yield and the green product was easily purified and isolated by silica gel chromatography, again using a very a-polar solvent system.

The remaining *meso*-free position of the porphyrin was brominated, again using NBS. Pyridine was added to prevent side reactions with the sensitive alkyne group present. A reaction was conducted in which the pyridine was not added. In this case, considerable degradation occurred producing a green-brown byproduct that was immobile in silica gel chromatography relative to the desired product.

At this point in the synthesis, all steps had proceeded in comparatively good yields and gram quantities of material were carried through each step. The Buchwald-Hartwig coupling of *p,p'*-diocytldiphenylamine proved to be difficult, despite considerable care being taken to exclude water and oxygen from the reactions performed. Reactions attempted using NaH were largely unsuccessful with only traces of product

being obtained. The analogous NaH method reported by Yella *et al*. for the synthesis of **YD2-*o*-C8** was attempted but without success. Analysis of the products revealed that debromination of the porphyrin was occurring without coupling to the diarylamine. Fortunately, the starting material could be regenerated by repeating the previous bromination step to provide material for further attempts.

After several attempts using different solvents and bases, the best yield was obtained using THF as the solvent and Cs_2CO_3 as the base. It was not determined if the poor yields obtained using reported literature procedures was as a result of poor preparation of solvents and reaction conditions or as a result of the differenced between the *p,p*'-dioctyldiphenylamine used as opposed to the *p,p*'-dihexyldiphenylamine used in the literature report[26].

Despite the shoddy, 13% yield achieved, sufficient material (500mg) of **5.18** had been obtained, which was sufficient to proceed with the next step. The primary goal of the synthesis was to make the dye **5.10** and determine its performance in a DSSC. Effort was not made to reproduce the literature yields that are typically upwards of 80%.

In the reported synthesis of **YD2-*o*-C8**, the product obtained on removal of the TIPS protecting group prior to coupling with 4-iodobenzoic acid is not purified or characterized but is used as a crude product immediately in the subsequent copper-free Sonogashira coupling. An effort was made to isolate this deprotected alkyne following treatment of **5.18** with 1M TBAF. The product did not fare well during silica gel chromatography and considerable degradation to produce an immobile green-brown product was observed. Consequently, efforts to isolate and characterize this intermediate

were abandoned and the literature protocol was followed in which a residue obtained following deprotection of **5.18** with 1M TBAF was used directly in the following step.

Scheme 5.6

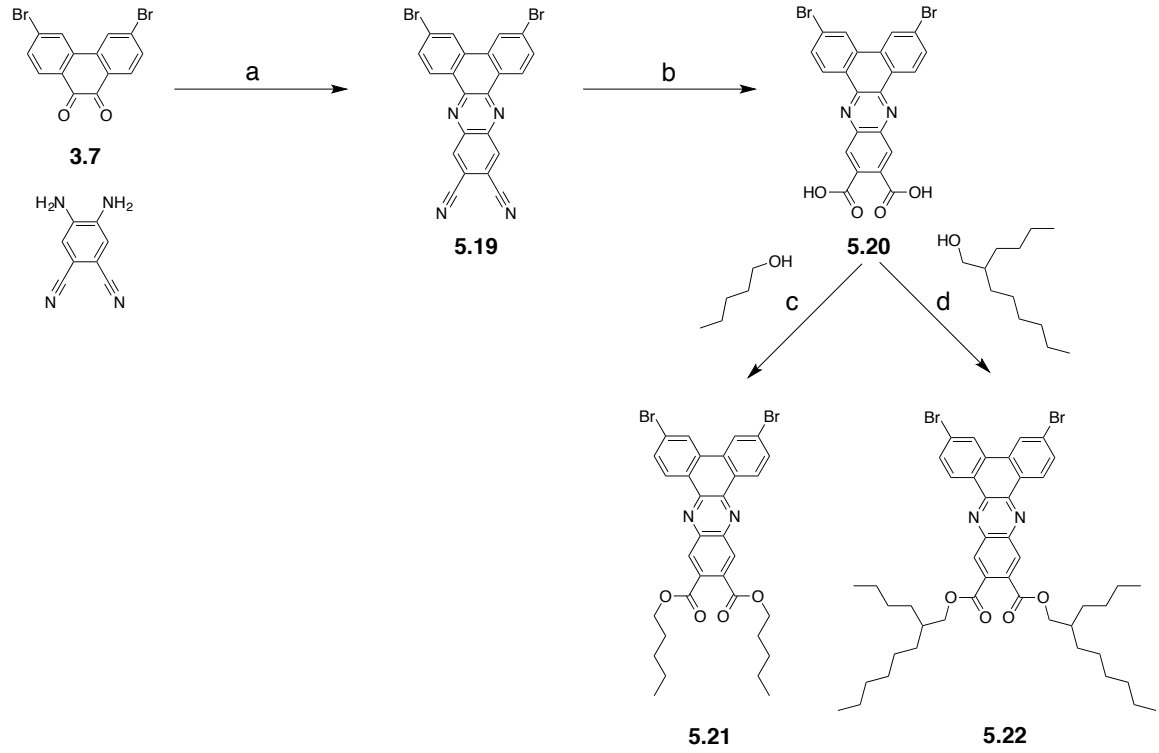

a) 1,2-dichlorobenzene:AcOH:EtOH (pressure tube), internal reflux, 2 days, 98% **b)** EtOH:H_2O (1:1), KOH, reflux, 98% **c)** Toluene, H_2SO_4 (cat.), reflux, overnight, >100% **d)** H_2SO_4 (cat.), 24h, 22%.

In the synthesis of **5.2**, the harsh conditions required to hydrolyze the nitrile groups to generate the corresponding carboxylic acid groups damaged the substituents on the porphyrin pigments. There was some concern that in employing a similar synthetic protocol for the synthesis of **5.10** as was used for the synthesis of **5.2**, that the more diversely functionalized porphyrin pigment would be damaged beyond repair during the hydrolysis of the nitrile groups. Consequently several efforts were made to design and

synthesize a building-block in which the fused-heteroaromatic core of spacer **A** is present, along with the presence of carboxylic acid group in protected ester form and two bromine atoms for attachment of chromophores by palladium-mediated cross coupling methodologies. Such a building block would increase the utility and facility of spacer **A(COOH)$_2$** in the synthesis of future dyes.

Bromine atoms have a tendency to diminish the solubility of aromatic compounds, and while **5.2** and **5.4** exhibited very good solubility, despite the presence of the extended aromatic core, without the porphyrin moieties present on these compounds, the propensity for the extended fused-heteroarmatics to stack, coupled with the diminished solubility imbued by the presence of bromine atoms would render a building-block as proposed above largely insoluble. Consequently, preliminary designs for the building-block described above featured solubilizing alkyl groups as the ester substituent. Scheme 5.6 shows the most successful designs and efforts made in producing such a building-block. **5.21** Features pentyl esters and **5.22** 2-butyl-octyl esters. The branched alkyl chain of **5.22** was hoped to confer a higher degree of solubility to the molecule than if 1-dodecanol had been used.

3,6-dibromophenanthrene-9,10-dione was condensed with 4,5-diaminophthaleonitrile to produce the largely insoluble dinitrile, dibromo heteroaromatic spacer core **5.19**. Various methods were investigated as routes to convert the nitrile groups to the corresponding acid esters. These include TFA/HCl and H_2SO_4 acid hyrolysis to the corresponding amides, which could then be converted to the desired esters. These reactions were not, however, as clean as the method shown in scheme 5.6 in which a suspension of **5.19** in ethanol containing KOH was refluxed for 2 days. More

work is required to fully characterize **5.20**, ensuring that the product obtained is free of any moisture or salts. For the purposes of this study, attention was not paid to these finer, though important details, as the primary goal was to see if the final compounds would be soluble and suitable for palladium mediated cross coupling reactions. Efforts to characterize **5.20** by NMR spectrometry failed due to insolubility, even in CF_3COOD heated to 65^oC.

A suspension of **5.20** in toluene was created and 1-pentanol was added along with a catalytic amount of H_2SO_4. Reflux of this solution using a Dean-Stark apparatus to remove water from the system produced **5.21**. The solubility of the product was poor in most common solvents but was considerably better than that of **5.20**. A ^1H NMR spectrum was obtained but required TFA as the solvent and heating to 65^oC to achieve a noisy spectrum. There was concern then, that in a reaction such as a Suzuki-coupling which is often performed in refluxing THF that the poor solubility of **5.21** would inhibit the reaction.

Consequently, the synthesis of **5.22** was attempted and produced mixed results. The reaction was conducted in 4-*n*-butyl-octan-1-ol without any solvent. Reflux of the suspension with a catalytic amount of H_2SO_4 added produced the product **5.22** along with the dianhydride dehydration product. After 24h of reflux, MS (MALDI-TOF) analysis of the reaction solution revealed that this dianhydride byproduct was stable and was not being converted to the desired product. Consequently, water was added to the reaction solution in an attempt to shift the equilibrium to convert the dianhydride back to the starting material. This seemed to help the problem somewhat but not completely, with subsequent analysis of the reaction solution still showing traces of the dianhydride

present. Following work up, attempts were made to characterize the product my NMR spectrometry but proved futile. It should be expected that the solubility of **5.22** would be considerably better than that of **5.21**, possibly even allowing for purification by column chromatography. This was not the case. As MALDI-TOF MS is not a quantitative technique, the proportion of the dianhydride contaminant in the product obtained could not be determined. It is safe to conclude that the proportion of the dianhydride byproduct decreased following the addition of water, but only under an unverified assumption that the byproduct and product are ionized to fly to the same degree could one conclude that more of product **5.22** was present. Nonetheless, MALDI-TOF analysis did affirm the synthesis of **5.22**, though further work is required to improve on the yield, purity and to complete the charaterization of the product. However, given that **5.22** could not be isolated apart from the byproduct by simple dissolution in any chlorinated attempted, it may not be worth conducting this work and redesigning the building block to feature an even more judiciously engineered entity to be soluble with a longer, and more highly branched alkyl chain than that used in **5.22**.

Scheme 5.7

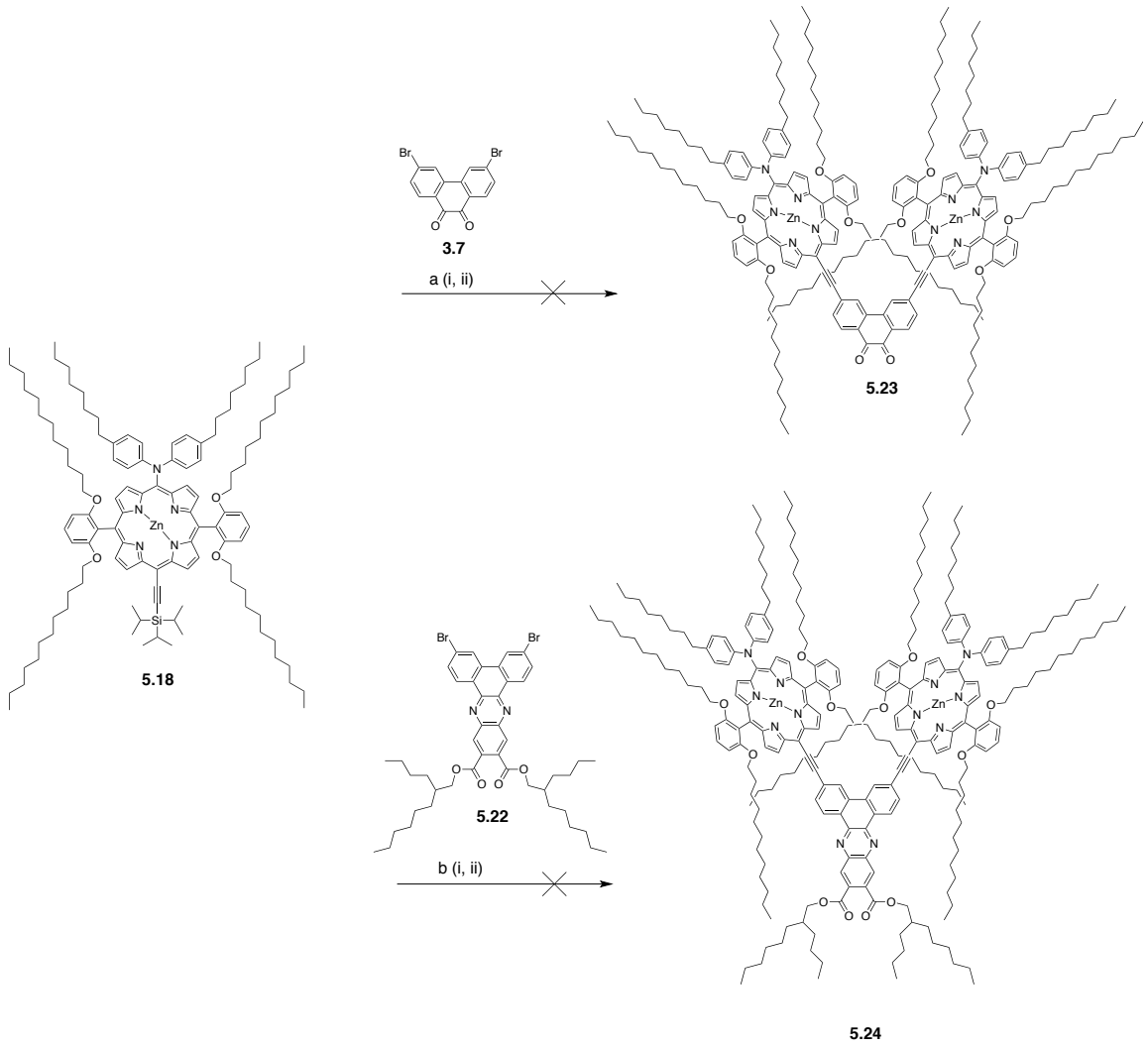

a) i THF, 1M TBAF, 30min, RT. **ii** THF (dry), $Pd_2(dba)_3$, $AsPh_3$, 80°C, Ar., 6h. **b) i** THF, 1M TBAF, 30min, RT. **ii** Toluene (dry), $Pd_2(dba)_3$, $AsPh_3$, 80°C, Ar., 6h.

Scheme 5.7 shows the two attempts that were made towards coupling the deprotected alkyne produced by treatment of **5.18** with 1M of TBAF. Both Copper-free Sonogashira cross-couplings failed. The synthesis of **5.23** was attempted as a control, to investigate if the reaction conditions were suitable for coupling the terminal alkyne with an aromatic dibromide similar to **5.22**. Sonogashira reactions show better cross-coupling yields with aromatic iodides and so it was useful to find that the reaction to produce **5.23**

failed. Thus, the failed attempt at synthesizing **5.24** was not attributed purely to the poor solubility of **5.22**. There is currently no example in the literature for the synthesis of the iodo analogue of **3.7**. All syntheses for the iodination of phenanthrene-9,10-dione present in the literature produce 2,7-diiodophenanthrene-9,10-dione and not 3,6-diiodophenanthrene-9,10-dione. Consequently, in order to produce the dye **5.10** work must be conducted to produce the iodinated analogue of **5.22**, which should also be engineered to be more soluble through altered ester functionality.

5.8 An Alternative Strategy for Introducing Carboxylic Acid Functionality into Spacer Building Blocks

The synthesis of **5.2** and the proposed synthesis of **5.10** both featured introduction of the carboxylic acid dye anchoring groups via hydrolysis of nitrile groups. An alternative route for producing fused heteroaromatic acenes terminating in *o*-carboxylic acid functionality was investigated. The high yielding and benign synthesis of **4.23** and related compounds in this work motivated finding a way to convert compounds like **4.23** to dyes that featured *o*-carboxylic acid functionality. There are several reports for the synthesis of **5.25** present in the literature together with its condensation with aromatic *o*-amines to produce ester functionalized pyrazine constructs. The synthesis of **5.25** was thus conducted according a report[186] for the production of a crude oil rich in **5.25** that employs NBS to oxidize L-diethyl tartrate in refluxing CCl_4.

Scheme 5.8

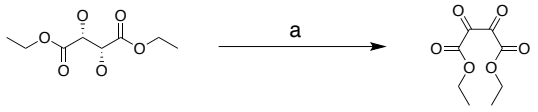

5.25

a) CCl_4, NBS, reflux, overnight, crude product obtained, not purified

Attempts were then made to condense **5.25** with compounds on hand, specifically **4.31** (scheme 5.9) and **4.23** (scheme 5.10) as part of two routes investigated for the synthesis of **5.27** from which hydrolysis of the ethyl esters present under basic conditions would produce a new dye, **5.28** (scheme 5.10). The dicarboxylic heteroaromatic spacer featured in **5.28** will be referred to as spacer **B(COOH)$_2$**. **B(COOH)$_2$** is one pyrazine ring longer that **spacer-A** and is comparable to the wire core of the series **A** molecules of chapter 4 of this dissertation.

Scheme 5.9

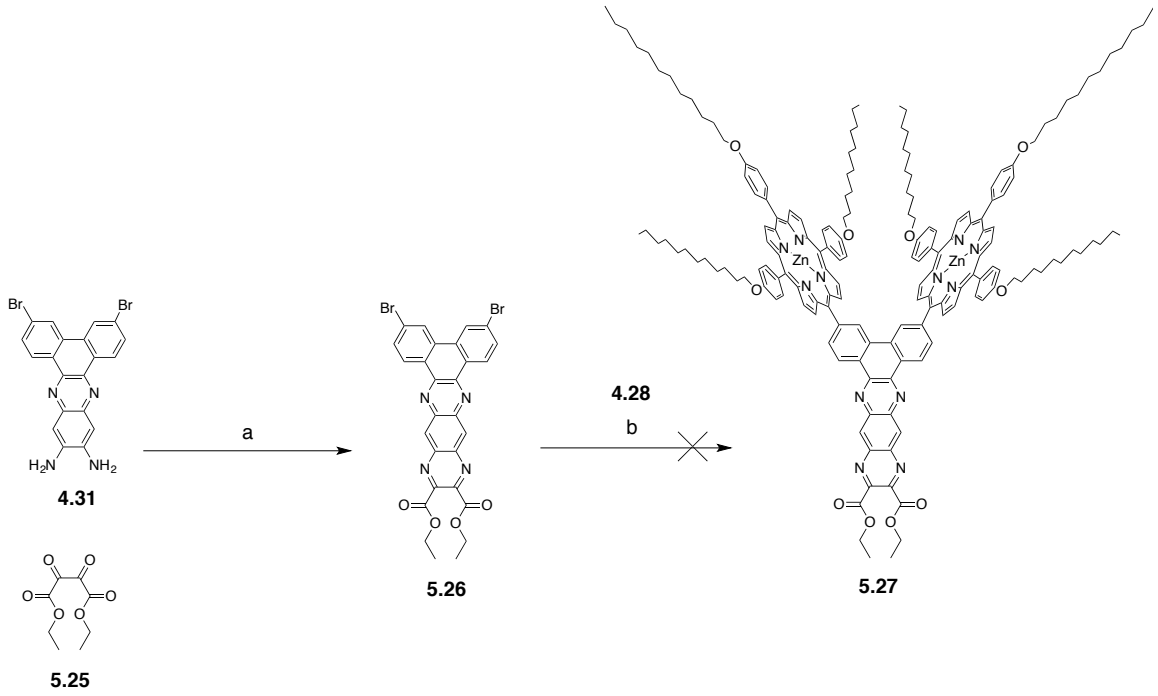

a) 1,2-Dichlorobenzene, AcOH (1:1), 110°C, 16h, 45%. **b)** $Pd(PPh_3)_4$, Cs_2CO_3, THF, 100°C, pressure tube, overnight. Debromination of **5.26** was observed.

In line with the project objectives to obtain a functional dye to test the function of spacer **B(COOH)$_2$** and to synthesize a building block that could be coupled via palladium-mediated cross coupling reactions with pigments and then hydrolyzed to produce a functional dyes, the synthesis of **5.26** (the building block) and **5.28** (the functional dye) were attempted. The crude oil obtained by the synthesis of scheme 5.8 was used to successfully synthesize the building block **5.26** (scheme 5.9) and **5.27** from **4.23** (scheme 5.10). Characterization of **5.26** by MALDI-TOF MS and by NMR spectroscopy was possible, despite it being largely insoluble in most solvents. A proton spectrum was acquired using 1,2-dichlorobenzene-*d*4 as the solvent and at 110°C.

Despite the poor solubility of **5.26**, a Suzuki-coupling of **5.26** with **4.28** was attempted. It was thought that a small fraction of the surface molecules of particulate **5.26**

present in the reaction may be able to react, and that in achieving coupling of one porphyrin entity onto the hetero-aromatic spacer, sufficient solubility would be imbued to the intermediate so that the second porphyrin would attach as in a normal solution state reaction. This did not seem to be the case and no product formation was observed.

Scheme 5.10

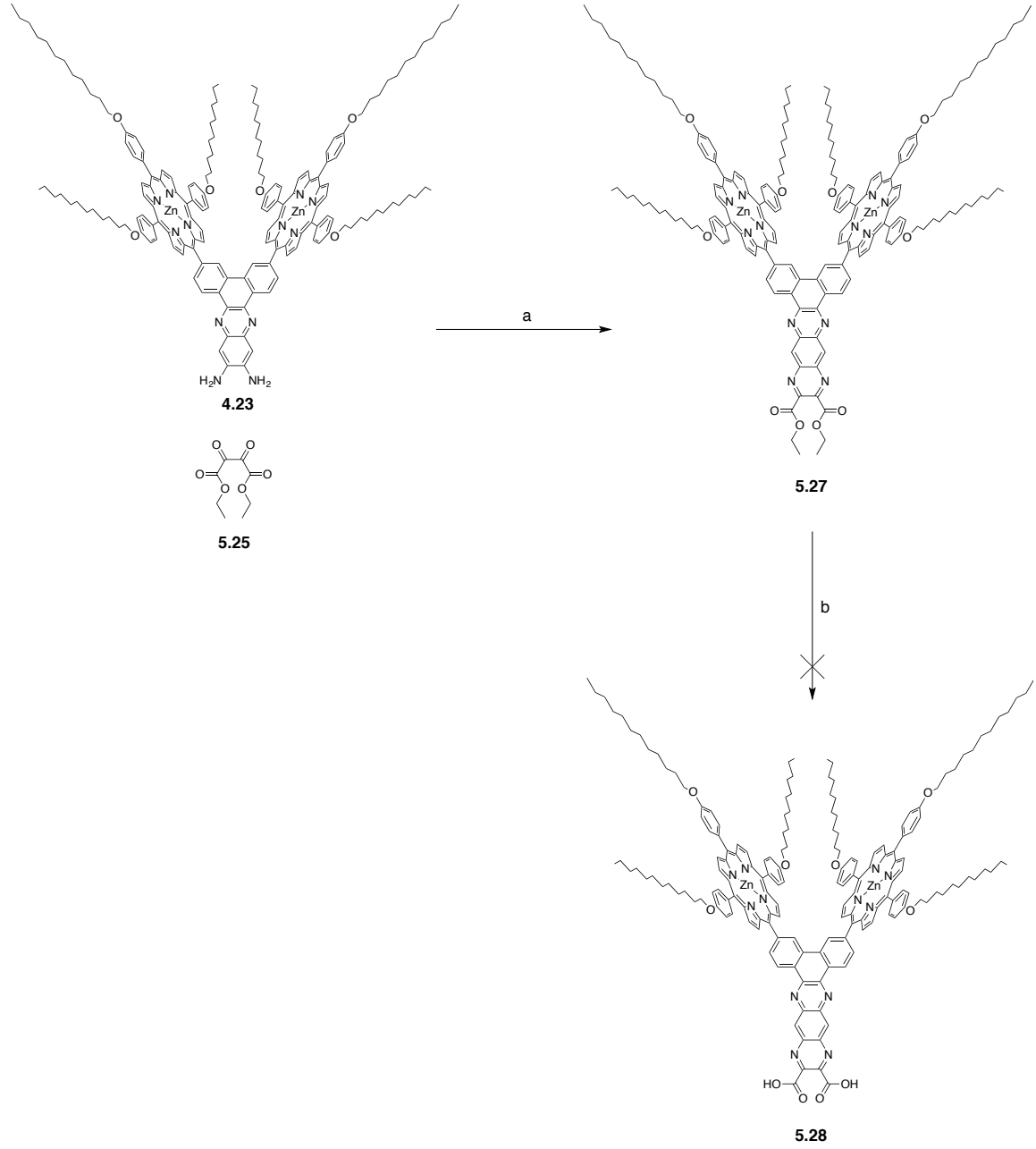

a) 1,2-Dichlorobenzene:AcOH (1:1), 110^{o}C, overnight, 58% **b)** KOH, THF/10% H_2O, reflux. Decomposition observed.

As shown in scheme 5.10, the synthesis of **5.27** can be achieved easily by heating and excess of **5.25** with **4.23** in acetic acid. The product is soluble in common chlorinated solvents which enabled characterization by NMR spectroscopy. In the subsequent

reaction in which **5.27** was treated with KOH to cleave the esters, to produce the carboxylic acid functionalities, the integrity of the terminal pyrazine appeared to have been compromised and a product was obtained with a lower mass than what was expected. No further work has been conducted to investigate what the strange product is or by what mechanism it could be produced.

5.9 Conclusions

It has been shown that the performance of a simple porphyrin chromophore can be dramatically enhanced through attachment to the fused aromatic spacer **A(COOH)$_2$**. A DSSC containing dye **5.2**, which incorporates **A(COOH)$_2$**, showed a 29% improvement in V_{OC}, a 181% improvement in $j_{\text{steady state}}$, and a 258% increase in η as compared to a DSSC with **5.1**. In addition to improving the DSSC performance, spacer **A(COOH)$_2$** presents the possibility of functionalizing the TiO_2 surface with two complementary chromophores in a well controlled 1:1 ratio. Judicious choice of chromophores in combination with the spacer **A(COOH)$_2$** would allow for testing of antenna complexes and represents the goal of future work. Exposing the porphyrins of **5.7** to the acidic conditions required to hydrolyze the dinitrile functionality is a less than ideal synthetic protocol considering the 3 steps required to regenerate the damaged dye and cleave the anhydride formed through dehydration of the dicarboxylic acid formed. To extend the use of the spacer to compounds featuring other dyes (especially more chemically sensitive chromophores), an alternative synthetic methodology is required. Further work is required to synthesize soluble spacer building blocks with the dicarboxylic acid

functionality present in masked ester form and which feature either bromine atoms for Suzuki-coupling or iodine atoms for Sonogashira-coupling methodologies.

5.10 Materials and Methods

5.10.1 General

Dichloromethane, chloroform, carbontetrachloride, hexanes, ethyl acetate, tetrahydrofuran, toluene and methanol were purchased from BDH. 200 PROOF ethanol was purchased from KOPTEC. DMF was purchased from Alfa Aesar and stored over sieves prior to use. 1,2-Dichlorobenzene and 1,4-dioxane were purchased from Sigma-Aldrich. Solvents were used without purification unless stated otherwise. Tetrahydrofuran was distilled over CaH under argon and stored over molecular sieves. 4-Forymyl-methylbenzoate, 4,5-diaminophthaleonitrile, 4-nitrobenzaldehyde, resorcinol, (triisopropylsilyl)acetylene, 1-pentanol and 2-*n*-butyl-octanol starting materials were purchased from Sigma-Aldrich. *p*-Dodecyloxybenzaldehyde and L-diethyltartrate starting materials were obtained for Alfa Aesar. *p,p'*-Dioctyldiphenylamine was purchased from MP Biomedical. $Zn(OAc)_2.2H_2O$ was purchased fro Mallinckrodt Baker. Et_3N and 1.6M *n*-butyllithium reagents were obtained from Alfa Aesar. N,N,N',N'-tetramethylethylenediamine, 1.6M *n*-butyllithium, copper iodide, DPEphos, *N*-bromosuccinimide, 2,3-dicholoro-5,6-benzoquinone, $BF_3.OEt_2$, $Pd_2(dba)_3$, 1M TBAF, $Pd(PPh_3)_4$, $Pd_2(PPh_3)_2Cl_2$ $Pd(OAc)_2$, $AsPh_3$ and Cs_2CO_3 reagents were purchased from Sigma Aldrich. Silica for silica gel chromatography was purchased from Silicycle.

Matrix assisted laser desorption/ionization time of flight (MALDI-TOF) mass spectra were acquired using an Applied Biosystems Voyager-DE STR workstation and acquired in reflector mode using terthiophene, diphenylbutadiene or dithranol as the matrix. NMR spectroscopy was conducted using a Varian (Agilent) MR 400 MHz NMR spectrometer operating at a 1H Lamor frequncy of 399.87 MHz, equipped with a 5 mm Broadband Observe Z-gradient probe.. UV-Vis spectra were acquired using a Shimadzu UV-Vis spectrometer.

5.10.2 Synthesis of Compounds

5.1 0.187g (0.155mmol) of **5.6** was taken up in 300ml dichloromethane to which 0.339g (1.55mmol) $Zn(AcO)_2.2H_2O$ dissolved in 30ml MeOH was added. The solution was allowed to reflux overnight. The solution was diluted with 100ml dichloromethane and washed with water. The organic layer was concentrated and chromatographed on silca gel using DCM/4% MeOH as the eluting solvent. A few drops of pyridine was added to prevent crystal formation at the silica solvent interface. Concentration and drying on hi-vac of appropriate fractions afforded 0.186g (0.146 mmol, yield: 94%). ^{1}H NMR (400 MHz, $CDCl_3$): δ 8.97 (d, J = 4.6Hz, 2H), 8.95 (bs, 4H), 8.86 (d, J = 4.6Hz, 2H), 8.51 (d, J = 8.0Hz, 2H), 8.35 (d, J = 8.0Hz, 2H), 8.10 (d, J = 8.3Hz, 6H), 7.25 (m, 6H), 4.23 (t, J = 6.5Hz, 6H), 1.97 (quin, J = 7.8Hz, 6H), 1.62 (quin, J = 7.8Hz, 6H), 1.53-1.20 (m, 48H), 0.90 (t, J = 6.7Hz, 9H). ^{13}C NMR (100 MHz, CDCl3): δ 171.5, 158.90, 150.84, 150.66, 150.59, 149.50, 150.44, 143.53, 135.61, 135.47, 135.44, 134.86, 132.35, 132.10, 131.98, 131.23, 128.42, 128.34, 122.36, 121.35,

121.03, 118.87, 112.64, 68.49, 32.12, 29.90, 29.85, 29.72, 29.56, 26.42, 22.88, 14.30. MS (MALDI-TOF) m/z: obsvd 1273.1544 $[M]^+$ calcd 1272.6980.

5.2 78.3mg of **5.7** was dissolved in 50ml of trifluoroacetic acid in a pressure tube. 50ml Of 12.1 M HCl was added carefully and the tube sealed quickly with a Teflon screw cap. The mixture was heated at reflux for 6 days after which it was cooled and the solution transferred to a separating funnel containing 300ml dichloromethane. The solution was neutralized with 3M NaOH. The organic layer was isolated and washed further with saturated $NaHCO_3$ prior to concentration and drying on hi-vac. overnight. MALDI-TOF analysis of the residue revealed that varying degrees of hydrolysis of the dodecyloxy groups had occurred. Consequently, the purple residue was taken up in 200ml of dry DMF, 0.25g of K_2CO_3 was added followed by 0.3ml of 1-bromododecane. The solution was stirred at 70^oC overnight, cooled, transferred into a sep. funnel containing 500ml H_2O and extracted with EtOAc. The organic layer was concentrated and the purple residue was dissolved in 300ml dichloromethane. 0.065g of $ZnAcO_2.H_2O$ dissolved in 50ml methanol was added and the solution was allowed to reflux overnight. The dichloromethane solution was cooled, washed with water and concentrated prior to being dissolved in 200ml THF. 1g of KOH and 20ml of H_2O were added and the solution was heated to reflux for 16 hours following which the solution was cooled, carefully neutralized with 4N hydrochloric acid and extracted with dichloromethane. In the extraction, glacial acetic acid was added as required to facilitate extraction. The isolated dichloromethane layer was washed with water, concentrated *in vacuo* and dried on hi-vac overnight. The residue was chromatographed on silica gel using dichloromethane followed by dichloromethane with 1 %, then 4 % MeOH and finally 6% MeOH with 1%

AcOH. ^{1}H NMR (400 MHz, 1,1,2,2-tetrachloroethane-*d*6): δ 9.94 (d, J = 7.6Hz, 2H), 9.54 (m, 2H), 9.16-8.63 (m, 18H), 8.05 (m, 8H), 7.79 (m, 4H), 7.26 (m, 8H), 7.00 (m, 4H), 4.27 (m, 8H), 4.08 (m, 4H), 1.96 (m, 12H), 1.66 (m, 12H), 1.61-1.08 (m, 96H), 0.96 (s, 18H). MS (MALDI-TOF) m/z: obsvd 2669.5184 $[M]^{+}$ calcd 2669.4030.

5.3. 5.8 (0.103g, 0.085mmol) was dissolved in 50ml DCM. To this, $Zn(AcO)_2.H_2O$ (0.187g, 0.85mmol) dissolved in 5ml MeOH was added and the solution warmed to reflux overnight. On cooling, the solution was washed with 200ml H_2O and the organic layer isolated and concentrated. The residue was taken up in DCM and passed through a short silica column using DCM. The eluent was concentrated affording 98.5mg (77.19μmol, 91% yield) of a purple residue. ^{1}H NMR (400 MHz, $CDCl_3$): δ 8.99 (m, 6H), 8.80 (d, J = 4.68Hz, 2H), 8.59 (d, 2H, J = 8.5Hz), 8.73 (d, J = 8.5Hz, 2H), 8.08 (m, 6H), 7.23 (d, J = 8.7Hz, 6H), 4.19 (t, J = 6.4Hz, 6H), 1.95 (quin, J = 7.6Hz, 6H), 1.60 (quin, J = 7.8Hz, 6H), 1.51-1.22 (m, 48H), 0.90 (t, J = 6.8Hz). ^{13}C NMR (100 MHz, $CDCl_3$): δ 159.05, 151.08, 150.86, 150.27, 149.17, 147.67, 135.55, 135.16, 134.91, 134.86, 132.83, 132.49, 132.32, 130.92, 122.04, 121.83, 121.58, 117.51, 112.82, 68.50, 32.11, 29.89, 29.84, 29.70, 29.66, 29.55, 26.40, 22.88, 14.30. MS (MALDI-TOF) m/z: obsvd 1273.6103 $[M]^{+}$ calcd 1273.6932.

5.4 61.6mg (24.50μmol) of **4.15**, 48.5mg (245.0μmol) of 1,2-dinitro-4,5-diaminobenze (**5.9**) were placed in a 100ml RBF along with 10ml of a 2:1:1 mixture of toluene:AcOH:EtOH. The flask was fitted with a reflux condenser and left to reflux overnight. The solution was diluted with 50ml toluene and transferred to a separating funnel to be washed with water. The organic layer was collected and concentrated. The resulting residue was purified by silica gel chromatography using DCM:Hex. (7:3→ 1:0)

as the eluting solvent. Concentration of relevant fractions afforded 63mg (23.54μmol, 96%)of the product. ^{1}H NMR (400 MHz, $CDCl_3$): δ 9.57 (d, J = 7.8Hz, 2H), 9.43 (s, 2H), 8.84 (s, J = 4.6Hz, 8H), 8.80 (d, J = 4.6Hz, 4H), 8.64 (m, 4H), 8.01 (d, J = 8.5Hz, 2H), 7.94 (m, 6H), 7.67 (d, J = 7.9Hz, 4H), 7.14 (m, 4H), 7.08 (d, J =8.2Hz, 4H), 6.85 (d, J = 7.2Hz, 4H), 4.13 (t, J = 6.4Hz,4H), 3.97 (t, J = 6.1Hz, 8H), 1.90 (quin, J = 7.6Hz, 4H), 1.81 (quin, J = 7.4Hz, 8H), 1.81 (quin, J = 7.4Hz, 8H), 1.60-1.09 (m, 108H), 0.88 (t, J = 6.9Hz, 18H). ^{13}C NMR (100 MHz, $CDCl_3$): δ 158.93, 158.81, 50.80, 150.65, 150.44, 149.45, 147.85, 146.66, 142.16, 141.65, 135.43, 135.30, 134.86, 134.71, 132.60, 132.25, 132.11, 131.67, 131.24, 129.83, 128.48, 127.40, 125.55, 121.65, 121.27, 118.92, 112.69, 112.64, 112.52, 68.42, 68.31, 32.10, 29.87, 29.84, 29.83, 29.82, 29.79, 29.66, 29.65, 29.56, 29.54, 29.53, 26.31, 22.87, 14.30, 14.29. MS (MALDI-TOF) m/z: obsvd 2669.5184 $[M]^+$ calcd 2669.4030

5.5 2.5l Of chloroform containing 18.75ml EtOH was deoxygenated with bubbling argon for 20 minutes. To this, 409mg (2.492mmol) methyl-4-formyl benzoate, 2.025g (4.984 mmol) of meso-(4-dodecyloxyphen-1-yl)-2,2í-dipyrromethane and 0.724g (2.49 mmol) 4-dodecyloxybenzaldehyde were added with stirring followed by 0.13ml (1.047mmol) $BF_3.OEt_2$. The solution was allowed to stir in the dark under argon for 3h following which 1.7g (7.49mmol) DDQ was added and stirred for 45 more minutes. The solution was filtered through a thick pad of silica, concentrated and the residue purified using silica gel chromatography employing hexane:DCM (1:1) to neat DCM as the eluting solvent system. Concentration of relevant fractions yielded 0.336g (0.274mmol: 11%) of product. ^{1}H NMR (400 MHz, $CDCl_3$): δ 8.88 (d, J = 5.6 Hz, 6H), 8.764 (d, J = 4.4 Hz, 2H), 8.42 (d, J = 8.0 Hz, 2H), 8.29 (d, J = 8.4 Hz, 2H), 8.09 (d, J = 8.4 Hz, 2H),

8.08 (d, *J* = 8.4 Hz, 4H), 7.23 (d, *J* = 8.0 Hz, 6H), 4.19 (t, *J* = 6.8 Hz, 6 H), 4.09 (s, 3H), 1.95 (p, *J*= 7.2 Hz, 6H), 1.60 (p, *J* = 7.2 Hz, 6H), 1.31 (bm, 54H), 0.91 (t, *J* = 6Hz, H), -2.7 (s, 2 H). ^{13}C NMR (100 MHz, CDCl3): δ 167.50, 159.17, 147.38, 135.84, 135.63, 134.89, 134. 45, 134.39, 129.62, 128.21, 127.87, 120.65, 120.31, 118.28, 113.11, 112.62, 68.71, 68.46, 68.21, 32.12, 29.89, 29.84, 29.65, 29.65, 29.56, 26.39, 22.88, 14.38, 14.23. MS (MALDI-TOF) m/z: obsvd 1224.9138 $[M]^+$, calcd 1224.8001.

5.6. 90ml of isopropanol and 40ml of 2M KOH were added to a round bottom flask containing 0.3346g (0.273mmol) of **5.5**. The flask was fitted with a condenser and allowed to reflux with stirring overnight. The solution was neutralized with 4M HCl and extracted with dichloromethane. The organic layer was concentrated and dried on hi-vac yielding 0.2905g (0.24mmol, 88%) of the carboxylic acid product. ^{1}H NMR (400 MHz, $CDCl_3$): δ 8.89 (m, 6H), 8.80 (d, *J* = 4.8Hz, 2H), 8.56 (d, *J* = 8.0Hz, 2H), 8.37 (d, *J* = 8.1Hz, 2H), 8.10 (m, 6H), 7.26 (m, 6H), 4.23 (m, 6H), 1.97 (m, 6H), 1.62 (m, 6H), 1.54-1.16 (m, 48H), 0.90 (t, *J* = 6.6Hz, 9H), -2.73 (s, 2H). ^{13}C NMR (100 MHz, $CDCl_3$): δ 159.20, 159.19, 148.30, 135.74, 134.90, 134.47, 134.38, 128.70, 120.71, 120.36, 118.10, 112.90, 68.52, 32.11, 29.89, 29.85, 29.71, 29.68, 26.41, 22.88, 14.30. MS (MALDI-TOF) m/z: obsvd 1210.5601 $[M]^+$ calcd 1210.7845.

5.7. 127mg (50.63 μmol) of **4.15** and 24mg (151.9 μmol) of 4,5-diaminophthalonitrile along with 20ml of toluene, 10ml of glacial acetic acid and 10ml ethanol were placed in a 100ml round bottom flask and allowed to reflux for 20h. The reaction solution was cooled, diluted with 100ml of toluene and transferred to a separating funnel. The solution was washed with 200ml of water, the organic layer collected, concentrated and dried on hi-vac.. The residue was taken up in DCM, loaded

onto a silica-gel column and chromatographed using DCM:Hexanes (3:2) as the eluting solvent. Appropriate fractions were concentrated yielding 124mg (46.8μmol, 93%) of the desired product. ^{1}H NMR (400 MHz, $CDCl_3$, 58^{o}C): δ 9.47 (d, J = 8.0Hz, 2H), 9.41 (s, 2H), 8.83 (m, 16H), 8.65 (d, J = 8.4 Hz, 2H), 8.60 (d, J = 8.0 Hz, 2H), 7.96 (m, 8H), 7.69 (d, J = 3.6 Hz, 4H), 7.16 (m, 4H), 7.09 (d, J = 6.4 Hz, 4H), 6.88 (d, J = 4.8 Hz, 4H), 4.16 (t, J = 6.8 Hz, 4H), 4.00 (t, 6.4 Hz, 8H), 1.91 (p, J = 8 Hz, 4H), 1.80 (p, J = 7.2Hz, 8H), 1.56 (p, J = 7.6Hz, 4H), 1.44 (p, J = 6.8Hz, 8H), 1.28 (bs, 48H), 0.864 (t, J = 7.2 Hz, 18H).^{13}C NMR (100 MHz, CDCl3): δ 159.21, 159.08, 151.00, 150.88, 150.59, 149.62, 147.81, 146.13, 141.39, 136.26, 135.62, 135.51, 135.07, 134.93, 132.72, 132.34, 132.17, 131.17, 131.27, 129.94, 128.67, 125.69, 121.83, 121.37, 119.08, 114.74, 112.97, 112.87, 112.69, 68.672, 68.55, 32.10, 29.87, 29.84, 29.82, 29.80, 29.78, 29.74, 29.69, 29.66, 29.51, 26.41, 26.35, 22.84, 14.18. MS (MALDI-TOF) m/z: obsvd 2630.1573 $[M]^{+}$ calcd 2631.4138.

5.8 To a 1l RBF containing $CHCl_3$ (750ml) and EtOH (5.7ml), 4-dodecyloxybenzaldehyde (0.536g, 1.85mmol), 4-nitrobenzaldehyde (0.279g, 1.85mmol), and **4.27** (1.5g, 3.69mmol) were added. In the dark, $BF_3.OEt_2$ (0.097ml, 0.775mmol) was added and the solution allowed to stir for 3h at RT. Following this period, DDQ (1.275g, 5.54mmol) was added and the solution left to stir for an additional hour. The dark solution was filtered through a pad of celite, concentrated and the residue purified by silica gel chromatography using DCM:Hex. (4:1) as the eluting solvent. Concentration of relevant fractions afforded 0.306g (0.253mmol, 14% yield) of the product **5.8**. ^{1}H NMR (400 MHz, $CDCl_3$): δ 8.86 (m, 6H), 8.65 (d, J = 4.7Hz, 2H), 8.50 (d, J = 8.6Hz, 2H), 8.27 (d, J = 8.6Hz, 2H), 8.04 (m, 6H), 7.19 (m, 6H), 4.13 (m, 6H), 1.92 (quin, J = 6.6Hz, 6H),

1.58 (quin, J = 6.6Hz, 6H), 1.49-1.23 (m, 48H), 0.90 (m, 9H), -2.72 (s, 2H). ^{1}H NMR (100 MHz, $CDCl_3$): δ 159.22, 149.48, 147.72, 136.39, 135.73, 135.35, 135.09, 134.28, 134.19, 131.68 (broad), 122.02, 121.73, 121.17, 120.62, 116.34, 113.06, 112.74, 68.43, 32.12, 29.90, 29.86, 29.70, 29.64, 29.56, 26.40, 22.89. MS (MALDI-TOF) m/z: obsvd 1211.8730 $[M]^+$ calcd 1211.7797.

5.9 Argon was bubbled through solution of 4ml H_2O and 40ml H_2SO_4 in a RBF. **3.11** (8.5g, 16.78mmol) was added, the flask fitted with reflux condenser and heated to stir under argon at 100^{o}C for 3.5h. The solution was then cooled and stored at 4^{o}C overnight. The solution was then poured into 500ml of crushed ice and further diluted with 400ml water. The solution was warmed gently with stirring to dissolve the yellow ppt. that had formed. The solution was filtered and the filtrate treated with solid $NaHCO_3$ until evolution of CO_2 ceased. The red ppt. formed in this step was isolated by filtration. The red solid was dissolved in 300ml of EtOH and 2.2l of water added causing a red precipitate to reform that was isolated by filtration and dried on hi-vac overnight. The filtrate was left to stand for 3days and subsequently filtered and dried. The solids obtained were combined for a total yield of 1.654g (8.345mmol, 50%). ^{1}H NMR (400 MHz, DMSO-*d*6): δ 7.06 (s, 2H), 6.09 (s, 4H). ^{13}C NMR (100 MHz, DMSO-*d*6): δ 138.53, 133.26, 107.64.

5.11 Resorcinol (25g, 227.05mmol) and K_2CO_3 (125.5g, 908.18mmol) were placed in a 1l, oven-dried, RBF containing a magnetic stirrer bar. Under a flow of argon, 600ml of anhydrous DMF was added followed by 1-bromododecane (130.8ml, 544.91mmol). The solution was heated to 80^{o}C and left to stir overnight under argon. The solution was cooled, 600ml H_2O was added and extracted with hexanes:EtOAc (1:1). The

organic layer was collected and concentrated. The residue obtained was dried on hi-vac. overnight and then purified by silica-gel chromatography using hexanes/5% EtOAc as the solvent system. Concentration of relevant fractions afforded 57.42g (128.53mmol, 57% yield) of a waxy white solid.

5.12 20g (44.77mmol) of 1,3-bis(dodecyloxy)benzene (**5.11**) was dissolved in 130ml dry THF in a 250ml RBF containing a magnetic stirrer bar. The flask was sealed with a rubber septum, 9ml of TMEDA was added and a needle was inserted to bubble argon through the solution for 20minutes. The flask was cooled to 0^{o}C and 33.58ml (53.72mmol) of 1.6M *n*-BuLi was added slowly via syringe over 5min. The solution was left to stir under argon at 0^{o}C for 1h and then was allowed to warm to RT and stir at that temperature for 3h. The solution was then cooled to 0^{o}C and 8.76ml of DMF was added and allowed to warm to RT to stir for 16h at that temperature under argon. The solution was transferred to a separating funnel, quenched and washed with water and extracted with ethyl acetate. The organic layer was concentrated and purified by silica gel chromatography using Hexanes/1% EtOAc as the eluting solvent. Concentration of relevant fractions afforded 22.74g, (47.88mmol, >100% yield) of the product. The product was dried on hi-vac but the dense, white waxy solid could not be dried further and was used as is. ^{1}H NMR (400 MHz, $CDCl_3$): δ 10.54 (s, 1H), 7.36 (t, J = 8.44Hz, 1H), 6.52 (d, J = 8.5Hz, 2H), 4.01 (t, J = 6.6Hz, 4H), 1.82 (quin, J = 8.0Hz, 4H), 1.46 (m, 4H), 1.39-1.18 (m, 32H), 0.88 (t, J = 7Hz, 6H). ^{13}C NMR (100 MHz, $CDCl_3$): δ 189.38, 161.77, 135.59, 114.89, 104.61, 69.03, 32.02, 29.76, 29.73, 29.71, 29.66, 29.45, 29.16, 26.08, 22.79, 14.20.

5.13 Argon was bubbled through a solution of 4l $CHCl_3$ and 30ml EtOH for 20minutes. 3.654g (25mmol) dipyrromethane (**2.5**), 11.869g (25mmol) **5.12** and 1.32ml (10.5mmol) were added sequentially and the solution left to stir under a blanket of argon in the dark for 3h. DDQ (17g, 75mmol) was then added and the solution left to stir for 1h further. The reaction solution was passed through a thick pad of silica, concentrated then purified by silica gel chromatography using neat DCM to elute the red product affording 8.151g (6.793mmol, 54%). ^{1}H NMR (400 MHz, $CDCl_3$): δ 10.13 (s, 2H), 9.25 (d, J = 4.6Hz, 4H), 8.97 (d, J = 4.6Hz, 4H), 7.67 (t, J = 8.4Hz, 2H), 7.00 (d, J = 8.48, 4H), 3.81 (t, J = 6.5Hz, 8H), 1.23 (m, 16H), 1.14 (m, 16H), 0.99 (quin, J = 7.6Hz, 8H), 0.87 (m, 28H), 0.70 (quin, J = 7.4Hz, 8H), 0.54 (m, 16H), 0.43 (m, 8H), -3.0 (s, 2H). ^{13}C NMR (100 MHz, $CDCl_3$): δ 160.30, 147.80, 145.09, 130.93, 130.57, 130.14, 120.14, 111.69, 105.44, 104.07, 68.82, 32.07, 29.66, 29.60, 29.48, 29.36, 29.22, 28.85, 28.76, 25.44, 22.86, 14.30.

5.14. 8.15g (6.793mmol) of **5.13** was dissolved in 500ml $CHCl_3$. With stirring, and in the dark, 1.209g (6.793mmol) of *N*-bromosuccinimide was added in small portions over 30minutes. The solution was allowed to stir for 1h in the dark and subsequently concentrated. The residue was purified by silica gel chromatography using DCM:Hex (1:9→2:8) as the eluting solvent. Concentration of the middle band afforded 5.121g (4.00mmol, 59% yield). ^{1}H NMR (400 MHz, $CDCl_3$): δ 10.0 (s, 1H), 9.61 (d, J = 4.8Hz, 2H), 9.15 (d, J = 4.6Hz, 2H), 8.87 (t, J = 4.4Hz, 4H), 7.70 (t, J = 8.4Hz, 2H), 7.00 (d, J = 8.4Hz, 4H), 3.82 (t, J = 6.5Hz, 8H), 1.22 (quin, J = 7.3Hz, 8H), 1.12 (m, 16H), 0.95 (sept. J = 8.3Hz, 16H), 0,84 (m, 20H), 0.68 (quin, J = 7.1Hz, 8H), 0.54 (m, 16H), 0.42 (quin, J = 6.2Hz, 8H), -2.87 (s, 2H).

5.15 5.057g (3.951mmol) of **5.15** was taken up in 500ml DCM. A solution of 8.672g (39.51mmol) $Zn(AcO).2H_2O$ in 50ml MeOH was added and heated to reflux overnight. The solution was washed with water and the organic layer concentrated. The residue was taken up in DCM and passed through a short silica gel column. The red eluent was concentrated affording 5.302g (3.95mmol, 100%). ^{1}H NMR (400 MHz, $CDCl_3$): δ 10.07 (s, 1H), 9.71 (d, J = 4Hz, 2H), 9.25 (d, J = 4.6Hz, 2H), 8.97 (t, J = 4.4Hz, 4H), 7.66 (t, J = 8.4Hz, 2H), 6.98 (d, J = 8.5Hz, 4H), 3.81 (t, J = 6.3Hz, 8H), 1.21 (quin, J = 7.3Hz, 8H), 1.10 (m, 16H), 0.92 (m, 16H), 0.84 (t, J = 7.1Hz, 12H), 0.78 (m, 8H), 0.58 (quin, 7.6Hz, 8H), 0.53-0.26 (24H). ^{13}C NMR (100 MHz, $CDCl_3$): δ 160.19, 151.26, 151.12, 150.14, 149.02, 132.60, 132.46, 132.40, 131.76, 130.01, 121.24, 113.80, 105.46, 103.82, 68.79, 32.06, 29.63, 29.53, 29.46, 29.34, 28.82, 28.75, 25.36, 22.86. MS (MALDI-TOF) m/z: obsvd 1276.6822 $[M]^+$ calcd 1276.8253.

5.16 4.72g (3.517mmol) of **5.15** was dissolved in 200ml of freshly distilled THF. Et_3N (30ml) was added and argon was bubbled through the solution for 20 minutes. Under an argon blanket, triisopropylacetylene (1.953ml, 8.792mmol), CuI (0.201g, 1.055mmol) and $Pd(PPh_3)_2Cl_2$ (0.494g, 0.703mmol) were added, the vessel fitted with a reflux condenser and heated to reflux under argon for 14h. The solution was then concentrated and the residue purified by silica gel chromatography (DCM:hex. = 1:4) affording 4.322g (2.994mmol, 85% yield). ^{1}H NMR (400 MHz, $CDCl_3$): δ 10.07 (s, 1H), 9.78 (d, J = 4.6Hz, 2H), 9.23 (d, J = 4.6Hz, 2H), 8.97 (m, 4H), 7.65 (t, J = 8.4Hz, 2H), 6.97 (d, J = 8.5Hz, 4H), 3.81 (t, J = 6.45 Hz, 8H), 1.47 (m, 21H), 1.20 (quin., J = 7.6Hz, 8H), 1.08 (m, 16H), 0.90 (m, 16H), 0.82 (t, J = 7.1Hz, 12H), 0.75 (m, 8H), 0.56 (quin., J = 7.6Hz, 8H), 0.51-0.27 (m, 24H). ^{13}C NMR (100 MHz, $CDCl_3$): δ 160.22, 152.30,

151.20, 150.58, 149.38, 132.26, 131.82, 131.61, 130.90, 129.96, 121.39, 114.09, 110.47, 106.54, 105.58, 99.34, 96.27, 68.89, 32.07, 29.65, 29.50, 29.46, 29.33, 29.15, 28.81, 28.78, 25.37, 22.88, 19.36, 14.31, 12.21. MS (MALDI-TOF) m/z: obsvd 1440.9378 $[M]^+$ calcd 1440.9617.

5.17 4.32g (2.99mmol) of **5.16** was dissolved in 1l of $CHCl_3$ and 40ml of pyridine added. With stirring, 0.46g (3.59mmol) of NBS was added in small portions over a 15min. period. After 30min. total reaction time, the reaction was quenched with 50ml of acetone and concentrated. The residue was purified by silica gel chromatography using DCM:hex. (1:4) as the eluting solvent. Concentration of relevant fractions afforded 3.94g (2.589mmol, 87% yield) of product. ^{1}H NMR (400 MHz, $CDCl_3$): δ 9.65 (m, 2H), 9.58 (m, 2H), 8.85 (m, 4H), 7.67 (t, J = 8.3Hz, 2H), 6.98 (d, J = 8.5Hz, 4H), 3.82 (d, J = 8.5Hz, 4H), 3.82 (t, J = 6.1Hz, 8H), 1.43 (m, 21H), 1.19 (m, 8H), 1.08 (m, 16H), 0.93 (m, 16H), 0.82 (m, 20H), 0.63 (quin., J = 6.4Hz, 8H), 0.48 (m, 16H), 0.37 (m, 8H). ^{1}H NMR (100 MHz, $CDCl_3$): δ 160.11, 153.03, 151.57, 150.82, 149.02, 143.87, 132.68, 132.54, 132.17, 131.12, 129.96, 121.95, 121.21, 114.99, 105.41, 68.83, 32.02, 29.62, 29.48, 29.42, 29.36, 29.17, 28.83, 28.79, 25.39, 22.83, 10.28. MS (MALDI-TOF) m/z: obsvd 1519.943 $[M+H]^+$, calcd 1519.8800.

5.18. An oven dried pressure tube containing a magnetic stirrer bar was charged with **5.17** (3.098g, 2.035mmol), *p,p'*-diocytldiphenylamine (2.884g, 7.325mmol), Cs_2CO_3 (0.928g, 2.85mmol) and 70ml of freshly distilled THF. The solution was cooled to 0^{o}C and argon was bubbled through it for 30min. Under a steady flow of argon, DPEphos (0.0822g, 0.1526mmol) and $Pd(OAc)_2$ (24.9mg, 0.1017mmol) were added, the tube was sealed with a Teflon screw cap and heated to 80^{o}C to stir overnight. On cooling,

the solution was concentrated and the residue was purified by silica gel chromatography using neat hexanes to elute the unreacted *p,p'*-dioctyldiphenylamine followed by DCM:hex (1:9) as the eluting solvent affording 500mg (0.272mmol, 13%) of **5.18**. ^{1}H NMR (400 MHz, $CDCl_3$): δ 9.73 (d, J = 4.4Hz, 9.24 (d, J = 4.5Hz, 2H), 8.92 (d, J = 4.3Hz, 2H), 8.73 (d, J = 4.6Hz, 2H), 7.70 (t, J = 8.5Hz, 4H), 7.30 (d, J = 8.3Hz, 4H), 7.20 (d, J = 8.5Hz, 4H), 7.02 (d, J = 8.4Hz, 4H), 3.88 (t, J = 6.2Hz, 8H), 1.70 (s, 4H), 1.53 (s, 21H), 1.36 (m, 14H), 1.25 (m, 8H), 1.20-1.02 (m, 24H), 0.97 (m, 10H), 0.87 (t, J = 6.9Hz, 20H), 0.78 (m, 16H), 0.73 (m, 12H), 0.63 (m, 12H), 0.54 (m, 8H). ^{13}C NMR (100 MHz, $CDCl_3$): δ 160.07, 152.62, 152.10, 150.69, 150.46, 150.29, 114.73, 132.18, 131.95, 126.71, 123.42, 121.76, 121.18, 114.30, 110.31, 105.41, 99.42, 96.23, 68.86, 57.39, 38.11, 32.54, 32.02, 31.93, 31.58, 29.64, 29.47, 29.43, 29.40, 29.15, 28.86, 28.69, 25.31, 22.82, 19.33, 14.27, 12.18. MS (MALDI-TOF) m/z: obsvd 1832.0592 $[M]^+$, calcd 1832.2856.

5.19 A pressure tube containing a magnetic stirrer bar was charged with 482mg (1.317mmol) of **3.7**, 250mg (1.581mmol) of 4,5-diaminophthaleonitrile and 30ml of a 1:1:1 mixture of 1,2-dichlorobenzene:AcOH:EtOH. The tube was sealed with a Teflon screw cap and heated to reflux internally overnight. The solution was then cooled, diluted with 100ml MeOH, which further promoted precipitation, and filtered. The yellow product obtained was washed with MeOH (300ml), DCM (200ml) and then dried on hi-vac. overnight yielding 629mg (1.288mmol, 98%). ^{1}H NMR (400 MHz, 1,1,2,2-tetrchloroethane-*d*2, 110^{o}C): δ 9.26 (bs, 2H), 8.85 (s, 2H), 8.68 (s, 2H), 8.01 (bs, 2H). MS (MALDI-TOF) m/z: obsvd 485.9510 $[M]^+$, calcd 485.9110.

5.20 500mg (1.024mmol) of **5.19** was placed in a 100ml RBF. EtOH (6ml), H_2O (6ml) was added followed by 0.862g (15.36mmol) of KOH. The flask was fitted with a reflux condenser, and with stirring, the solution was heated to reflux for 2 days. On cooling, 4N HCL was used to acidify the solution. The solid precipitant was isolated by filtration and washed with H_2O, MeOH and finally dried on hi-vac. overnight. 0.64g (1.222mmol, 120%) Of **5.20** was obtained implying that the product was not properly dried. All efforts to characterize the product by NMR failed due to insolubility. The product was used as is in the proceeding reactions. MS (MALDI-TOF) m/z: obsvd 523.9199 $[M]^+$, calcd 523.9002.

5.21 To a 100ml RBF containing a magnetic stirrer bar, 225mg (0.415mmol) of **5.20** was added along with toluene (5ml), 1-pentanol (2ml) and H_2SO_4 (0.05ml). The flask was fitted with a Dean-Stark apparatus connected to a dry argon line. The solution was heated to reflux overnight. On cooling, solid $NaHCO_3$ was added to neutralize the solution followed by 40ml MeOH. The solution was filtered and the solid product obtained washed with water (3 x 100ml) and MeOH (2 x 100ml). The beige solid was dried on hi-vac. overnight yielding 0.3145g (0.472mmol, 114%). Again a >100% yield reveals the difficulty in drying this class of compounds. ^{1}H NMR (400 MHz, TFA-*d*1, 65^{o}C): δ 9.62 (bs, 2H), 9.51 (bs, 2H), 9.31 (s, 2H), 8.58 (s, 2H), 5.09 (s, 4H), 2.41 (bs, 4H), 1.96 (m, 8H), 1.44 (t J = 6.5Hz, 6H). MS (MALDI-TOF) m/z: obsvd 664.9956 $[M+H]^+$, calcd 665.0645.

5.22 To an oven dried RBF containing 113mg (0.215mmol) of **5.20**, 5ml of 2-butyl-1-octanol was added followed by 0.25ml of H_2SO_4. The flask was fitted with a condenser and the suspension heated to reflux overnight with stirring. After 24h,

MALDI-TOF MS analysis revealed that some of the starting material had dehydrated to form the corresponding dianhydride. Consequently, 1ml H_2O was added and the solution left to reflux for 24h. This effectively hydrolyzed the dianhydride freeing it up to react with the alcohol present. The solution was cooled, diluted with 50ml MeOH and filtered. The solid obtained was washed with MeOH, H_2O and dried on hi-vac. overnight yielding 40mg (0.0464, 22%) of a beige product. Attempts to characterize the product by NMR were futile. MS (MALDI-TOF) m/z: obsvd 861.1890 $[M+H]^+$, calcd 861.2836.

Attempted synthesis of 5.23. 125.9mg (68.6μmol) of **5.18** was taken up in 10ml of dry THF. Under a blanket of argon, 0.343ml of 1M TBAF in hexanes was added and stirred at RT for 30min. The reaction was quenched by addition of water and extracted with dichloromethane. The organic layer was dried over $MgSO_4$, filtered, concentrated and dried on hi-vac. The residue was dissolved in 18ml dry THF, transferred to a pressure tube and 3.5ml Et_3N added. Argon was bubbled through the solution at 0^oC for 30min prior to the addition of 10mg (0.027mmol) 3,6-dibromo-phenanthrene-9,10-dione (**3.13**), $Pd_2(dba)_3$ (18.8mg, 20.6μmol) and $AsPh_3$ (46.2mg, 151μmol). The tube was filled with argon, sealed with a Teflon screw-cap and heated to 80^oC for 6h. MALDI-TOF MS analysis of the crude reaction mixture revealed that the reaction was unsuccessful.

Attempted synthesis of 5.24. 64mg (34.87μmol) of **5.18** was taken up in 6ml of dry THF. Under a blanket of argon, 0.173ml of 1M TBAF in hexanes was added and stirred at RT for 30min. The reaction was quenched by addition of water and extracted with dichloromethane. The organic layer was dried over $MgSO_4$, filtered, concentrated and dried on hi-vac. The residue was dissolved in 10ml dry toluene, transferred to a pressure tube and 2ml Et_3N added. Argon was bubbled through the solution at 0^oC for

30min prior to the addition of 12.3mg (13.95μmol) of **5.22**, $Pd_2(dba)_3$ (9.58mg, 10.46mol) and $AsPh_3$ (23.5mg, 76.7μmol). The tube was filled with argon, sealed with a Teflon screw cap and heated to 80°C for 6h. MALDI-TOF MS analysis of the crude reaction mixture revealed that the reaction was unsuccessful.

5.25 The synthesis of **5.25** followed a known literature procedure[186] for the production of a crude oil that is used without purification or characterization. Accordingly, 20g (96.99mmol) L-diethyl tartrate was combined with 100ml CCl_4 and 49.66g (388mmol) of NBS in a 250ml RBF containing a large magnetic stirrer bar. The flask was fitted with a reflux condenser, and with stirring, the suspension was heated to reflux overnight. During this period the suspension turned a deep red due to the production of Br_2. On cooling, 100ml Et_2O was added and the suspension filtered. The cake of succinimide was washed with Et_2O and the combined filtrates were concentrated yielding an orange oil that was used without further purification. ^{1}H NMR (400 MHz, $CDCl_3$): δ 4.30 (dq, J = 7.3, 0.9 Hz, 4H), 1.32 (t, J = 7.1Hz, 6H).

5.26. 57mg (0.122mmol) Of **4.31** and 0.123g (0.609mmol) of **5.25** were added to a RBF containing 5ml AcOH. The solution was heated to 110°C and left to stir for 16h. On cooling, 80ml of MeOH was added, the solid isolated by filtration, washed with MeOH (300ml) and dried on hi-vac. overnight yielding 41mg (64.6μmol, 54%) of a yellow-beige solid. ^{1}H NMR (400 MHz, 1,2-dichlorobenzene-*d*4, 110°C): δ 9.15 (m, 4H), 8.33 (s, 2H), 7.72 (d, J = 7.5Hz, 2H), 2.89 (m, 4H). MS (MALDI-TOF) m/z: obsvd 632.9499 $[M+H]^+$, calcd 632.9768.

5.27 22mg (8.41μmol) of **4.23** and 70mg of the crude oil containing **5.25** was combined in a 100ml RBF and 1,2-dichlorobenzene (10ml) and glacial acetic acid (10ml)

added. The solution was heated to 110°C and left to stir for 16h. The solution was washed with water, extracted with dichloromethane and concentrated. The residue was purified by silica gel chromatography using DCM:Hexanes (6:4→8:2) as the eluting solvent affording 13.6mg (4.89μmol, 58%). ^{1}H NMR (400 MHz, $CDCl_3$): δ 9.94 (d, J = 8.0Hz, 2H), 9.49 (s, 2H), 9.37 (s, 2H), 8.97 (d, J = 4.2Hz, 4H), 8.85 (m, 12H), 8.72 (d, J = 8.2Hz, 2H), 8.01 (m, 6H), 7.95 (d, J = 8.1Hz, 2H), 7.80 (d, J = 8.2Hz, 4H), 7.19 (m, 8H), 7.04 (d, J = 7.9Hz, 4H), 4.67 (q, J = 6.8Hz, 4H), 4.17 (m, 12H), 1.93 (m, 12H), 1.58 (m, 18H), 1.50 (bs, 12H), 1.44 (m, 12H), 1.41-1.20 (m, 84H), 0.88 (m, 18H). MS (MALDI-TOF) m/z: obsvd 2776.66 calc 2777.4721

5.10.3 Solar cells

The preparation of the dye-sensitized solar cells prepared in this study followed methodologies established in the literature[24,187-189]. In brief, the transparent conducting fluorine doped tin oxide (FTO) based photoanodes were prepared by first applying a spray coating of TiO_2[189] followed by treatment with $TiCl_4$ [187], deposition of a mesoporous TiO_2 layer[188], and a final treatment with $TiCl_4$. The thus prepared FTO-TiO_2 electrodes were immersed in DCM solutions of **5.1** or **5.2** overnight (12 h) resulting in the fully prepared photoanodes. The fully assembled solar cell consisted of this photoanode and an FTO-Pt cathode formed after applying a solution of chloroplatinic acid to the FTO surface and treating at 450 °C for 30 min. The two electrodes were attached using heat shrink plastic (Solaronix), and the electrolyte was introduced to the internal cavity of the cell via small ports drilled in FTO-Pt cathode. The electrolyte consisted of 1:1

acetonitrile:valeronitrile with 0.2 M lithium iodide, 0.05 M iodine, 0.2 M tetrabutylammonium iodide, and 0.5 M 4-tertbutylpyridine.

Photocurrent and photovoltage measurement of the cells were taken using a 300 W Xe lamp with a 400 nm longpass and AM 1.5 filters, with the cells positioned to receive light intensity of 100 mW cm^{-2}. The geometric area of the cell exposed to illumination measured 0.20 cm^2. Incident photon to current efficiency (IPCE) measurements used a Jobin Yvon monochromator, with photocurrents measured in 4 nm intervals from 800 to 380 nm, and the intensity at each wavelength was determined with a Newport 818-UV photodiode in the same context as the DSSCs studied.

Chapter 6: Synthesis of a Highly Soluble, Red-Absorbing, Pyrazine-Containing Phthalocyanine

6.1 Design of a Highly-Soluble Extended Phthalocyanine

To date, the most efficient dye sensitized solar cells reported employ dyes that do not absorb beyond 700nm. Analysis of the AM1.5 spectrum reveals that considerable photon flux is present beyond 700nm. While the red and near infra-red photons are less energetic than their blue and green counterparts, the cumulative power from the flux of these photons cannot be ignored. The red-most absorbing feature in the absorption spectrum of porphyrins are the Q-bands, a spectroscopically forbidden transition. Phthalocyanines, on the other hand, exhibit strong absorptions into the red and near-IR. Consequently, strategies to red-shift the phthalocyanine absorption spectrum further towards the red are better suited to produce dyes that absorb strongly in the region of interest than strategies to red-shift the weak porphyrin absorption spectrum.

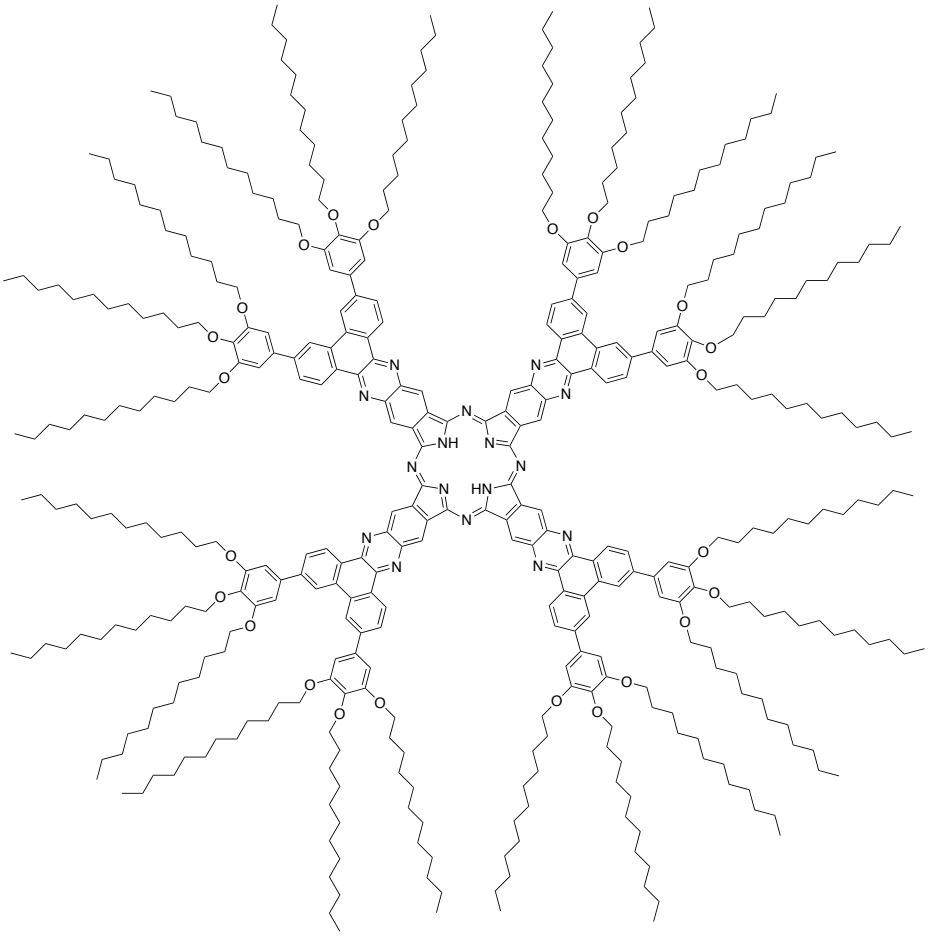

6.1

Figure 6.1. Structure of a 6+kDa extended phthalocyanine for the use in artificial photosynthetic applications.

Figure 6.1 shows the structure of a large, novel, highly soluble extened-phthalocyanine (**6.1)** that exhibits absorption far past the red portion of the spectrum, tailing off out to 900nm. This phthalocyanine is D_{4h} symmetric and features 24 dodecyloxy groups, making it a strong candidate for a liquid crystal or discotic. Rusanova et al. reported the synthesis and purification of a large extended pthalocyanine [190] with a similar aromatic core structure. Their structure was appended with phenanthrolines as opposed to functionalized phenanthrenes. As would be expected, their

phthalocyanine's extensive conjugation imbued it with a high propensity to stack strongly, rendering it largely insoluble and required dissolution in CF_3COOD to acquire and NMR spectrum.

Condensation of *o*-diketones with *o*-amines provides a simple avenue for producing extended, rigid, planar and importantly, diversely functionalized heteroaromatic structures. Formation of the acene analogues of pyrazine-containing heteroaromatics are difficult to synthesize and functionalize, exhibiting susceptibility to oxidation and cycloadition reactions. The electronegativity of pyrazine in pyrazine-containing heteroaromatics is believed to stabilize the systems[95]. Orthodiketone and *o*-amine building blocks can be functionalized diversely prior to condensation to form the pyrazine containing heteroaromatic species. This allows for the potential synthesis of a wide array of rigid, functionalized scaffolds and a route to forming arrays for solar energy harvesting in which the scaffold itself is optically active and features HOMO and LUMO energy levels aptly poised to participate in the photophysics of the system.

6.2 Synthesis of a Highly-Soluble Extended Phthalocyanine

Scheme 6.1

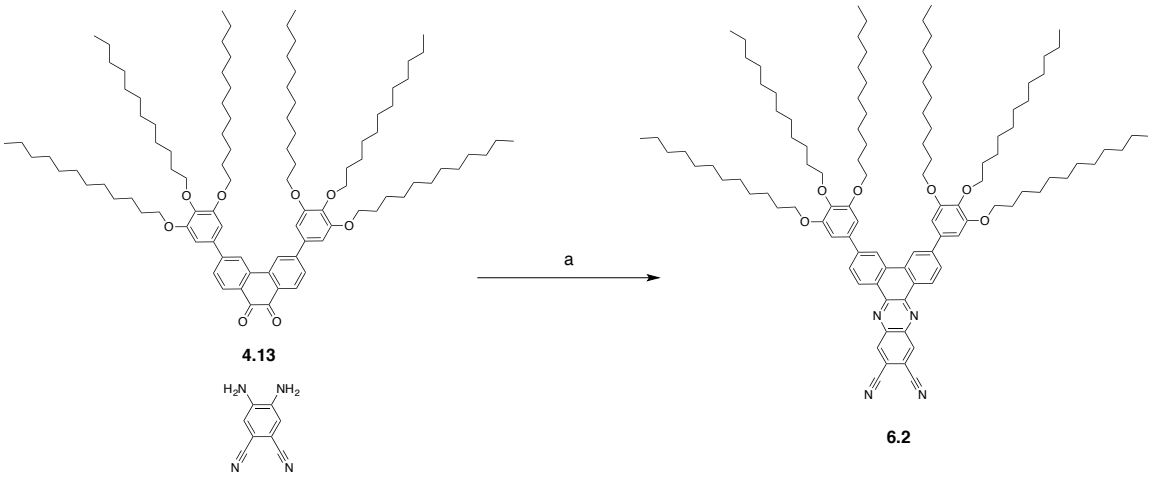

a) Toluene:EtOH:AcOH (2:1:1), reflux, overnight, 91% yield.

The synthesis (scheme 6.1) of the necessary dinitrile, **6.2**, was achieved by refluxing **4.13** together with 4,5-diaminophthaleonitrile in a 2:1:1 mixture of toluene:EtOH:AcOH. The product, **6.2** was obtained in 91% yield.

Scheme 6.2

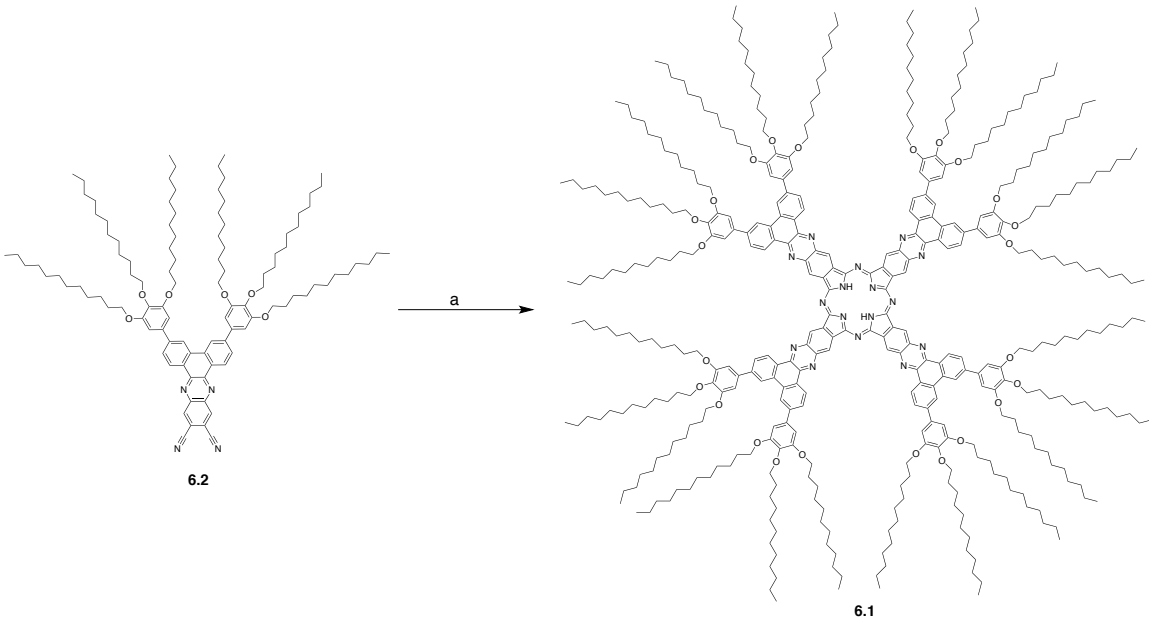

a) Li (flakes), *n*-butanol, reflux, 2h, 20% yield

The synthesis of **6.1** employed addition of freshly crushed Li metal to a refluxing solution of **6.2** in *n*-butanol. Unlike the similar compound reported by Rusanova[190]*et al.* the product **6.1** was soluble in many common laboratory solvents, including hexanes. Despite the considerable planar π-conjugated surface area **6.1**, the considerable alkylation results in the high solubility of **6.1**, allowing for purification by column chromatography.

6.3 UV-Vis Absorption Characteristics of the Extended Phthalocyanine

The 6+ kDa phthalocyanine produced exhibits strong absorption (shown in figure 6.2) tailing out to 900nm. The absorption differs from simpler phthalocyanine spectra in that it exhibits pronounced and broad absorption from 200nm to 500nm. The characteristic green trough of phthalocyanines is red-shifted and is disrupted by a small

peak around 575nm. The red-most transition is not as sharp as those exhibited by simple pthalocyanines. The broadness of the feature peaking at 755nm is advantageous for collecting more of the red end of the solar spectrum.

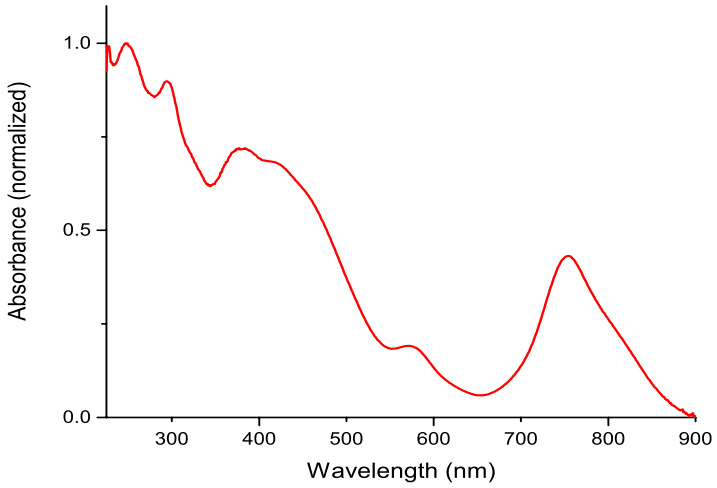

Figure 6.2 The UV-Vis absorption spectrum of **6.1** in dichloromethane.

6.4 Materials and Methods.

6.4.1 General

Dichloromethane, hexanes, ethylacetate, tetrahydrofuran and toluene were purchased from BDH and 200 PROOF ethanol from KOPTEC. n-Butanol was purchased form Sigma Aldrich. Li metal pellets were purchased from Sigma-Aldrich.

Matrix assisted laser desorption/ionization time of flight (MALDI-TOF) mass spectra were acquired using an Applied Biosystems Voyager-DE STR workstation and acquired in reflector mode using terthiophene, diphenylbutadiene or dithranol as the

matrix. NMR spectroscopy was conducted using a Varian (Agilent) MR 400 MHz NMR spectrometer operating at a 1H Lamor frequncy of 399.87 MHz, equipped with a 5 mm Broadband Observe Z-gradient probe. UV-Vis spectra were acquired using a Shimadzu UV-310PC UV-VIS-NIR spectrophotometer.

6.4.2 Synthesis of Compounds

6.1. A suspension of **6.2** (216.6mg, 136.4μmol) in 15ml of anhydrous *n*-butanol was heated to reflux under argon. Under a stream of argon, 40mg of freshly crushed lithium pellets were added quickly to the hot solution, which turned green within seconds of the addition. The solution was left to reflux for 2h. On cooling, 20ml of acetic acid was added to the dark green solution and left to stir at RT overnight. The solution was diluted with hexanes, washed with water, sat. $NaHCO_3$ (aq.) and finally brine before being collected and concentrated. The residue was chromatographed using DCM as the solvent. MALDI-TOF MS analysis revealed that Li was still present on the macrocycle. The residue obtained from chromatography was dissolved in 200ml DCM and 100ml TFA added. The solution was left to stir at RT for 30min, washed with water and sat. $NaHCO_3$(aq.) prior to being concentrated. The residue was passed through a second silica gel column using DCM as the solvent yielding 45mg (7.1μmol, 20%) of the highly soluble phthalocyanine. ^{1}H NMR (400 MHz, $CDCl_3$, 58^{o}C): δ 10.10 (s, 8H), 9.57 (d, J = 7.4Hz, 8H), 8.36 (s, 8H), 7.86 (d, J = 7.4Hz, 8H), 6.82 (s, 12H), 4.06 (m, 48H), 1.90 (m, 48H), 1.62 (m, 48H), 1.52-1.11 (m, 384H), 0.90 (m, 84), -1.10 (s, 2H). MS (MALDI-TOF) m/z: obsvd 6356.2876 (highest intensity peak) $[M]^+$ calcd 6355.1451 (highest

intensity peak). Resolved mass peak could not be determined as the individual isotopic peaks are coalesced.

6.2 150mg (0.102mmol) of **4.13** was added to a 100ml RBF along with 32.4mg (0.205mmol) of 4,5-diaminophthaleonitrile, toluene (6ml), EtOH (3ml) and AcOH (3ml). The solution was heated to reflux overnight under argon. The solution was concentrated and dried on hi-vac.. The residue obtained was purified by silica gel chromatography using DCM:Hex (3:2→ 4:1) as the eluting solvent. Concentration of relevant fractions afforded 0.16g (0.101mmol, 99%) of a waxy orange solid. ^{1}H NMR (400 MHz, $CDCl_3$): δ 9.04 (d, J = 8.6Hz, 2H), 8.71 (s, 2H), 8.05 (s, 1.81), 7.95 (d, J = 8.4Hz, 2H), 7.06 (s, 4H), 4.17 (t, J = 6.1Hz, 8H), 4.09 (t, J = 6.3Hz, 4H), 1.87 (m, 12H), 1.56 (m, 12H), 1.46-1.18 (m, 96H), 0.89 (m, 18H). ^{13}C NMR (400 MHz, $CDCl_3$): δ 153.91, 146.23, 144.81, 141.22, 139.20, 136.44, 135.52, 133.04, 128.09, 127.67, 127.26, 121.68, 115.26, 112.65, 106.68, 73.80, 69.61, 32.11, 32.08, 30.63, 29.97, 29.95, 29.91, 29.88, 29.87, 29.85, 29.76, 29.72, 29.57, 29.54, 26.44, 26.38, 22.86, 22.83, 14.26, 14.24. MS (MALDI-TOF) m/z: obsvd 1588.6195 $[M+H]^+$ calcd 1588.2567.

References

(1) Broecker, W. S. *Science* **1975**, *189*, 460–463.

(2) McCright, A. M.; Dunlap, R. E. *The Sociological Quarterly* **2011**, *52*, 155–194.

(3) Hansen, J.; Sato, M.; Ruedy, R. *Proc. Natl. Acad. Sci. U.S.A.* **2012**, *109*, E2415–23.

(4) Semenza, J. C.; Hall, D. E.; Wilson, D. J.; Bontempo, B. D.; Sailor, D. J.; George, L. A. *Am J Prev Med* **2008**, *35*, 479–487.

(5) Rahmstorf, S.; Cazenave, A.; Church, J. A.; Hansen, J. E.; Keeling, R. F.; Parker, D. E.; Somerville, R. C. J. *Science* **2007**, *316*, 709.

(6) Solomon, S.; Plattner, G.-K.; Knutti, R.; Friedlingstein, P. *Proc. Natl. Acad. Sci. U.S.A.* **2009**, *106*, 1704–1709.

(7) Root, T. L.; Price, J. T.; Hall, K. R.; Schneider, S. H.; Rosenzweig, C.; Pounds, J. A. *Nature* **2003**, *421*, 57–60.

(8) Bellard, C.; Bertelsmeier, C.; Leadley, P.; Thuiller, W.; Courchamp, F. *Ecol. Lett.* **2012**.

(9) Meinshausen, M. M.; Meinshausen, N. N.; Hare, W. W.; Raper, S. C. B. S.; Frieler, K. K.; Knutti, R. R.; Frame, D. J. D.; Allen, M. R. M. *Nature* **2009**, *458*, 1158–1162.

(10) Hansen, J.; Ruedy, R.; Sato, M.; Lo, K. *Reviews of Geophysics* **2010**, *48*, RG4004.

(11) Rockström, J.; Steffen, W.; Noone, K.; Persson, A.; Chapin, F. S.; Lambin, E. F.; Lenton, T. M.; Scheffer, M.; Folke, C.; Schellnhuber, H. J.; Nykvist, B.; de Wit, C. A.; Hughes, T.; van der Leeuw, S.; Rodhe, H.; Sörlin, S.; Snyder, P. K.; Costanza, R.; Svedin, U.; Falkenmark, M.; Karlberg, L.; Corell, R. W.; Fabry, V. J.; Hansen, J.; Walker, B.; Liverman, D.; Richardson, K.; Crutzen, P.; Foley, J. A. *Nature* **2009**, *461*, 472–475.

(12) Heil, M. T.; Wodon, Q. T. *The Journal of Environment & Development* **1997**, *6*, 426–452.

(13) CO2 EMISSIONS FROM FUEL COMBUSTIONHIGHLIGHTS http://www.iea.org/publications/freepublications/publication/CO2EmissionsFromFuelCombustionHighlights2013.pdf (accessed Nov 23, 2013).

(14) Liao, H.; Cao, H. S. *Glob Environ Change* **2013**.

(15) Lewis, N. S.; Nocera, D. G. *Proc. Natl. Acad. Sci. U.S.A.* **2006**, *103*, 15729–15735.

(16) Kasha, M. *Discussions of the Faraday Society* **1950**, *9*, 14–19.

(17) IUPAC Gold Book - Kasha rule http://goldbook.iupac.org/K03370.html (accessed Nov 3, 2013).

(18) Shockley, W.; Queisser, H. J. *J. Appl. Phys.* **1961**, *32*, 510–519.

(19) Solar Spectral Irradiance: Air Mass 1.5 http://rredc.nrel.gov/solar/spectra/am1.5/ (accessed Nov 6, 2013).

(20) *rredc.nrel.gov*.

(21) Martí, A.; Araújo, G. L. *Solar Energy Materials and Solar Cells* **1996**, *43*, 203–222.

(22) Krause, G. H.; Weis, E. *Annual review of plant biology* **1991**, *42*, 313–349.

(23) Aro, E.-M.; Virgin, I.; Andersson, B. *Biochimica et Biophysica Acta (BBA)-Bioenergetics* **1993**, *1143*, 113–134.

(24) O'regan, B.; Grfitzeli, M. *Nature* **1991**, *353*, 24.

(25) Grätzel, M. *Journal of Photochemistry and Photobiology C: Photochemistry Reviews* **2003**, *4*, 145–153.

(26) Yella, A. A.; Lee, H.-W. H.; Tsao, H. N. H.; Yi, C. C.; Chandiran, A. K. A.; Nazeeruddin, M. K. M.; Diau, E. W.-G. E.; Yeh, C.-Y. C.; Zakeeruddin, S. M. S.; Grätzel, M. M. *Science* **2011**, *334*, 629–634.

(27) Dimitrov, S. D.; Durrant, J. R. *Chem. Mater.* **2013**.

(28) Gust, D.; Moore, T. A.; Moore, A. L.; Macpherson, A. N.; Lopez, A.; DeGraziano, J. M.; Gouni, I.; Bittersmann, E.; Seely, G. R. *J. Am. Chem. Soc.* **1993**, *115*, 11141–11152.

(29) Gust, D.; Moore, T. A.; Moore, A. L.; Leggett, L.; Lin, S.; DeGraziano, J. M.; Hermant, R. M.; Nicodem, D.; Craig, P. *The Journal of Physical Chemistry* **1993**, *97*, 7926–7931.

(30) Gust, D.; Moore, T. A.; Moore, A. L.; Seely, G.; Liddell, P.; Barrett, D.; Harding, L. O.; Ma, X. C.; Lee, S.-J.; Gao, F. *Tetrahedron* **1989**, *45*, 4867–

4891.

(31) Gust, D.; Moore, T. A.; Liddell, P. A.; Nemeth, G. A.; Makings, L. R.; Moore, A. L.; Barrett, D.; Pessiki, P. J.; Bensasson, R. V. *J. Am. Chem. Soc.* **1987**, *109*, 846–856.

(32) Hung, S.-C.; Lin, S.; Macpherson, A. N.; DeGraziano, J. M.; Kerrigan, P. K.; Liddell, P. A.; Moore, A. L.; Moore, T. A.; Gust, D. *Journal of Photochemistry and Photobiology A: Chemistry* **1994**, *77*, 207–216.

(33) Kuciauskas, D.; Liddell, P. A.; Hung, S.-C.; Lin, S.; Stone, S.; Seely, G. R.; Moore, A. L.; Moore, T. A.; Gust, D. *J. Phys. Chem. B* **1997**, *101*, 429–440.

(34) Maniga, N. I.; Sumida, J. P.; Stone, S.; Moore, A. L.; Moore, T. A.; Gust, D. *J. Porphyrins Phthalocyanines* **1999**, *3*, 32–44.

(35) Moore, A. L.; Liddell, P. A.; Nemethl, G. A. *J Phys Chem* **1987**.

(36) Gust, D.; Moore, T. A.; Moore, A. L. *Acc. Chem. Res.* **2001**, *34*, 40–48.

(37) Gust, D. D.; Moore, T. A. T.; Moore, A. L. A. *Acc. Chem. Res.* **2009**, *42*, 1890–1898.

(38) Megiatto, J. D.; Antoniuk-Pablant, A.; Sherman, B. D.; Kodis, G.; Gervaldo, M.; Moore, T. A.; Moore, A. L.; Gust, D. *Proc. Natl. Acad. Sci. U.S.A.* **2012**, *109*, 15578–15583.

(39) Moore, G. F.; Hambourger, M.; Gervaldo, M.; Poluektov, O. G.; Rajh, T.; Gust, D.; Moore, T. A.; Moore, A. L. *J. Am. Chem. Soc.* **2008**, *130*, 10466–10467.

(40) Savolainen, J.; Dijkhuizen, N.; Fanciulli, R.; Liddell, P. A.; Gust, D.; Moore, T. A.; Moore, A. L.; Hauer, J.; Buckup, T.; Motzkus, M.; Herek, J. L. *J. Phys. Chem. B* **2008**, *112*, 2678–2685.

(41) Miller, M. A.; Lammi, R. K.; Prathapan, S.; Holten, D.; Lindsey, J. S. *J. Org. Chem.* **2000**, *65*, 6634–6649.

(42) Song, H.-E.; Kirmaier, C.; Taniguchi, M.; Diers, J. R.; Bocian, D. F.; Lindsey, J. S.; Holten, D. *J. Am. Chem. Soc.* **2008**, *130*, 15636–15648.

(43) Sazanovich, I. V.; Balakumar, A.; Muthukumaran, K.; Hindin, E.; Kirmaier, C.; Diers, J. R.; Lindsey, J. S.; Bocian, D. F.; Holten, D. *Inorg. Chem.* **2003**, *42*, 6616–6628.

(44) Yang, S. I.; Prathapan, S.; Miller, M. A.; Seth, J.; Bocian, D. F.; Lindsey, J. S.; Holten, D. *J. Phys. Chem. B* **2001**, *105*, 8249–8258.

(45) Prathapan, S.; Yang, S. I.; Seth, J.; Miller, M. A.; Bocian, D. F.; Holten, D.; Lindsey, J. S. *J. Phys. Chem. B* **2001**, *105*, 8237–8248.

(46) Kirmaier, C.; Yang, S. I.; Prathapan, S.; Miller, M. A.; Diers, J. R.; Bocian, D. F.; Lindsey, J. S.; Holten, D. *Research on chemical intermediates* **2002**, *28*, 719–740.

(47) Li, J.; Lindsey, J. S. *J. Org. Chem.* **1999**, *64*, 9101–9108.

(48) Hsiao, J.-S.; Krueger, B. P.; Wagner, R. W.; Johnson, T. E.; Delaney, J. K.; Mauzerall, D. C.; Fleming, G. R.; Lindsey, J. S.; Bocian, D. F.; Donohoe, R. J. *J. Am. Chem. Soc.* **1996**, *118*, 11181–11193.

(49) Peet, J.; Heeger, A. J.; Bazan, G. C. *Acc. Chem. Res.* **2009**, *42*, 1700–1708.

(50) Beek, W. J.; Wienk, M. M.; Janssen, R. A. *Adv. Funct. Mater.* **2006**, *16*, 1112–1116.

(51) Crossland, E. J. W.; Kamperman, M.; Nedelcu, M.; Ducati, C.; Wiesner, U.; Smilgies, D. M.; Toombes, G. E. S.; Hillmyer, M. A.; Ludwigs, S.; Steiner, U.; Snaith, H. J. *Nano Lett.* **2009**, *9*, 2807–2812.

(52) Atienzar, P.; Ishwara, T.; Illy, B. N.; Ryan, M. P.; O'Regan, B. C.; Durrant, J. R.; Nelson, J. *J. Phys. Chem. Lett.* **2010**, *1*, 708–713.

(53) Olson, D. C.; Lee, Y. J.; White, M. S.; Kopidakis, N.; Shaheen, S. E.; Ginley, D. S.; Voigt, J. A.; Hsu, J. W. P. *J. Phys. Chem. C* **2007**, *111*, 16640–16645.

(54) Hardin, B. E.; Snaith, H. J.; McGehee, M. D. *Nature Photon* **2012**, *6*, 162–169.

(55) Furukawa, H.; Cordova, K. E.; O'Keeffe, M.; Yaghi, O. M. *Science* **2013**, *341*, 1230444.

(56) Yaghi, O. M.; O'Keeffe, M.; Ockwig, N. W.; Chae, H. K.; Eddaoudi, M.; Kim, J. *Nature* **2003**, *423*, 705–714.

(57) Eddaoudi, M.; Moler, D. B.; Li, H.; Chen, B.; Reineke, T. M.; O'Keeffe, M.; Yaghi, O. M. *Acc. Chem. Res.* **2001**, *34*, 319–330.

(58) Eddaoudi, M.; Kim, J.; Rosi, N.; Vodak, D.; Wachter, J.; O'Keeffe, M.; Yaghi, O. M. *Science* **2002**, *295*, 469–472.

(59) Rosi, N. L.; Eckert, J.; Eddaoudi, M.; Vodak, D. T.; Kim, J.; O'Keeffe, M.; Yaghi, O. M. *Science* **2003**, *300*, 1127–1129.

(60) Yaghi, O. M.; Li, H.; Davis, C.; Richardson, D.; Groy, T. L. *Acc. Chem. Res.* **1998**, *31*, 474–484.

(61) Ockwig, N. W.; Delgado-Friedrichs, O.; O'Keeffe, M.; Yaghi, O. M. *Acc. Chem. Res.* **2005**, *38*, 176–182.

(62) Rowsell, J. L.; Yaghi, O. M. *Microporous and Mesoporous Materials* **2004**, *73*, 3–14.

(63) Rosi, N. L.; Kim, J.; Eddaoudi, M.; Chen, B.; O'Keeffe, M.; Yaghi, O. M. *J. Am. Chem. Soc.* **2005**, *127*, 1504–1518.

(64) Chen, B.; Eddaoudi, M.; Hyde, S. T.; O'Keeffe, M.; Yaghi, O. M. *Science* **2001**, *291*, 1021–1023.

(65) Shekhah, O.; Wang, H.; Strunskus, T.; Cyganik, P.; Zacher, D.; Fischer, R.; Wöll, C. *Langmuir* **2007**, *23*, 7440–7442.

(66) Shekhah, O.; Wang, H.; Kowarik, S.; Schreiber, F.; Paulus, M.; Tolan, M.; Sternemann, C.; Evers, F.; Zacher, D.; Fischer, R. A.; Wöll, C. *J. Am. Chem. Soc.* **2007**, *129*, 15118–15119.

(67) Zacher, D.; Shekhah, O.; Wöll, C.; Fischer, R. A. *Chem. Soc. Rev.* **2009**, *38*, 1418–1429.

(68) So, M. C.; Jin, S.; Son, H.-J.; Wiederrecht, G. P.; Farha, O. K.; Hupp, J. T. *J. Am. Chem. Soc.* **2013**, *135*, 15698–15701.

(69) Son, H.-J.; Jin, S.; Patwardhan, S.; Wezenberg, S. J.; Jeong, N. C.; So, M.; Wilmer, C. E.; Sarjeant, A. A.; Schatz, G. C.; Snurr, R. Q.; Farha, O. K.; Wiederrecht, G. P.; Hupp, J. T. *J. Am. Chem. Soc.* **2013**, *135*, 862–869.

(70) Weiss, E. A.; Wasielewski, M. R.; Ratner, M. A. **2005**, 103–133.

(71) Emberly, E. G.; Kirczenow, G. *Physical Review B* **1998**, *58*, 10911.

(72) Nitzan, A.; Ratner, M. A. *Science* **2003**, *300*, 1384–1389.

(73) Davis, W. B.; Svec, W. A.; Ratner, M. A.; Wasielewski, M. R. *Nature* **1998**, *396*, 60–63.

(74) Tao, N. J. *Nature Nanotechnology* **2006**, *1*, 173–181.

(75) Diez-Perez, I.; Hihath, J.; Hines, T.; Wang, Z.-S.; Zhou, G.; Müllen, K.; Tao, N. **2011**, 1–6.

(76) Xu, B. Q.; Li, X. L.; Xiao, X. Y.; Sakaguchi, H.; Tao, N. J. *Nano Lett.* **2005**, *5*, 1491–1495.

(77) Joachim, C.; Ratner, M. A. *Proc. Natl. Acad. Sci. U.S.A.* **2005**, *102*, 8801–8808.

(78) Solomon, G. C.; Andrews, D. Q.; Van Duyne, R. P.; Ratner, M. A. *J. Am. Chem. Soc.* **2008**, *130*, 7788–7789.

(79) Ricks, A. B.; Solomon, G. C.; Colvin, M. T.; Scott, A. M.; Chen, K.; Ratner, M. A.; Wasielewski, M. R. *J. Am. Chem. Soc.* **2010**, *132*, 15427–15434.

(80) Creager, S.; Yu, C. J.; Bamdad, C.; O'Connor, S.; MacLean, T.; Lam, E.; Chong, Y.; Olsen, G. T.; Luo, J.; Gozin, M. *J. Am. Chem. Soc.* **1999**, *121*, 1059–1064.

(81) la Torre, de, G.; Giacalone, F.; Segura, J. L.; Martín, N.; Guldi, D. M. *Chemistry* **2005**, *11*, 1267–1280.

(82) Weiss, E. A.; Ahrens, M. J.; Sinks, L. E.; Gusev, A. V.; Ratner, M. A.; Wasielewski, M. R. *J. Am. Chem. Soc.* **2004**, *126*, 5577–5584.

(83) Albinsson, B.; Eng, M. P.; Pettersson, K.; Winters, M. U. *Phys. Chem. Chem. Phys.* **2007**, *9*, 5847–5864.

(84) Goldsmith, R. H.; Sinks, L. E.; Kelley, R. F.; Betzen, L. J.; Liu, W.; Weiss, E. A.; Ratner, M. A.; Wasielewski, M. R. *Proc. Natl. Acad. Sci. U.S.A.* **2005**, *102*, 3540–3545.

(85) Atienza-Castellanos, C.; Wielopolski, M.; Guldi, D. M.; van der Pol, C.; Bryce, M. R.; Filippone, S.; Martín, N. *Chem. Commun.* **2007**, 5164–5166.

(86) Giacalone, F.; Segura, J. L.; Martín, N.; Guldi, D. M. *J. Am. Chem. Soc.* **2004**, *126*, 5340–5341.

(87) Nakamura, T.; Fujitsuka, M.; Araki, Y.; Ito, O.; Ikemoto, J.; Takimiya, K.; Aso, Y.; Otsubo, T. *J. Phys. Chem. B* **2004**, *108*, 10700–10710.

(88) Molina-Ontoria, A.; Wielopolski, M.; Gebhardt, J.; Gouloumis, A.; Clark, T.; Guldi, D. M.; Martín, N. *J. Am. Chem. Soc.* **2011**, *133*, 2370–2373.

(89) Nitzan, A. *J. Phys. Chem. A* **2001**, *105*, 2677–2679.

(90) Guo, H.; Liu, L.; Lao, K.-Q. *Chemical Physics Letters* **1994**, *218*, 212–220.

(91) McConnell, H. M. *J. Chem. Phys.* **1961**, *35*, 508.

(92) Gust, D. **1994**.

(93) Onipko, A. *Chemical Physics Letters* **1998**, *292*, 267–272.

(94) Ratner, M. A. *The Journal of Physical Chemistry* **1990**, *94*, 4877–4883.

(95) Gao, B.; Wang, M.; Cheng, Y.; Wang, L.; Jing, X.; Wang, F. *J. Am. Chem. Soc.* **2008**, *130*, 8297–8306.

(96) *laserfocusworld.com*.

(97) Scharber, M. C.; Mühlbacher, D.; Koppe, M.; Denk, P.; Waldauf, C.; Heeger, A. J.; Brabec, C. J. *Adv. Mater. Weinheim* **2006**, *18*, 789–794.

(98) Shockley, W.; Queisser, H. J. *J. Appl. Phys.* **1961**, *32*, 510–519.

(99) Closs, G. L.; Miller, J. R. *Science* **1988**, *240*, 440–447.

(100) Closs, G. L.; Calcaterra, L. T.; Green, N. J.; Penfield, K. W.; Miller, J. R. *The Journal of Physical Chemistry* **1986**, *90*, 3673–3683.

(101) Moses, D.; Leclerc, M.; Lee, K.; Heeger, A. J. **2009**.

(102) Silvestri, F. F.; Irwin, M. D. M.; Beverina, L. L.; Facchetti, A. A.; Pagani, G. A. G.; Marks, T. J. T. *Audio, Transactions of the IRE Professional Group on* **2008**, *130*, 17640–17641.

(103) Bertho; Janssen; Cleij; Conings; Moons; Gadisa; Goovaerts; Lutsen; Manca; Vanderzande *Solar Energy Materials and Solar Cells* **2008**, *92*, 8–8.

(104) Brédas, J.-L.; Norton, J. E.; Cornil, J.; Coropceanu, V. *Acc. Chem. Res.* **2009**, *42*, 1691–1699.

(105) Liang, Y.; Yu, L. *Acc. Chem. Res.* **2010**, *43*, 1227–1236.

(106) Brabec, C. J.; Gowrisanker, S.; Halls, J. J.; Laird, D.; Jia, S.; Williams, S. P. *Adv. Mater. Weinheim* **2010**, *22*, 3839–3856.

(107) Cravino, A.; Sariciftci, N. S. *J. Mater. Chem.* **2002**, *12*, 1931–1943.

(108) Hauch; Schilinsky; Choulis; Childers; Biele; Brabec *Solar Energy Materials and Solar Cells* **2008**, *92*, 5–5.

(109) Rohand, T.; Dolusic, E.; Ngo, T. H.; Maes, W.; Dehaen, W. *Arkivoc* **2007**, *10*, 307–324.

(110) Mulholland, A. R.; Woodward, C. P.; Langford, S. J. *Chem. Commun. (Camb.)* **2011**, *47*, 1494–1496.

(111) Laha, J. K.; Dhanalekshmi, S.; Taniguchi, M.; Ambroise, A.; Lindsey, J. S. *Org. Process Res. Dev.* **2003**, *7*, 799–812.

(112) Maggini, M.; Scorrano, G.; Prato, M. *J. Am. Chem. Soc.* **1993**, *115*, 9798–9799.

(113) Gvozdenović, M. M.; Jugović, B. Z.; Stevanović, J. S.; Trišović, T. L.; Grgur, B. N. *Electropolymerization* **2011**, 77–96.

(114) Wielopolski, M.; de Miguel Rojas, G.; van der Pol, C.; Brinkhaus, L.; Katsukis, G.; Bryce, M. R.; Clark, T.; Guldi, D. M. *ACS Nano* **2010**, *4*, 6449–6462.

(115) Guldi, D. M.; Illescas, B. M.; Atienza, C. M.; Wielopolski, M.; Martín, N. *Chem. Soc. Rev.* **2009**, *38*, 1587–1597.

(116) Wessendorf, F.; Grimm, B.; Guldi, D. M.; Hirsch, A. *J. Am. Chem. Soc.* **2010**, *132*, 10786–10795.

(117) Arnold, F. E. *Journal of Polymer Science Part A□1: Polymer Chemistry* **1970**, *8*, 2079–2089.

(118) Torres-Garcia, G.; Luftmann, H.; Wolff, C.; Mattay, J. *J. Org. Chem.* **1997**, *62*, 2752–2756.

(119) Zhang, J.; Wang, X.; Su, Q.; Zhi, L.; Thomas, A.; Feng, X.; Su, D. S.; Schlögl, R.; Müllen, K. *J. Am. Chem. Soc.* **2009**, *131*, 11296–11297.

(120) Hu, J.; Zhang, D.; Harris, F. W. *J. Org. Chem.* **2005**, *70*, 707–708.

(121) Suzuki, K.; Yamada, N.; Ueno, K. **2009**.

(122) Tabatabaeian, K.; Mamaghani, M.; Mahmoodi, N. O.; Khorshidi, A. *Catalysis Communications* **2008**, *9*, 416–420.

(123) Proust, N.; Gallucci, J. C.; Paquette, L. A. *J. Org. Chem.* **2009**, *74*, 2897–2900.

(124) Cheeseman, G. *Journal of the Chemical Society (Resumed)* **1962**, 1170–1176.

(125) Shirai, Y.; Osgood, A. J.; Zhao, Y.; Yao, Y.; Saudan, L.; Yang, H.; Yu-Hung, C.; Alemany, L. B.; Sasaki, T.; Morin, J.-F.; Guerrero, J. M.; Kelly, K. F.; Tour, J. M. *J. Am. Chem. Soc.* **2006**, *128*, 4854–4864.

(126) Burley, G. A.; Keller, P. A.; Pyne, S. G.; Ball, G. E. *Chem. Commun.* **2001**, 563–564.

(127) Hazen, J. R. *J. Org. Chem.* **1970**, *35*, 973–978.

(128) Starnes, S. D.; Rudkevich, D. M.; Rebek, J. *J. Am. Chem. Soc.* **2001**, *123*, 4659–4669.

(129) Imai, K.; Kurihara, M.; Mathias, L.; Wittmann, J.; Alston, W. B.; Stille, J. K. *Macromolecules* **1973**, *6*, 158–162.

(130) Khoury, T.; Crossley, M. J. *Chem. Commun.* **2007**, 4851–4853.

(131) Nageswar, Y. V. D.; Reddy, K. H. V.; Ramesh, K.; Murthy, S. N. *Organic Preparations and Procedures International* **2013**, *45*, 1–27.

(132) Raad, F. S.; El-Ballouli, A. O.; Moustafa, R. M.; Al-Sayah, M. H.; Kaafarani, B. R. *Tetrahedron* **2010**, *66*, 2944–2952.

(133) Rahmatpour, A. *Heteroatom Chem.* **2012**, *23*, 472–477.

(134) Stille, J. K.; Mainen, E. L. *Macromolecules* **1968**, *1*, 36–42.

(135) Wang, X.; Zhou, Y.; Lei, T.; Hu, N.; Chen, E.-Q.; Pei, J. *Chem. Mater.* **2010**, *22*, 3735–3745.

(136) Zhu, Y.; Yen, C.-T.; Jenekhe, S. A.; Chen, W.-C. *Macromol. Rapid Commun.* **2004**, *25*, 1829–1834.

(137) Kulisic, N.; More, S.; Mateo-Alonso, A. *Chem. Commun. (Camb.)* **2011**, *47*, 514–516.

(138) Lee, D.-C.; Jang, K.; McGrath, K. K.; Uy, R.; Robins, K. A.; Hatchett, D. W. *Chem. Mater.* **2008**, *20*, 3688–3695.

(139) Dogutan, D. K.; Zaidi, S. H. H.; Thamyongkit, P.; Lindsey, J. S. *J. Org. Chem.* **2007**, *72*, 7701–7714.

(140) Gajiwala, H. M.; Zand, R. *Polymer* **2000**, *41*, 2009–2015.

(141) Yasuda, T.; Shimizu, T.; Liu, F.; Ungar, G.; Kato, T. *J. Am. Chem. Soc.* **2011**, *133*, 13437–13444.

(142) Secondo, P.; Fages, F. *Org. Lett.* **2006**, *8*, 1311–1314.

(143) Takahashi, R.; Kobuke, Y. *J. Org. Chem.* **2005**, *70*, 2745–2753.

(144) PAWAR, O. B.; CHAVAN, F. R.; SURYAWANSHI, V. S.; SHINDE, V. S.; D SHINDE, N. *Journal of Chemical Sciences* **2013**, 1–5.

(145) Hagfeldt, A.; Gratzel, M. *Acc. Chem. Res.* **2000**, *33*, 269–277.

(146) Ardo, S.; Meyer, G. J. *Chem. Soc. Rev.* **2009**, *38*, 115–164.

(147) Cahen, D.; Hodes, G.; Grätzel, M.; Guillemoles, J. F.; Riess, I. *J. Phys. Chem. B* **2000**, *104*, 2053–2059.

(148) Yella, A.; Lee, H. W.; Tsao, H. N.; Yi, C.; Chandiran, A. K.; Nazeeruddin, M. K.; Diau, E. W. G.; Yeh, C. Y.; Zakeeruddin, S. M.; Gratzel, M. *Science* **2011**, *334*, 629–634.

(149) Grätzel, M. *Acc. Chem. Res.* **2009**, *42*, 1788–1798.

(150) Horiuchi, T.; Miura, H.; Sumioka, K.; Uchida, S. *J. Am. Chem. Soc.* **2004**, *126*, 12218–12219.

(151) Mishra, A.; Fischer, M. K.; Bäuerle, P. *Angew. Chem. Int. Ed.* **2009**, *48*, 2474–2499.

(152) Gao, F.; Wang, Y.; Shi, D.; Zhang, J.; Wang, M.; Jing, X.; Humphry-Baker, R.; Wang, P.; Zakeeruddin, S. M.; Grätzel, M. *J. Am. Chem. Soc.* **2008**, *130*, 10720–10728.

(153) Hara, K.; Sato, T.; Katoh, R.; Furube, A.; Ohga, Y.; Shinpo, A.; Suga, S.; Sayama, K.; Sugihara, H.; Arakawa, H. *J. Phys. Chem. B* **2003**, *107*, 597–606.

(154) Kim, S.; Lee, J. K.; Kang, S. O.; Ko, J.; Yum, J.-H.; Fantacci, S.; De Angelis, F.; Di Censo, D.; Nazeeruddin, M. K.; Grätzel, M. *J. Am. Chem. Soc.* **2006**, *128*, 16701–16707.

(155) Robertson, N. *Angew. Chem. Int. Ed. Engl.* **2006**, *45*, 2338–2345.

(156) Campbell, W. M.; Burrell, A. K.; Officer, D. L.; Jolley, K. W. *Coordination Chemistry Reviews* **2004**, *248*, 1363–1379.

(157) Kitamura, T.; Ikeda, M.; Shigaki, K.; Inoue, T.; Anderson, N. A.; Ai, X.; Lian, T.; Yanagida, S. *Chem. Mater.* **2004**, *16*, 1806–1812.

(158) Hagberg, D. P.; Yum, J.-H.; Lee, H.; De Angelis, F.; Marinado, T.; Karlsson, K. M.; Humphry-Baker, R.; Sun, L.; Hagfeldt, A.; Grätzel, M. *J. Am. Chem. Soc.* **2008**, *130*, 6259–6266.

(159) Zeng, W.; Cao, Y.; Bai, Y.; Wang, Y.; Shi, Y.; Zhang, M.; Wang, F.; Pan, C.; Wang, P. *Chem. Mater.* **2010**, *22*, 1915–1925.

(160) Campbell, W. M.; Jolley, K. W.; Wagner, P.; Wagner, K.; Walsh, P. J.; Gordon, K. C.; Schmidt-Mende, L.; Nazeeruddin, M. K.; Wang, Q.; Gratzel, M.; Officer, D. L. *J. Phys. Chem. C* **2007**, *111*, 11760–11762.

(161) Imahori, H.; Umeyama, T.; Ito, S. *Acc. Chem. Res.* **2009**, *42*, 1809–1818.

(162) Lee, C.-W.; Lu, H.-P.; Lan, C. M.; Huang, Y. L.; Liang, Y. R.; Yen, W. N.; Liu, Y. C.; Lin, Y. S.; Diau, E. W.-G.; Yeh, C.-Y. *Chem. Eur. J.* **2009**, *15*, 1403–1412.

(163) Koumura, N.; Wang, Z.-S.; Mori, S.; Miyashita, M.; Suzuki, E.; Hara, K. *J. Am. Chem. Soc.* **2006**, *128*, 14256–14257.

(164) Yella, A.; Lee, H.-W.; Tsao, H. N.; Yi, C.; Chandiran, A. K.; Nazeeruddin, M. K.; Diau, E. W.-G.; Yeh, C.-Y.; Zakeeruddin, S. M.; Grätzel, M. *Science* **2011**, *334*, 629–634.

(165) Wu, S.-L.; Lu, H.-P.; Yu, H.-T.; Chuang, S.-H.; Chiu, C.-L.; Lee, C.-W.; Diau, E. W.-G.; Yeh, C.-Y. *Energy Environ. Sci.* **2010**, *3*, 949.

(166) Mathew, S.; Iijima, H.; Toude, Y.; Umeyama, T.; Matano, Y.; Ito, S.; Tkachenko, N. V.; Lemmetyinen, H.; Imahori, H. *J. Phys. Chem. C* **2011**, *115*, 14415–14424.

(167) Wu, S.-L.; Lu, H.-P.; Yu, H.-T.; Chuang, S.-H.; Chiu, C.-L.; Lee, C.-W.; Diau, E. W.-G.; Yeh, C.-Y. *Energy Environ. Sci.* **2010**, *3*, 949.

(168) Yum, J.-H.; Jang, S.-R.; Walter, P.; Geiger, T.; Nüesch, F.; Kim, S.; Ko, J.; Grätzel, M.; Nazeeruddin, M. K. *Chem. Commun.* **2007**, 4680–4682.

(169) Guo, M.; Diao, P.; Ren, Y.-J.; Meng, F.; Tian, H.; Cai, S.-M. *Solar Energy Materials and Solar Cells* **2005**, *88*, 23–35.

(170) Kuang, D.; Walter, P.; Nüesch, F.; Kim, S.; Ko, J.; Comte, P.; Zakeeruddin, S.

M.; Nazeeruddin, M. K.; Grätzel, M. *Langmuir* **2007**, *23*, 10906–10909.

(171) Colonna, D.; Capogna, V.; Lembo, A.; Brown, T. M.; Reale, A.; Carlo, A. D. *Appl. Phys. Express* **2012**, *5*, 022303.

(172) Chen, Y.; Zeng, Z.; Li, C.; Wang, W.; Wang, X.; Zhang, B. *New J. Chem.* **2005**, *29*, 773–776.

(173) Rochford, J.; Chu, D.; Hagfeldt, A.; Galoppini, E. *J. Am. Chem. Soc.* **2007**, *129*, 4655–4665.

(174) Alex, S.; Santhosh, U.; Das, S. *Journal of Photochemistry and Photobiology A: Chemistry* **2005**, *172*, 63–71.

(175) Lu, H.-P.; Tsai, C.-Y.; Yen, W. N.; Hsieh, C.-P.; Lee, C.-W.; Yeh, C.-Y.; Diau, E. W.-G. *J. Phys. Chem. C* **2009**, *113*, 20990–20997.

(176) Ito, S.; Miura, H.; Uchida, S.; Takata, M.; Sumioka, K.; Liska, P.; Comte, P.; Péchy, P.; Grätzel, M. *Chem. Commun.* **2008**, 5194–5196.

(177) Morandeira, A.; López-Duarte, I.; O'regan, B.; Martínez-Díaz, M. V.; Forneli, A.; Palomares, E.; Torres, T.; Durrant, J. R. *J. Mater. Chem.* **2009**, *19*, 5016–5026.

(178) Mori, S.; Nagata, M.; Nakahata, Y.; Yasuta, K.; Goto, R.; Kimura, M.; Taya, M. *J. Am. Chem. Soc.* **2010**, *132*, 4054–4055.

(179) He, J.; Benkö, G.; Korodi, F.; Polívka, T.; Lomoth, R.; Åkermark, B.; Sun, L.; Hagfeldt, A.; Sundström, V. *J. Am. Chem. Soc.* **2002**, *124*, 4922–4932.

(180) Lu, M.; Liang, M.; Han, H.-Y.; Sun, Z.; Xue, S. *J. Phys. Chem. C* **2010**, *115*, 274–281.

(181) Basham, J. I.; Mor, G. K.; Grimes, C. A. *ACS Nano* **2010**, *4*, 1253–1258.

(182) Forster, T. *Naturwissenschaften* **1946**, *33*, 166–175.

(183) Cong, J.; Yang, X.; Liu, J.; Zhao, J.; Hao, Y.; Wang, Y.; Sun, L. *Chem. Commun. (Camb.)* **2012**, *48*, 6663–6665.

(184) Ambrosio, F.; Martsinovich, N.; Troisi, A. *J. Phys. Chem. Lett.* **2012**, *3*, 1531–1535.

(185) Kleineweischede, A.; Mattay, J. *Eur. J. Org. Chem.* **2006**, *2006*, 947–957.

(186) Gawrys, P.; Marszalek, T.; Bartnik, E.; Kucinska, M.; Ulanski, J.; Zagorska, M. *Org. Lett.* **2011**, *13*, 6090–6093.

(187) Ito, S.; Murakami, T. N.; Comte, P.; Liska, P.; Grätzel, C.; Nazeeruddin, M. K.; Grätzel, M. *Thin Solid Films* **2008**, *516*, 4613–4619.

(188) Kang, M. G.; Park, N.-G.; Park, Y. J.; Ryu, K. S.; Chang, S. H. *Solar Energy Materials and Solar Cells* **2003**, *75*, 475–479.

(189) Kavan, L.; Grätzel, M. *Electrochimica Acta* **1995**, *40*, 643–652.

(190) Rusanova, J.; Pilkington, M.; Decurtins, S. *Chem. Commun.* **2002**, 2236–2237.

APPENDIX A

NMR and MASS SPECTRAL DATA FOR SYNTHESIZED COMPOUNDS OF CHAPTER 2

Monomer **2.1**

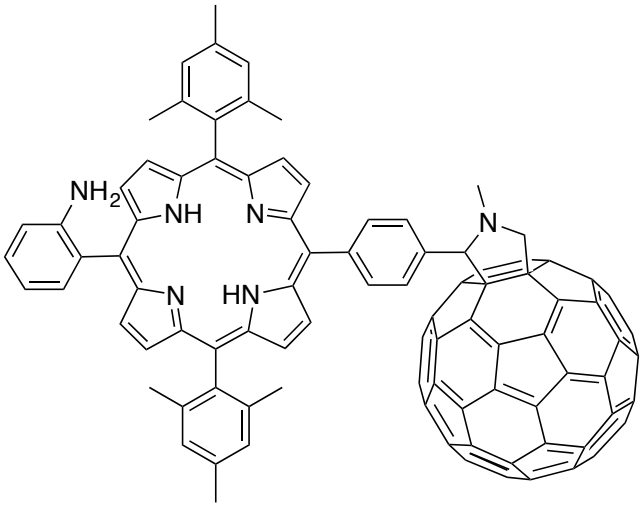

2.1

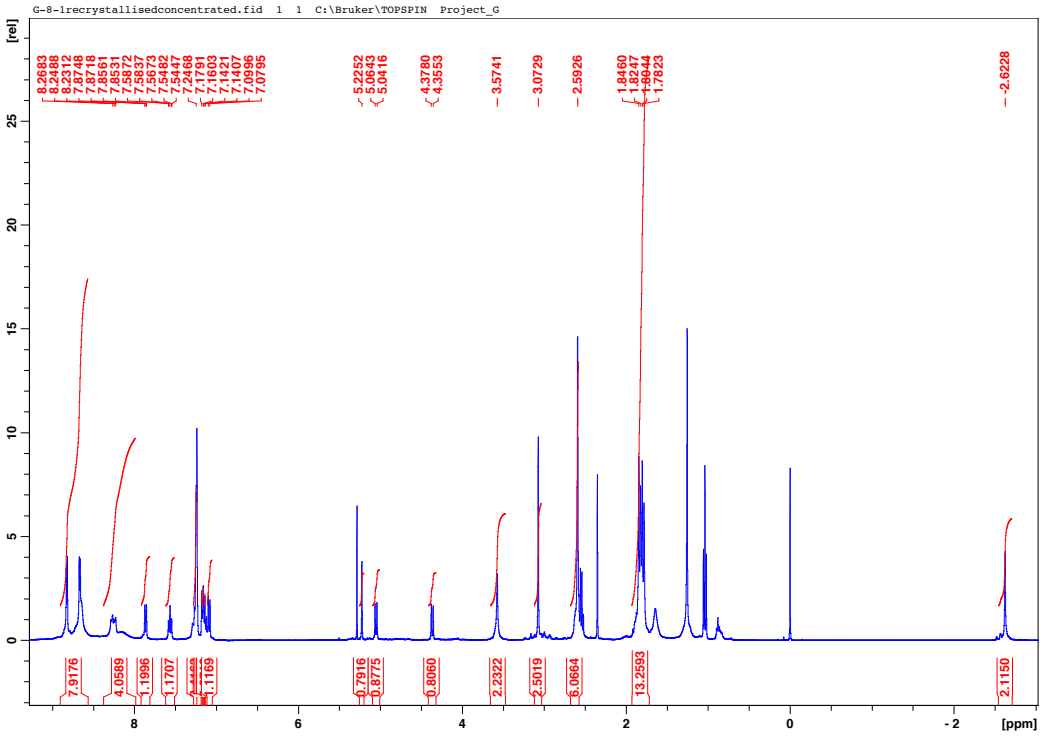

^{1}H NMR spectrum of **2.1** in $CDCl_3$ at 25^{o}C

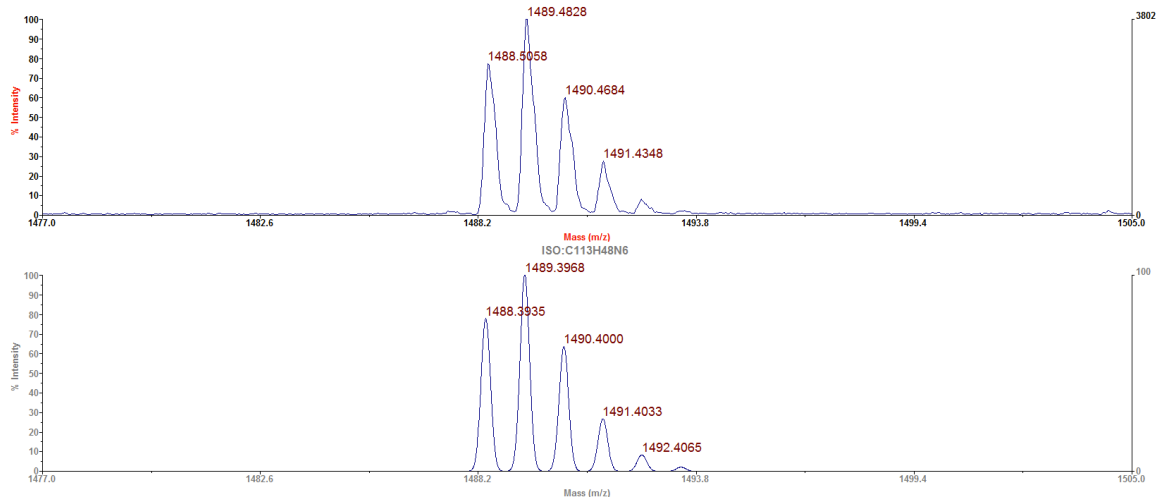

MALDI-TOF mass spectrum for **2.1**. The top trace shows the observed spectrum and the bottom trace shows the theoretical spectrum for chemical formula $C_{113}H_{48}N_6$ $[M]^+$.

2.2

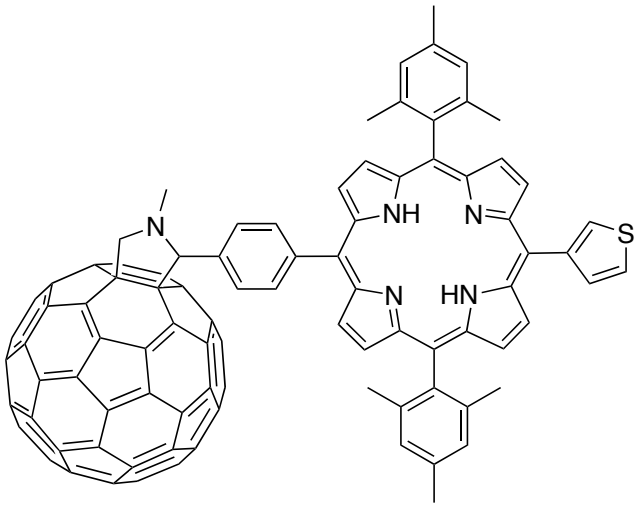

2.2

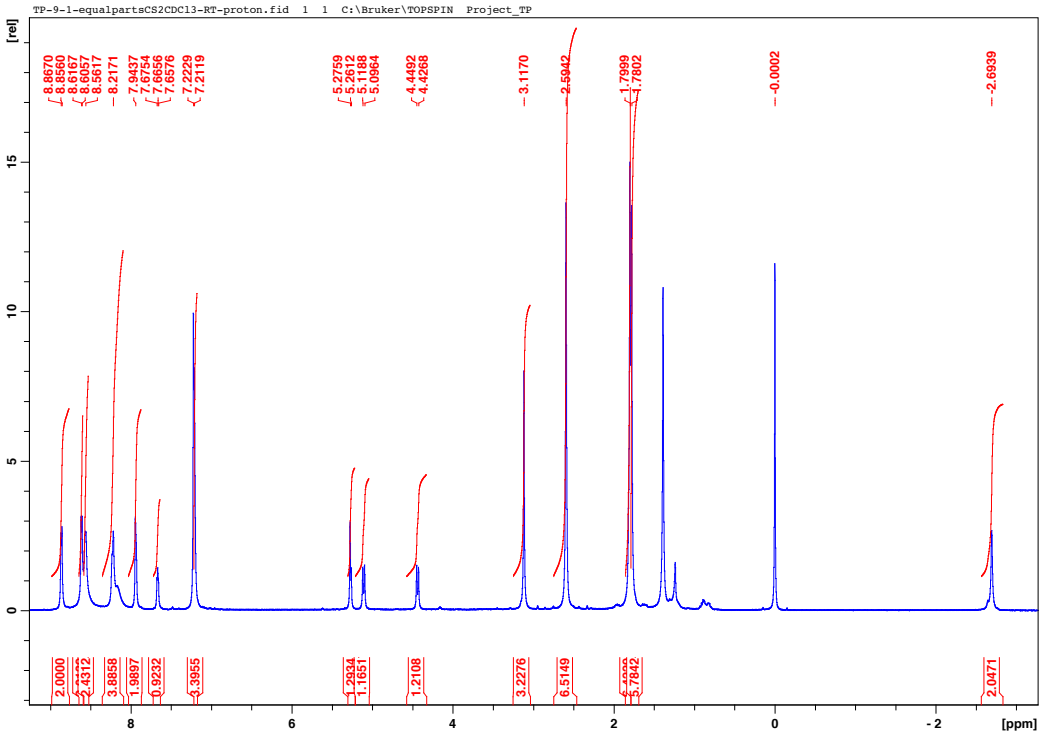

^{1}H NMR spectrum of **2.2** in CS_2:$CDCl_3$ (1:1) at 25^{o}C

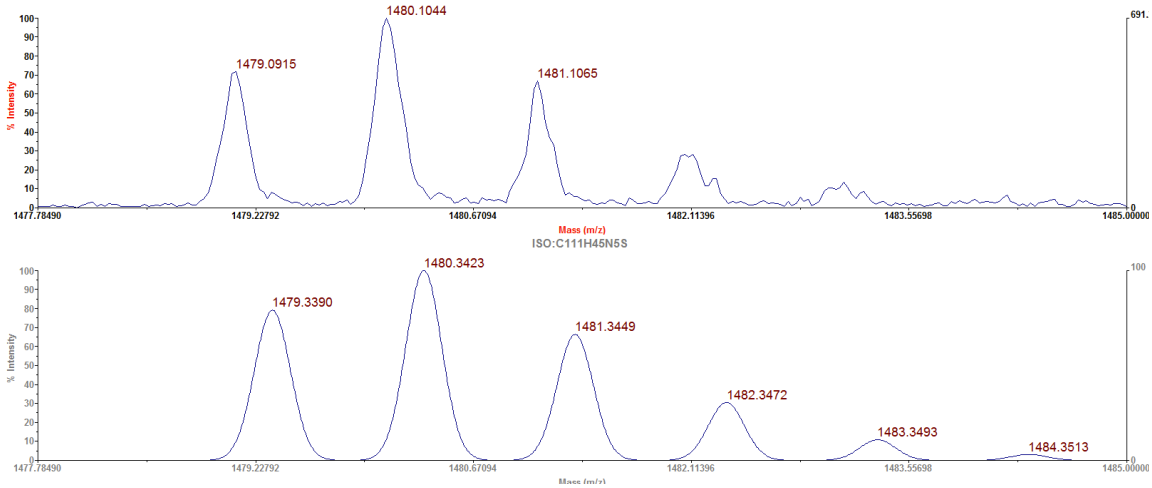

MALDI-TOF mass spectrum for **2.2**. The top trace shows the observed spectrum and the bottom trace shows the theoretical spectrum for chemical formula $C_{111}H_{45}N_5S$ $[M]^+$.

Monomer 2.3

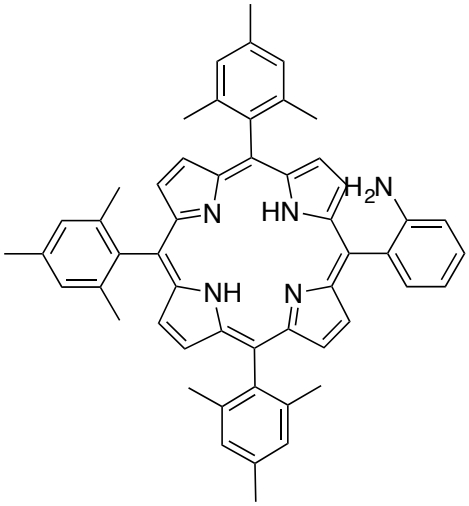

2.3

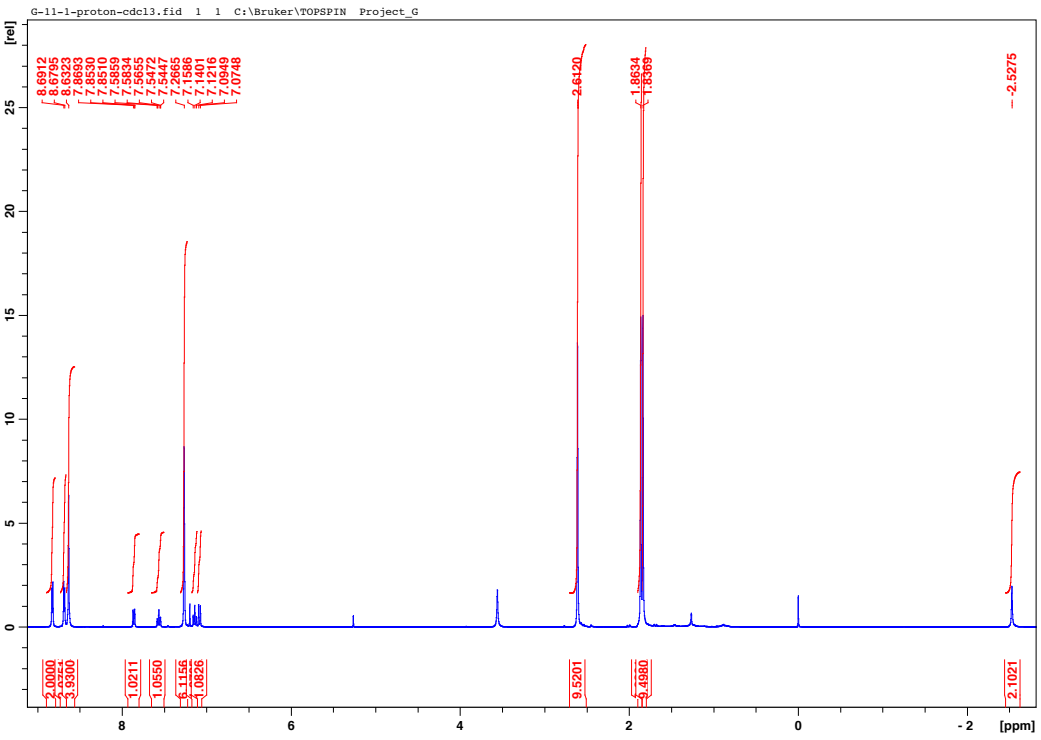

^{1}H NMR spectrum of **2.3** in $CDCl_3$ at 25^{o}C

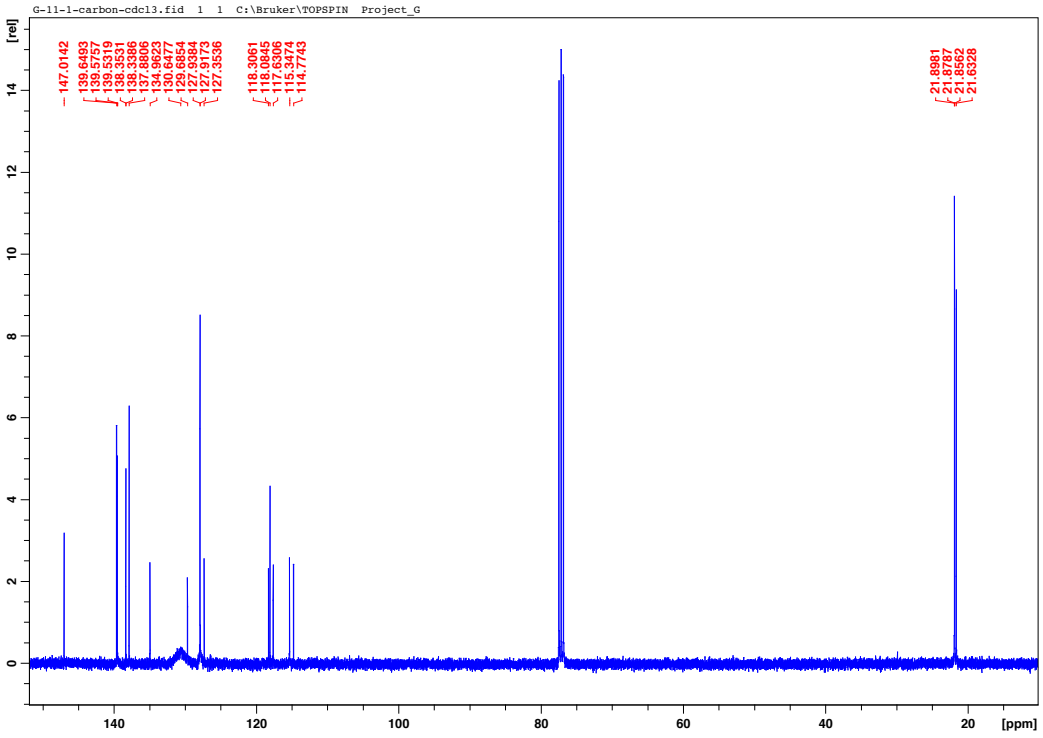

^{13}C NMR spectrum of **2.3** in $CDCl_3$ at 25°C

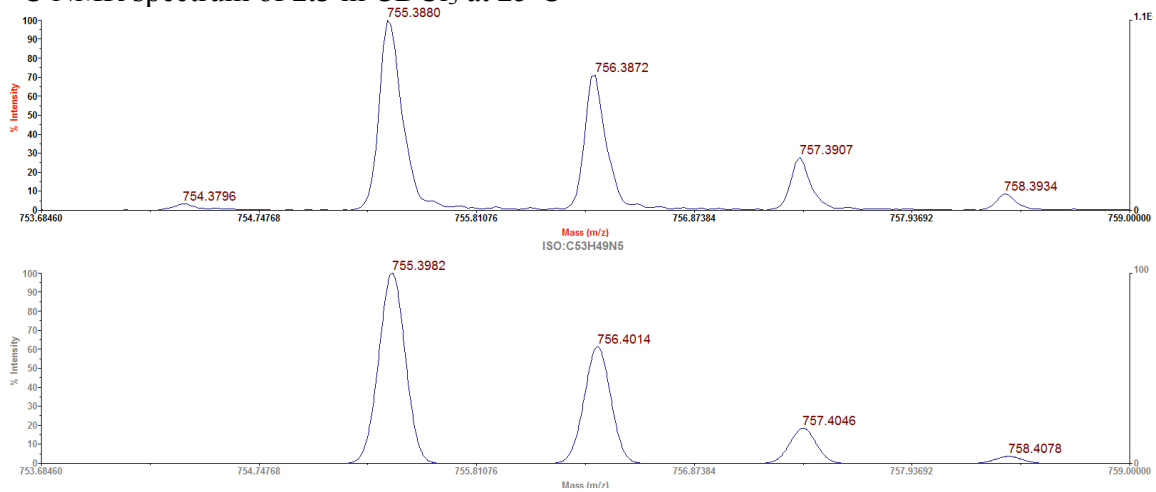

MALDI-TOF mass spectrum for **2.3**. The top trace shows the observed spectrum and the bottom trace shows the theoretical spectrum for chemical formula $C_{53}H_{49}N_5S$ $[M]^+$.

Monomer 2.4

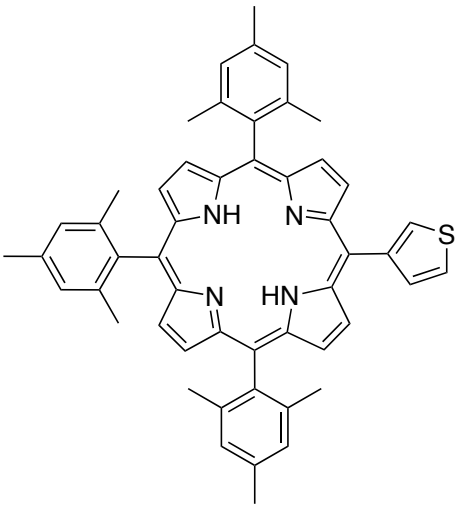

2.4

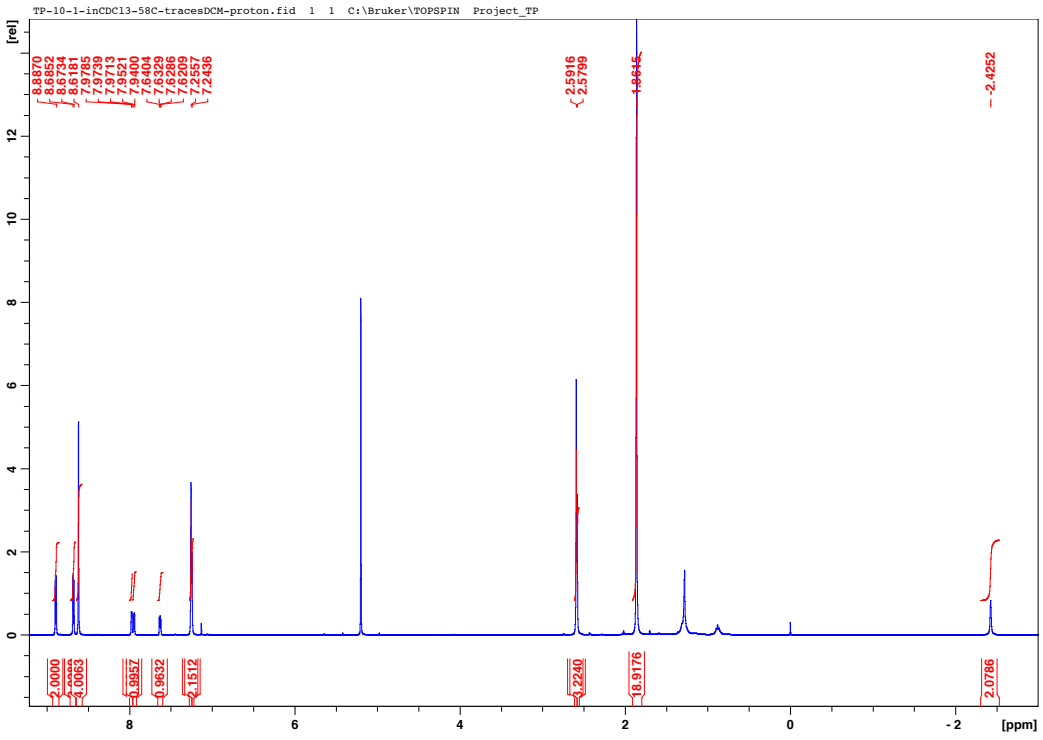

^{1}H NMR spectrum of **2.4** in $CDCl_3$ at 25^{o}C

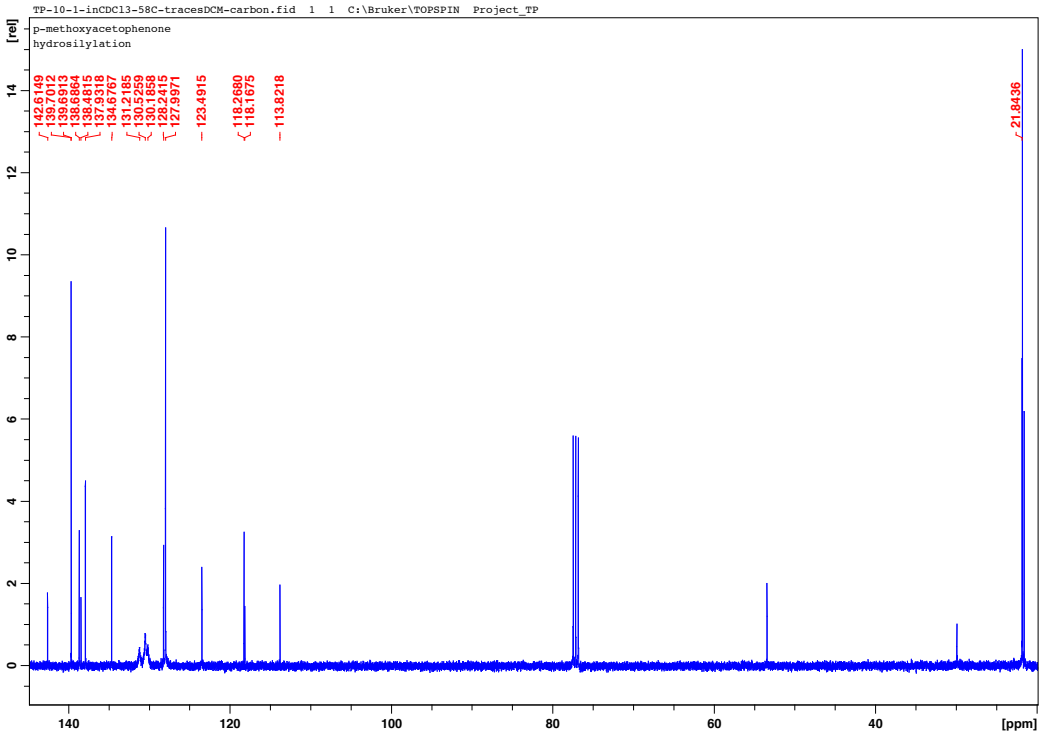

^{13}C NMR spectrum of **2.4** in $CDCl_3$ at 25°C

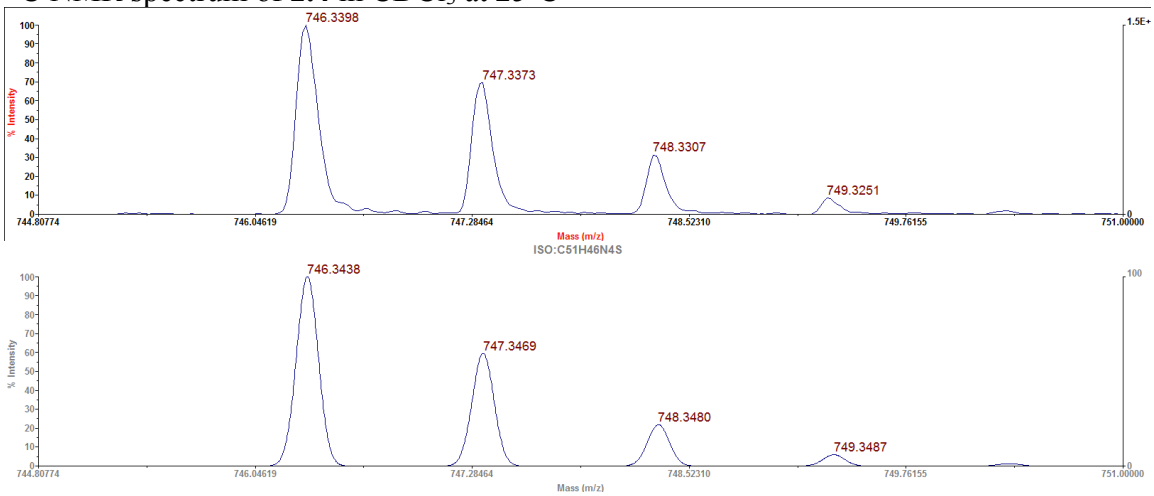

MALDI-TOF mass spectrum for **2.4**. The top trace shows the observed spectrum and the bottom trace shows the theoretical spectrum for chemical formula $C_{51}H_{46}N_4S$ $[M]^+$.

***Meso*-(*p*-methylbenzoate)dipyrromethane (2.5)**

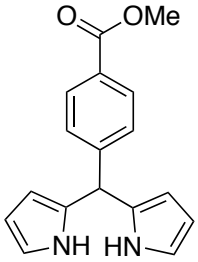

2.5

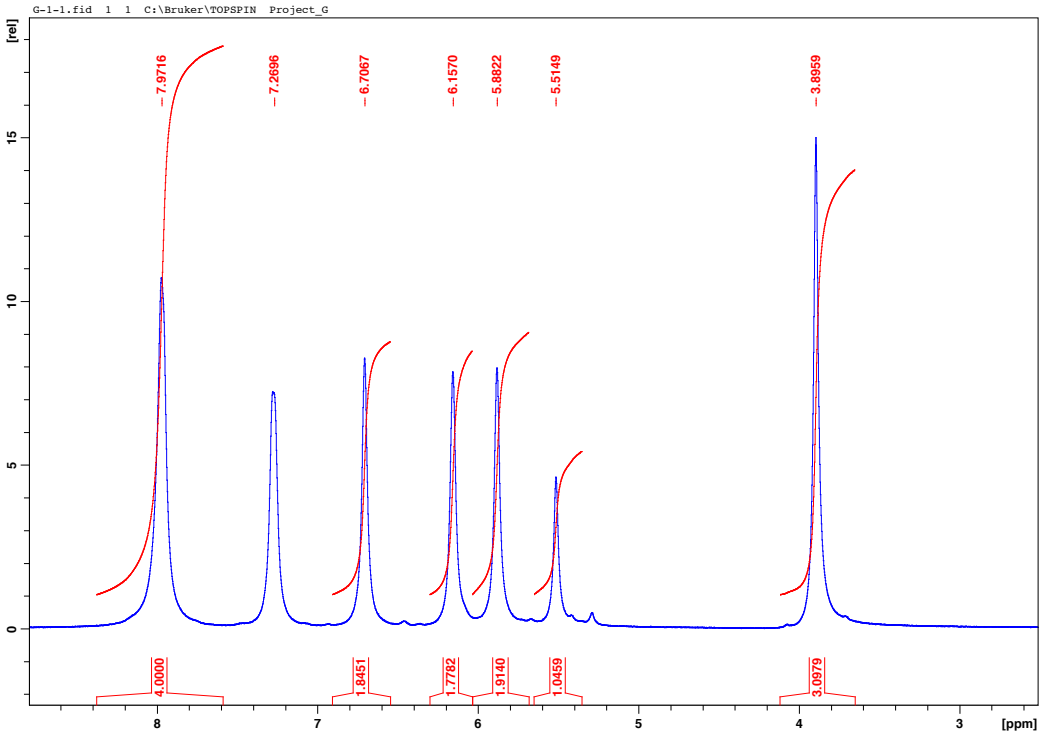

^{1}H NMR spectrum of **2.5** in $CDCl_3$ at 25^{o}C

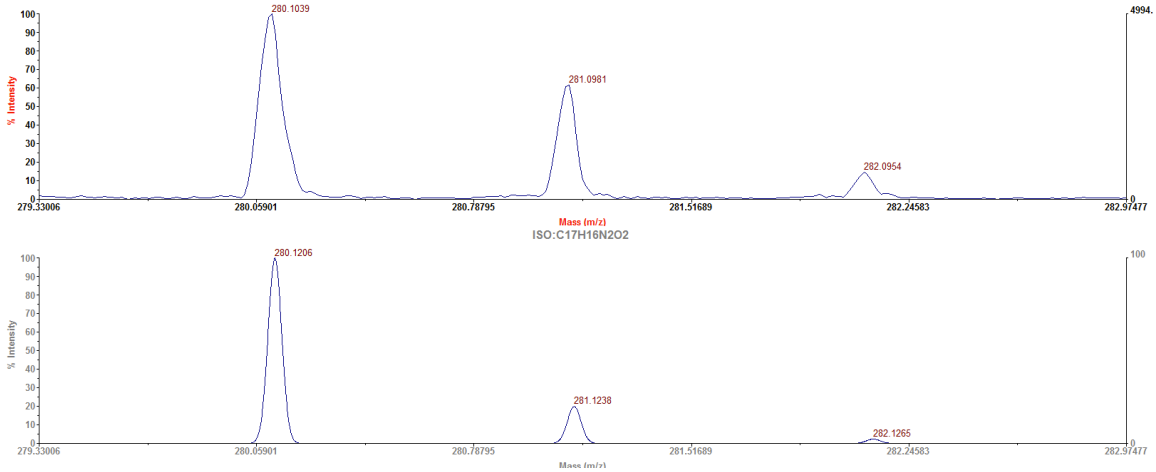

MALDI-TOF mass spectrum for **2.5**. The top trace shows the observed spectrum and the bottom trace shows the theoretical spectrum for chemical formula $C_{17}H_{16}N_2O_2$ $[M]^+$.

Dipyrromethane (2.6)

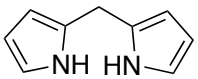

2.6

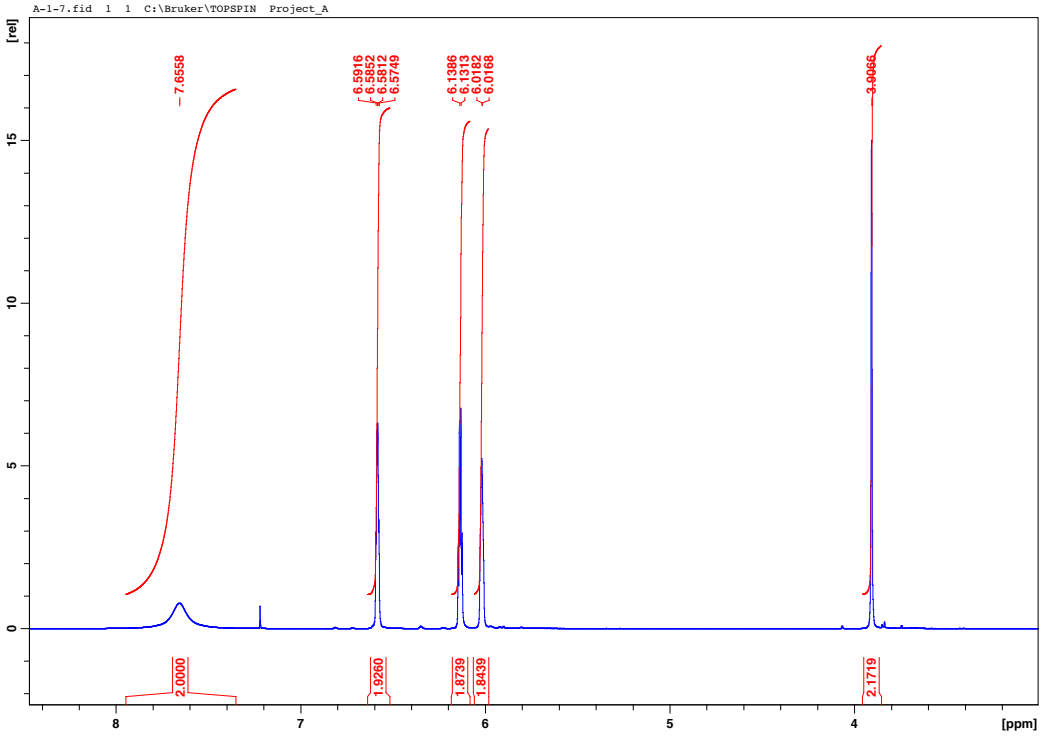

^{1}H NMR spectrum of **2.6** in $CDCl_3$ at 25°C

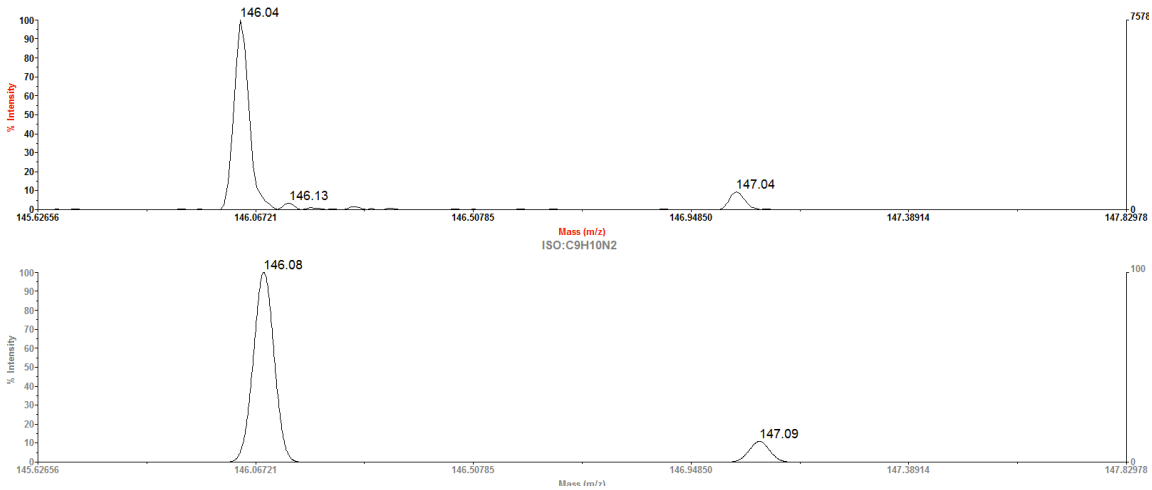

MALDI-TOF mass spectrum for **2.6**. The top trace shows the observed spectrum and the bottom trace shows the theoretical spectrum for chemical formula $C_9H_{10}N_2$ $[M]^+$.

Porphyrin (2.7)

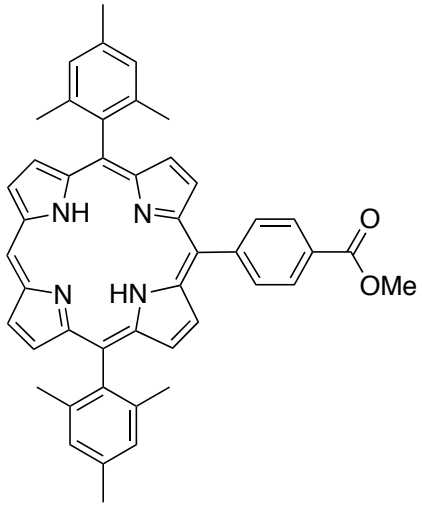

2.7

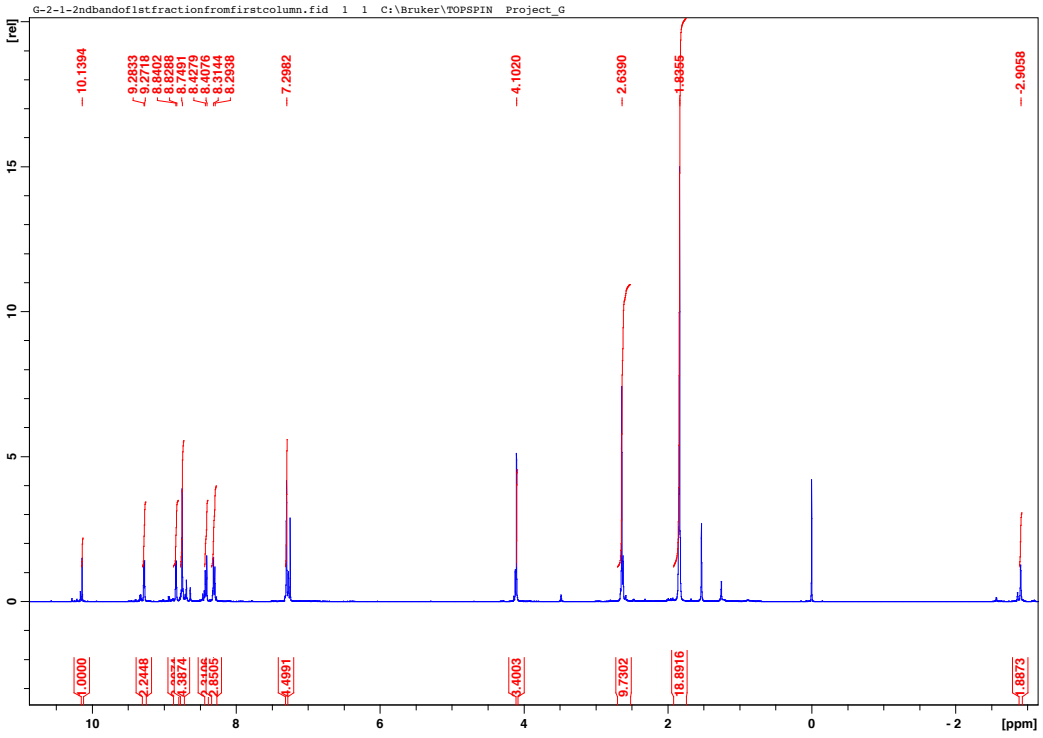

^{1}H NMR spectrum of **2.7** in $CDCl_3$ at 25^{o}C

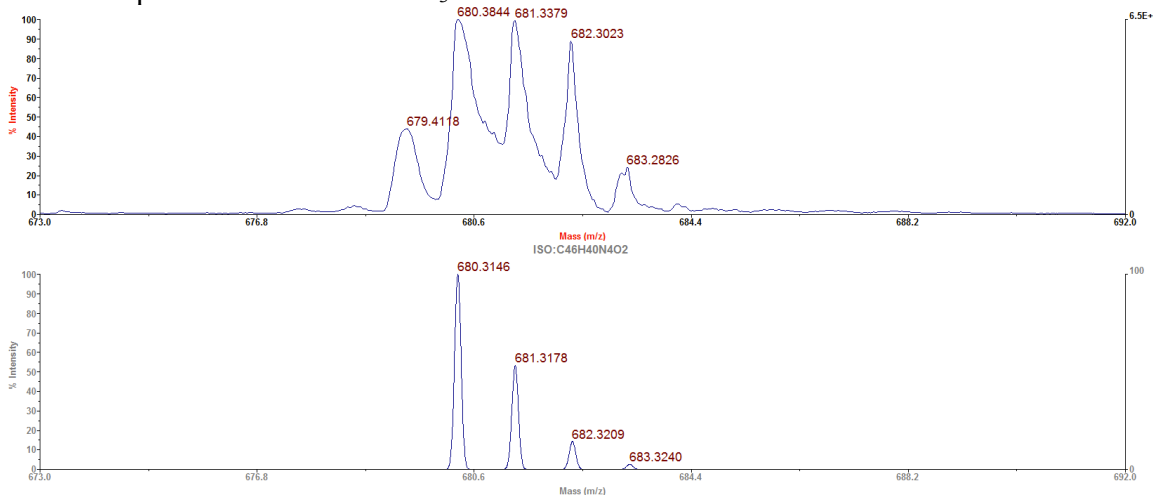

MALDI-TOF mass spectrum for **2.7**. The top trace shows the observed spectrum and the bottom trace shows the theoretical spectrum for chemical formula $C_{46}H_{40}N_4O_2$ $[M]^{+}$.

2.8

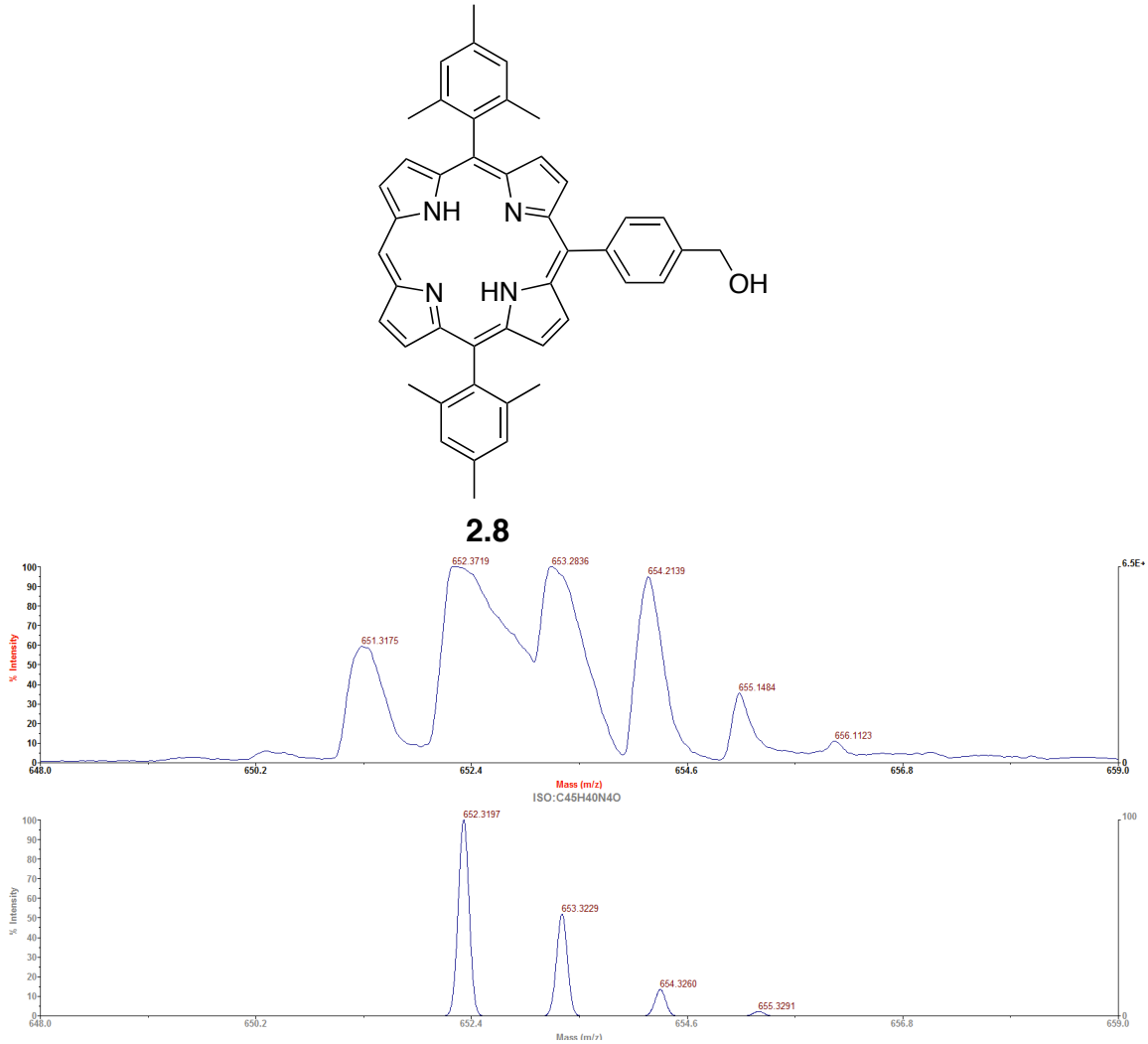

MALDI-TOF mass spectrum for **2.8**. The top trace shows the observed spectrum and the bottom trace shows the theoretical spectrum for chemical formula $C_{44}H_{40}N_4O$ $[M]^+$.

Porphyrin 2.9

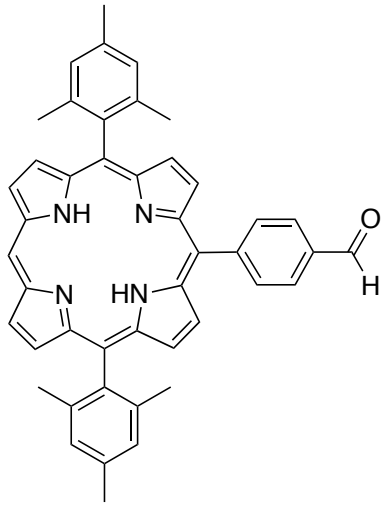

2.9

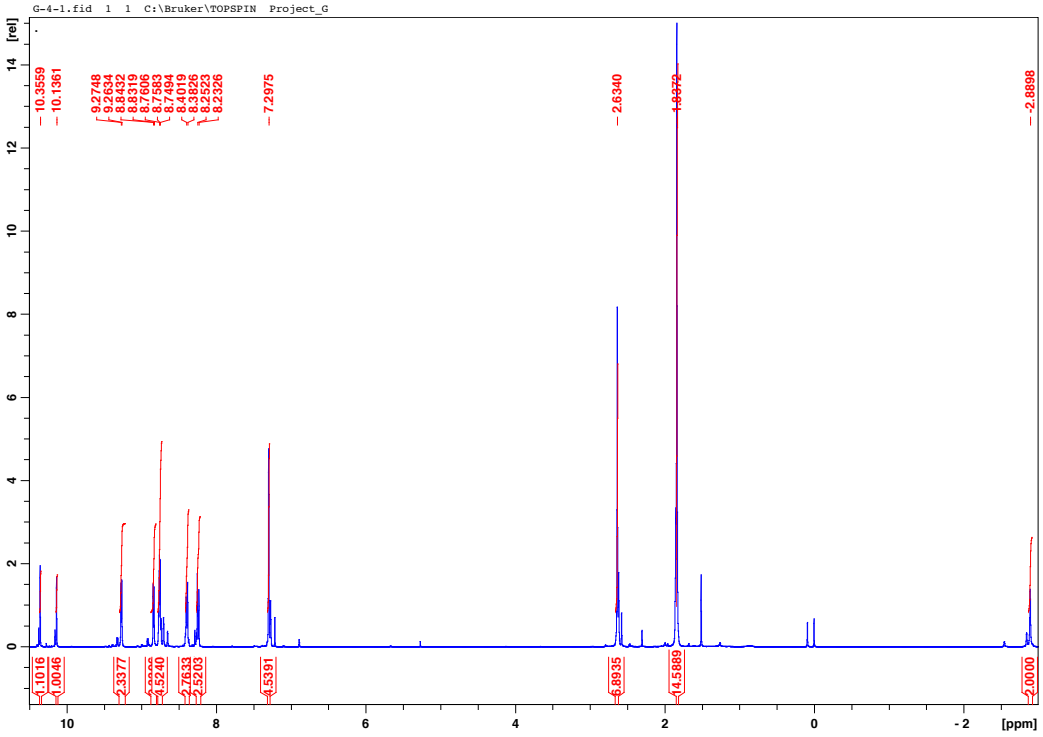

^{1}H NMR spectrum of **2.9** in $CDCl_3$ at 25^{o}C

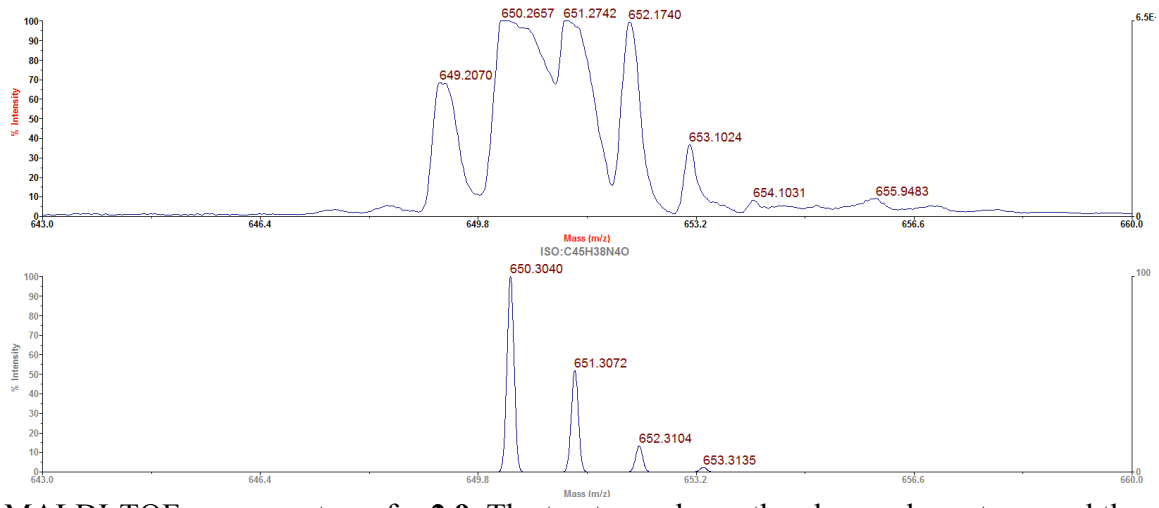

MALDI-TOF mass spectrum for **2.9**. The top trace shows the observed spectrum and the bottom trace shows the theoretical spectrum for chemical formula $C_{45}H_{38}N_4O$ $[M]^+$.

Porphyrin 2.10

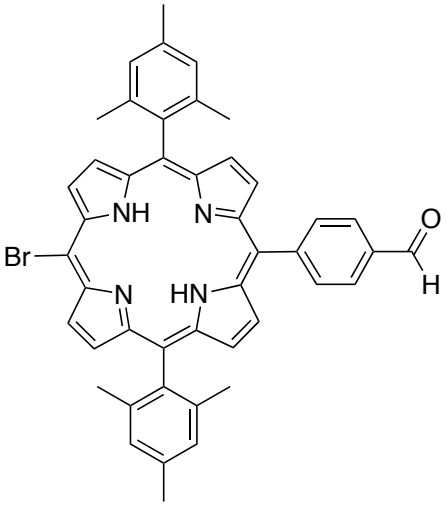

2.10

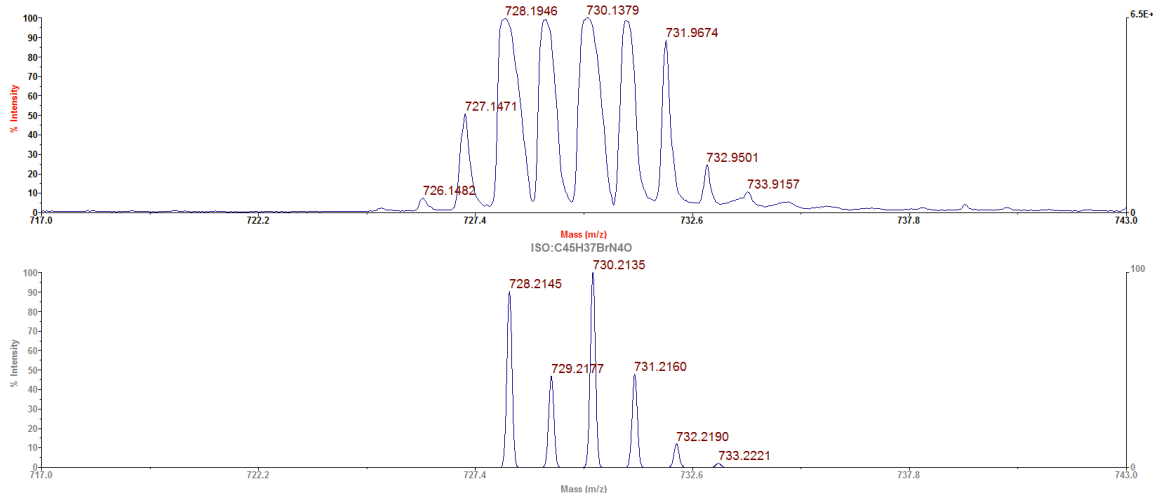

MALDI-TOF mass spectrum for **2.10**. The top trace shows the observed spectrum and the bottom trace shows the theoretical spectrum for chemical formula $C_{45}H_{37}N_4O$ $[M]^+$.

Porphyrin 2.11

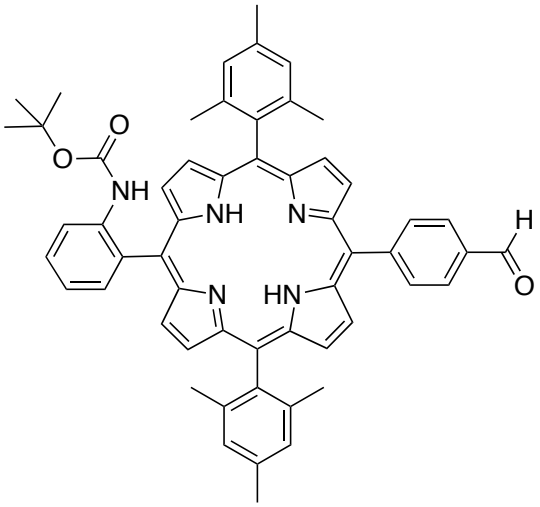

2.11

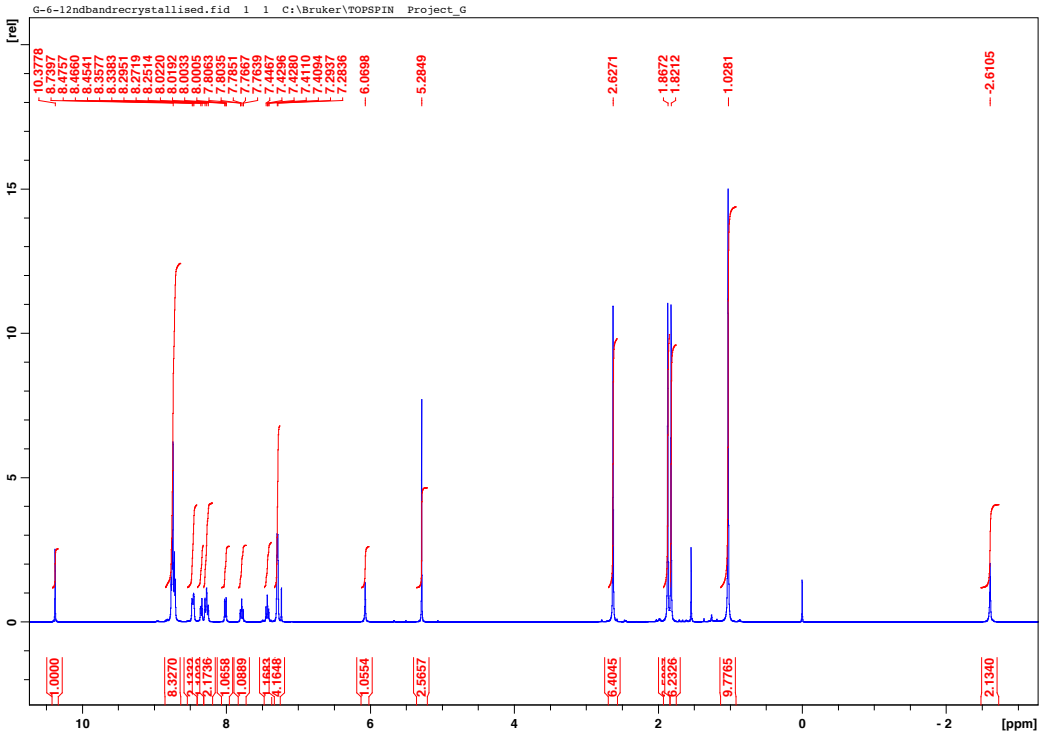

^{1}H NMR spectrum of **2.11** in $CDCl_3$ at 25^{o}C

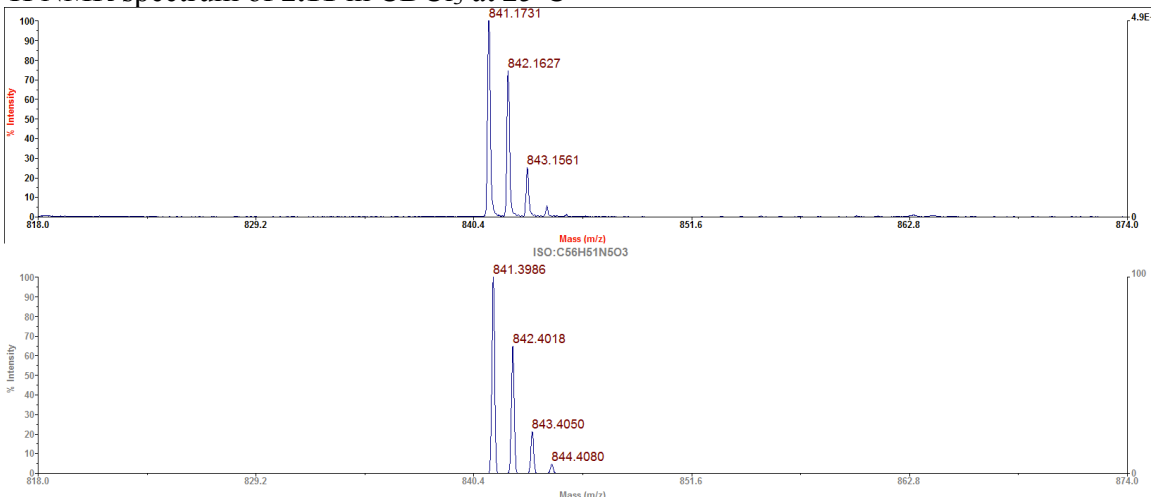

MALDI-TOF mass spectrum for **2.11**. The top trace shows the observed spectrum and the bottom trace shows the theoretical spectrum for chemical formula $C_{56}H_{51}N_5O_3$ $[M]^+$.

Porphyrin 2.12

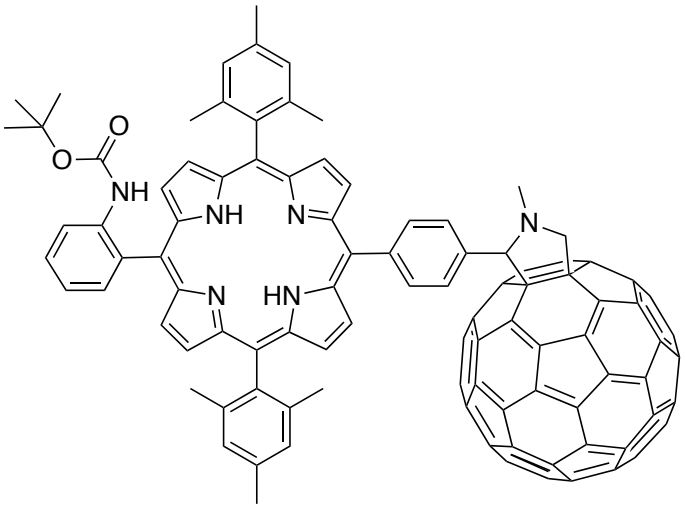

2.12

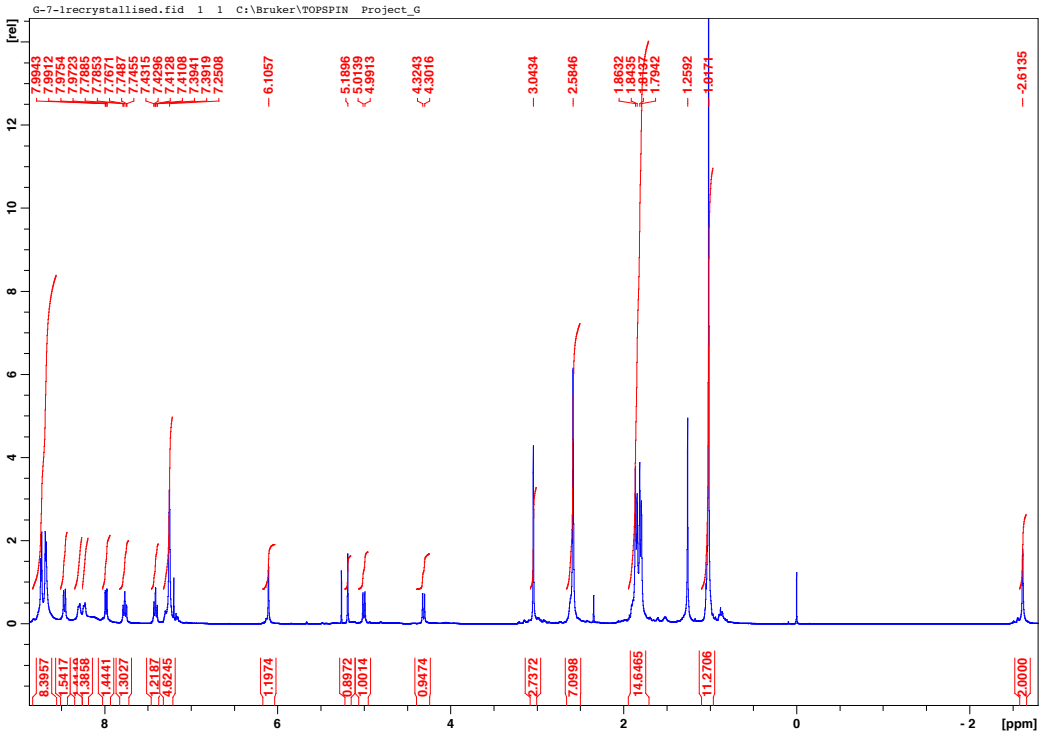

^{1}H NMR spectrum of **2.12** in $CDCl_3$ at 25^{o}C

***Meso*-(mesityl)dipyrromethane 2.13**

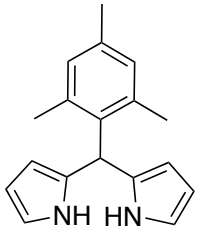

2.13

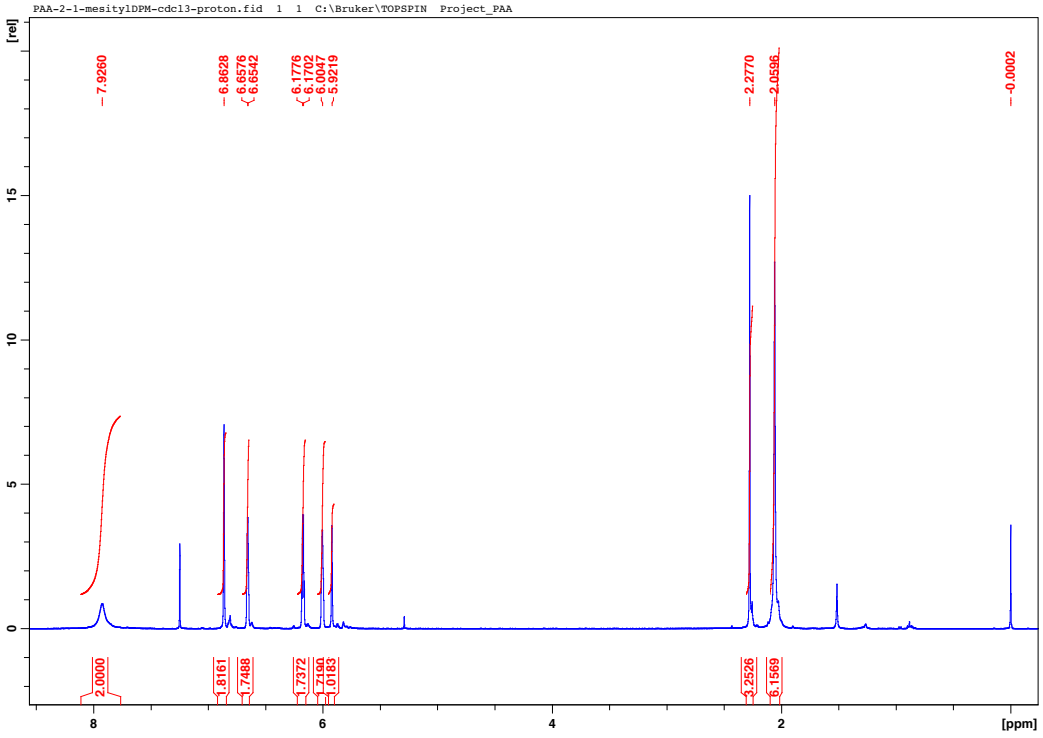

^{1}H NMR spectrum of **2.13** in $CDCl_3$ at 25^{o}C

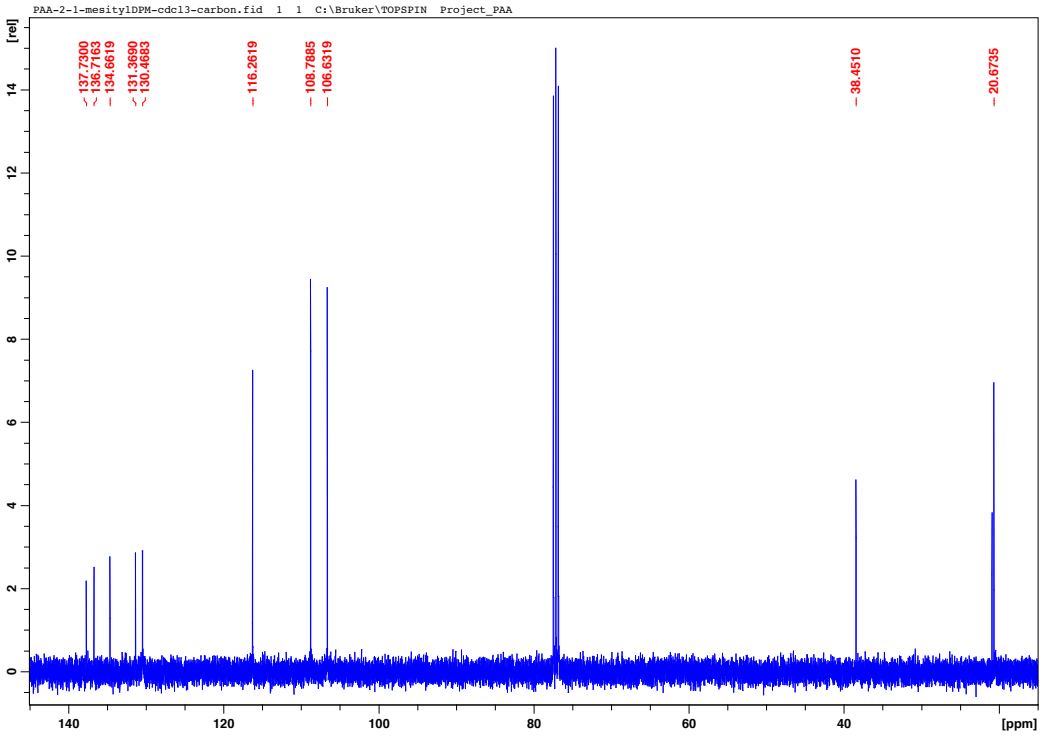

^{13}C NMR spectrum of **2.13** in $CDCl_3$ at 25°C

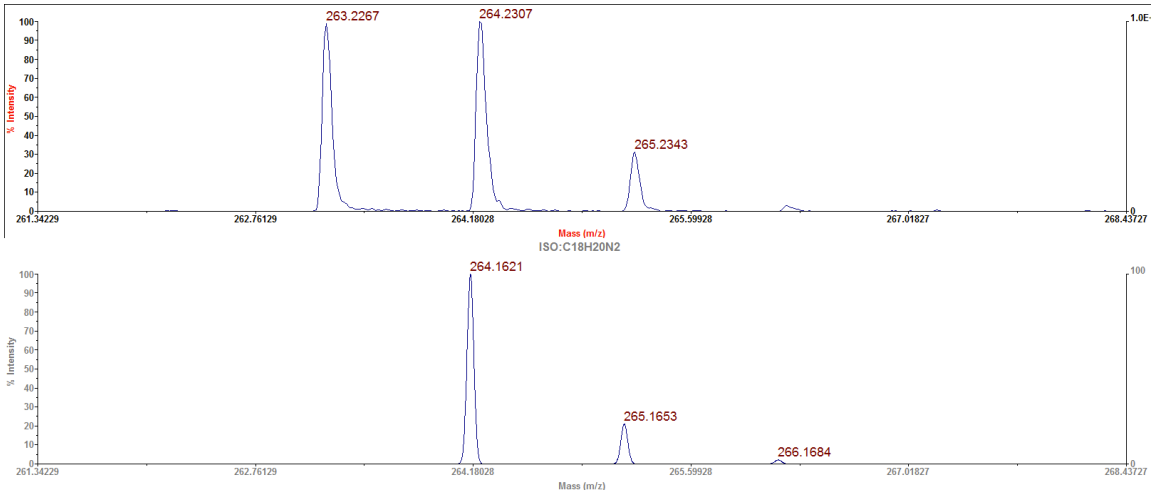

MALDI-TOF mass spectrum for **2.13**. The top trace shows the observed spectrum and the bottom trace shows the theoretical spectrum for chemical formula $C_{18}H_{20}N_2$ $[M]^+$.

Porphyrin 2.14

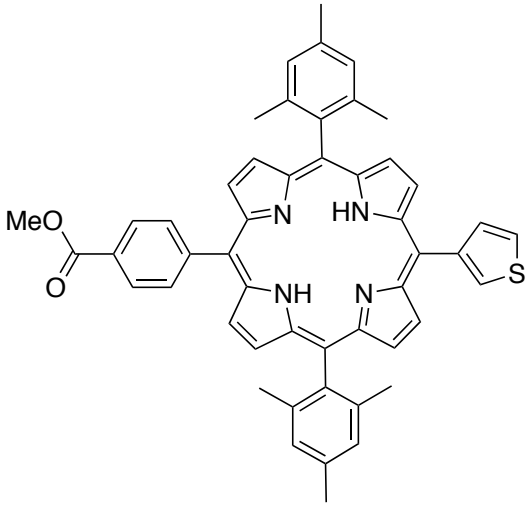

2.14

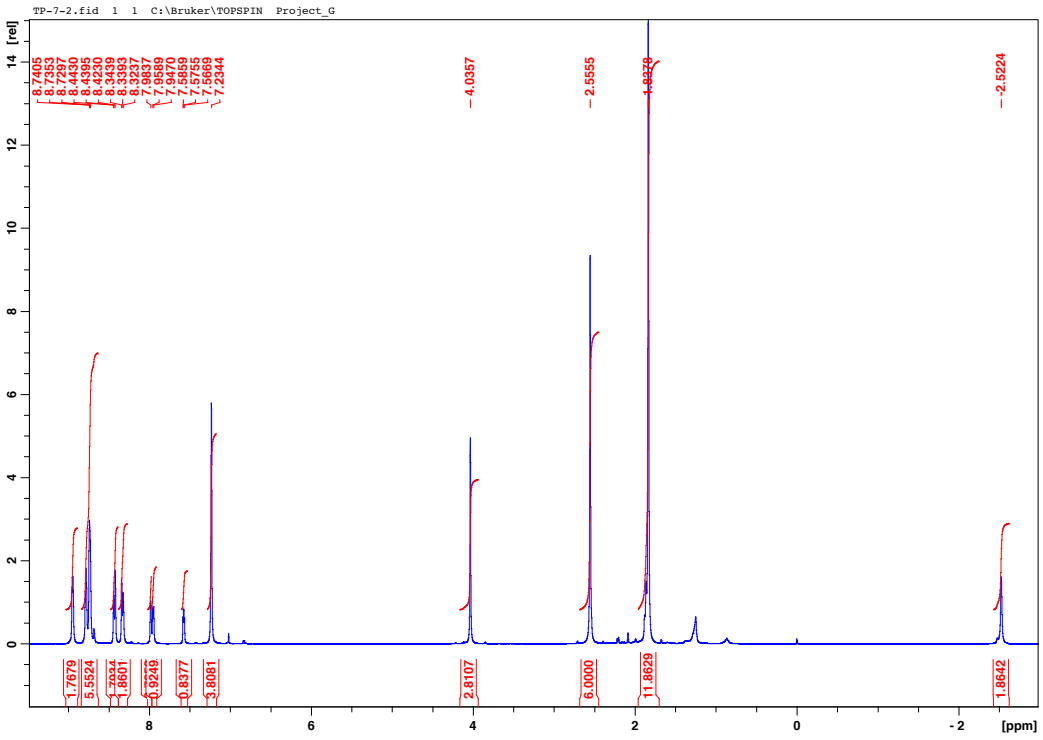

^{1}H NMR spectrum of **2.14** in $CDCl_3$ at 25^{o}C

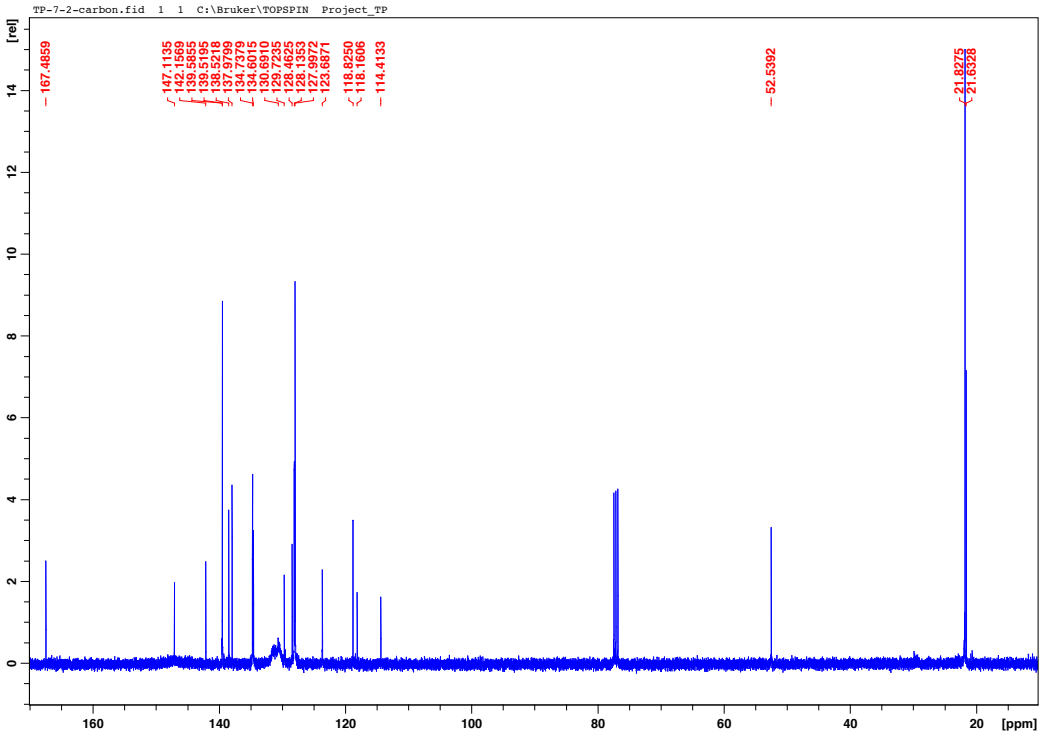

^{13}C NMR spectrum of **2.14** in $CDCl_3$ at 25°C

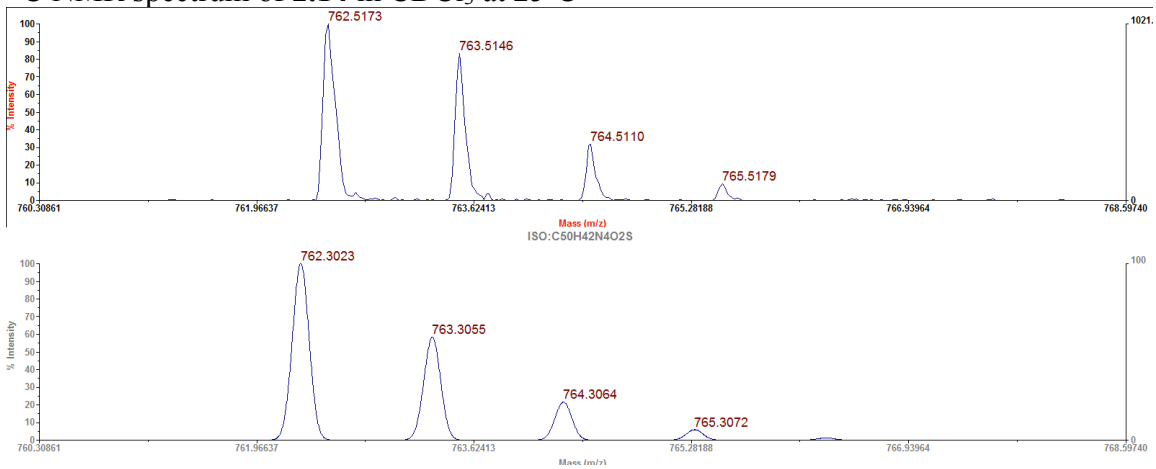

MALDI-TOF mass spectrum for **2.14**. The top trace shows the observed spectrum and the bottom trace shows the theoretical spectrum for chemical formula $C_{50}H_{42}N_4O_2S$ $[M]^+$.

Porphyrin 2.15

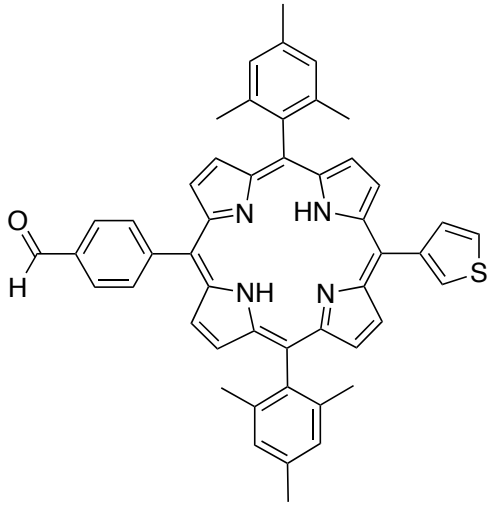

2.15

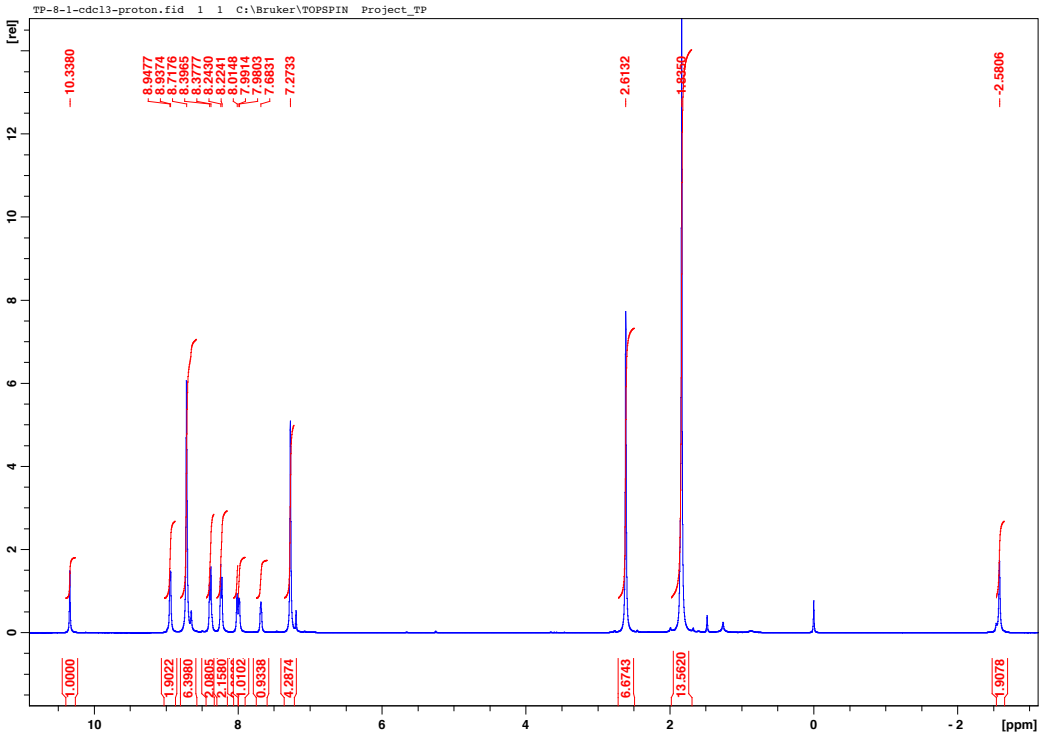

^{1}H NMR spectrum of **2.15** in $CDCl_3$ at 25^{o}C

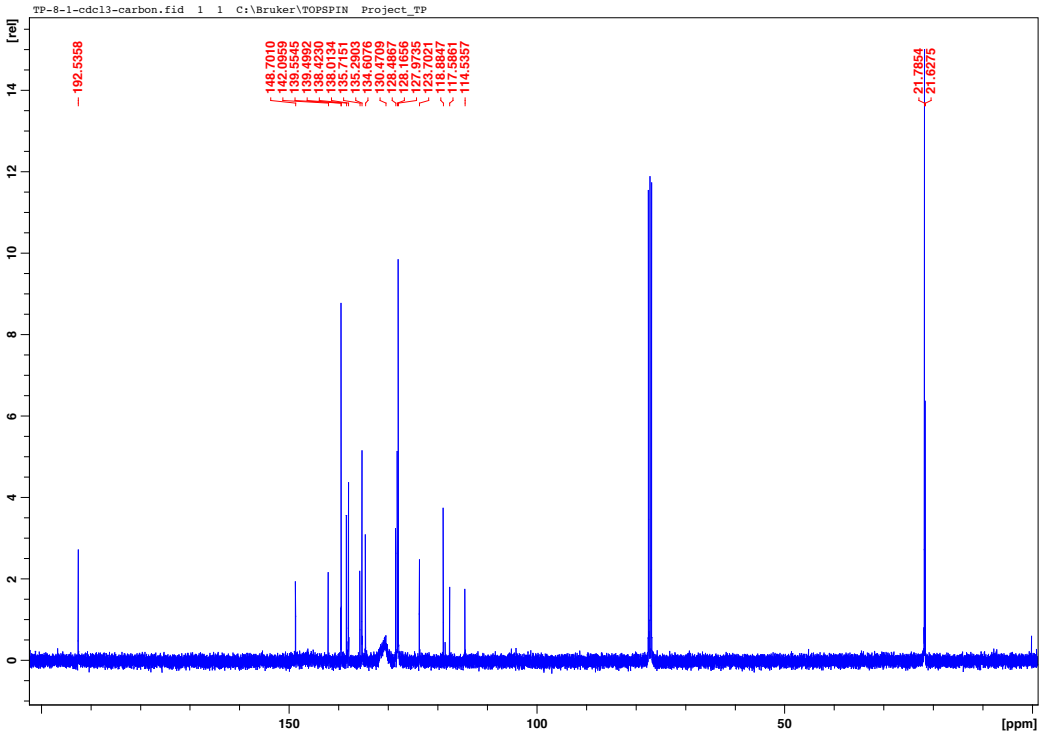

^{13}C NMR spectrum of **2.15** in $CDCl_3$ at 25°C

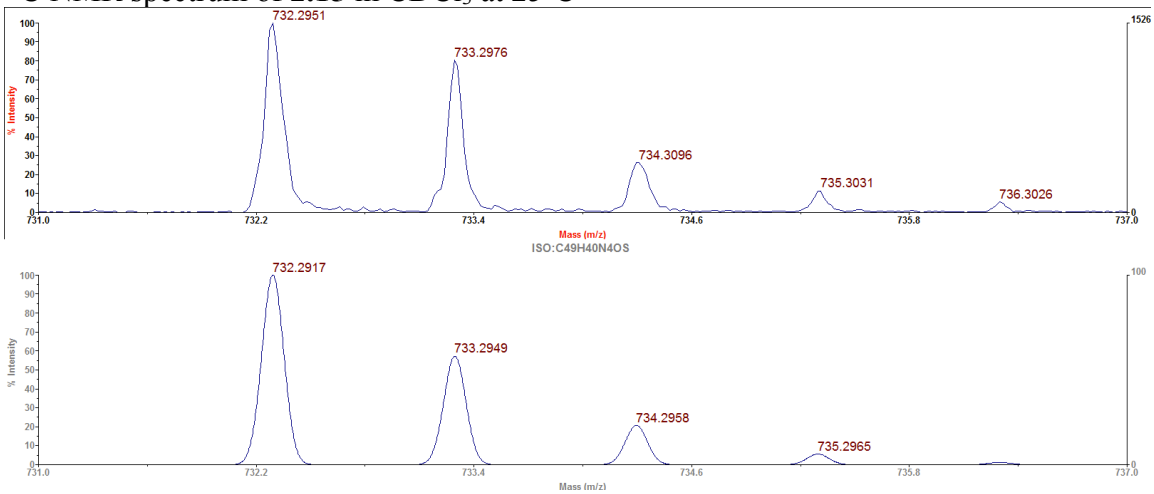

MALDI-TOF mass spectrum for **2.15**. The top trace shows the observed spectrum and the bottom trace shows the theoretical spectrum for chemical formula $C_{49}H_{40}N_4OS$ $[M]^+$.

Porphyrin 2.16

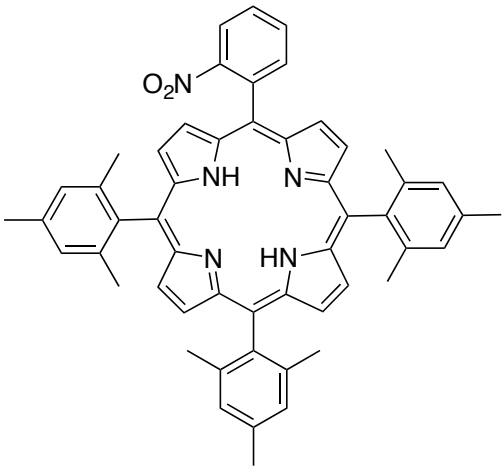

2.16

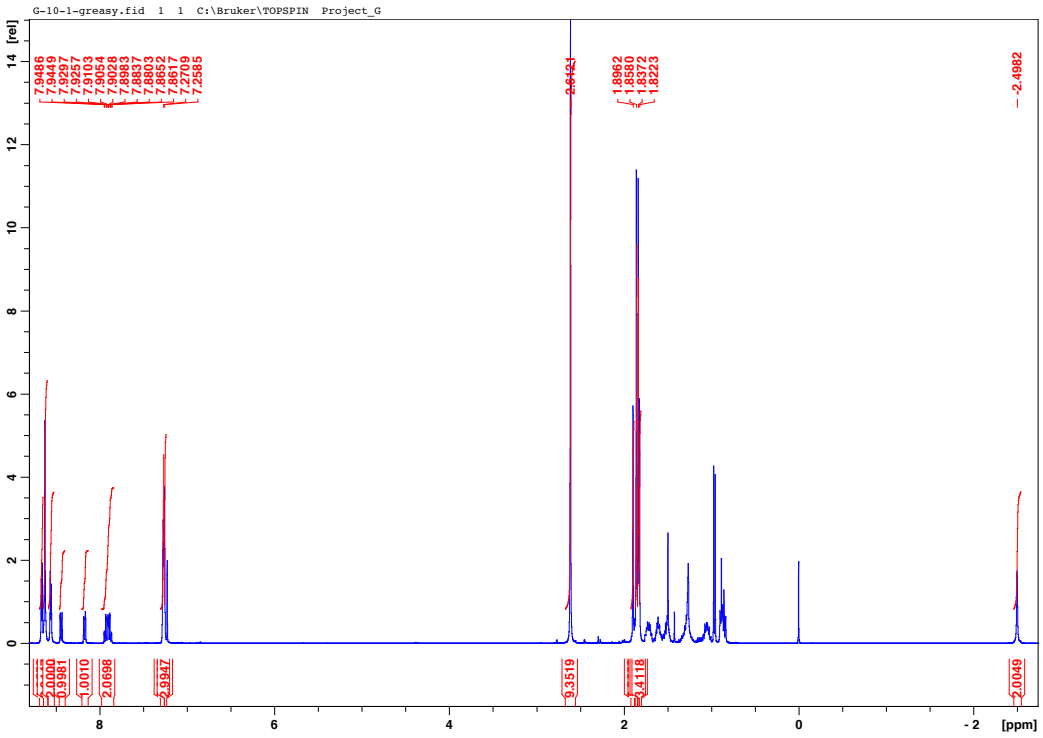

^{1}H NMR spectrum of **2.16** in $CDCl_3$ at 25°C

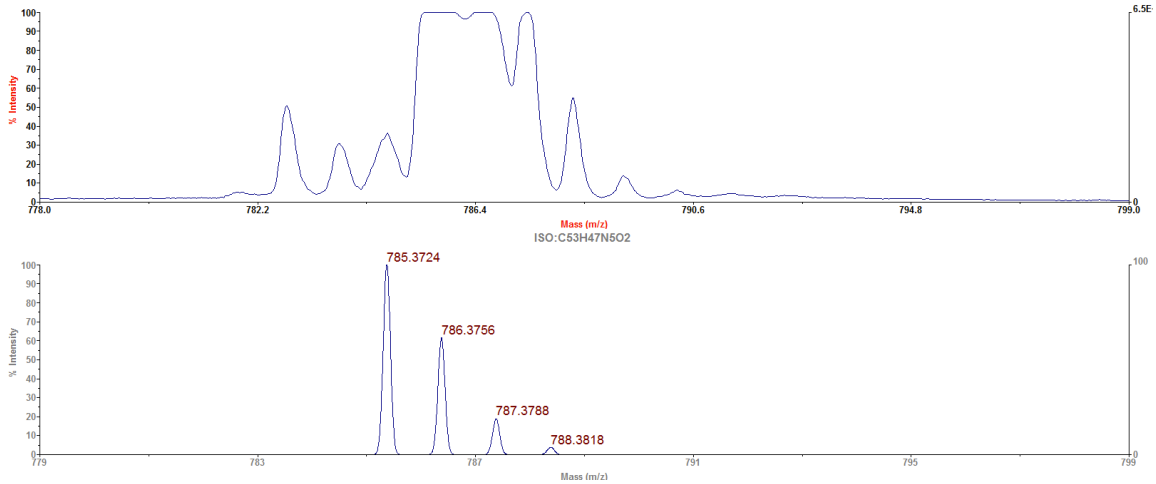

MALDI-TOF mass spectrum for **2.16**. The top trace shows the observed spectrum and the bottom trace shows the theoretical spectrum for chemical formula $C_{53}H_{47}N_5O_2$ $[M]^+$.

Porphyrin 2.17

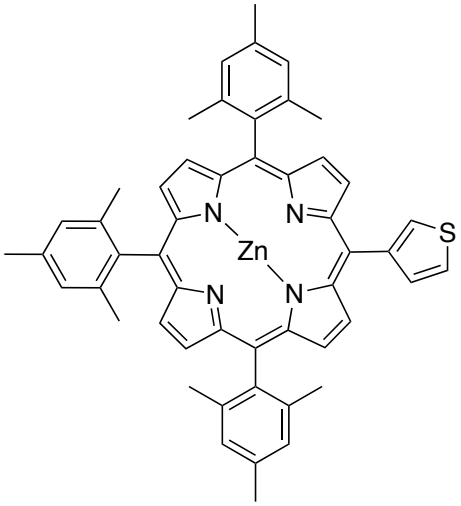

2.17

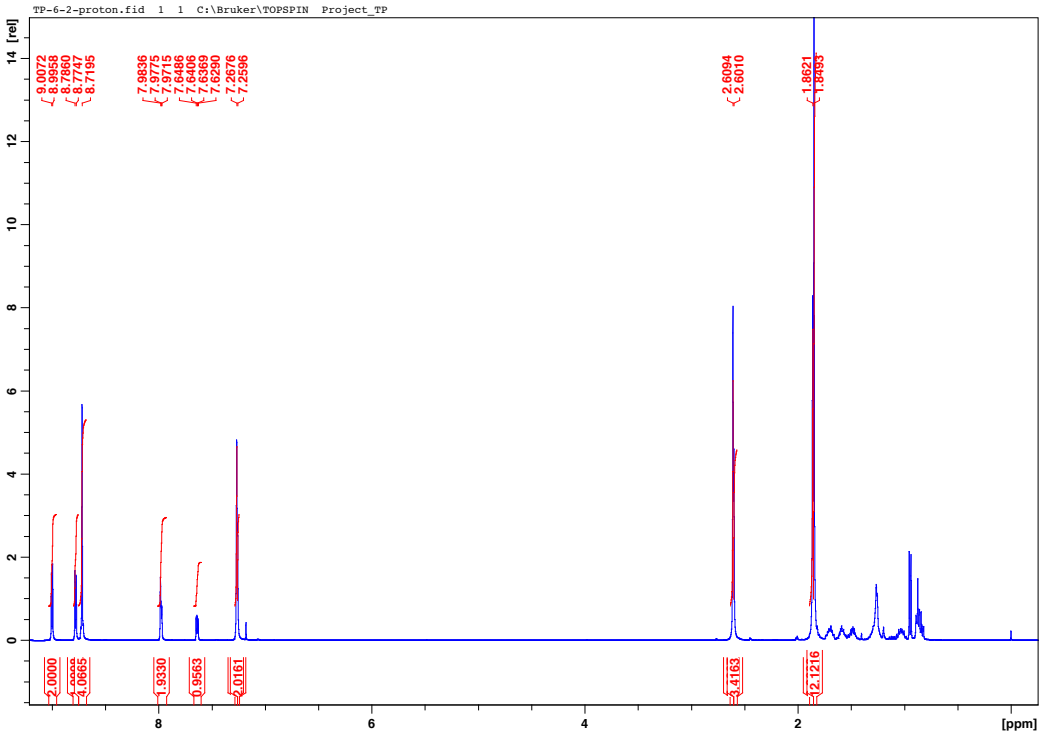

^{1}H NMR spectrum of **2.17** in $CDCl_3$ at 25^{o}C

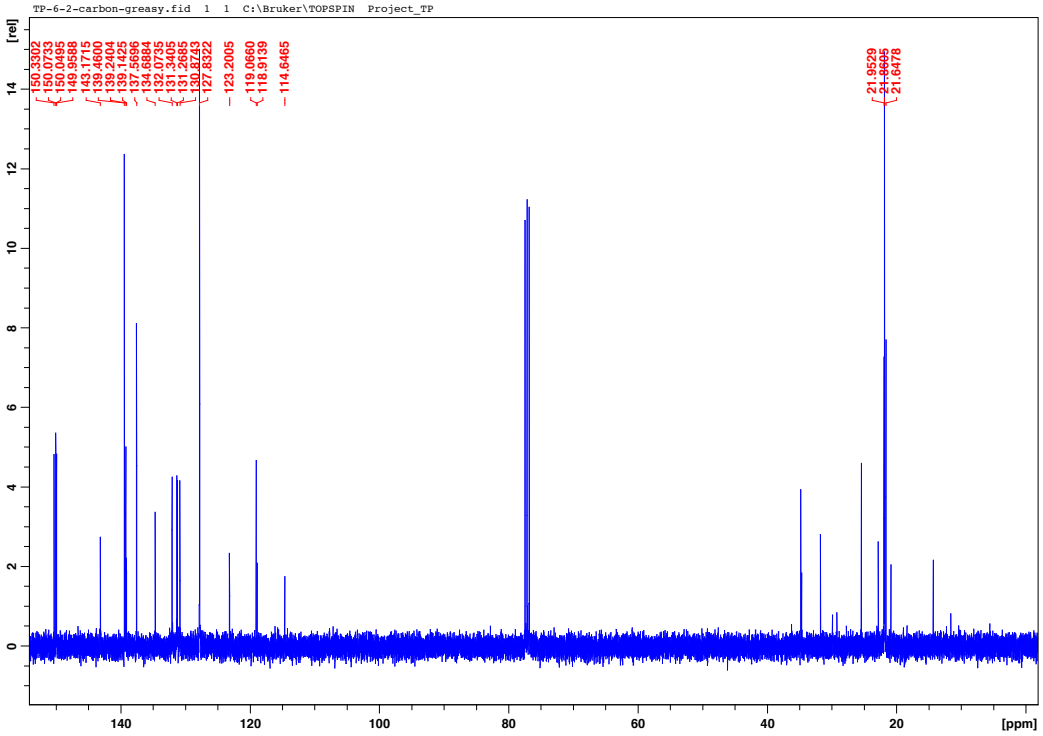

^{13}C NMR spectrum of **2.17** in $CDCl_3$ at 25°C

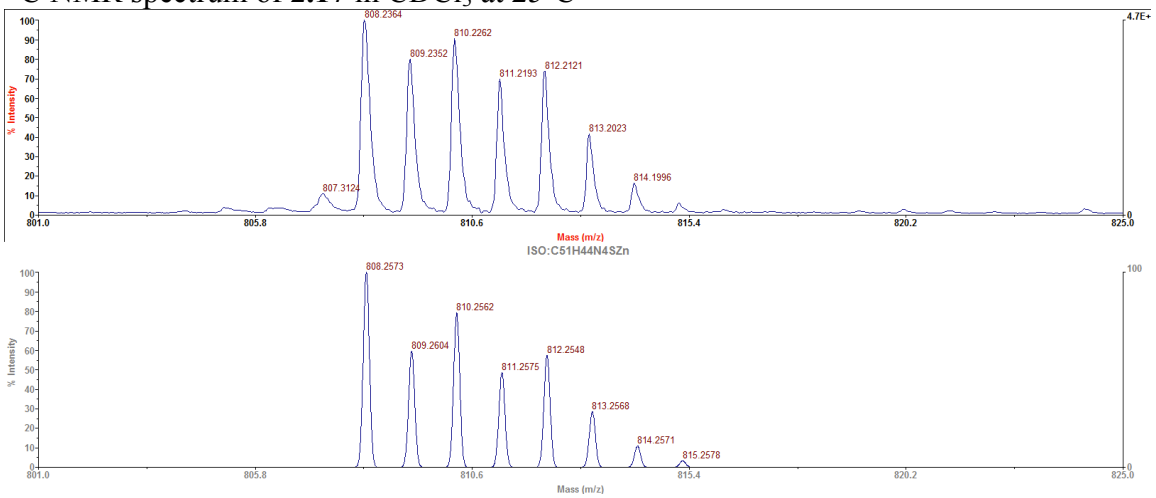

MALDI-TOF mass spectrum for **2.17**. The top trace shows the observed spectrum and the bottom trace shows the theoretical spectrum for chemical formula $C_{51}H_{44}N_4SZn$ $[M]^+$.

APPENDIX B

NMR and MASS SPECTRAL DATA FOR SYNTHESIZED COMPOUNDS OF CHAPTER 3

3.1

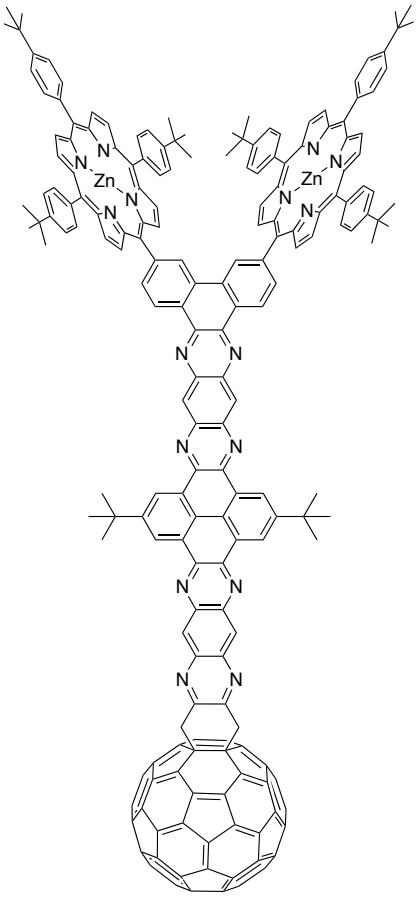

3.1

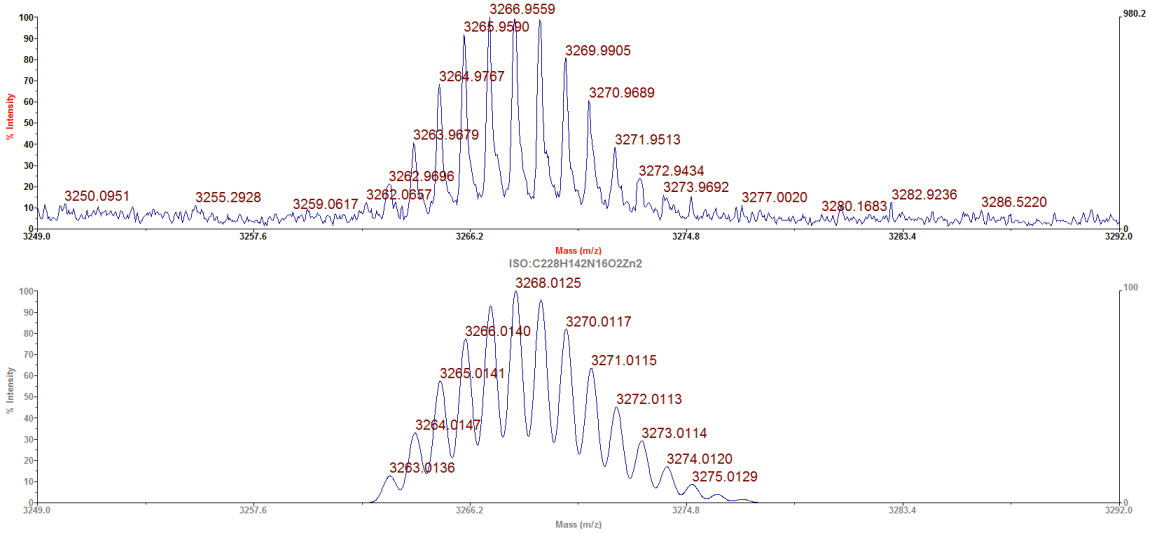

MALDI-TOF Mass Spectrum of possible structure, **3.1**. The top trace is the observed spectrum while the bottom trace is the theoretical spectrum for molecular formula $C_{228}H_{142}N_{16}O_2Zn_2$ $[M]^+$.

3.2

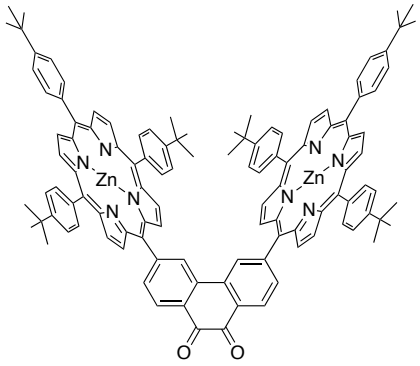

3.2

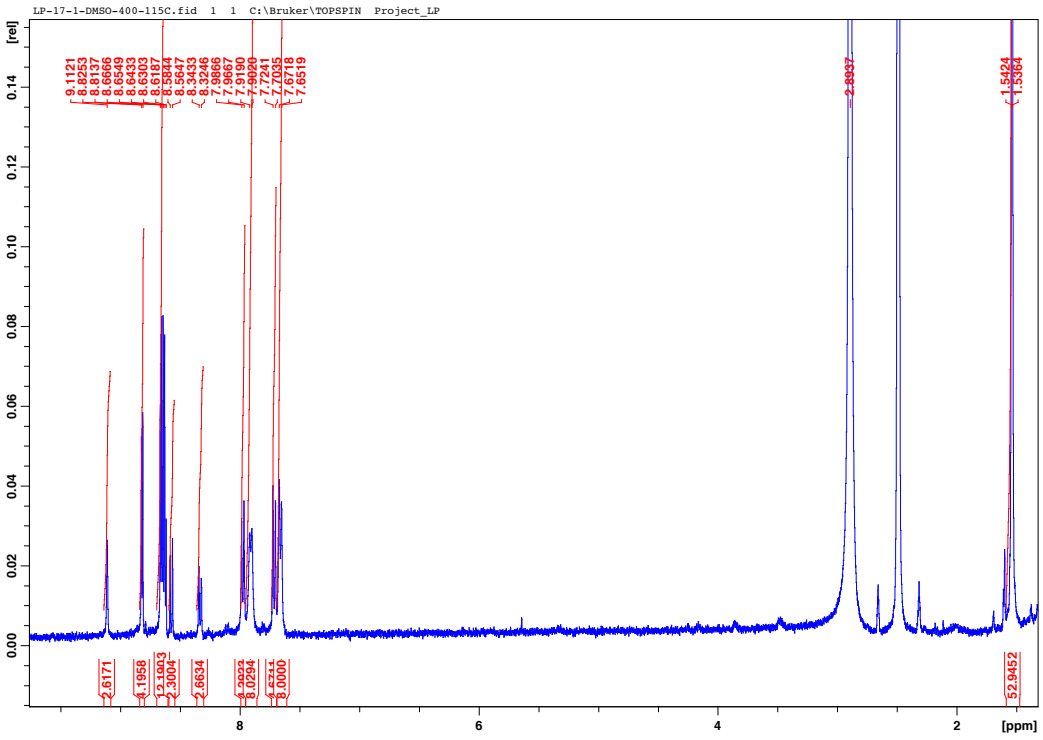

^{1}H NMR spectrum of **3.4** in $CDCl_3$ at 115^{o}C.

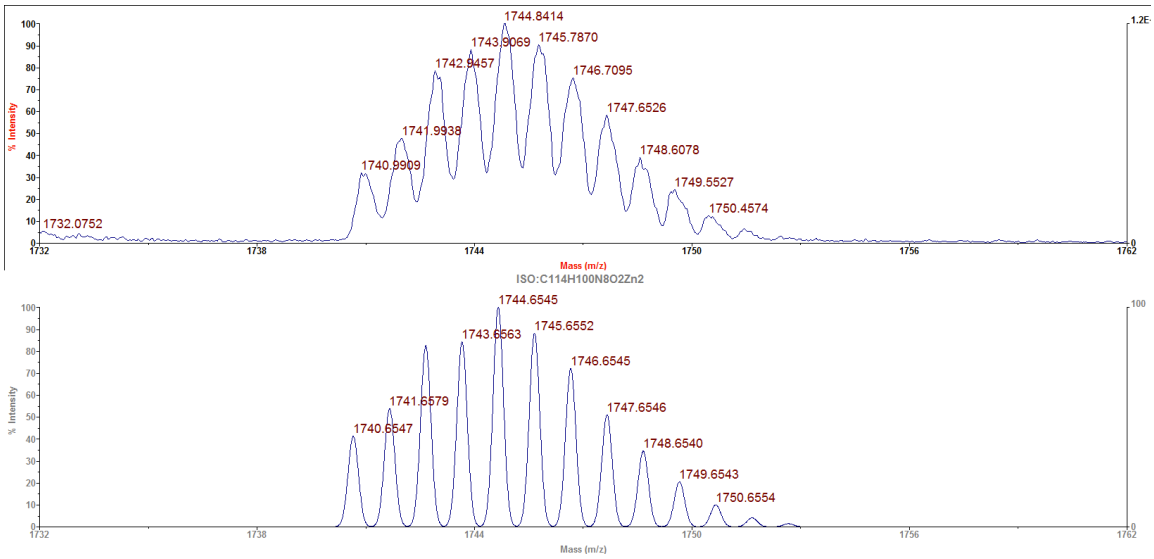

MALDI-TOF MS spectrum of **X**. The top trace is the observed spectrum and the bottom trace is the theoretical spectrum form molecular formula $C_{114}H_{100}N_8O_2Zn_2$ $[M]^+$

3.3

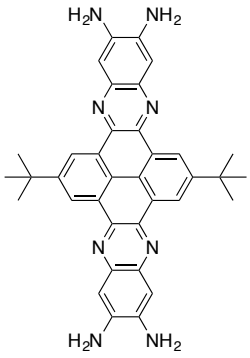

3.3

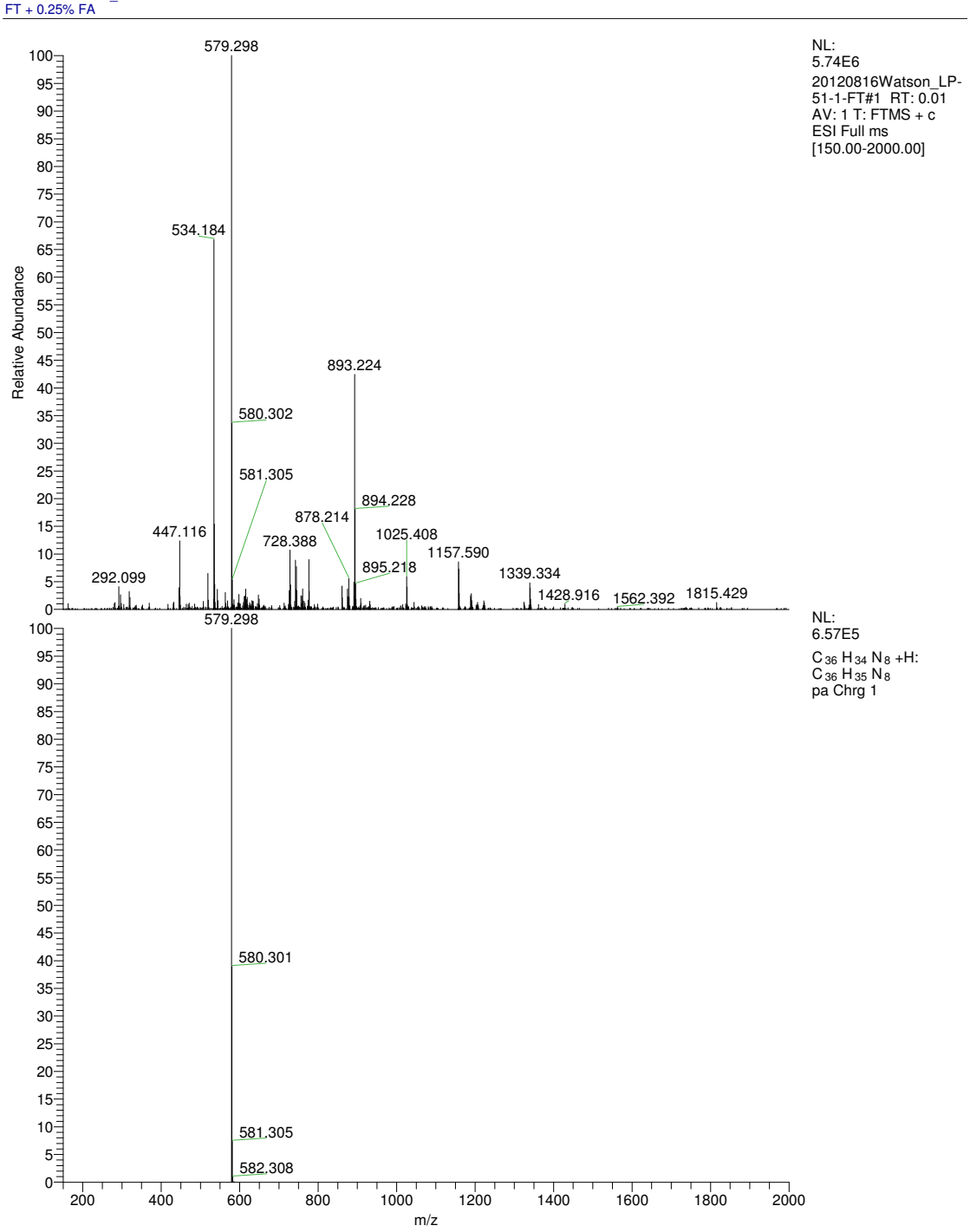

High Resolution Mass Spectrum of **3.11**. The top trace is the observed spectrum and the bottom trace is the theoretical spectrum form molecular formula $C_{36}H_{35}N_8$ $[M+H]^+$.

3.4

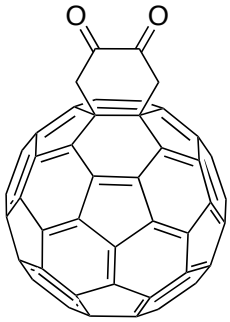

3.4

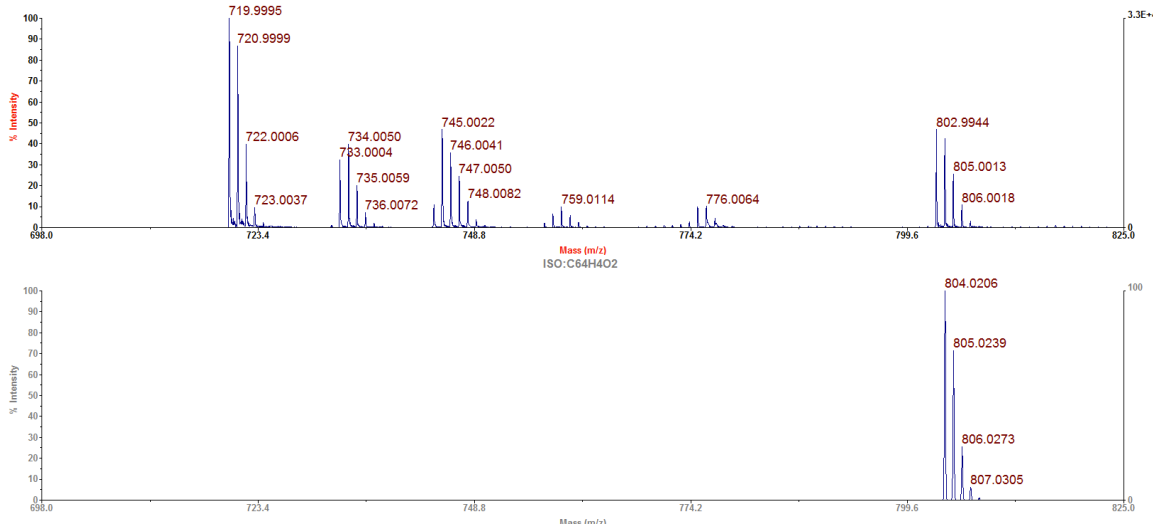

MALDI-TOF MS spectrum of **3.4**. The top trace is the observed spectrum and the bottom trace is the theoretical spectrum form molecular formula $C_{64}H_4O_2$ $[M]^+$.

***Meso*-(*p-tert*-butylphenyl)dipyrromethane (3.5)**

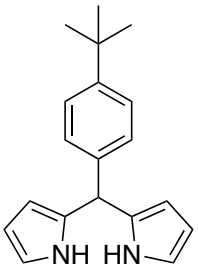

3.5

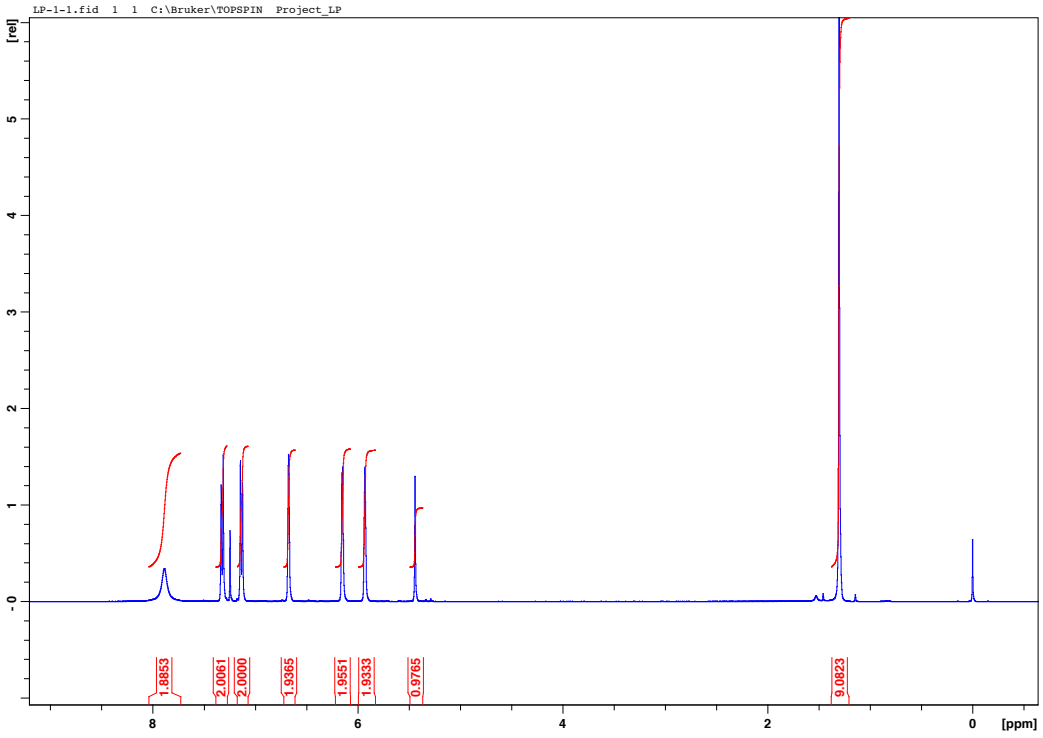

^{1}H NMR spectrum of **3.5** in $CDCl_3$ at RT.

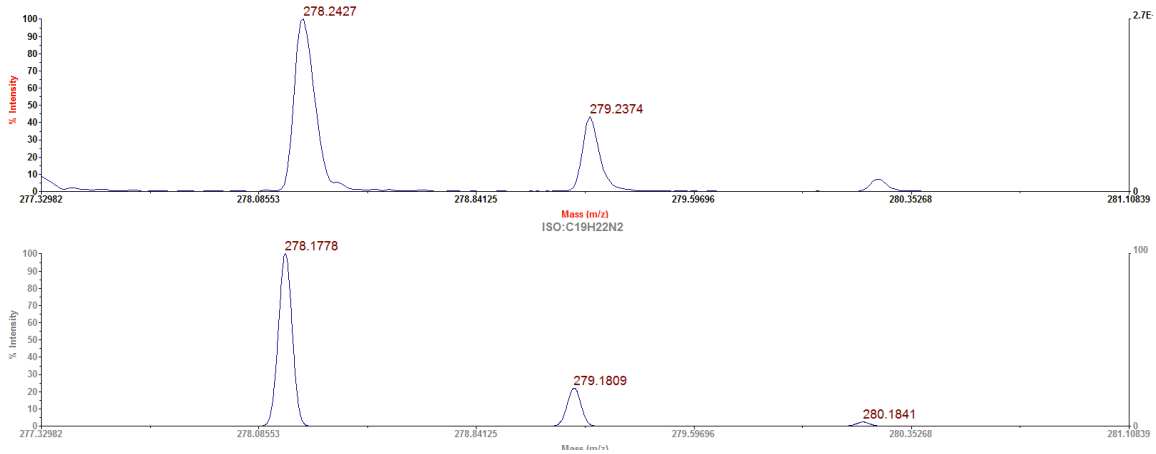

MALDI-TOF MS of **3.5**. The top trace is the observed spectrum. The bottom trace is the calculated theoretical spectrum for molecular formula: $C_{19}H_{22}N_2$. $[M]^+$

3.6

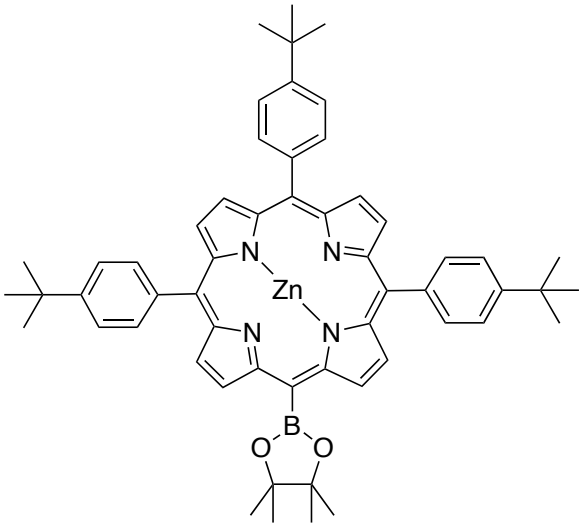

3.6

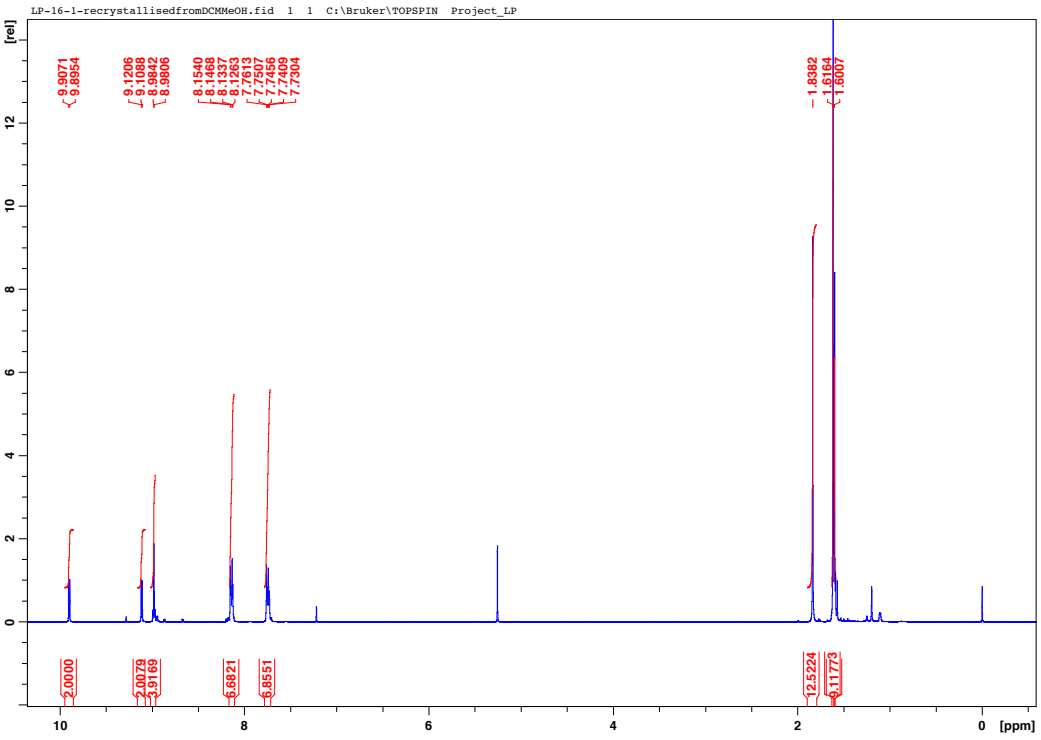

^{1}H NMR spectrum of **3.6** in $CDCl_3$ at RT.

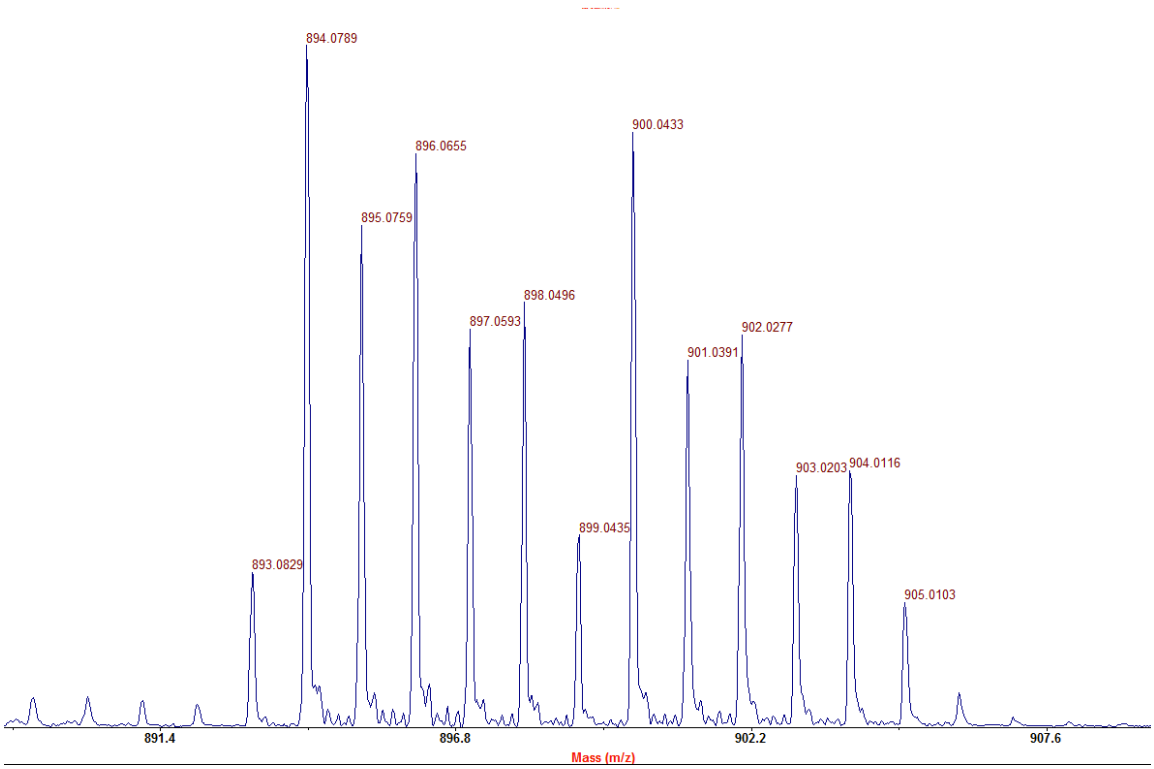

MALDI-TOF MS spectrum of **3.6** (spectrum is of the crude mixture and [tetramesitylporphyrinato]Zn(II) is also present.

3,6-dibromophenanthrene-9,10-quinone (3.7)

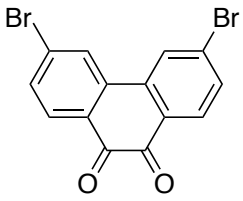

3.7

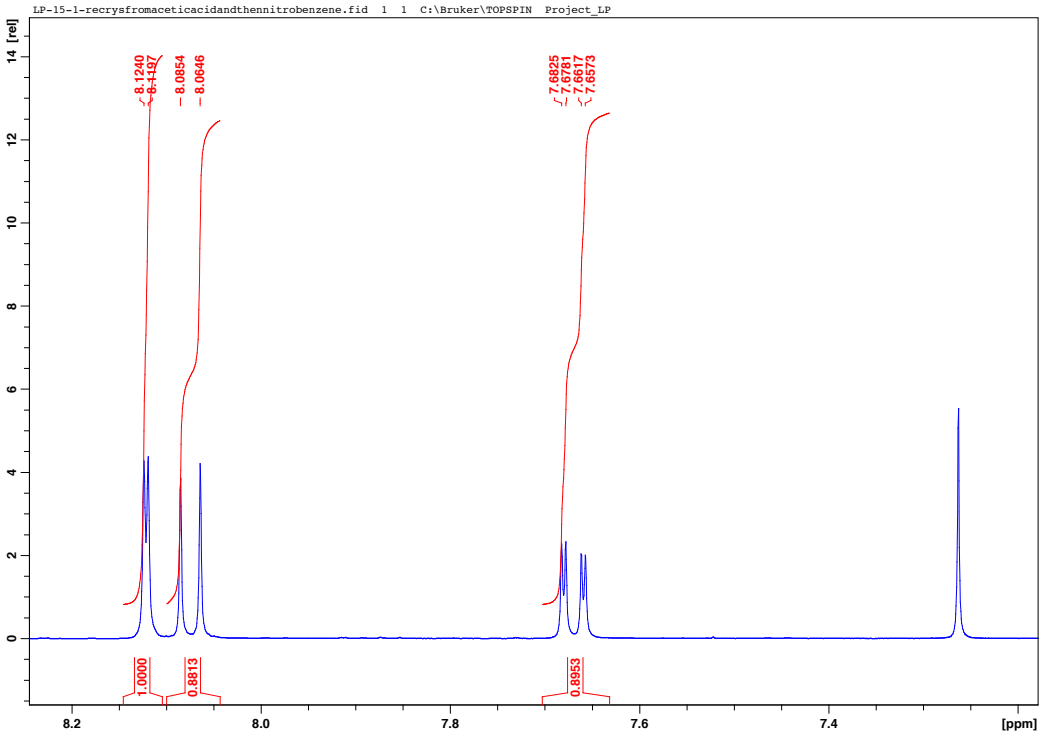

^{1}H NMR spectrum of **3.7** in $CDCl_3$ at RT.

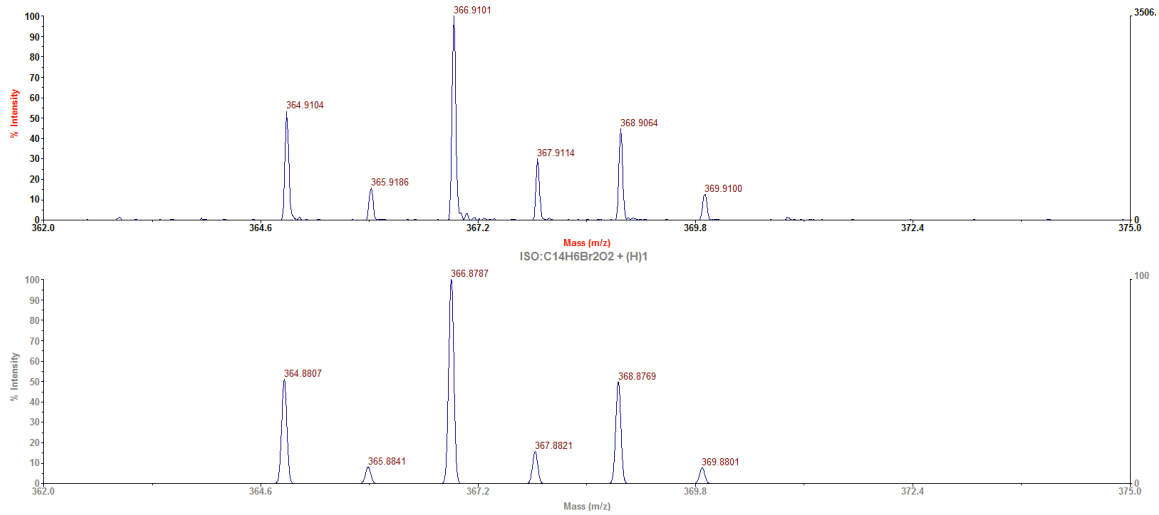

MALDI-TOF MS of **3.7**. The top trace is the observed spectrum. The bottom trace is the calculated theoretical spectrum for molecular formula: $C_{14}H_7Br_2O_2$. $[M+H]^+$

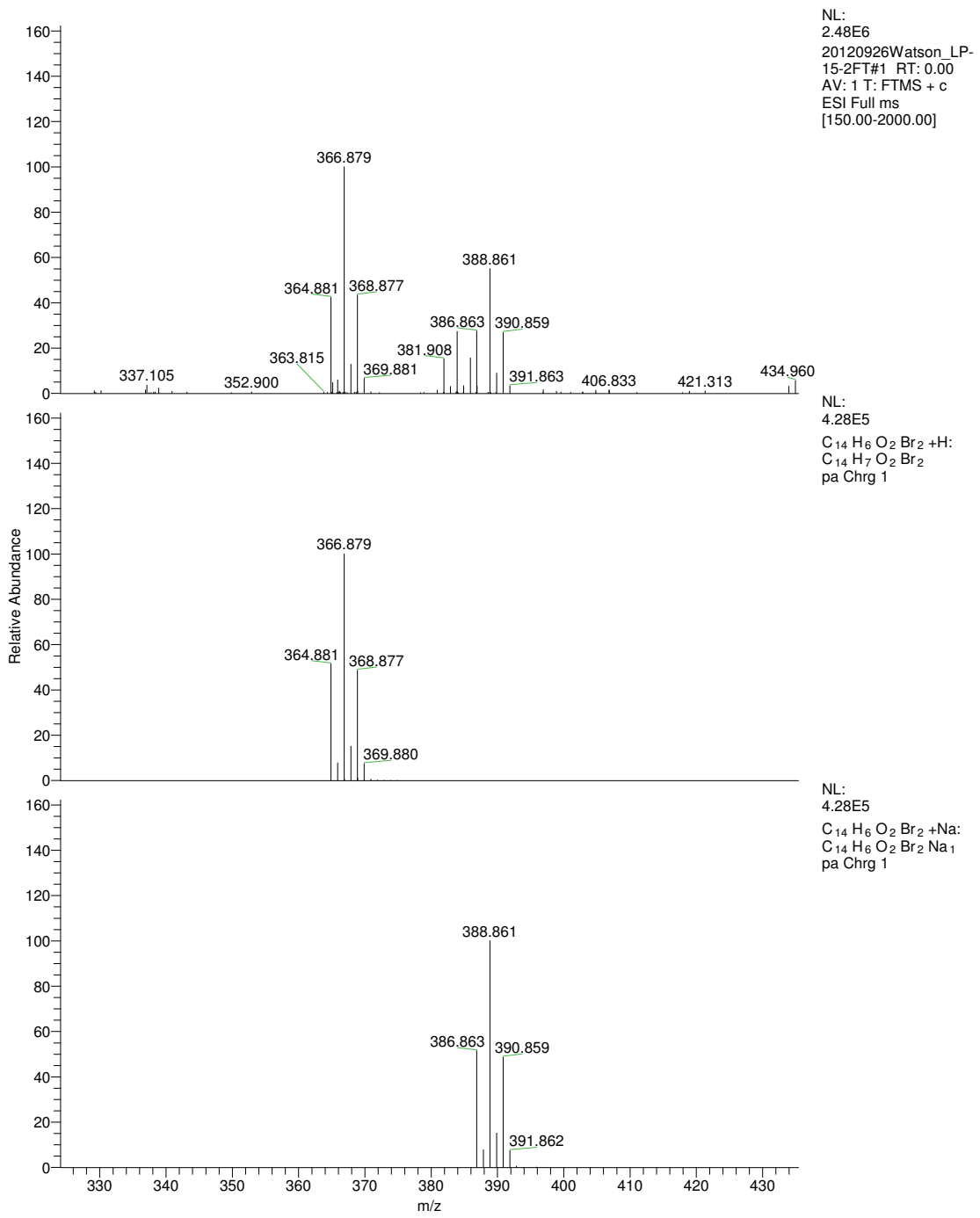

High Resolution MS of **3.7**. The top trace is the observed spectrum. The bottom traces are the calculated theoretical spectrum for molecular formula: $C_{14}H_6Br_2O_2$. $[M+H]^+$ and $C_{14}H_6Br_2O_2$. $[M+Na]^+$.

2,7-di-*tert*-butylpyrene (3.8)

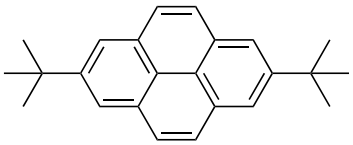

3.8

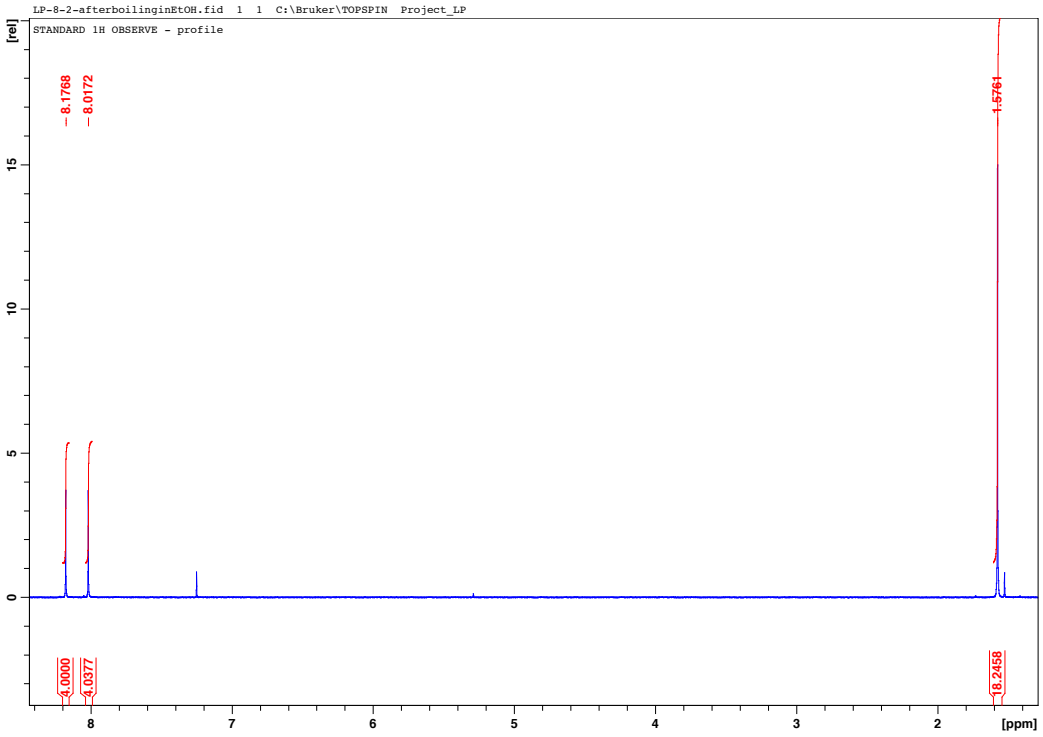

^{1}H NMR spectrum of **3.8** in $CDCl_3$ at RT.

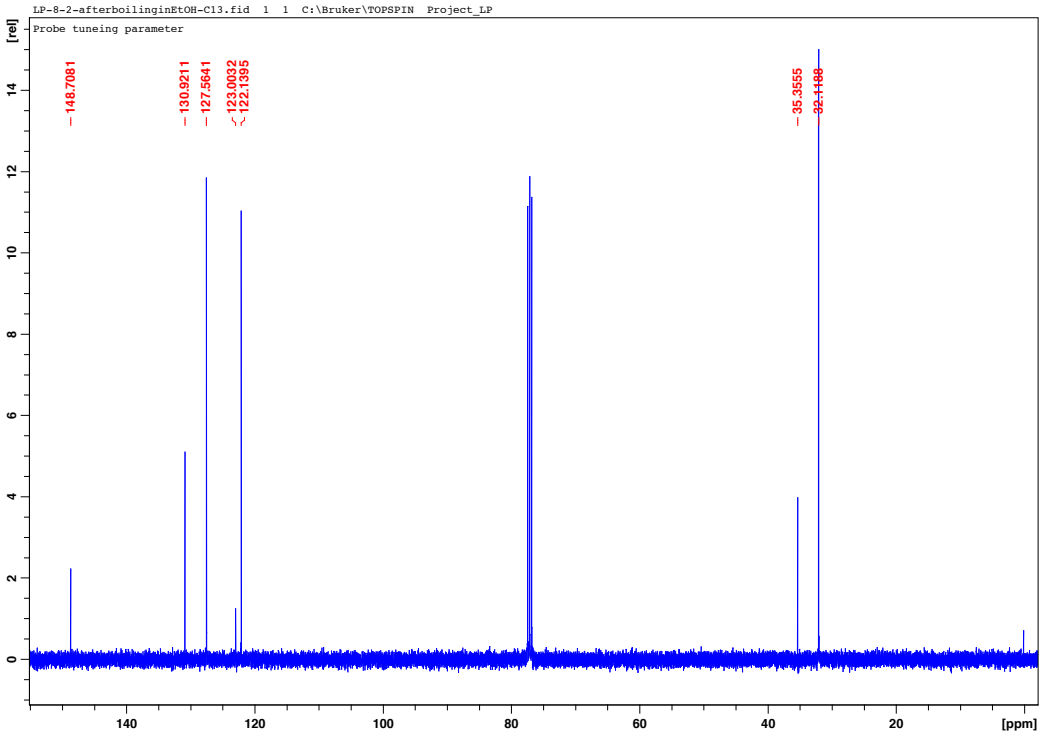

^{13}C NMR spectrum of **3.8** in $CDCl_3$ at RT.

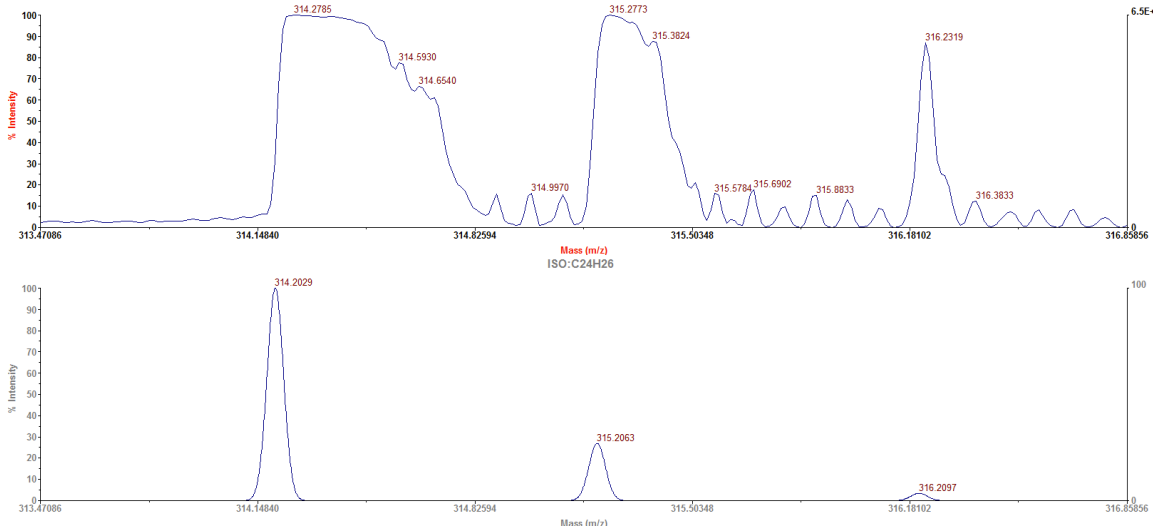

MALDI-TOF MS spectrum of **3.8**. The top trace is the observed spectrum and the bottom trace is the theoretical spectrum form molecular formula $C_{114}H_{100}N_8O_2Zn_2$.

2,7-di-*tert*-butyl-4,4,9,10-tetraketopyrene (3.9)

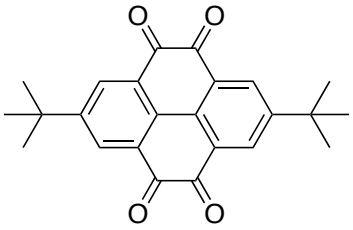

3.9

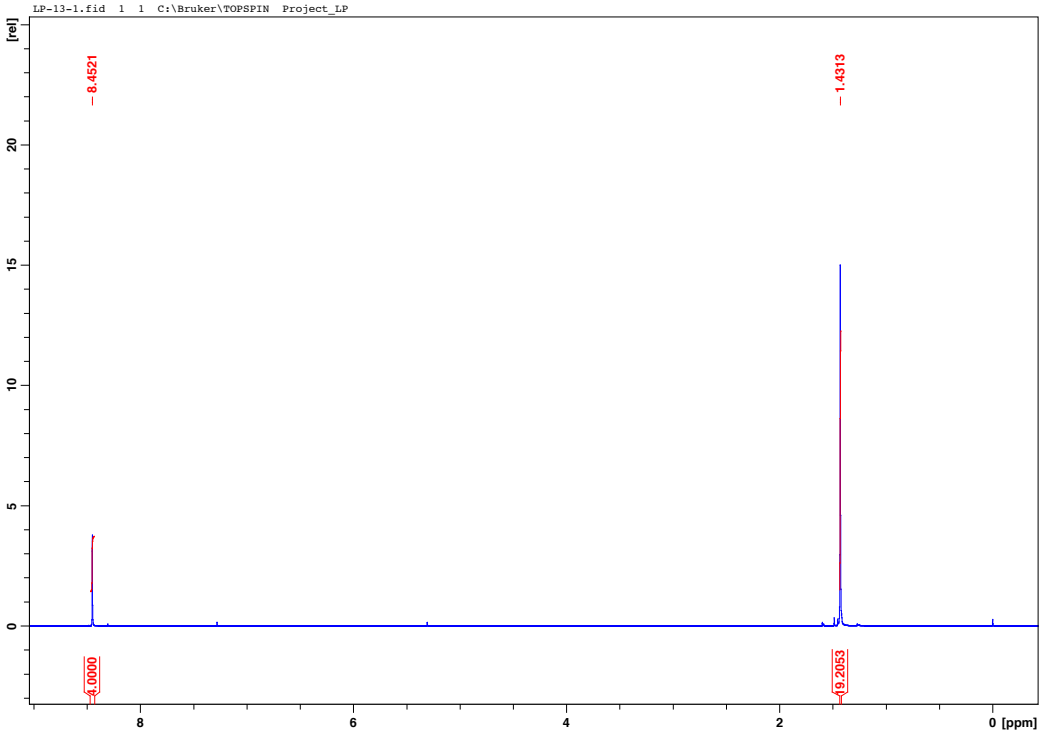

^{1}H NMR spectrum of **3.9** in $CDCl_3$ at RT.

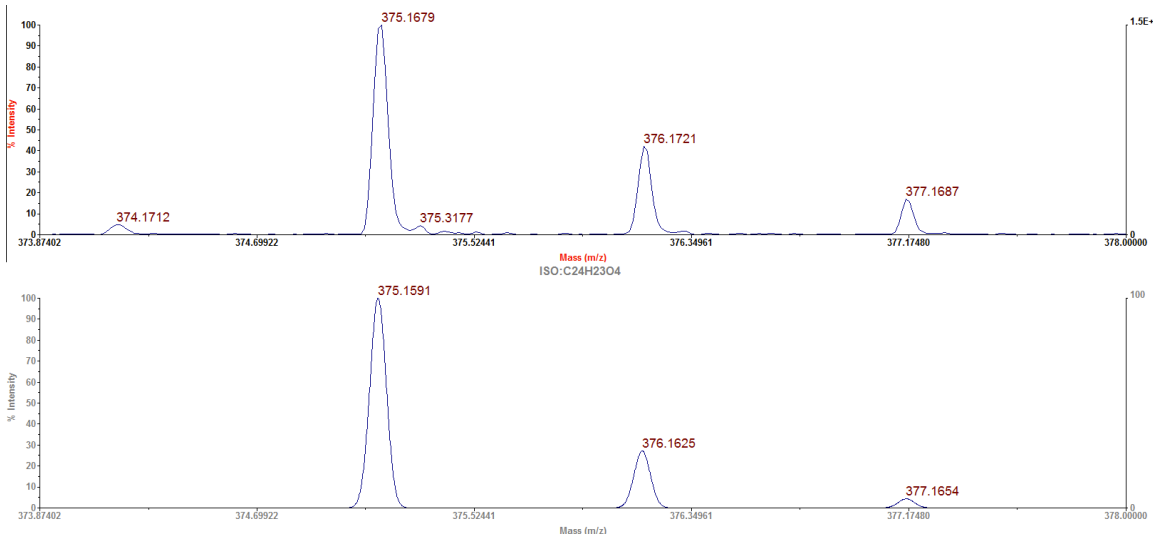

MALDI-TOF MS spectrum of **3.9**. The top trace is the observed spectrum and the bottom trace is the theoretical spectrum form molecular formula $C_{24}H_{23}O_4$ $[M+H]^+$.

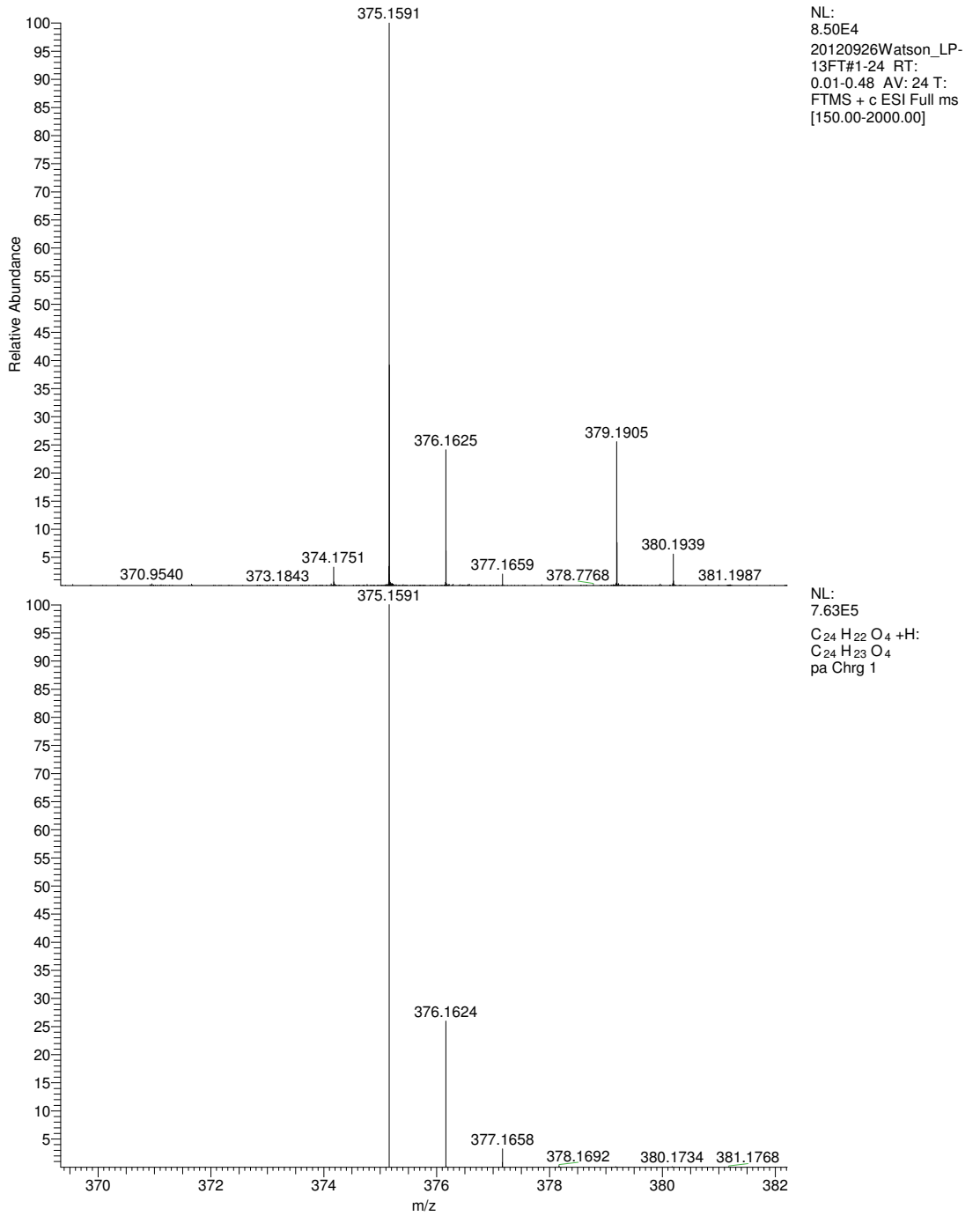

High Resolution Mass Spectrum of **3.9**. The top trace is the observed spectrum and the bottom trace is the theoretical spectrum form molecular formula $C_{24}H_{23}O_4$ $[M+H]^+$.

3.10

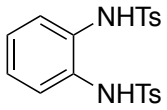

3.10

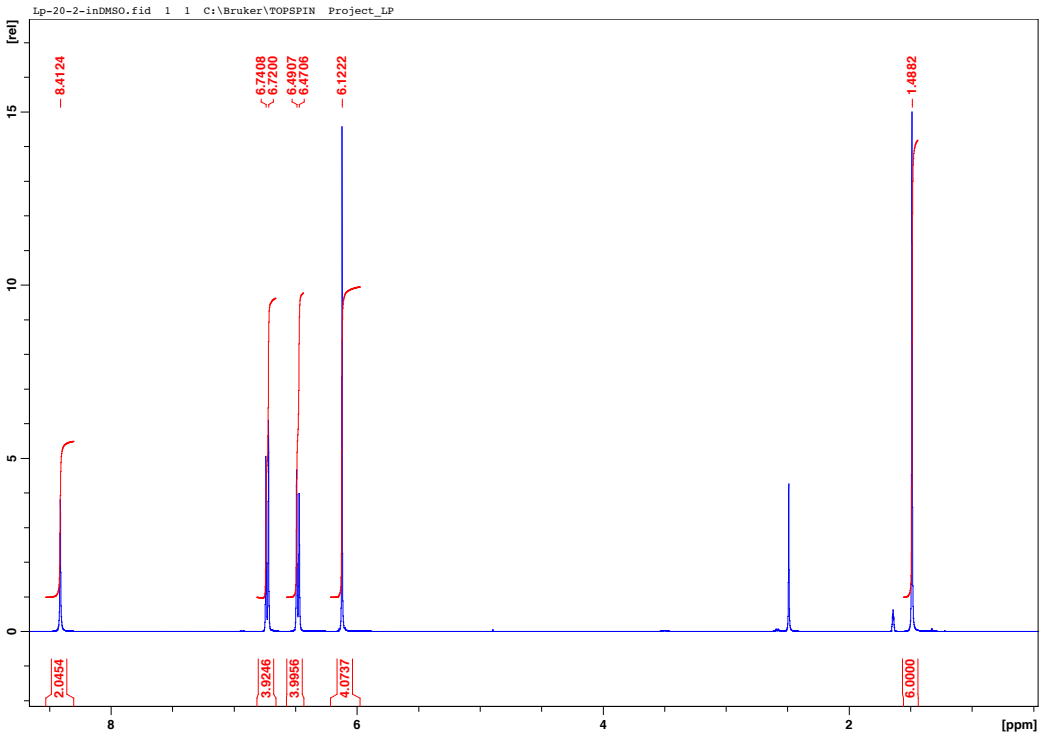

^{1}H NMR spectrum of **3.10** in DMSO-*d*6 at RT.

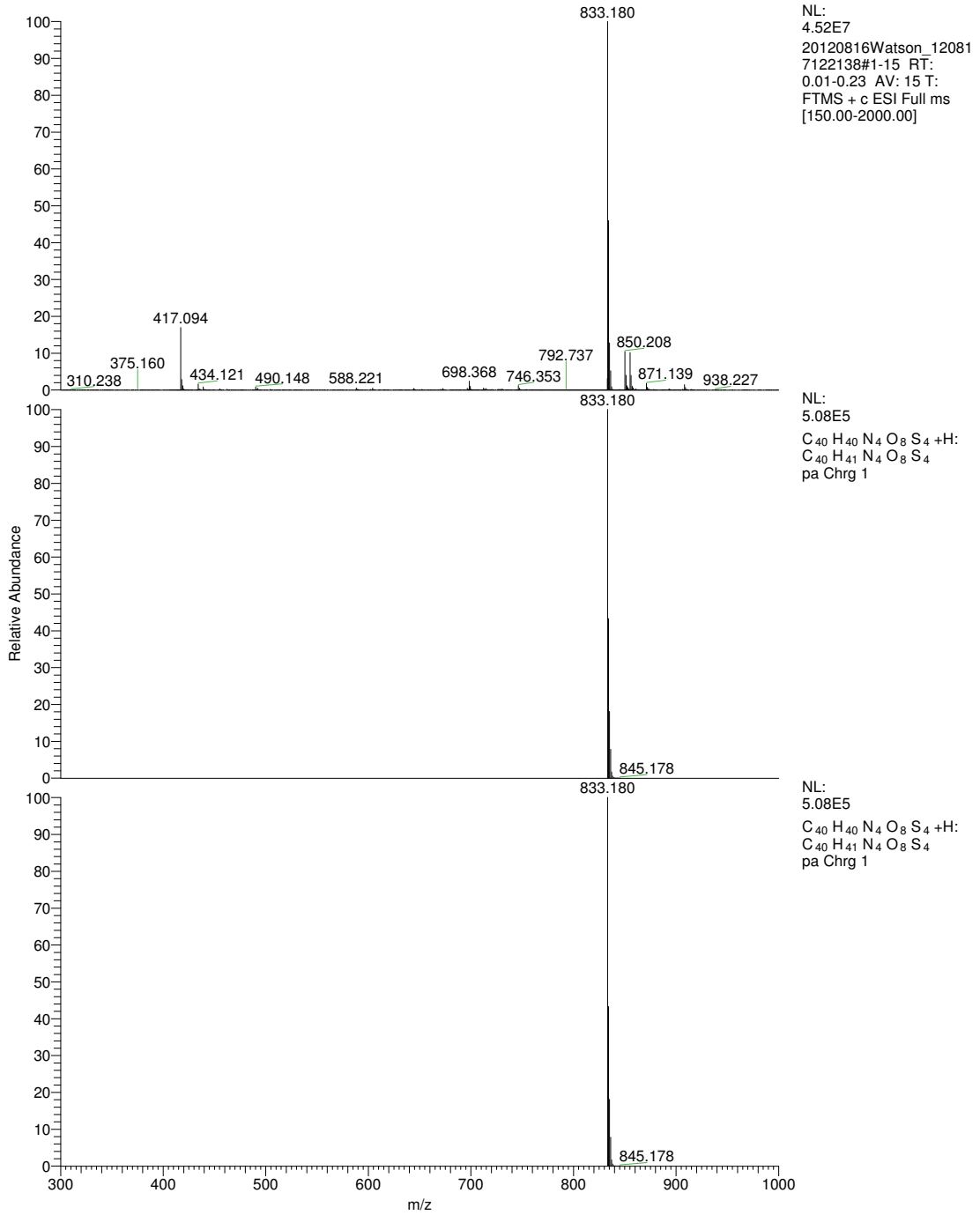

High-Resolution MS spectrum of **3.10**. The top trace is the observed spectrum and the bottom two traces are the theoretical spectrum form molecular formula $C_{40}H_{41}N_4O_8S_4$ $[2M+H]^+$.

3.11

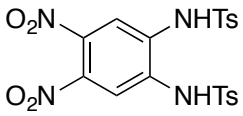

3.11

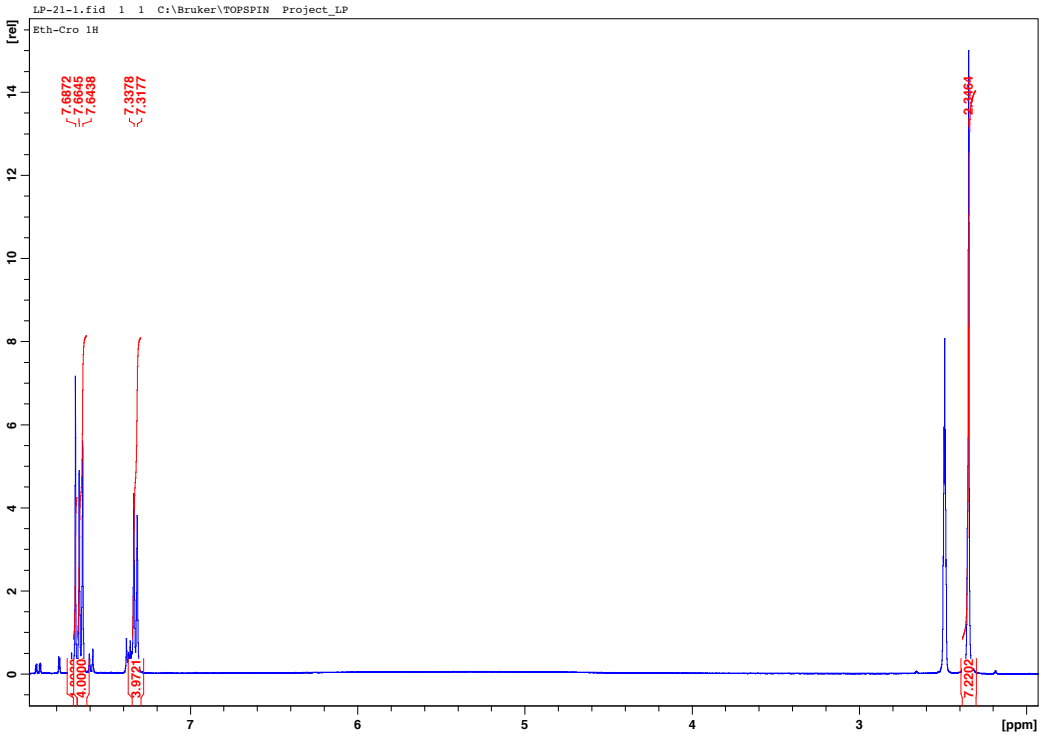

^{1}H NMR spectrum of **3.11** in DMSO-*d*6 at RT.

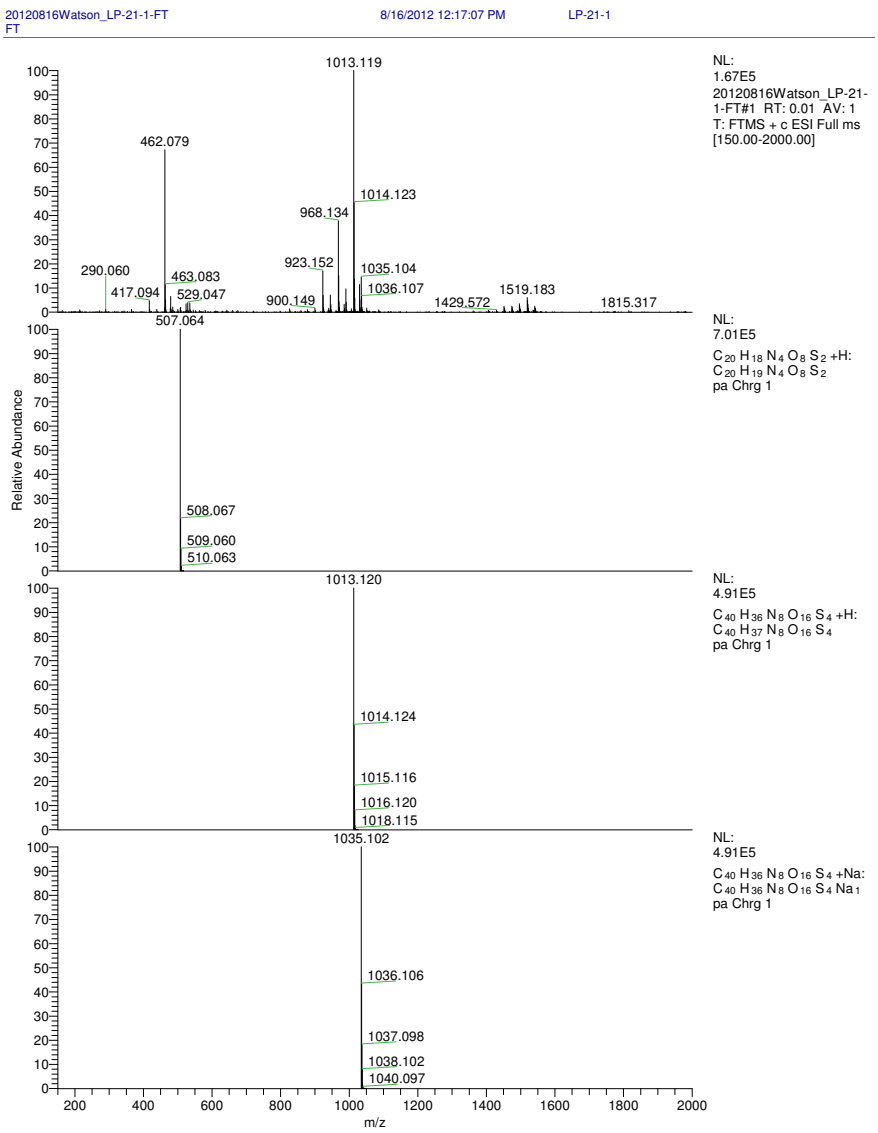

High-Resolution Mass Spectrum of **3.11**. The top trace is the observed spectrum and the bottom traces are the theoretical spectra for various dimers and adducts of the product. $C_{40}H_{37}N_8O_{16}S_4$ $[2M+H]^+$ observed.

3.12

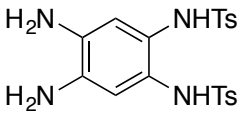

3.12

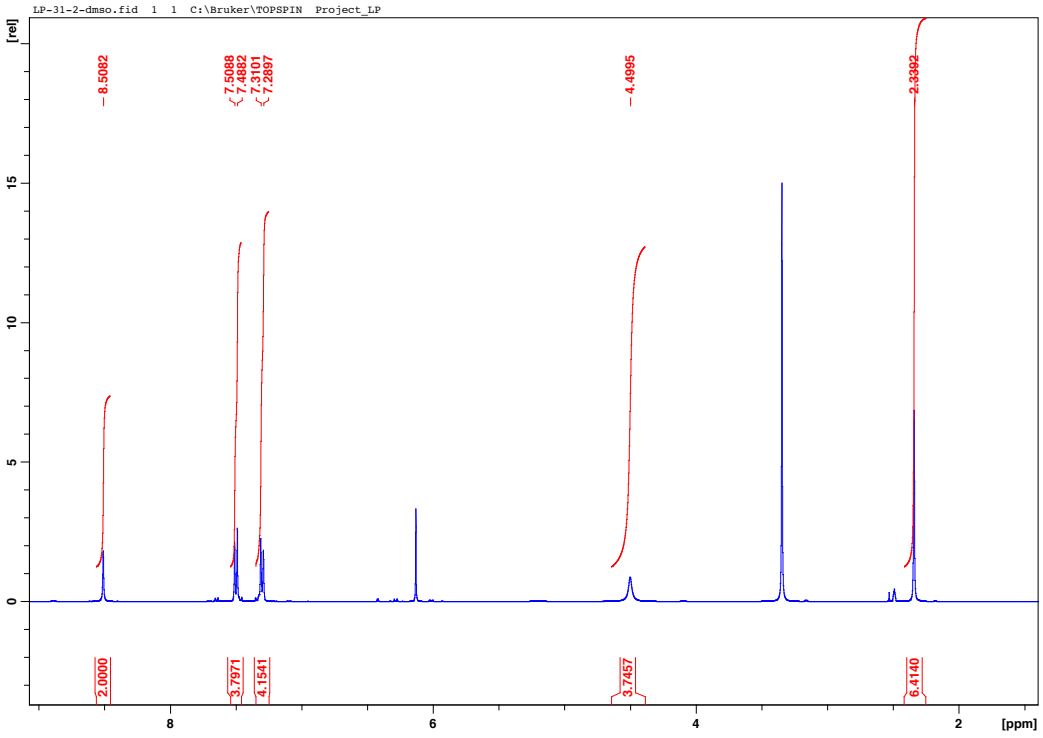

^{1}H NMR spectrum of **3.12** in DMSO-*d6* at RT.

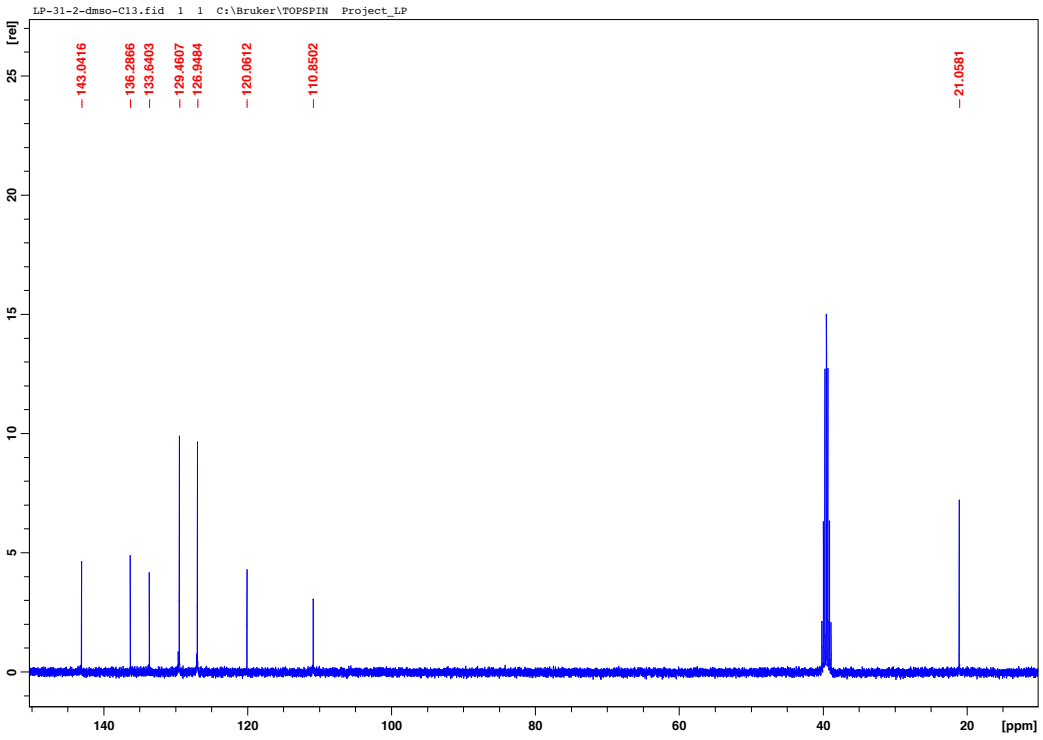

^{13}C NMR spectrum of **3.12** in DMSO-*d6* at RT.

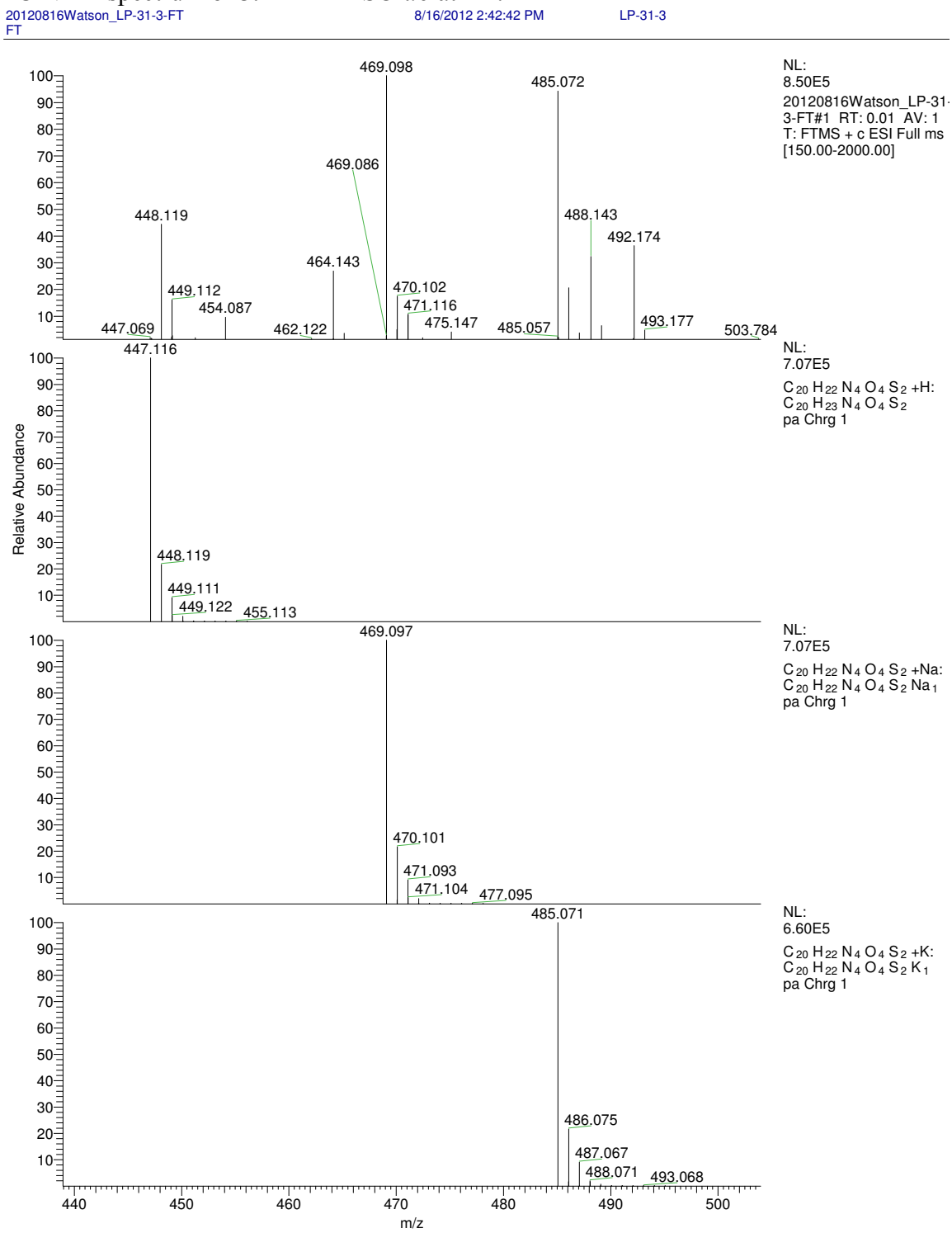

High Resolution Mass Spectrum of **3.12**. The top trace is the observed spectrum and the bottom traces are theoretical spectra of various adducts of the product. Observed: $C_{20}H_{22}N_4O_4S_2Na_1$ $[M+Na]^+$.

3.13

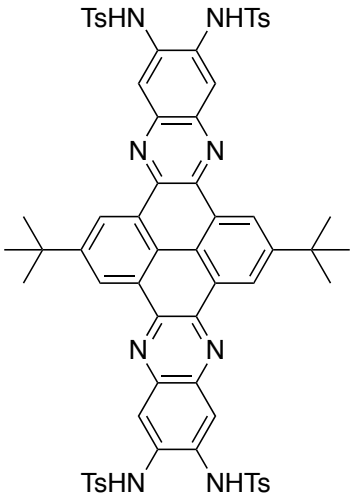

3.13

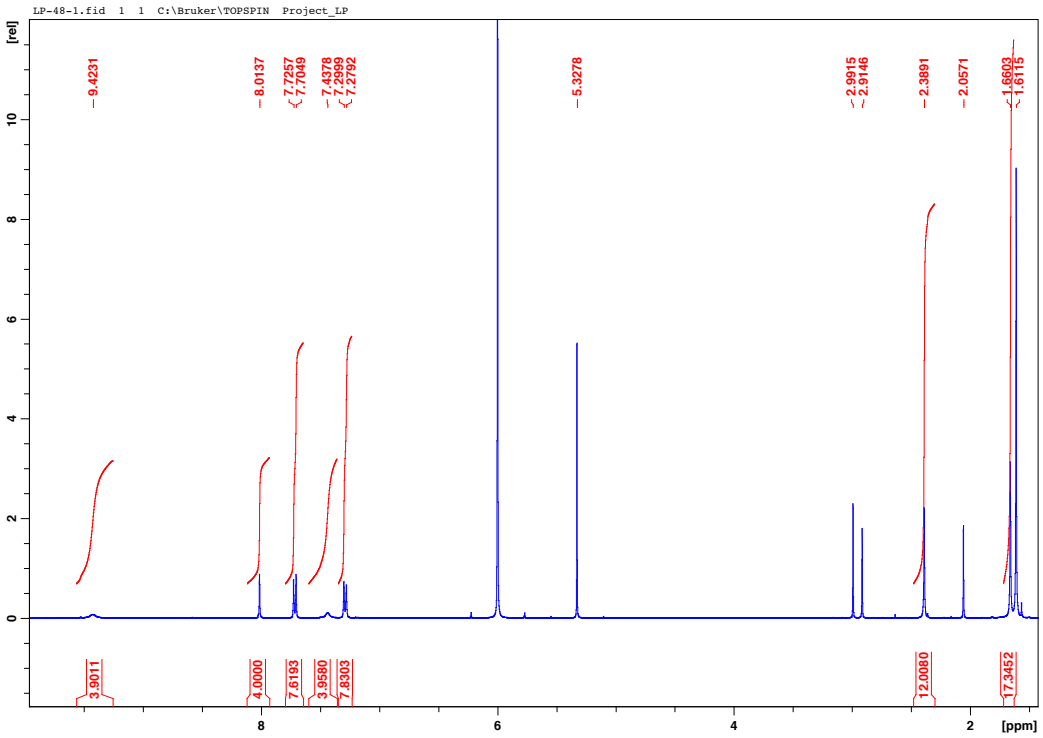

^{1}H NMR spectrum of **3.13** in 1,1,2,2-tetrachloroethane-*d*2 at RT.

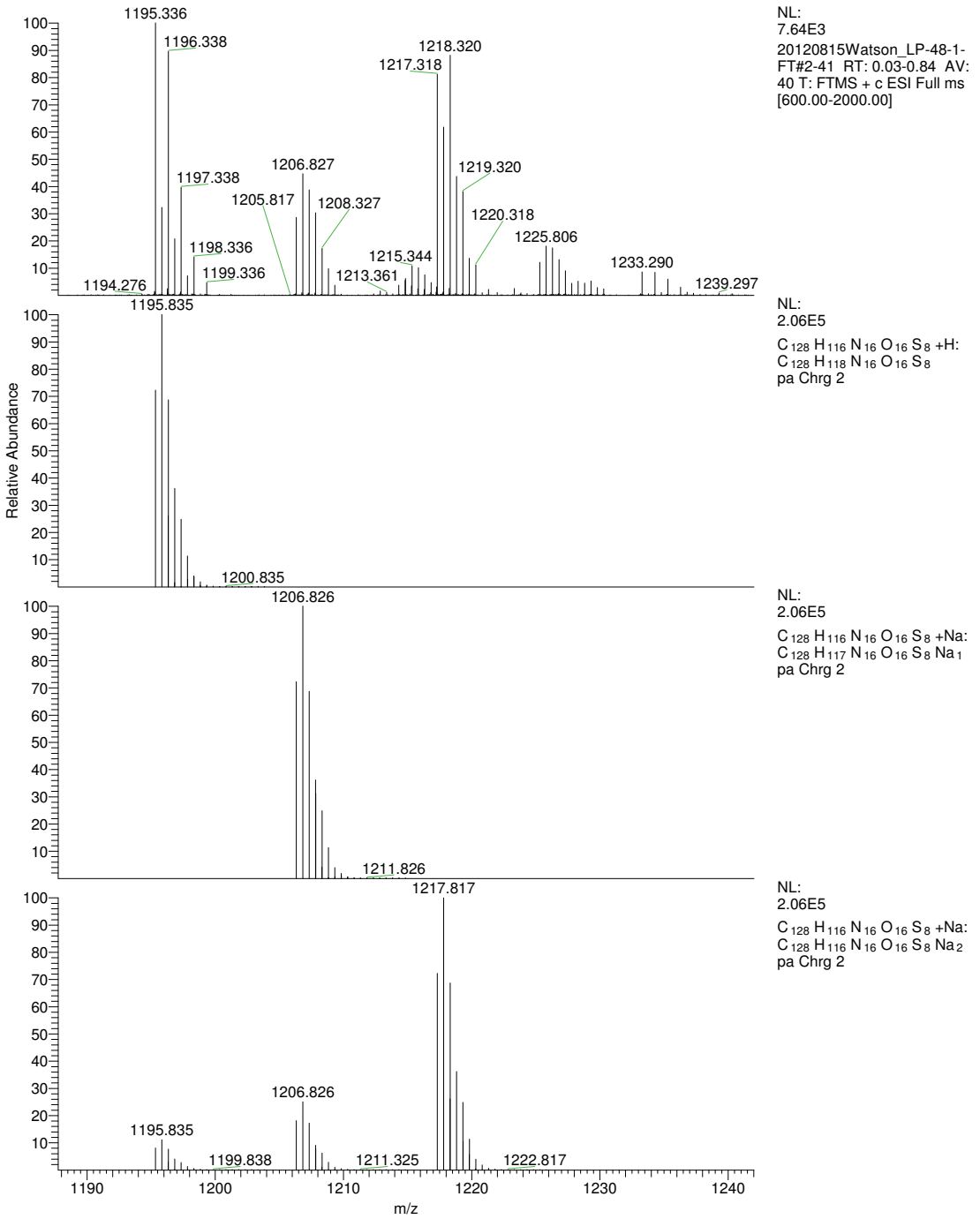

High Resolution Mass Spectrum of **3.13**. The top trace is the observed spectrum and the bottom traces are theoretical spectra for various adducts of the product. Observed $C_{128}H_{117}N_{16}O_{16}S_8$ $[M+H]^+$.

1,2-Bistrimethoxysiloxy-1-cyclobutane (3.14)

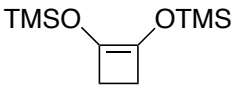

3.14

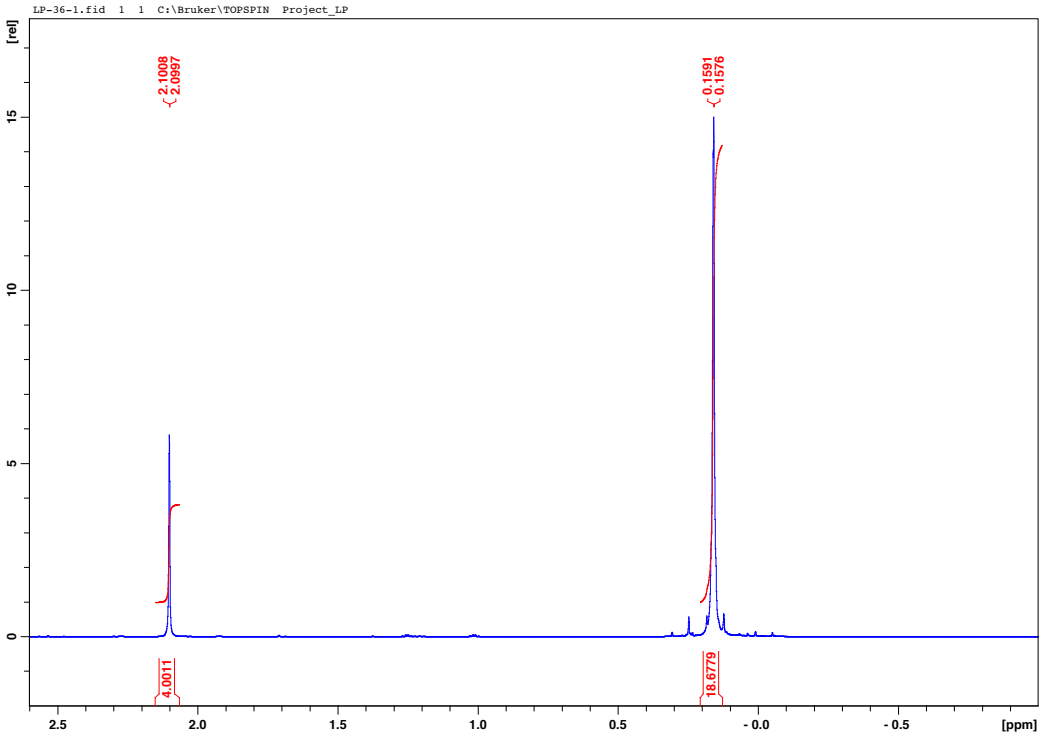

^{1}H NMR spectrum of **3.14** in $CDCl_3$ at RT.

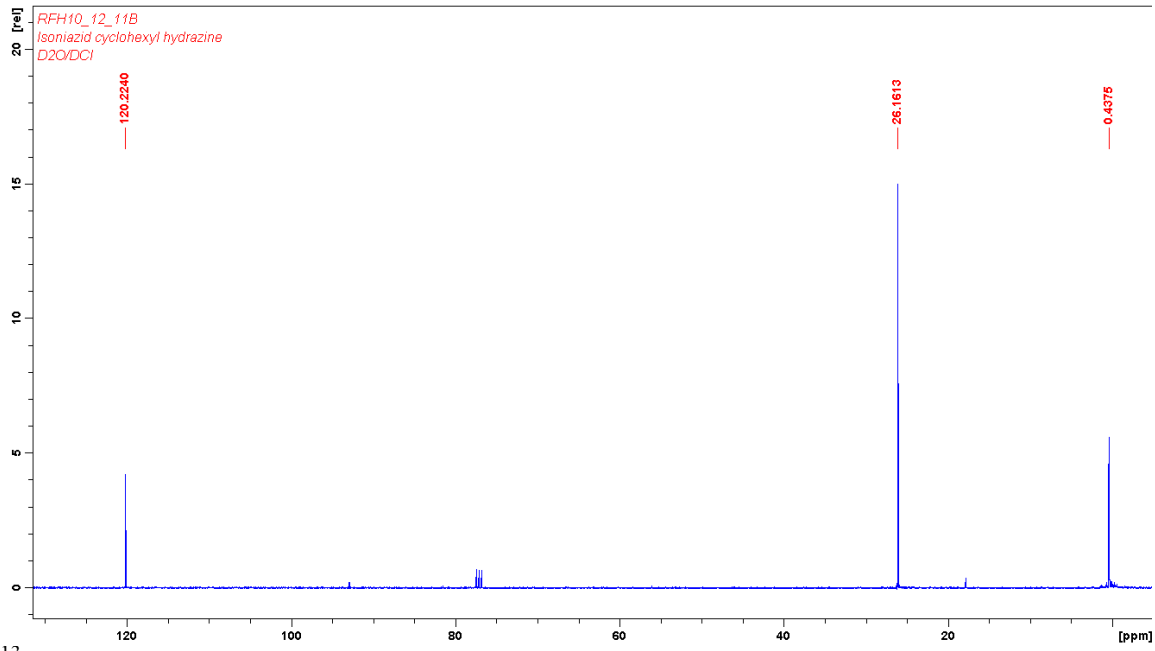

^{13}C NMR spectrum of **3.14** in $CDCl_3$ at RT.

3.15

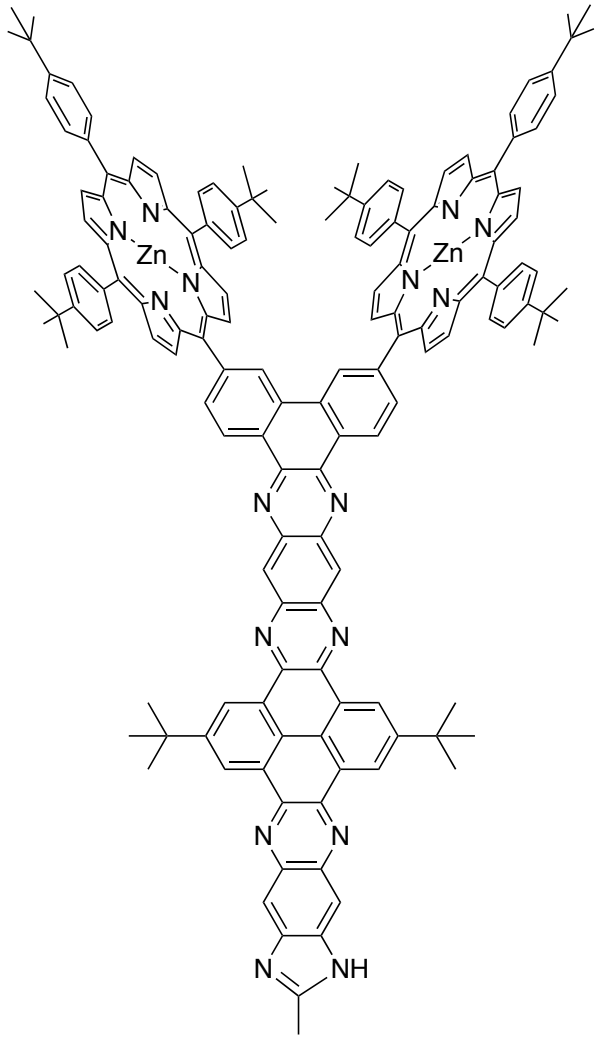

3.15

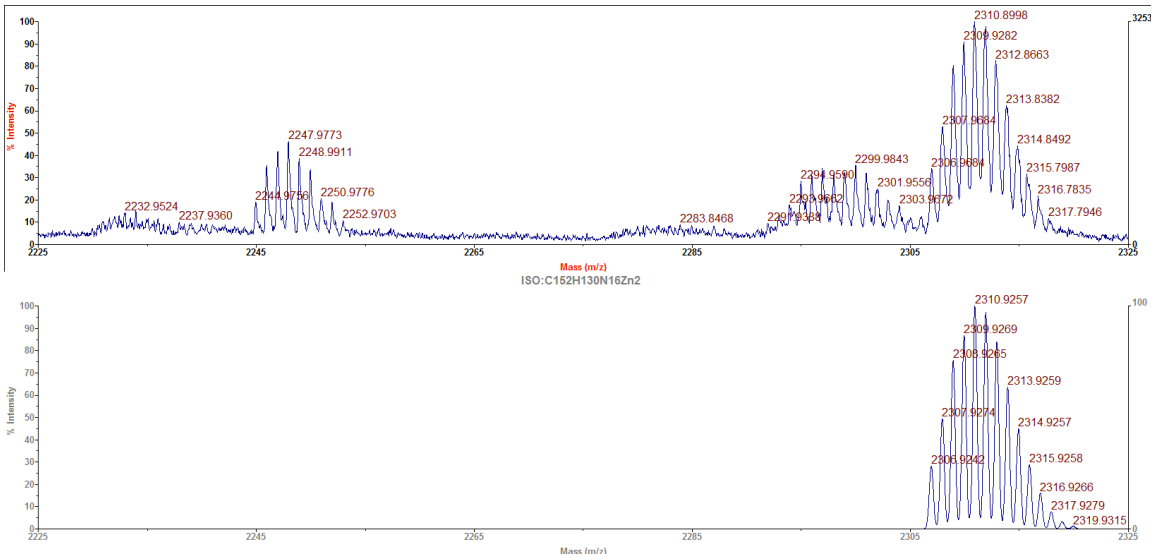

MALDI-TOF MS spectrum of **3.15**. The top trace is the observed spectrum and the bottom trace is the theoretical spectrum form molecular formula $C_{152}H_{130}N_{16}Zn_2$.

3.16

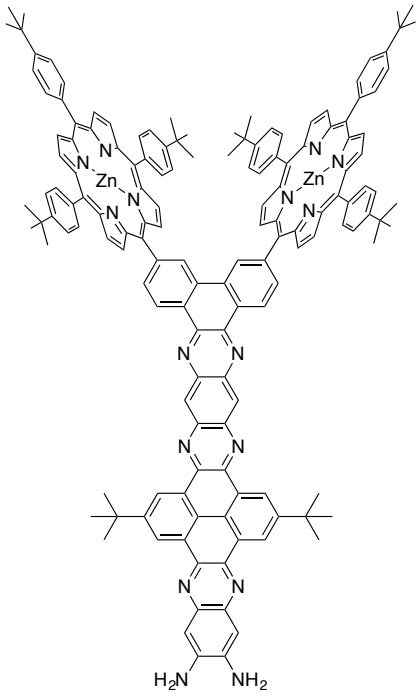

3.16

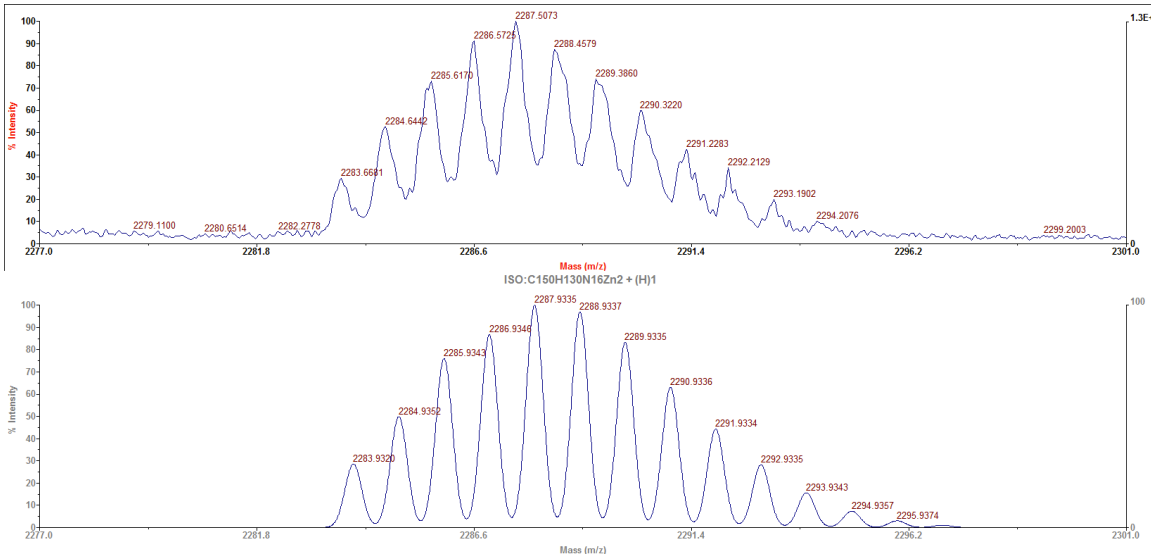

MALDI-TOF Mass Spectrum of **3.16**. The top trace is the observed spectrum while the bottom trace is the theoretical spectrum for molecular formula $C_{150}H_{131}N_{16}Zn_2$ $[M+H]^+$.

3.17

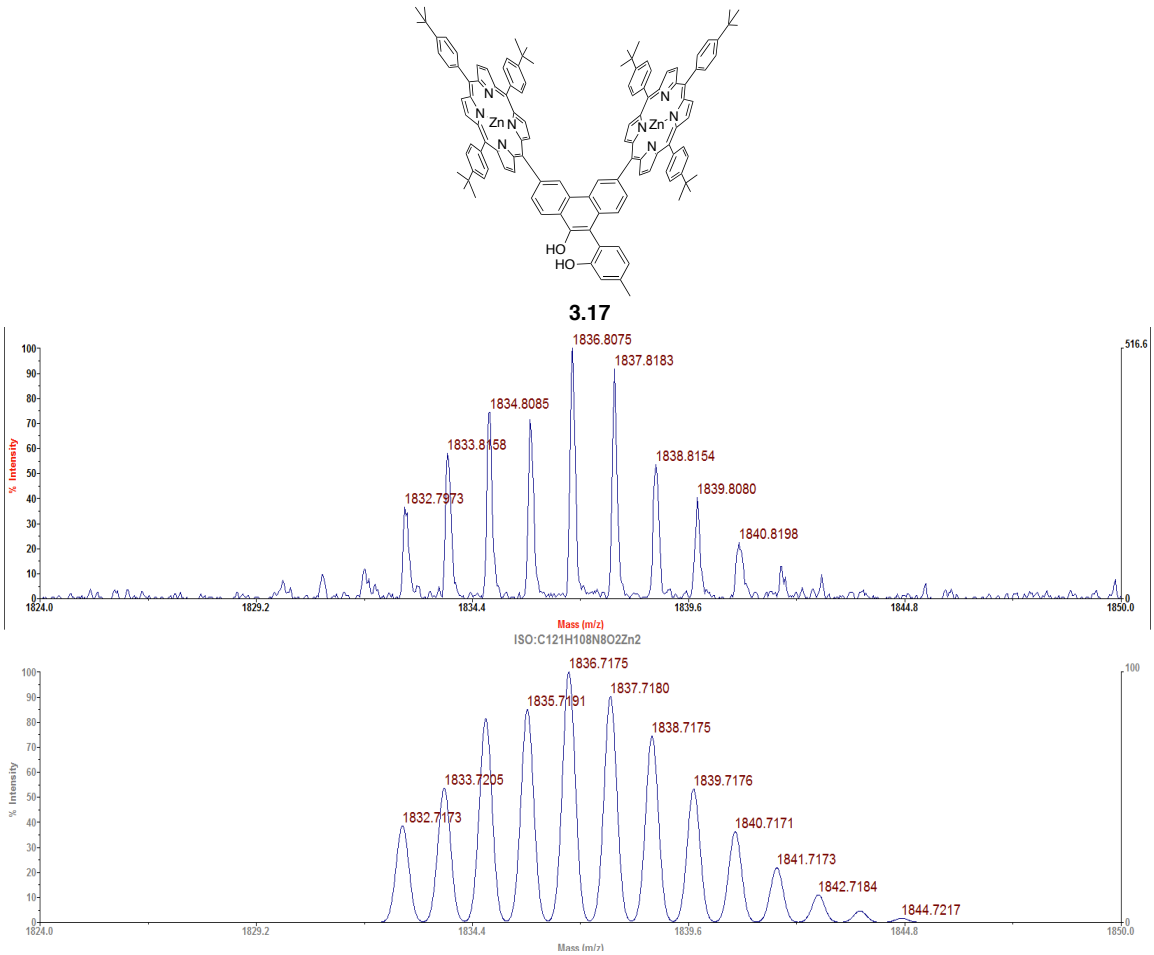

MALDI-TOF Mass Spectrum of possible structure, **3.17**. The top trace is the observed spectrum while the bottom trace is the theoretical spectrum for molecular formula $C_{121}H_{108}N_8O_2Zn_2$ $[M]^+$.

3.18

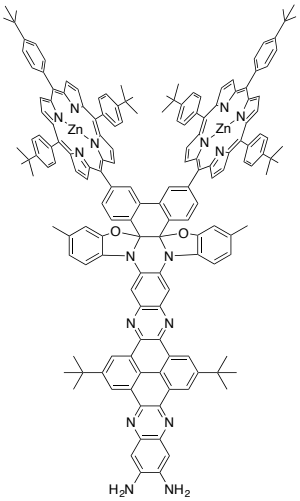

3.18

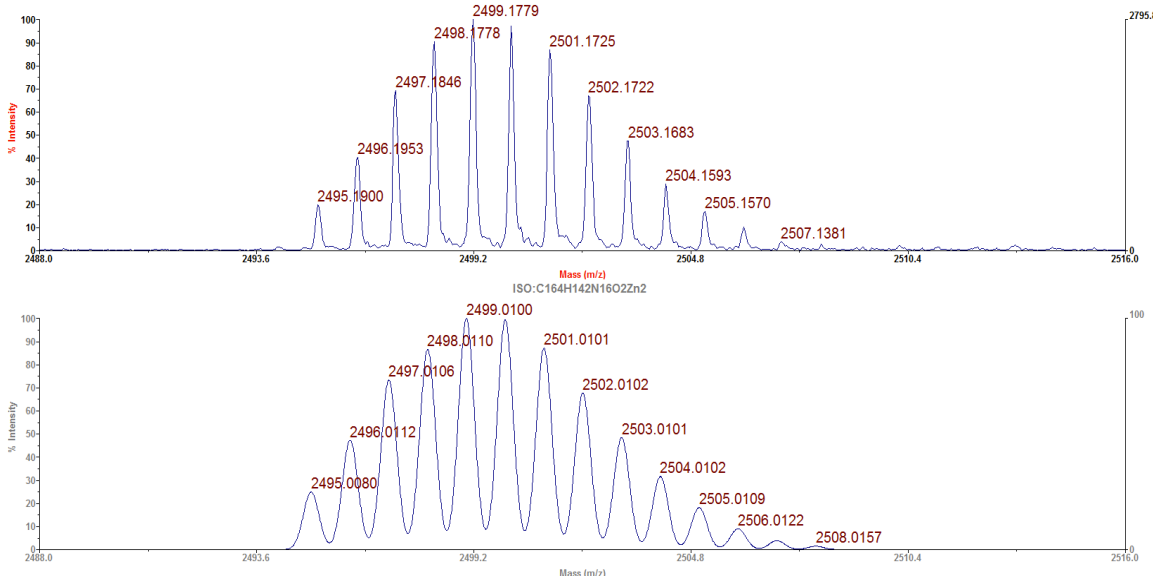

MALDI-TOF Mass Spectrum of possible structure, **3.18**. The top trace is the observed spectrum while the bottom trace is the theoretical spectrum for molecular formula $C_{164}H_{142}N_{16}O_2Zn_2$ $[M]^+$.

APPENDIX C

NMR AND MASS SPECTRAL DATA FOR SYNTHESIZED COMPOUNDS OF CHAPTER 4

4.1

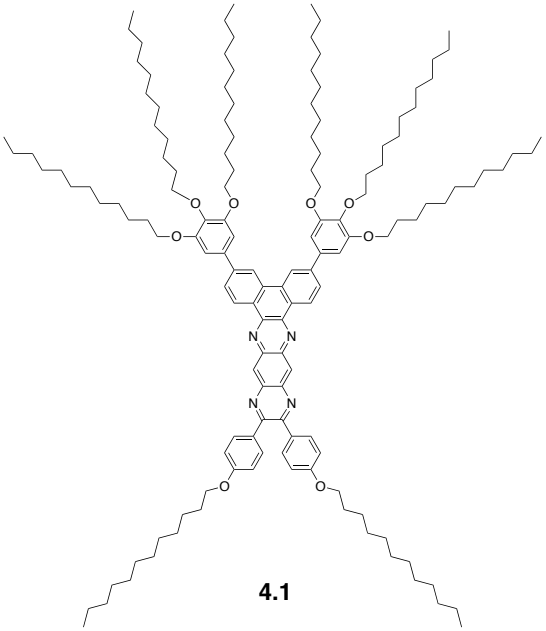

4.1

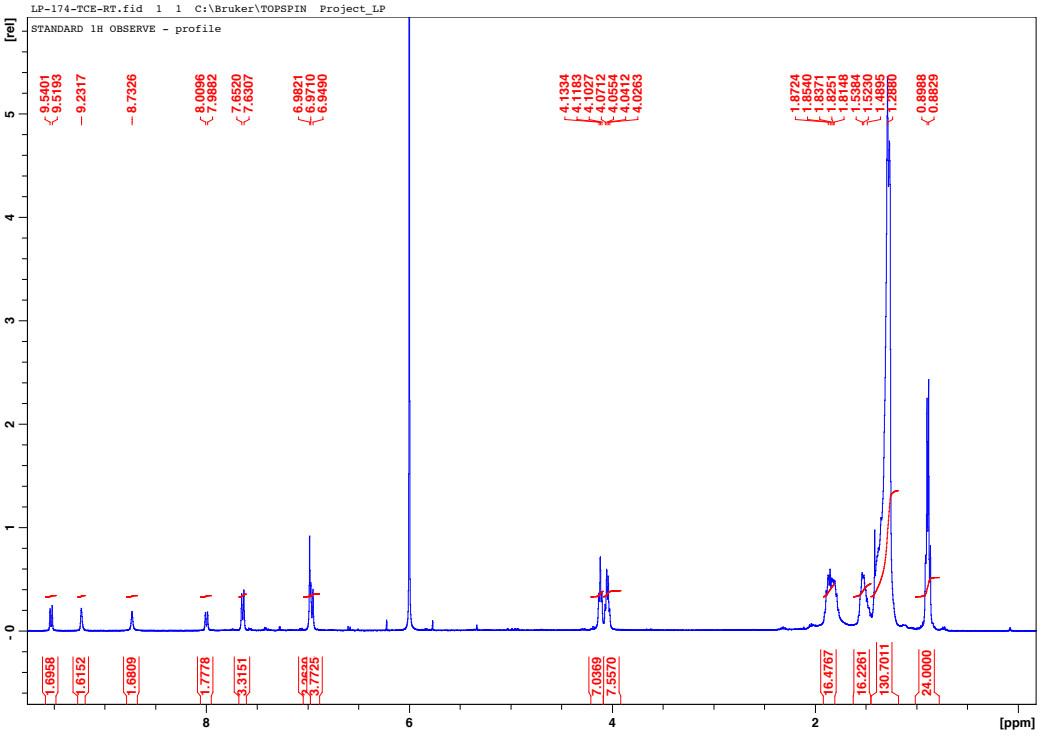

^{1}H NMR spectrum of **4.1** in $CDCl_3$ at RT.

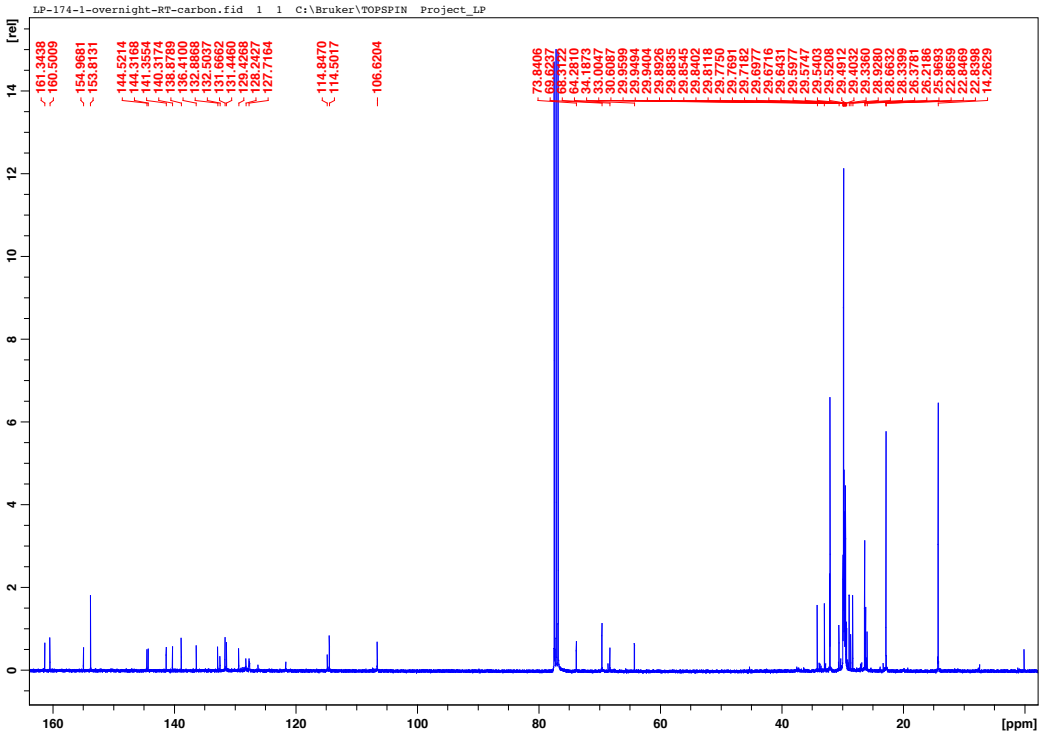

^{13}C NMR spectrum of **3.12** in $CDCl_3$ at RT.

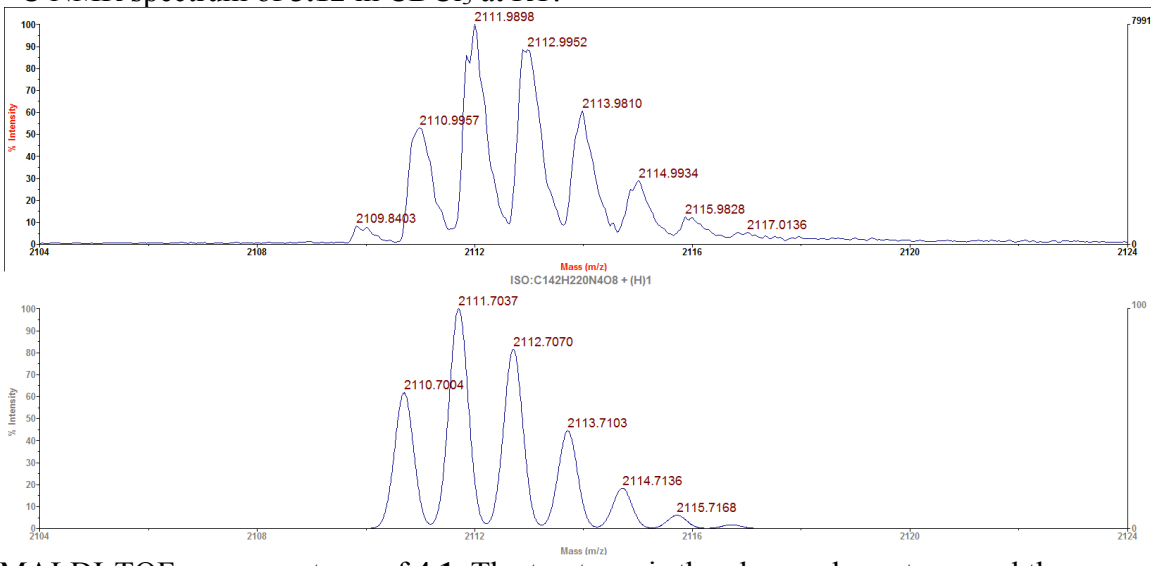

MALDI-TOF mass spectrum of **4.1**. The top trace is the observed spectrum and the bottom trace is the theoretical spectrum form molecular formula $C_{142}H_{223}N_4O_8$ $[M+H]^+$.

4.2

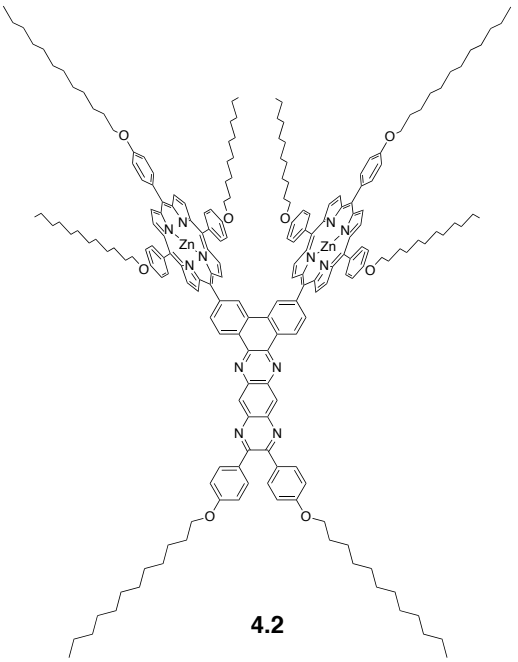

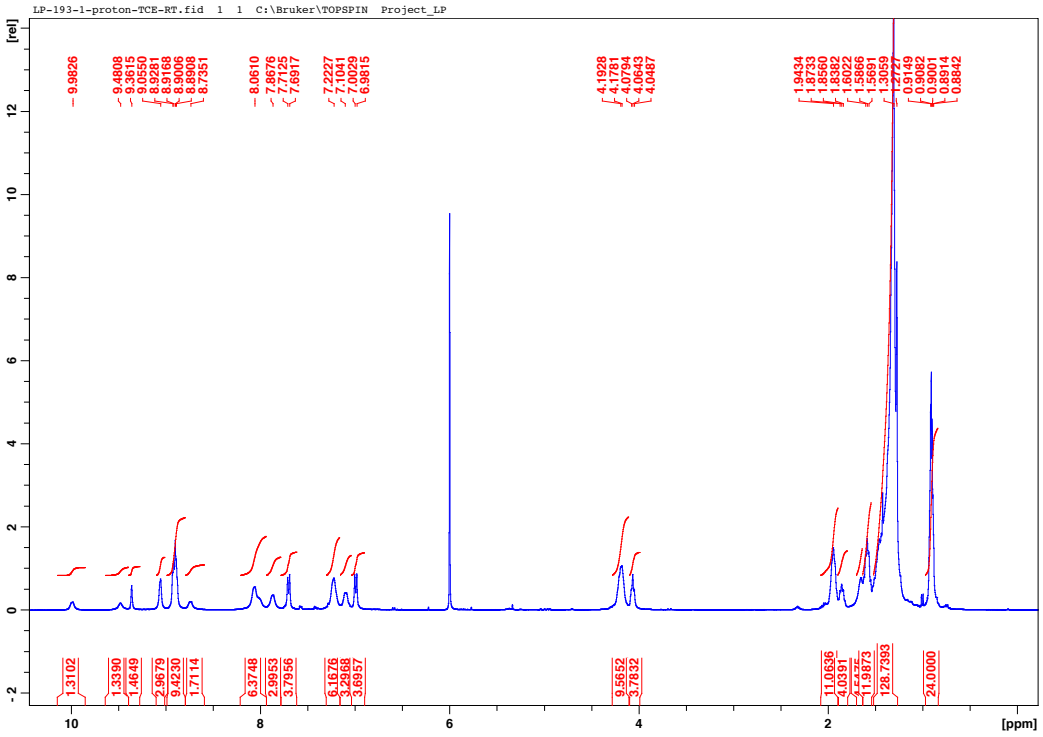

^{1}H NMR spectrum of **4.2** in 1,1,2,2-tetrachloroethane at RT.

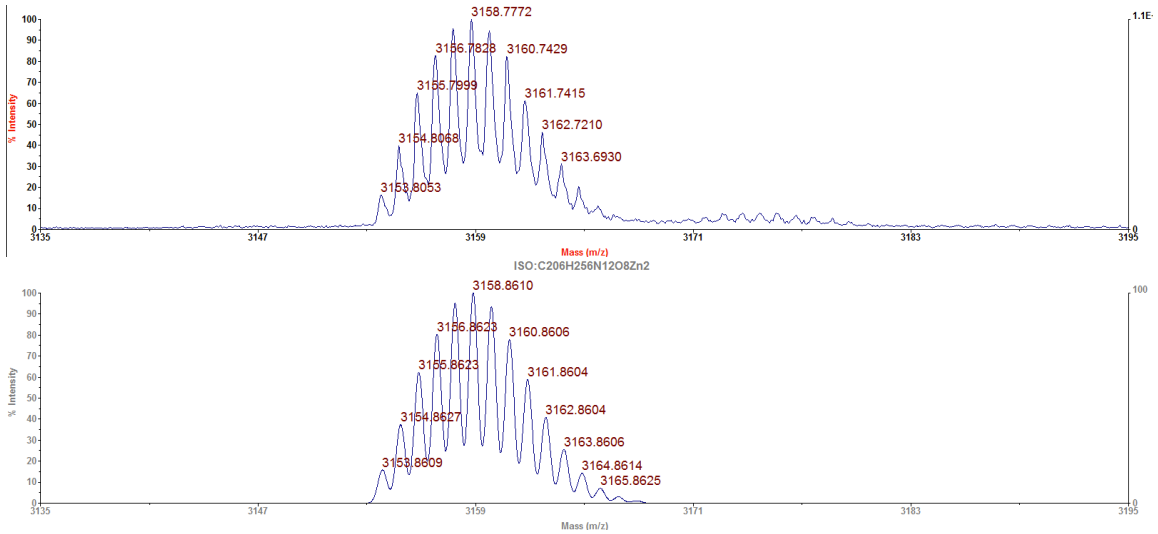

MALDI-TOF mass spectrum of **4.2**. The top trace is the observed spectrum and the bottom trace is the theoretical spectrum for molecular formula $C_{206}H_{256}N_{12}O_8Zn_2$ $[M]^+$.

4.3

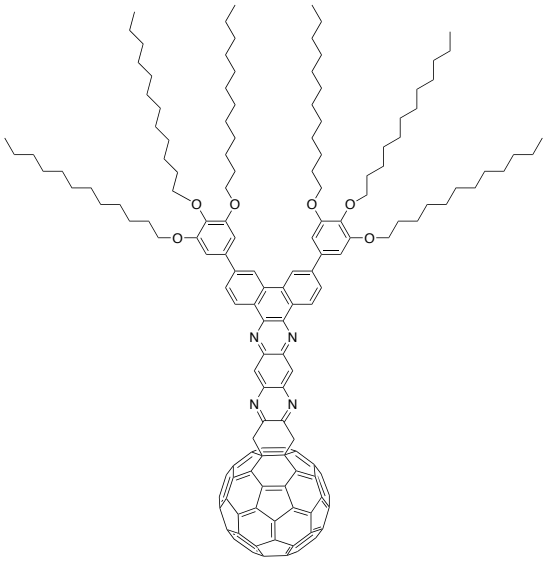

4.3

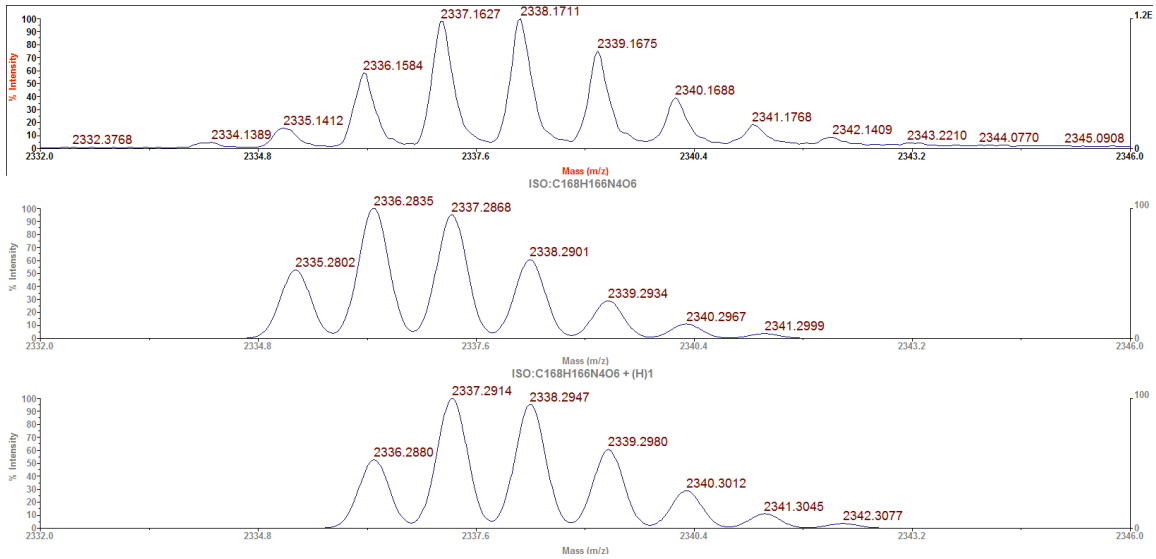

MALDI-TOF mass spectrum of **4.3**. The top trace is the observed spectrum and the bottom two traces are the theoretical spectrum form molecular formula $C_{168}H_{166}N_4O_6$ $[M]^+$ and $C_{168}H_{167}N_4O_6$ $[M+H]^+$.

4.4

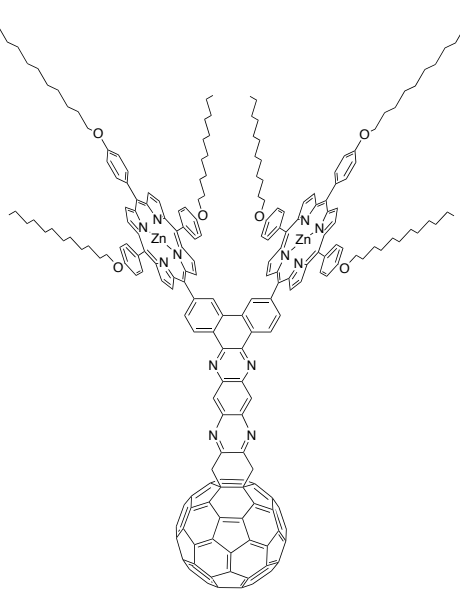

4.4

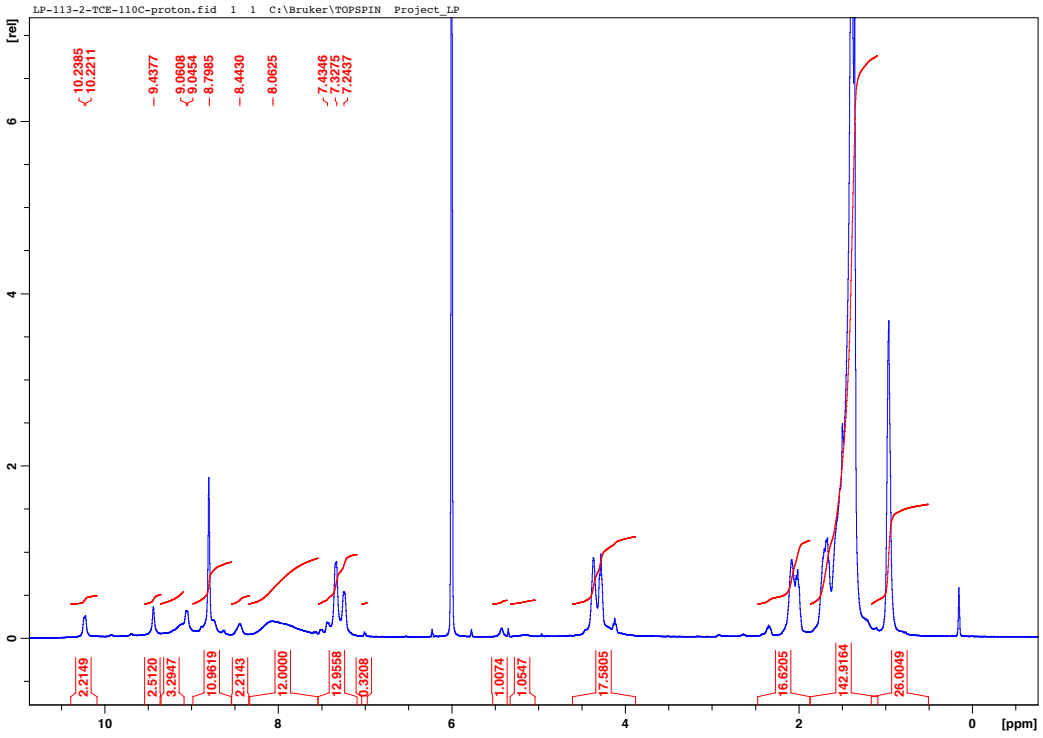

^{1}H NMR spectrum of **4.4** in 1,1,2,2-tetrachloroethane-*d*2 at 110^{o}C.

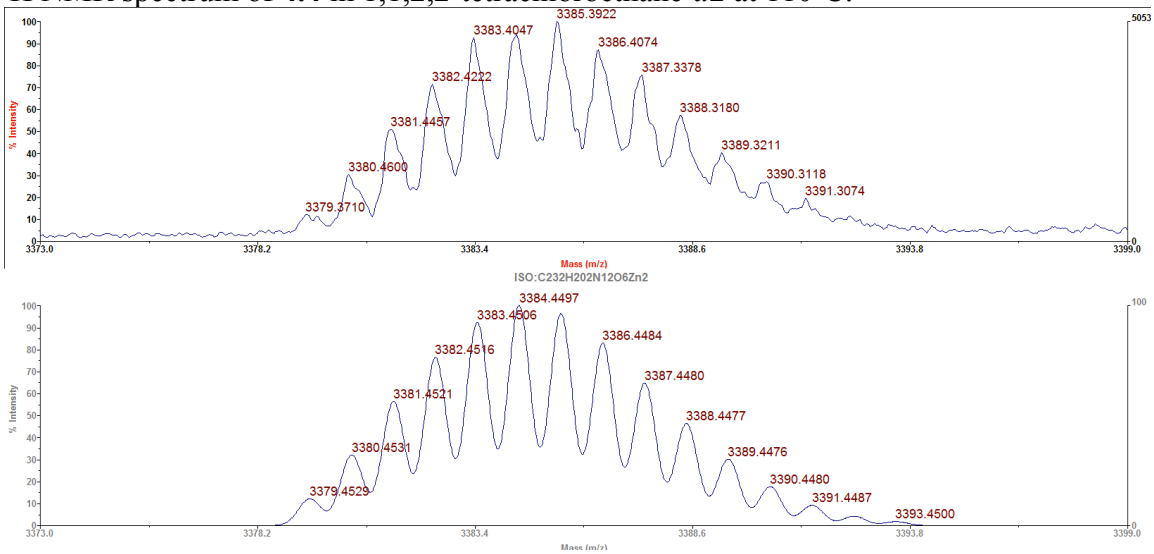

MALDI-TOF mass spectrum of **4.4** synthesized by scheme 4.110-a. The top trace is the observed spectrum and the bottom trace is the theoretical spectrum for molecular formula $C_{232}H_{202}N_{12}O_6Zn_2$ $[M]^+$.

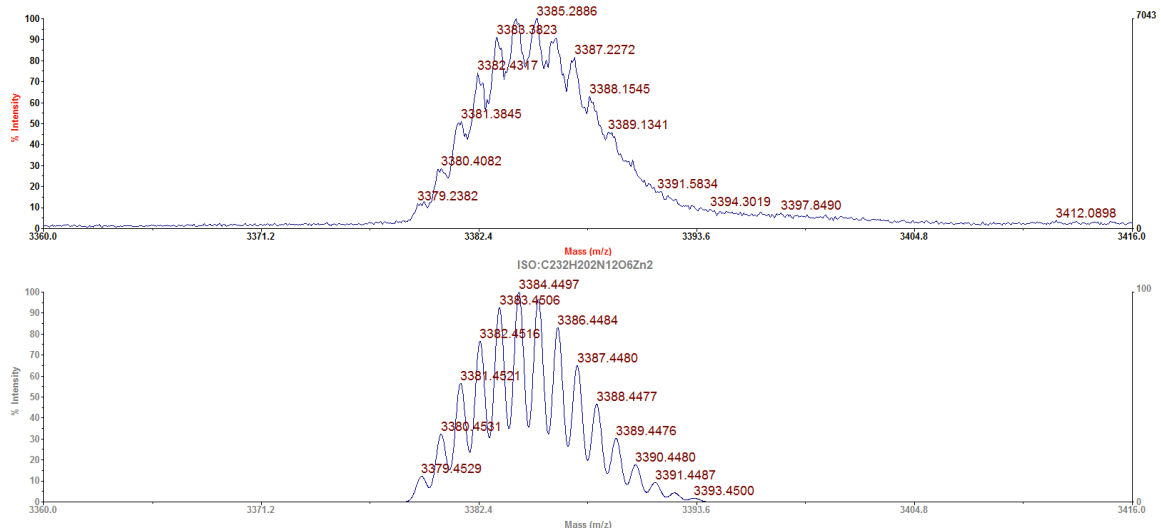

MALDI-TOF mass spectrum of **4.4** synthesized by scheme 4.11-b. The top trace is the observed spectrum and the bottom trace is the theoretical spectrum for molecular formula $C_{232}H_{202}N_{12}O_6Zn_2$ $[M]^+$.

4.5

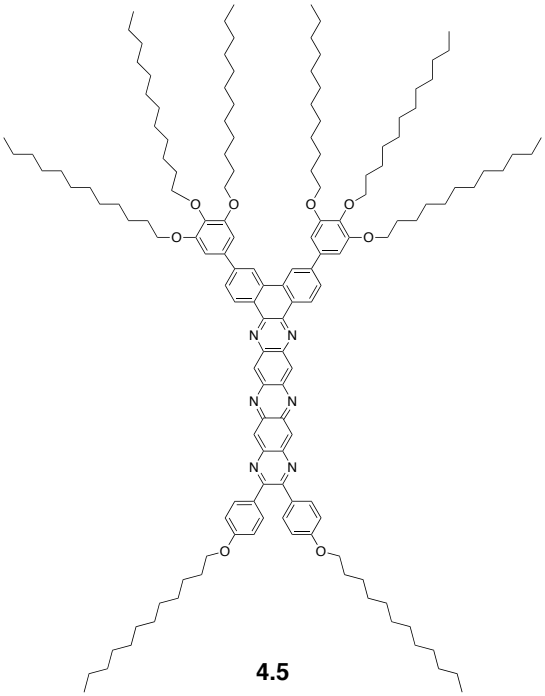

4.5

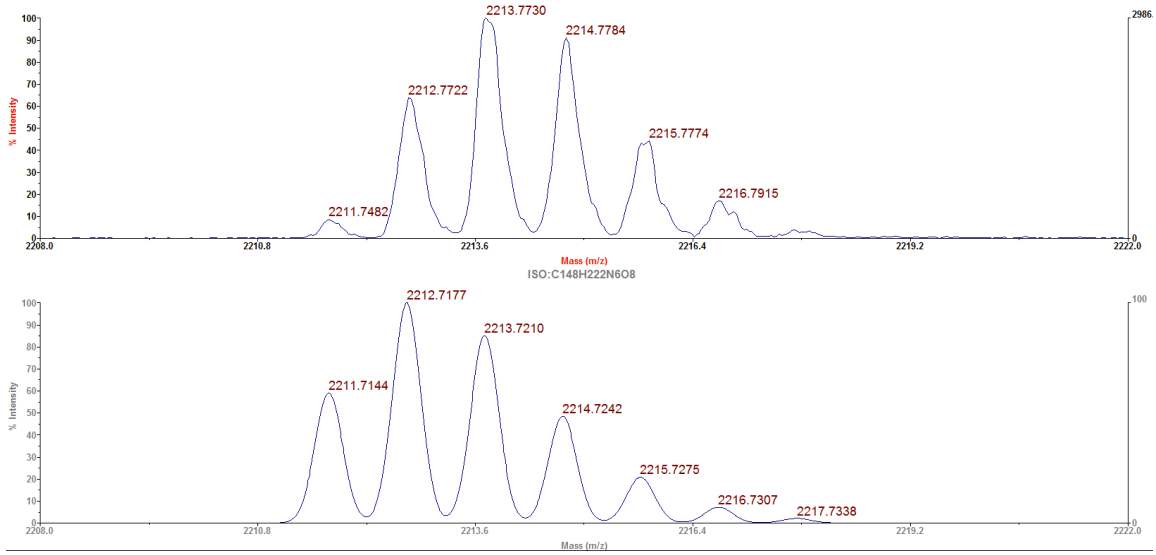

MALDI-TOF mass spectrum of **4.5**. The top trace is the observed spectrum and the bottom trace is the theoretical spectrum for molecular formula $C_{148}H_{222}N_6O_8$ $[M]^+$.

4.7

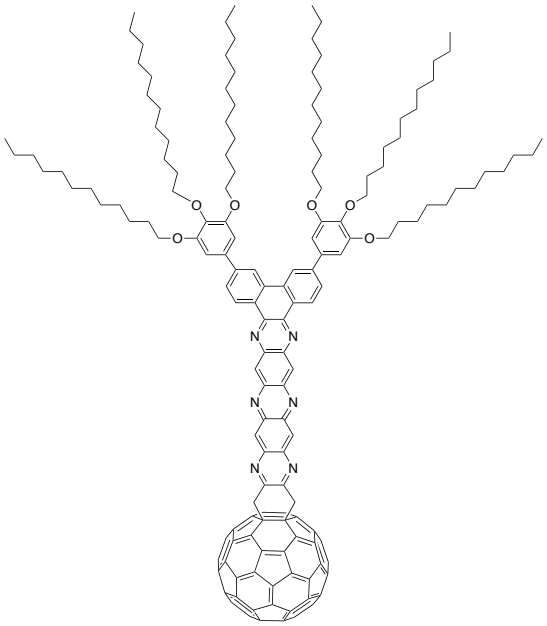

4.7

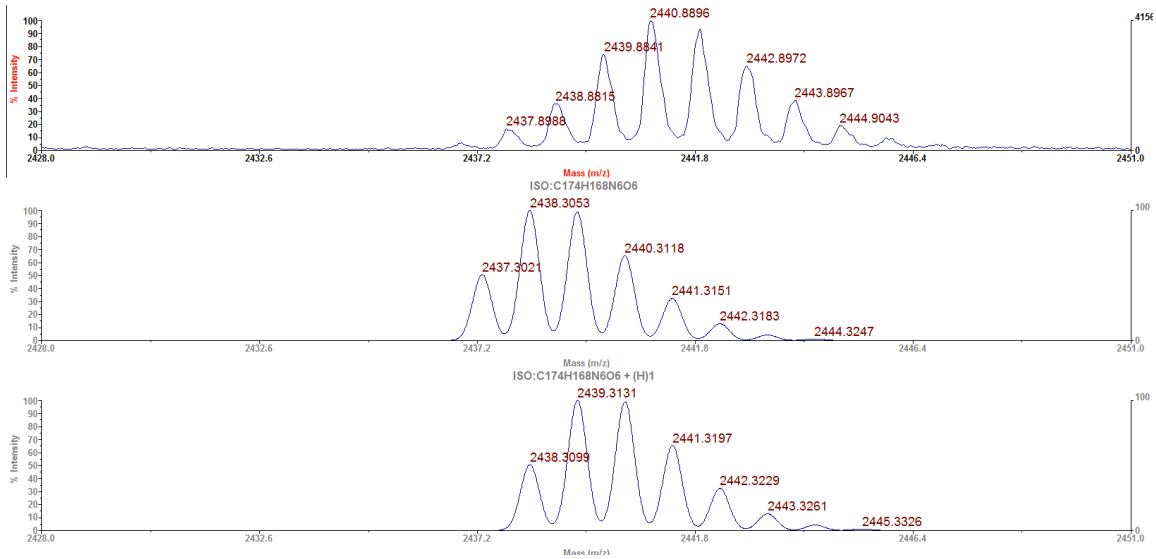

MALDI-TOF mass spectrum of **4.7**. The top trace is the observed spectrum and the bottom two traces are the theoretical spectra for molecular formula $C_{174}H_{168}N_6O_6$ $[M]^+$ and $C_{174}H_{169}N_6O_6$ $[M+H]^+$ respectively. The observed spectrum has been assigned as a superposition of these two theoretical spectra.

4.8

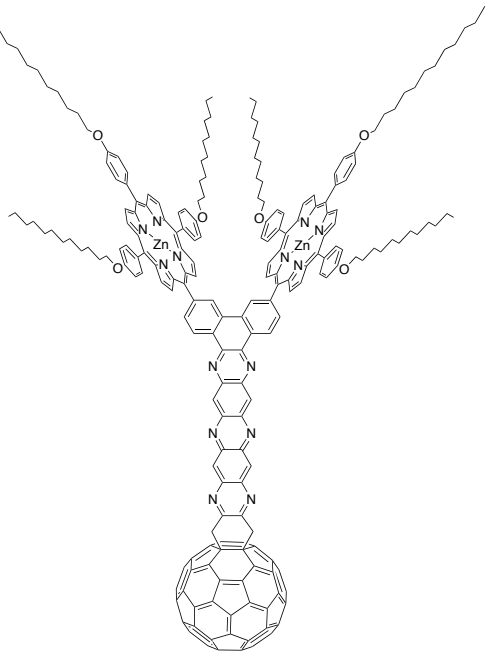

4.8

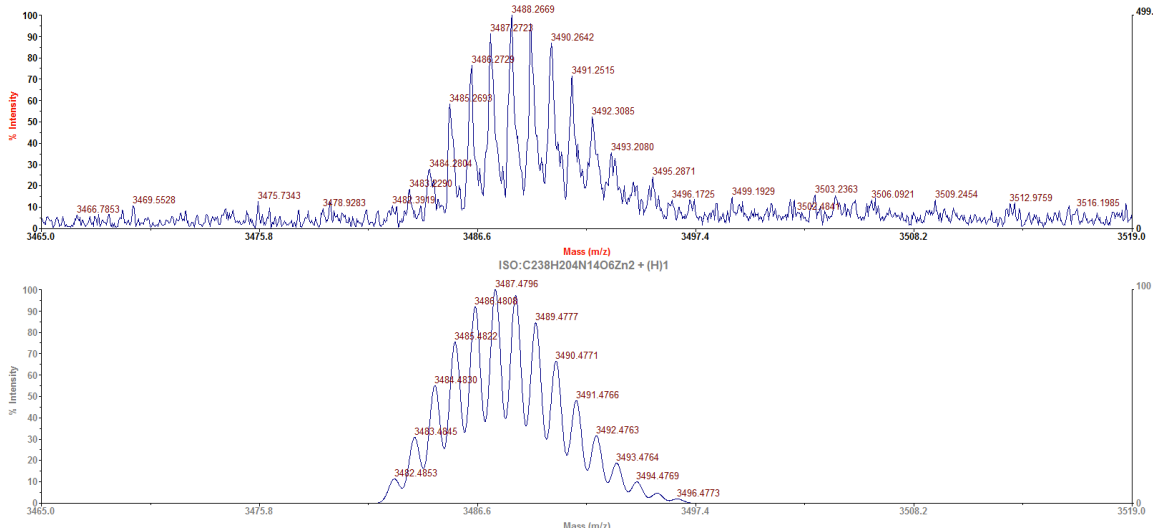

MALDI-TOF mass spectrum of **4.8**. The top trace is the observed spectrum and the bottom trace is the theoretical spectrum for molecular formula $C_{232}H_{205}N_{14}O_6Zn_2$ $[M+H]^+$.

4.9

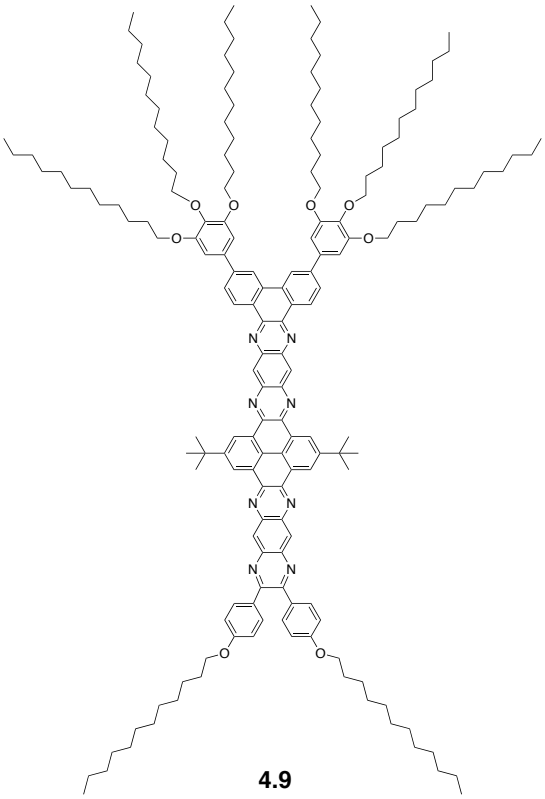

4.9

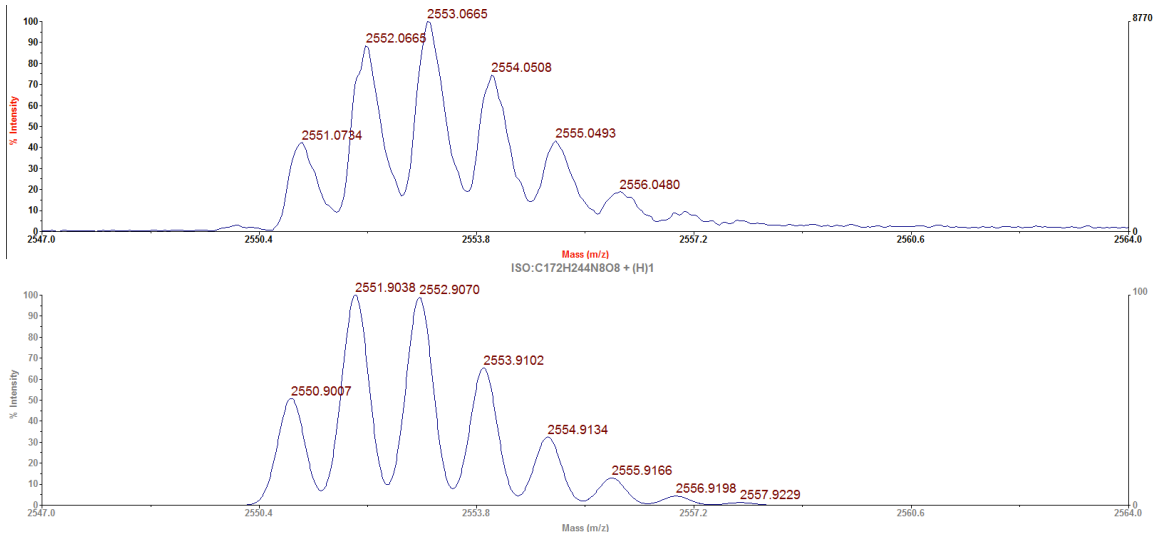

MALDI-TOF mass spectrum of **4.9**. The top trace is the observed spectrum and the bottom trace is the theoretical spectrum for molecular formula $C_{172}H_{245}N_8O_8$ $[M+H]^+$.

4.10

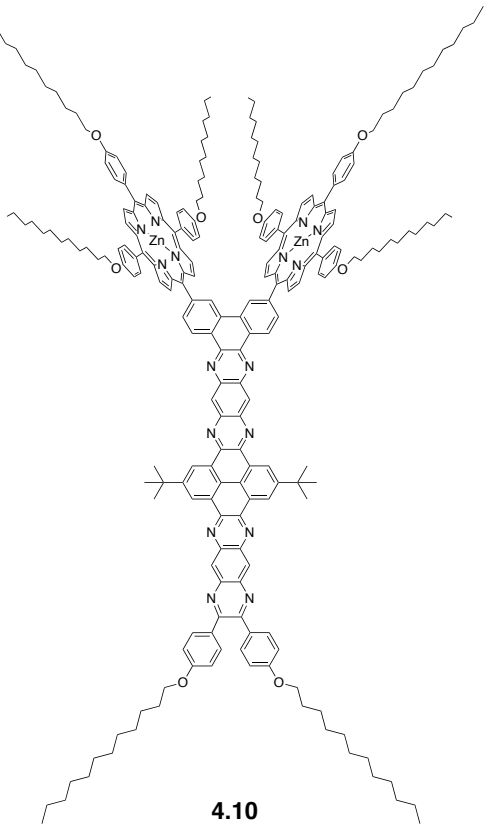

4.10

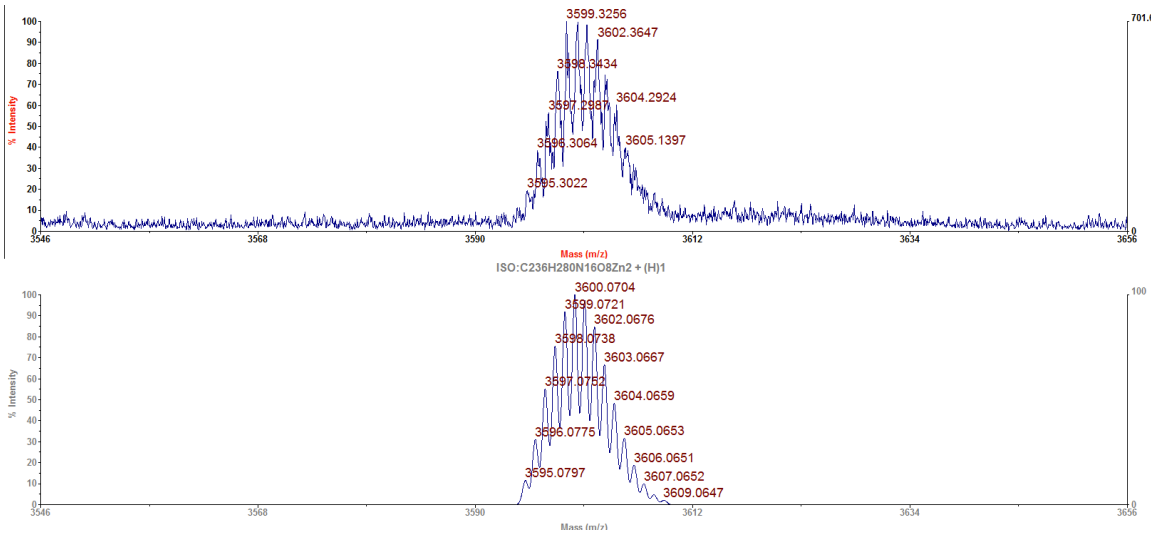

MALDI-TOF mass spectrum of **4.10**. The top trace is the observed spectrum and the bottom trace is the theoretical spectrum for molecular formula $C_{236}H_{281}N_{16}O_8Zn_2$ $[M+H]^+$.

4.11

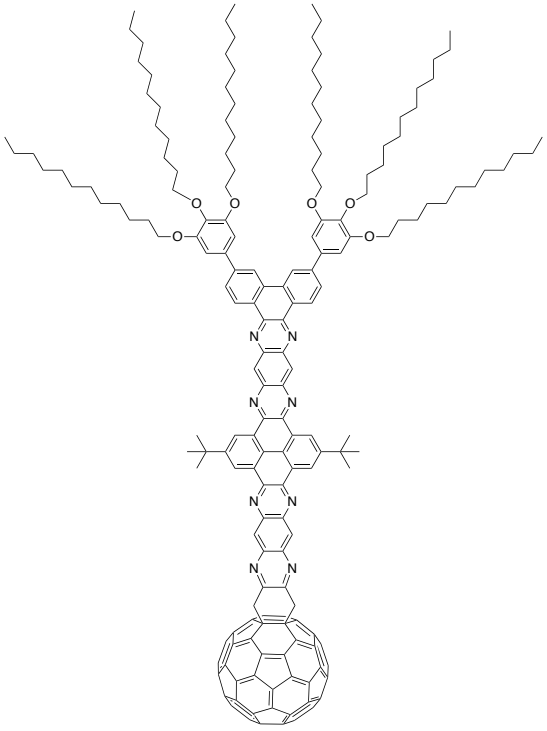

4.11

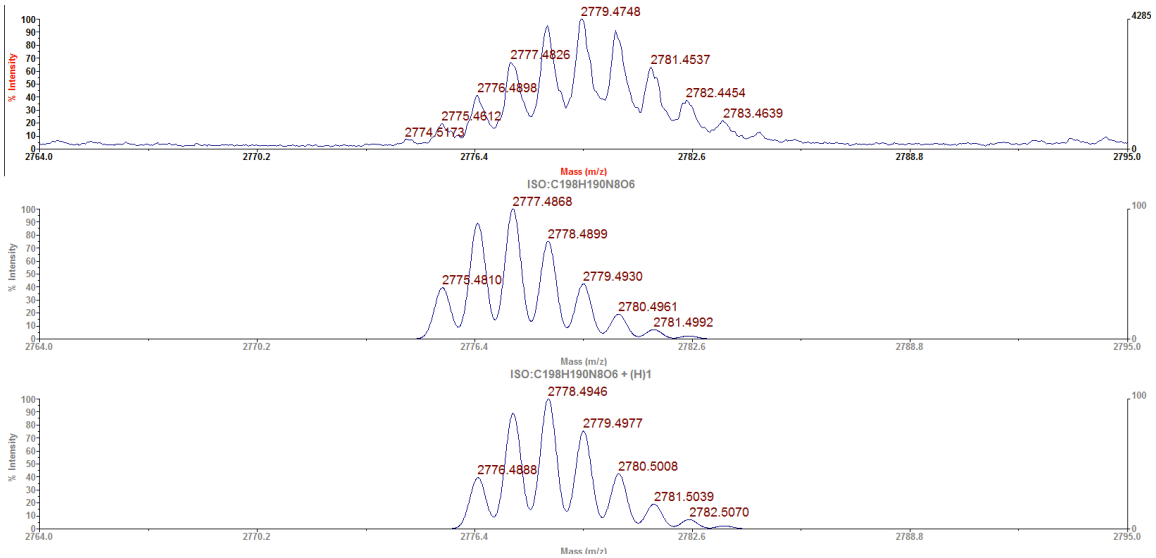

MALDI-TOF mass spectrum of **4.11**. The top trace is the observed spectrum and the bottom two traces are the theoretical spectra for molecular formula $C_{198}H_{190}N_8O_6$ $[M]^+$ and $C_{198}H_{191}N_8O_6$ $[M+H]^+$. It is proposed that the observed spectrum is a superposition of the bottom two spectra.

4.12

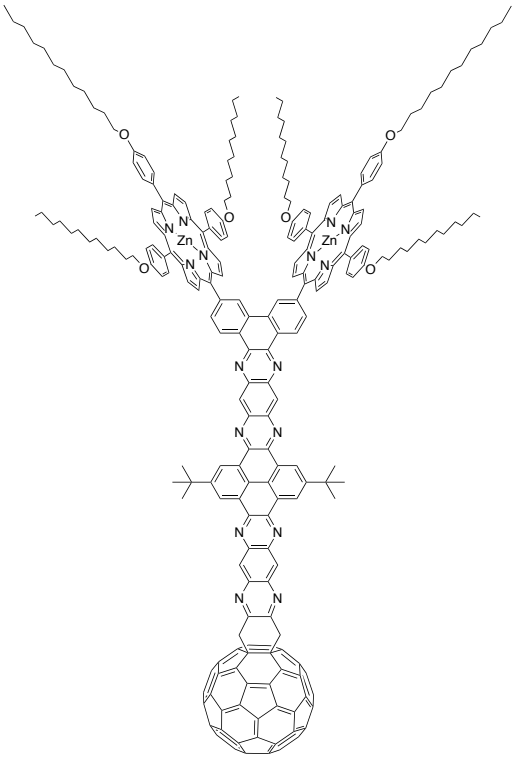

4.12

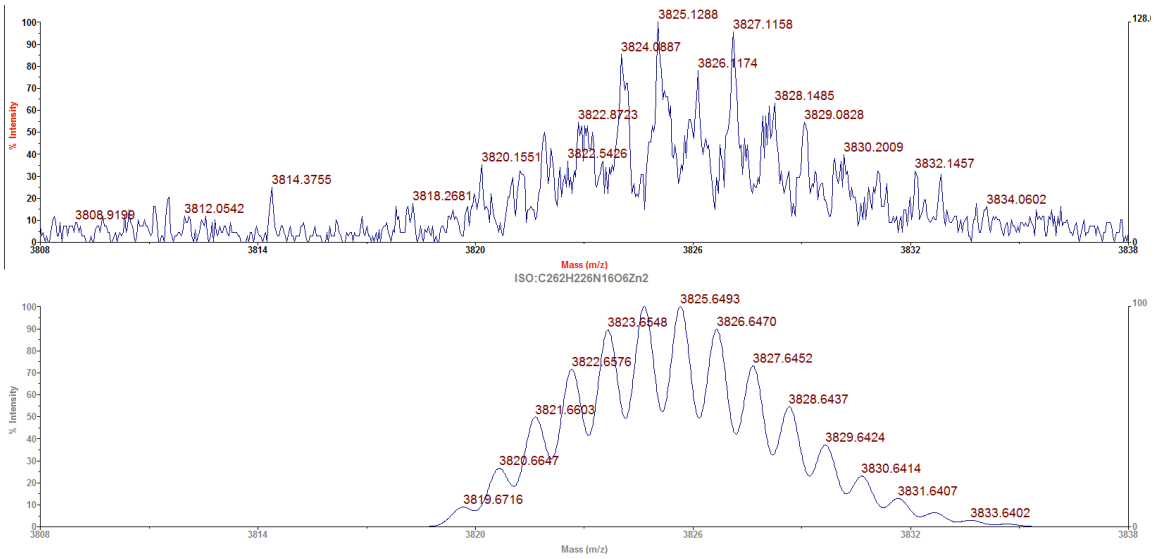

MALDI-TOF mass spectrum of **4.12**. The top trace is the observed spectrum and the bottom trace is the theoretical spectrum for molecular formula $C_{262}H_{226}N_{16}O_6Zn_2$ $[M]^+$.

4.13

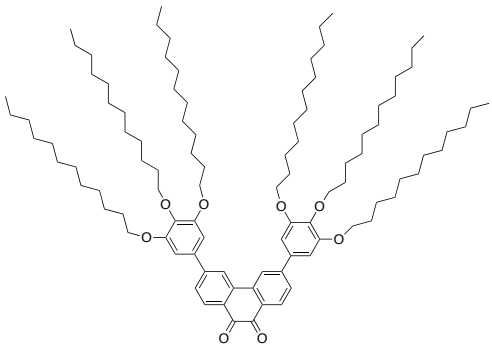

4.13

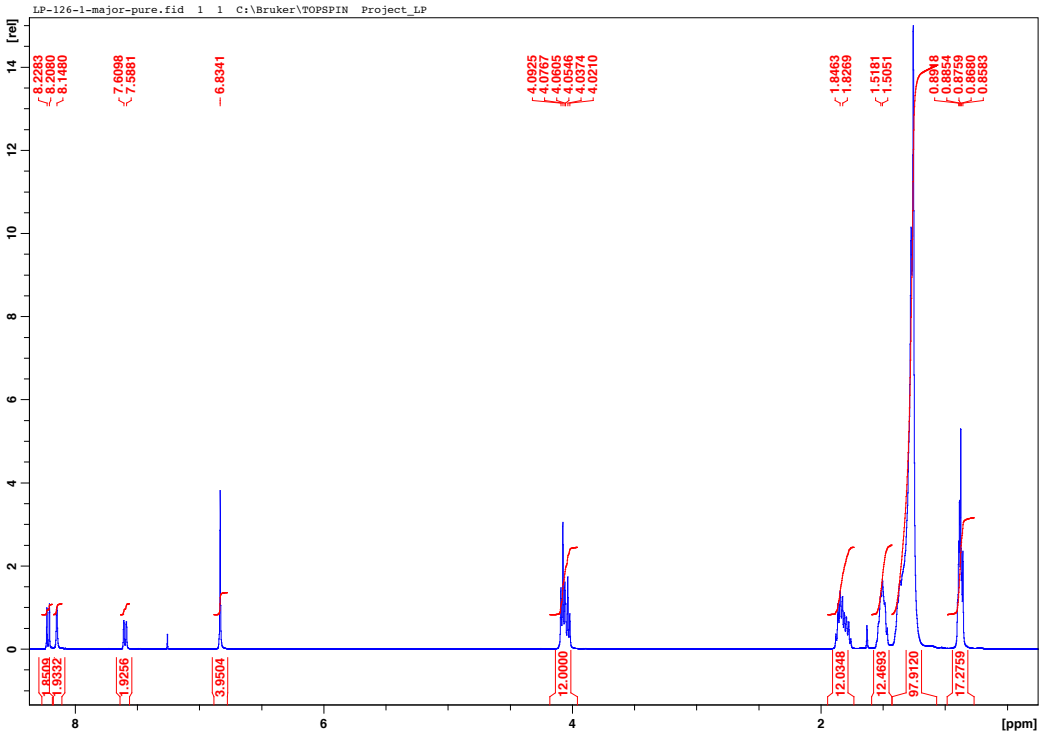

^{1}H NMR spectrum of **4.13** synthesized by scheme 4.2 in $CDCl_3$ at RT.

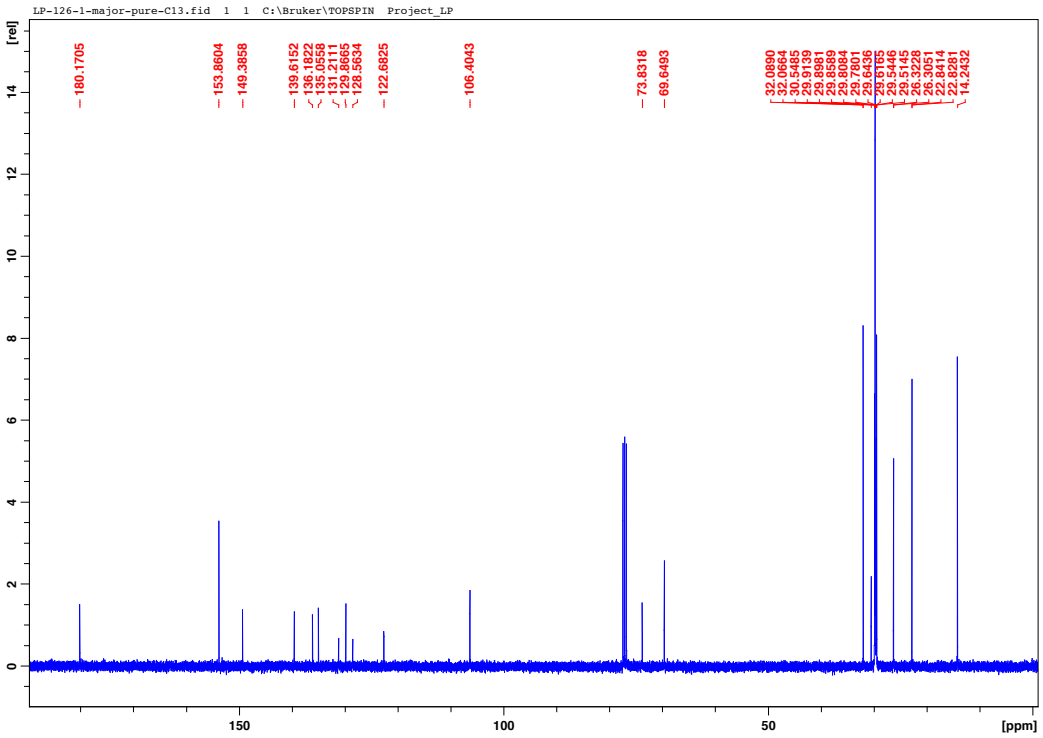

^{13}C NMR spectrum of **4.13** synthesized by scheme 4.2 in $CDCl_3$ at RT.

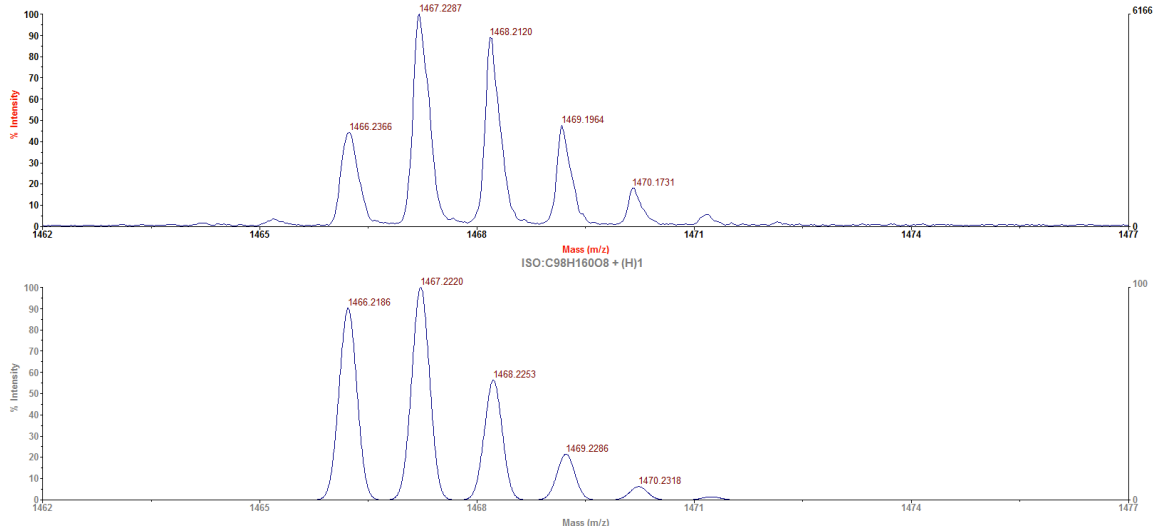

MALDI-TOF mass spectrum of **4.13** by scheme 4.2. The top trace is the observed spectrum and the bottom trace is the theoretical spectrum for molecular formula $C_{98}H_{161}O_8$ $[M+H]^+$.

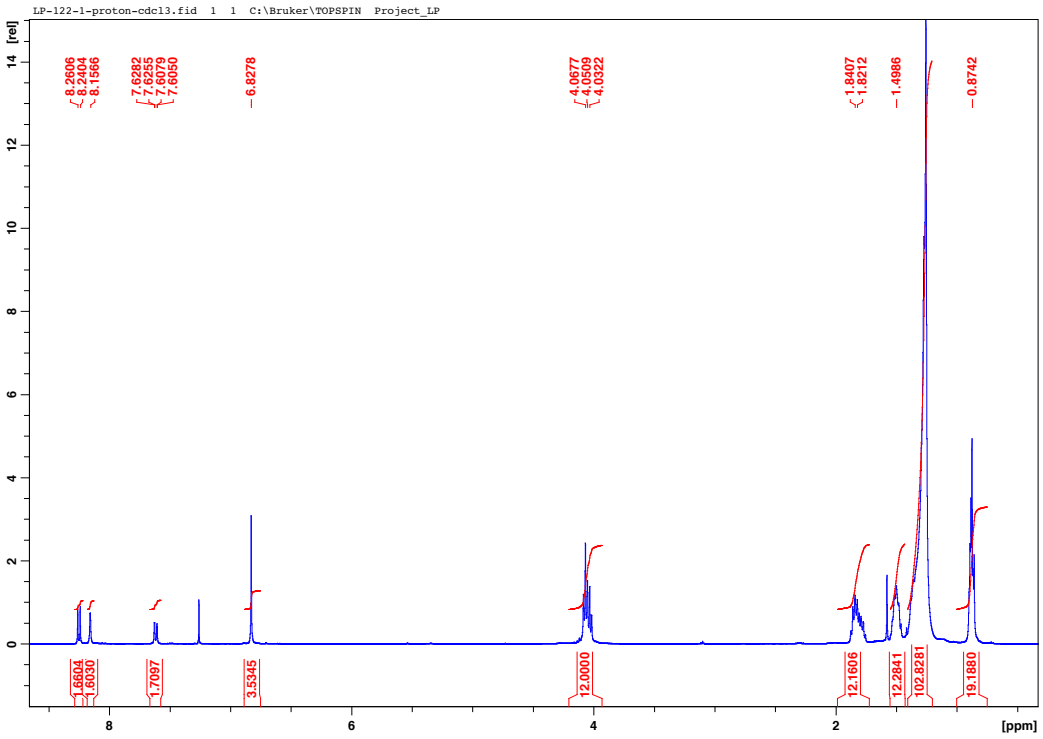

^1H NMR spectrum of **4.13** synthesized by scheme 4.3 in $CDCl_3$ at RT.

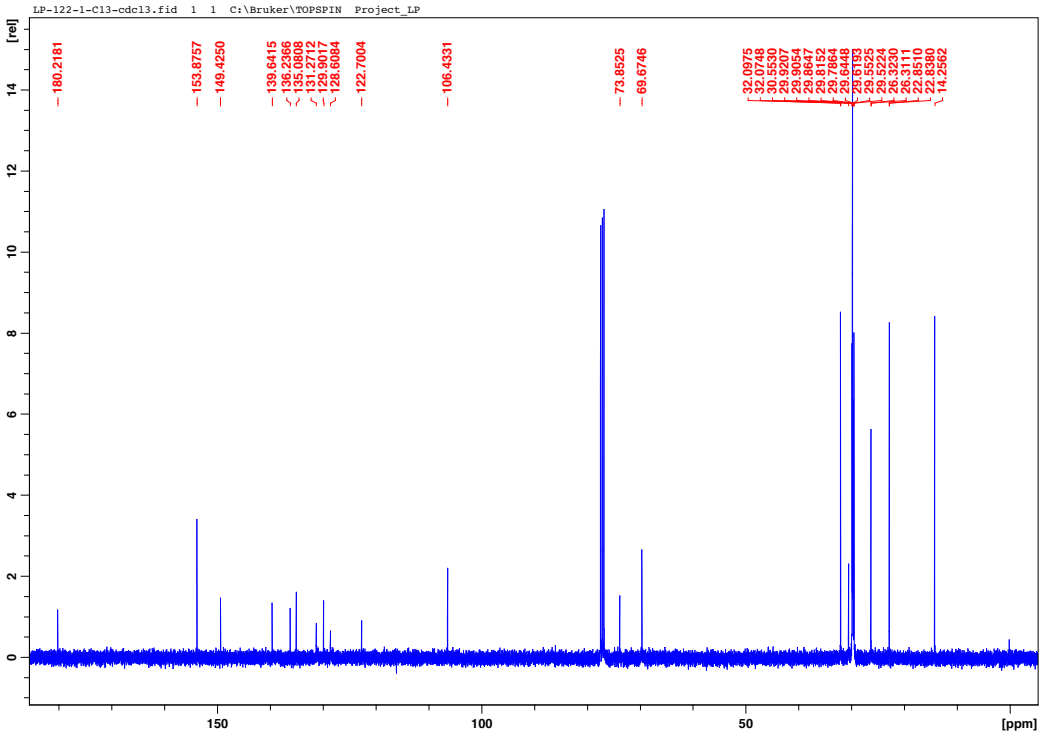

^{13}C NMR spectrum of **4.13** synthesized by scheme 4.3 in $CDCl_3$ at RT.

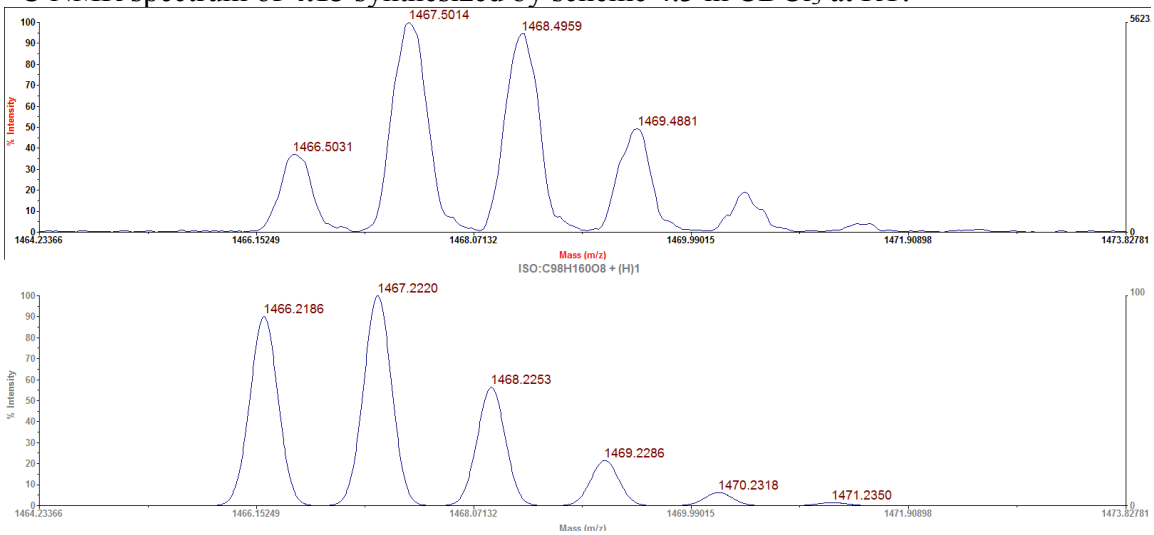

MALDI-TOF mass spectrum of **4.13** by scheme 4.3. The top trace is the observed spectrum and the bottom trace is the theoretical spectrum for molecular formula $C_{98}H_{161}O_8$ $[M+H]^+$.

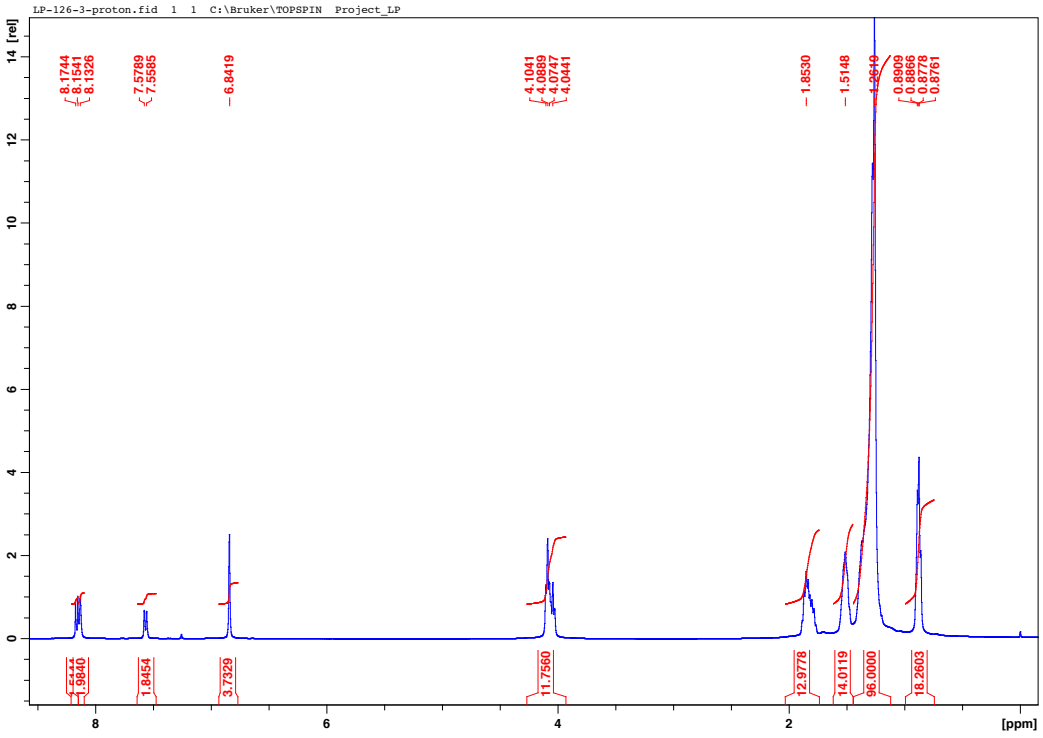

^{1}H NMR spectrum of **4.13** synthesized by scheme 4.4 in $CDCl_3$ at RT.

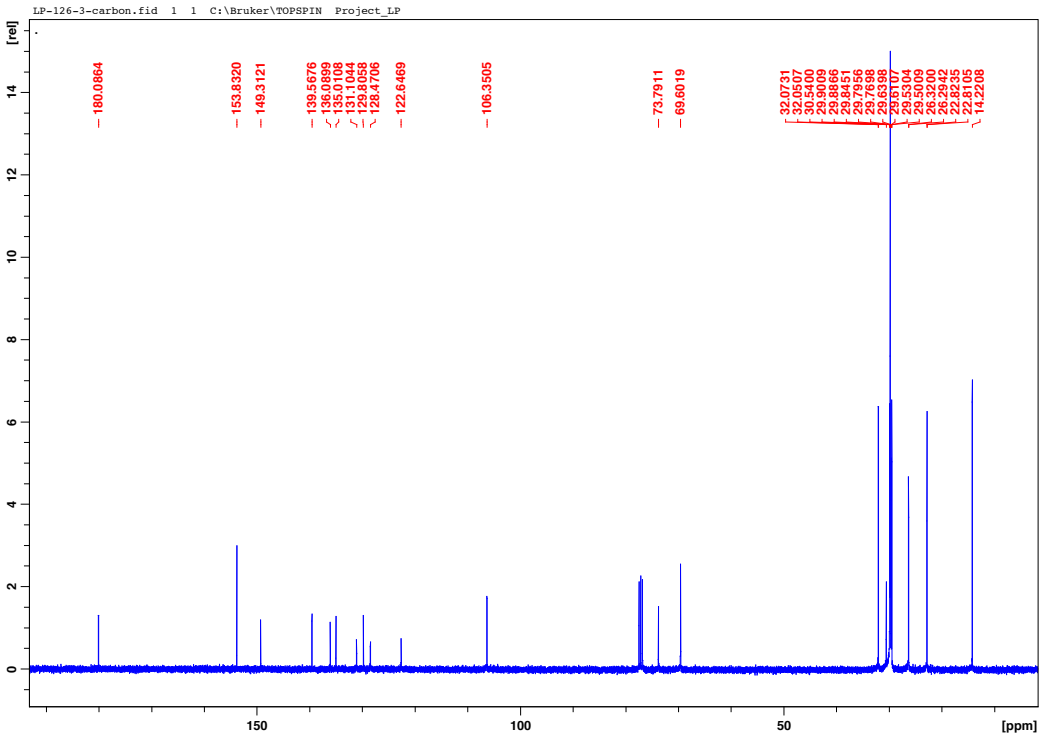

^{13}C NMR spectrum of **4.13** synthesized by scheme 4.4 in $CDCl_3$ at RT.

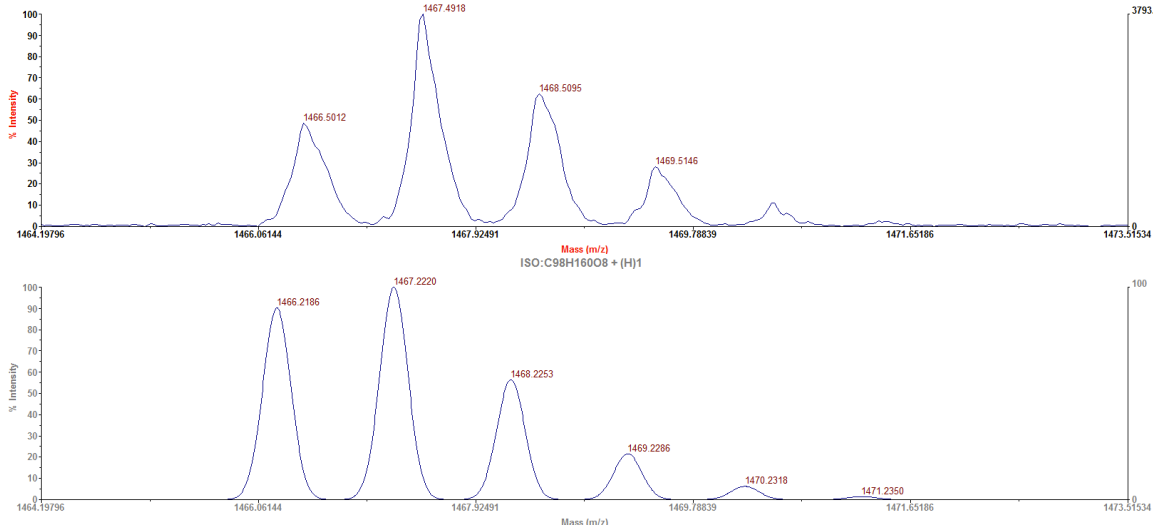

MALDI-TOF mass spectrum of **4.13** by scheme 4.4. The top trace is the observed spectrum and the bottom trace is the theoretical spectrum for molecular formula $C_{98}H_{161}O_8$ $[M+H]^+$.

4.14

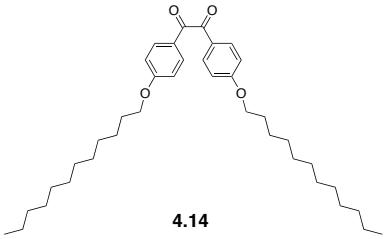

4.14

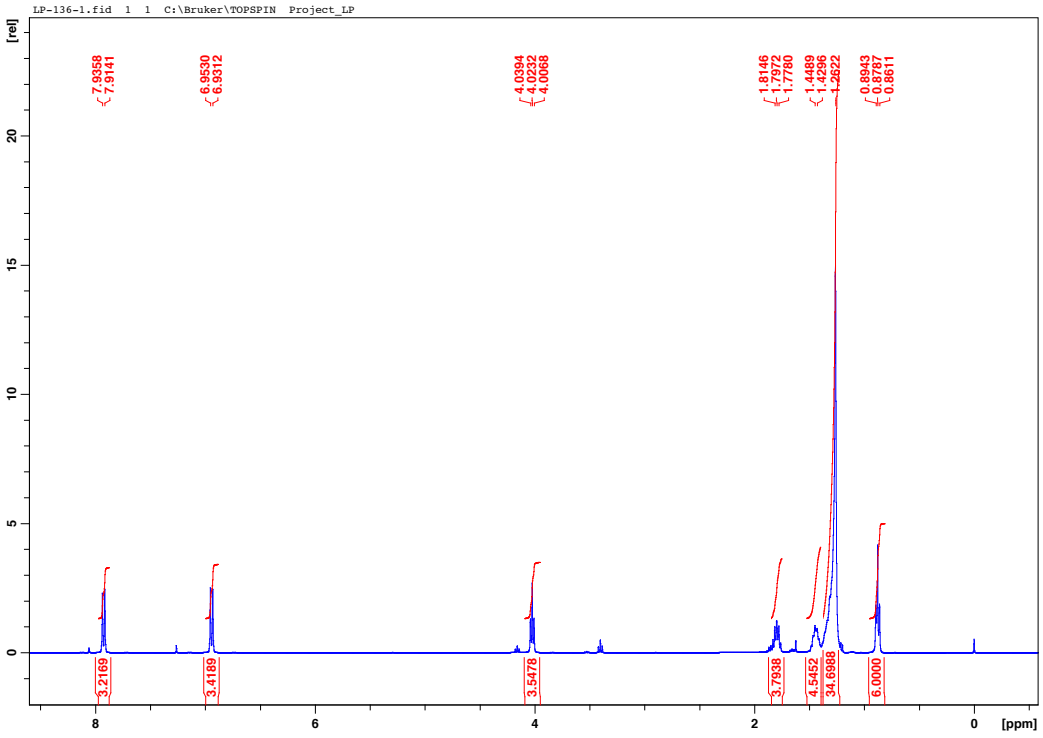

^{1}H NMR spectrum of **4.14** in $CDCl_3$ at RT.

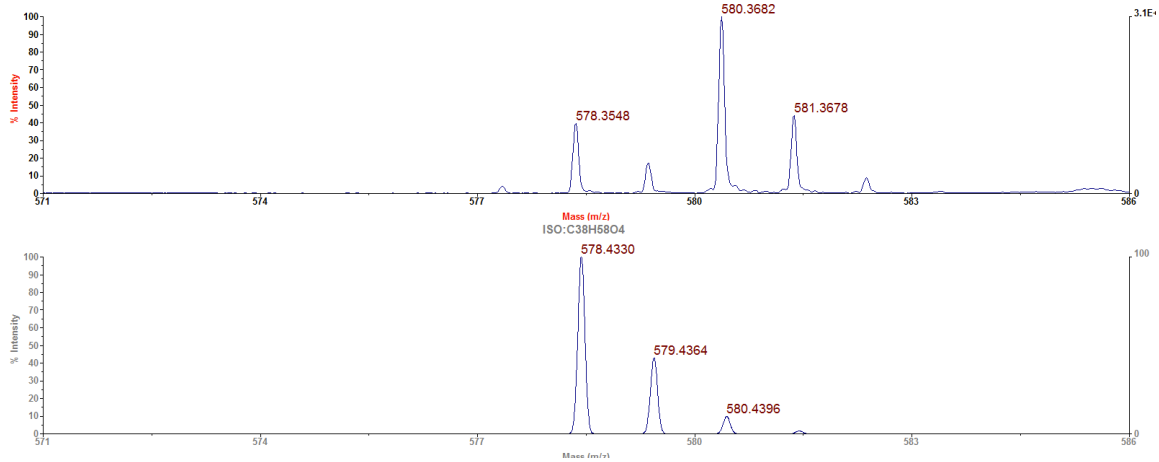

MALDI-TOF mass spectrum of **4.14**. The top trace is the observed spectrum and the bottom trace is the theoretical spectrum form molecular formula $C_{38}H_{58}O_4$ $[M]^+$.

4.15

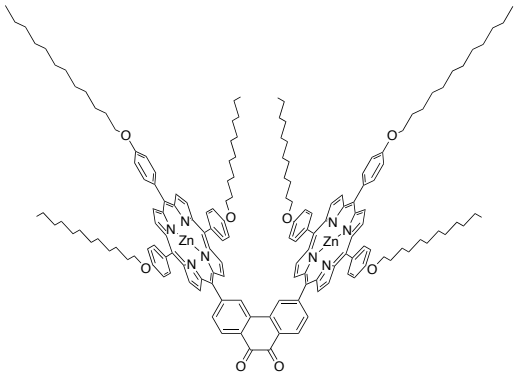

4.15

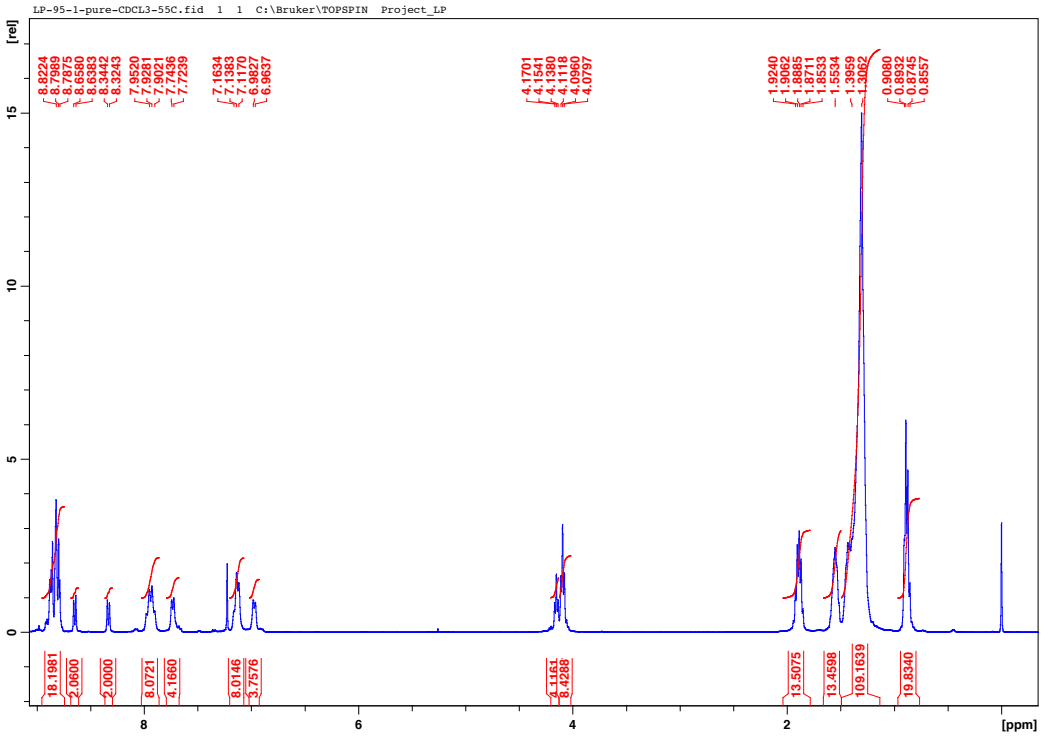

^{1}H NMR spectrum of **4.15** in $CDCl_3$ at 55°C.

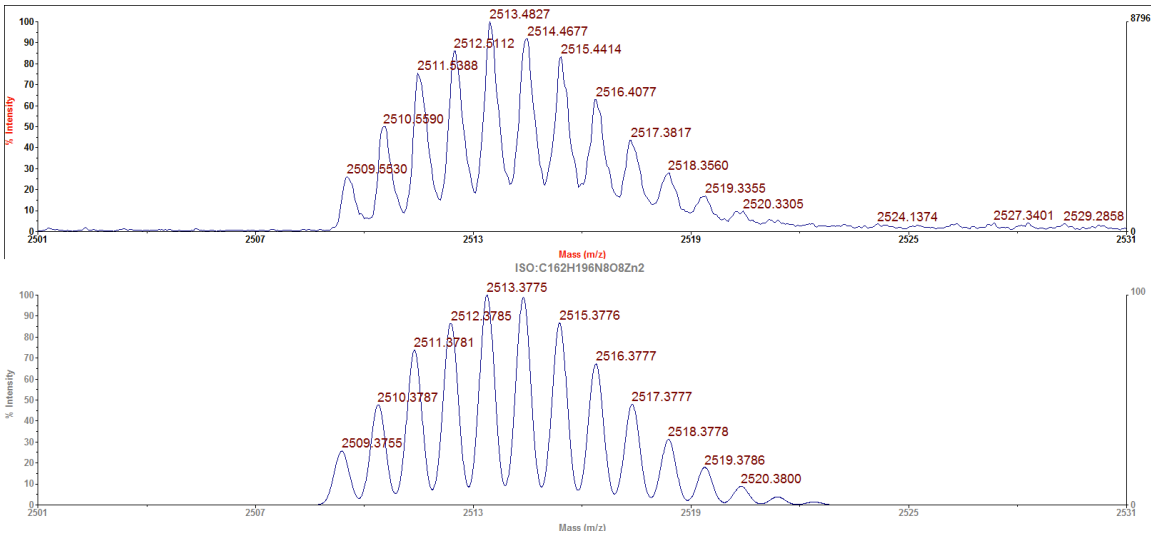

MALDI-TOF mass spectrum of **4.15**. The top trace is the observed spectrum and the bottom trace is the theoretical spectrum for molecular formula $C_{162}H_{196}N_8O_8Zn_2$ $[M]^+$.

4.16

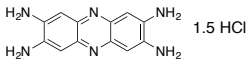

4.16

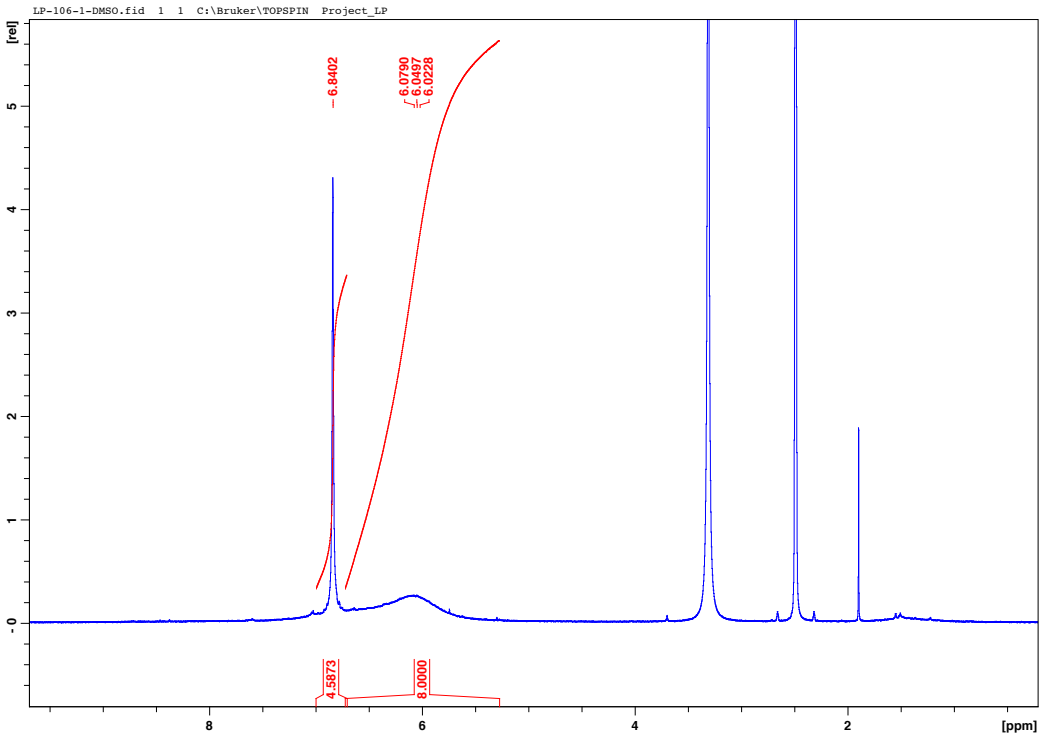

^{1}H NMR spectrum of **4.16** in DMSO at RT.

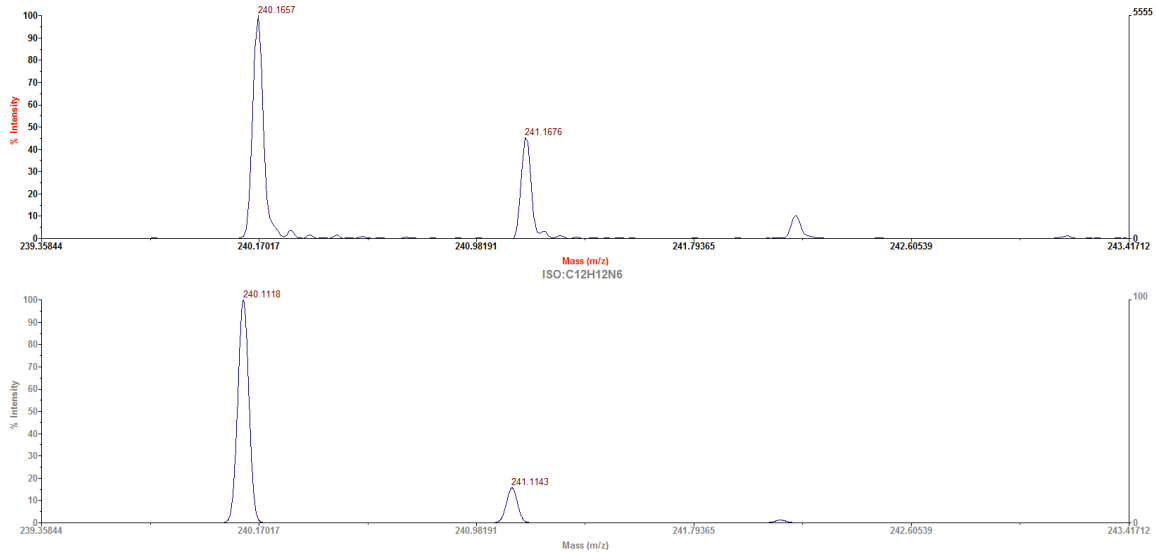

MALDI-TOF mass spectrum of **4.16**. The top trace is the observed spectrum and the bottom trace is the theoretical spectrum for molecular formula $C_{12}H_{12}N_6$ $[M]^+$.

4.17

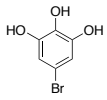

4.17

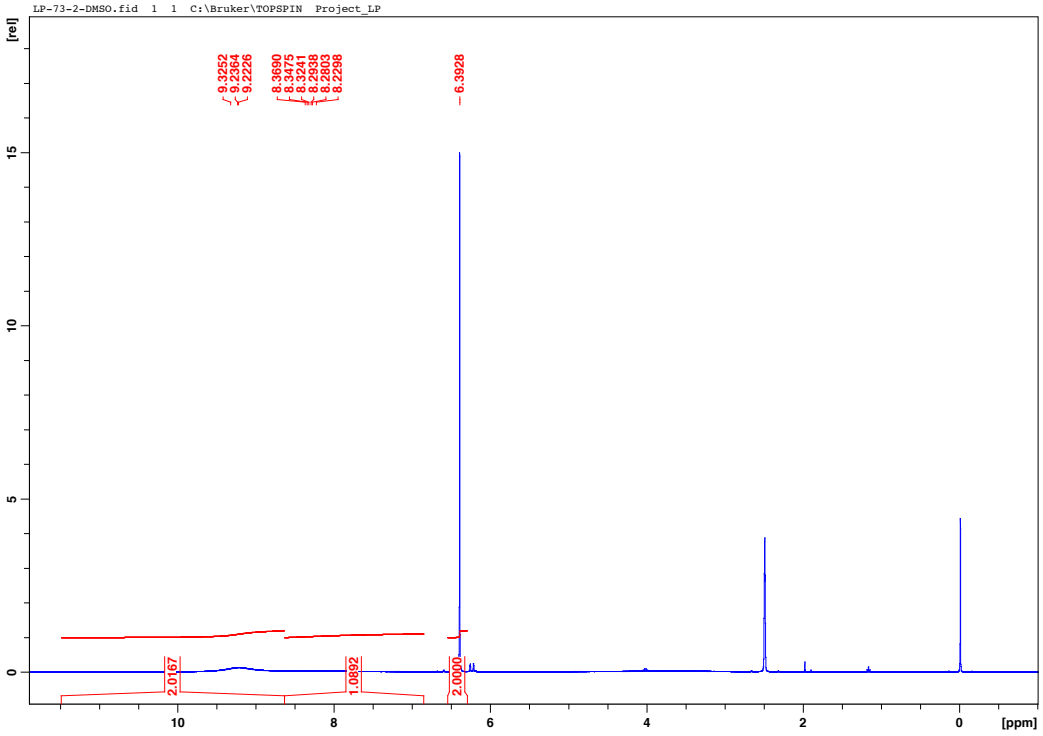

^{1}H NMR spectrum of **4.17** in DMSO-*d*6 at RT.

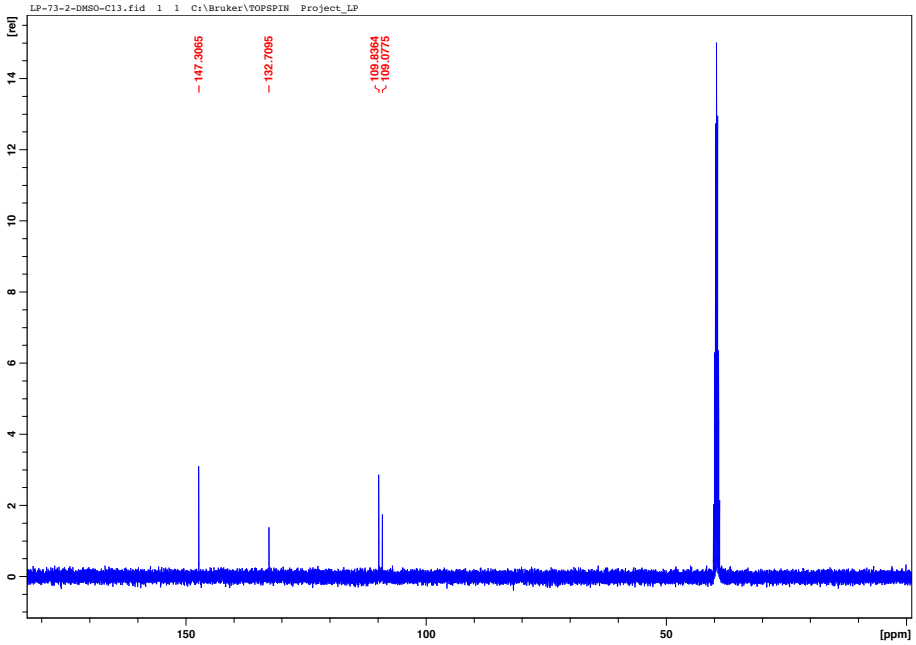

^{13}C NMR spectrum of **4.17** in DMSO-*d*6 at RT.

4.18

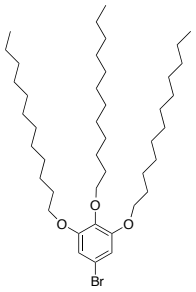

4.18

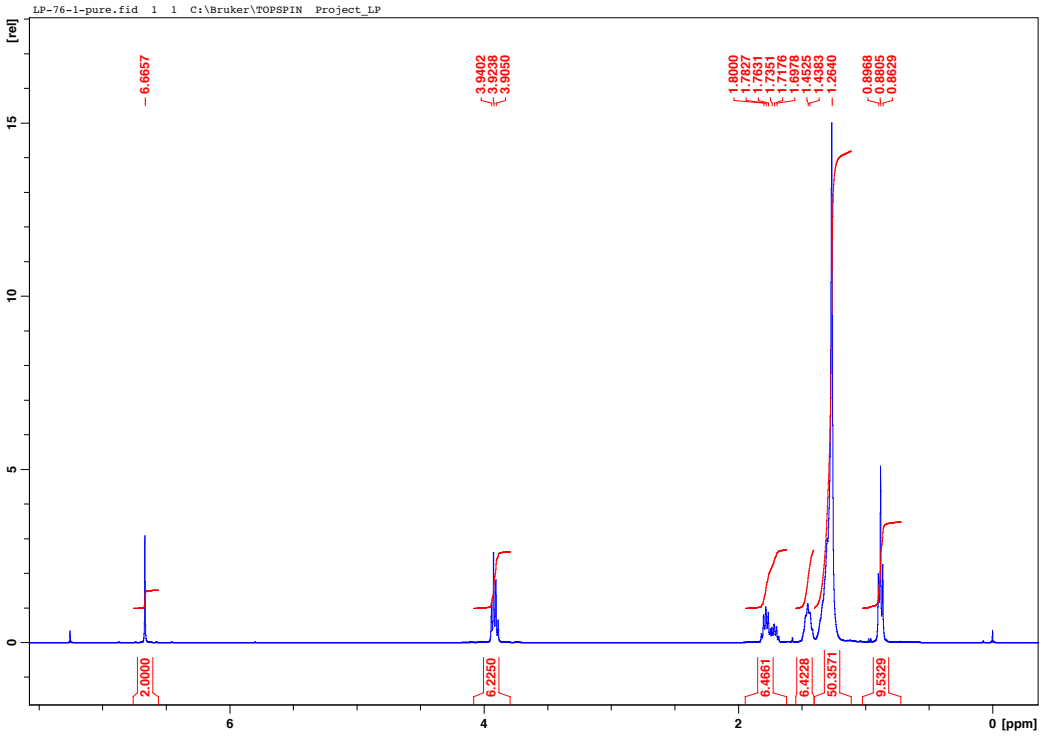

^{1}H NMR spectrum of **4.18** in $CDCl_3$ at RT.

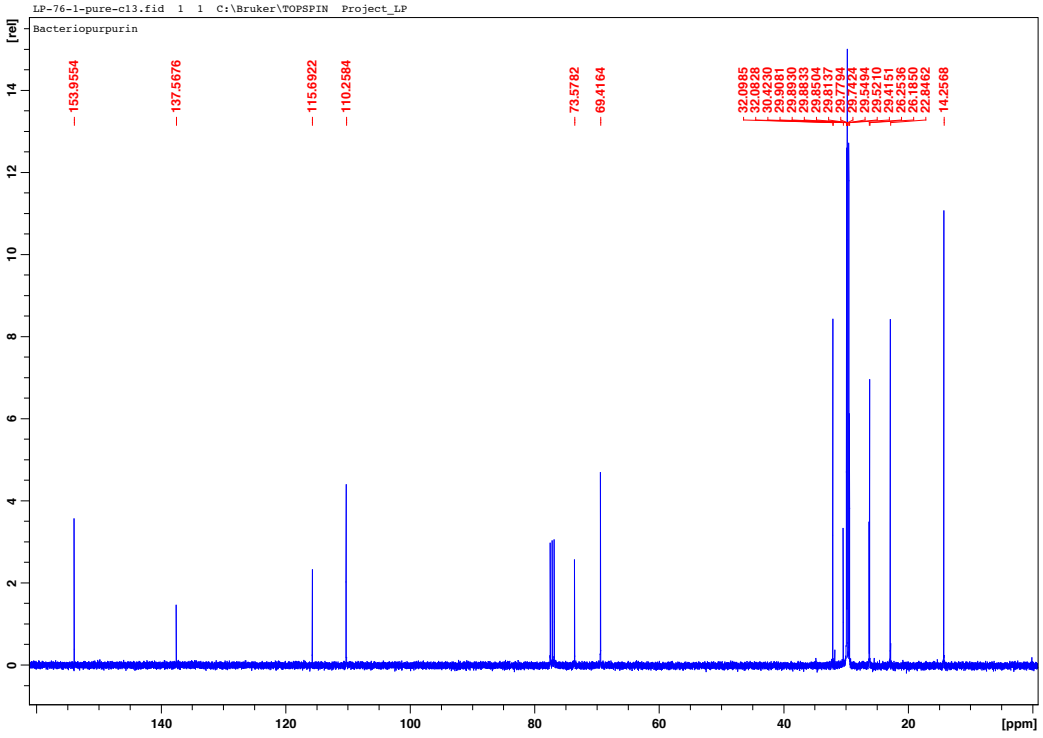

^{13}C NMR spectrum of **4.18** in $CDCl_3$ at RT.

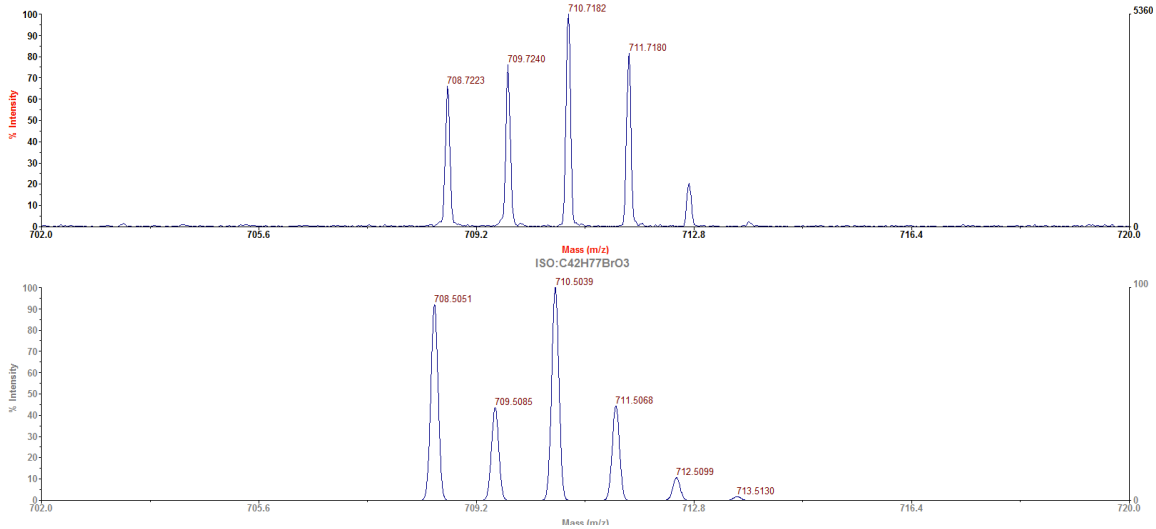

MALDI-TOF mass spectrum of **4.18**. The top trace is the observed spectrum and the bottom trace is the theoretical spectrum form molecular formula $C_{42}H_{77}BrO_3$ $[M]^+$.

4.19

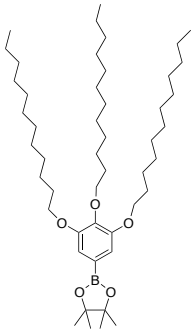

4.19

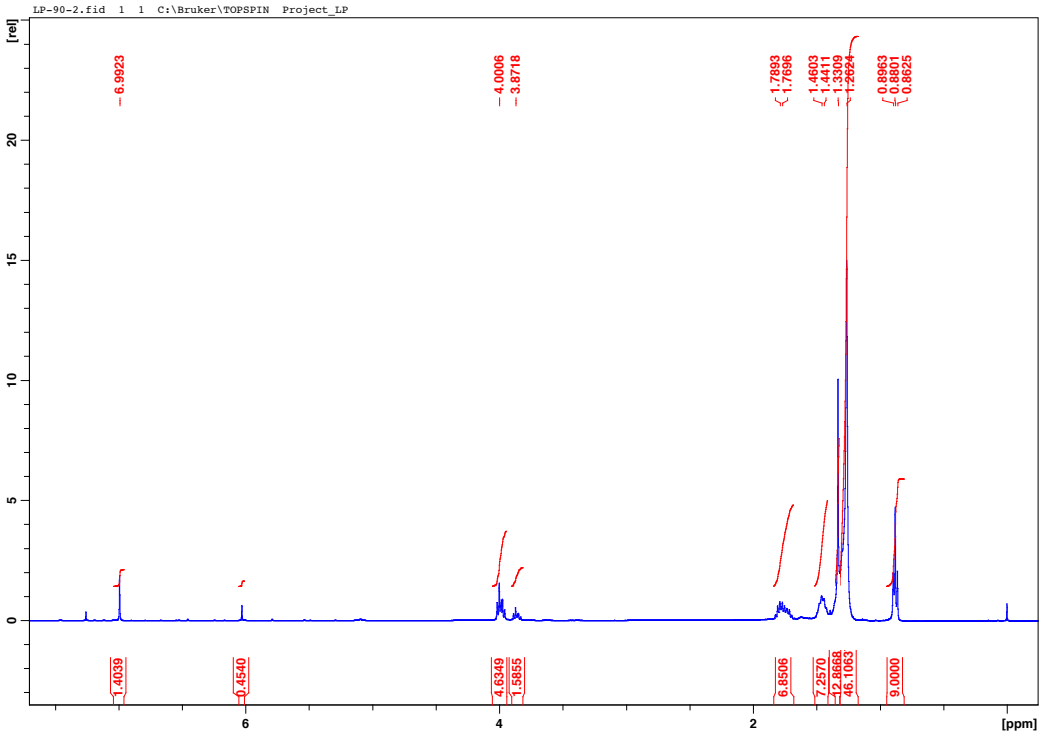

^{1}H NMR spectrum of **4.19** in $CDCl_3$ at RT.

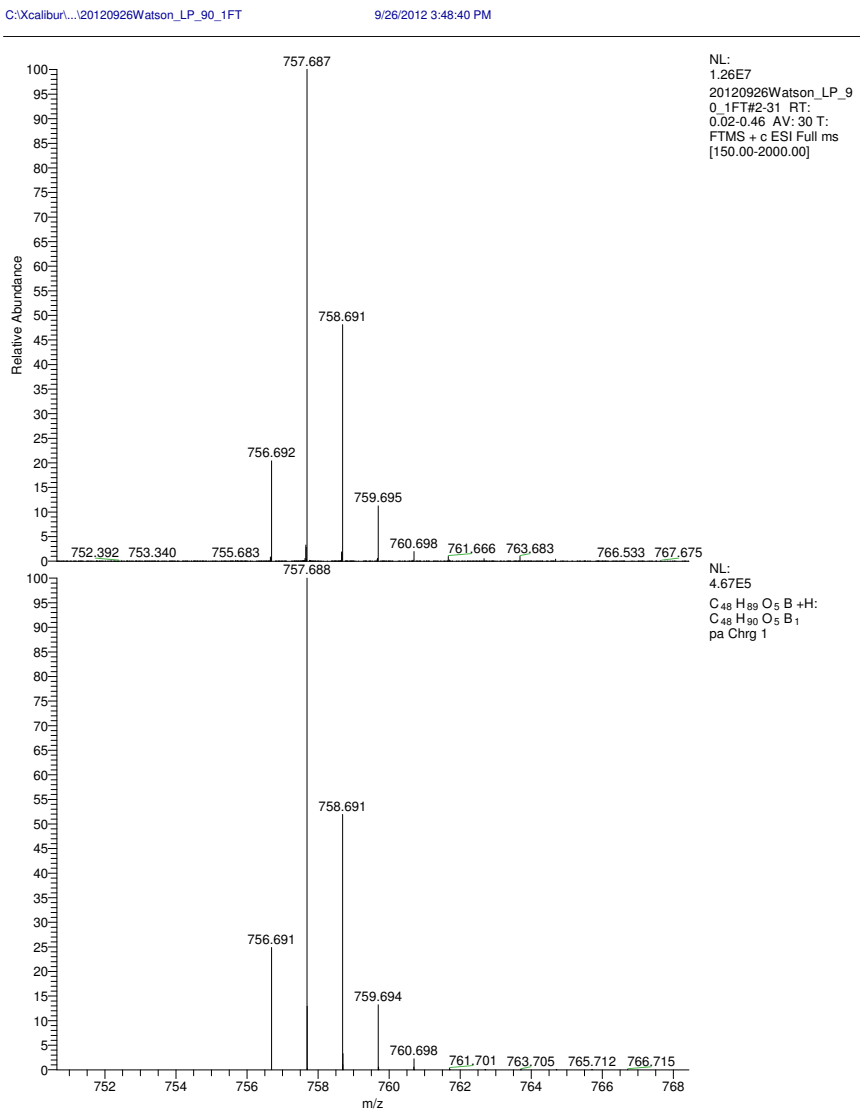

High-Resolution MS of **4.19**. The top trace is the observed spectrum and the bottom trace is the theoretical spectrum form molecular formula $C_{48}H_{90}O_8B$ $[M+H]^+$.

4.20

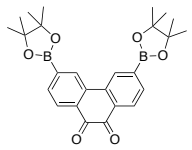

4.20

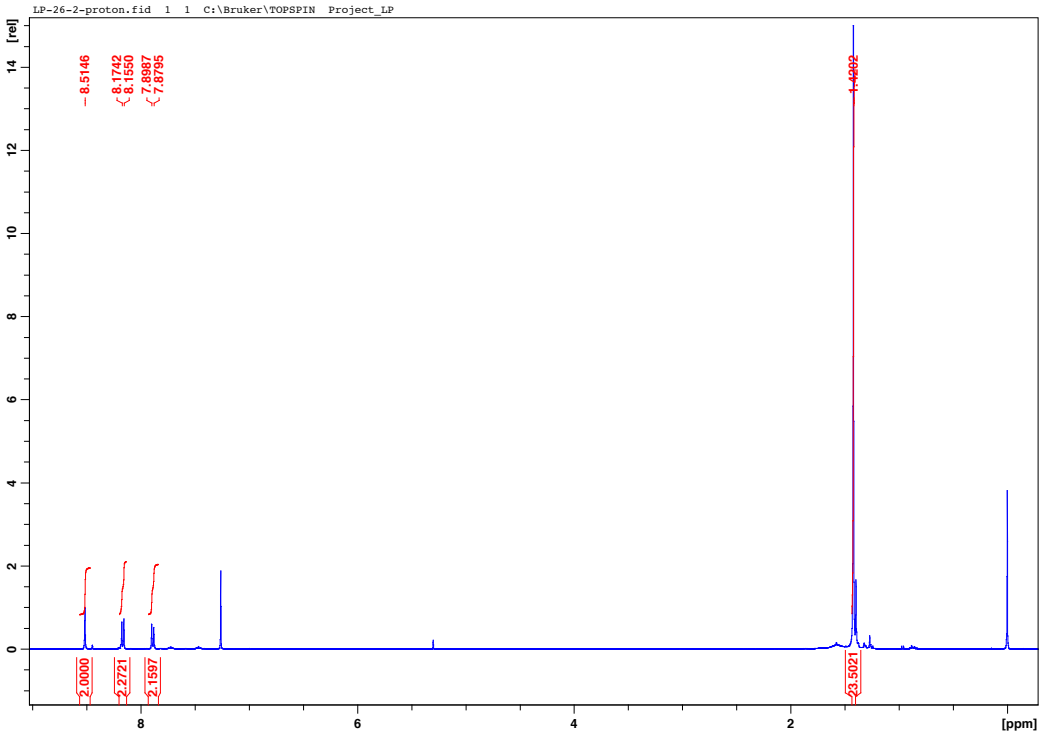

^{1}H NMR spectrum of **4.20** in $CDCl_3$ at RT.

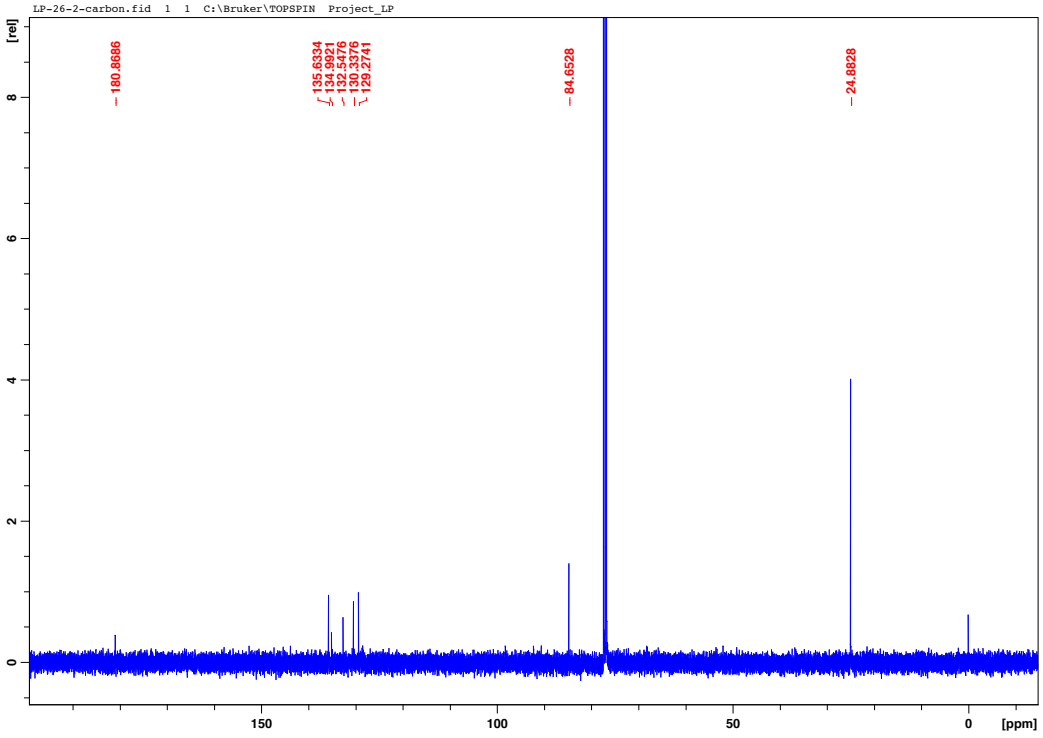

^{13}C NMR spectrum of **4.20** in $CDCl_3$ at RT.

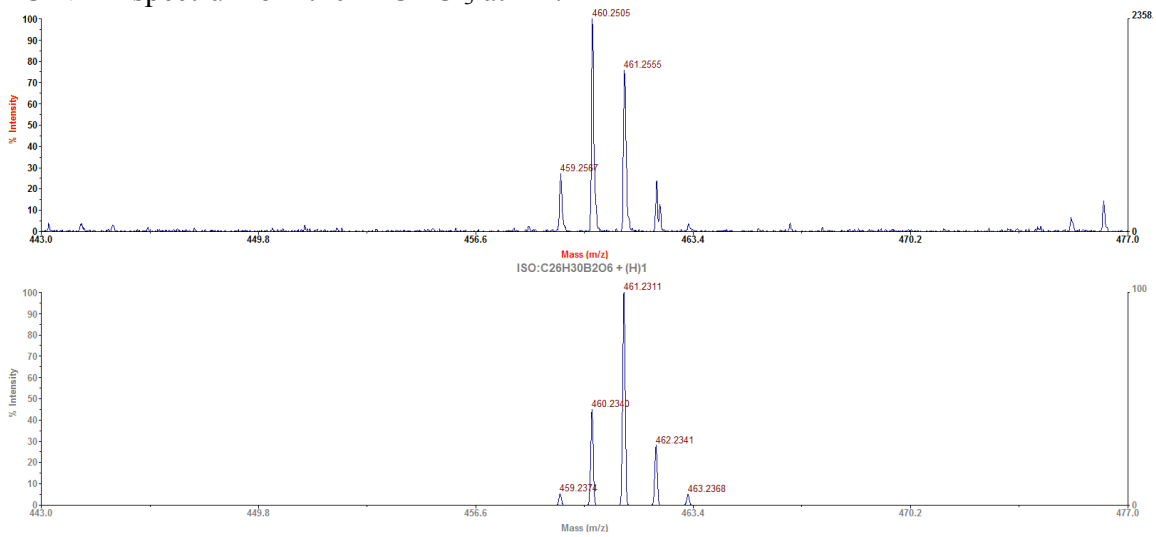

MALDI-TOF mass spectrum of **4.20**. The top trace is the observed spectrum and the bottom trace is the theoretical spectrum for molecular formula $C_{26}H_{31}B_2O_6$ $[M+H]^+$.

4.21

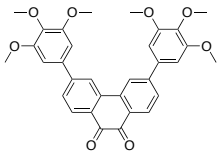

4.21

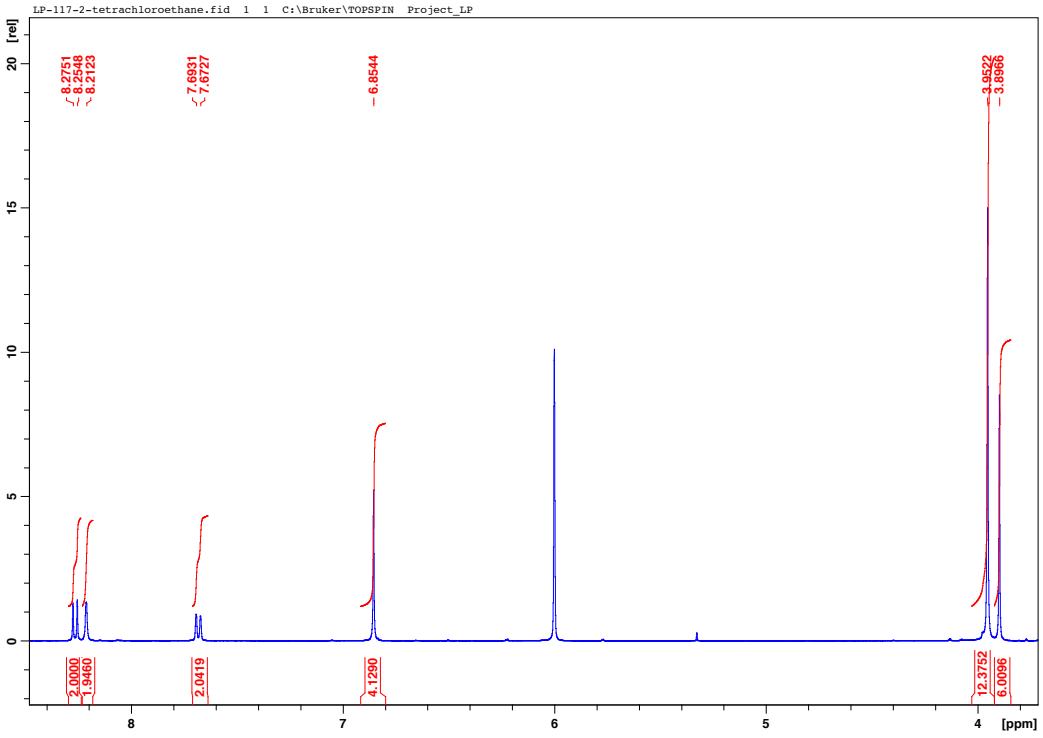

^{1}H NMR spectrum of **4.21** in $CDCl_3$ at RT.

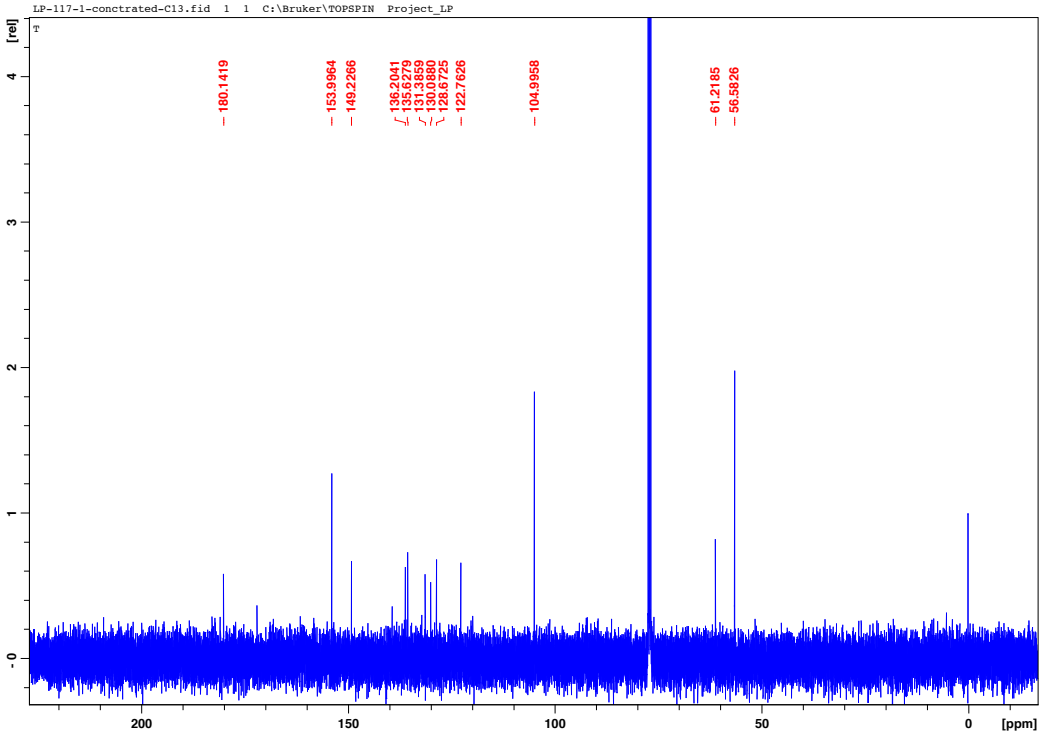

^{13}C NMR spectrum of **4.21** in $CDCl_3$ at RT.

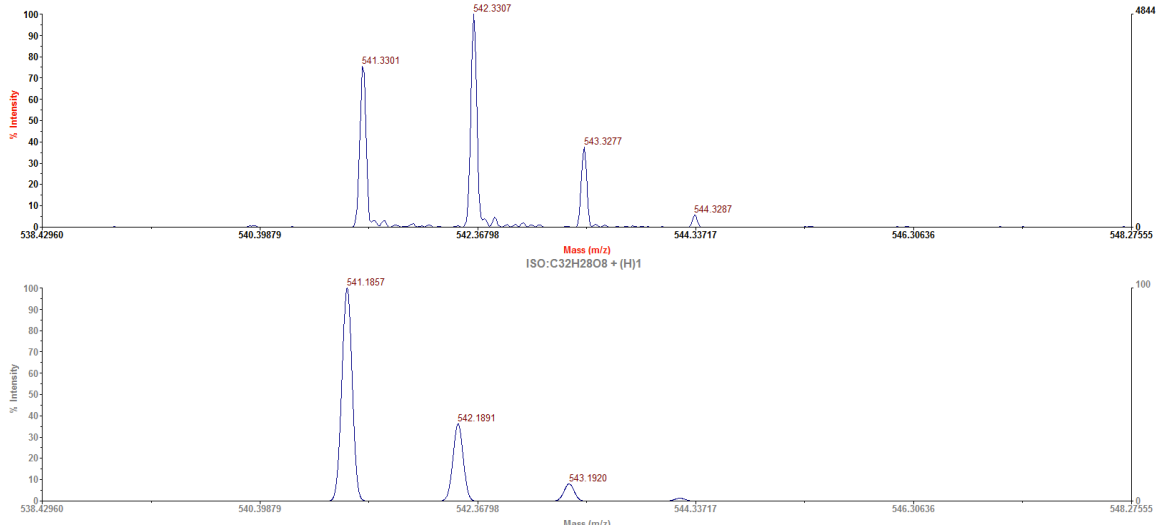

MALDI-TOF mass spectrum of **4.21**. The top trace is the observed spectrum and the bottom trace is the theoretical spectrum for molecular formula $C_{32}H_{29}N_4O_8$ $[M+H]^+$.

4.25

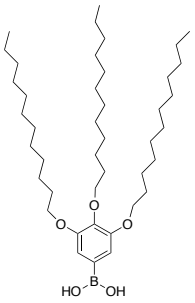

4.25

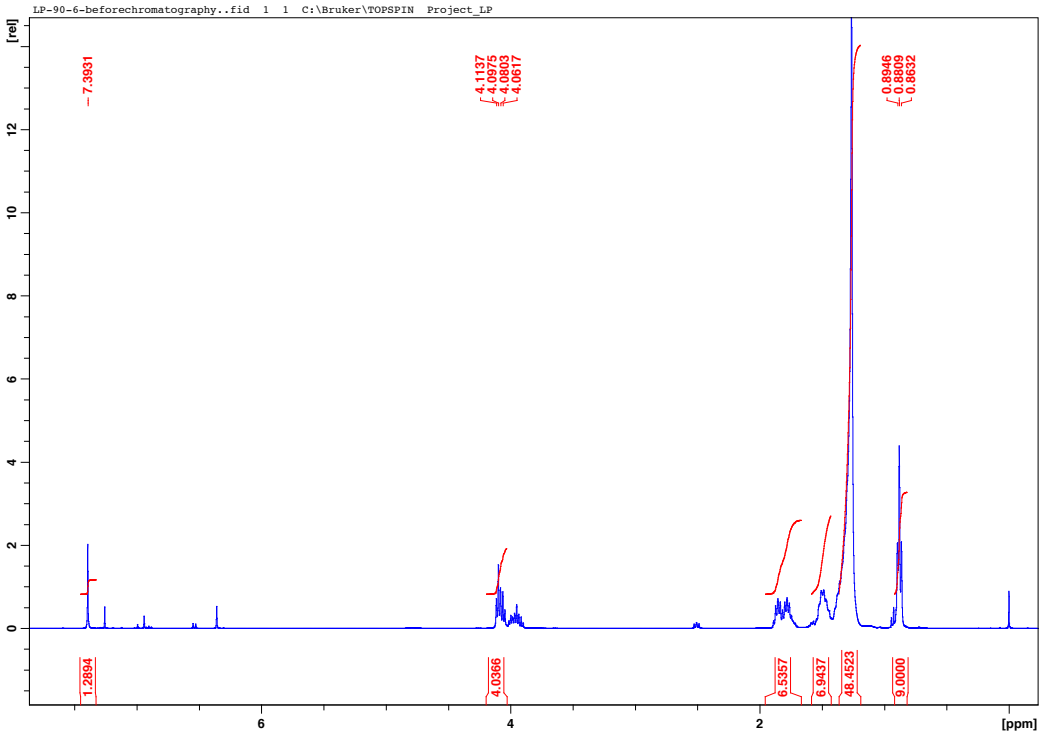

^{1}H NMR spectrum of **4.25** in $CDCl_3$ at RT.

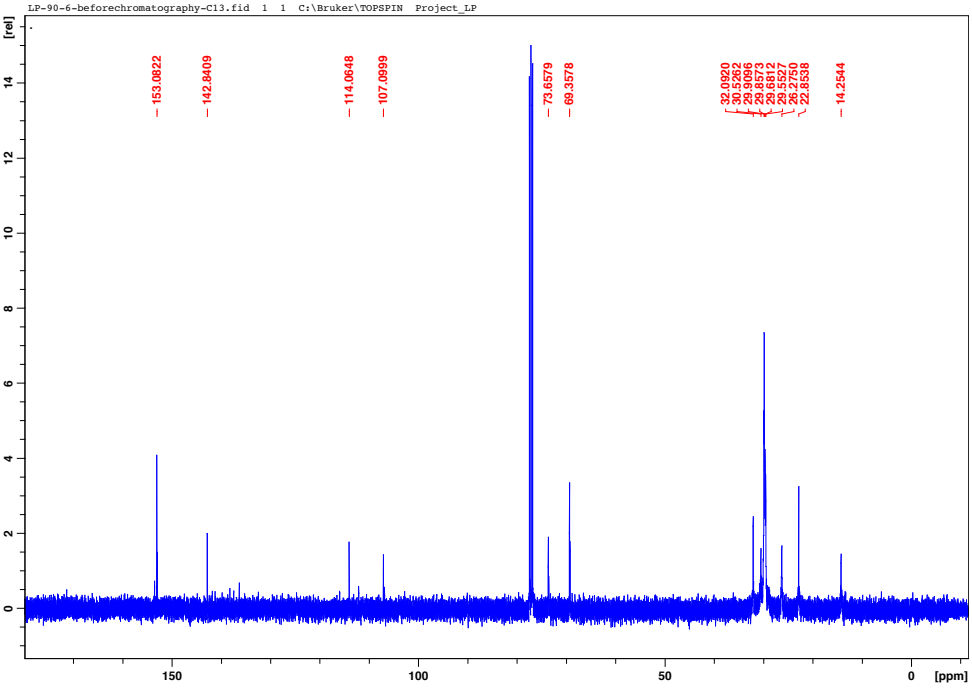

^{13}C NMR spectrum of **4.25** in $CDCl_3$ at RT.

4.26

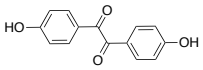

4.26

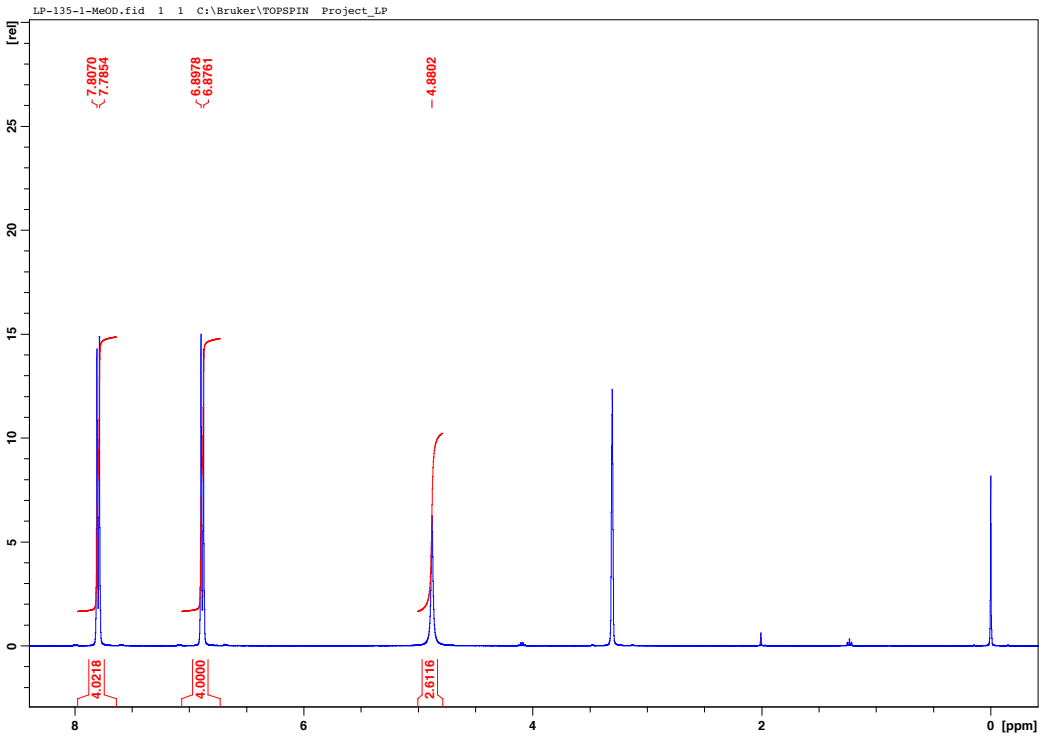

^{1}H NMR spectrum of **4.26** in MeOD at RT.

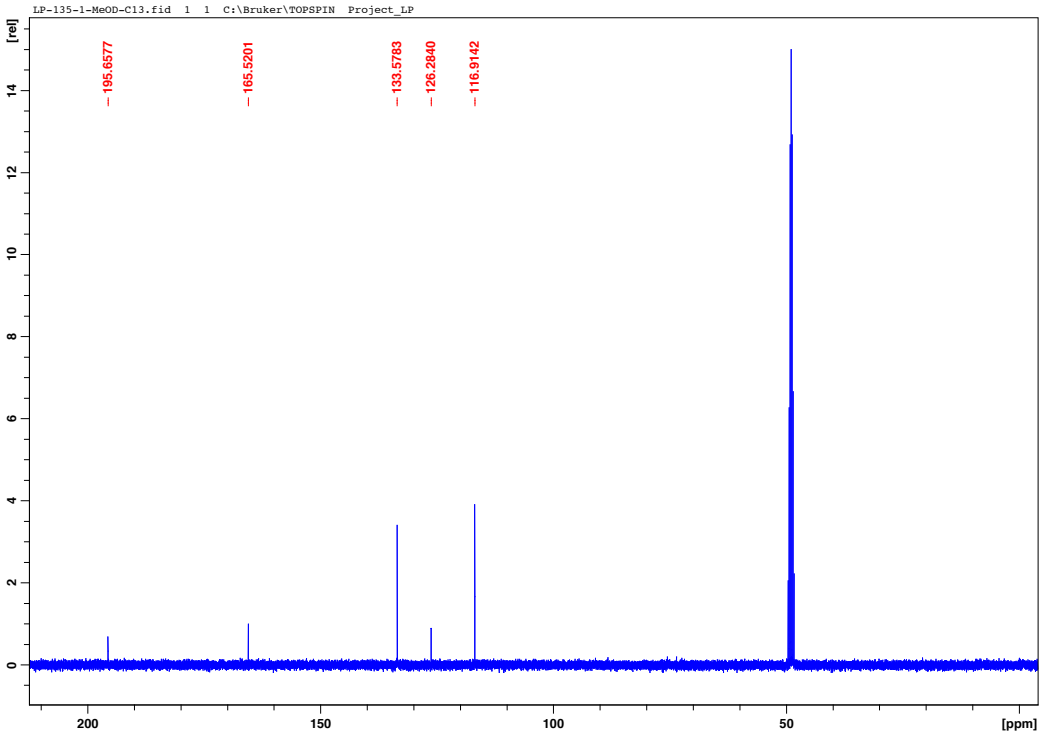

^{13}C NMR spectrum of **4.26** in MeOD at RT.

4.27

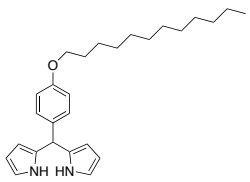

4.27

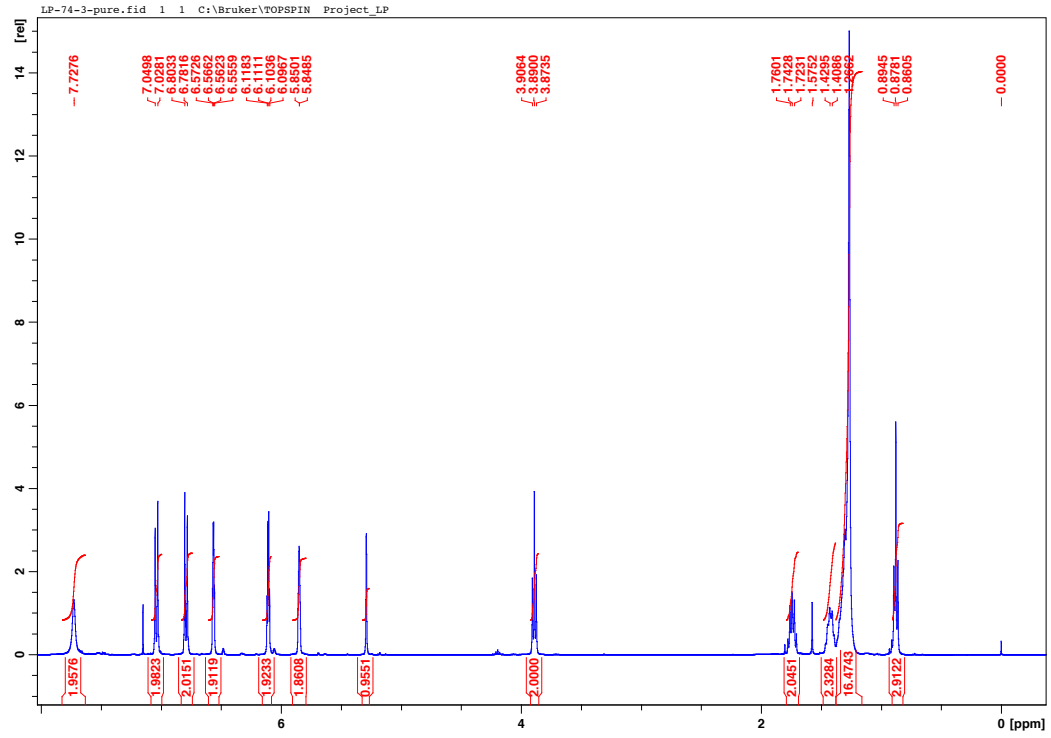

^{1}H NMR spectrum of **4.27** in $CDCl_3$ at RT.

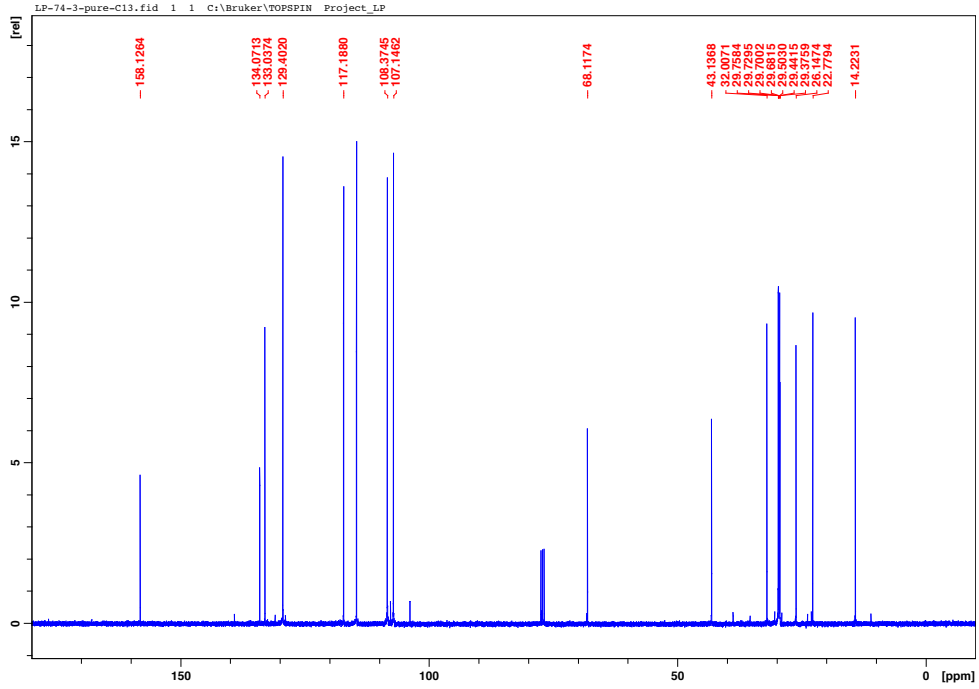

^{13}C NMR spectrum of **4.27** in $CDCl_3$ at RT.

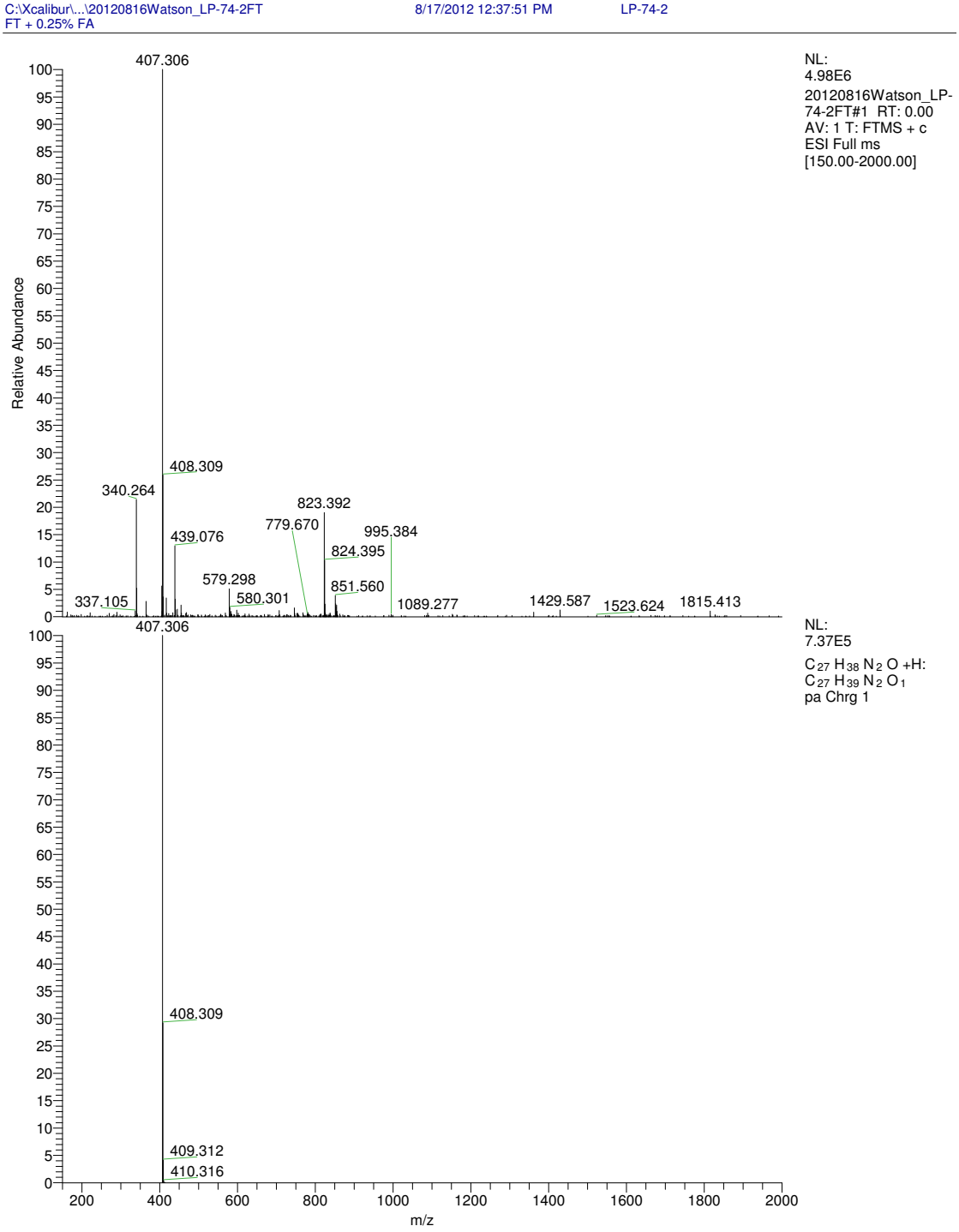

High-Resolution mass spectrum of **4.27**. The top trace is the observed spectrum and the bottom trace is the theoretical spectrum for molecular formula $C_{27}H_{39}N_2O_1$ $[M+H]^+$.

4.28

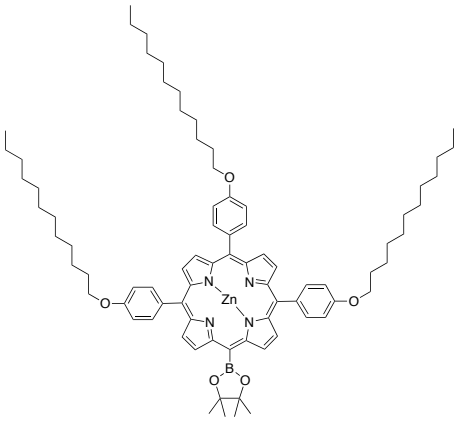

4.28

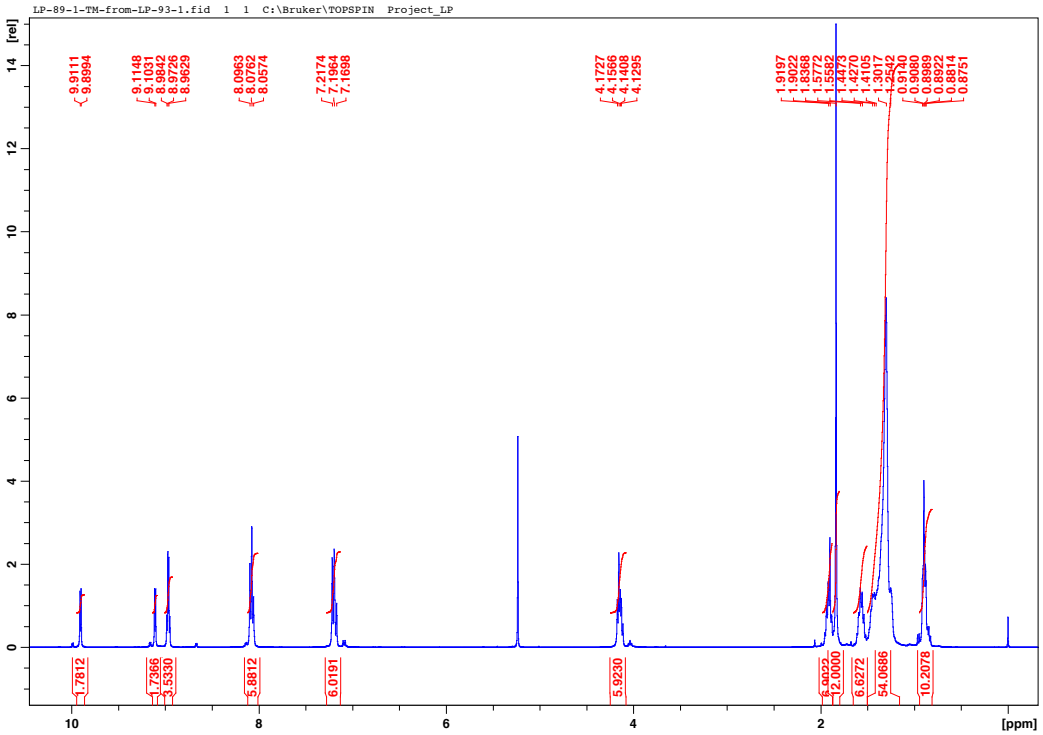

^{1}H NMR spectrum of **4.28** in $CDCl_3$ at RT.

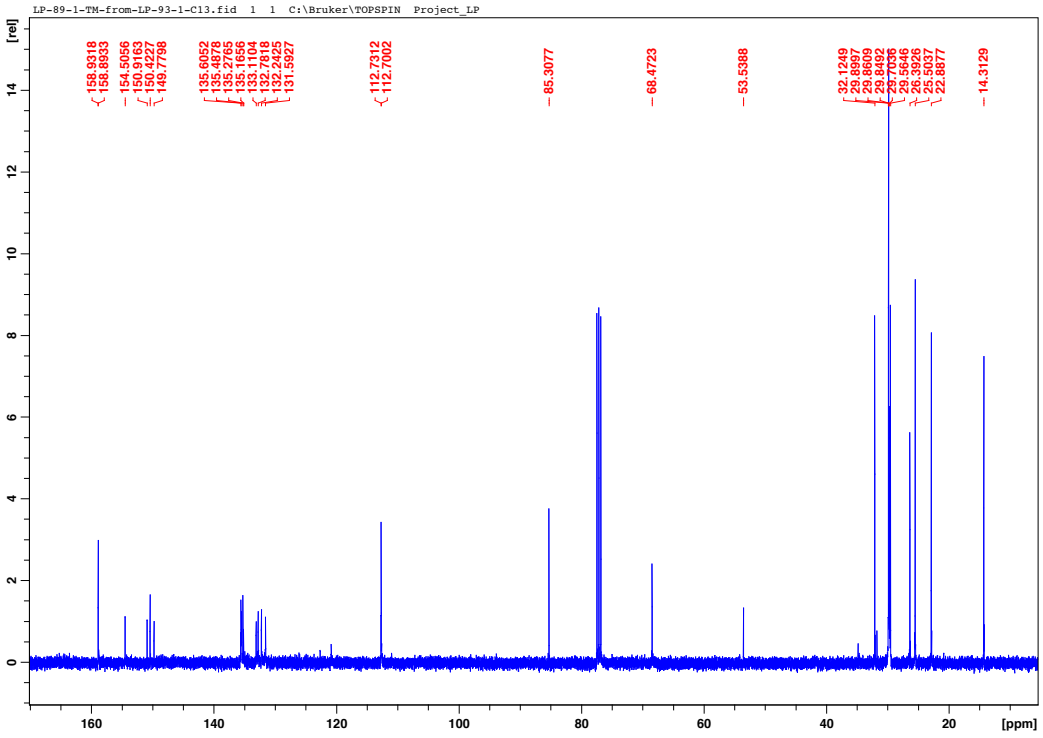

^{13}C NMR spectrum of **4.28** in $CDCl_3$ at RT.

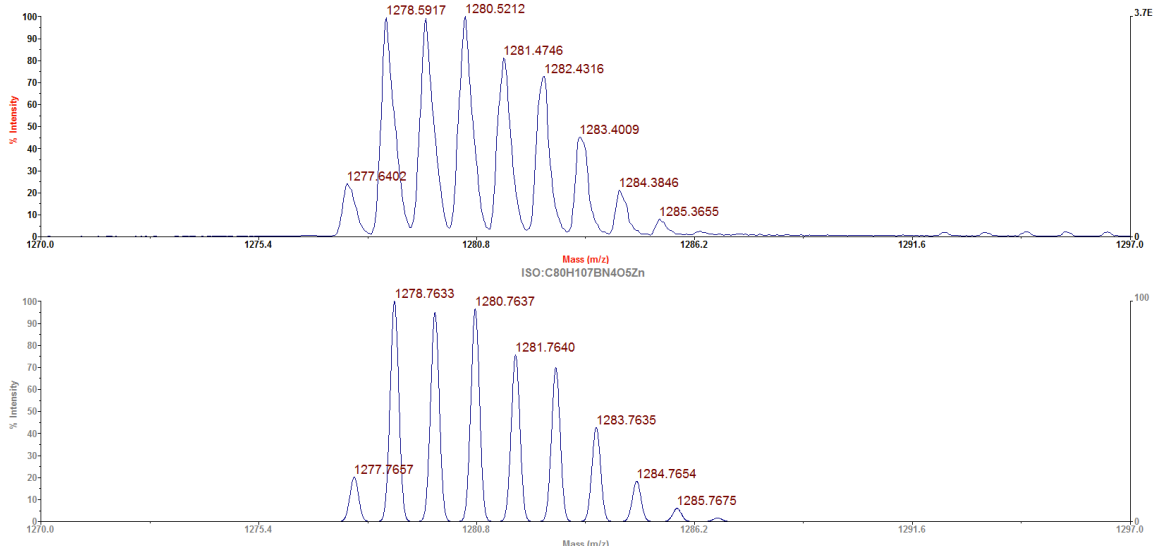

MALDI-TOF mass spectrum of **4.28**. The top trace is the observed spectrum and the bottom trace is the theoretical spectrum for molecular formula $C_{80}H_{107}BN_4O_5Zn$ $[M]^+$.

4.29

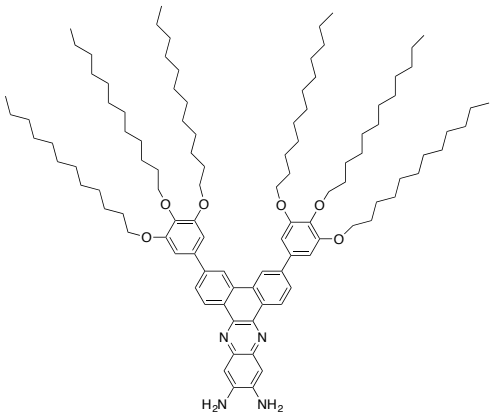

4.29

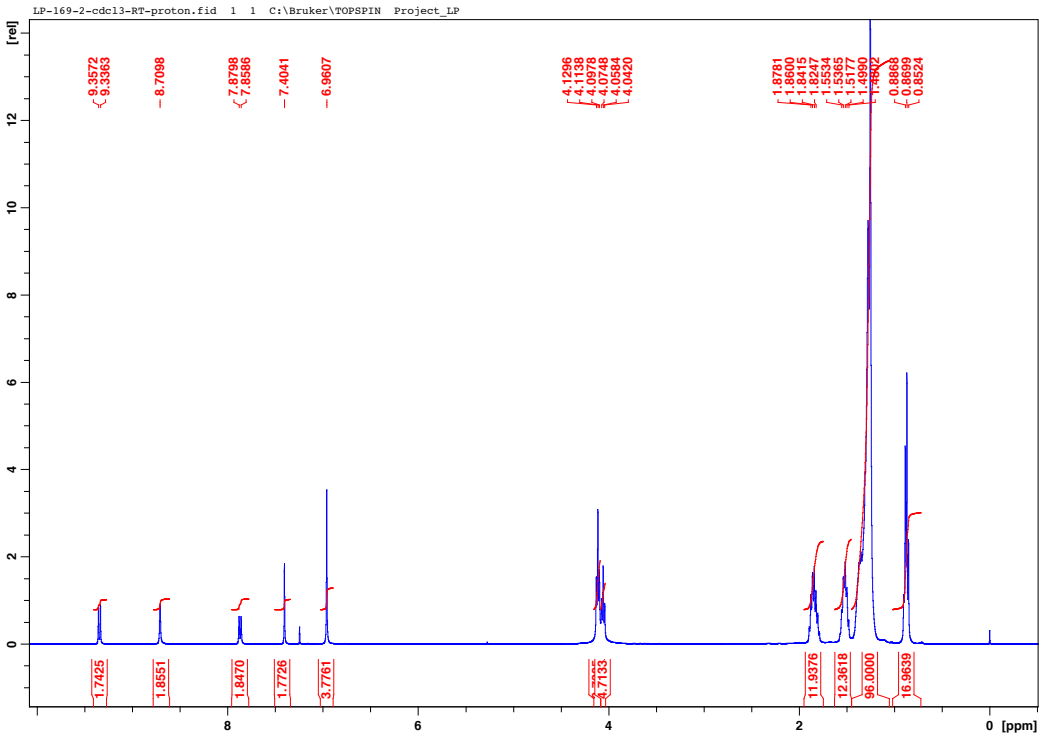

^{1}H NMR spectrum of **4.29** in $CDCl_3$ at RT.

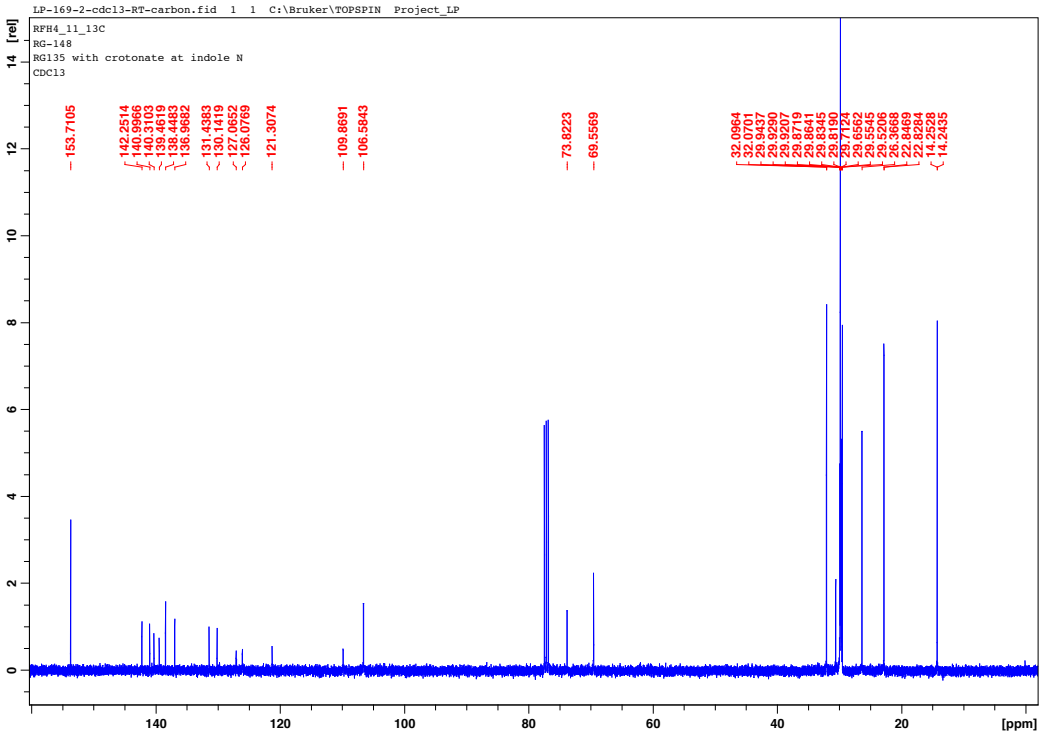

^{13}C NMR spectrum of **4.29** in $CDCl_3$ at RT.

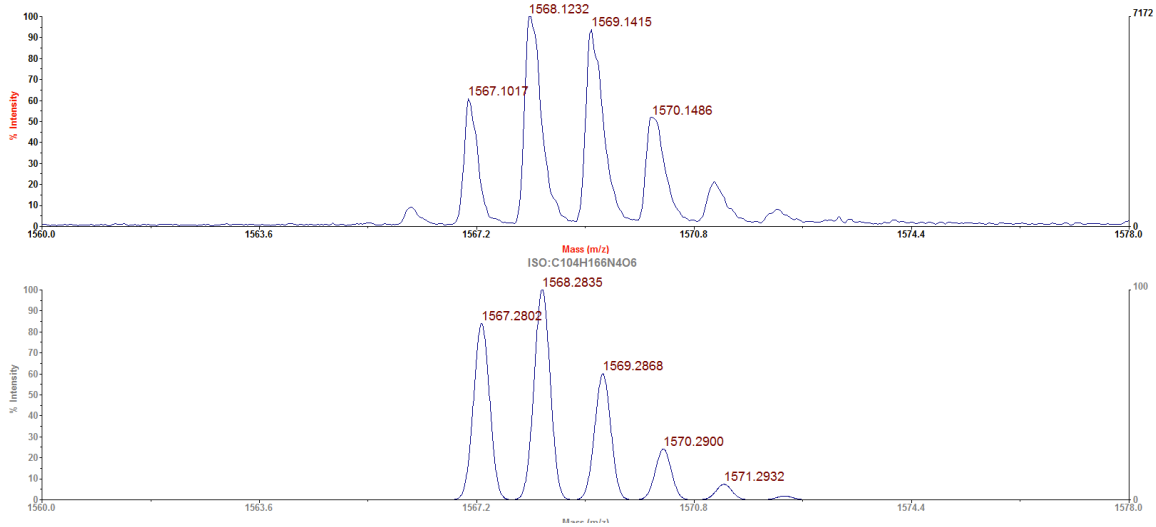

MALDI-TOF mass spectrum of **4.29**. The top trace is the observed spectrum and the bottom trace is the theoretical spectrum for molecular formula $C_{104}H_{166}N_4O_6$ $[M]^+$.

4.30

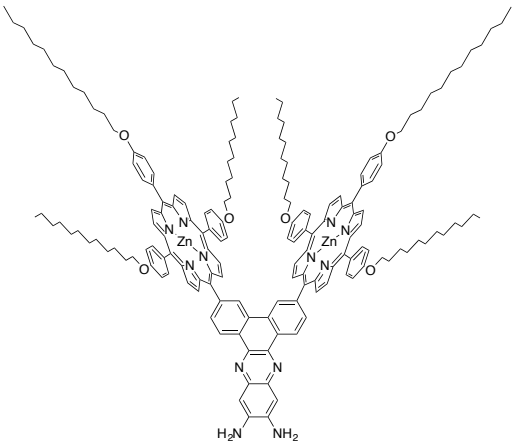

4.30

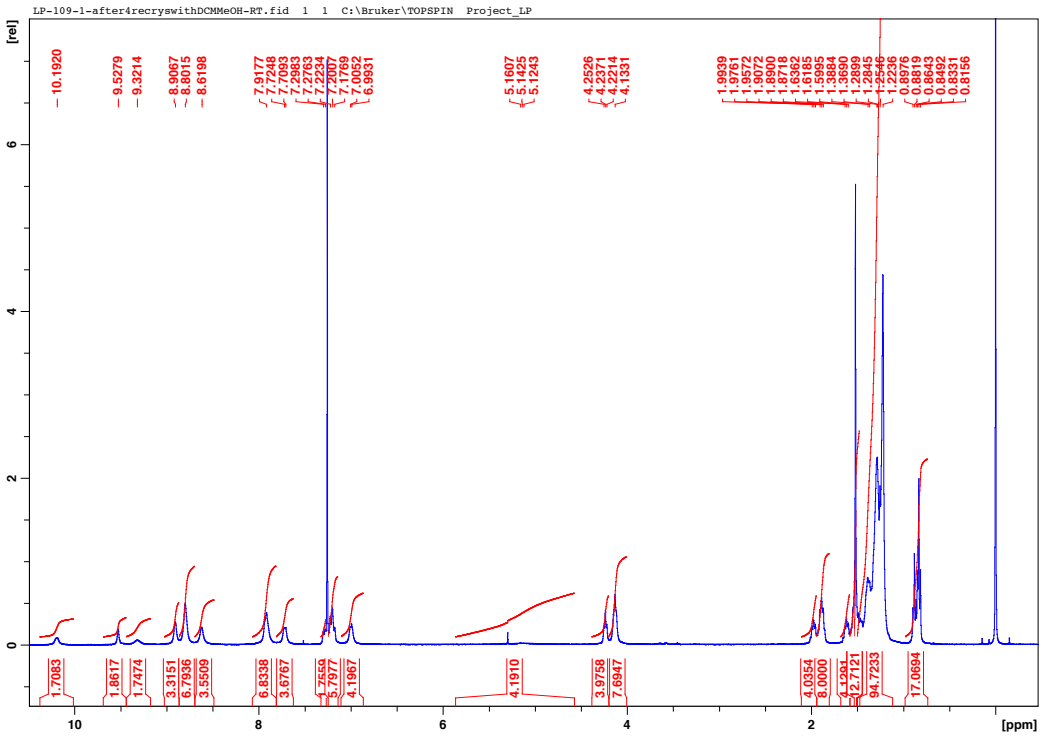

^{1}H NMR spectrum of **4.30** in $CDCl_3$ at RT.

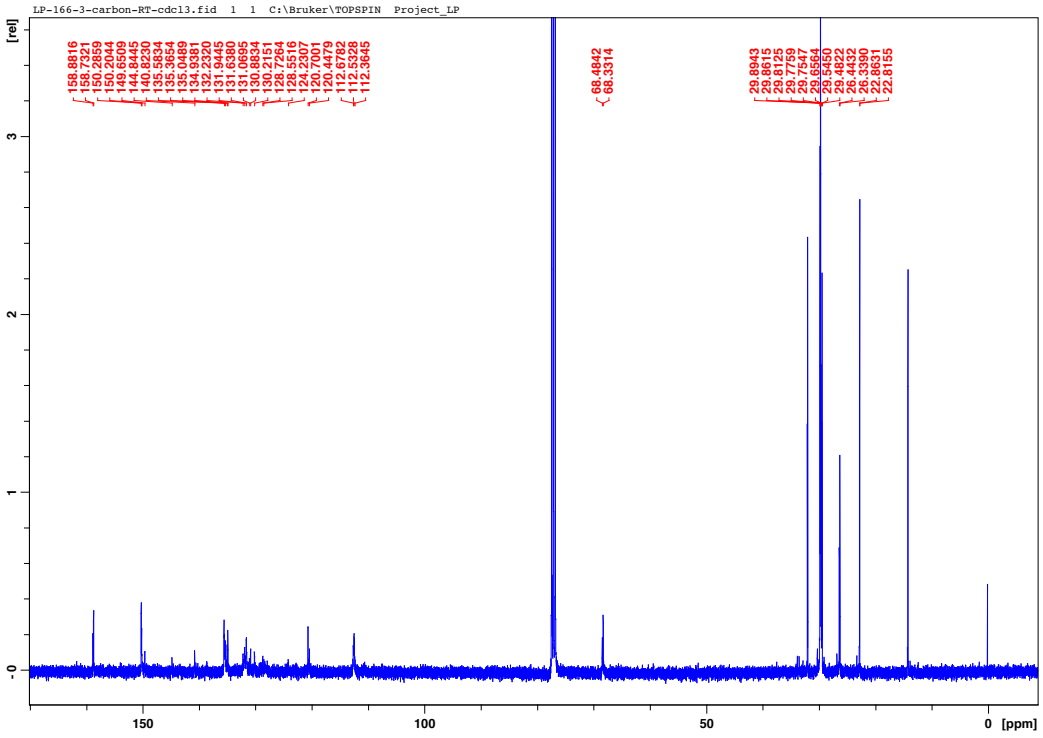

^{13}C NMR spectrum of **4.30** in $CDCl_3$ at RT.

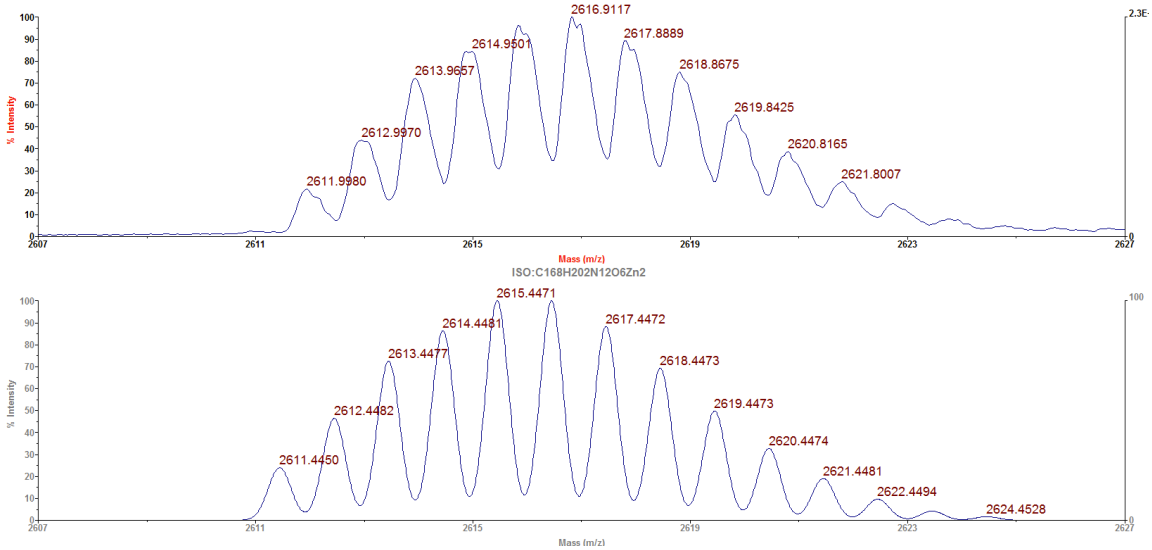

MALDI-TOF mass spectrum of **4.30**. The top trace is the observed spectrum and the bottom trace is the theoretical spectrum for molecular formula $C_{168}H_{202}N_{12}O_6Zn_2$ $[M]^+$.

4.31

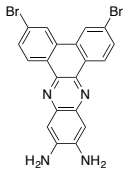

4.31

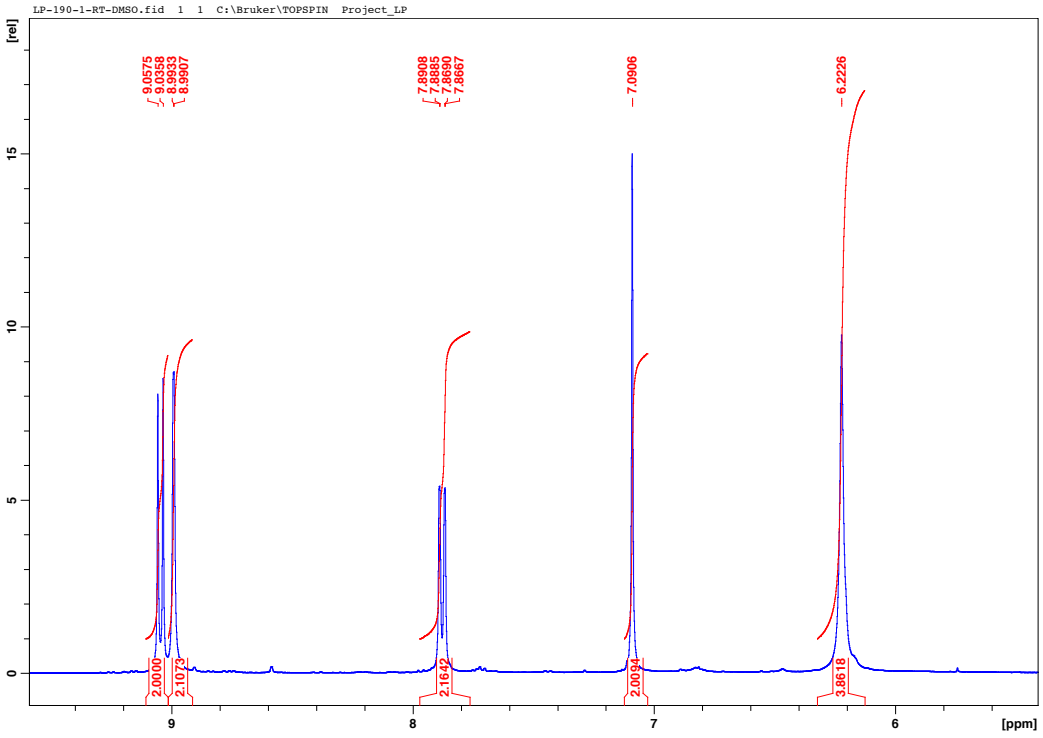

^{1}H NMR spectrum of **4.31** in DMSO-*d*6 at RT.

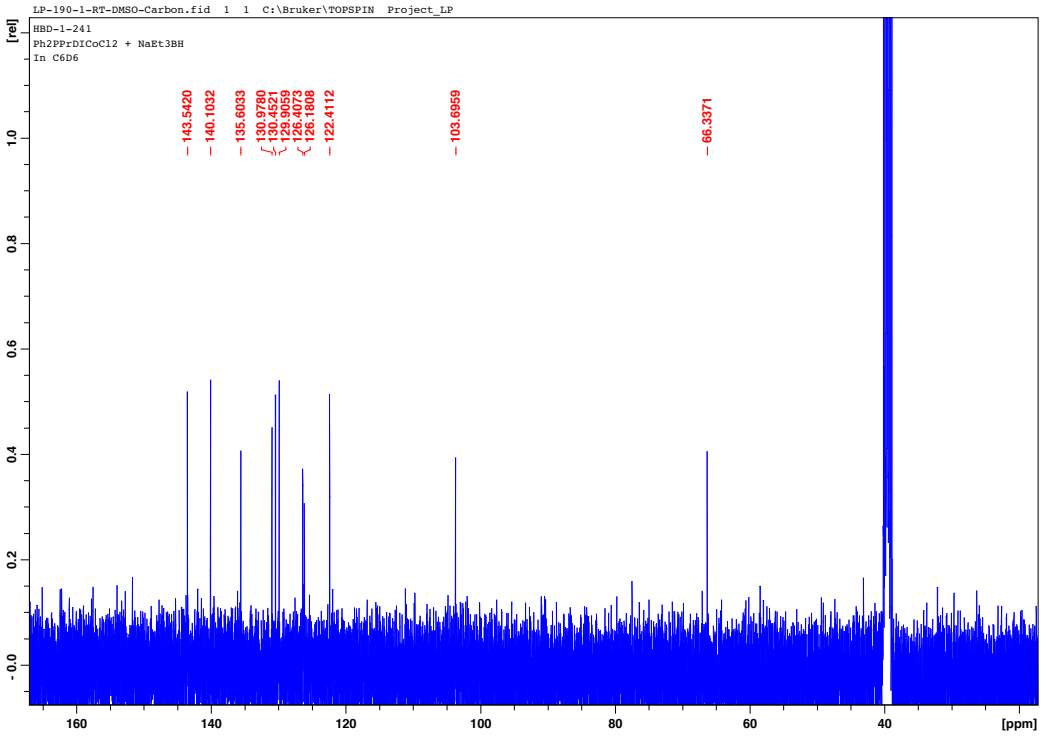

^{13}C NMR spectrum of **4.31** in DMSO-*d6* at RT.

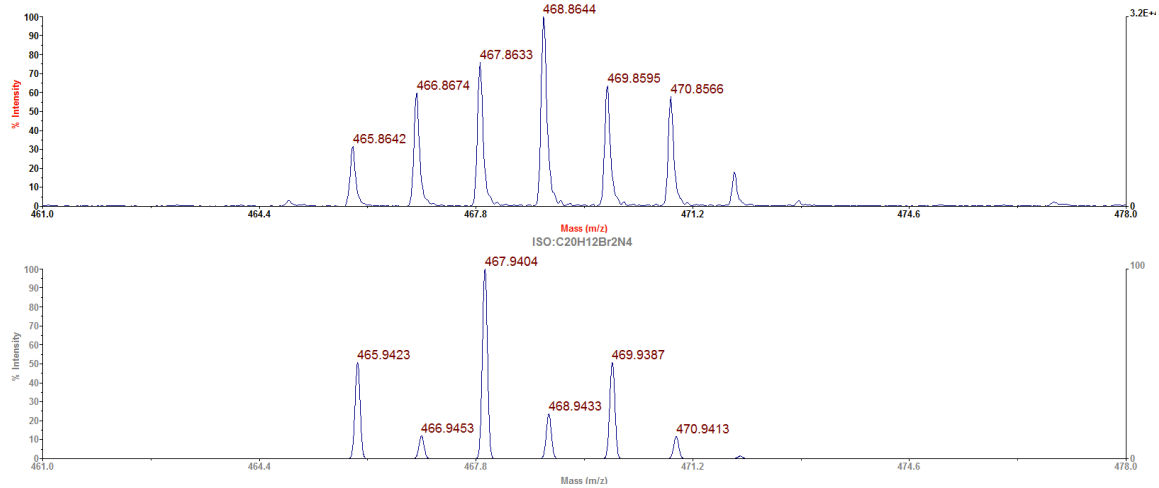

MALDI-TOF MS spectrum of **4.31**. The top trace is the observed spectrum and the bottom trace is the theoretical spectrum form molecular formula $C_{20}H1_2N_4$ $[M]^+$.

4.32

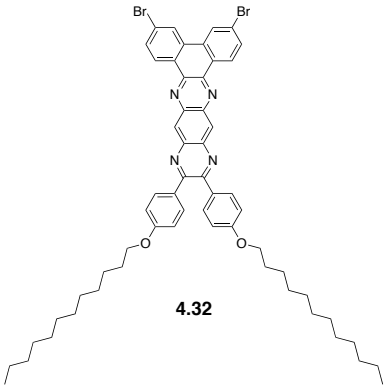

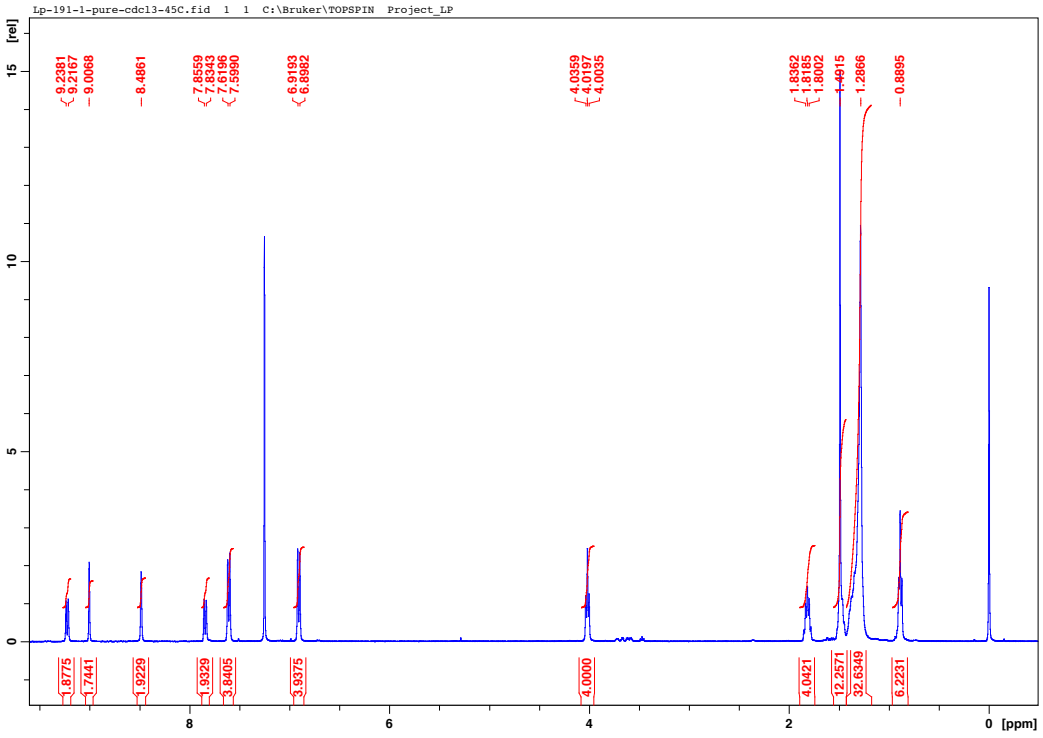

^{1}H NMR spectrum of **4.32** in $CDCl_3$ at 45^{o}C.

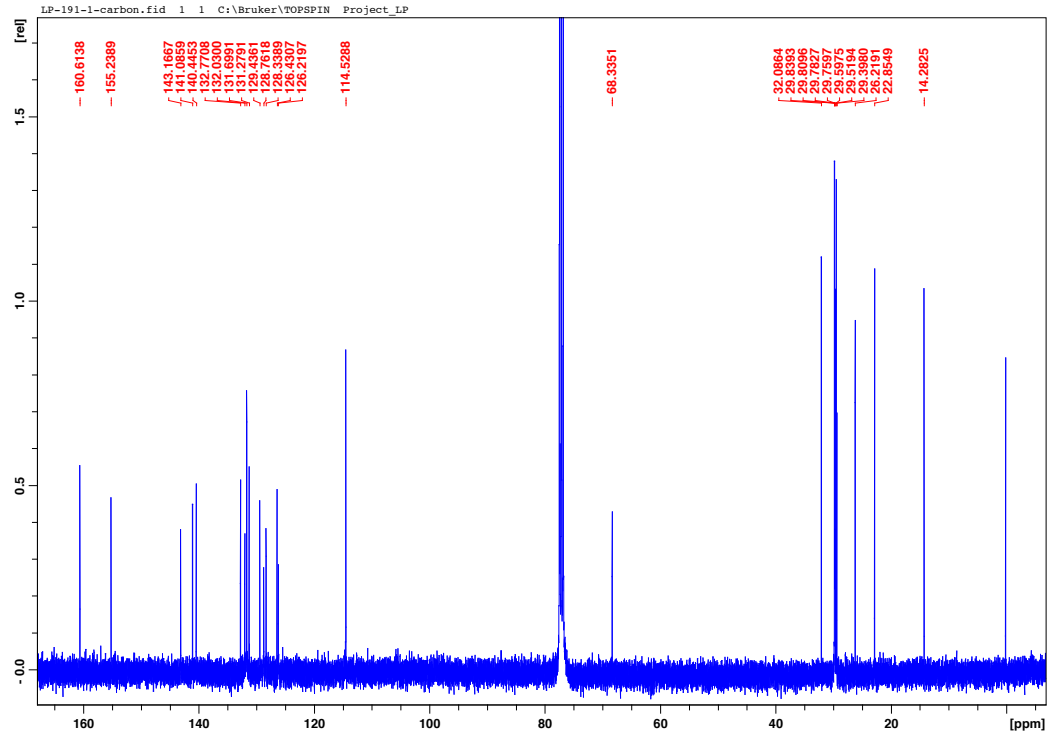

^{13}C NMR spectrum of **4.32** in $CDCl_3$ at RT.

4.33

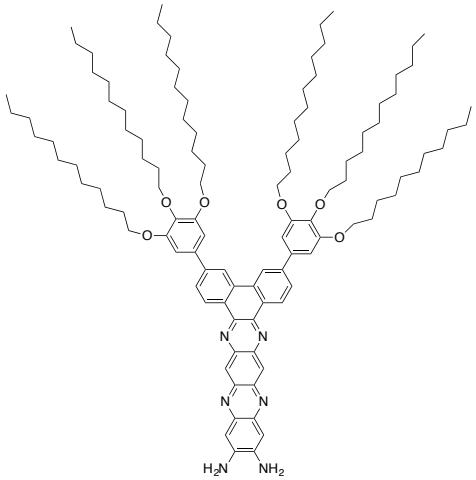

4.33

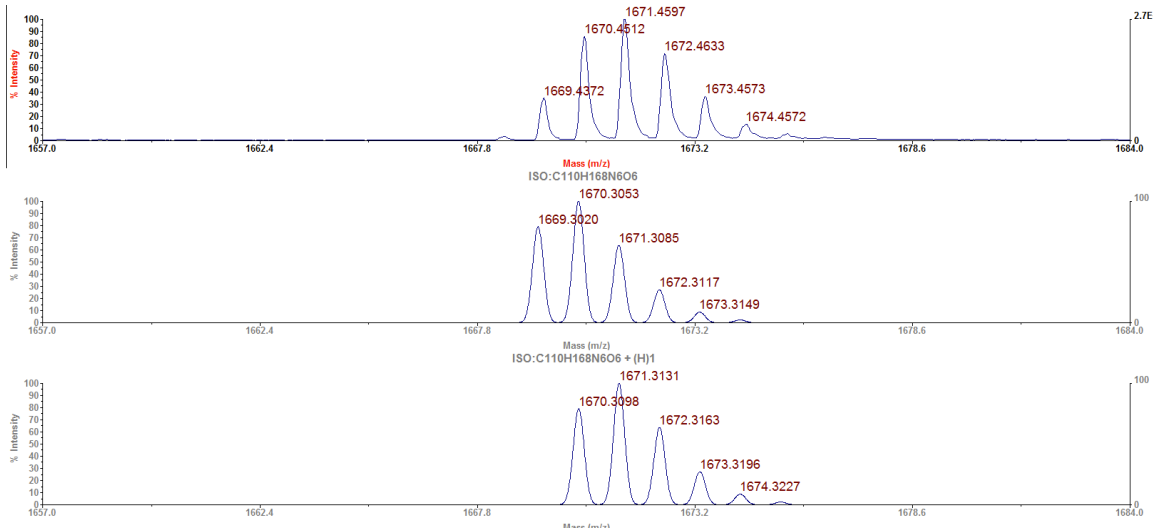

MALDI-TOF mass spectrum of **4.33**. The top trace is the observed spectrum and the bottom two traces are the theoretical spectra for molecular formula $C_{110}H_{168}N_6O_6$ $[M]^+$ and $C_{110}H_{169}N_6O_6$ $[M+H]^+$.

4.34

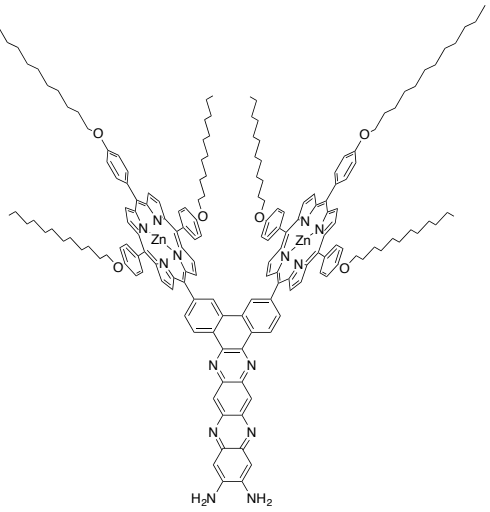

4.34

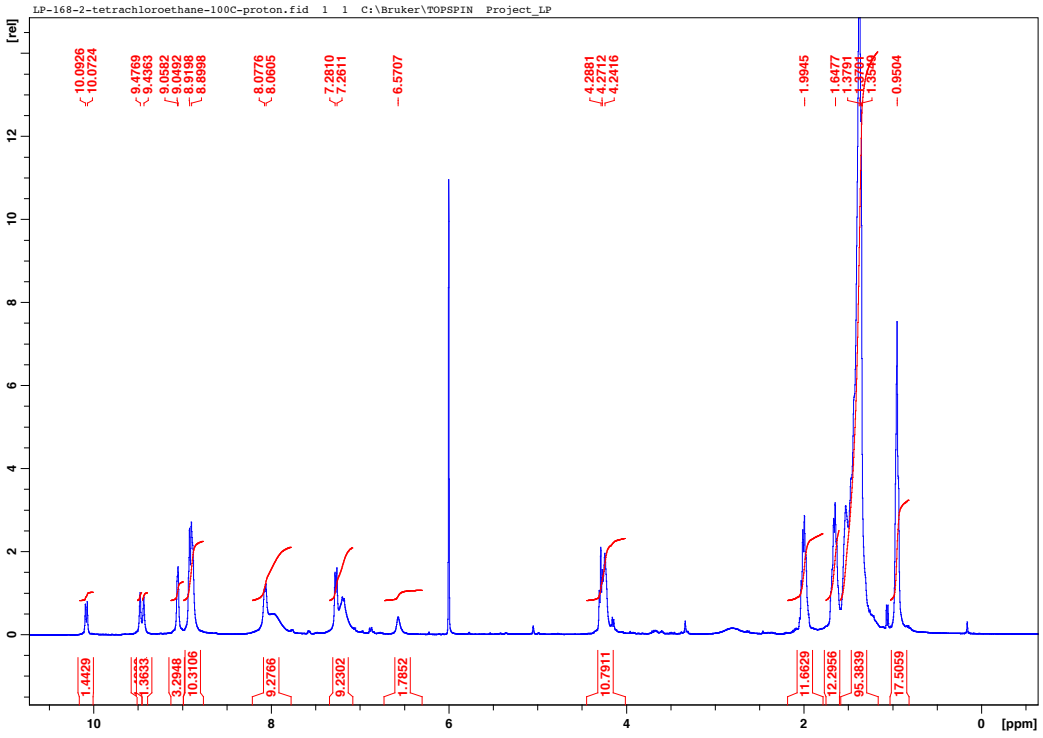

^{1}H NMR spectrum of **4.34** in 1,1,2,2-tetrachloroethane-*d*2 at 100°C.

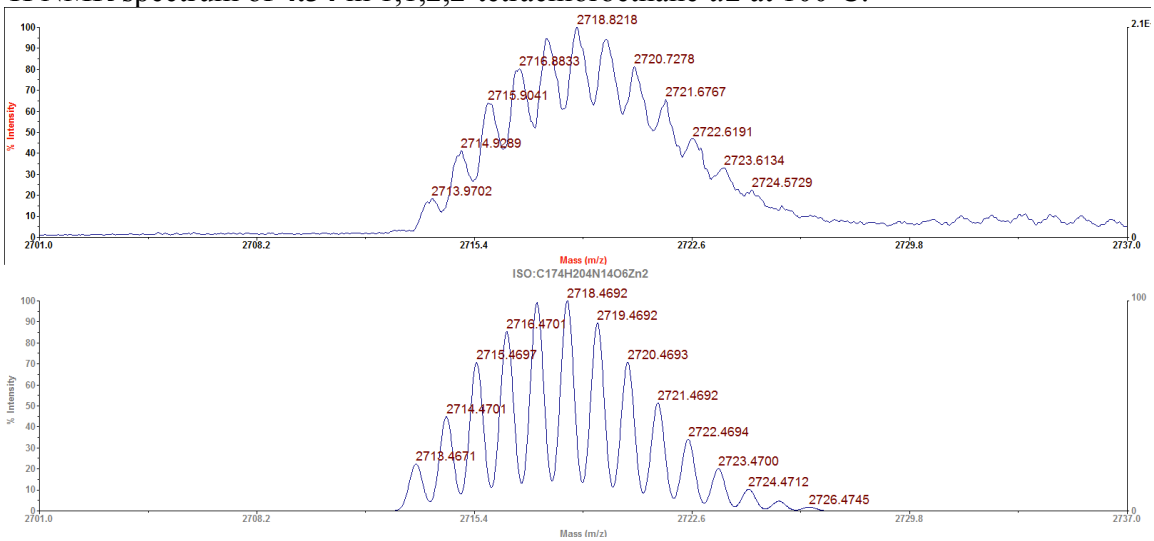

MALDI-TOF mass spectrum of **4.34**. The top trace is the observed spectrum and the bottom trace is the theoretical spectrum for molecular formula $C_{174}H_{204}N_{14}O_6Zn_2$ $[M]^+$.

4.35

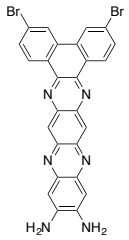

4.35

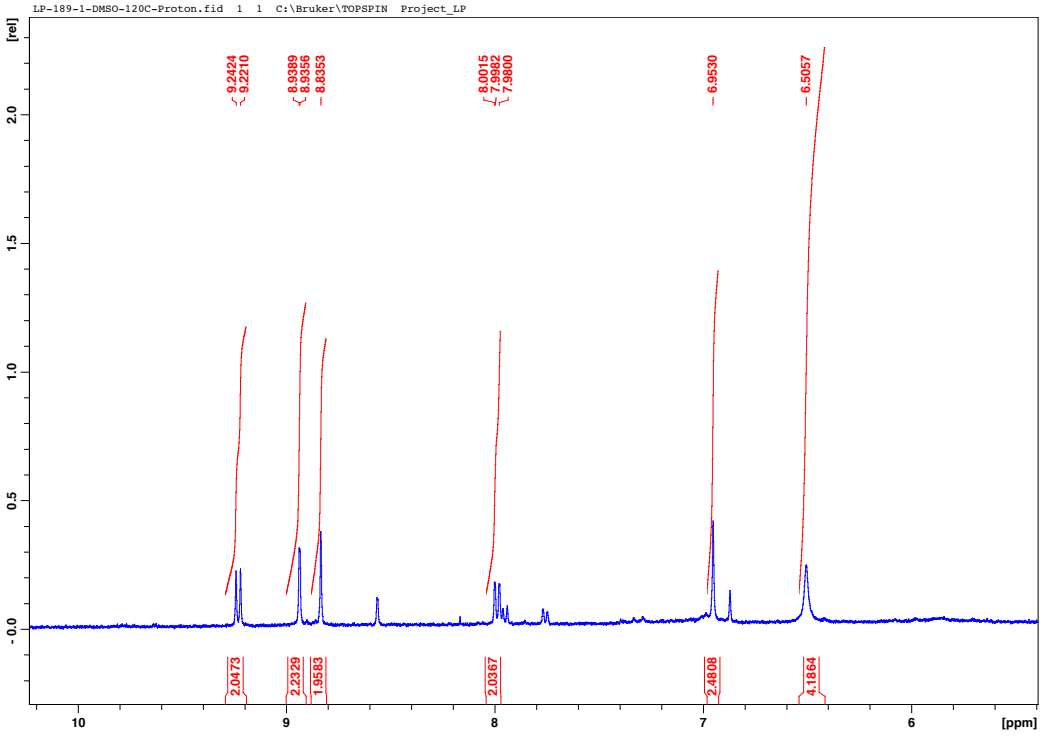

^{1}H NMR spectrum of **4.35** in DMSO-*d*6 at 120^{o}C.

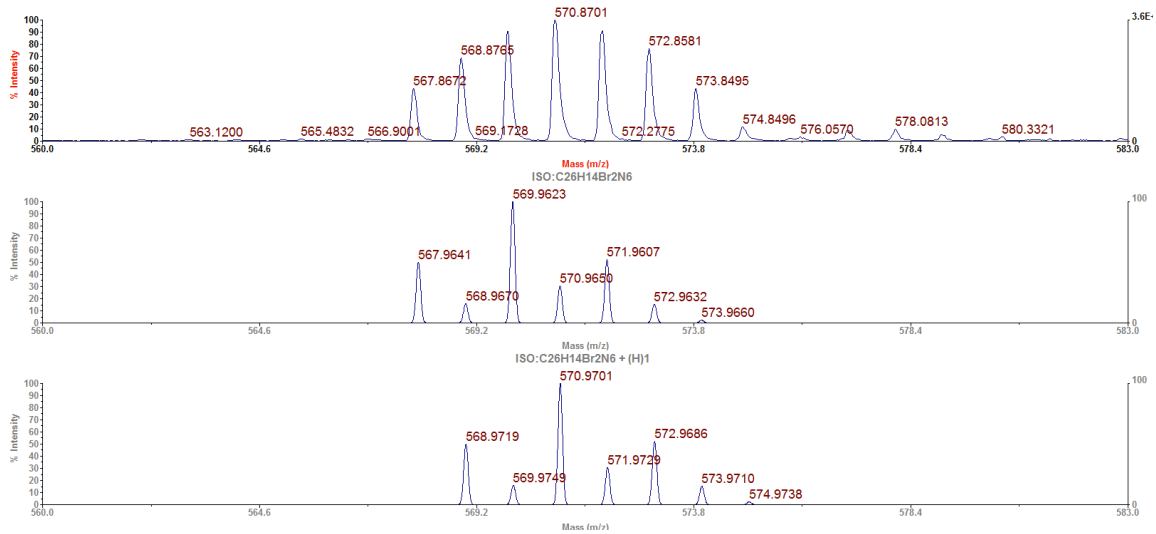

MALDI-TOF mass spectrum of **4.35**. The top trace is the observed spectrum and the bottom two traces are the theoretical spectra for molecular formula $C_{26}H_{14}Br_2N_6$ $[M]^+$, $C_{26}H_{14}Br_2N_6$ $[M+H]^+$. It is proposed that the observed spectrum is a superposition of these two species.

4.36

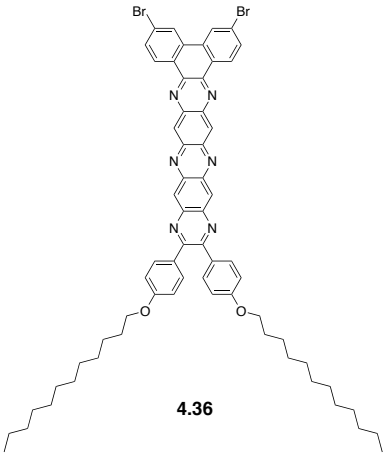

4.36

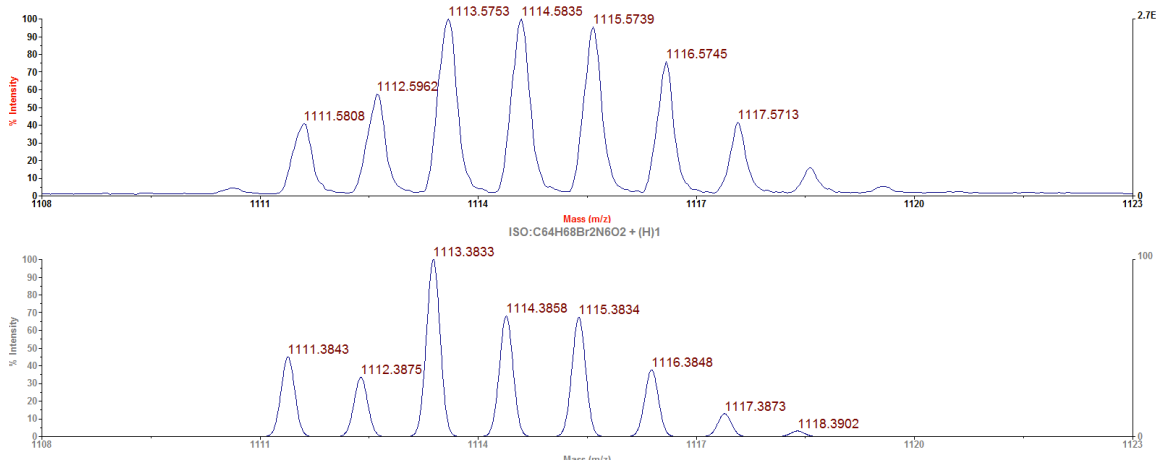

MALDI-TOF mass spectrum of **4.36**. The top trace is the observed spectrum and the bottom trace is the theoretical spectrum form molecular formula $C_{64}H_{69}NBr_2N_6O_2$ $[M+H]^+$.

4.37

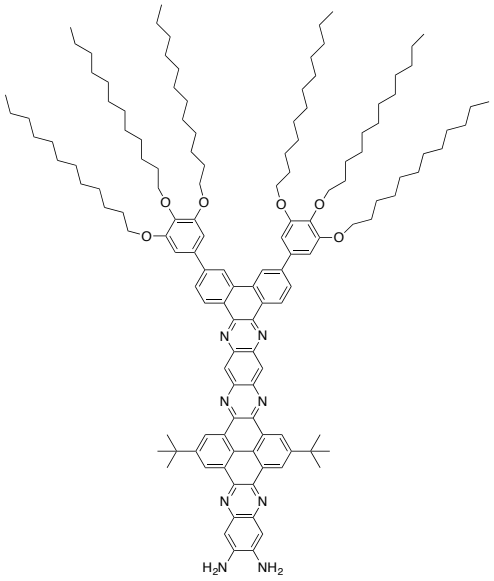

4.37

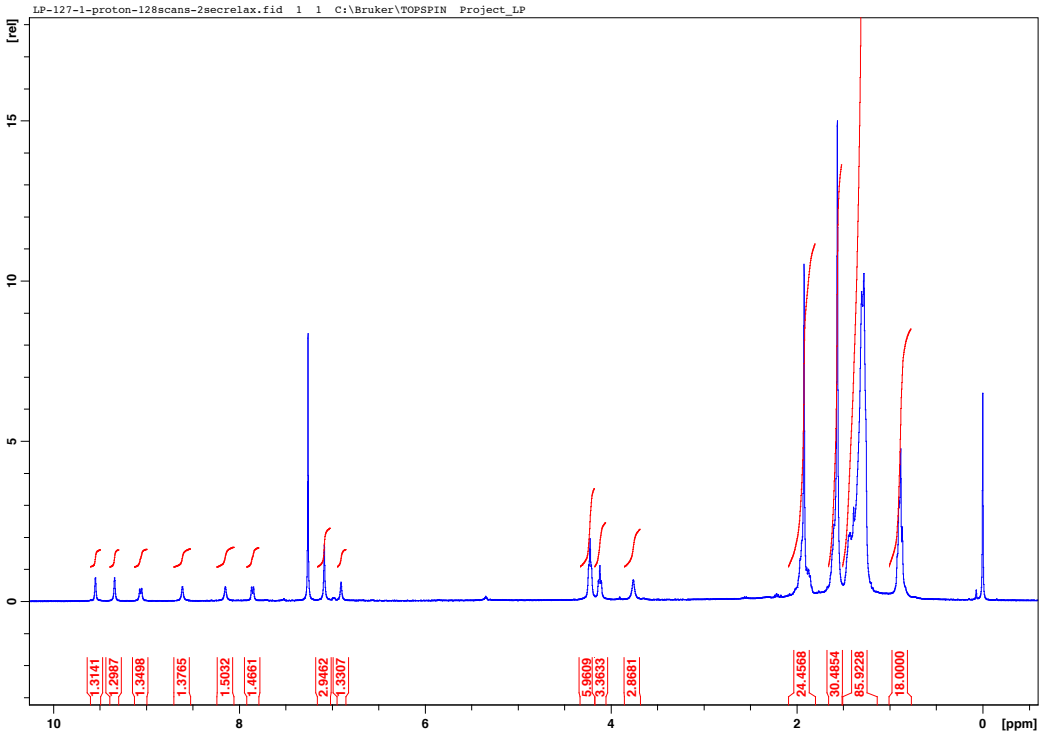

^{1}H NMR spectrum of **4.37** in $CDCl_3$ at RT.

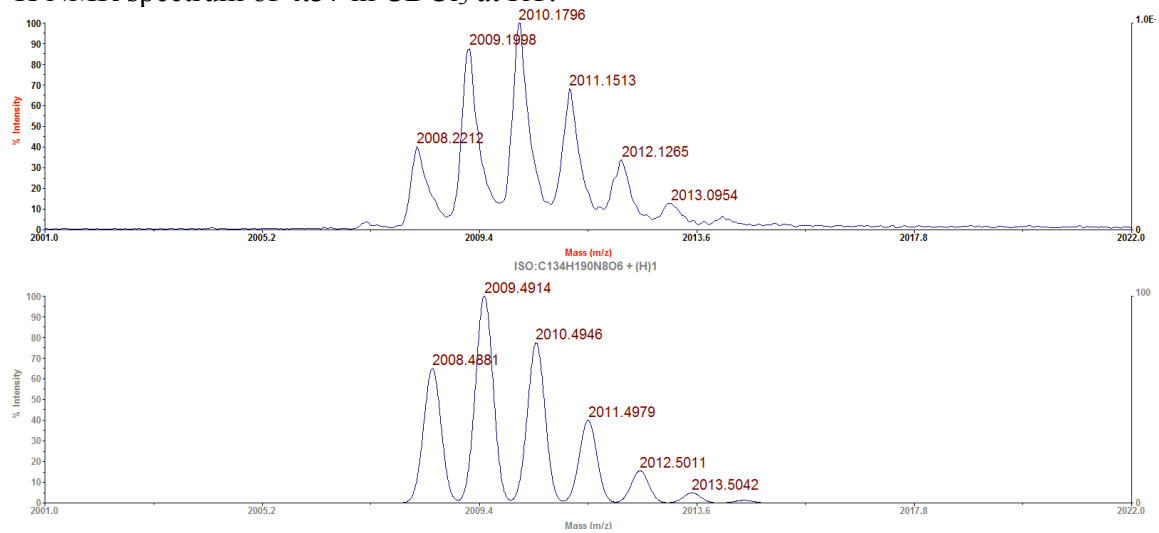

MALDI-TOF mass spectrum of **4.37**. The top trace is the observed spectrum and the bottom trace is the theoretical spectrum for molecular formula $C_{134}H_{191}N_8O_6$ $[M+H]^+$.

4.38

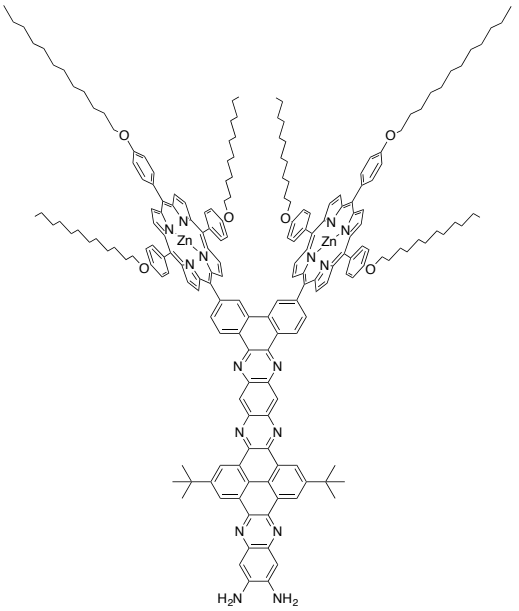

4.38

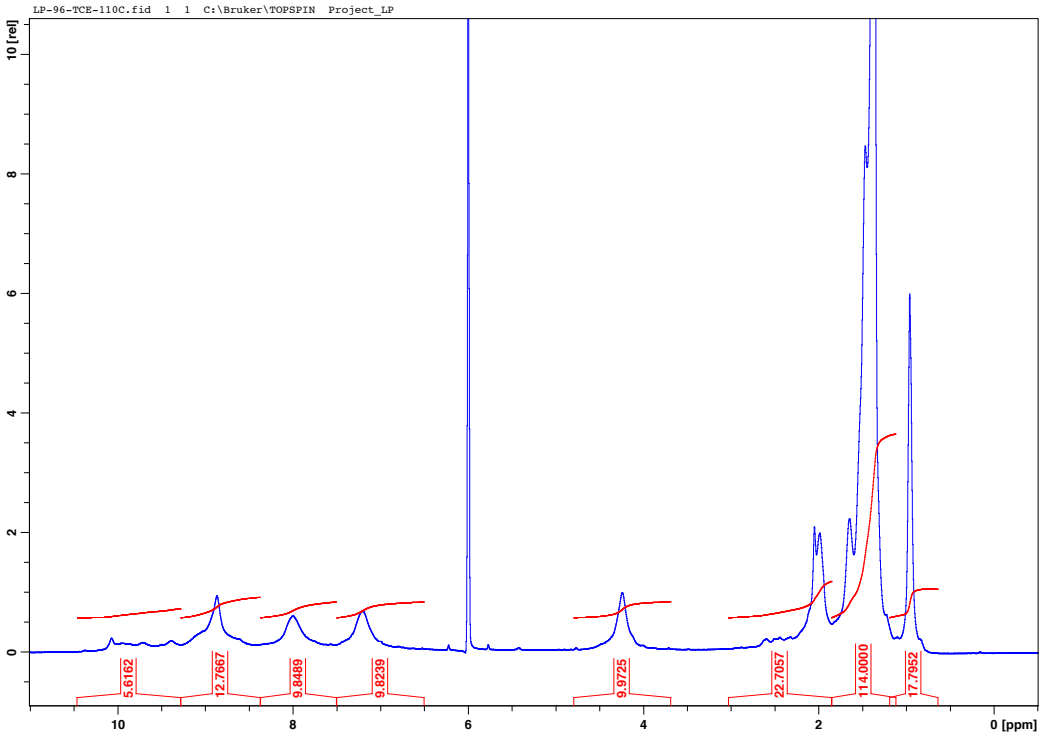

^{1}H NMR spectrum of **4.38** in 1,1,2,2-tetrachloroethane-*d*2 at 110^{o}C.

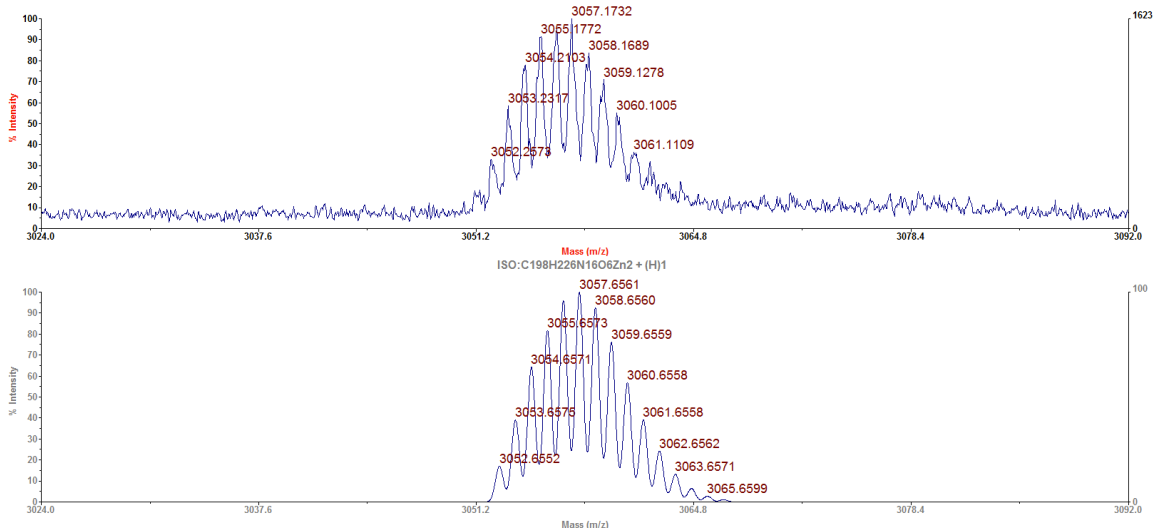

MALDI-TOF mass spectrum of **4.38**. The top trace is the observed spectrum and the bottom trace is the theoretical spectrum for molecular formula $C_{198}H_{227}N_{16}O_6Zn_2$ $[M+H]^+$.

APPENDIX D

NMR AND MASS SPECTRAL DATA FOR SYNTHESIZED COMPOUNDS OF CHAPTER 5

5.1

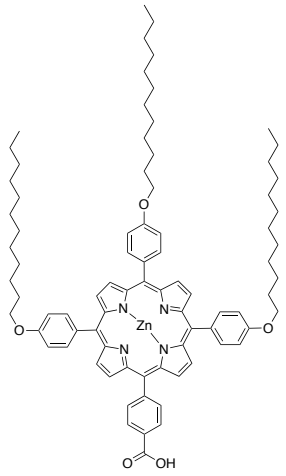

5.1

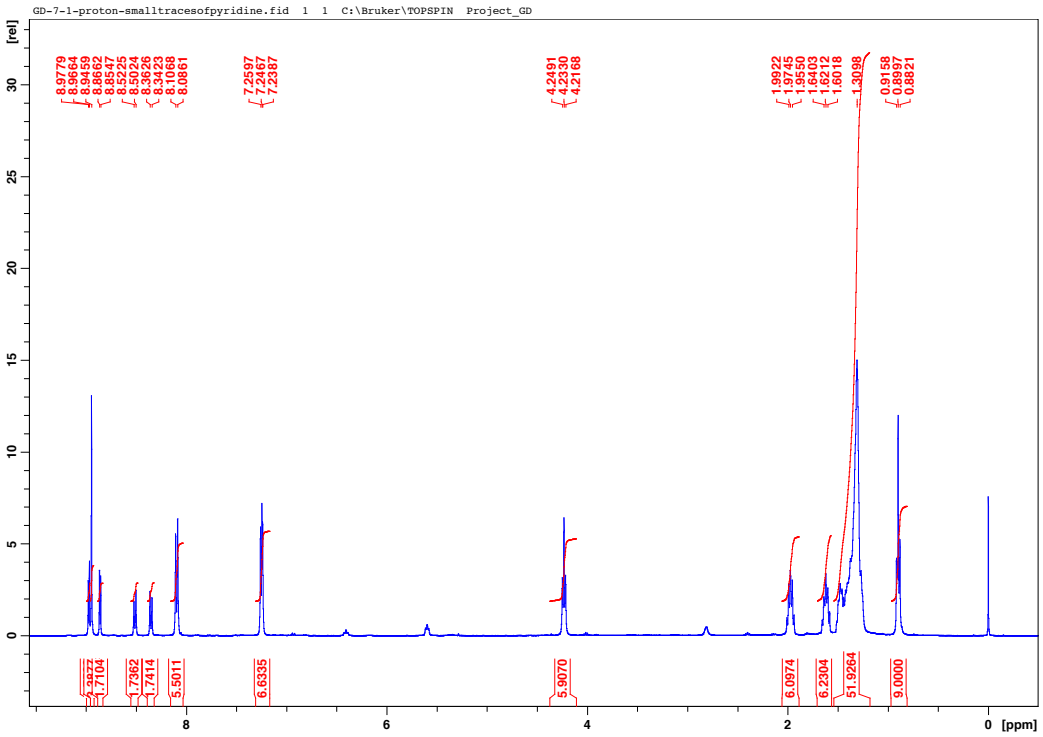

^{1}H NMR spectrum of **5.1** in $CDCl_3$ at RT.

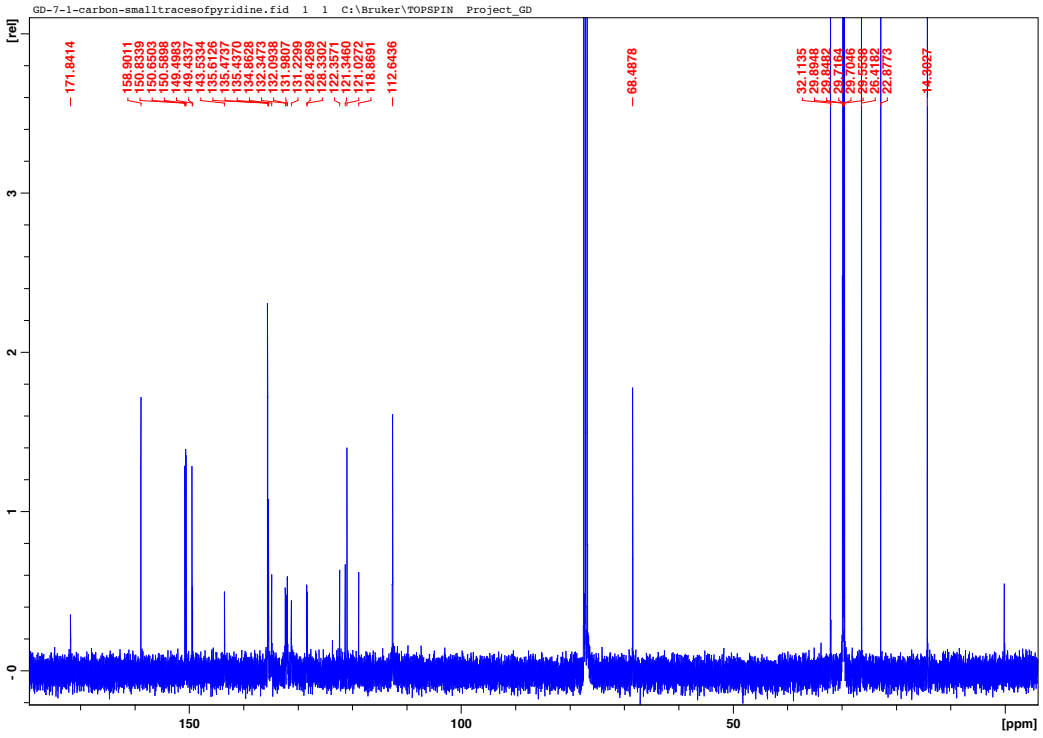

^{13}C NMR spectrum of **5.1** in $CDCl_3$ at RT.

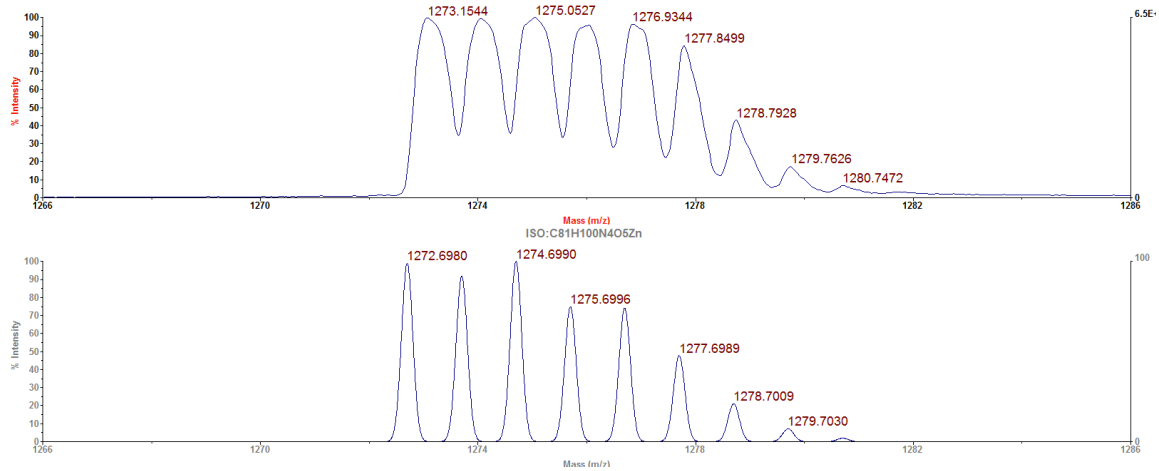

MALDI-TOF mass spectrum for **5.1**. The top trace shows the observed spectrum and the bottom trace shows the theoretical spectrum for chemical formula $C_{81}H_{100}N_4O_5Zn$ $[M]^+$.

5.2

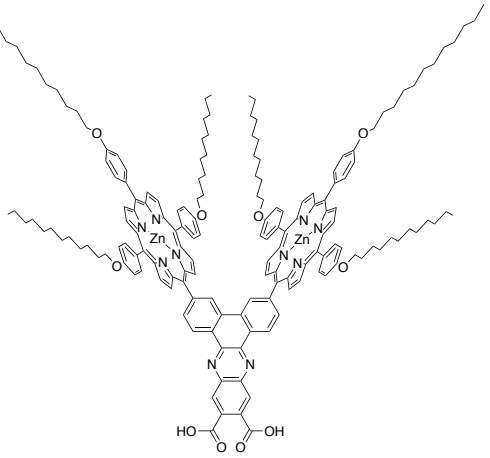

5.2

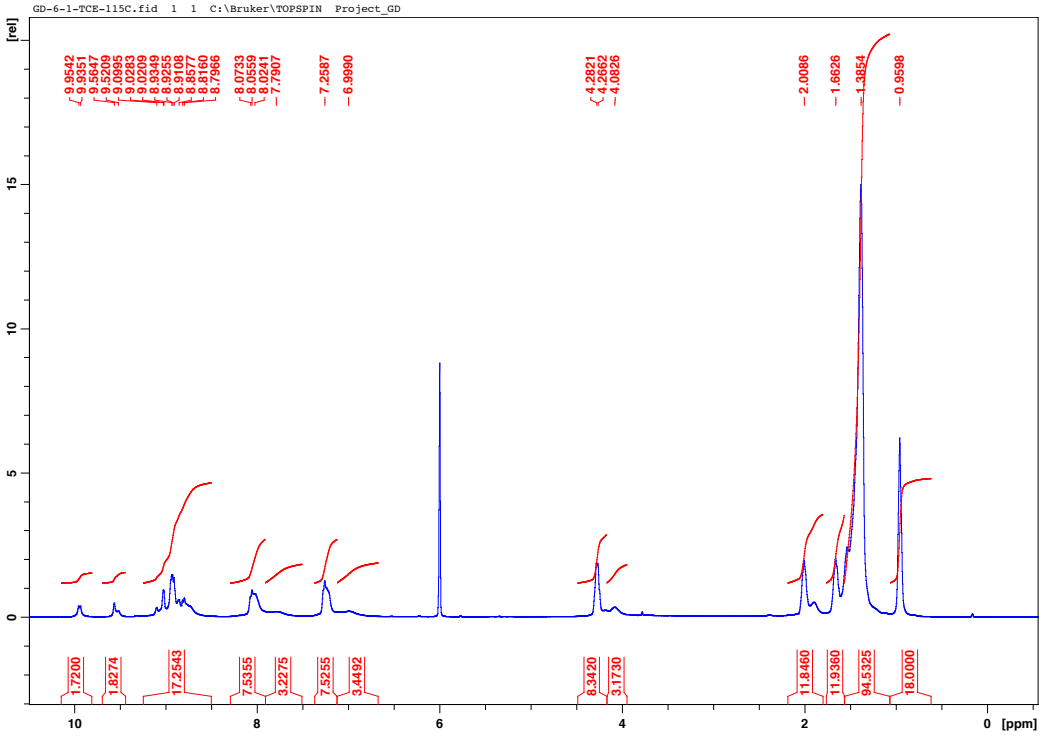

^{1}H NMR spectrum of **5.2** in 1,1,2,2-tetrachloroethane-*d*2 at 115^{o}C.

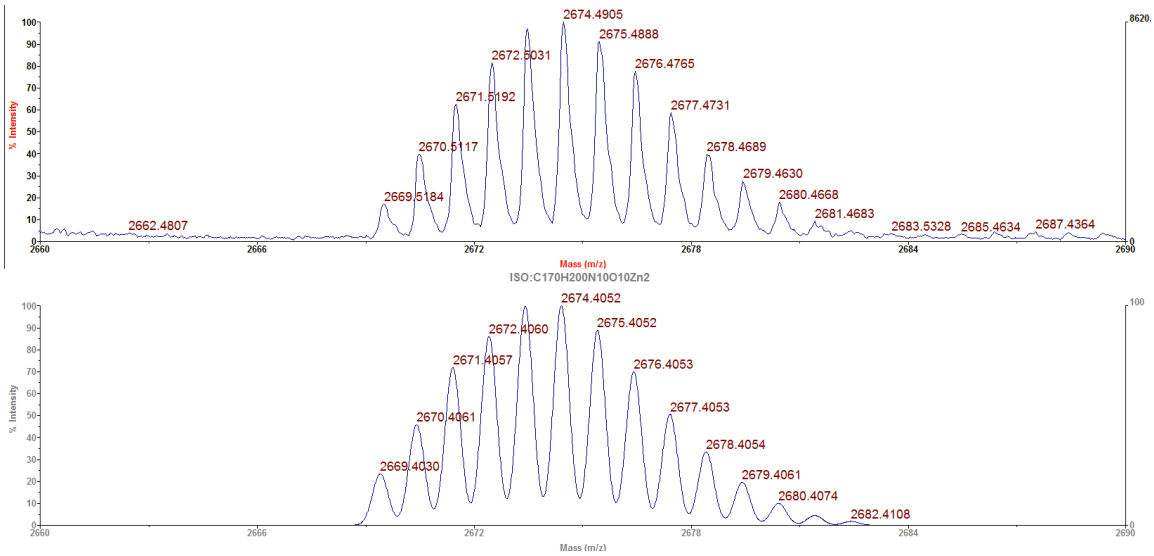

MALDI-TOF mass spectrum for **5.2**. The top trace shows the observed spectrum and the bottom trace shows the theoretical spectrum for chemical formula $C_{170}H_{200}N_{10}O_{10}Zn_2$ $[M]^+$.

5.3

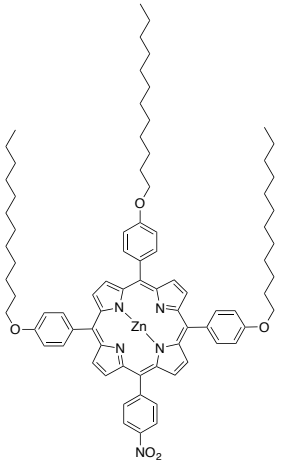

5.3

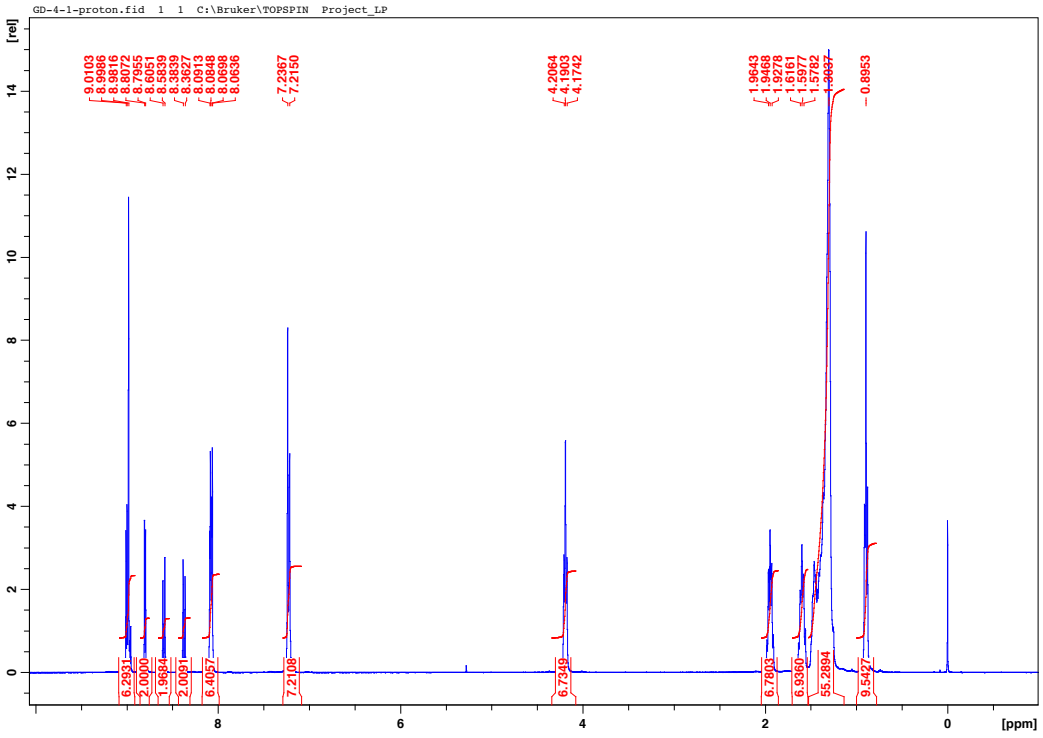

^{1}H NMR spectrum of **5.3** in $CDCl_3$ at RT.

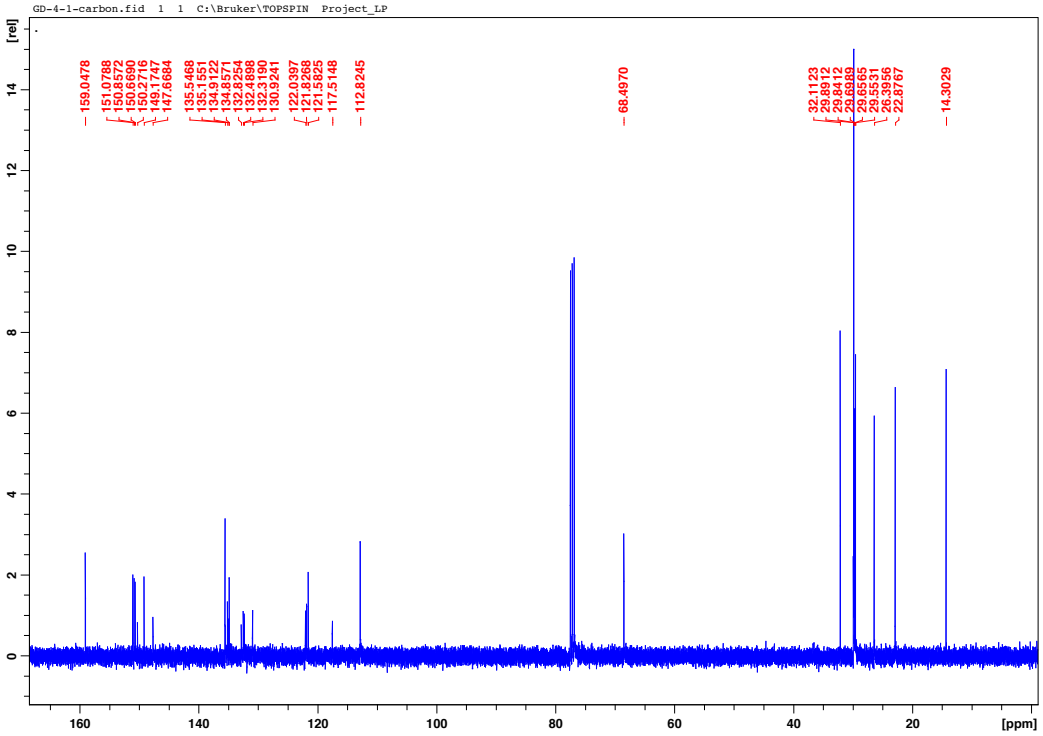

^{13}C NMR spectrum of **5.3** in $CDCl_3$ at RT.

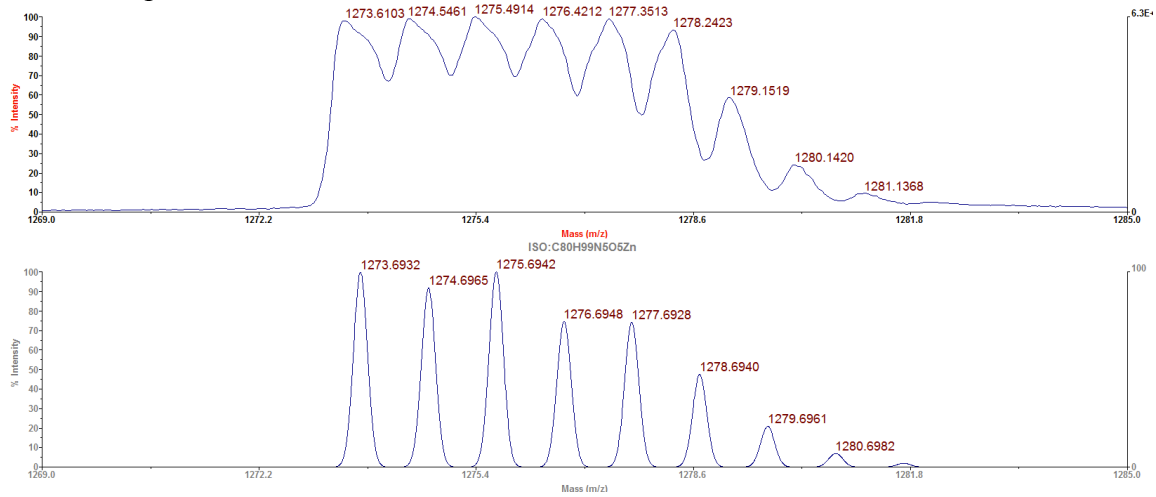

MALDI-TOF mass spectrum for **5.3**. The top trace shows the observed spectrum and the bottom trace shows the theoretical spectrum for chemical formula $C_{80}H_{99}N_5O_5Zn$ $[M]^+$.

5.4

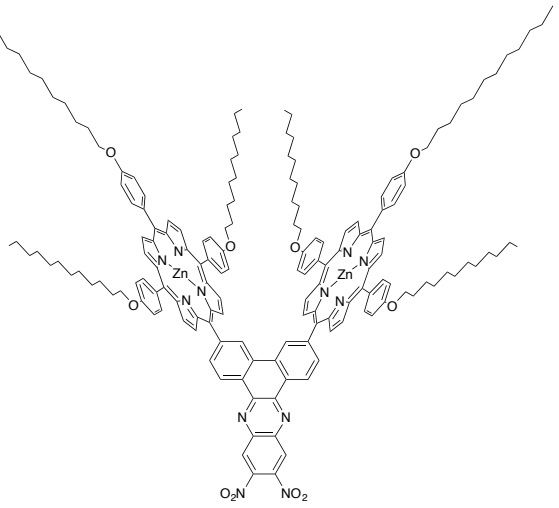

5.4

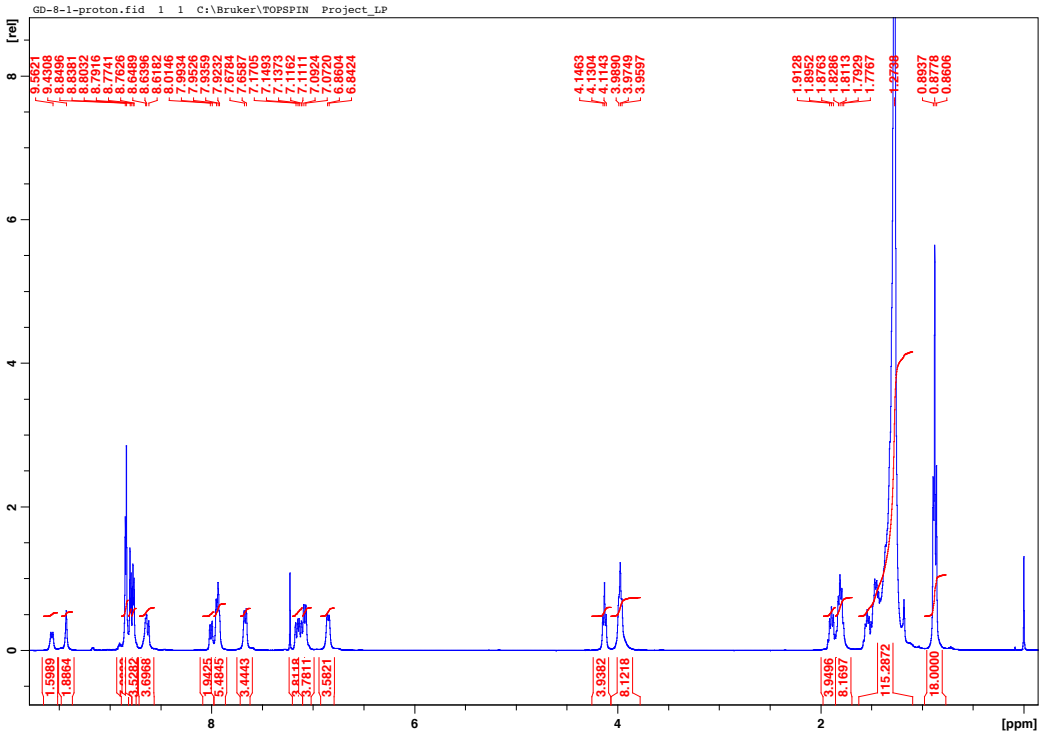

^{1}H NMR spectrum of **5.4** in $CDCl_3$ at RT.

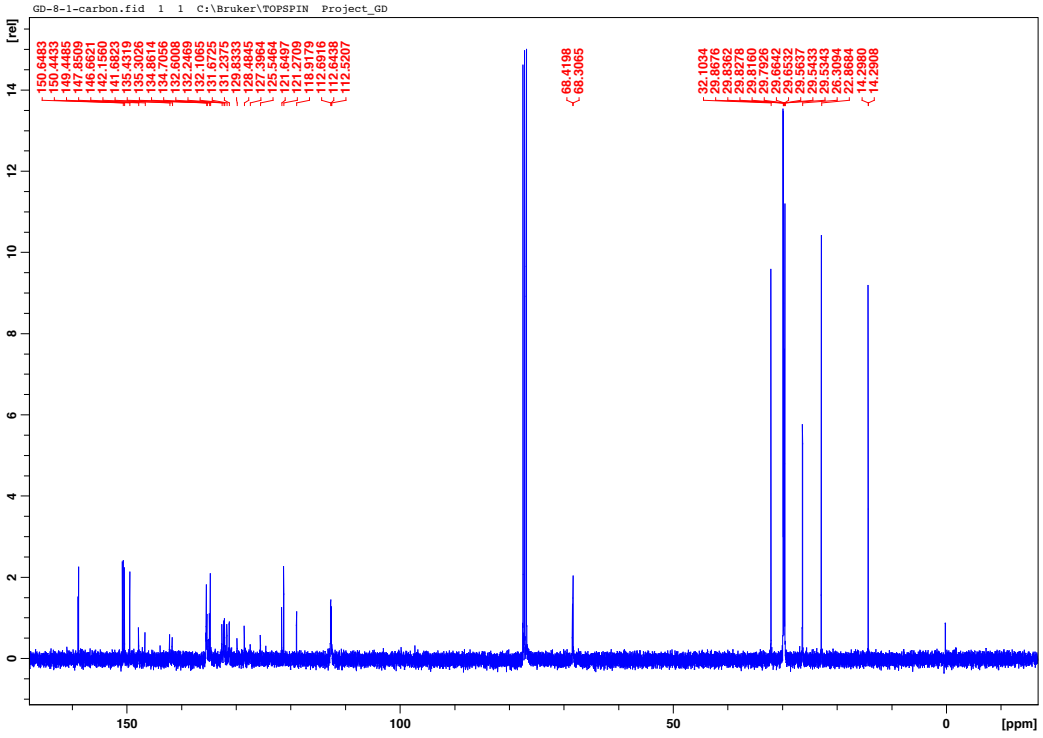

^{13}C NMR spectrum of **5.4** in $CDCl_3$ at RT.

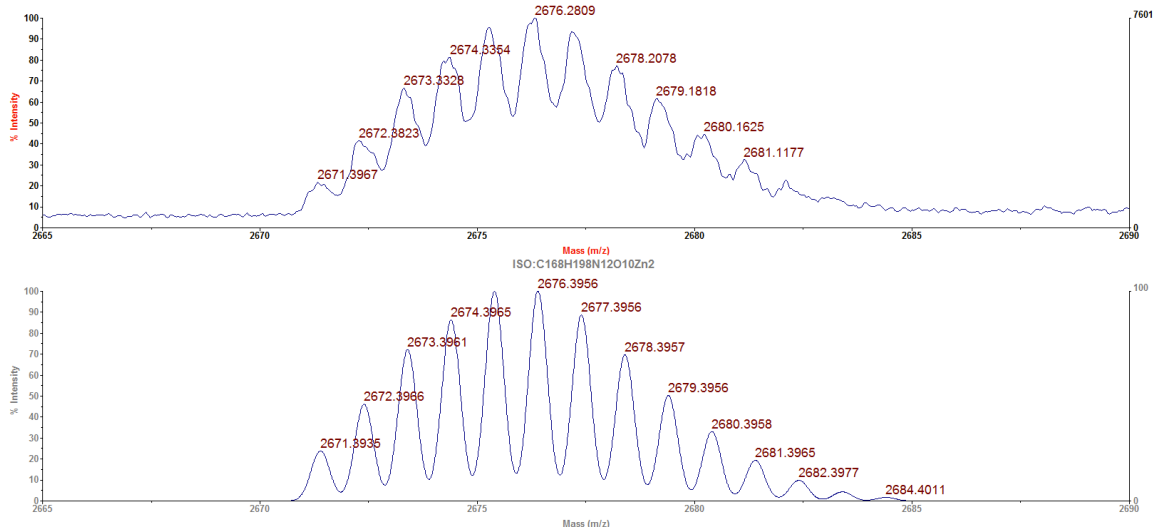

MALDI-TOF mass spectrum for **5.4**. The top trace shows the observed spectrum and the bottom trace shows the theoretical spectrum for chemical formula $C_{168}H_{198}N_{12}O_{10}Zn_2$ $[M]^+$.

5.5

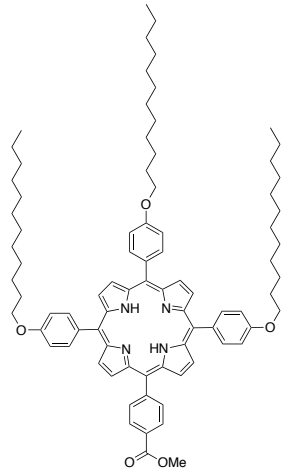

5.5

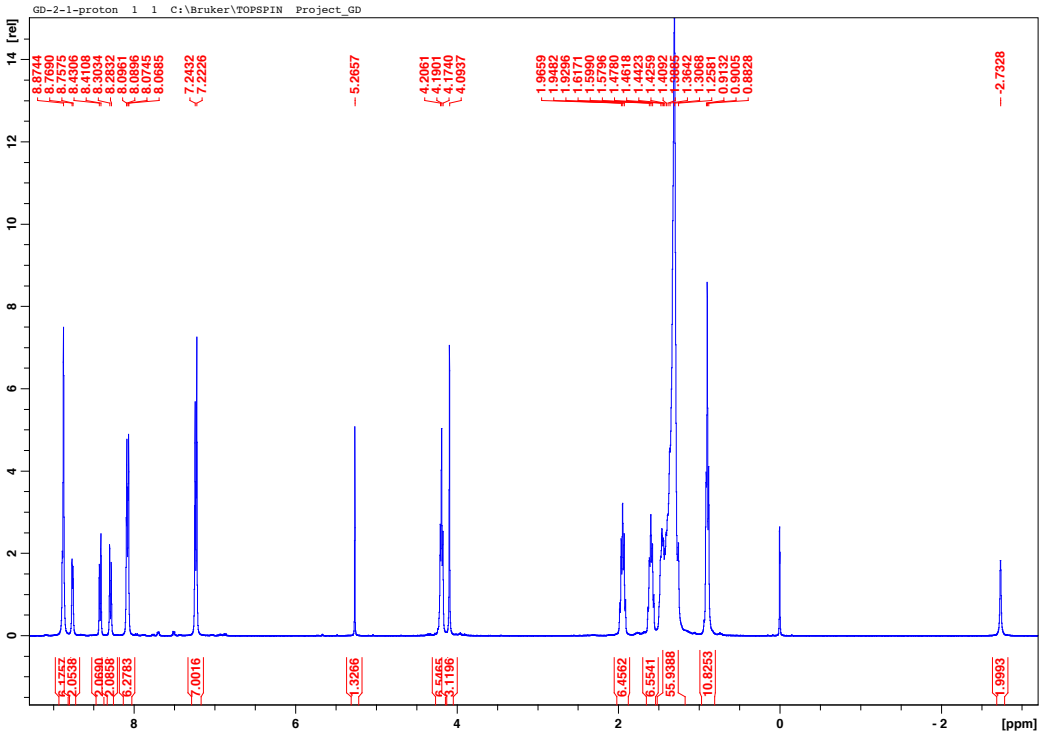

^{1}H NMR spectrum of **5.5** in $CDCl_3$ at RT.

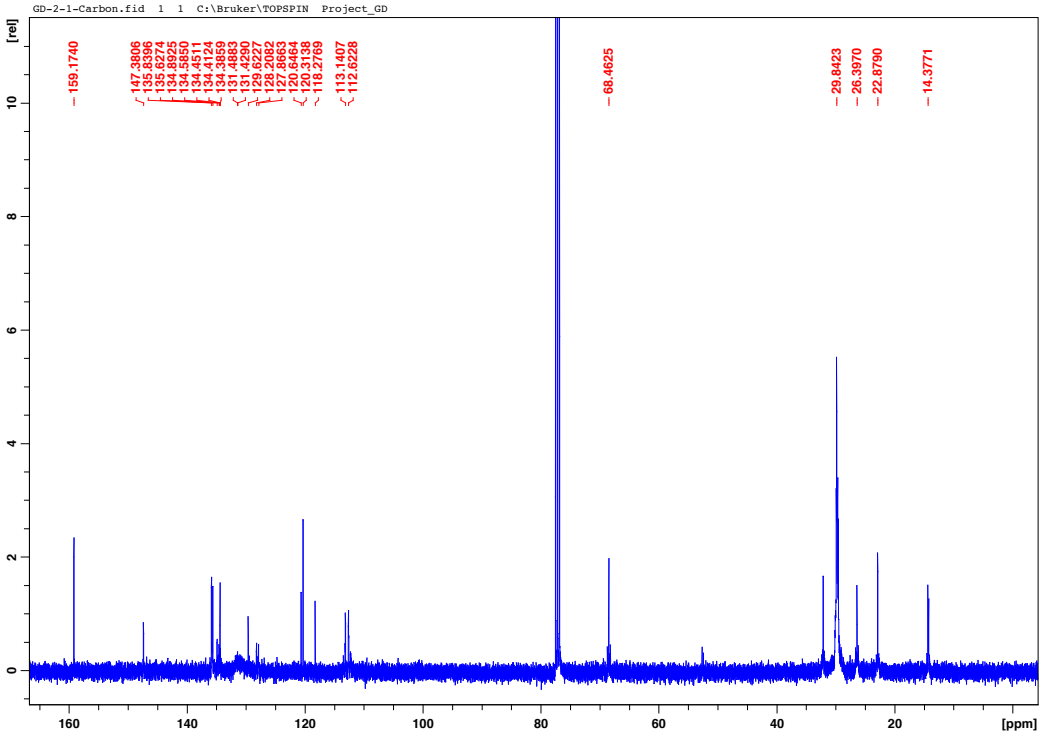

^{13}C NMR spectrum of **5.5** in $CDCl_3$ at RT.

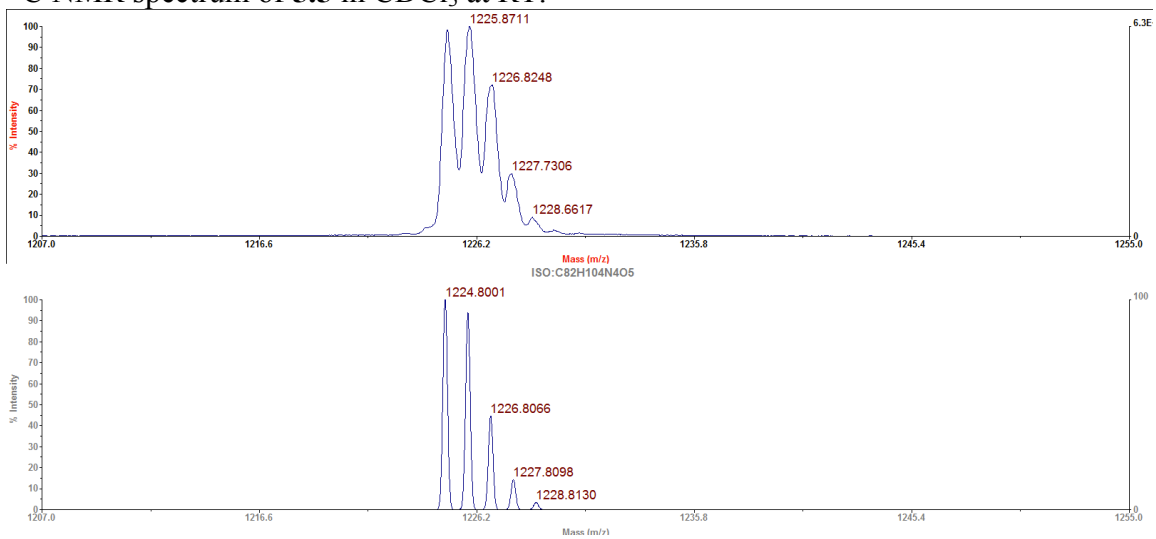

MALDI-TOF mass spectrum for **5.5**. The top trace shows the observed spectrum and the bottom trace shows the theoretical spectrum for chemical formula $C_{82}H_{104}N_4O_5$ $[M]^+$.

5.6

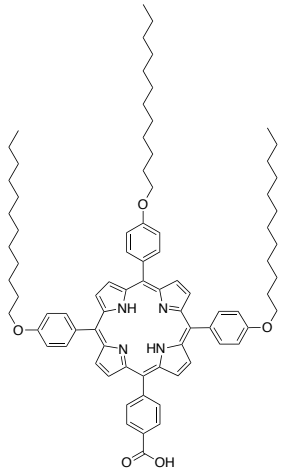

5.6

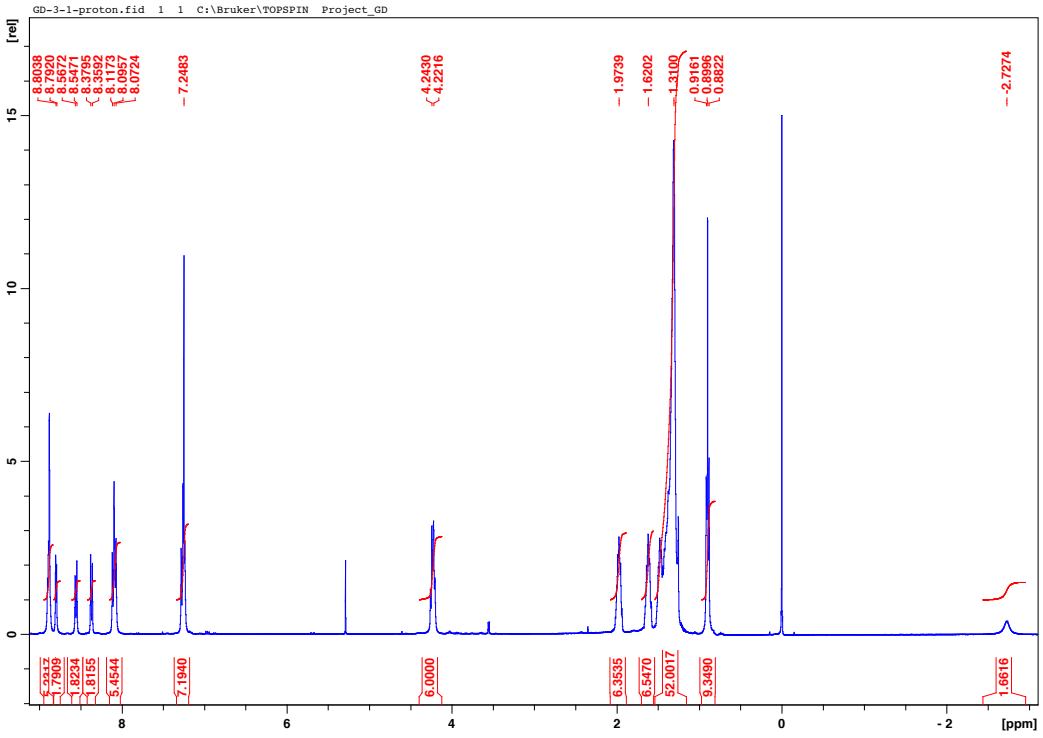

^{1}H NMR spectrum of **5.6** in $CDCl_3$ at RT.

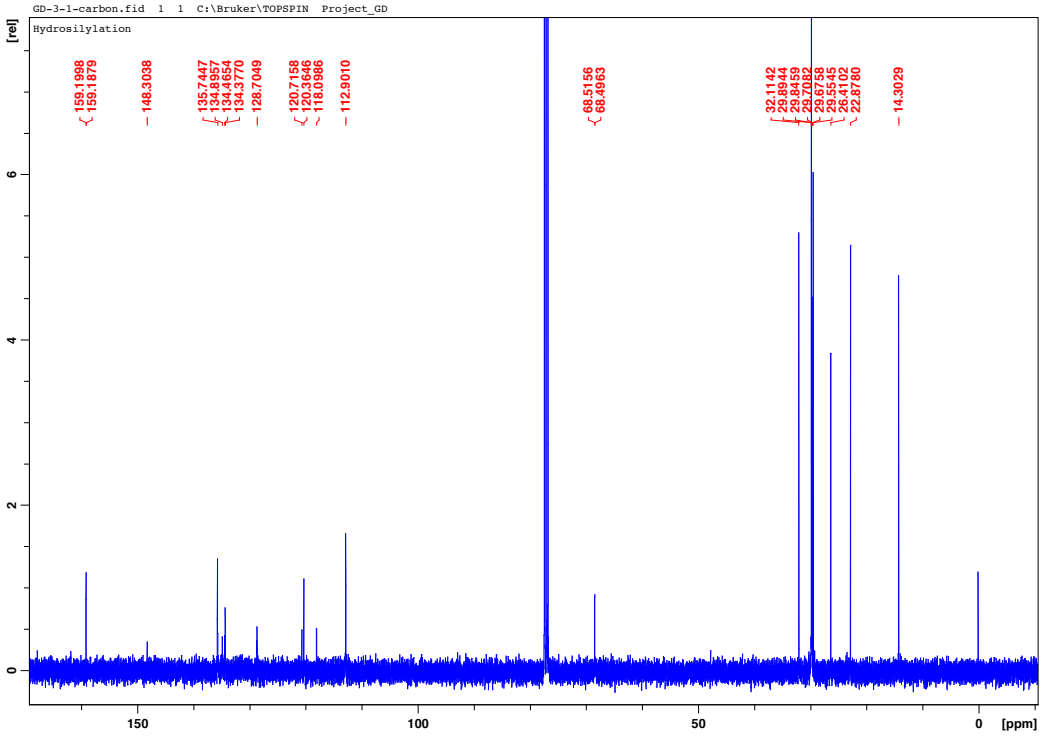

^{13}C NMR spectrum of **5.6** in $CDCl_3$ at RT.

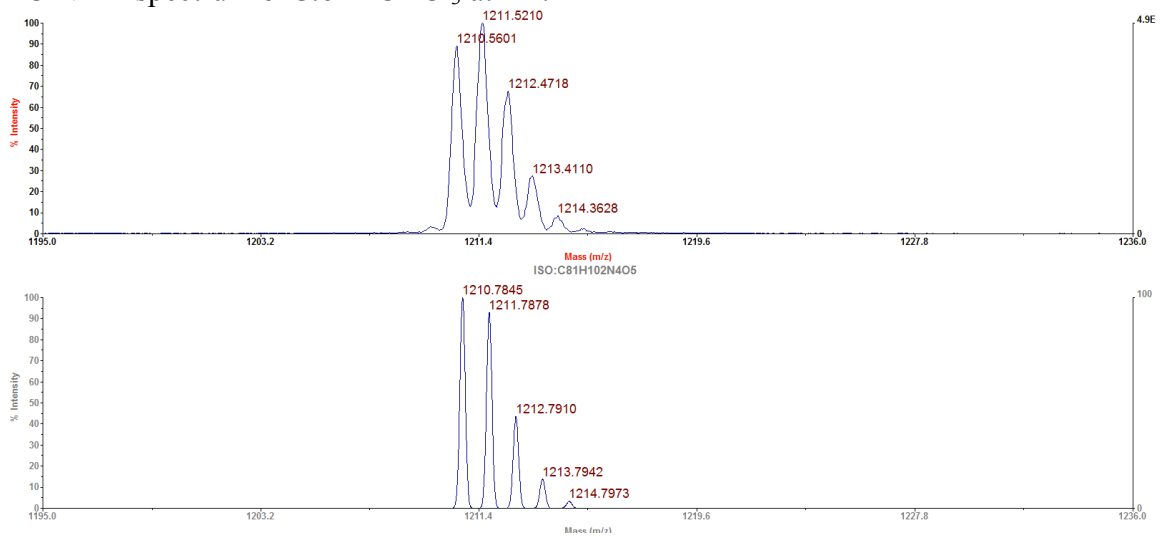

MALDI-TOF mass spectrum for **5.6**. The top trace shows the observed spectrum and the bottom trace shows the theoretical spectrum for chemical formula $C_{81}H_{102}N_4O_5$ $[M]^+$.

5.7

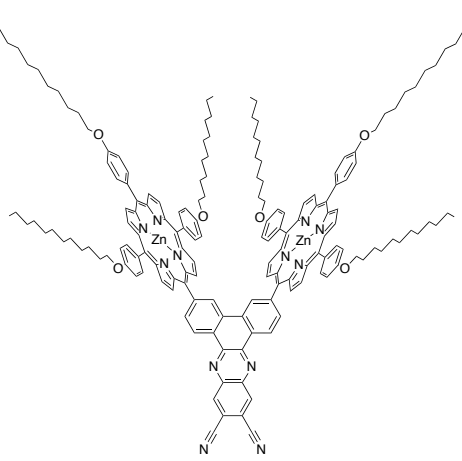

5.7

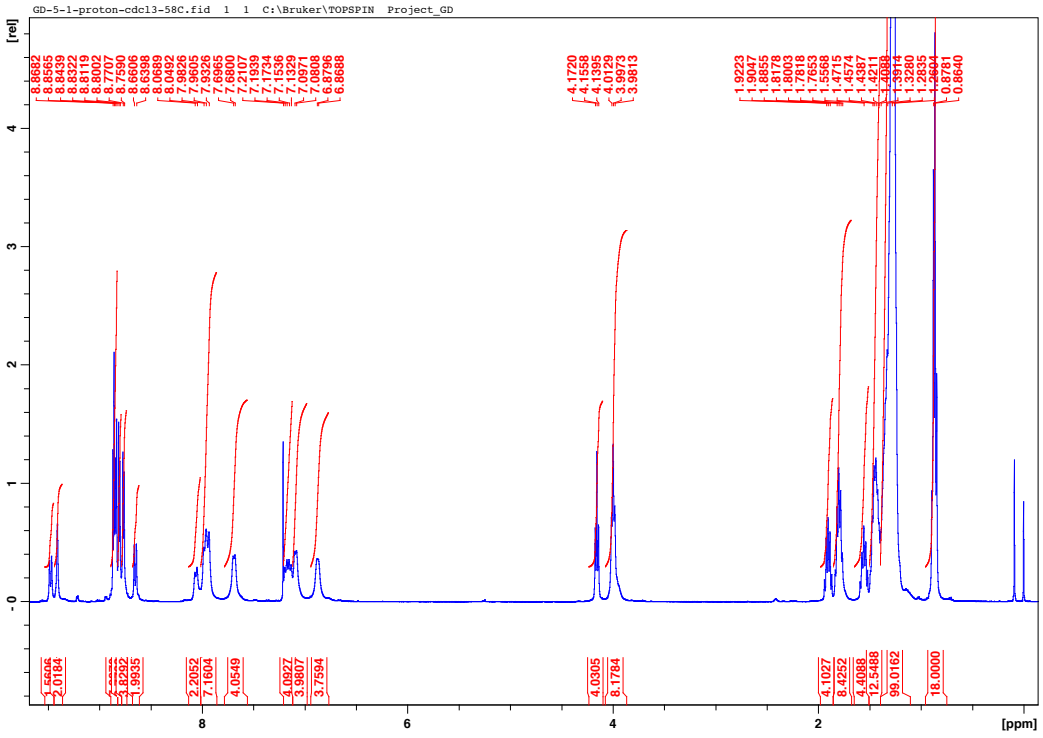

^{1}H NMR spectrum of **5.7** in $CDCl_3$ at RT.

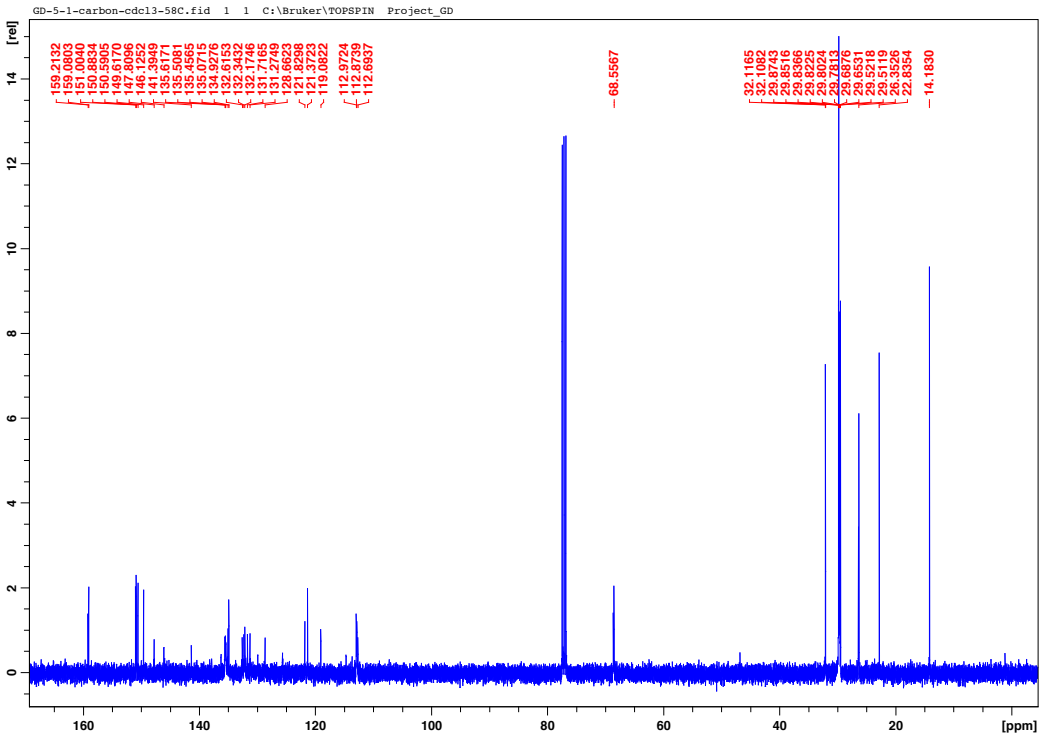

^{13}C NMR spectrum of **5.7** in $CDCl_3$ at RT.

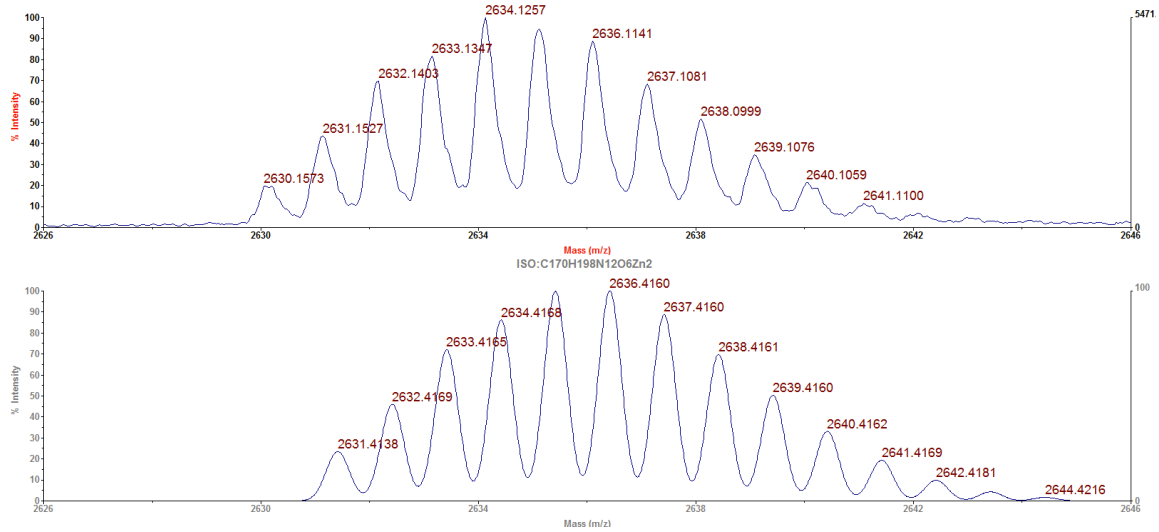

MALDI-TOF mass spectrum for **5.7**. The top trace shows the observed spectrum and the bottom trace shows the theoretical spectrum for chemical formula $C_{170}H_{198}N_{12}O_6Zn_2$ $[M]^+$.

5.8

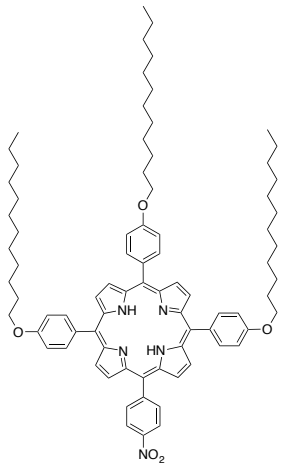

5.8

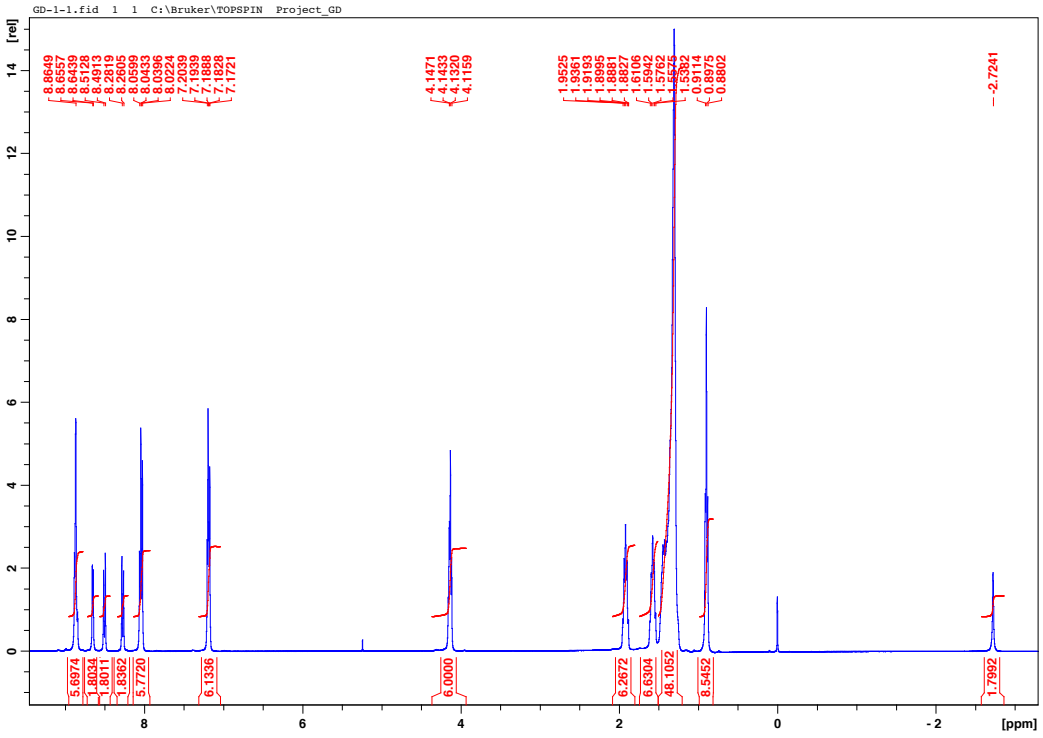

^{1}H NMR spectrum of **5.8** in $CDCl_3$ at RT.

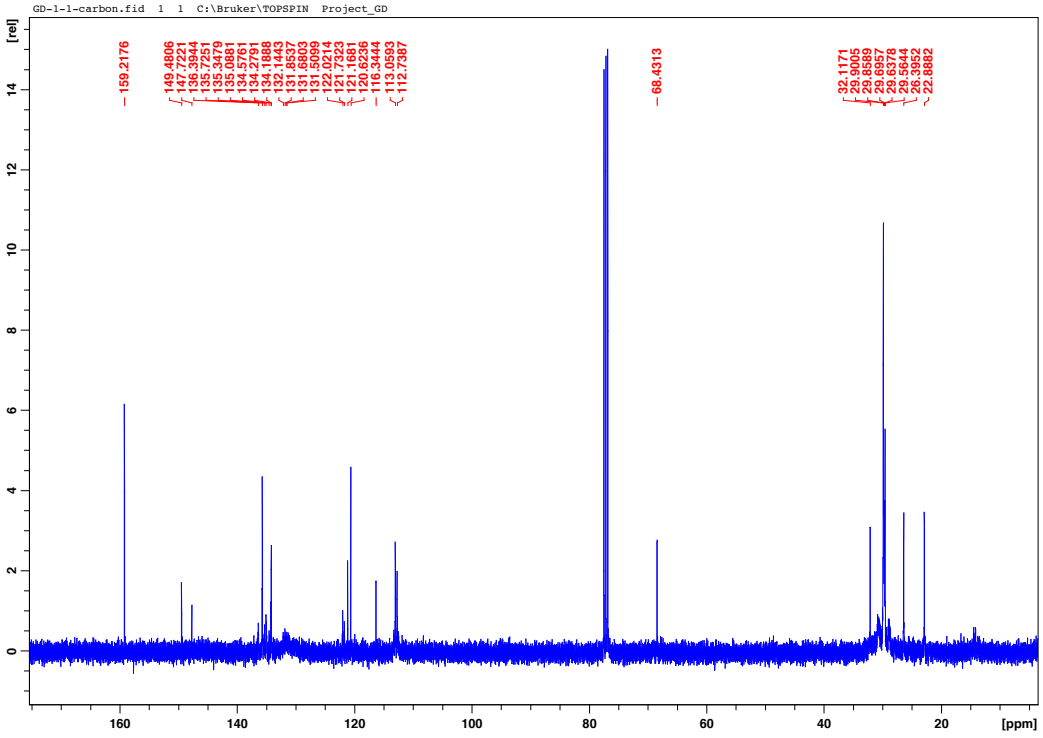

^{13}C NMR spectrum of **5.8** in $CDCl_3$ at RT.

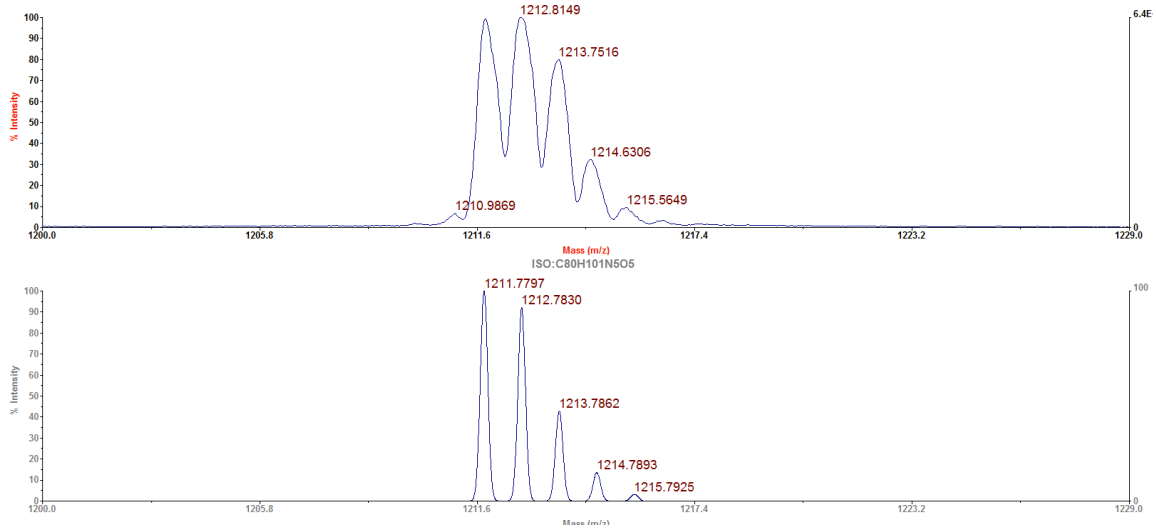

MALDI-TOF mass spectrum for **5.8**. The top trace shows the observed spectrum and the bottom trace shows the theoretical spectrum for chemical formula $C_{80}H_{101}N_5O_5[M]^+$.

5.9

5.9

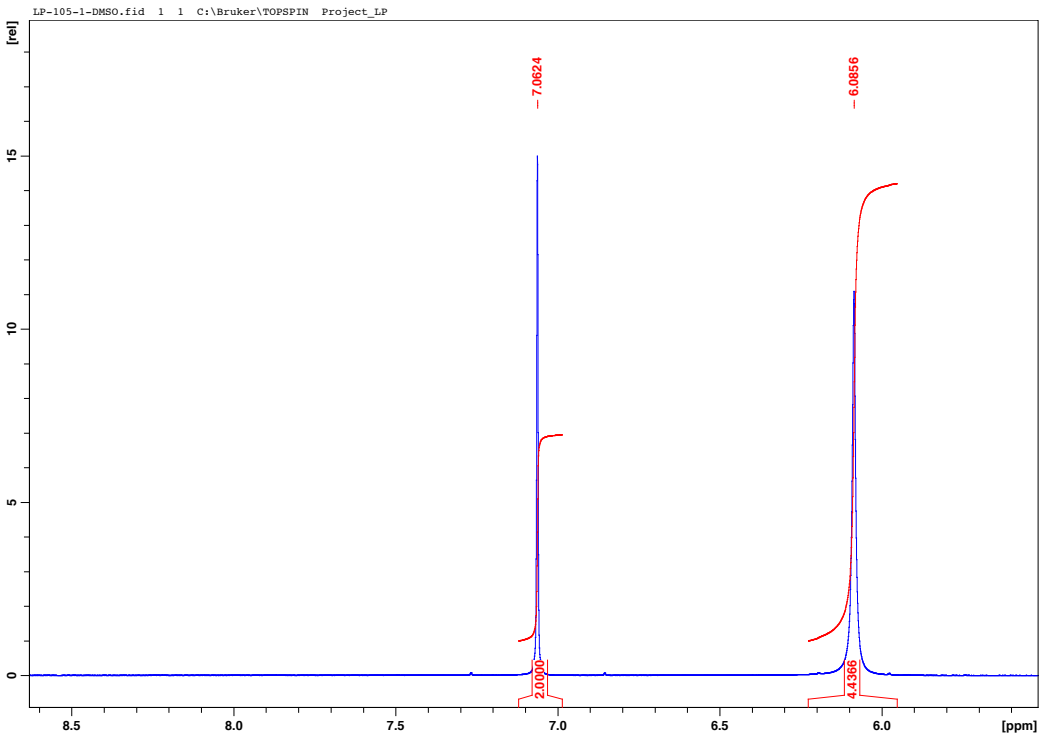

^{1}H NMR spectrum of **5.9** in DMSO-*d*6 at RT.

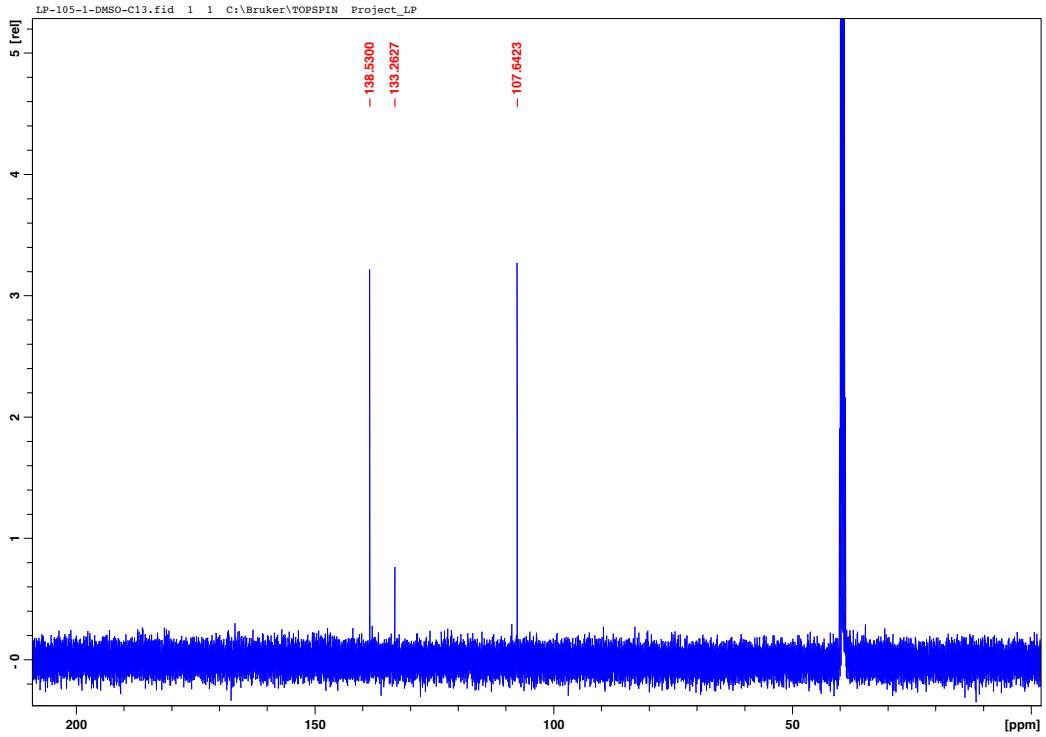

^{13}C NMR spectrum of **5.9** in DMSO-*d*6 at RT.

5.12

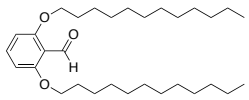

5.12

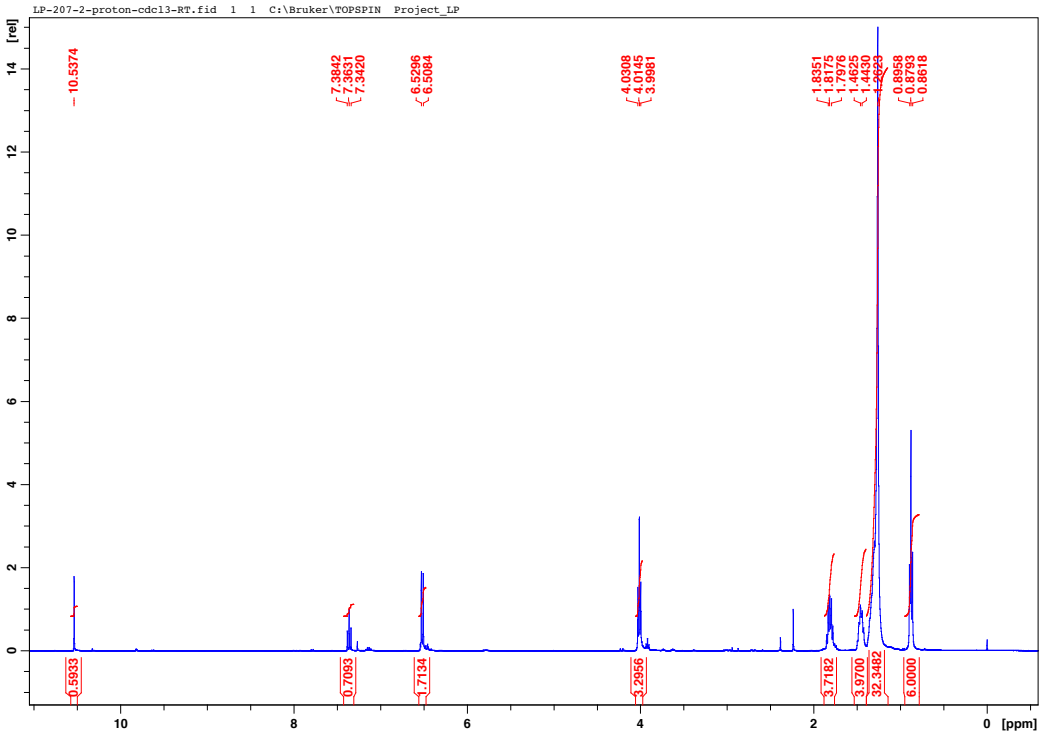

^{1}H NMR spectrum of **5.12** in $CDCl_3$ at RT.

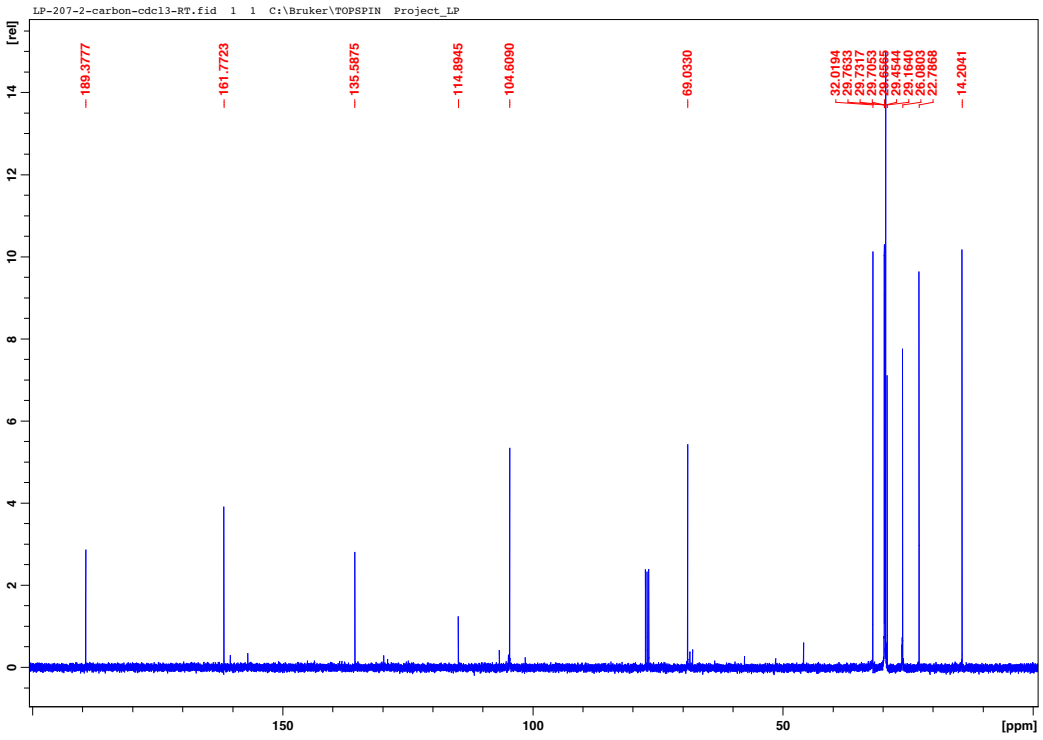

^{13}C NMR spectrum of **5.12** in $CDCl_3$ at RT.

5.13

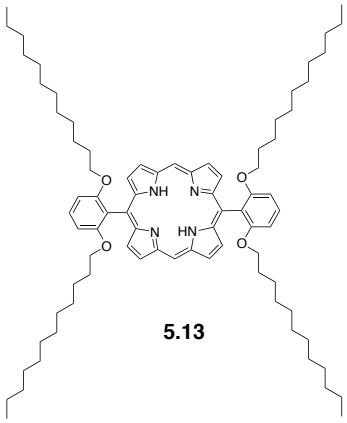

5.13

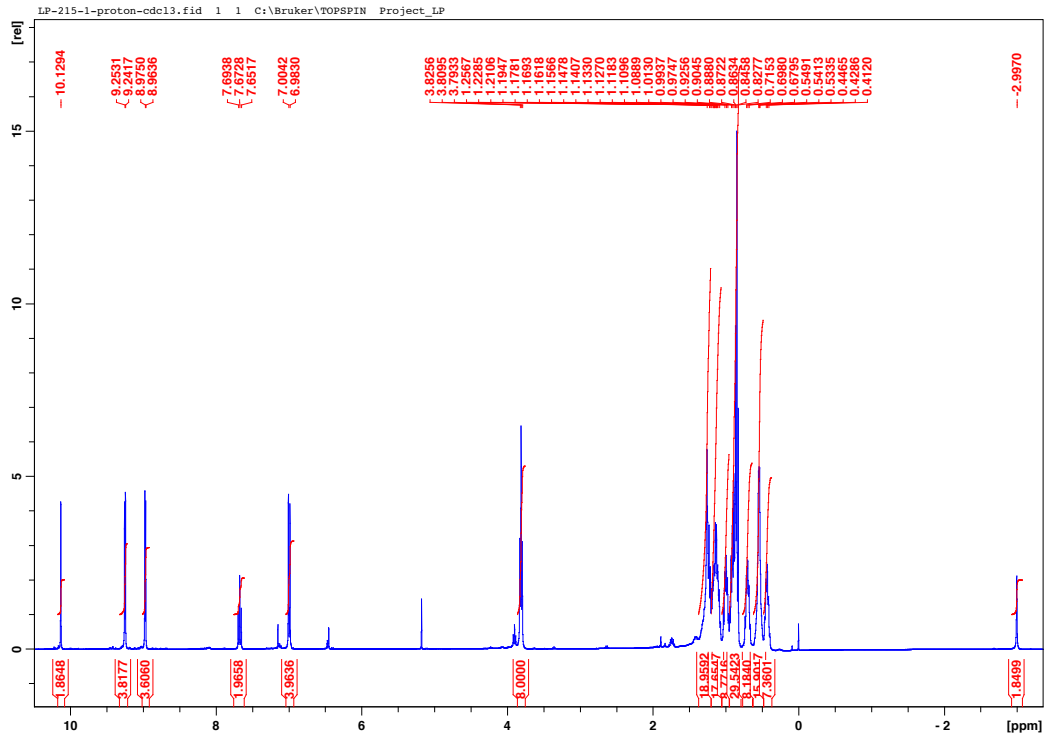

^{1}H NMR spectrum of **5.13** in $CDCl_3$ at RT.

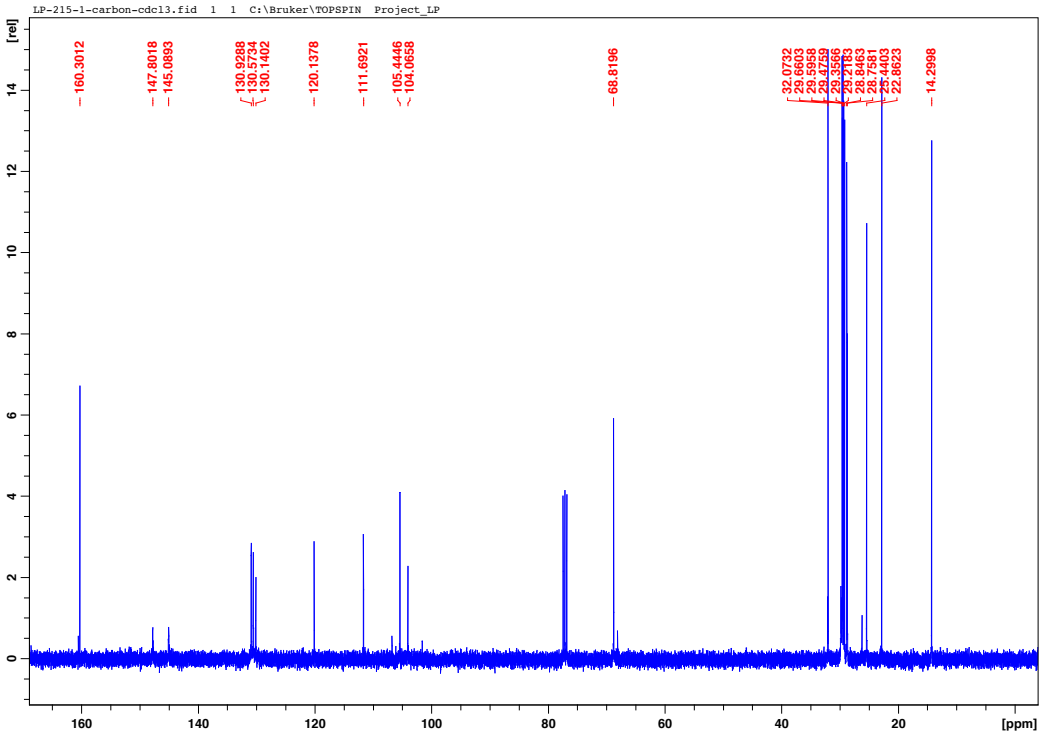

^{13}C NMR spectrum of **5.13** in $CDCl_3$ at RT.

5.14

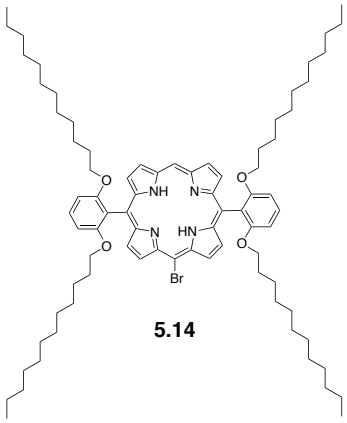

5.14

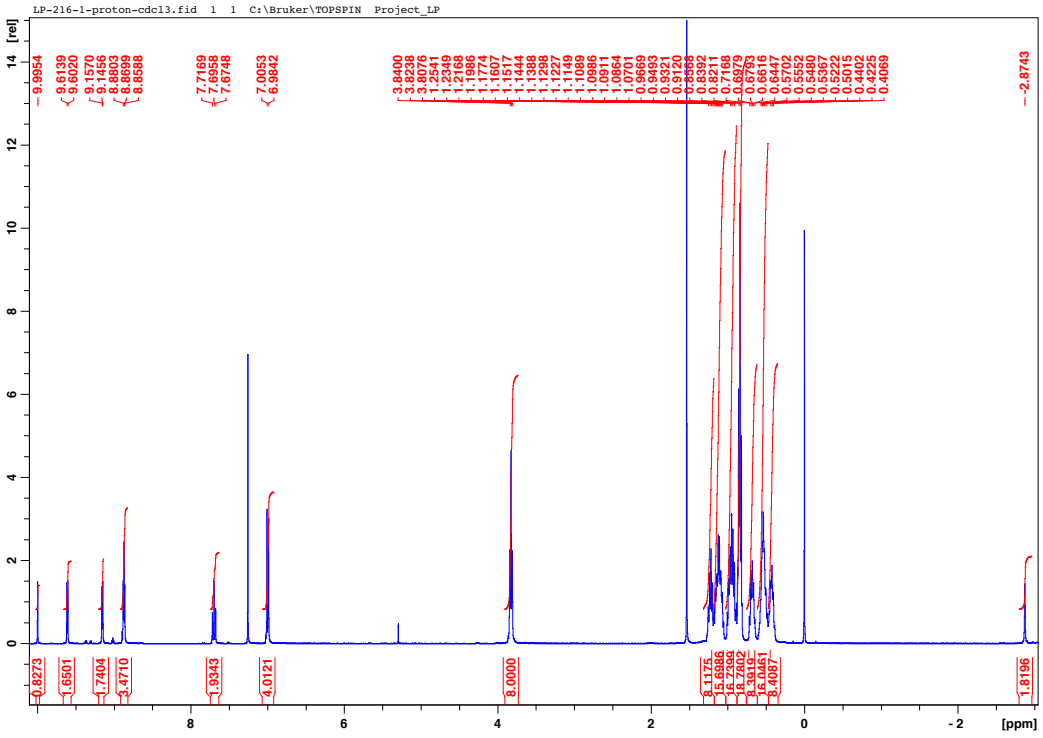

^{1}H NMR spectrum of **5.14** in $CDCl_3$ at RT.

5.15

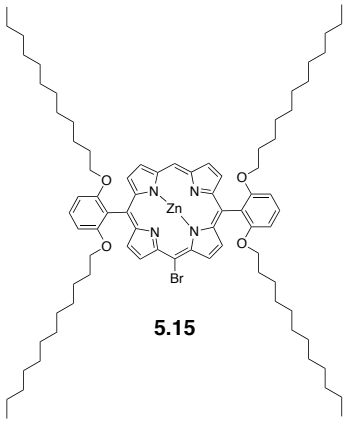

5.15

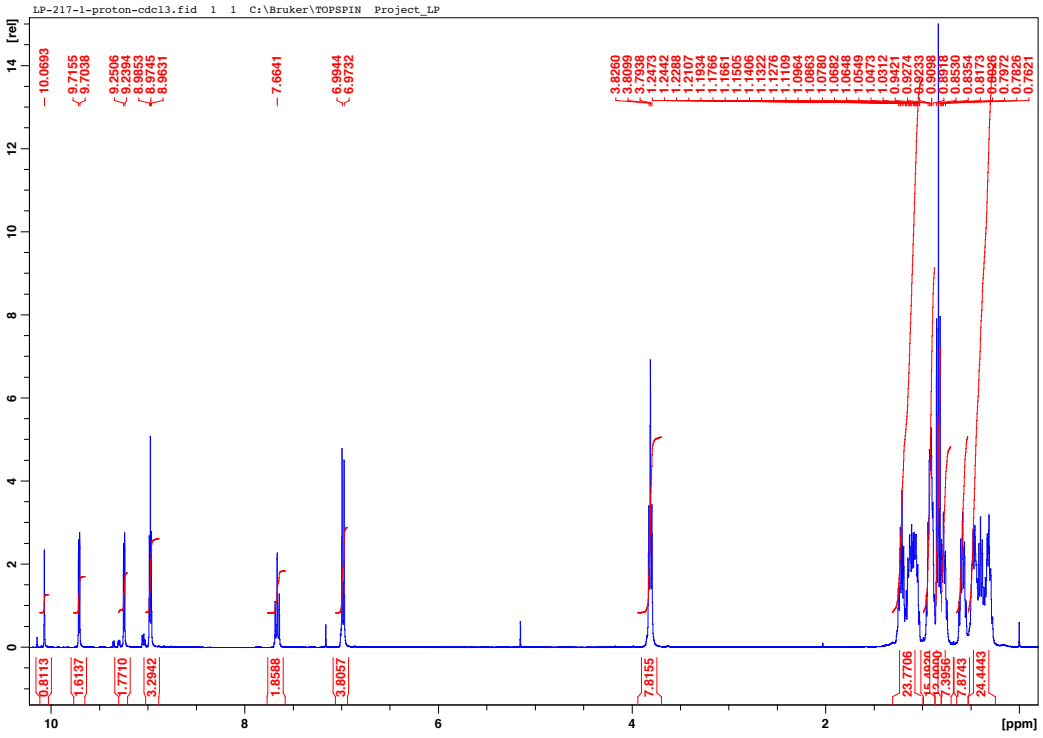

^{1}H NMR spectrum of **5.15** in $CDCl_3$ at RT.

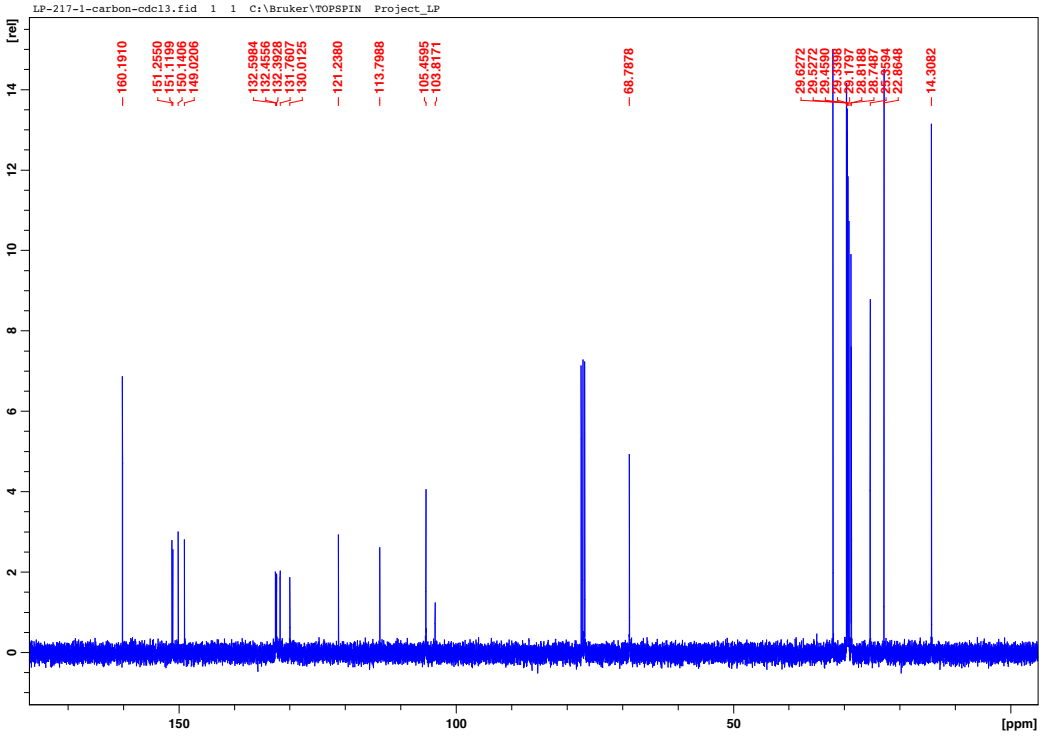

^{13}C NMR spectrum of **5.15** in $CDCl_3$ at RT.

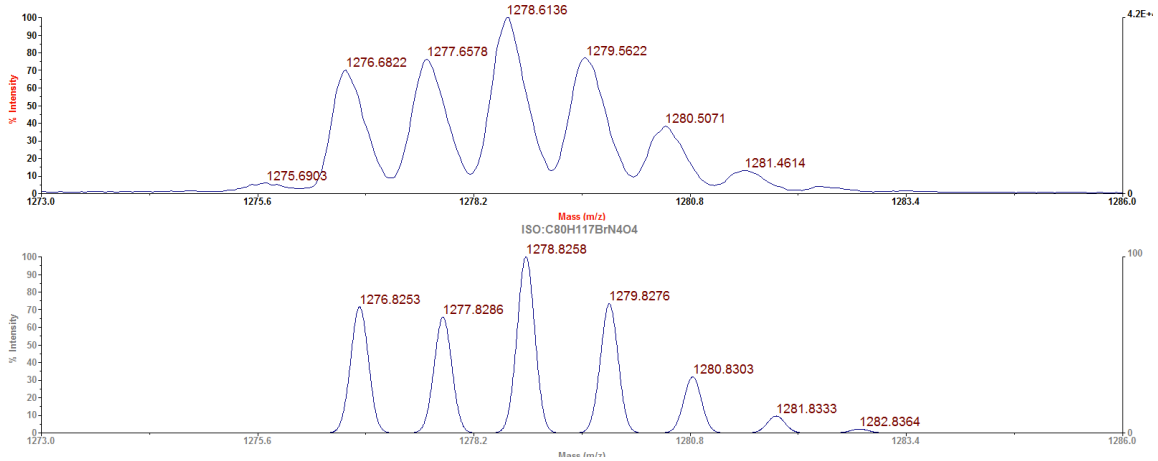

MALDI-TOF mass spectrum for **5.15**. The top trace shows the observed spectrum and the bottom trace shows the theoretical spectrum for chemical formula $C_{80}H_{117}BrN_4O_4$ $[M]^+$.

5.16

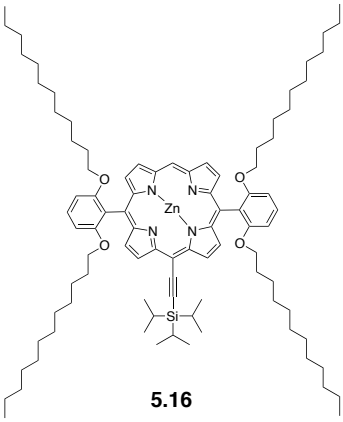

5.16

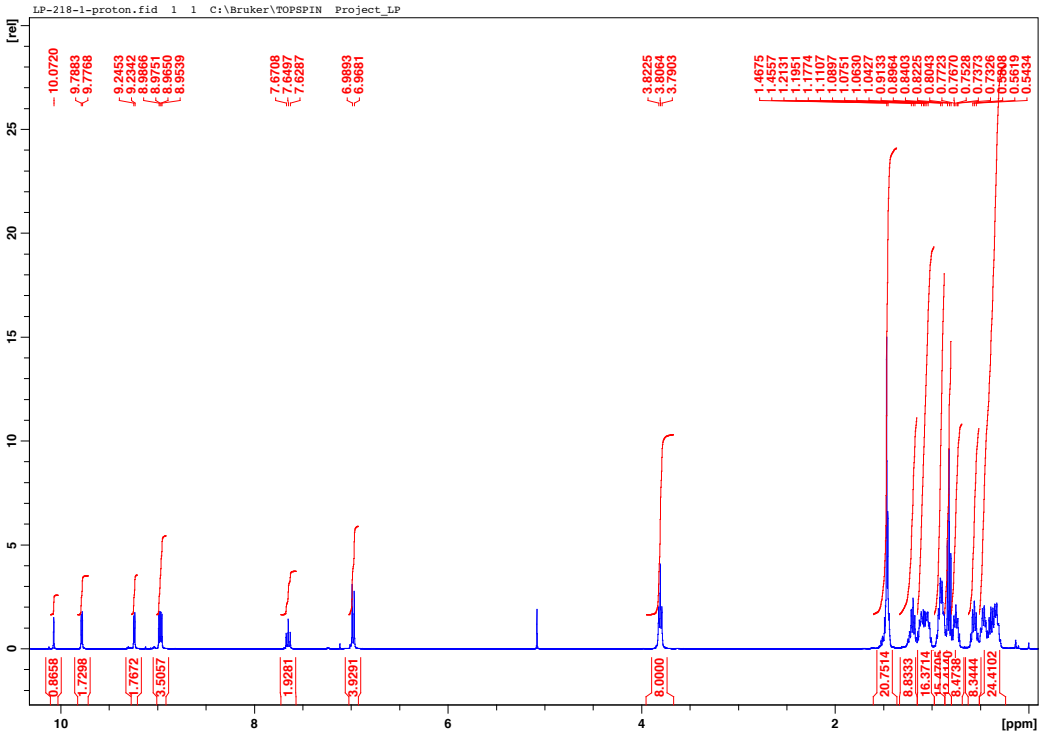

^{1}H NMR spectrum of **5.16** in $CDCl_3$ at RT.

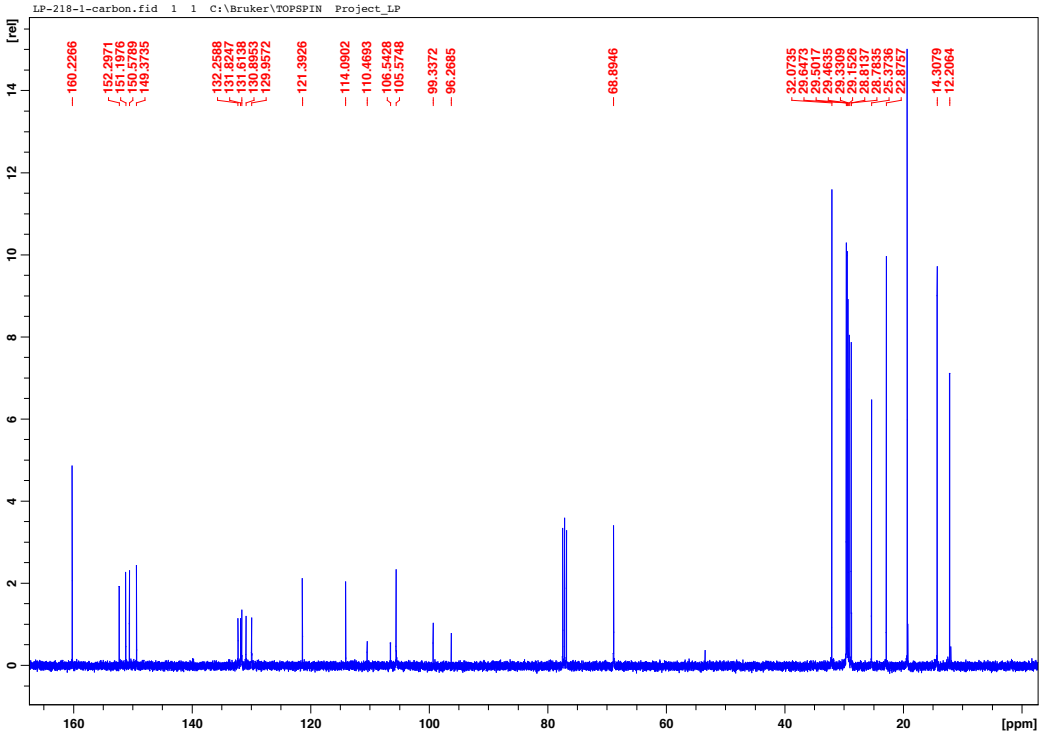

^{13}C NMR spectrum of **5.16** in $CDCl_3$ at RT.

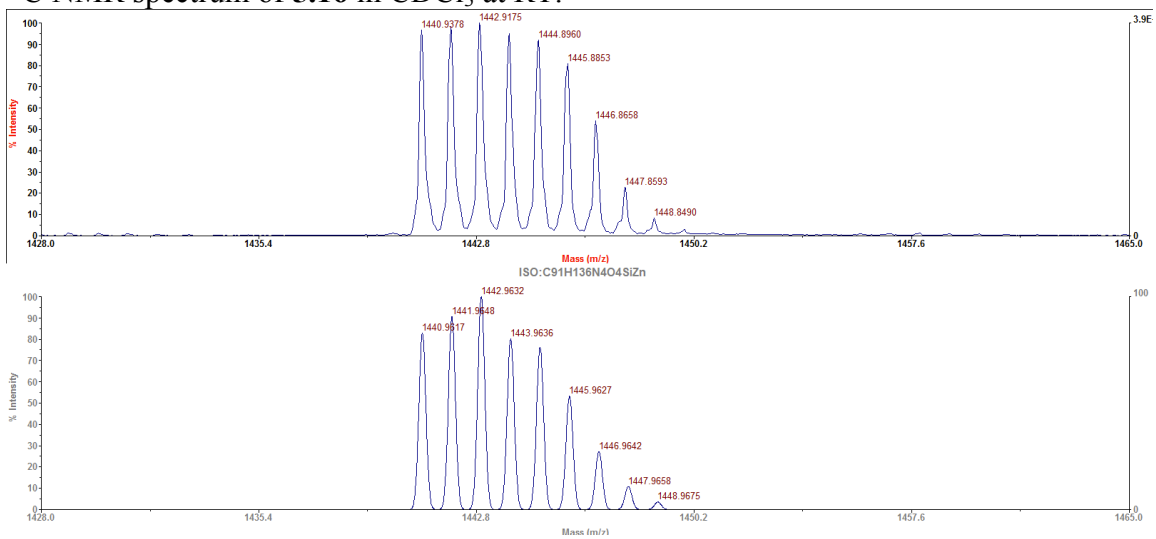

MALDI-TOF mass spectrum for **5.16**. The top trace shows the observed spectrum and the bottom trace shows the theoretical spectrum for chemical formula $C_{91}H_{136}N_4O_4SiZn$ $[M]^+$.

5.17

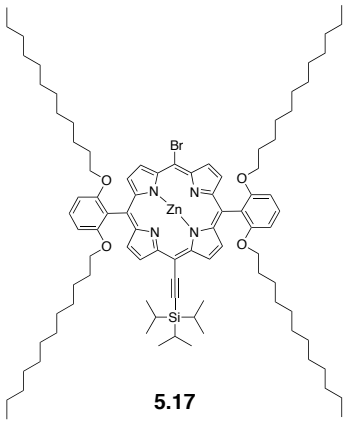

5.17

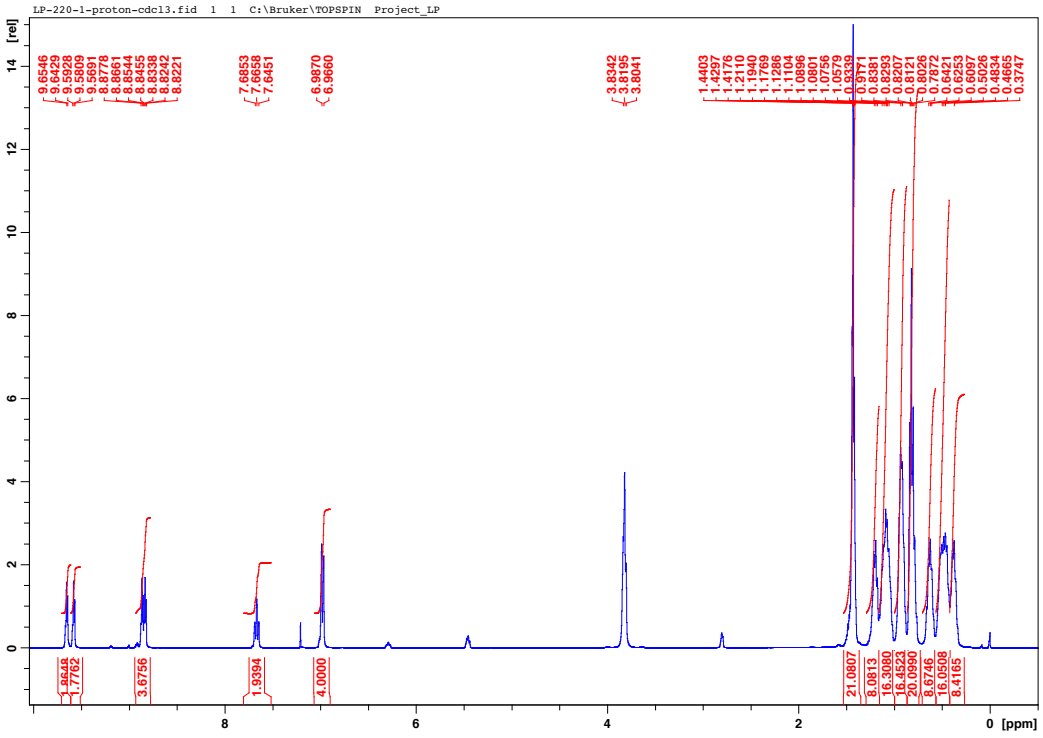

^{1}H NMR spectrum of **5.17** in $CDCl_3$ at RT.

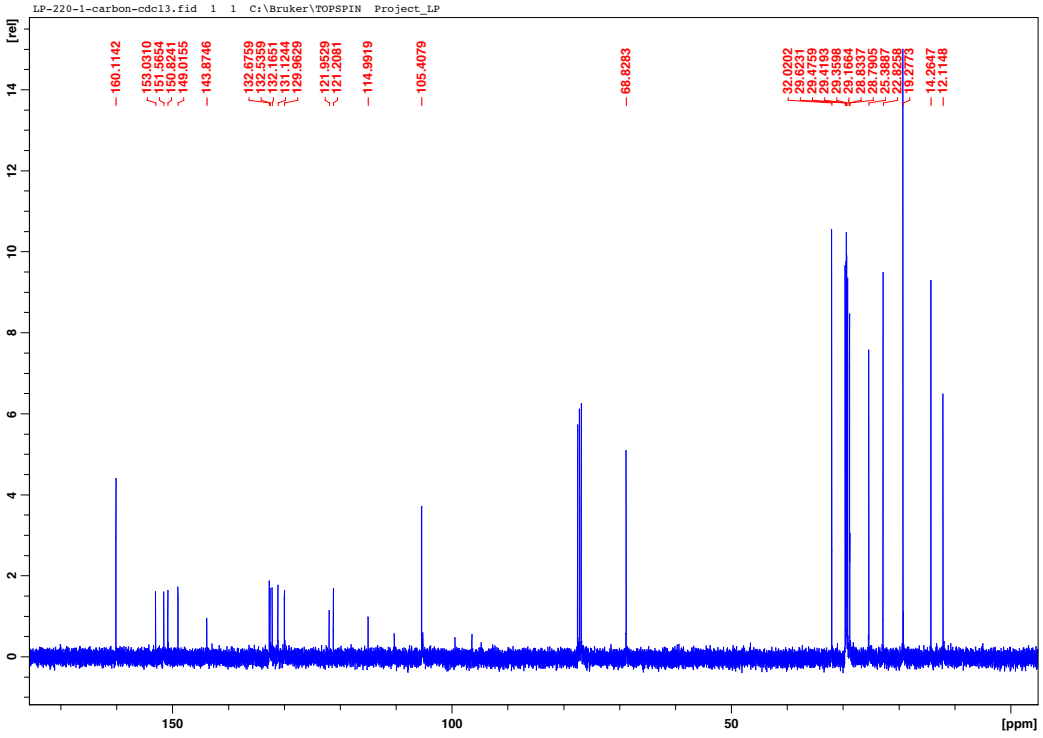

^{13}C NMR spectrum of **5.17** in $CDCl_3$ at RT.

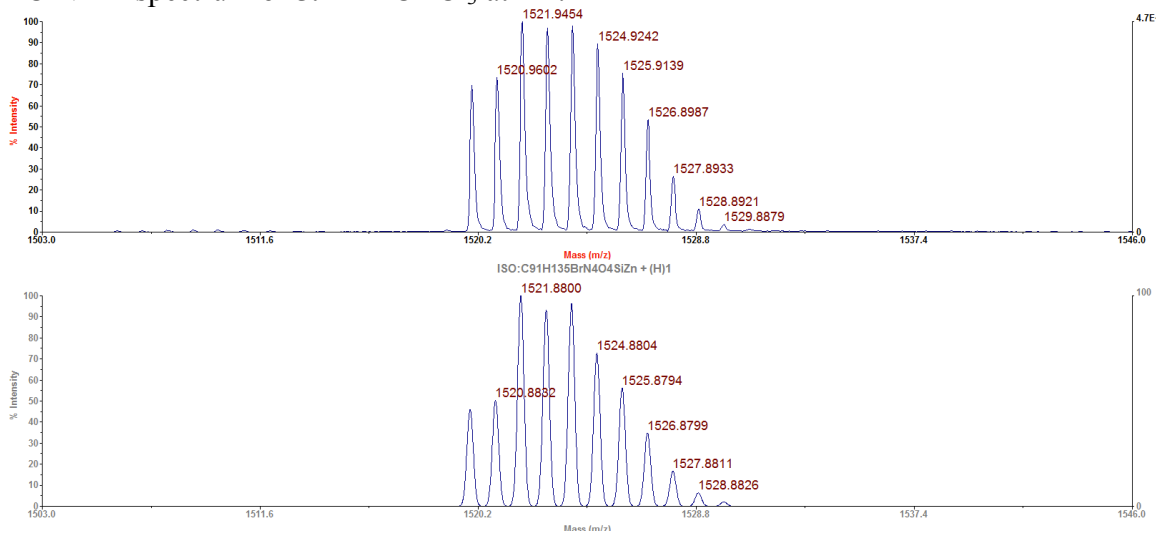

MALDI-TOF mass spectrum for **5.17**. The top trace shows the observed spectrum and the bottom trace shows the theoretical spectrum for chemical formula $C_{91}H_{136}BrN_4O_4SiZn$ $[M+H]^+$.

5.18

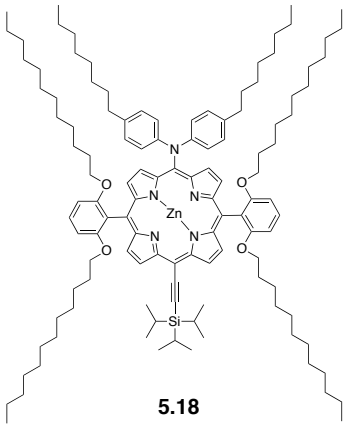

5.18

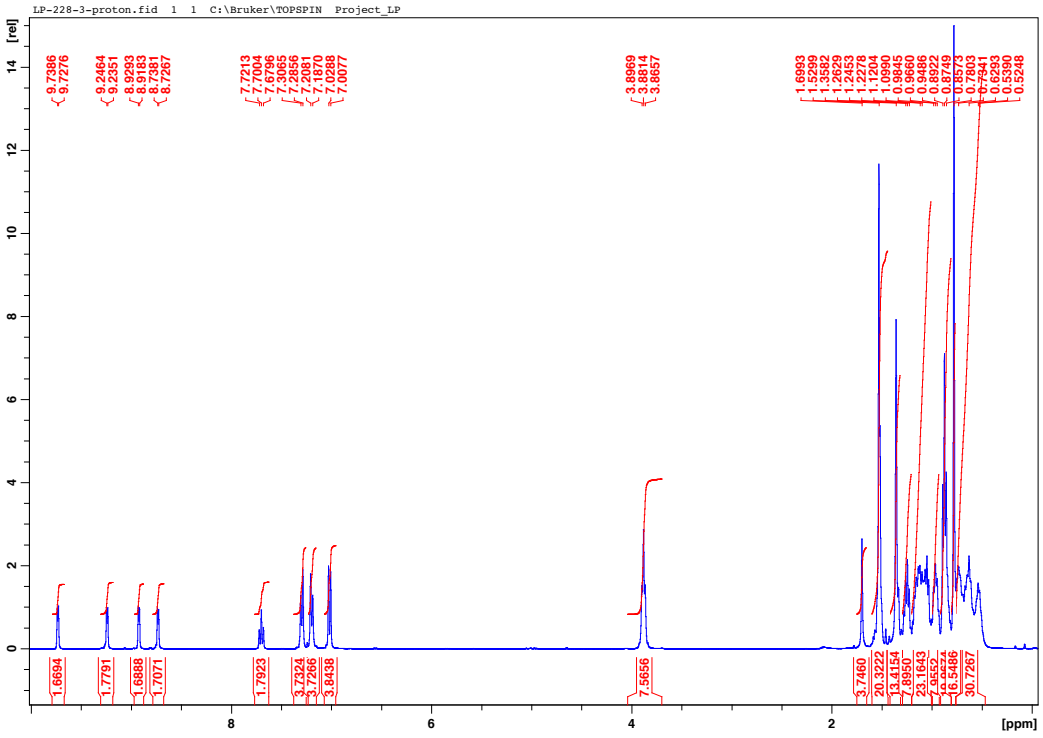

^{1}H NMR spectrum of **5.18** in $CDCl_3$ at RT.

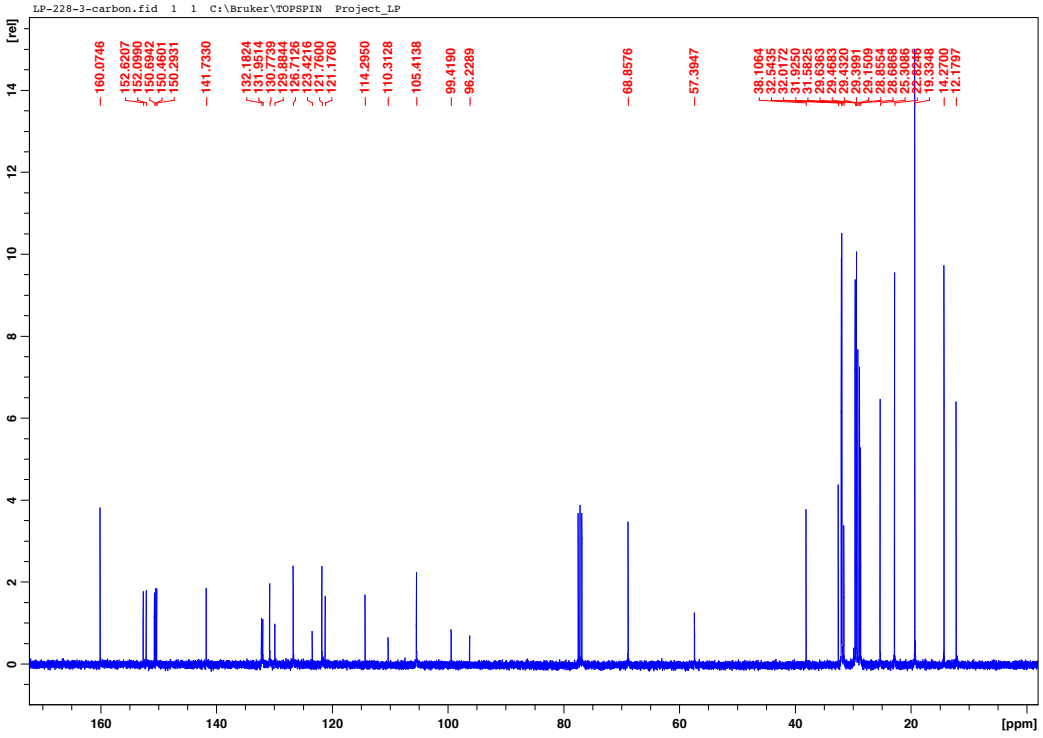

^{13}C NMR spectrum of **5.18** in $CDCl_3$ at RT.

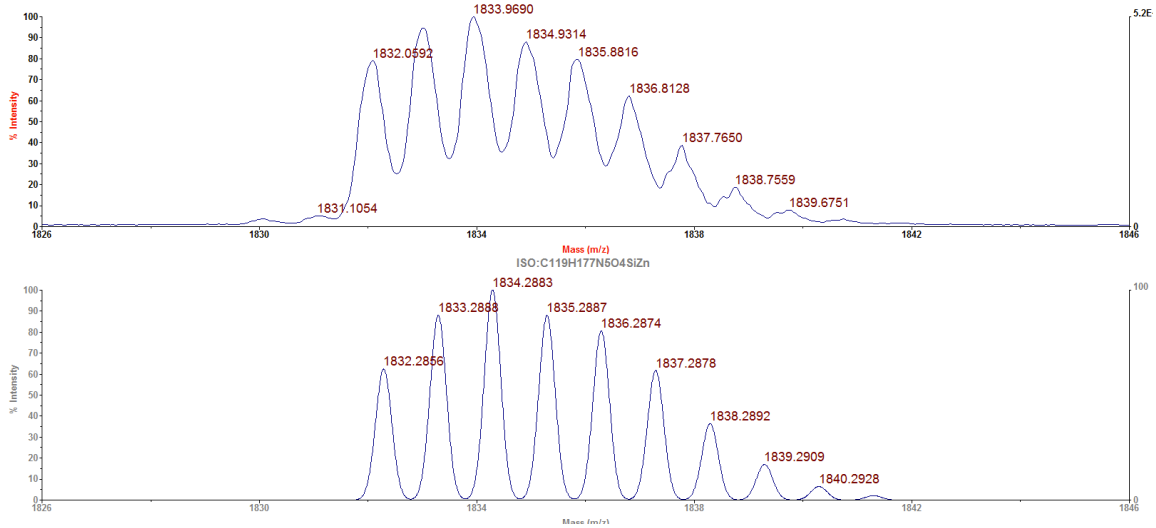

MALDI-TOF mass spectrum for **5.18**. The top trace shows the observed spectrum and the bottom trace shows the theoretical spectrum for chemical formula $C_{119}H_{177}N_5O_4SiZn$ $[M]^+$.

5.19

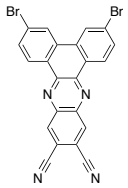

5.19

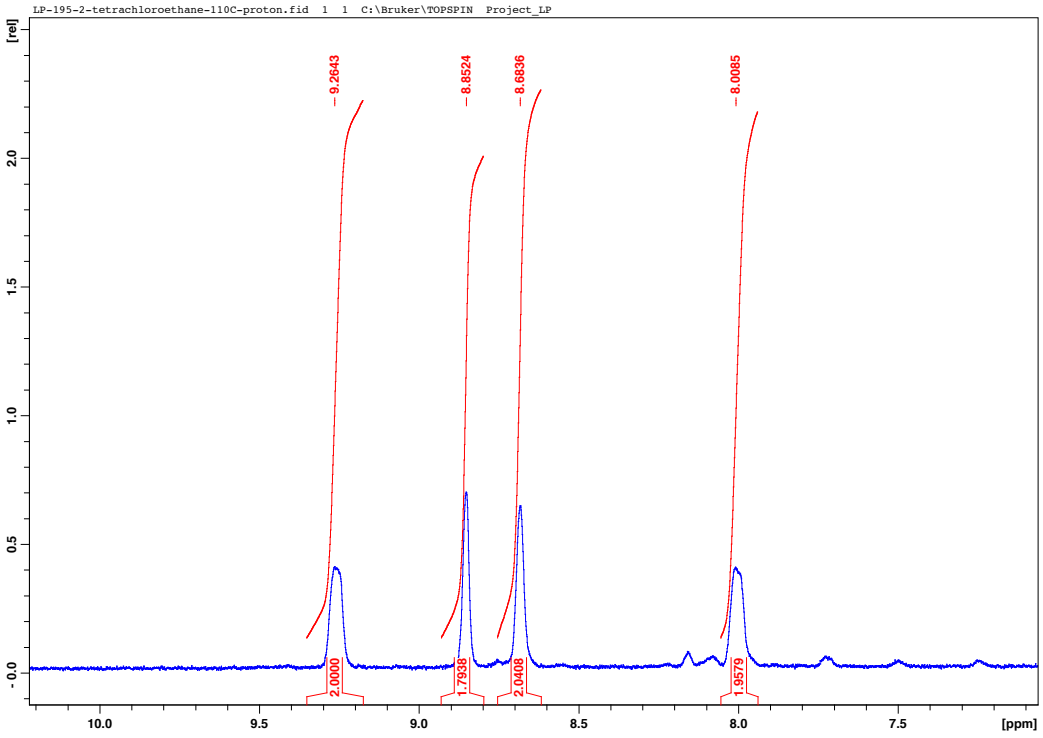

^{1}H NMR spectrum of **5.19** in 1,1,2,2-tetrachloroethane-*d*2 at 110^{o}C.

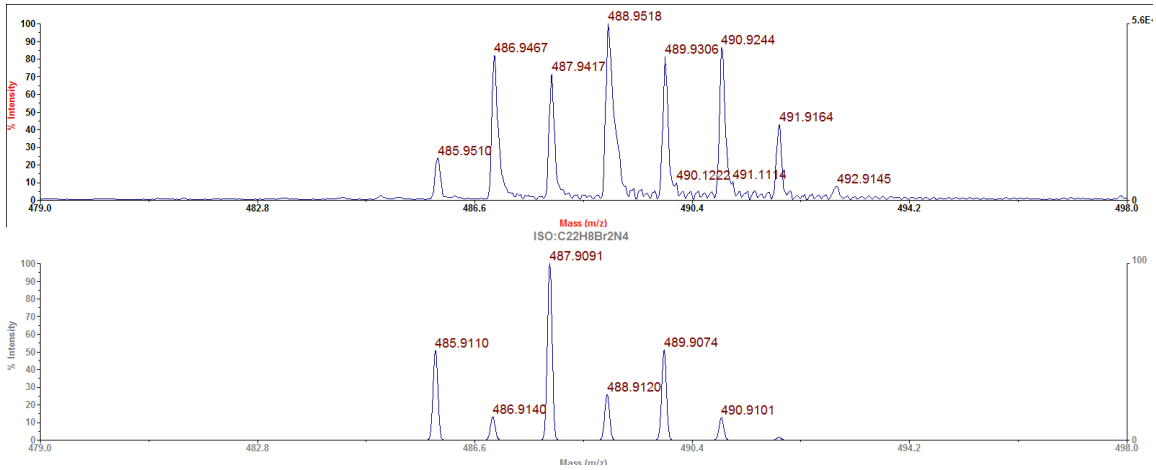

MALDI-TOF mass spectrum for **5.19**. The top trace shows the observed spectrum and the bottom trace shows the theoretical spectrum for chemical formula $C_{22}H_8Br_2N_4$ $[M]^+$.

5.20

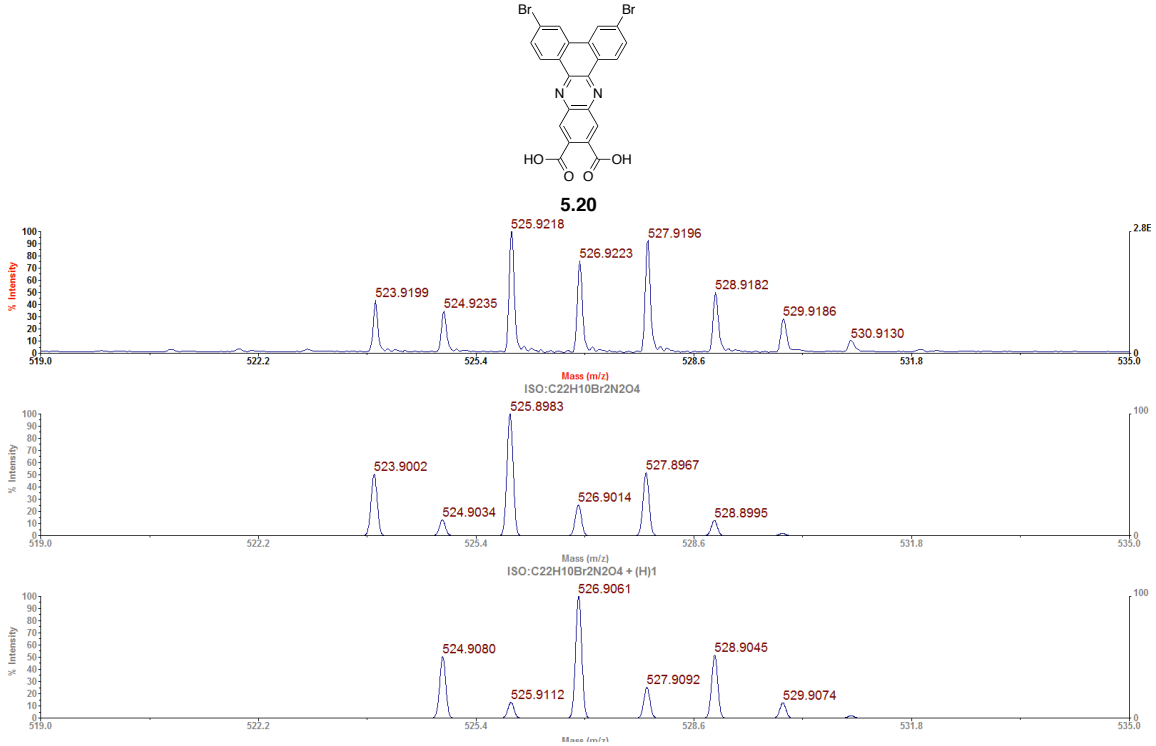

MALDI-TOF mass spectrum for **5.20**. The top trace shows the observed spectrum and the bottom traces show the theoretical spectrum for chemical formula $C_{22}H_{10}Br_2N_2O_4$ $[M]^+$ and $C_{22}H_{11}Br_2N_2O_4$ $[M+H]^+$. It is proposed that the observed spectrum is a superposition of the two theoretical spectra shown.

5.21

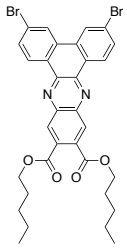

5.21

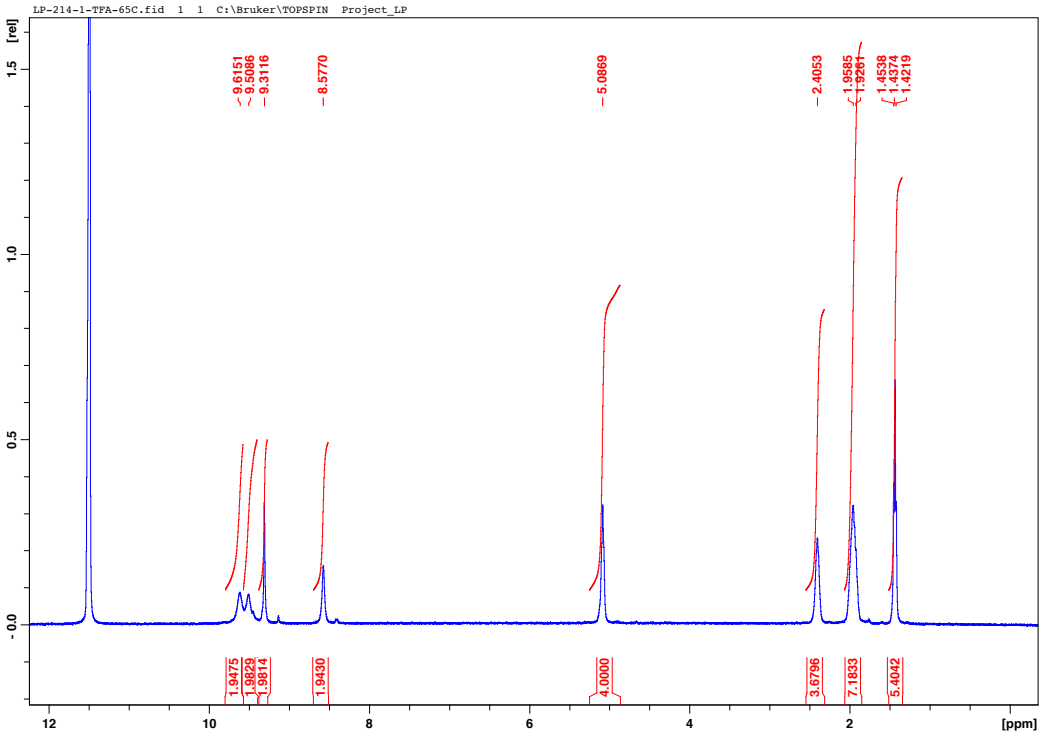

^{1}H NMR spectrum of **5.21** in $CDCl_3$ at RT.

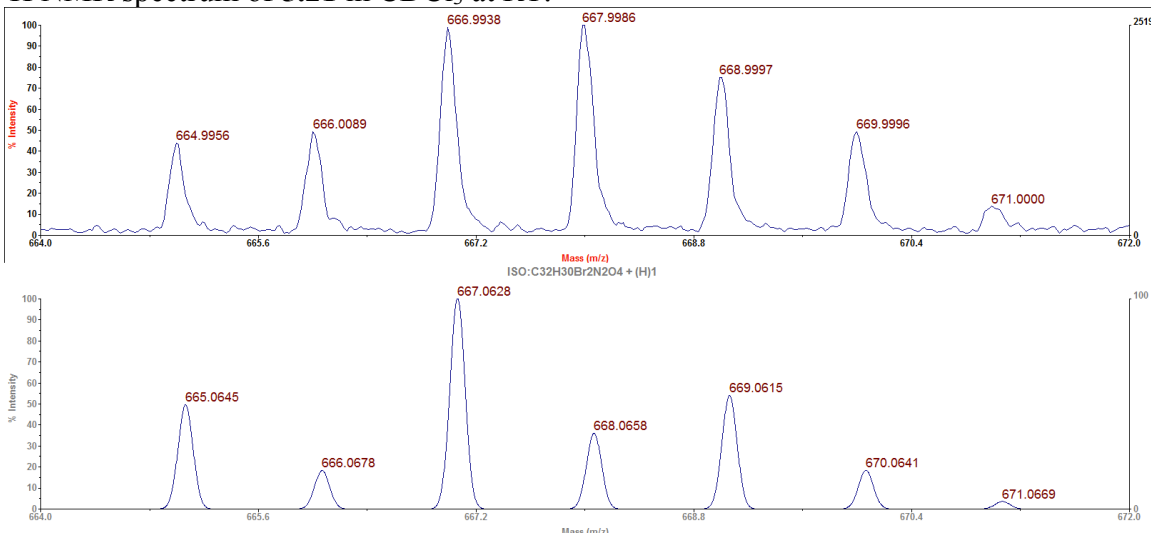

MALDI-TOF mass spectrum for **5.21**. The top trace shows the observed spectrum and the bottom trace shows the theoretical spectrum for chemical formula $C_{32}H_{30}Br_2N_2O_4$ $[M]^+$.

5.22

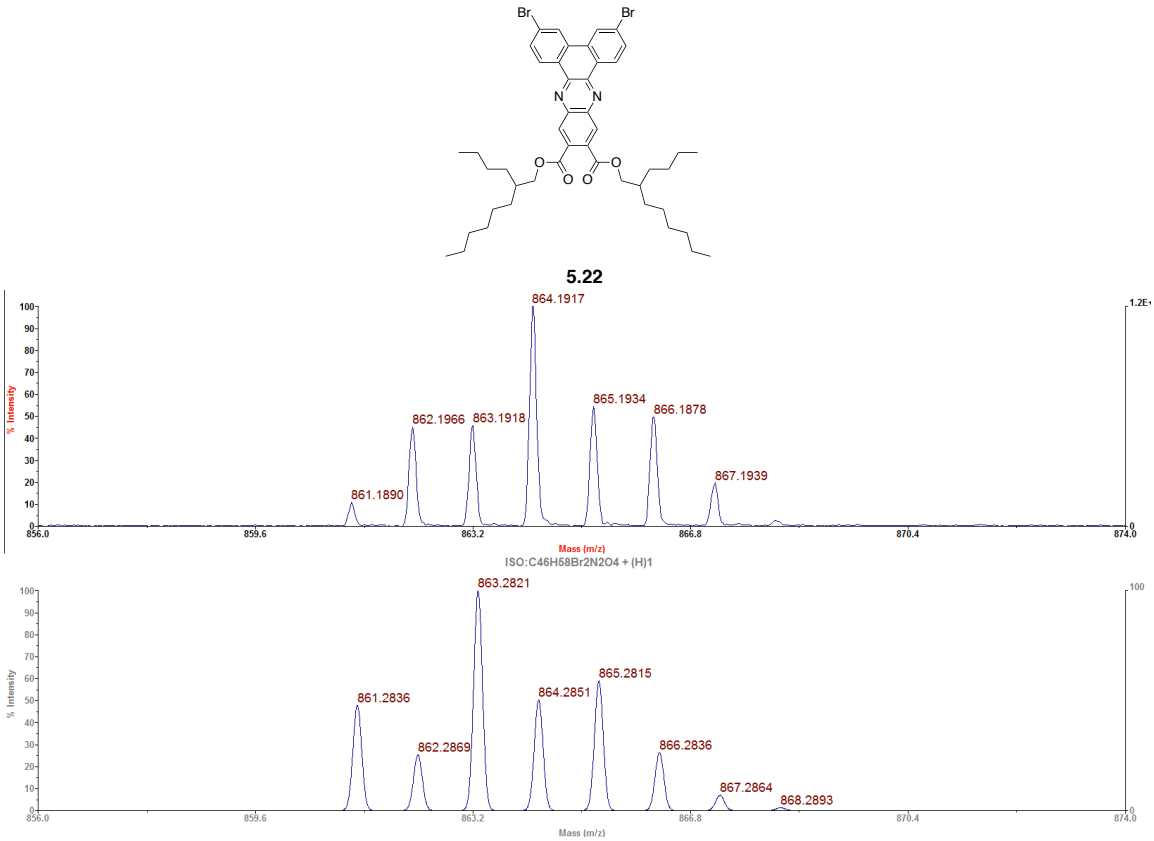

MALDI-TOF mass spectrum for **5.22**. The top trace shows the observed spectrum and the bottom trace shows the theoretical spectrum for chemical formula $C_{46}H_{59}Br_2N_2O_4$ $[M]^+$.

5.25

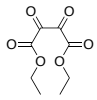

5.25

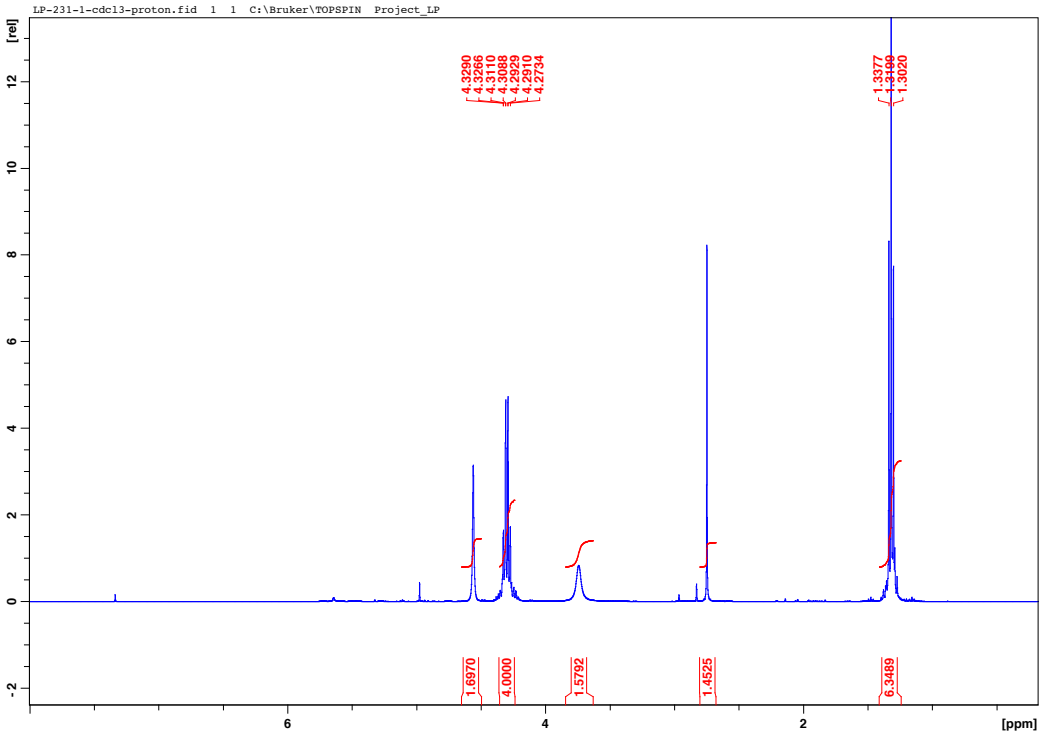

^{1}H NMR spectrum of **5.25** in $CDCl_3$ at RT.

5.26

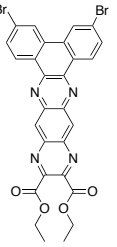

5.26

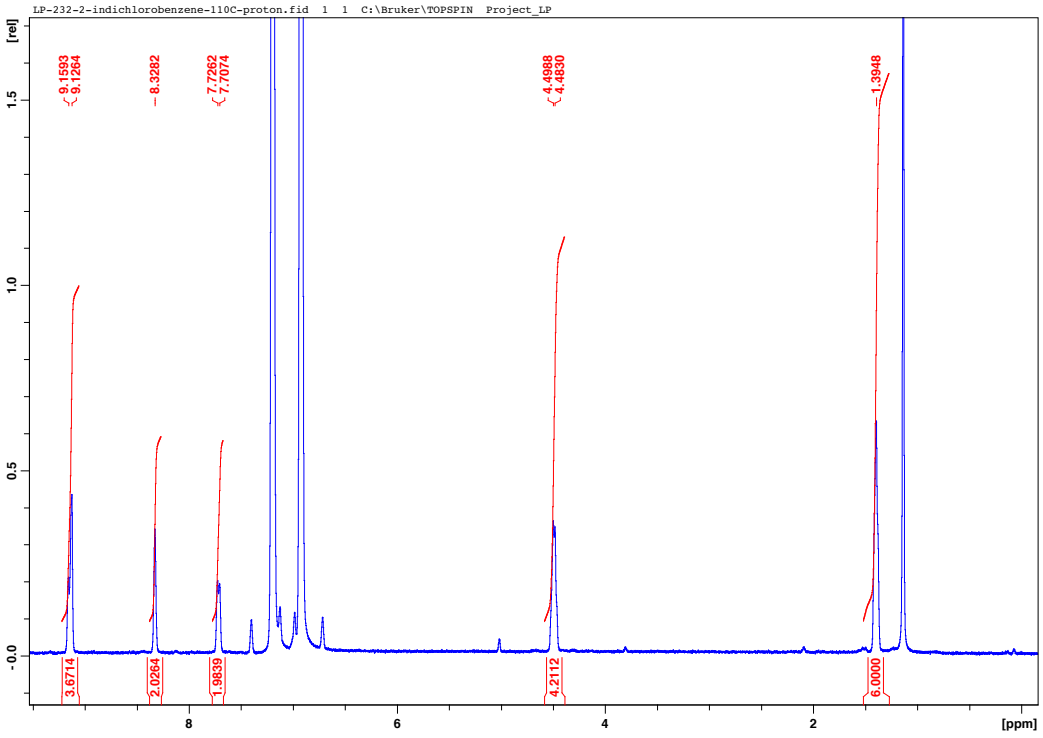

^{1}H NMR spectrum of **5.26** in 1,2-dichlorobenzene-*d*4 at 110^{o}C.

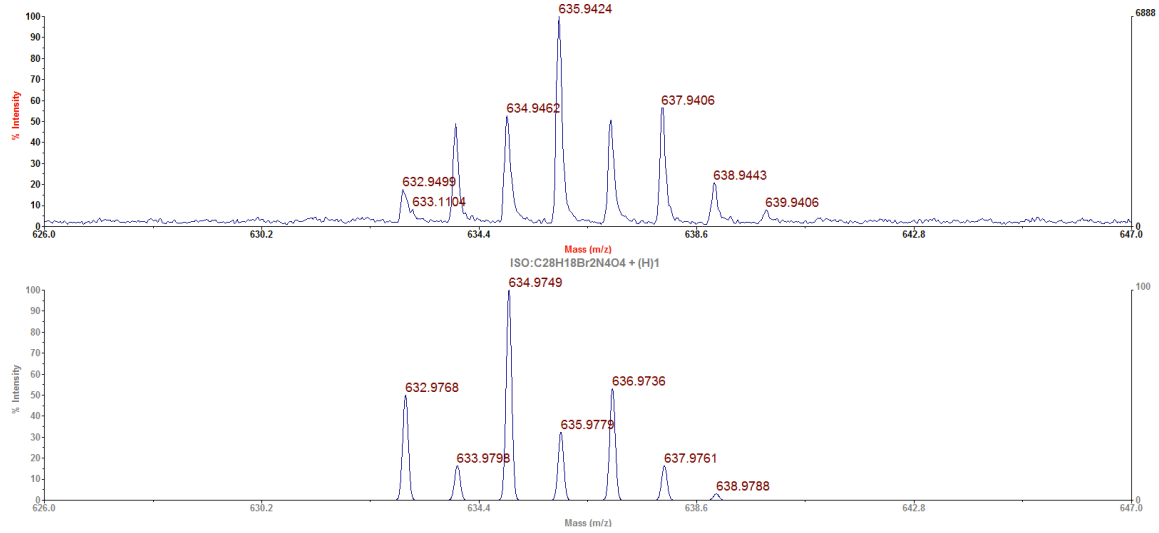

MALDI-TOF mass spectrum for **5.26**. The top trace shows the observed spectrum and the bottom trace shows the theoretical spectrum for chemical formula $C_{28}H_{19}Br_2N_{14}O_4$ $[M+H]^+$.

5.27

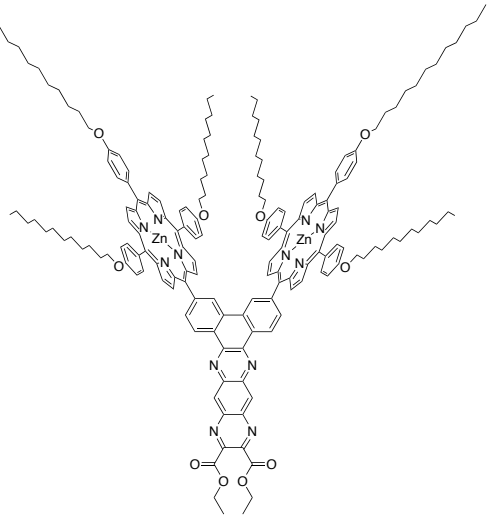

5.27

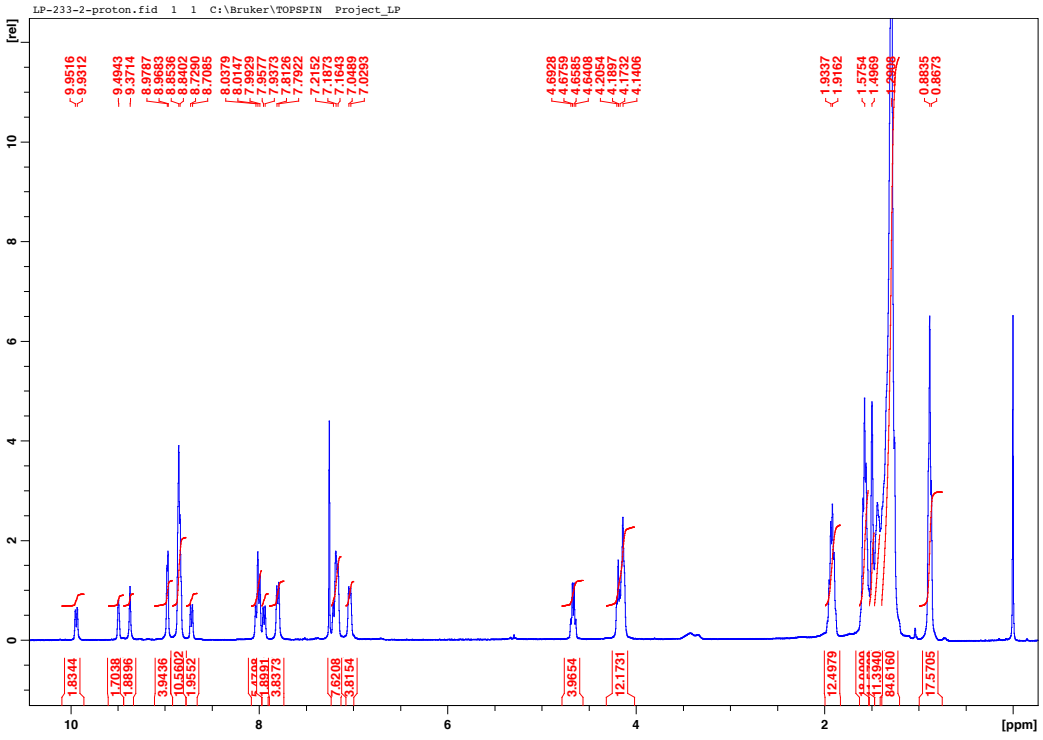

^{1}H NMR spectrum of **5.27** in $CDCl_3$ at RT.

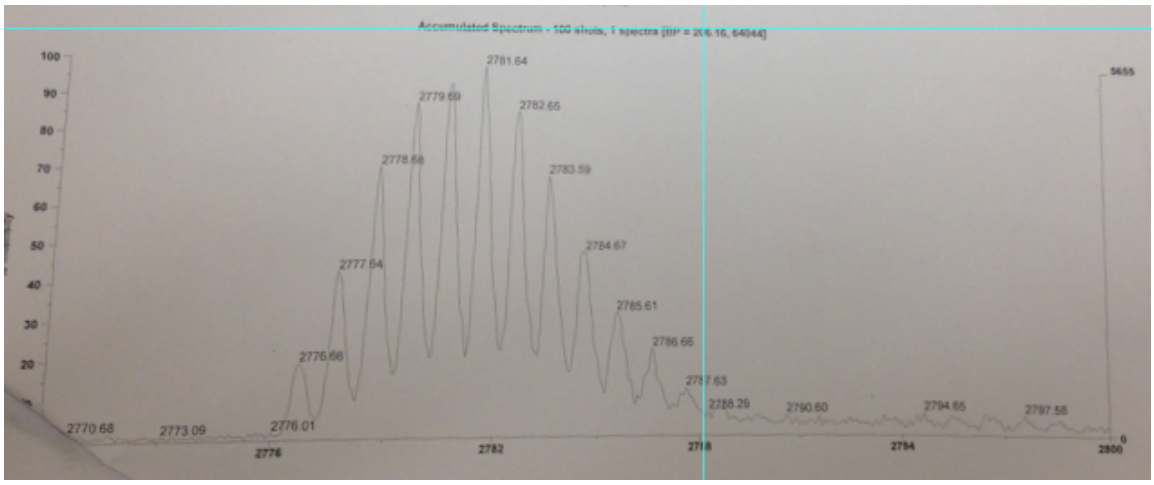

MALDI-TOF mass spectrum for **5.27** . The top trace shows the observed spectrum.

APPENDIX E

NMR and MASS SPECTRAL DATA FOR SYNTHESIZED COMPOUNDS OF CHAPTER 6

6.1

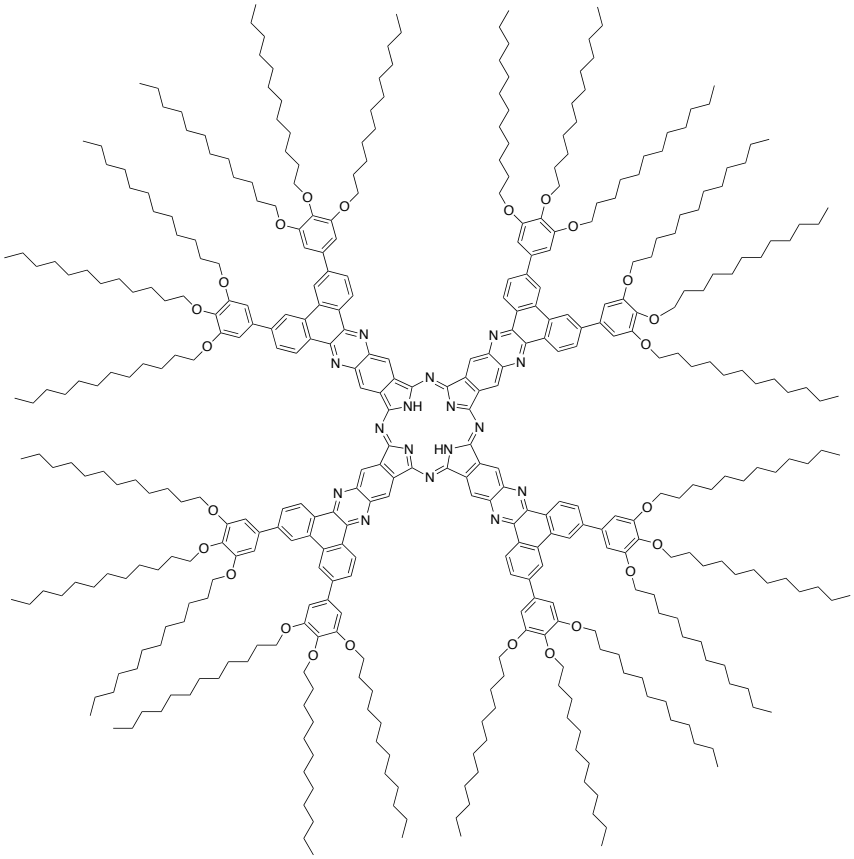

6.1

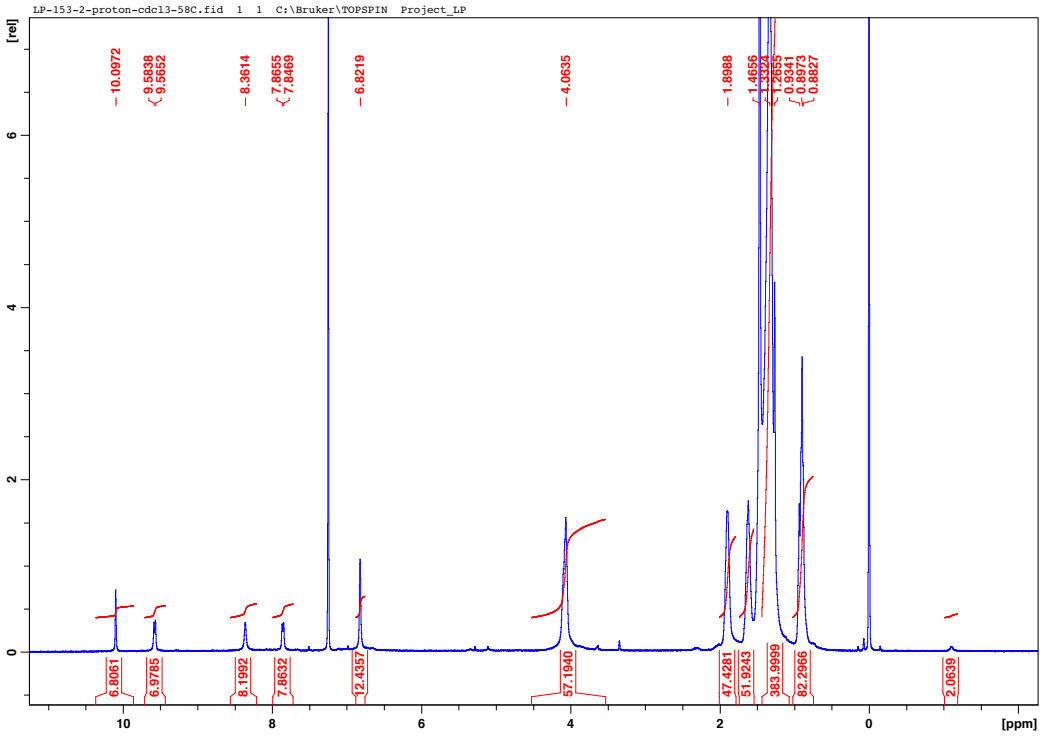

^{1}H NMR spectrum of **6.1** in $CDCl_3$ at 58^{o}C.

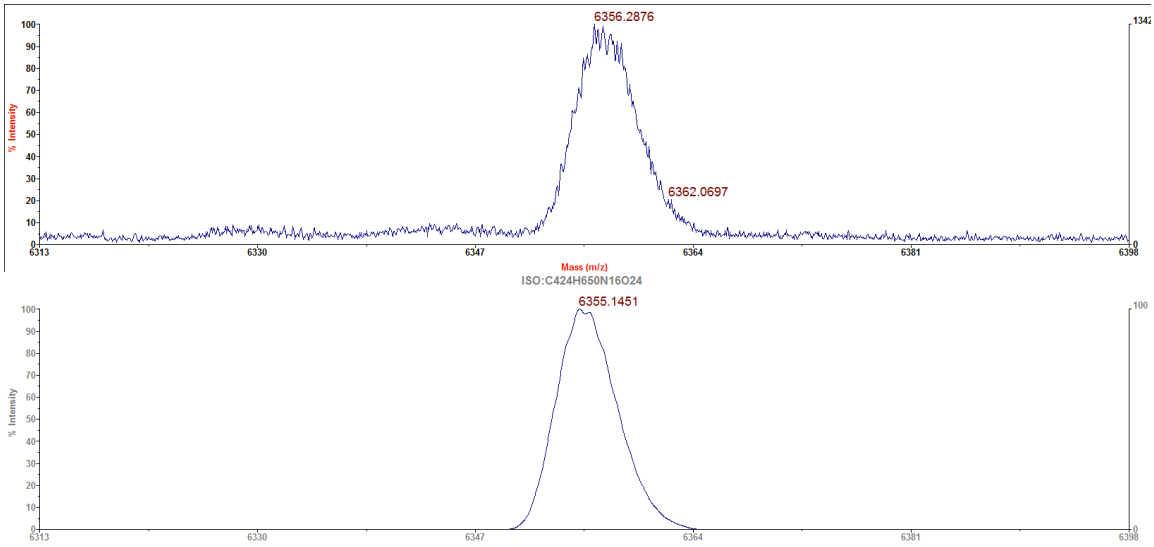

MALDI-TOF mass spectrum for **6.1**. The top trace shows the observed spectrum and the bottom trace shows the theoretical spectrum for chemical formula $C_{424}H_{650}N_{16}O_{24}[M]^{+}$.

6.2

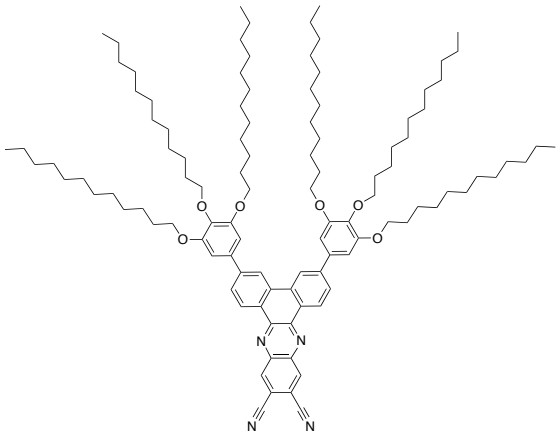

6.2

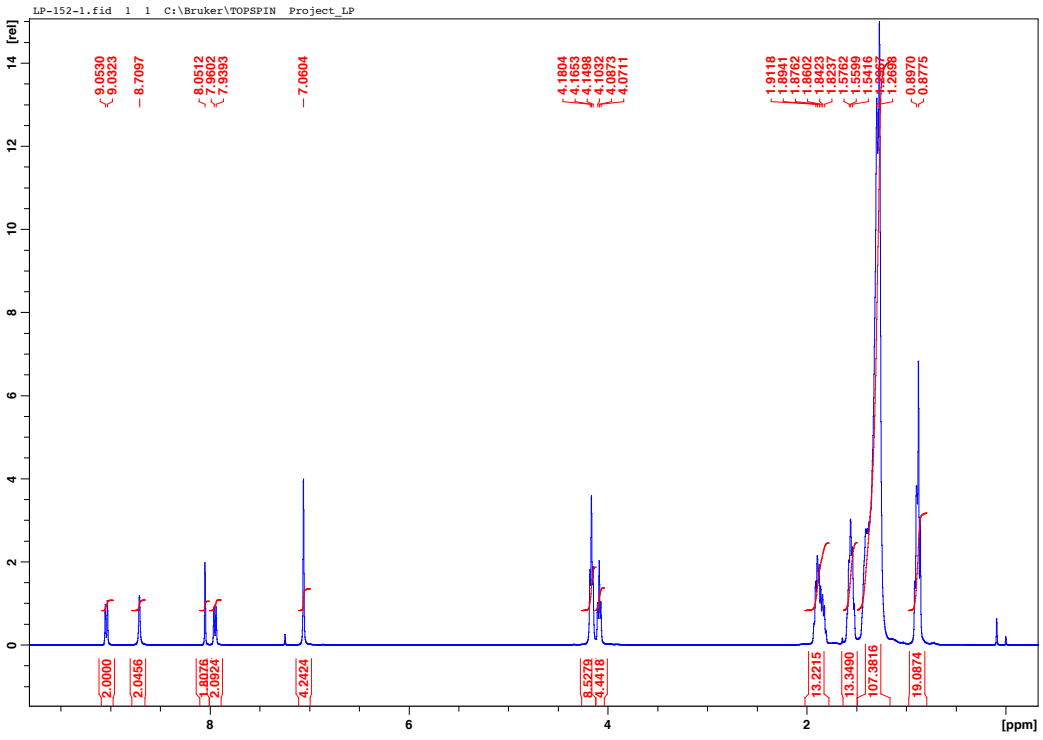

^{1}H NMR spectrum of **6.2** in $CDCl_3$ at RT.

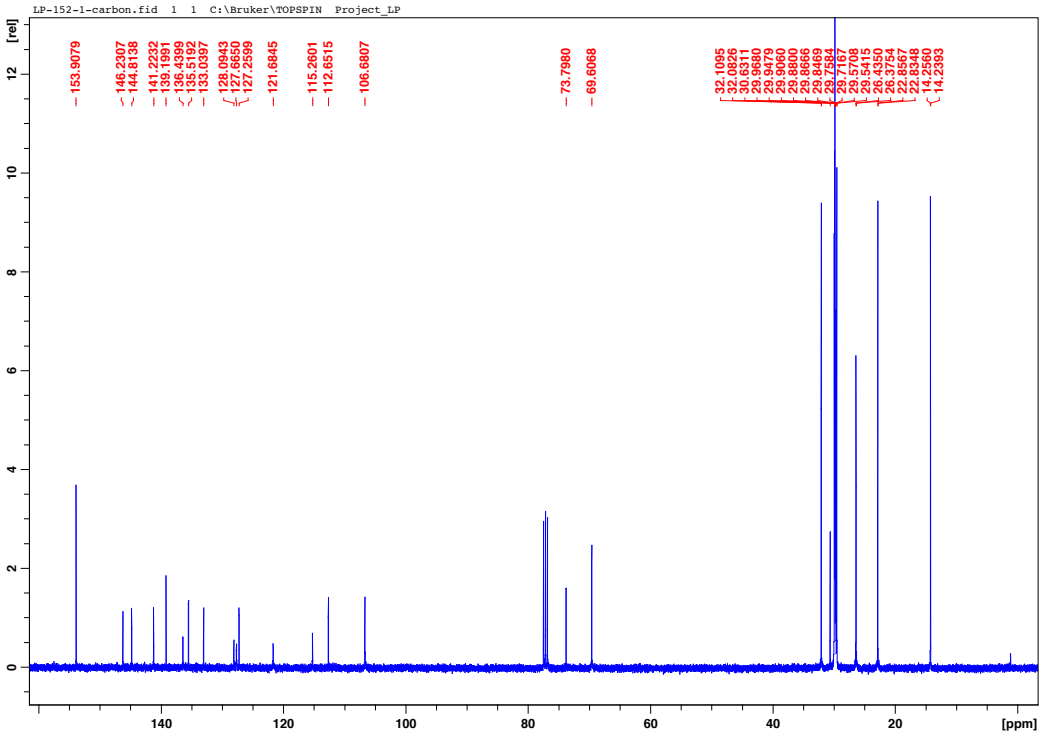

^{13}C NMR spectrum of **6.2** in $CDCl_3$ at RT.

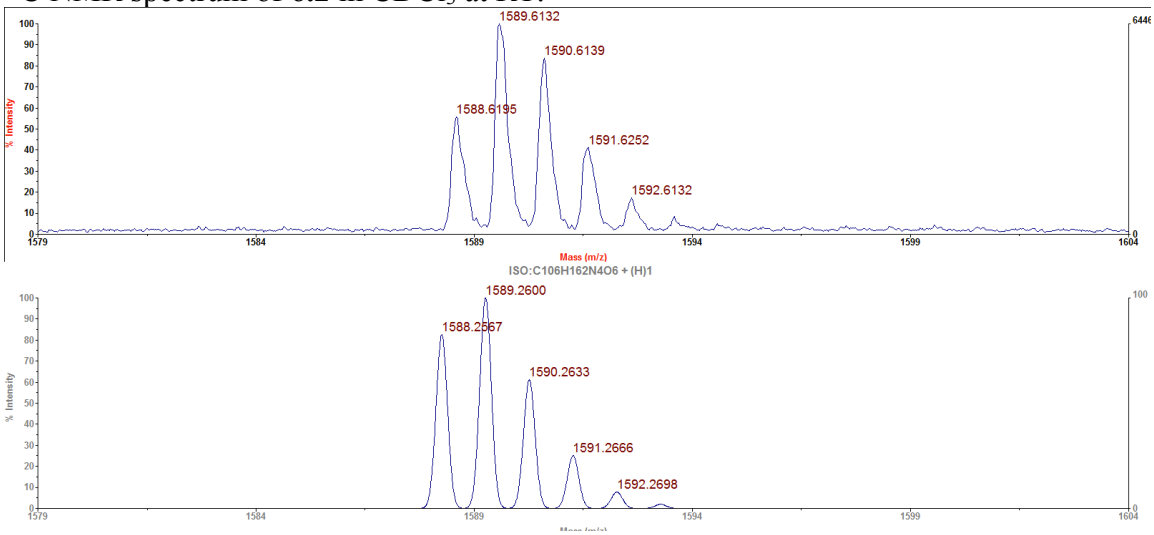

MALDI-TOF mass spectrum for **6.2**. The top trace shows the observed spectrum and the bottom trace shows the theoretical spectrum for chemical formula $C_{106}H_{163}N_4O_6$ $[M+1]^+$.